WORKSHOP ON

Advanced PEM Fuel Cell Membranes and Membrane-Electrode Assemblies for Non-Conventional Fuels.

April 28 - May 1, 1998

Edited by

Charles W. Martin
Department of Chemistry

And

Darryl D. DesMarteau
Department of Chemistry

Clemson University
P. O. Box 1905
Clemson, SC 29634-1905

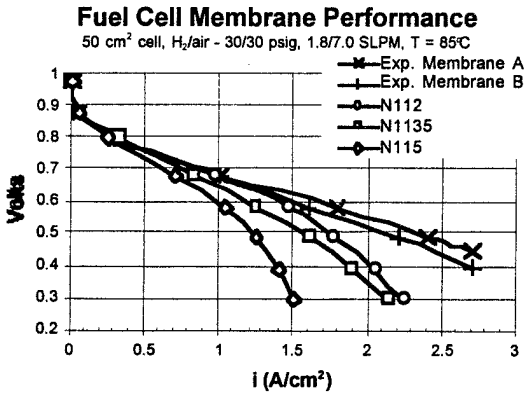

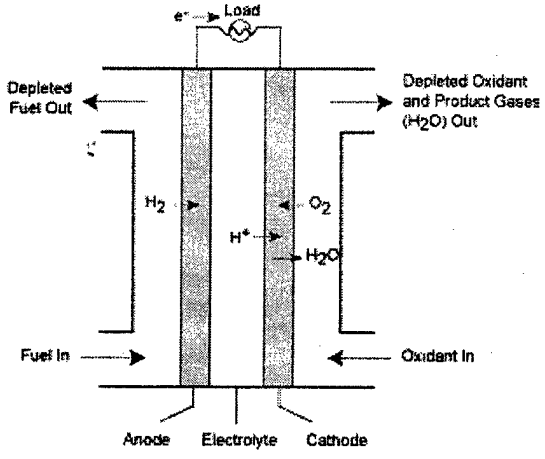

The views, opinions, and /or findings contained in this report are those of the author(s) and should not be construed as an official Department of Defense position, policy, or decision, unless so designated by other documentation.

DISTRIBUTION STATEMENT A
Approved for Public Release
Distribution Unlimited

REPORT DOCUMENTATION PAGE

Form Approved
OMB NO. 0704-0188

Public Reporting burden for this collection of information is estimated to average 1 hour per response, including the time for reviewing instructions, searching existing data sources, gathering and maintaining the data needed, and completing and reviewing the collection of information. Send comment regarding this burden estimates or any other aspect of this collection of information, including suggestions for reducing this burden, to Washington Headquarters Services, Directorate for information Operations and Reports, 1215 Jefferson Davis Highway, Suite 1204, Arlington, VA 22202-4302, and to the Office of Management and Budget, Paperwork Reduction Project (0704-0188,) Washington, DC 20503.

1. AGENCY USE ONLY (Leave Blank)	2. REPORT DATE July 1999	3. REPORT TYPE AND DATES COVERED Final Report

4. TITLE AND SUBTITLE
Workshop on Advanced PEM Fuel Cell Membranes and Membrane-Electrode Assemblies for Non-Conventional Fuels

5. FUNDING NUMBERS
DAAG55-98-1-0204

6. AUTHOR(S)
Charles W. Martin

7. PERFORMING ORGANIZATION NAME(S) AND ADDRESS(ES)
Clemson University
Clemson, SC 29634-1095

8. PERFORMING ORGANIZATION REPORT NUMBER

9. SPONSORING / MONITORING AGENCY NAME(S) AND ADDRESS(ES)
U. S. Army Research Office
P.O. Box 12211
Research Triangle Park, NC 27709-2211

10. SPONSORING / MONITORING AGENCY REPORT NUMBER
ARO 38702.1-CH-CF

11. SUPPLEMENTARY NOTES
The views, opinions and/or findings contained in this report are those of the author(s) and should not be construed as an official Department of the Army position, policy or decision, unless so designated by other documentation.

12 a. DISTRIBUTION / AVAILABILITY STATEMENT
Approved for public release; distribution unlimited.

12 b. DISTRIBUTION CODE

13. ABSTRACT

The workshop was organized to examine the problem of utilizing fuels alternative to neat hydrogen. Sponsors included the U. S. Army Research Office (ARO), the U. S. Office of Naval Research (ONR), and the Defense Advanced Research Projects Agency (DARPA). The Organizing Committee consisted of Professors Charles Martin and Darryl DesMarteau (Clemson University), Drs. Peter Fedkiw and Dick Paur (ARO), Dr. Richard Carlin (ONR) and Dr. Bob Nowak (DARPA). A group of 69 scientists and engineers from industry, academia and government laboratories were assembled at the Holiday Inn Boardwalk in Las Vegas, NV, April 28 – May 1, 1998. Their objective was to examine the state-of-the-art of current PEM fuel cell systems for alternate fuels, to identify the most important factors limiting the efficient use of these fuels, and to recommend the most promising directions for future research to overcome those limitations.

14. SUBJECT TERMS

15. NUMBER OF PAGES

16. PRICE CODE

17. SECURITY CLASSIFICATION OR REPORT	18. SECURITY CLASSIFICATION ON THIS PAGE	19. SECURITY CLASSIFICATION OF ABSTRACT	20. LIMITATION OF ABSTRACT
UNCLASSIFIED	UNCLASSIFIED	UNCLASSIFIED	UL

WORKSHOP ON

Advanced PEM Fuel Cell Membranes and Membrane-Electrode Assemblies for Non-Conventional Fuels.

April 28 - May 1, 1998

Edited by

Charles W. Martin
Department of Chemistry

And

Darryl D. DesMarteau
Department of Chemistry

Clemson University
P. O. Box 1905
Clemson, SC 29634-1905

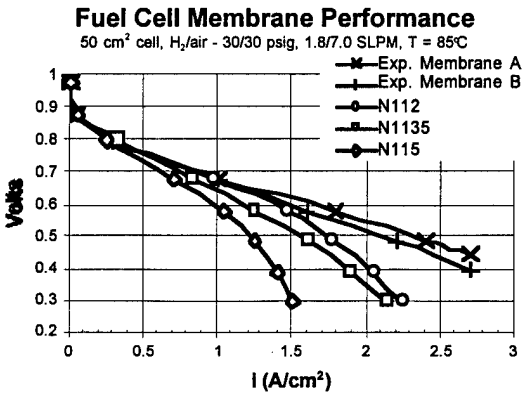

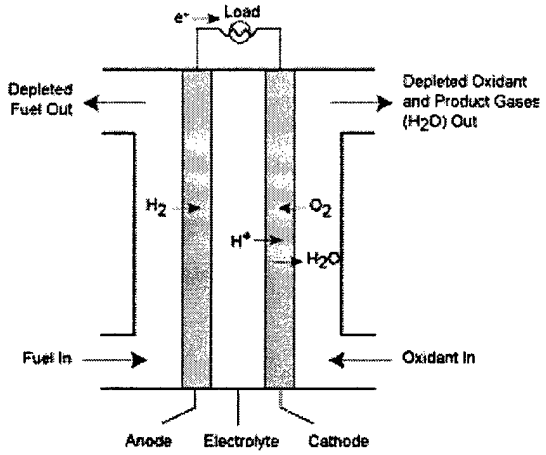

The views, opinions, and /or findings contained in this report are those of the author(s) and should not be construed as an official Department of Defense position, policy, or decision, unless so designated by other documentation.

DTIC QUALITY INSPECTED 4

19991101 067

Table of Contents

	Page
Preface	1
Executive Summary	4
Report on Working Group Discussions	7
Agenda	22
Workshop Participants	25
Plenary Session	31
Army/DARPA Power Perspective (Paur)	31
DARPA Advanced Energy Technologies (Nowak)	42
Navy Research and Development Programs (Carlin)	56
The Army After Next Project (Jones) (Background article reprinted from *"Army RD&A"* May-June, 1998)	66
Soldier Portable Hybrid Electrical Power Systems (Brandhorst)	102
Satisfying the Commercial Requirements for Alternative Energy Applications (Bartelt)	112
Advanced Components for PEM Fuel Cells (Rusch)	129
Technology Update Session I	155
Membrane Electrode Assemblies (Gottesfeld)	155
Structure of the Pt/Ru catalyst for DMFC (Wieckowski)	178
Structure of Perfluorinated Ionomer Solutions (Pineri)	214
Electrocatalyst-Membrane Interface (Mukerjee)	224
Water Uptake by Nafion® Membranes (Zawodzinski)	252
Transport in PFSA Membranes: Computational Studies (Zawodzinski)	261
Methanol Barrier Membranes (Cussler)	278
Direct Methanol Fuel Cells at LANL (Gottesfeld)	286
Organic/Inorganic Nanocomposites (Mauritz)	304
Hydrocarbon PEMs Revisited (Wnek)	343

Technology Update Session II 363

Sulfonated Polyimides Membranes (Pineri) **363**

High Temperature PEM Fuel Cells (Savinell) **384**

High Temperature Functional Fluoropolymers (DesMarteau) **406**

Development of Higher Temperature Proton Exchange Membranes (Datta) **438**

Sulfonated Polyphosphazenes (Pintauro) **456**

An Overview of Ionomer Membrane Stability (Martin) **476**

Preface

The proton exchange membrane (PEM) fuel cell is a highly efficient, environmentally benign power source that has many potential advantages in portable and mobile applications. Practical units with power outputs ranging from less than 100 watts to greater than 10^5 watts have been designed and constructed. One very significant impediment to the implementation of this technology in military and commercial applications, however, is the transport and storage of the primary fuel, hydrogen. If pure hydrogen were as readily available and as easily transported as liquid hydrocarbons, the military and commercial development of PEM fuel cells would proceed at a rapid rate.

The workshop was organized to examine the problem of utilizing fuels alternative to neat hydrogen. Sponsors included the U. S. Army Research Office (ARO), the U. S. Office of Naval Research (ONR), and the Defense Advanced Research Projects Agency (DARPA). The Organizing Committee consisted of Professors Charles Martin and Darryl DesMarteau (Clemson University), Drs. Peter Fedkiw and Dick Paur (ARO), Dr. Richard Carlin (ONR) and Dr. Bob Nowak (DARPA). A group of 69 scientists and engineers from industry, academia and government laboratories were assembled at the Holiday Inn Boardwalk in Las Vegas, NV, April 28 – May 1, 1998. Their objective was to examine the state-of-the-art of current PEM fuel cell systems for alternate fuels, to identify the most important factors limiting the efficient use of these fuels, and to recommend the most promising directions for future research to overcome those limitations.

The alternate fuels of interest here are any readily available, easily transportable materials that could serve directly or indirectly as a fuel. They include hydrogen rich materials such as hydrocarbons or alcohols. Transported as liquids, these fuels have a high hydrogen content per unit mass. As discussed below, the state-of-the-art membrane electrode assembly (MEA) imposes significant limitations on the efficient utilization of these alternate fuels.

Additional Technical Background

The heart of the PEM fuel cell is the proton conducting membrane, which serves a number of important functions in the state-of-the-art membrane electrode assembly (MEA). These include:

1) Ion (proton) conductor.
2) Barrier to fuel and oxidant crossover
3) Transport of water from cathode to anode.
4) Physical support and separator for the electrodes.
5) Electronic insulator.
6) Catalyst interface for proton transfer.

7) Bonding agent to form a robust MEA structure.

In a typical design for a hydrogen/oxygen PEM fuel cell, the porous, platinum-catalyzed electrodes are laminated to each side of the membrane and this membrane-electrode assembly (MEA) is sandwiched between 2 sheets of an electrically conductive, porous carbon paper. This structure is compressed between electrically conductive plates having channels to allow gas flow to reach the surface of the MEA through the porous carbon paper. Hydrogen gives up two electrons at the anode and the resulting protons are transported across the membrane to the cathode. There, the protons combine with oxygen and electrons from the external circuit to form water. The cell voltage is typically on the order of 0.6 - 0.8 V depending on the operating temperature and current density.

The evolution of PEM fuel cell technology is well advanced for operation on pure hydrogen at 90°C or below. Below 60°C, sulfonated hydrocarbon membranes have adequate lifetime and performance for many applications[1]. For operation in the 70-90°C region, perfluorinated[2] or partially fluorinated[3] sulfonic membranes give very good performance and long operating life.

In general, there is a trade off between conductivity, which depends on ionic content and hydration, and strength, which depends on the continuous hydrophobic, amorphous region and the crystallinity. The hydration is important for two reasons. Water ionizes the acid groups and provides for the transport of the protons as H_3O^+. The water also swells the ionic clusters and increases the connective channels through the hydrophobic polymer matrix. Below 90°C, conventional sulfonic functional membranes are highly hydrated and highly conductive. Above 100 °C, these membranes dehydrate and the resistance to proton transport increases due to the loss of both hydration and connectivity through the membrane[4,5,6]. The high temperature conductivity would be enhanced if more functional groups were incorporated into the polymers but physical strength would be reduced.

UTILIZATION OF ALTERNATE FUELS.

Reformer Hydrogen & CO Poisoning

One approach to the problem of hydrogen generation is to reform a hydrogen rich fuel to form hydrogen, carbon dioxide and carbon monoxide. The level of carbon monoxide is a key factor in the cost-effective utilization of reformer hydrogen. The catalytic activity of platinum is reduced by the presence of CO even in the low ppm range. Tolerance to CO can be increased in a number of ways including addition of air to the reformer feed and/or adding ruthenium to the catalyst. Each of these extracts a cost and/or performance penalty and still provides only limited tolerance to CO. Reducing the CO to low levels requires an additional step in the reforming process and thus increases the cost and complexity.

Catalyst sensitivity to CO poisoning is inversely proportional to operating temperature. The higher the operating temperature, the less sensitive typical catalysts are to CO

poisoning. Thus the temperature limitation of current membranes is an important factor in limiting the tolerance of CO in the fuel.

Direct Electrochemical Oxidation

If methanol is fed directly to the anode side of a PEM fuel cell, a voltage is produced. However, even the best catalytic electrode gives[7] only about 440 mV at 300 mA/cm^2 below 100°C. Also, the fuel efficiency is drastically reduced by the phenomena of crossover. Methanol and water are miscible. Thus, a highly hydrated proton exchange membrane rapidly transports the methanol from the anode to the cathode where it is oxidized directly to produce only heat.

Thus, it is clear that limitations of current proton exchange membranes and membrane electrode assemblies are a significant impediment to the utilization of alternate fuel.

Executive Summary

The current state-of-the-art MEA for hydrogen-fueled PEM fuel cells is a fluorinated sulfonic acid membrane laminated to a catalytic platinum electrode. Operating in a highly hydrated environment below 90° C on pure hydrogen, these MEA's have demonstrated high efficiencies and long operating life. However, these MEA's have serious limitations for utilizing alternate fuels. For this conference, the organizing committee decided to focus on the two most promising alternate fuels – reformer hydrogen containing carbon monoxide and direct methanol. The Working group topics were chosen to address the most important limitations:

Working Group Topics.

Working Group A addressed the problem of membranes designed for high temperature operation. The potential advantages of high temperature are clear. They include improved electrode kinetics (CO tolerance), advantages in system integration and waste heat recovery, reduced methanol crossover in the low hydration environment, and potential for internal reforming of methanol. The challenges are equally clear. The Group considered three major problems that must be addressed in the design of membranes for high temperature operation: Conductivity at low relative humidity; chemical stability in an aggressive oxidative environment; and physical stability. Their recommendations for the most promising avenues of research are summarized below.

Working Group B addressed the problem of membrane barrier properties with the focus on methanol crossover. The problem of methanol crossover is a fundamental one for current state-of-the-art membranes. Good proton conductivity is dependent on high hydration. Methanol is highly soluble and highly mobile in this hydrated environment and is easily transported across the membrane to the cathode. Their recommendations are outlined below.

Working Group C addressed the structure-performance of the membrane electrode assembly. Alloy catalysts such as platinum/ruthenium are key part of improved resistance to CO poisoning and direct oxidation of methanol. Performance is affected by the structural features of the catalyst from the atomic level up to the meso-scale structure of the catalyst-membrane interface. Their recommendations identify the need for a better fundamental understanding of both electrocatalyst structure and electrode structure in order to improve the design of the membrane electrode assemblies. Improved catalysts for both anode and cathode are needed.

Group A Recommendations

- **High temperature, low hydration conductivity**
  - Polyprotic acids
  - Novel super acids

- Alternate proton acceptors
- Composites & blends
- Improved models of conductivity & morphology needed

♦ **Maintain chemical stability of polymer backbone**
- Fluorocarbon
- Deactivated aromatic

♦ **Maintain physical stability (dimensional)**
- Composites & blends
- Chemical crosslinking
- High Tg or semi-crystalline materials

Group B Recommendations

♦ **Improved selectivity for proton flux relative to methanol**
- Asymmetric membranes
  - Thin, highly selective layer
- High-temperature membranes
  - Low hydration, low MeOH solubility
  - MeOH vapor feed
- Composite membranes
  - Inorganic conductor
  - Lower hydration

Group C Recommendations

♦ **Electrode Structure**
- Systematic characterization needed
  - Physical & mathematical model
  - Correlate materials/fabrication/performance
- Integrate nano-engineered materials into meso-scale electrode structure

♦ **Characterize Pt/Ru catalysts**
- Unsupported for direct MeOH
- Supported for reformate

♦ **Optimize new Pt/Mo catalysts**

♦ **New oxygen reduction catalysts**
- Currently 200-300 mV loss

Summary.

All three groups concluded that membranes that operate at temperatures above 100° C with low hydration should be a primary focus of future research. This will require a conduction mechanism not dependent on the membrane being swollen with water. The higher temperatures would enhance electrode kinetics and reduce sensitivity to catalyst poisons such as CO. If the membrane is not highly swollen with water, the problem of methanol crossover should be substantially reduced.

It is important to note that most of the recommendations here involve questions of fundamental science rather than technological implementation. Working Group C structured their recommendations in terms of short- and long-term goals with the "short" including up to 5 years. There are some promising new materials on the horizon today but most of the recommended research initiatives will require a sustained effort.

REPORT ON WORKING GROUP DISCUSSIONS.

Working Group A. Dr. Darryl DesMarteau, Chair

Working Group A considered many options and suggestions for improving proton conductivity in membranes at higher temperatures and lower humidity.

I. We considered the greatest advantages of going to higher temperature to be:

- Ability to have higher performance operating on reformate.
- While direct methanol does not require higher temperature, methanol cross -over may be decreased by higher temperatures and lower humidity.
- Potential for internal reforming of methanol.
- Minor gains in heat removal.
- Useful waste heat.

II. The major disadvantages of higher temperature operation were considered to be:

- Decreased conductivity at higher temperatures due to lower hydration.
- Decreased membrane stability for polymer based membranes, especially membranes containing aliphatic hydrogen.
- Decrease in desirable mechanical properties of membranes and resistance to plastic deformation.
- Increased crossover / permeability of H_2 and O_2.

III. Numerous issues relating to proton conductivity in membranes were considered. It was concluded that based on the state of knowledge at present and the currently available acid functions, water is required for effective proton transport and the number of water / proton is greater than 1 and probably greater than 5. It was concluded that increasing the acidity of the acid functions in the membrane material could increase proton conductivity at lower hydration and increased self ionization of the acid functions could lower the water dependence. However, it was generally agreed that some acceptor (water or other) is required to promote proton transport.

In considering higher temperature operation we considered several temperature domains:

- < 90C: current situation for PEM FC, existing sulfonic acid based polymers work well.
- 90-100C: significant gains in performance but current membrane materials begin to dehydrate and conductivity decreases for ambient or low-pressure operations.
- 120-150C: PROX requirements are decreased for elimination of CO in reformate, possible or potential useful waste heat. Hydration and proton conductivity become major issues.
- 200C: Useful waste heat, PROX requirements eliminated. Catalyst support stability becomes an issue and proton conductivity in membrane materials will be difficult

Possible solutions to effective higher temperature operation of PEM FC were based on:

- Chemical stability under FC operating conditions are most likely to be demonstrated by deactivated aromatics and fluoropolymers.
- New acid functions capable of maintaining hydration at elevated temperatures such as polyprotic acids.
- Composite membranes based on hydrophilic materials supported in an ionomer.
- Hybrid anion exchange membranes such as phosphoric acid doped heteroaromatics as the backbone polymer or as pendant functions in ionomers.
- New very strong acids containing very weakly coordinating anions as a basis for mitigation of water in proton transport.
- New concepts for development of hydroxide anion exchange materials as alternatives.
- Better understanding by modeling and theory of proton transport in PEM's.
- Polymer blends for improved mechanical properties and/or alternative proton acceptors to promote proton transport.
- Low EW polymer membranes utilizing crosslinking for better mechanical properties.
- The effect of polymer morphology on water structure and conductive pathways.

Working Group B. Dr. Ed Cussler, Chair.

Decoupling Proton Conductivity and Methanol Crossover

This group was to explore how current membrane structures could be improved to make them more methanol impermeable while retaining proton conductivity. We were to discuss different chemical structures, different testing procedures and targets by which we could judge progress. We were also to explore where we are currently ignorant, i.e. where additional research effort is indicated.

The meeting was co-chaired by Ed Cussler, University of Minnesota, Joan Bartelt, Dupont, and Peter Pintauro, Tulane University.

We met three times. The first two meetings were devoted to deciding what we believed the current situation was and where we believed we were ignorant. The third session aimed at answering more specific questions put to us by the organizers. Jokingly, we referred to the first two sessions as a search for truth and the third session as a concession to reality.

Session #1: The Search for a Better Membrane

This session was a wide-ranging discussion aimed at new membranes. In this discussion, we implicitly adopted two axioms. First, we assumed that whatever membrane we chose would not cause problems with the catalysis: The catalysts could be easily bound to the membrane or protected from the membrane. One way in which we imagined this protection was to put any new membrane as the meat in a sandwich made of Nafion. The new membrane was the meat inside the sandwich: the Nafion was the bread on the outside of the sandwich.

Our second axiom, suggested by Figure 1, underscored our expectation that proton conductivity and methanol resistance would be inversely related. For example, Nafion and polyvinyl alcohol show dramatically different conductivities and methanol resistances, but their selectivity, the product of these two, is actually about the same. We sought a membrane with a better selectivity, i.e., both with a high proton conductivity and a high methanol resistivity.

Figure 1

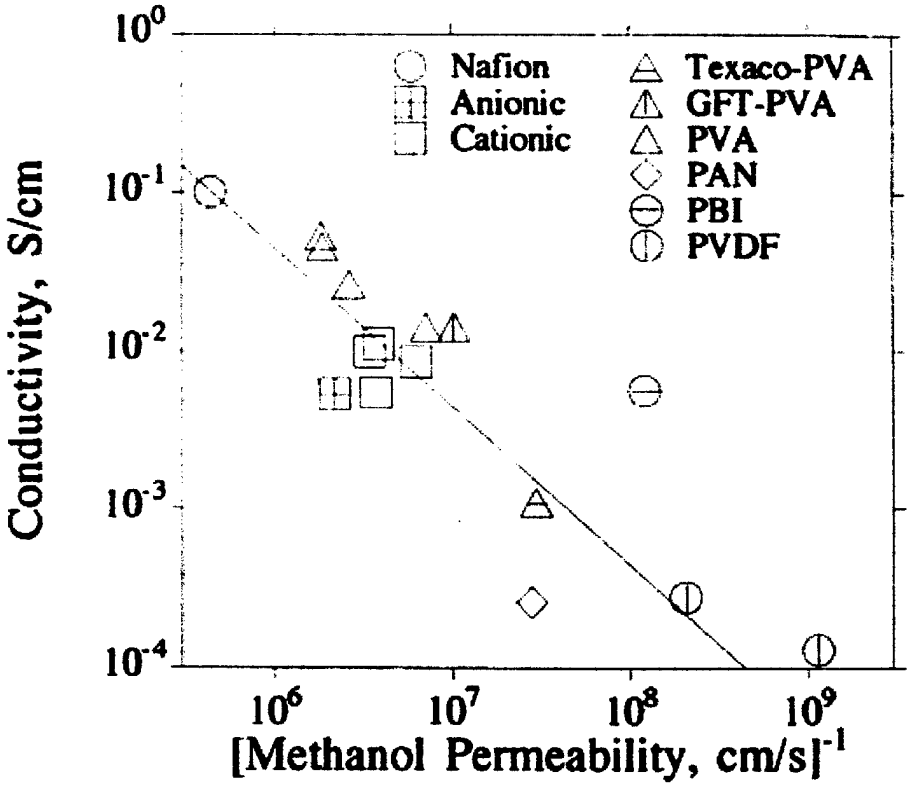

Our discussion of the solutions to this problem centered on the role of water in the membrane. Here our opinions differed widely. We could not even decide whether we

wanted excess water or very little water. This lead us to explore a wide variety of alternatives implying different amounts of membrane hydration. Among the alternatives we discussed were, in order of water content, a Nafion with more charged groups; a polyvinyl pyrolidene, which would be protonated under operating conditions; polybenzimidizol, the most attractive of the current membranes; composite membranes containing silica structures like MCM-41, as synthesized by Mobil; and composite membranes of inorganic oxides, like those of antimony. While we did struggle with the mechanisms in this extremely broad variety of membranes, we did not come up with any cogent conclusions. We did recognize that we were discussing primarily differences in transport rates and how they might lead to superior selectivity.

We also discussed membranes which might have altered equalibria and hence exclude methanol not on the basis on rates but on the basis of equilibrium solubility. This discussion included a variety of non-aqueous materials and of materials that might not be wetted by methanol. One of the more intriguing was an imaginary "super hydrophilic material" which would somehow dissolve water but not methanol.

Other aspects of our discussions were less organized but equally important. We were concerned with membrane start up, especially where we imagined operating the membranes at high temperature. We fussed about chemical degradation of our new selective membranes even when they were presumably protected by Nafion coatings. And we were worried about the problem of catalysis attachment even though we more or less agreed to defer this issue while we sought new membrane chemistries.

Session #2: Our Wish List

The second session used as its focus one question from each of the participants. These questions were a list of what we most wanted from the meeting. In other words, they were the questions that we most hoped the meeting would answer.

Interestingly, these questions, given verbatim in Appendix A broke into three groups. The first group was desire for better understanding of the membranes that we currently have. The second group sought a more effective membrane chemistry. And the third group asked for a criterion for success. Each of these groups of questions was then discussed in detail.

What understanding is needed?

Our most impassioned discussions centered on this issue and in particular on the mechanism of proton transport. Proton transport almost certainly occurs by two parallel routes. The first of these is, "jump" or Grotthuss mechanism assumes a proton adds to one side of a water molecule and causes a proton to jump off the other side of the molecule. (I recognize that I'm oversimplifying this mechanism, that it involves chemical reaction, molecular rotation and bond bending). The second proton transport mechanism, a "vehicle" mechanism, assumes a proton adds to a water cluster, as H_3O^+

or $H_7O_3^+$, and then diffuses intact. Methanol presumably diffuses only by a vehicle mechanism. As a result, our goal was to shut down both vehicle mechanisms, but to allow the jump mechanism to continue unaltered.

Our discussion was impassioned. We argued chemical details, and we suggested experimental methods that might be appropriate for this study. Two points seemed to have special value. First, methanol and for that matter diethyl ether, can serve as a stronger base then water itself. This implies that methanol may compete as a vehicle for proton, and could explain the apparent correlation of methanol transport and proton conductivity. NMR spectra apparently can show the relative importance of the jump and vehicle mechanisms. If so, NMR can be a valuable screening technique for future membranes.

What a better membrane would be? On this topic we had more conflicting opinions than participants. Everyone had his own favorite new membrane. New chemistries frequently depended on additives within existing membranes: dendrimers, zeolites, and inorganic ion exchangers. Other membranes took physical changes as the key to progress. These included putting Nafion or other conducting polymers in aerogels to inhibit swelling, making polystyrene sulfonate-Nafion sandwiches, and building membranes with highly conducting flakes. The discussion contained an enormous number of creative ideas, though these ideas were rarely described in sufficient detail to allow careful evaluation. They seemed rather like an orchard whose fruit is far short of being ripe.

What is Success. On this third topic we reached much more definite conclusions. We decided that our standard for success should be a membrane that was ten times better than Nafion 117. By better, we mean that its selectivity is ten times better. It could have a conductivity ten times less than Nafion if it had a methanol permeability which is reduced by more then ten times.

Session #3: More specific goals.

In the third session, we switched to the more specific challenges required to make methanol fuel cells effective. Our three more specific challenges dealt with how fuel cells would develop for different sizes and missions, for the factors limiting the potential of PEM fuel cells and for the best targets for further research. The variations of size and mission were a problem that our group did not tackle effectively. We didn't know enough about it and we didn't know what the technical challenges would be. For example, we felt that we could answer the question of how a membrane would have to be altered if it were operated at 20° C higher temperature, but we did not know if a temperature increase of 20° was indicated.

We did much better on the limits of the PEM fuel cells. We felt that the goal of ten times better selectivity, suggested in our second session, was obtainable within five years. We also felt that a more ambitious goal would be ten times better selectivity at

120° C. Such improved selectivity would reduce problems with carbon monoxide and hence make the direct methanol cell more attractive relative to reforming the methanol as hydrogen. Our group was remarkably sanguine about these goals, perhaps naively so. Still, they were almost unanimously felt to be reasonable.

Finally, we turned to the question of future research. This research hinged on the selectivity of the membranes in these fuel cells. Because the selectivity β has not always been carefully defined, we used the definition:

$$\beta = \frac{D_H [H^+]}{D_{CH_3OH} K_{CH_3OH} [CH_3OH]}$$

where D_H and D_{CH3OH} are the diffusion coefficients of protons and methanol within the membrane, respectively; $[H^+]$ is the concentration of hydrogen within the membrane; and K_{CH3OH} is the partition coefficient of methanol into the membrane and $[CH_3OH]$ is the methanol concentration outside the membrane. This definition allowed us to focus our discussion on rate processes - the diffusion coefficients-versus equilibrium properties - the proton and methanol concentrations. While we were concerned that our discussions emphasized rate processes at the expense of equalibria, we had more ideas about rate.

But as our discussions developed, they took on a somewhat surprising tone. We realized that we lacked fundamental information about how these fuel cells operate. We didn't know what the different mechanisms were. Our methods of membrane development - our favorite inventions - often were really guesses without a lot of careful thought. As a result, we came down wanting to know more fundamental information about existing transport processes within these fuel cells. We felt that this fundamental information could accelerate our development of more applied and more effective fuel cells.

Appendix A: Our Wish List

- CH_3OH fuel cell which works at a higher temperature using gaseous form of CH_3OH.
- Change the characteristics of CH_3OH so that it does not migrate through the membrane.
- Selectively modify the functional groups of the membrane so that the cross-over rate of CH_3OH is decreased.
- Put some coatings on the membrane to decrease cross-over.
- Can we construct an integral asymmetric membrane with low porosity/low conductivity/low methanol permeability layer within (not at surface) a membane from a single casting solution?

- Can one use interfacial polymerization to construct such an "internal" barrier?
- H^+ is charged; CH_3OH is not. Why aren't we able to pass one in a membrane without blocking the other?
- How to modify conductive channel of PEM to repel/hold methanol water and H^+ to move.
- What is the ideal channel diameter and how to orient them?
- What about methanol? I.e., Is there a difference in the way methanol and water interact with Nafion?
- Recent data suggest that a substantial amount of methanol enters the hydrophobic region. Blasphemy? Reconsider the backbone.
- If we wanted to use some kind of molecular engineering to design a MEA for a "liquid-fuel" fuel cell:
    1) Should we do CH_3OH or look at other fuels?
    2) What kind of theory/modeling do we bring in?
    3) What kinds of generalities in self-assembly or super molecular chemistry are known that would help guide us?
- Some way of incorporating conductive inorganic materials in membrane to replace $-SO_3H$ group?
- Developing a composite polymer possessing non-sulfonic conductive organic functional groups?
- Composite organic/inorganic membranes with selectivity and oxidation resistance?
    Selectivity for H_2O over CH_3OH
    Peroxide resistance via additives (e.g. "Vitamin E")
    Possible addition of suitable inorganic atoms on polymer chains
    Nanophase adducts.
- Can CH_3OH transport through PEM be modulated via a "CH_3OH sponge"?
- Crazy idea: Use methyl acetate in feed with water; CH_3OH released on hydrolysis & oxidized @anode; (what to do with CH_3COOH?) re-esterify waste CH_3OH?
- Is it possible to make a membrane without water that would still be proton conducting?
- Can you alter the property of membrane bound water such that it would be conducting with methanol?
- Can we define the proper metric for this cross-over phenomenon? I don't believe it is strictly CH_3OH permeation, but a measure of overall fuel efficiency or power output.
- I wish I could have a screening test to select promising candidates for a CH_3OH impermeable layer.
- Wish to separate PEM's into CH_3OH, liquid or gas, at high T and H_2 PEM for <100°C as two different products. The H_2 product as latter stage development and

the CH_3OH product is in conceptual stage. Could look at it as an improvement over both PEM & phosphoric acid.

Work Group C. Dr. Robert Savinell, Chairman

We had lively discussions over the last two days – lot of opinions & thoughts aired. We have distilled them down to the eight attached slides.

Recommendations come in two categories: The issues related to catalyst used in MEA's and the issue of the electrode structures of the MEA's containing the catalyst. Depending on the process used, the MEA may include a backing material such as the carbon paper. The recommendations are grouped into short term (2-5 years) and longer term.

It is important to understand that electrode reproducibility is typically on the order of ±15%. Using the same procedure, different individuals and different labs will fabricate electrodes that vary significantly.

MEMBRANE ELECTRODE ASSEMBLIES.

Our consensus is that Nafion MEA structures are well developed with efficient utilization of catalyst. However, the details of microstructure and nanostructure of these electrodes are not well defined, and the study and optimization of each new candidate component of an MEA is still a matter of trial an error composed of both art and science.

Short Term Recommendations:

1. A systematic and thorough characterization of the state-of-the-art anode and cathode structures for both liquid fed and gas fed electrodes is needed. Each combination has different characteristics and problems. This should lead to an understanding of a physical model of the form and distribution of the materials in the electrode structure. This physical understanding should lead to a mathematical model that takes into account the basic material properties, geometric factors, etc. to allow one to elucidate and correlate material properties with the fabrication method leading to the high performance electrodes.

   This recommendation includes the concept of understanding and evaluating the various layers and components of an MEA independently. For example, the fundamental properties of the ionomer incorporated with the anode catalyst, e.g., surface tension, wetting properties, glass transition temperature, etc. will influence the optimum fabrication method leading to the ideal three-dimensional structure for

a high performance anode. The anode layer must then form an interface with a membrane that may be the same or different ionomer. Finally on the other side of the membrane, we have the cathode catalyst and ionomer, both of which may be optimally different from those in the anode.

2. One specific problem that needs to be addressed short term is that of water flooding in cathodes. This is a significant problem for direct methanol systems in which you are feeding methanol-water to the anode.
3. While the flow field is not a part of this Workshop, the optimum flow field design is probably interactive with and dependent on the electrode structure. Therefore, characterization and optimization of the flow field design should be carried out concurrently with that of the electrodes

Long Term Recommendations:

1. Develop and integrate nano-engineered materials into the meso-scale electrode structure. Currently, standard electrode structures are a fairly random agglomeration of materials. Integrating a more uniform support structure such as an aerogel, etc. would potentially enhance the performance and reproducibility of a designed electrode structure.
2. Develop new backing materials and structures to replace the carbon paper typically used today. Perhaps the gas distribution and electrical conductivity functions of the backing paper could be integrated into an extended electrode structure.
3. Eliminate micropore structures in electrodes. Micropores are not accessible to electrolyte, so catalysts on surfaces within micropores are not utilized.

CATALYST.

The state-of-the-art in direct methanol and CO tolerant catalysts is platinum-ruthenium although lower cost Pt/Mo combinations have shown promise. The optimum state-of-the-art for Pt/Ru is very fuel dependent. For reformate, supported Pt/Ru catalysts work best, but for direct methanol, high loadings of unsupported Pt/Ru catalysts are preferred. Further, incorporation of ionomer in the electrode is not beneficial to the performance of the unsupported Pt/Ru. We see a performance limit at about 150 mV positive of the hydrogen reference for methanol oxidation. Adding to the complexity of the current state-of-the-art is the variation in catalyst made by different vendors.

The purity of methanol that would be available through bulk commercial distribution is another concern for the future commercialization of direct methanol technology. Another concern raised that related to the eventual commercialization of direct methanol was that of the effect of impurities. In the laboratory, we tend to use reagent grade chemicals for research purposes. In the real world, bulk methanol will be used and it will not be made and transported in glass. There will be numerous opportunities

for contaminants and impurities that could affect performance of the fuel cell both short and long term.

On the cathode side, there exists a 200-300 mV over potential even in pure hydrogen systems that is perhaps the largest inefficiency in fuel cell systems.

Short Term Recommendations:

1. Characterize state-of-the-art Pt/Ru catalyst for both reformate and direct methanol.
2. Elucidate the role of the hydrous oxide coating in the conduction of protons in the catalyst layer and the effect of processing temperature on its formation.
3. Establish specifications for catalyst quality based on the above characterization.
4. Determine the effect of impurities in commercial methanol and establish tolerance levels.
5. Optimize Pt/Mo for CO-tolerant anodes and elucidate the mechanism by which Mo functions.

Intermediate Term Recommendations:

1. Development of engineered nano-particles with controlled geometry and particle size.
2. Develop electrochemical and spectroscopic techniques for *in situ* and *ex situ* characterization of electrode structures.
3. Elucidate structure-performance relationship.

Long Term Recommendations:

1. Fundamental studies of anode catalyst systems
   a. Pt/Ru and other binary and ternary catalysts.
   b. Combine experimental and computational studies of electronic effects.
   c. Structural effects of well defined crystal planes and methods of maximizing the most active crystal planes in nano-particles in the electrode.
1. Fundamental studies of oxygen electrocatalysts.
   a. Understand and overcome the 200-300 mV of cathodic overpotential.
   b. Develop methanol-tolerant cathode catalysts.

Slide 1

Work Group C

Membrane Electrode Assemblies:

Structure & Performance

Slide 2

Perspective

- Short term (≈ 2 yr.) & long term (≈ 10 yr.)
- Electrode Structures (MEA)
- Catalyst

Slide 3

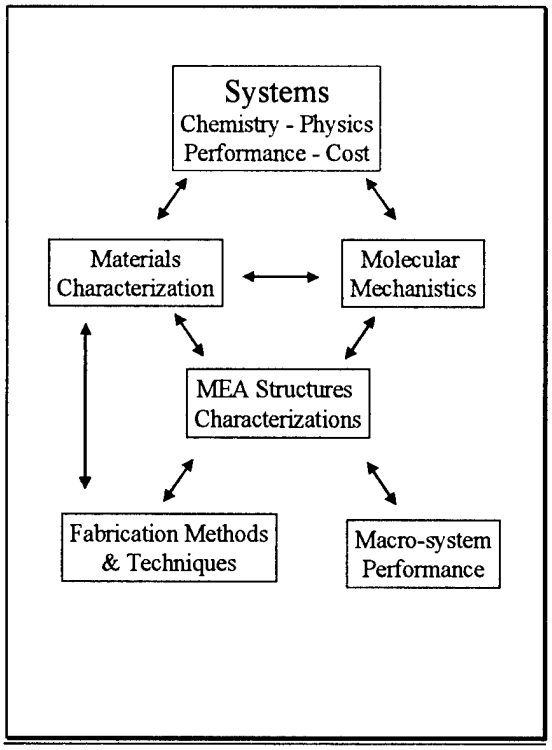

Slide 4

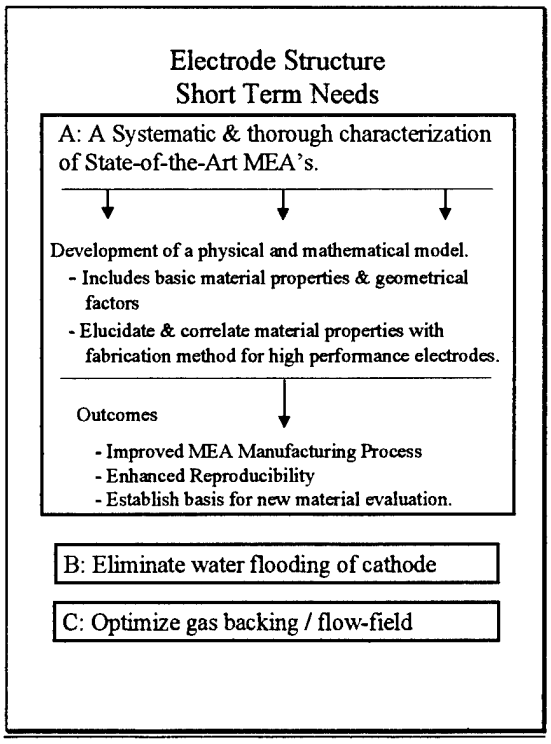

Slide 5

Electrode Structures - Long Term

- Integrate nano - engineered materials into meso-scale electrode structures.
- Alternate backing materials
- Eliminate micropore structures to maximize catalyst utilization

Slide 6

Catalysts - Short Term

- Characterize state-of-the-art Pt/Ru catalyst
  - Supported (reformate) & unsupported (dir. MeOH)
  - Elucidate role of hydrous oxide proton conduction
  - Determine effect of processing temperature
  - Establish specifications for catalyst quality.
- Establish tolerance level to impurities in commercial MeOH.
- Optimize Pt/Mo for CO tolerant anode
  - Mechanistic studies

Slide 7

Catalysts - Short Term (cont.)

- Engineered nano-particles and electrochemical evaluation
  - Control geometry & particle size
  - *In situ* & *ex situ* spectroscopic and electrochemical techniques
  - Structure - performance relationships

Slide 8

Catalysts - Long Term

- Fundamental Studies:
  - Electronic effects of Pt-Ru & other binary and ternary catalysts.
  - Experimental + computational methods
  - Structural effects
    - Well defined crystal planes
    - Nano-particles
- Oxygen electrocatalysis
  - eliminate the 200 - 300 mv loss

[1] Ehrenberg, S. G.; Serpico, J. M.; Sheikh-Ali, B. M.; Tangredi, T. N.; Zador, E.; Wnek, G. E. *Hydrocarbon PEM/electrode assemblies for low-cost fuel cells: development, performance and market opportunities,* New Mater. Fuel Cell Mod. Battery Syst. II, Proc. Int. Symp., 2nd Ed.: Savadogo, O. (Ed), Roberge, P. R (Ed), p 828-835,: Ecole Polytechnique de Montreal, Montreal, Que, (1997).

[2] Pourcelly, G and Gravach, C. in *Proton Conductyors. Solids, Membranes, and Gels - Materials and Devices,* Columban, P., (Ed.), Cambridge University Press, Cambridge, UK (1992).

[3] Wei; J., Stone; C., Steck; A. E., *Trifluorostyrene and substituted trifluorostyrene copolymeric compositions and ion-exchange membranes formed therefrom,* U.S. 5,422,411 (1995.).

[4] Zawodzinski, T. A.; Springer, T. E.; Uribe, F.; and Gottesfeld, S.; *Solic State Ionics,* **60,** 199-211, (1993).

[5] Stone, Y.; Ekdunge, P.; and Simonsson, K.; *J. Electrochem. Soc.,* **143**, 1254-1259 (1996)

[6] Opekar, F.; and Svozil, D.; *J. Electroanal. Chem.,* **385**, 269 (1995).

[7] Narayanan, S. R.; Kindler, A.; Jeffries-Nakamura, B.; Chun, W.; Frank, H.; Smart, M.; Surampudi, S.; Halpert, G. *Performance of PEM liquid-feed direct methanol-air fuel cells,* Proc. - Electrochem. Soc. (1995), 95-23 (Proton Conducting Membrane Fuel Cells I), 261-6

Workshop Agenda

Advanced PEM Fuel Cell Membranes and MEA's for Non-Conventional Fuels.

April 28 – May 1, 1998

Tuesday	5:30-6:45	April 28
Registration	Conference Center	
Reception	Conference Center	

Plenary Session	6:45 - 9:30	
ARO perspective	Dick Paur	ARO
DARPA perspective	Bob Nowak	DARPA
ONR perspective	Rich Carlin	ONR
Army After Next (ANN)	Ken Jones	ARO
Hybrid Power Electrical Power Systems - Overview	Henry Brandhorst	AUSPI
Break		
Satisfying the Commercial Requirements for Alternative Energy Applications"	Joan Bartelt	Dupont
Advanced components for PEM fuel cells	Greg Rusch	Gore

April 29: Continental Breakfast 7:00 – 8:00

Wednesday Morning	8:00 - 12:30	April 29
MEA Fundamentals	Shimshon Gottesfeld	LANL
Structure of the Pt/Ru Catalyst for DMFC	Andrzej Wieckowski	U. of Ill

Ionomer Solutions	**Michel Pineri**	**CEA (France)**
Investigations of Electrocatalyst - Membrane Interface	**Sangev Murkerjee**	**BNL**

Break

Modeling of Ionomer Membranes	**Tom Zawodzinski**	**LANL**
Pervaporation Membranes In Direct Methanol Fuel Cells	**Ed Cussler**	**U. Minn.**
Direct Methanol fuel cells	**Shimshon Gottesfeld**	**LANL**
Ionomer/Sol-gel Nanophase Composites	**Ken Mauritz - U. So. Miss**	**U. So. Miss.**
Hydrocarbon Membranes Revisited	**Gary Wnek**	**Va. Com. U.**

Wednesday Afternoon 2:00 - 4:00 April 29

Informal Poster Session

Buffet Dinner 6:00 - 7:00 Holiday Inn Boardwalk

Wednesday Evening 7:00 – 10:00 April 29

Evaluation of Sulfonated Polyimides in PEM Fuel Cells	**Michel Pineri**	**CEA (France)**
Phos Acid-polyimidazoles	**Bob Savinell**	**Case Western**
High Temp Functional Perfluoropolymers	**Darryl DesMarteau**	**Clemson U.**

Break

High Temperature Fuel Cell	**Ravi Datta**	**U. Iowa**
Phospazine Ionomers/Direct MeOH	**Peter Pintauro**	**Tulane U.**

April 30: Continental Breakfast *7:00 – 8:00*

Thursday Morning	**8:00 - 12:00**	**April 30**
Stability of PEM Membranes: Chemical, Thermal & Physical	**Charlie Martin**	**Clemson U.**
Working Group Discussions		

Thursday Evening	**7:00 – 10:00**	**April 30**
Working Group Discussions		

May 1: Continental Breakfast *7:00 – 8:00*

Friday AM	**8:00 - 12:00**	**May 1**
Working Group Summary Report Preparation	**All**	**8:00 - 9:30**
Reports from Session Chairs		**9:30 – 12:00**

WORKSHOP PARTICIPANTS
ADVANCED FUEL CELL MEMBRANES
LAS VEGAS, NV
APRIL 28-MAY 1, 1998

BRIAN BARNETT
VICE PRESIDENT
ARTHUR D. LITTLE, INC.
15 ACORN PARK
CAMBRIDGE, MA 02140
617-498-5307
FX 617-498-7012
E-MAIL: barnett.b@edlittle.com

JOAN BARTELT
SENIOR CHENUST
DUPONT NAFION
P.O. DRAWER Z, HWY 87 SOUTH
FAYETTEVELLE, NC 28302
910-678-1545
FX: 910-678-1496
E-MAIL: Joan.E.Bartelt-1@usa.dupont.com

HENRY BRANDHORST
CCDS DIRECTOR
AUBURN UNIVERSITY
SPACE POWER INSTITUTE
231 LEACH CENTER
AUBURN, AL 36849
334-844-5894
FX 334-844-5900
E-MAIL: brandhh@mail.auburn.edu

RICHARD CARLIN
PROGRAM OFFICER
OFFICE OF NAVAL RESEARCH
800 N QUINCY ST
CODE 331
ARLINGTON, VA 22217
703-696-5075
FX: 703-696-6887
E-MAIL: carlinr@onr.navy.mil

BISWAJIT CHOUDHURY
RESEARCH SCIENTIST
BALLARD ADVANCED MATERIALS
9000 GLENLYON PARKWAY
BURNABY, BC, CANADA V5J 5J9
604412-7948
FX: 6044124704
E-MAIL: bischo@ballard.com

DERYN CHU
RESEARCH CHEMIST
ARMY RESEARCH LAB
2800 POWDER MILL RD
MS: AMSRL-SE-DC
AMLPFI, MD 20783-1197
301-721-3451
FX: 301-721-3402
E-MAIL: dchu@arl.mil

H. YOUNG CHUNG
FELLOW
DONALDSON CO., INC
PO BOX 1299
MINNEAPOLIS, MN 55440
612-887-3456
FX 612-887-3937
E-MAIL hychung@mail.donaldson.com'

AL CISAR
MANAGER
LYNNTECH, INC.
7610 EASTMARK DR
SUITE 105
COLLEGE STATION, TX 77840
409-693-0017
FX: 409-764-7479
E-MAIL: lynntech@myriad.net

STEVE CREAGER
PROFESSOR
CLEMSON UNIVERSITY
DEPT OF CHEMISTRY
CLEMSON, SC 29634
864-656-4995
FX: 864-656-6613
E-MAIL: screage@clemson.edu

CECILIA CROPLEY
ASSOC. DIRECTOR
GINER, INC.
14 SPRING STREET
WALTHAM MA 02154-4497
781-899-7270
FX 781-894-2762
E-MAIL: ginerinc@compuserve.com

WILLIAM CURLEY
STAFF ENGINEER
CINERGY CORP.
1000 E. MAIN ST.
PLAINFIELD, IN 46168
317-838-2589
FX: 317-838-1985
E-MAIL: wcurley@cinergy.com

R.L. CUSSLER
PROFESSOR
UNIVERSITY OF MINNESOTA
DEPT OF CHEM ENGR & MAT SC
421 WASHINGTON AVE. S.E.
MINNEAPOLIS, MN 55455
612-625-1596
FX: 612-626-7246
E-MAIL: cuss1001@tc.umn.edu

RAVINDRA DATTA
PROFESSOR
UNIVERSITY OF IOWA
DEPARTMENT OF CHEM &
BIOCHEMICAL ENGINEERING
IOWA CITY, IA 52242
319-335-1395
FX: 319-335-1415
EMAIL: yadatta@icaen.uiowa.edu

DARRYL D. DESMARTEAU
PROFESSOR OF CHEMISTRY
CLEMSON UNIVERSITY
BOX 341905, HUNTER HALL
CLEMSON, SC 29634-1905
864-656-4705
FX: 864-656-0627
E-MAIL: fluorin@clemson.edu

HARI DHAR
PRESIDENT
BCS TECHNOLOGY, INC.
2812 FINFEATHER RD
BRYAN, TX 77801
409-823-7138
FX: 409-823-8475
E-MAIL: bcstech@txcyber.com

CHARLES EDMONDSON
ASST. PROFESSOR
UNITED STATES NAVAL ACADEMY
DEPT. OF PHYSICS
572 HOLLOWAY RD
ANNAPOLIS, MD 21402-5062
410-293-6661
FX: 410-293-3729
E-MAIL: edmond@nadn.navy.mil

MOHAMMAD ENAYETULLAH
VP TECHNOLOGY
ICET INC
916 PLEASANT STREET
NORWOOD, MA 02062
781-769-6064
FX: 781-762-8204
E-MAIL: icetinc@ibm.net

BOBBY EZZELL
RESEARCH FELLOW
DOW CHEMICAL
1776 BLDG
MIDLAND, MI 48674
517-636-1924
FX: 517-638-9350
E-MAIL: brezzell@dow.com

PETER FEDKIW
US ARMY RESEARCH OFFICE
4300 S MIAMI BLVD
PO BOX 12211
RTP, NC 27709
919-549-4209
FX: 919-549-4310
E-MAIL: fedkiw@aro-emh1.army.mil

JOHN FONTANELLA
PROFESSOR
US NAVAL ACADEMY
PHYSICS DEPARTMENT
ANNAPOLIS, MD 21402
410-293-5507
FX: 410-293-3729
E-MAIL: jjf@arctic.nadn.navy.mil

RICHARD FORMATO
DESIGN ENGR
FOSTER-MILLER INC
195 BEAR HILL RD
WALTHAM, MA 02154-1196
781-684-4127
FX: 781-290-0693
E-MAIL: bformato@foster-miller.com

DON GERVASIO
STAFF SCIENTIST
MOTOROLA
2100 EAST ELLIOT ROAD
MD EL703
TEMPE, AZ 85284
602-413-6094
FX: 602-413-4952
E-MAIL: a275ab@email.sps.mot.com

SHIMSHON GOTTESFELD
PROJECT LEADER
LOS ALAMOS NATIONAL LABORATORY
P.O. BOX 1663, MS D429, MST-11
LOS ALAMOS. NM 87545
505-667-0853
FX- 505-665-4292
E-MAIL: gottesfeld@lanl.gov

CARLA GROT
SOLUTION TECHNOLOGY, INC.
4 BYRON COURT
CHADDS FORD, PA 19317
610-388-6201
FX: 610-388-6974
E-MAIL: grot@esvax-mail.es.dupont.com

WALTER GROT
CG PROCESSING. INC
4 BYRON COURT
CHADDS FORD, PA 19317
610-388-6201
FX: 610-388-6974
E-MAIL: grot@esvax-mail.es.dupont.com

JAMES GUCINSKI
SUPVY ENGINEER
CRANE DIVISION
NAVAL SUR-FACE WARFARE CNTR
300 1EG14WAY 361
CRANE, IN 47522
812-854-6150
FX: 812-854-1212
E-MAIL: gucinski_j@crane.navy.mil

STEVEN HAMROCK
RESEARCH SPECIALIST
3M
3M CENTER
201-IW-28
SAINT PAUL. MN 55144
612-733-4254
FX- 612-737-5335
E-MAIL: sjhamrock@mmm.com

MATHIAS HECHT
ELECTROCHEMIST
MER CORP.
7960 S. KOLB RD,
TUCSON, AZ 85706
PH 520-574-1980
FX 520-574-1983
E-MAIL: hecht@opusl.com

JERRY HUANG
STAFF RESEARCH SCIENTIST
GM GLOBAL R & D OPERATIONS
PHYSIC & PHYSICAL CHEMISTRY DEPT.
30500 MOUND ROAD
WARREN, MI 48090-9055
810-986-0767
FX: 810-986-2244
E-MAIL: chaojung_huang@notes.gmr.com

KENNETH L. JONES
TECHNOLOGY INTEGRATION MANAGER
U.S. ARMY RESEARCH OFFICE
302 BONNIEWOOD DR.
CARY, NC 27511-8964
919-549-4200
FX: 919-549-4248
E-MAIL: jones@aro-emh1.army.mil

G. SANJIV KAMATH
PRINCIPAL RESEARCH SCIENTIST
HRL LABORATORIES, LLC
3011 MALIBU CANYON RD.
MALIBU, CA 90265
310-317-5210
FX 310-317-5840
E-MAIL: gskamath@hrl.com

LARRY KEPLEY
ADVANCE SCIENTIST
TPL, INC.
3921 ACADEMY PKWY NORTH, NE
ALBUQUERQUE, NM 87109
505-342-4474
FX: 505-345-8155
E-MAIL: sensors@tplinc.com

THOMAS KELLY
VP
TPL
CHEVY CHASE STATION
PO BOX 42415
WASHINGTON, DC 20015
202-966-7197
FX: 202-287-3662
E-MAIL: tkelly3@erols.com

MICHEAL KRUMPELT
SENIOR CHEMIST
ARGONNE NATIONAL LAB
9700 S CASS AVE
ARGONNE, IL 60439-4837
630-252-8520
FX- 630-252-4176
E-MAIL: krumpelt@cmt.anl.gov

R. O. LOUTFY
PRESIDENT
MER CORPORATION
7960 S. KOLB RD.
TUCSON, AZ 85706
520-574-1980 EXT. 12
FX: 520-574-1983
E-MAIL: rloutfy@opusl.com

SANJIV MALHOTRA
PROJECT MANAGER
H POWER CORP
C/O SM-ALC/EM BLDG 335
MC CLELLAN AFB. CA 95652
916-924-6650
FX: 916-924-3266
E-MAIL: smalho6428@aol.com

MATTHEW MARROCCO
VP, R&D
MAXDEM INCORPORATED
140 EAST ARROW HIGHWAY
SAN DIMAS. CA 91773
909-394-0644
FX: 909-394-0615
E-MAIL: mmarrocco@maxdem.com

CHARLES MARTIN
ASSOCIATE
W. L. GORE & ASSOCIATES, INC
201 AIRPORT ROAD
ELKTON, MD 21922-1488
410-506-7553
FX: 410-506-7633
E-MAIL: cwmartin@wlgore.com

MARK MATHIAS
STAFF RESEARCH ENGR
GENERAL MOTORS
GLOBAL ALTERNATIVE PROPULSION
285 METRO PARK
ROCHESTER, NY 14623
716-239-7348
FX: 716-239-73 10
E-MAIL: mathiasmf@aol.com

LOTHAR MATEJCEK
GLOBAL ALTERNATIVE PROPULSION CNTR
ADAM OPEL AG
IPC 81-90
RUESSELSHEIM, GERMANY D-65423
++49-6142-7-75748
FX: ++49-6142-7-76093
E-MAIL: lolbe.lmatejol@gmeds.com

KENNETH MAURITZ
PROFESSOR OF POLYMER SCIENCE
UNIVERSITY OF SOUTHERN MISSISSIPPI
DEPT OF POLYMER SCIENCE
SOUTHERN STATION BOX 10076
HATTESBURG, MS 39406
601-266-5595
FX: 601-266-5635
E-MAIL: kenneth.mauritz@usm.edu

JOSEF MICHL
PROFESSOR
UNIVERSITY OF COLORADO
DEPT OF CHEM/BIOCHEM
UNIVERSITY OF COLORADO
CB215
BOULDER, CO 80309-0215
303-492-6519
FX- 303-492-0799
E-MAIL: michl@ecfus.colorado.edu

NGUYEN MINH
MANAGER. FUEL CELLS
ALLIED SIGNAL AEROSPACE
2525 WEST 190TH ST
MS: TOR36-1-93140
TORRANCE, CA 90504-6099
310-512-3515
FX: 310-512-4128
E-MAIL: nguyen.minh@alliedsignal.com

ROBERT MOORE
ASSOCIATE PROFESSOR
UNIVERSITY OF SOUTHERN MISSISSIPPI
DEPT OF POLYMER SCIENCE
P.O. BOX 10076
HATTESBURG MS 39406
601-266-4480
FX: 601-266-5501
E-MAIL: rbmoore@ocean.st.usm.edu

SANJEEV MUKERJEE
ASSISTANT SCIENTIST
BROOKHAVEN NATIONAL LABORATORY
BUILDING 480
DEPT, OF APPLIED SCIENCE
UPTON, N.Y. 11973
516-344-4973
FX: 516-344-4071
E-MAIL: mukerjee@bnl480.das.bnl.gov

OLIVER MURPHY
PRESIDENT
LYNNTECH, INC.
7610 HASTMARK DRIVE
SUITE 105
COLLEGE STATION, TX 77840
409-693-0017
FX: 409-764-7479
E-MAIL: ojmurphy@myriad.net

ROBERT NOWAK
PROGRAM MANAGER
DARPA
3701 N FAIRFAX DR
ARLINGTON. VA 22203-1714
703-696-7491
FX: 703-696-3999
E-MAIL: rnowak@darpa.mil

RICHARD PAUR
CHIEF, ELECTROCHEM &
ADV ENERGY CONVERSION
ARMY RESEARCH OFFICE
P.O. BOX 12211
RTP, NC 27709
919-549-4208
FX: 919-549-4310
E-MAIL: paur@aro-emh1.army.mil

DVORA PERAHIA
CLEMSON UNIVERSITY
CHEMISTRY DEPARTMENT
CLEMSON, SC 29634
864-656-7903
FX: 864-656-6613
E-MAIL: dperahia@clemson.edu

MICHEL PINERI
CEA
DEM/SPCM CEA GRENOBLE
17 RUE DES MARTYRS
GRENOBLE, FRANCE F38054
FRANCE
33476884323
FX: 33476885198
E-MAIL: pineri@chartreuse.cea.fr

PETER PINTAURO
PROFESSOR
TULANE UNIVERSITY
DEPT OF CHEM ENGR
NEW ORLEANS, LA 70118
504-865-5872
FX: 504-865-0744
E-MAIL: peter.pintauro@tulane.edu

WILLIAM RISEN
PROFESSOR
BROWN UNIVERSITY
BOX H. DEPT OF CHEMISTRY
PROVIDENCE, RI 02912
401-836-2611
FX.- 401-863-2594
E-MAIL: wrisen@brown.edu

DEBRA ROLISON
NAVAL RESEARCH LABORATORY
4555 OVBRLOOK AVE SW
CODE 6170
WASHINGTON, DC 20375
202-767-3617
FX: 202-767-3321
E-MAIL: rolison@nrl.navy.mil

GREG RUSCH
PROD. DEV. ASSOC.
WL GORE & ASSOCIATES. INC
PO BOX 2200
402 VIEVES WAY
ELKTON, MD 21622-2200
410-5064071
FX: 410-5064090
E-MAIL: grusch@wlgore.com

SARANG SARANGAPANI
EXEC VP
ICET INC
916 PLEASANT STREET
NORWOOD, MA 02062
781-769-6064
FX: 781-762-8204
E-MAIL: icetinc@ibm.net

ROBERT SAVINELL
PROFESSOR
CASE WESTERN RESERVE UNIV
DEPT CHEMICAL ENGR
10900 EUCLID AVE
A.W. SMITH BLDG
CLEVELAND, OH 44106
216-368-2728
FX: 216-368-3016
E-MAIL: frsz@po.cwru.edu

STUART SCHWAB
SUPERVISOR
TPL, INC
3921 ACADEMY PKWY NORTH, NE
ALBUQUERQUE, NM 87109
505-342-4435
FX: 505-343-1797
E-MAIL: stschwab@tplinc.com

BRUNO SCROSATI
PROFESSOR
UNIVERSITY LA SAPIENZA
PIAZZA A MORO 5
ROME, ITALY 00185
39-6-4462866
FX: 39-6-491769
E-MAIL: scrosati@axrrma.uniromas.it

GREG SHAFER
GRAD STUDENT
CLEMSON UNIVERSITY
HL HUNTER HALL
BOX 341905
CLEMSON SC 29634-1905
864-656-5030
FX:
E-MAIL: gshafer@clemson.edu

STAN SIMPSON
SR PROJECT ENGINEER
ALLIED SIGNAL AEROSPACE
2525 WEST 190TH ST
TORRANCE, CA 90504
310-512-4804
FX: 310-512-4128
FX: 310-512-4128
E-MAIL: stan.simpson@alliedsignal.com

MARSHALL SMART
JET PROPULSION LABORATORY
4800 OAK GROVE DRIVE
PASADENA, CA 91109
PH 818-354-9374
FX 818-395-6951

EUGENE SMOTKTN ASSOCIATE PROFESSOR
ILLINOIS INSTITUTE OF TEC
10 WEST 33RD ST
CHICAGO, IL 60616-3793
312-567-7032
FX:312-567-8882
E-MAIL: esmotkin@charlie.cns.iit.edu

JESSE WAINRIGHT
SR RESEARCH ASSOC.
CASE WESTERN RESERVE UNIV
10900 EUCLID AVE
DEPT OF CHEM ENGR
CLEVELAND, OH 44106-7217
216-368-4072
FX: 216-368-3016
E-MAIL: jsw7.@po.cwru.edu

HENRY WHITE
PROFESSOR
UNIVERSITY OF UTAH
DEPARTMENT OF CHEMISTRY
SALT LAKE CITY, UT 84112
801-585-6256
FX: 801-585-3207
E-MAIL: white@chemistry.utah.edu

ANDRZEJ WIECKOWSKI
PROFESSOR
UNIVERSITY OF ILLINOIS
DEPARTMENT OF CHEMISTRY
600 S. MATHEWS AVE, BOX 56-5
URBANA, IL 61801
217-333-7943
FX: 217-244-8068
E-MAIL: andrzej@aries.scs.uiuc.edu

GARY WNEK
PROFESSOR
VA COMMONWEALTH UNIV
DEPT OF CHEMICAL ENGR
PO BOX 843028
RICHMOND,. VA 23284-3028
804-828-7789
FX: 804-828-4269
E-MAIL: gewnek@saturn.vcu.edu

DELIANG YANG
RESEARCH ENGINEER
INTERNATIONAL FUEL CELLS
195 GOVERNOR'S HIGHWAY
SOUTH WINDSOR. CT 06074
860-727-2278
FX: 860-727-2319
E-MAIL: yangjam@ifc.hsd.utc.com

DAVID YLITALO
3M
3M CTR
BLDG 201-25-05
ST PAUL, MN 55082
612-737-1157
FX: 612-737-2590
E-MAIL: daylitato@mmm.com

TOM ZAWODZINSKI
TEAM LEADER
LOS ALAMOS NATL LAB
PO BOX 1663
MS D42 9, MST- I I
LOS ALAMOS, NM 87545
505-667-0925
FX: 505-665-4292
E-MAIL: zawod@lanl.gov

Army/DARPA Power Perspective

Dr. Richard J. Paur
ARO / Electrochemistry & Advanced Energy Conversion

Dr. Robert Nowak
DARPA / DSO

The modern soldier needs significant electrical energy to power the various pieces of electronic gear that he carries. Battery technology is relatively mature, and there is little reason to expect any dramatic increase in the energy density of batteries in the future. Development of power sources with significant improvements in energy density will almost certainly require the use of fuels such as hydrogen, methanol, or hydrocarbons. These fuels, when reacted with oxygen from the ambient air, can produce 10-100 times the energy of battery chemistry. To make use of this energy, we will have to develop light weight energy conversion systems - for very light converters, the energy density of the system will approach that of the fuel.

Among the most highly developed small, quiet energy converters are PEM fuel cells. The hydrogen/air fuel cells are available in 15-150 W sizes, which covers the power ranges likely to be needed by the soldier. The polymer electrolytes used, typically Nafion or some other perfluorinated membrane with sulfonic acid ionic sites, can function over most of the desired temperature range and in all but the driest climates. In very dry air, and particularly at higher temperatures, dehydration of the membranes can lead to loss of ionic conductivity. For direct oxidation of methanol fuel cells, the *standard' membrane electrolytes suffer from the fact that they are quite permeable to methanol. The result is loss of fuel and interference with the function of the cathode catalysts.

We hope that this workshop will be able to suggest promising avenues of research for improved membrane electrolytes for the small fuel cells that may give our soldiers the improved power sources they need.

Army/DARPA Power Perspective

presented at the

Advanced Fuel Cell Membranes for Non-Conventional Fuels Workshop

28 Apr - 1 May, 1998
Las Vegas, NV

Dr Richard J Paur
ARO / Electrochemistry & Advanced Energy Conversion
919-549-4208; fax -4310; paur@aro-emh1.army.mil

Dr Robert Nowak
DARPA / DSO
703-696-7491; fax -9780; rnowak@darpa.mil

COMPACT POWER SOURCES

FUTURE MILITARY APPLICATIONS

- UAVS (E.G., μ-UAV)
- AUTONOMOUS OCEAN SAMPLING NETWORK (UUVs)
- UNATTENDED GROUND SENSORS
- SMALL UNIT OPERATIONS
- ARMY AFTER NEXT
- URBAN WARFARE
- THINGS WE HAVEN'T THOUGHT OF BUT WILL UNDOUBTABLY REQUIRE MORE POWER

COMPACT POWER SOURCES

SPECIFIC ENERGY (Wh/kg)

SOURCE	SPECIFIC ENERGY (Theoretical)	SPECIFIC ENERGY (Practical)
Rechargeable Batteries		35-200
Primary Li/SO_2	1,400	175
Primary $Li/SOCl_2$	1,400	300
TNT	1,400	N/A
Methanol	6,200	1,500-3,100
Diesel	13,200	1,320-5,000
Hydrogen	33,000	1,150-23,000
Nuclear	2,800,000	190,000

COMPACT POWER SOURCES
Lessons

- All useful systems contain enough energy to cause considerable damage in the event of an accident - safety engineering is essential
- 'Standard' battery systems can be improved in various ways (ie, cold weather performance, shelf life, rechargeable battery performance) but no dramatic improvements (more than doubling) in energy density are foreseen
- Lightweight, high efficiency energy conversion devices which can use air as the oxidizer are the key to making use of the high energy density of convenient liquid fuels --> fuel cells, thermophotovoltaics, micro turbines.... Caveate: systems need to be designed for tactical robustness, i.e., submersion in water...
- The relatively advanced state of the art of hydrogen/air fuel cells and the very high energy density of hydrogen justify the present significant DoD effort to find new ways to deliver hydrogen to the soldier
- Fueled systems will likely be hybrid systems - they will likely need batteries
- Power management through more efficient electronics

COMPACT POWER SOURCES

Partners:

- DARPA / DSO
- ARMY
  - ARO, ARL
  - CECOM RDEC, LRC, PM MEP, TRADOC FORSCOM
    - MICOM, ARDEC, TACOM, ATCOM
    - AAN Technology Panels, CASCOM
    - Dismounted Battlespace Battle Lab
- Intelligence Agencies
- Other Services - Navy, Air Force, Special Operations
- Other Agencies - DOE, NIST, National Laboratories
- Interagency Advanced Power Group
- The University Community
- The Industrial Base

COMPACT POWER SOURCES
Recent and/or Planned Workshops

- Small Fuel Cells - Oct-Nov 1994
- Disposable Fuel Cells - April 1996
  - DARPA,CECOM, ARL ... participation
- Thermophotovoltaics - July 1996
  - DARPA,CECOM, ARL ... participation
- Hydrogen Storage/Generation - April 1997
  - CIA co-sponsorship, DARPA,CECOM, ARL, DBBL ... participation
- Human Powered Systems - Nov 1997
  - DARPA,CECOM, ARL, SSCOM, SOCOM ... participation
- Hybrid Systems - 1-3 Apr 1998
  - DARPA, CIA co-sponsorship
- Membrane Electrolytes - 29 Apr-1May 1998
  - ONR, DARPA co-sponsorship

COMPACT POWER SOURCES

H-Power Fuel Cell Stack for SINCGARS Experiment

ARO/DARPA/CECOM
Compact Power Program

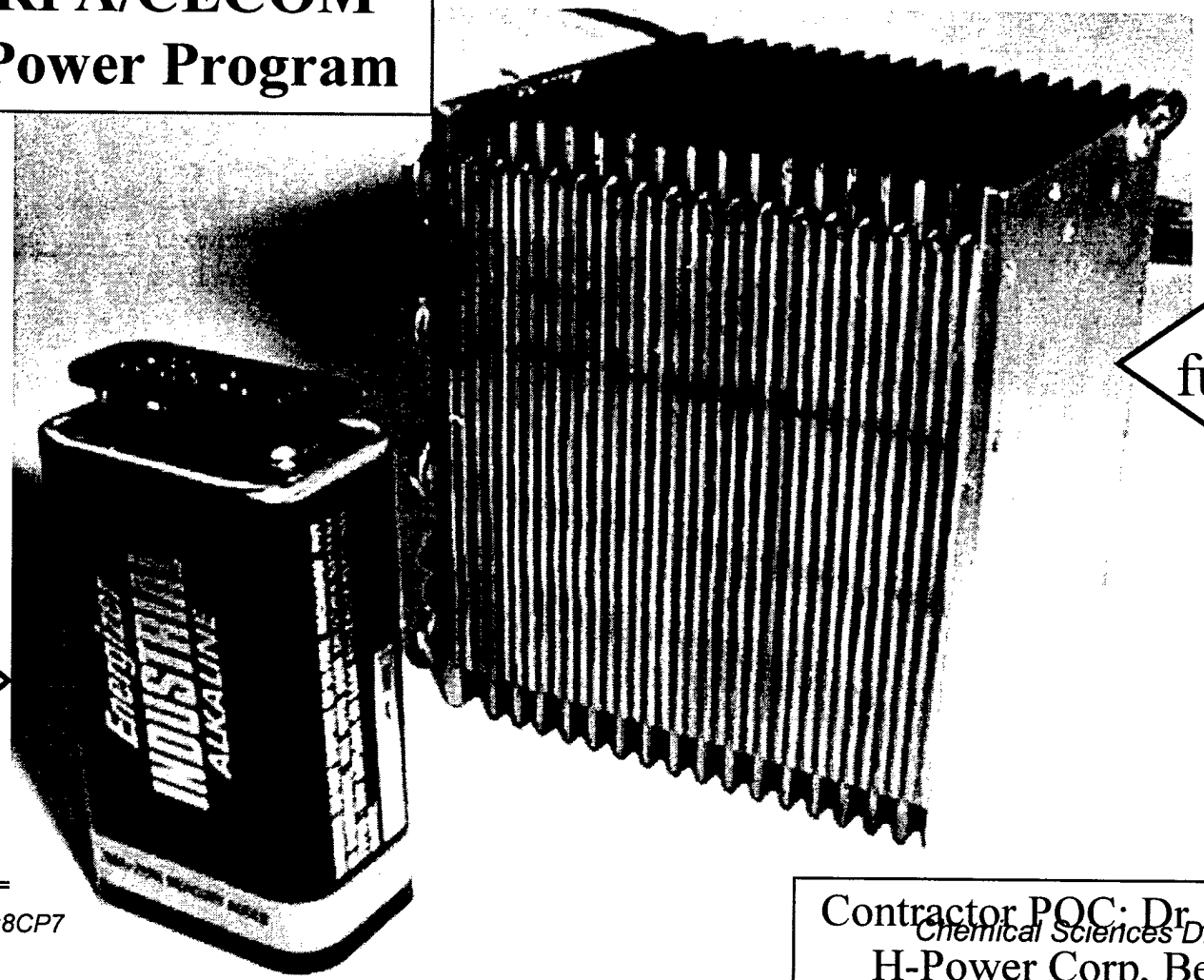

50 watt
fuel cell stack

9 volt
battery

Contractor POC: Dr Art Kaufmann
Chemical Sciences Division
H-Power Corp, Belleville, NJ

COMPACT POWER SOURCES
Improved Fuel Cells and Batteries - 2

1996 State-of-the-Art Fuel Cell fitted into BA5590 Battery Case

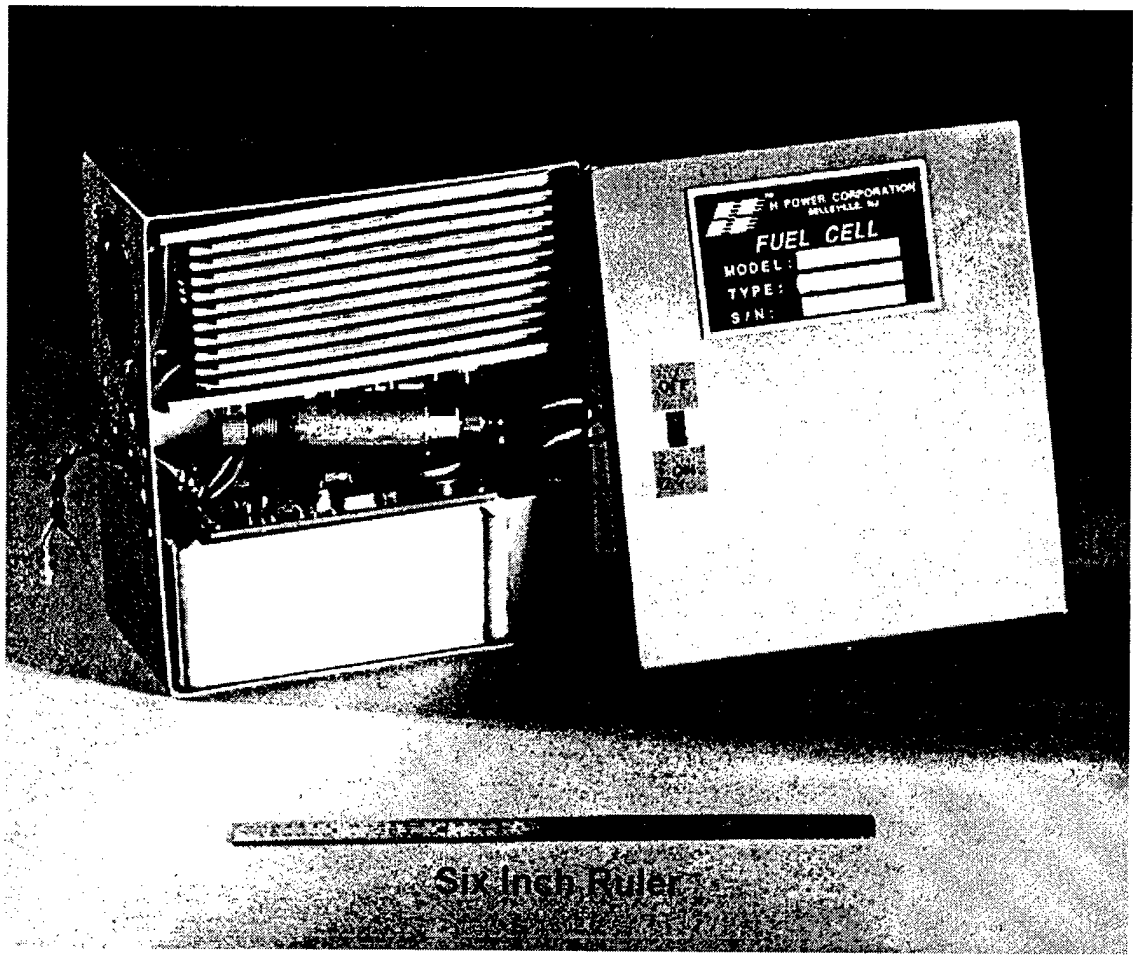

COMPACT POWER SOURCES
Improved Fuel Cells and Batteries - 3

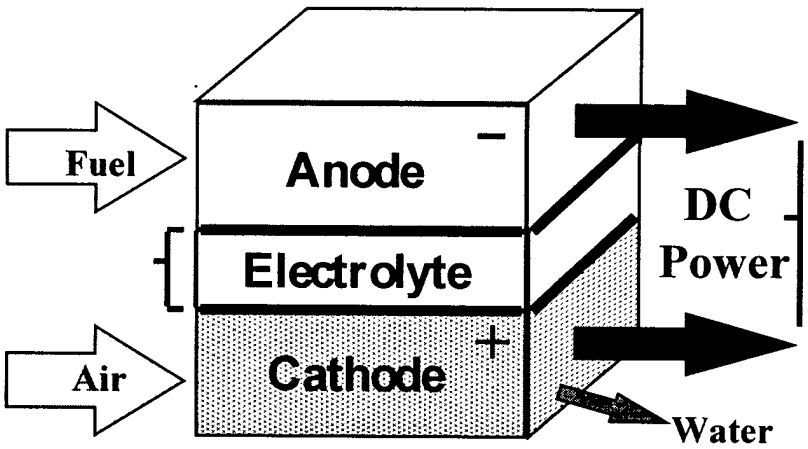

- **STATE-OF-THE-ART**
  - catalyst applied by spray, brush, or decale transfer - uniformity
  - fuel and air passages milled in bipolar plates, secondary passages in carbon paper electrode material
  - contacts formed by pressing carbon paper, membrane electrolyte, and catalysts together in high temperature press - very random process
  - catalysts appear to be only about one percent as active as similiar materials in processes like petroleum refining

COMPACT POWER SOURCES
Improved Fuel Cells and Batteries - 6

- Present knowledge about nanostructures can provide basis for systhesizing electrode structures in which small scale components such as catalyst particles can be precisely positioned to optimize catalysis and electron transfer

- Larger structures such as air and fuel passages can be formed using bicontinuous microemulsion approaches developed under chemical decomtamination programs

- Identification of catalysts by combinatorial approaches and synthesis using organometallic precursors to provide stoichiometric control should greatly improve catalysis

DARPA
Advanced Energy Technologies

"Advanced Fuel Cell Membranes For Non-conventional Fuel Sources"
April 28 - May 1, 1998

Dr. Robert J. Nowak
DARPA/DSO
(703) 696-7491 (voice)
(703) 696-3999 (fax)
RNOWAK@darpa.mil

Advanced Energy Technologies

Power for the Military

Mobile Electric Power
2 - 100 kW

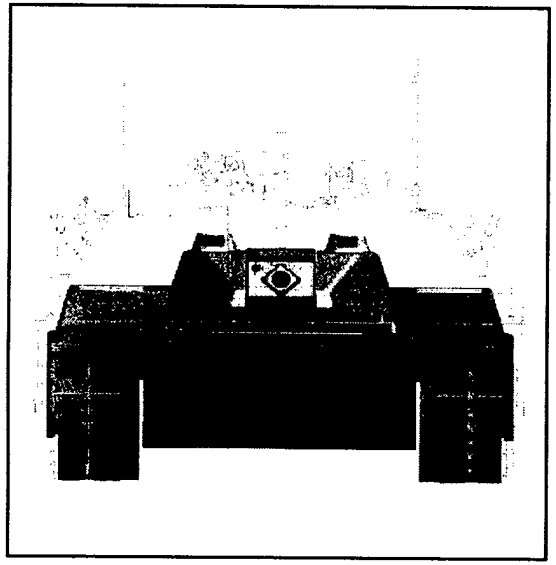

- Silent Watch
- Field Power Stations

Portable Power
50 - 500 W

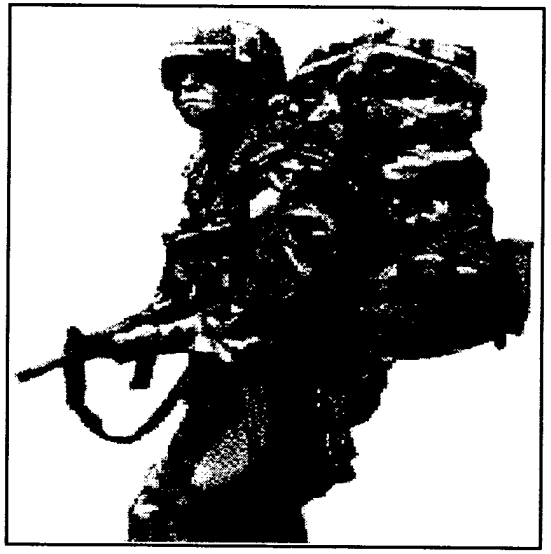

- Battery Replacement
- Micro-Climate Cooling
- Battery Charging

Energy Harvesting
< 5 W

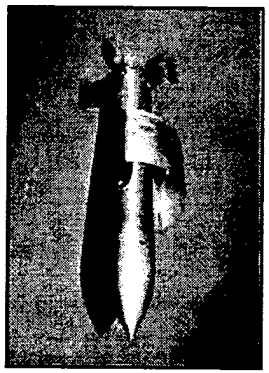

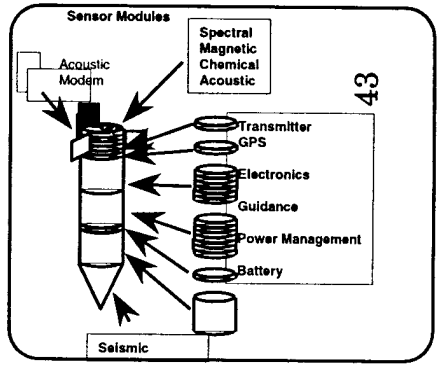

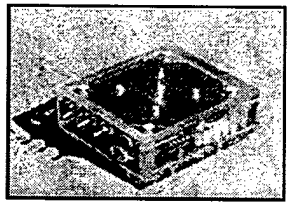

- Ground Sensors
- Micro - Robots

NOWAK280498

Weight Trade-Off: *Adding electronics and batteries is at the expense of other mission-essential items*

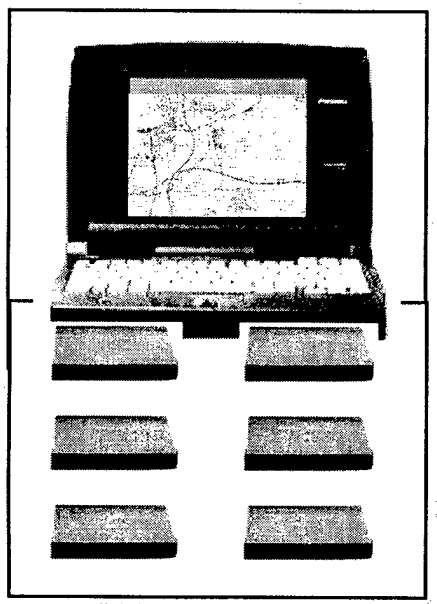

Laptop Computer and 2 Day Supply of Batteries ***(Approx. 12.4 lbs.)***

=

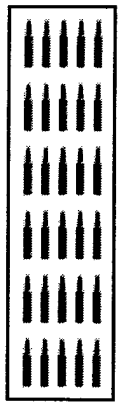

402 Rounds of 5.56 mm Ammo ***(13.4 30-Round Magazines)***

=

4 Day Supply of Food ***(12 1-lb. MRE's)***

=

Protective Mask

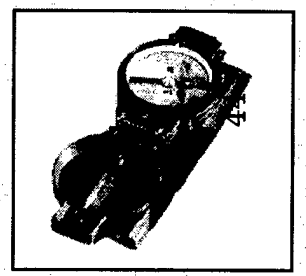

Compass

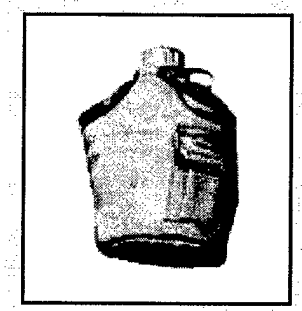

Canteen

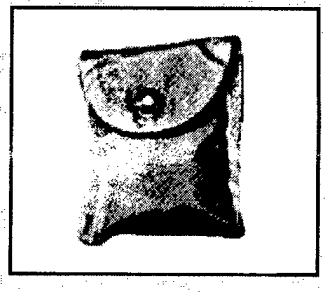

First Aid Kit

NOWAK280498

LI BATTERY PROGRAM TRANSITION
(Ultralife Batteries Inc.)

SOCOM Combat Management System

DARPA
ETO/URBAN

GPS Module
- Antenna
- Rockwell PLGR GPS Engine
- Size 4.5" x 3" x 1"

CPU Module
- 133MHz Pentium CPU
- 64MB DRAM
- 2 GB Hard Drive
- 2 PCMCIA Slots
- 2 RS-232 Ports
- Universal Serial Bus
- Size 6" x 7.25' x 1.25"
- Weight 10.78 Lbs. (est)

Wireless LAN
- Proxim RangeLAN2
- 1.6 Mbps data rate
- Range 1000 ft. LOS
- 2.4 - 2.4835 GHz Spread Spectrum

Battery on Back
- Solid Lithium Ion Polymer
- 9.6 Amp Hour
- System Operation at Least 6 Hrs

MXF-610 Radio
- Computer Control
- Voice
- Data (16Kbps)
- Range > 5KM

Advances In Energy Density of Sealed Rechargeable Batteries

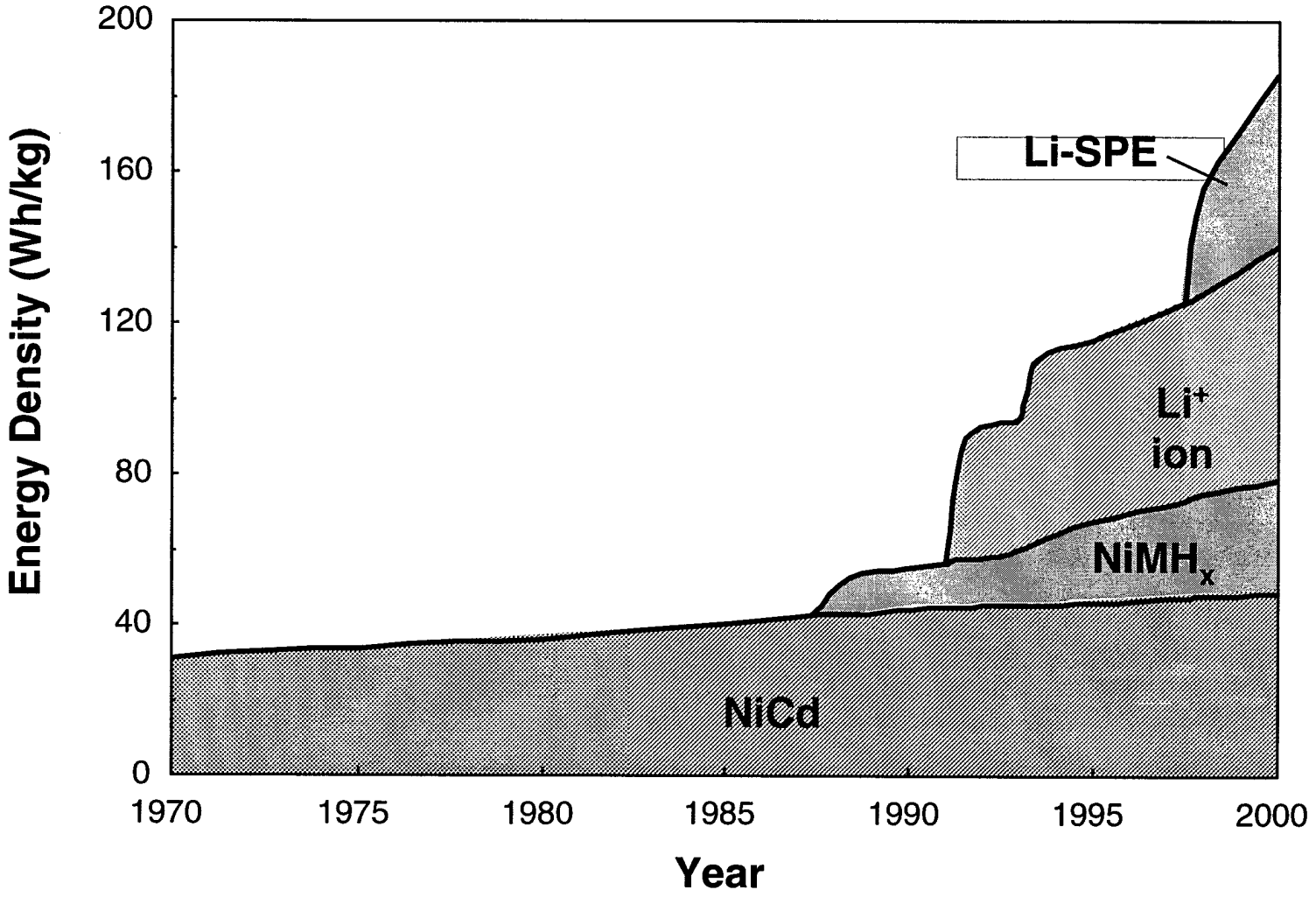

Energy Conversion vs. Energy Storage

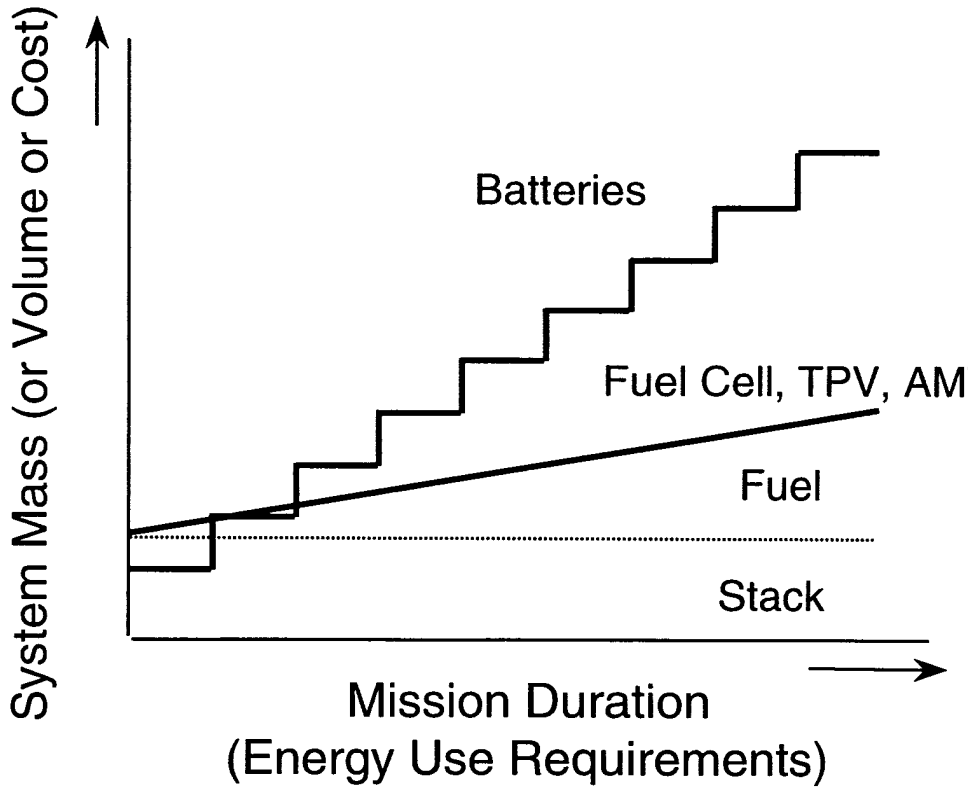

Energy Density of Selected Fuels and Batteries

Fuel:	Energy Density
Diesel Fuel/Jet Fuel	12,000 Wh/kg
Methanol	5,000
High Explosive	1,000

Battery:	
Primary Battery (est. max.)	500
Rechargeable (est. max.)	200
Li/SO_2 Battery (primary)	176
Alkaline Battery (primary)	80
Nickel-Cadmium (secondary)	40

47

Driving Force: Substantially decreased size, weight, and cost with improved safety and environmental compliance → Increased force mobility

NOWAK280498

Fuel Cell Operation on High Energy Density Liquid Fuels

Conventional Approach

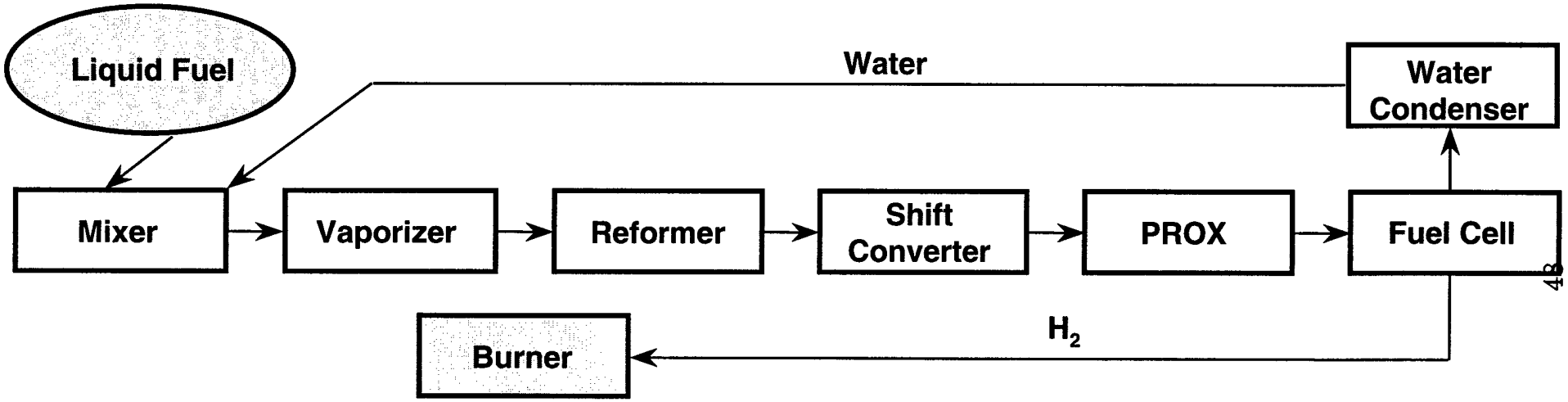

- Reduced complexity by a factor of 4-6
- Reduced weight and volume by 25-50%
- Improved reliabilty and lower maintenance
- Rapid start capability, rapid transient response
- Reduced capital and operating costs
- Lower thermal signature

Direct Oxidation

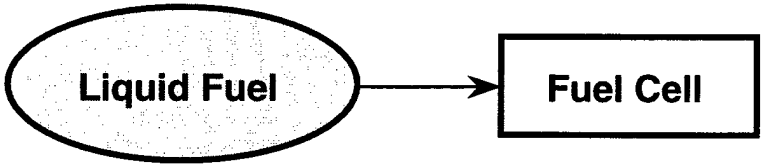

⇒ Increased applicability of fuel cells to DoD missions

Schematic Diagram of a Low-Temperature, Direct Methanol Oxidation Fuel Cell

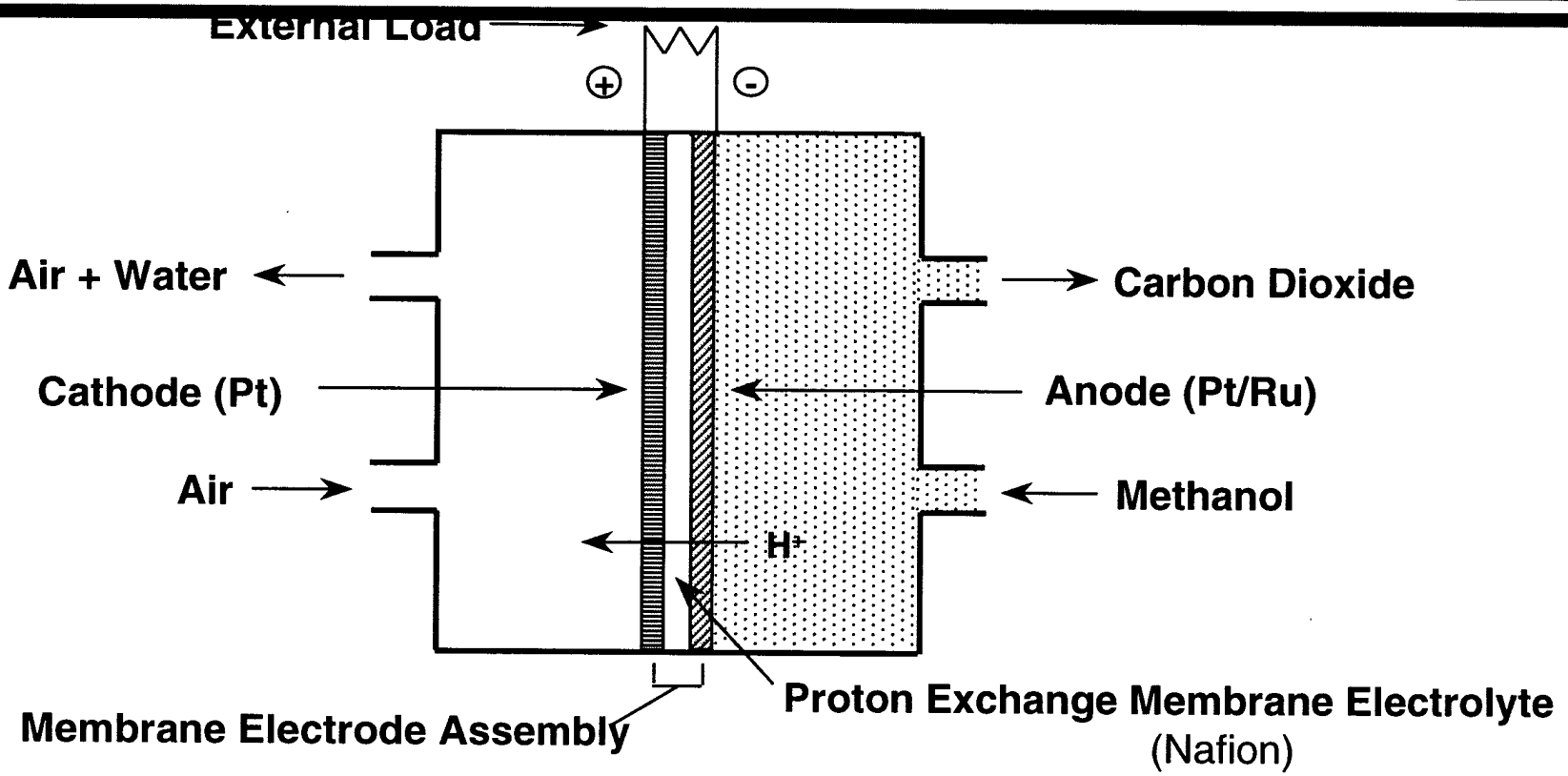

Anode	$CH_3OH + H_2O \rightarrow CO_2 + 6H^+ + 6e^-$
Cathode	$1.5O_2 + 6H^+ + 6e^- \rightarrow 3H_2O$
Cell	$CH_3OH + 1.5O_2 \rightarrow CO_2 + 2H_2O$

NOWAK280498

Progress In Direct Methanol Oxidation PEM Fuel Cells

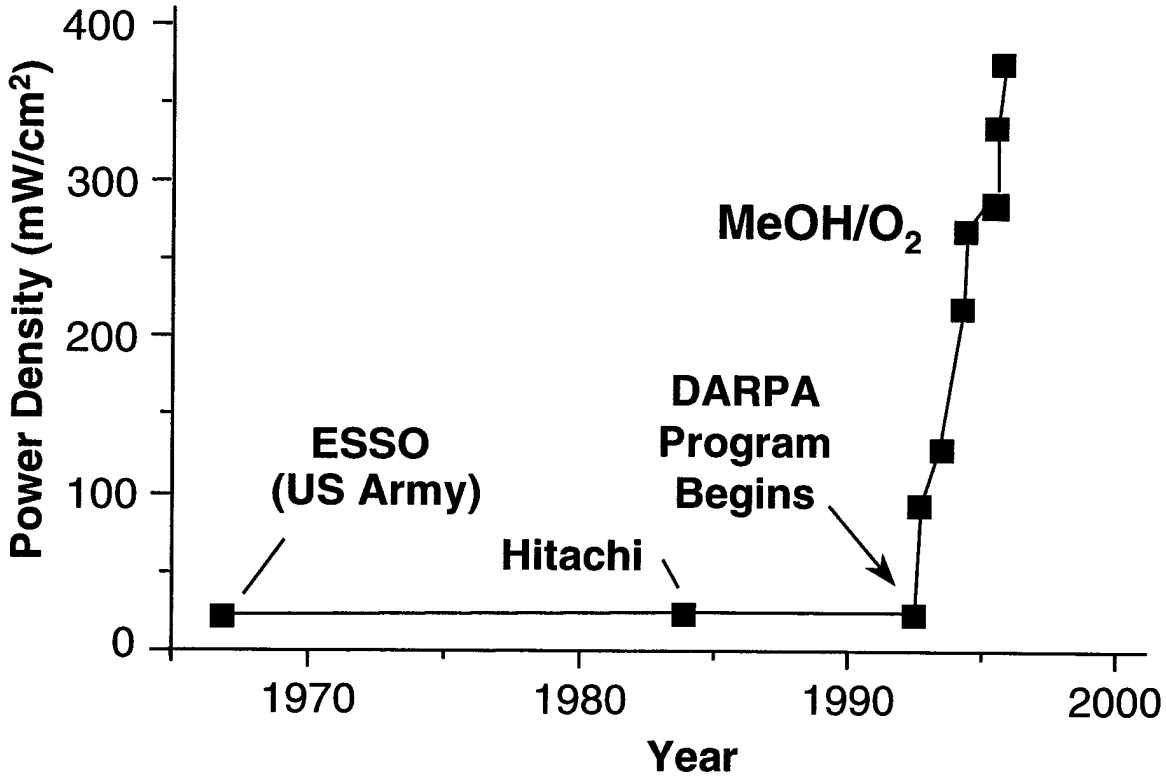

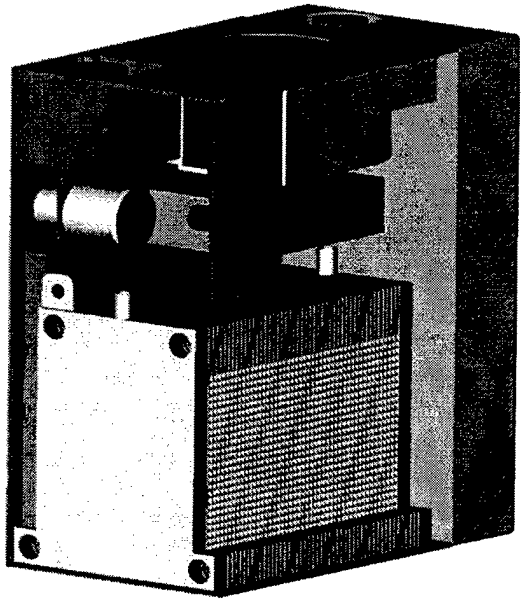

50

NOWAK280498

Direct Methanol Oxidation Fuel Cell Program:
Technology Challenges

GOAL: Increase power density and system efficiency to levels comparable with those of other fuel cells.

ISSUES:

- Solve methanol cross-diffusion problem
- Novel membrane chemistry (improve water management, lower cost, higher/lower temperature operation)
- New methods for preparing optimized Pt/Ru and other alloy catalysts and low-loaded electrodes
- System life, reliability, reproducibility
- Low-cost, light weight materials for substrates, separators, flow fields, and end plates
- Air vs. O_2 operation, ambient vs. elevated pressure, high efficiency compressors
- Water management and/or recycling, balance-of-plant
- Corrosion, methanol fuel specs

Portable Power
50 - 500 W

TPV

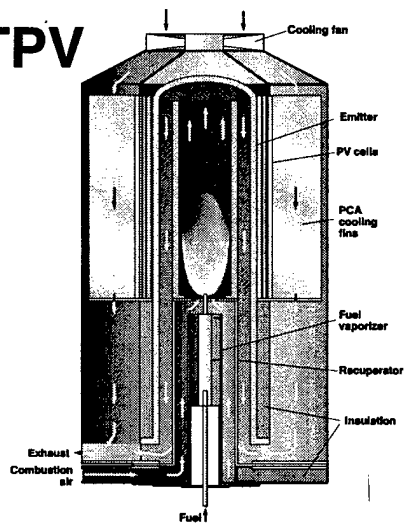

micro-Turbine Generator

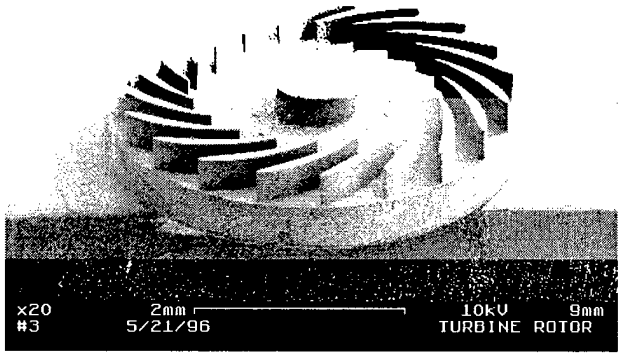

AMTEC

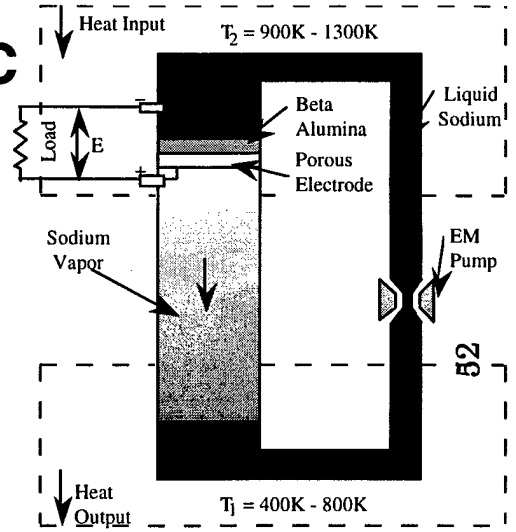

500 W Battery Charger

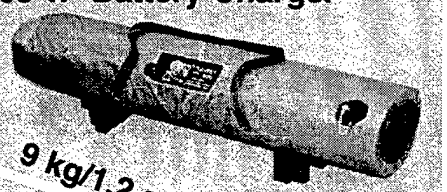

Planar SOFC

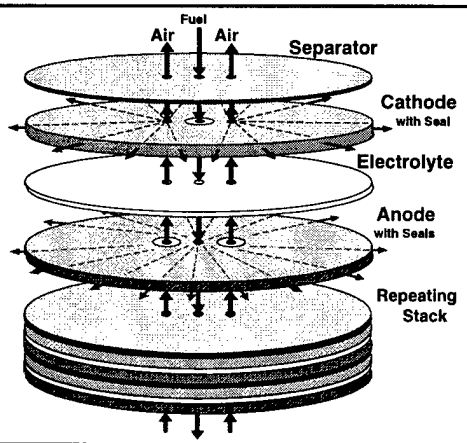

DMFC

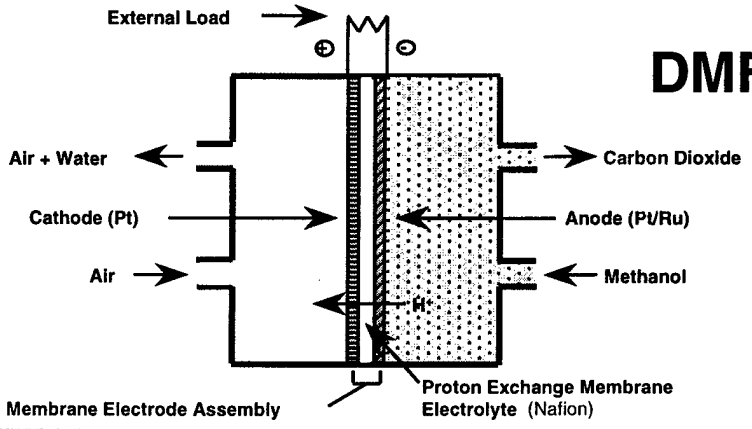

NOWAK280498

System Mass vs. Mission Duration
Portable Power - 500 W

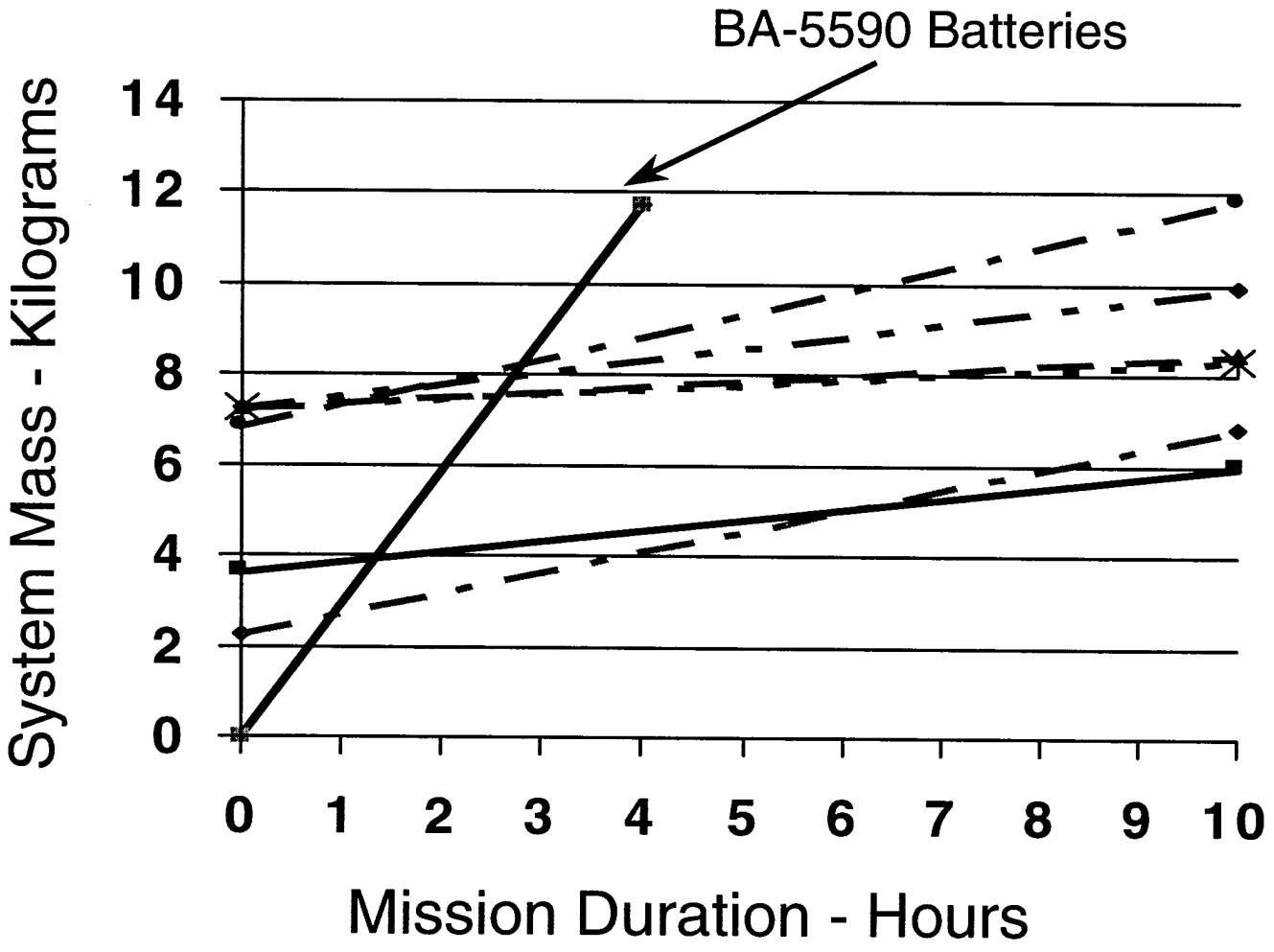

IC Engine

TPV

AMTEC,
Planar SOFC

} Logistics Fuel

PEM - Hydrogen (10%)

PEM - Methanol

53

5000 W-hr of
BA-5590 Batteries
would weigh 29 Kg

NOWAK280498

Energy from the Environment

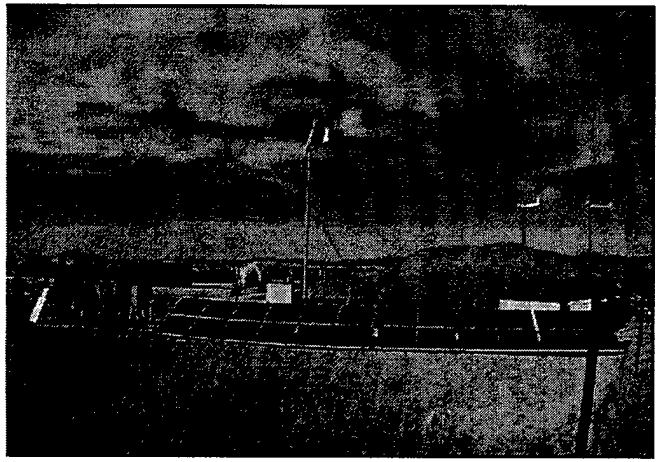

Marine Corps
Solar - PV; Wind
6 kW

DARPA CIS
Flexible PV
18 W

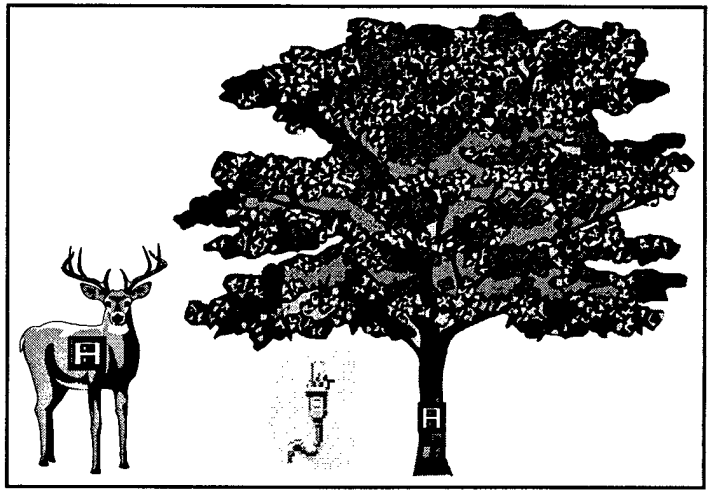

DARPA Energy Harvesting
Bio, Mechanical, Solar,
Gradients, EM, Transmission
Line, Human Activity, etc.
< 5 W

Energy Harvesting - *Opportunities and Issues*

- Realistic harvesting concepts - on and off the soldier
- Critical and credible application
- Compatible energy storage and power conditioning
- Power management vs. duty cycle
- Materials and/or fuels processing
- Reliability of technology and source
- Compact size, weight (footprint, impact), low cost

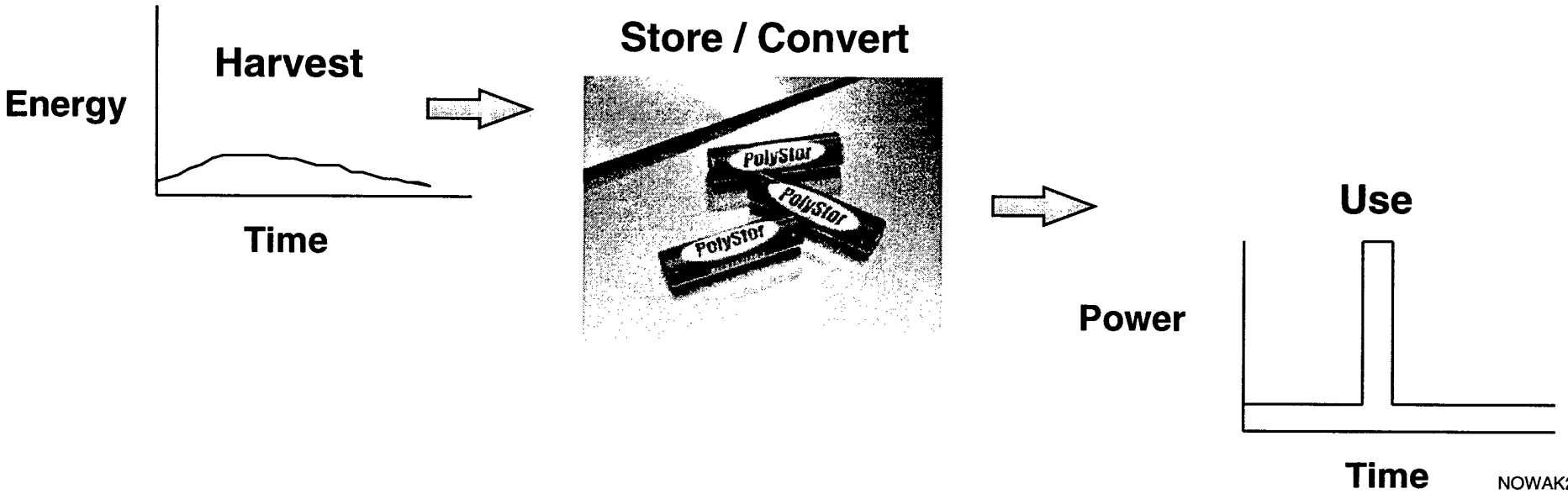

Navy Fuel Cell Research and Development Programs

Richard T. Carlin
Program Officer, Electrochemistry S&T Program

ABSTRACT

Fuel cells provide a unique opportunity to enhance the performance of future Navy platforms while concurrently meeting affordability and environmental quality demands. A major focus of the Navy fuel cell applied research and advanced technology development programs is ship service power, where output in the megawatt range is needed. For such shipboard applications, the fuel cell must operate on Naval logistic diesel fuels and provide quality power under stressful at-sea conditions; therefore, current research components include diesel reforming, sulfur removal/tolerance, shock/vibration testing, and systems modeling. The Navy also is integrating its shipboard program with a land based 250 kW PEM advanced development program being performed in collaboration with industrial and academic partners. As fuel cells become ingrained in the Navy's power technology, platform designers will look for increased fuel cell performance at lower costs. These future Naval capability options can only be realized through innovations from the S&T research community.

SLIDE NARRATIONS

Slide 1. Fuel cells are envisioned as clean, cost-effective power sources for Naval ships, land based facilities, and a variety of undersea platforms.

Slide 2. Academia, private industry, and Navy and other federal laboratories form the transitional bridge between S&T and future Naval mission capabilities and technology options. The Office of Naval Research ensures that this critical interconnect is maintained by recognizing and promoting S&T opportunities and maintaining support of S&T areas for which the Navy has assumed national leadership and responsibility.

Slide 3. At the present time, ONR has two ongoing applied research and advanced technology development programs examining fuel cells as power plants for ships and land based facilities. The first of these addresses the technical issues arising from operating commercial fuel cell technologies under the harsh conditions encountered in a marine environment. The second is evaluating a prototype land-based PEM fuel cell as a facilities power plant. As advances in fuel cells continue, opportunities to apply appropriate fuel cell technologies to other Navy platforms will arise, while adaptation of air-breathing fuel cells to undersea operation remains a technological challenge.

Slide 4. In terms of fuel utilization efficiency, fuel cells outperform gas turbines across all load levels. Even advanced designs, such as the intercooled recuperated gas turbine, can not match the overall performance of a PEM fuel cell.

Slide 5. Fuel cells operate with higher efficiencies and at lower temperatures than gas turbines and diesel engines. Therefore, they dramatically reduce emissions of NO_x, CO, and unburned hydrocarbons, while decreasing CO_2 release by approximately 30%. These benefits lead to lower ship operating costs, reduced environmental impact, and decreased ship signature.

Slide 6. Because the Navy operates worldwide, fuel cells on Navy ships must utilize marine diesels as the primary fuel. This requirement leads to new challenges in fuel cell tolerances, reformer operation, and system integration and performance - all of which are being addressed in ONR's ship service fuel cell program.

Slide 7. The electrochemistry basic research program at ONR provides a fundamental understanding of the phenomena that govern fuel cell performance, such as transport in polyelectrolytes and electrocatalysis. Moreover, the program seeks to expand the concepts of fuel cell generated electrical power by supporting research in advanced electrochemical materials and promoting the application of nanometer scale designs to device concepts.

Slide 8. Electrochemistry at ONR is an integrated program in which basic research and technological advancement join to transform scientific understanding into future electric power sources.

ONR Perspective

Richard T. Carlin

Electrochemistry S&T Program, Code 331

E. Ashey, ONR, Code 334; J. Woerner, M. Cervi, NSWCCD

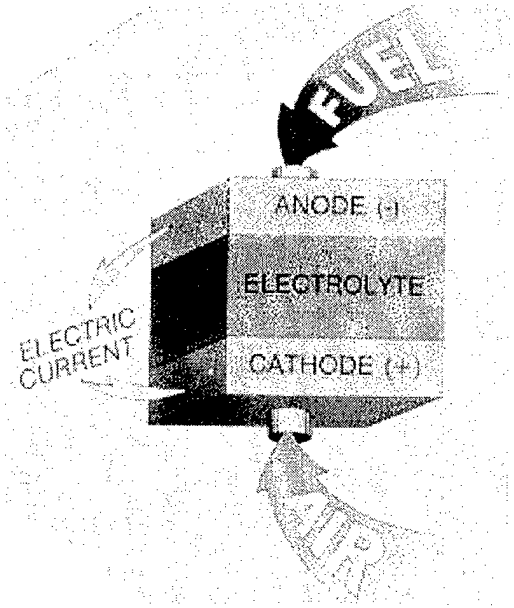

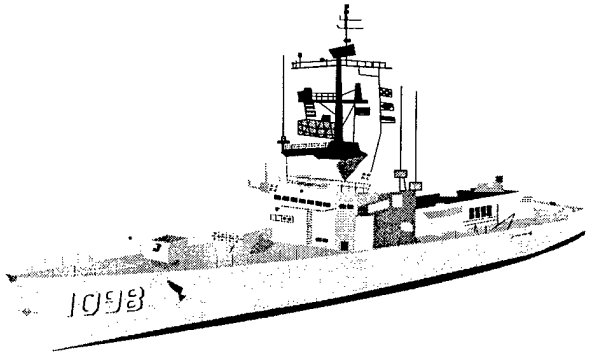

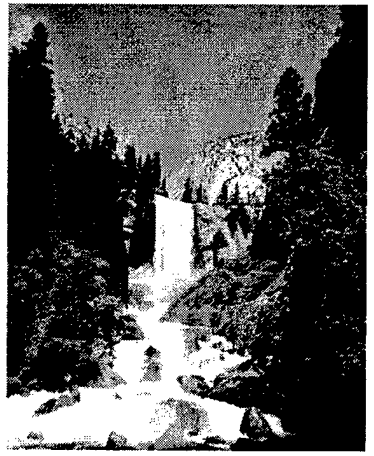

Transition Bridge

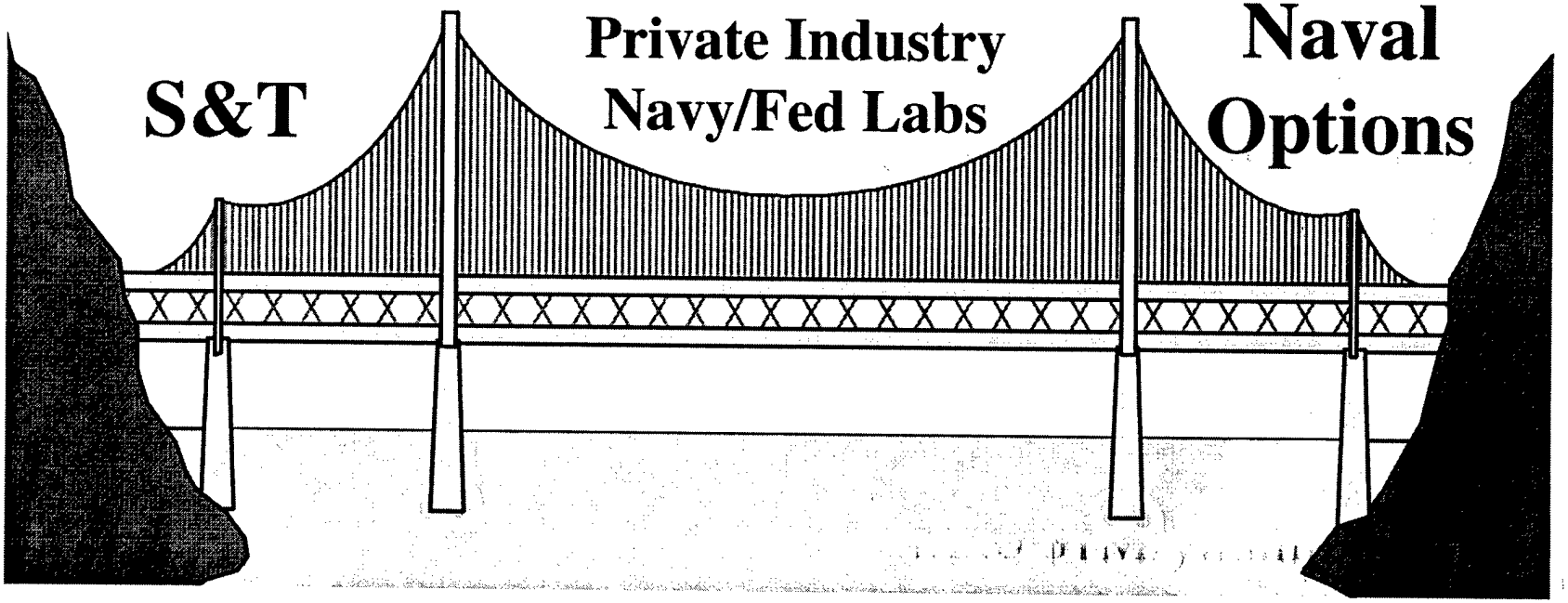

Fulfilling National Obligations
Utilizing S&T Opportunities

Applied Research and Advanced Technology Development

- Ship Surface Fuel Cell (SSFC) Power
  - » Demonstration of 0.5 MW fuel cell operating on reformed diesel fuel in marine environment
  - » Design of 2.5 MW SSFC

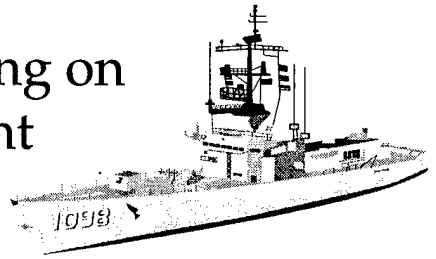

- Evaluate 250 kW PEM for land based power

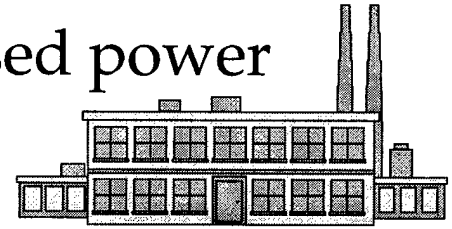

- Opportunities
  - » Unmanned Undersea Vehicle (UUV) Propulsion
  - » Power for portable sensors: batteries comprise ¼ to ½ weight

Fuel Rate Comparison
(Electrical Power Output)

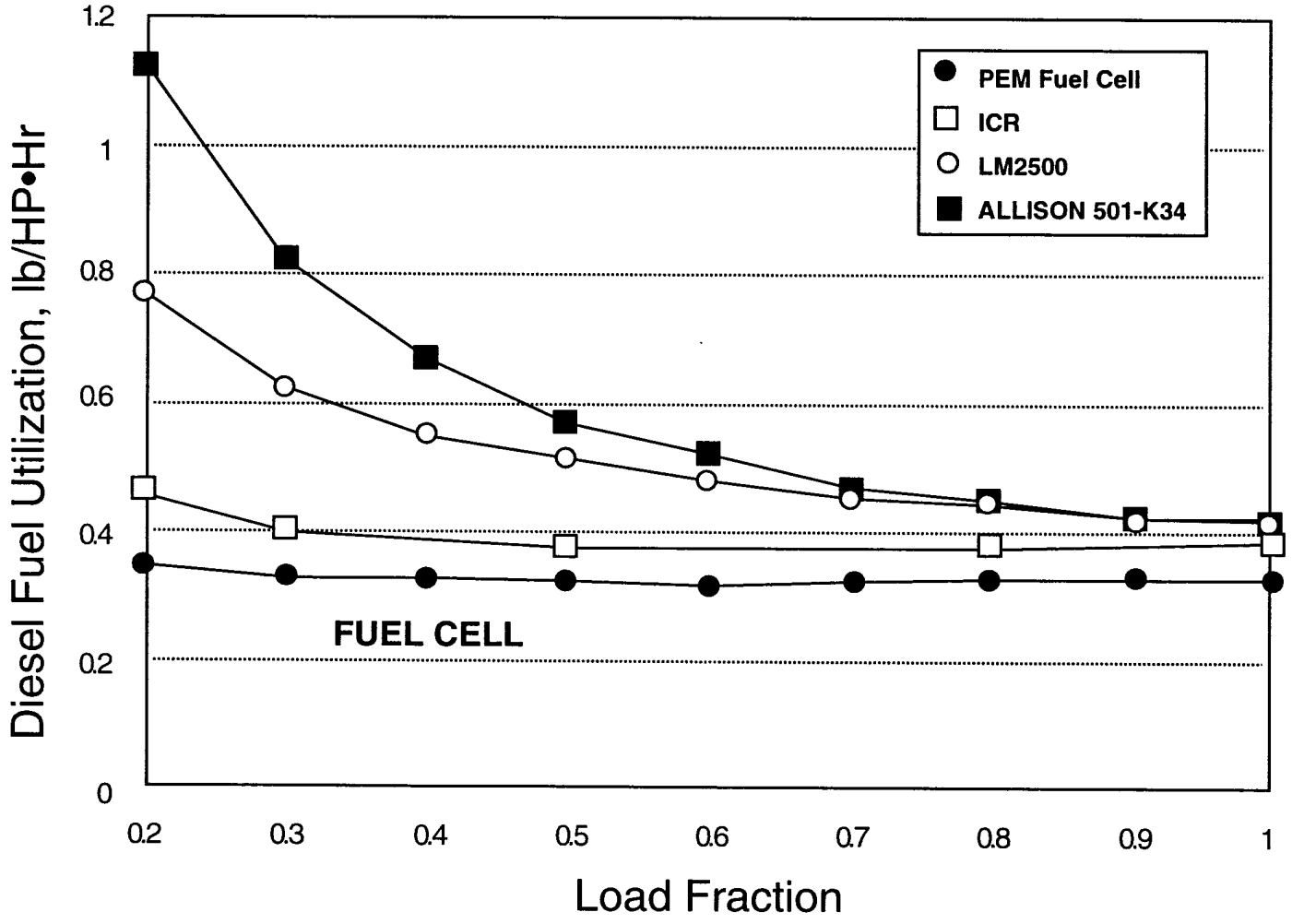

Fuel Cells for Ship Service Power

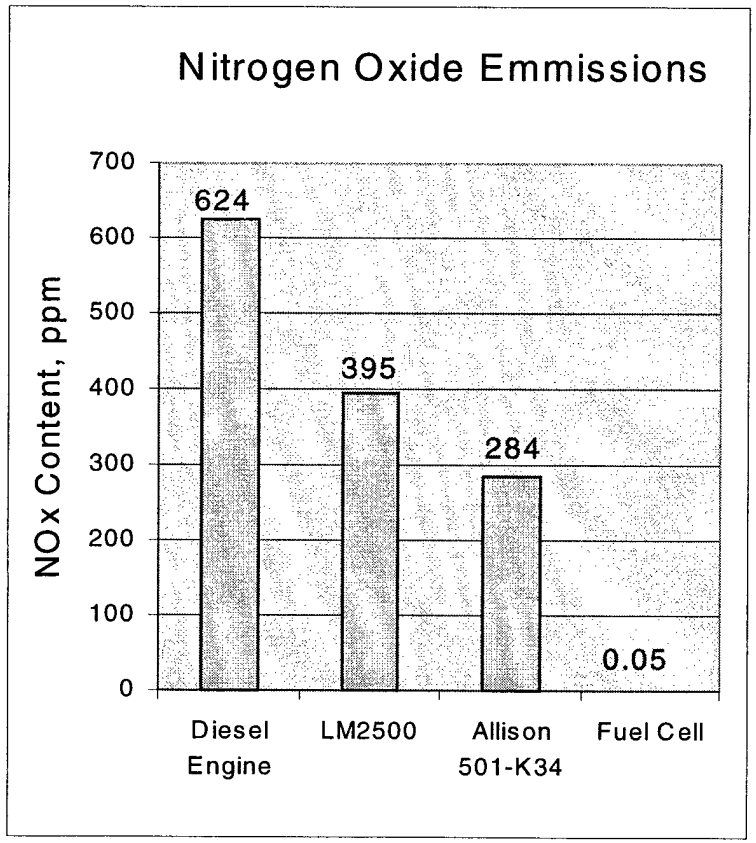

Operate with Higher Efficiencies and at Lower Temperatures

- ✔ 96% Reduction in NO_x, CO and HC Emissions
- ✔ 30% Reduction in CO_2 Emissions
- ✔ $0.6M to $1M/yr/ship Savings
- ✔ >75% Cooler Exhaust
- ✔ 60% Reduced Stacks

MUST Operate on Logistic Diesel Fuel (NATO F-76) with up to 1 wt% Sulfur)

Challenges

- Sulfur/CO Tolerance
- Reformer
- Reformate Cleanup (Contaminant Removal)
- Efficient System Integration
- High Specific Power
- Transient Response

Basic Research

- Current Programs
  - » Transport in polyelectrolytes
  - » Electro-oxidation of organic molecules
  - » Electrocatalysis at surface step-sites
- Future Directions
  - » Nanoarchitectural designs for power sources
  - » Novel membrane structures and applications

Research and Technology

Water-Derived Power
Advanced Propulsors
Electrochem Energy
Thermal Energy

Advanced Materials
MicroElectroMechanical Systems
Metal/Water Chemistry
Nanotechnology

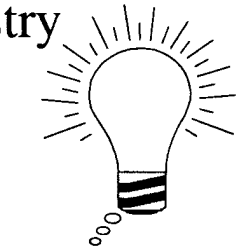

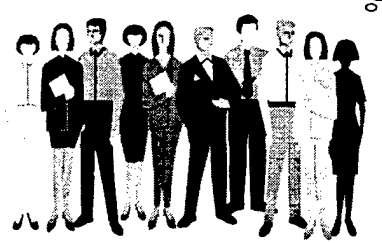

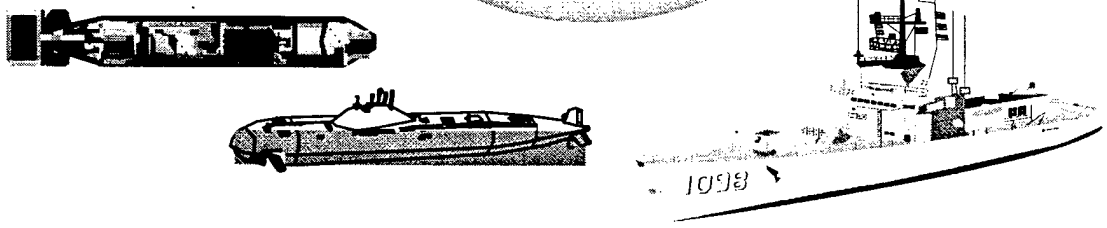

THE ARMY AFTER NEXT

Intertwining Military Art, Science, And Technology Out To The Year 2025

By MG Robert H. Scales Jr.
and Dr. John A. Parmentola
Army RD&A May-June 1998

Introduction

The Army After Next (AAN) Project Office at Headquarters, U.S. Army Training and Doctrine Command (TRADOC) is con-ducting broad studies of future warfare for the year 2025 timeframe. The purpose is to isolate the issues vital to the develop-ment of the Army. The vision generated from these studies will be integrated into future TRADOC combat developments programs.

Several important dimensions motivate the focus on the 2025 timeframe for AAN. First, given our available lead time and the rapid pace of economic development in a number of evolving countries, it is likely that the United States will encounter a major military competitor or, at the very least, con-front significant asymmetric threats in this period.

Second, the year 2025 enables military art and technology experts to divert their thinking from concepts and capabilities associated with the pro-grammed force of Army 2010 to more novel approaches to achieve the AAN vision. It also provides ample lead time to incorporate innovative technologiesand unanticipated revolutionary discoveries into this vision.

Finally, it provides an opportunity to refocus Army basic and applied research on efforts that have significant potential for advancing critical AAN enabling technologies. Thus, TRADOC ● s AAN efforts will enable the Army to refine its choices as a function of time and optimize its investment decisions to achieve critical AAN warfighter capabilities.

This article describes the assump-tions, arguments, and challenges that form the basis for conceptualizing the Army ● s warfighting capabilities out to the year 2025 and the science and tech-nology support and activities that will enable the Army to eventually realize these capabilities.

Speed, Knowledge And The Lessons Of History

Cycles of change in warfare are particularly difficult to comprehend and even more difficult to anticipate because, unlike endeavors in finance, medicine, or law, active experience in war is, thankfully, infrequent. Because warfare is not frequently practiced, soldiers must rely on the laboratory of past experiences to gain vicarious experience in war. To be sure, the frenetic pace of technological change in the modern world has compressed the interval and stretched the amplitude of the cycles of change. Nonetheless, undeniable cycles remain and we should be able to search the recent past to identify new cycles.

With the rise of industrial production and the appearance of precision warmaking machinery such as rifled weapons in the mid-19th century, tech-nology began to dominate patterns of change. Such weapons extended the deadly zone, or the distance that sol-diers had to cross to engage a defender, from 150 meters in Napoleon ● s day to 1,000 meters or more by the end of the American Civil War. As the deadly zone increased by nearly a factor of 10, the risks of crossing it were further multi-plied by the lethality induced through the precision and volume from the massive proliferation of repeating arms. Thus, technology favored the defender. Images of the terrible slaughter of

World War I remain as testimony to the cost in blood exacted by an operational method that relied on a killing effect to achieve decisive results.

The Germans first conceptualized the solution in 1918, and it was deceptively simple: short, highly intense doses of firepower to prepare the assault, small units to exploit the shock effect of fire-power to infiltrate and bypass centers of resistance, and operational formations to move through exposed points of weakness and push deep into enemy lines. After the war, the further development of the internal combustion engine provided the means to translate the theory into effective action and restore the dominance of the offensive. Motorized armored vehicles allowed soldiers to cross the deadly zone pro-tected by enormously greater speed while employing blitzkrieg to gain victory. This was achieved through psycho-logical paralysis induced by movement,
rather than through butchery induced by massive application of firepower.

After World War II, the challenge was to halt a Soviet-style blitzkrieg across the Northern German Plain. Tactical forces needed defensive killing power to absorb the initial Soviet-armored shock and hold their defensive positions. This led to the defensive forces ● return to dominance. The operational problem,
however, was to strike deep offensively to slow the rate of arrival of follow-on armored forces at the front line. The resulting AirLand Battle Doctrine of the 1980s suggested a swing of the pendulum back toward offensive forces. Operation Desert Storm added momentum to the pendulum swing with ground and air forces overwhelming static defenses with unprecedented speed and intensity. Nonetheless, even Desert
Storm produced troubling hints that evolving defensive systems threaten to reimpose strategic and operational paralysis. Iraq ● s SCUD missile attacks on Saudi Arabia and Israel, had they been more accurate or included chemical or biological warheads, might have strengthened Iraq ● s defense considerably.
The proliferation of such systems will substantially raise the stakes of future interventions.

Two key attributes of future U.S. Armed Forces, if harmoniously devel-oped, would firmly re-establish the killing zone, deliver metal on target, and provide timely logistic support to the battleforce. To that end, information technologies will allow us to position outside the combat zone all but those forces necessary to move, observe, and kill. The imperative for speed in this new form of warfare begins at home ports, airfields, and installations. A highly lethal force, shorn of its Cold War impedimenta, will be able to project itself from the homeland or from strategic points overseas in days rather than weeks or months and arrive in the operational theater ready to fight. Strategic speed will allow theater war to take the form of a coup de main. Our goal in applying firepower must be to exploit its substantial paralytic effects to gain advantage. To win quickly and decisively at low cost in the future, we must have the means to conduct the battle quickly and end it cleanly, preferably at the moment when the dominance of the offensive forces. The information revolution will likely allow us to define and track the elements of a force with exquisite clarity and detail, but knowledge of the enemy, alone, is not enough. We must possess the means to act on what we know, and action depends on speed. The combination of knowledge and speed of movement will allow a future battle force to anticipate enemy movement and turn costly force-on-force engagements of past wars into surer and less costly engagements by choice.

Much like the evolution of military and private sector capabilities in the 20th century, an important physical parameter influencing the Army After Next is the compression of time. For the Army, this means taking advantage of future advancements in information technologies while concurrently increasing speed or equivalently reducing the time required to strategically deploy, tactically maneuver, traverse the
the killing zone, deliver metal on targe, and provide timely logistic support to the battleforce. To that end, information technologies will allow us to position outside the combat zone all but those forces necessary to move, observe, and kill.

The imperative for speed in this new form of warfare begins at home ports, airfields, and installations. A highly lethal force, shorn of its Cold War impedimenta, will be able to project itself from the homeland or from strategic points overseas in days rather than weeks or months and arrive in the operational theater ready to fight. Strategic speed will allow theater war to take the form of a coup de main.

Our goal in applying firepower must be to exploit its substantial paralytic effects to gain advantage. To win quickly and decisively at low cost in the future, we must have the means to conduct the battle quickly and end it cleanly, preferably at the moment when the paralytic effect of firepower is greatest.

Victory is best guaranteed through maneuver of forces on the ground. Psychological collapse, the breaking of an enemy ● s will to resist, comes when an opponent is challenged and blocked at all points. A commander with the dual

advantage of speed of maneuver and killing power will dominate the battlefield. If these two essential elements of combat power are orchestrated skillfully, an unfettered battle force will be able to strike multiple vital points simultaneously or in a sequence of their choosing. In a very short time, perhaps only hours, such a force would be able to quickly disintegrate an enemy ● s warfighting structures, producing an unequivocal military decision with minimum cost.

The fourth cycle of war, therefore, should seek to exploit the information age to increase the velocity of maneuver. Speed must be the essential ingredient of a future landpower force. Speed will be achieved by creating a highly mobile force unimpeded by terrain and unburdened by an agility sapping logistical yoke. To achieve the speed of maneuver necessary to wage 21st century knowledge-based warfare will require a new concept of mechanized warfare that will free forces of maneuver inhibiting restrictions. The exploitation of knowledge via increased air and ground mobility will rsult in unprecedented tactical and operational maneuverability.

Such "air mechanized" battle units would be mechanized combined arms echelons of maneuver capable of air assault to operational depths to attack regimental size units and defend against division sized attacks. These units and the personnel and systems they contain will combine extreme speed with superior knowledge to provide precise maneuverability that takes optimum advantage of deadly accurate firepower. The employment of more maneuverable air mechanized battle forces in advance of potent Army XXI forces would create the capacity for 21st century strategic blitzkrieg. Once again, offensive forces would dominate warfare.

Intertwining To The Year 2025 And Beyond

The process for intertwining military art and technology for the AAN is depicted in Firgure 2. This process is comprehensive, highly coordinated, and relies on significant levels of cooperation among its participants. It starts with the annual AAN strategic and tactical war games that explore and assess novel concepts of operations and capabilities and then pass through a number of coordinated technolgy activities and eventually feed back into the AAN war games. This nonlinear process continues until the AAN military art innovations and proposed supporting technologies and systems converge to a feasible, affordable, and militarily significant set of AAN capabilities.

One important output of each yearly cycle of this process is a TRADOC approved short list of critical AAN enabling technologies that is used to establish new AAN Science and Technology Objectives (STOs) that directly involve private sector participation. This is designed to cultivate a growing private sector involvement in advancing technologies in support of challenging AAN capabilities.

Very early in the AAN study process, the Army recognized that team building among the military art and technology experts was crucial to the overall success of the AAN effort. This observation led to the concept of Integrated Idea Teams (IITs). The objective of these teams is to assess, from a technological perspective, the concepts, capabilities, and notional systems, including tradeoffs, that support AAN operational characteristics and ideas developed through AAN war games. IITs are managed by the Army Materiel Command (AMC) through the Army Research Laboratory (ARL) and are composed of technical experts from Army laboratories, National Laboratories, the private sector, the Defense Advanced Research Projects Agency (DARPA) and the other Services, and academia, as well as those more involved in the military art side of the AAN.

Once the IIT has developed such con-cepts, these notional system concept designs are then played in force-on-force/ system-of-systems high resolution modeling and simulation exercises conducted in collaboration with Rand Corp., the TRADOC Analysis Center (TRAC), TRADOC, the IIT, and Office of the Assistant Secretary of the Army (Research, Development and Acquisition) (OASARDA). The purpose of this is to assess the military significance of these systems within a larger set of warfighting systems and to determine system performance parameters that make a difference on the battle-field. This effort recognizes that maximizing individual system performance does not necessarily result in a more capable and affordable system.

The final step in this process is to assess the feasibility and affordability of selected concepts through a team of experts from the military laboratories, national laboratories, the private sector, and academia. The objective of this effort is to evaluate the IIT notional sys-tem designs, in concert with the above force-on-force results, with respect to feasibility (laws of physics, maturity of concept, and schedule) and affordability (development cost, production cost, operations and support costs, and leveraging with the private sector and the other Services and agencies). This effort also provides positive feedback to the IIT on their notional system con-cept designs. These assessments are then forwarded to TRADOC for review and assessment and the results are

used to decide on the role of these notional system concept designs in the next round of the AAN war games.

An example of an emerging insight from the AAN war gaming that was fleshed out through the IIT process is the concept of air mechanization, which was mentioned earlier. To achieve the requisite speed and agility, 21st century air mechanization will have to derive from new combinations of air and ground vehicles. A plausible option to provide the tactical and operational maneuverability required for the 21st century is to include an advanced airframe designed to be both a lifting and fighting vehicle. It would be able to lift, conformably, members of a family of light advanced ground vehicles with long-range, lightweight, highly accurate armaments. The advanced airframe would connect quickly to an advanced ground vehicle while its crew remains inside. The advanced airframe would transport the vehicle anywhere on the battlefield out to a combat radius within hours and deploy it combat ready. In addition to lifting advanced ground vehicles, the advanced airframe would lift or employ a variety of other mission modules.

All advanced ground vehicles would rarely be required to face main battle tanks head-on, which makes it possible to limit their weight by reducing the need for heavy armor. They will survive through a combination of speed, agility, active protection, signature management and control, comprehensive situational understanding, terrain masking, deception, and indirect fire. Greater ground speed on and off roads will be possible because of advanced suspension systems, power trains, and engines. Greater fuel economies will result from significant weight reduction and advanced propulsion system designs.

Thus far, the AAN study has focused on the challenging air mechanization concept involving a high-speed tiltrotor and several versions of a lightweight, highly lethal, mobile companion ground craft. This concept addresses the following: the need to overcome the limitations of ground vehicle speed by transporting the ground craft at high speed via the tiltrotor within theater; the need for a lightweight ground craft to limit the size of the tiltrotor; and the need to overcome the possible absence of an airfield in theater through the self-deployment of the tiltrotor and ground craft combination from CONUS. This system approach to the AAN air mechanization concept has not completed its first cycle through the AAN process depicted in Figure 2. However, the results so far are very encouraging. The first complete assessment will occur sometime in the summer of 1998.

In addition to this process, a comple-mentary set of activities involving the Army Science Board (ASB) and the National Research Council●s Board on Army Science and Technology (BAST) are currently under way. The ASB is investigating opportunities to advance strategic deployment capabilities out to the year 2025, while the BAST is constructing an investment roadmap for the Army Basic and Applied Research Programs for the development of technologies that will significantly reduce logistics demand. Finally, OASARDA, in partnership with TRADOC, is planning to initiate a series of technology-based war games that will assist in determining the most productive investment options to support AAN capabilities.

Conclusions

We believe the Army has seized upon a highly compelling vision of its future role in land warfare. It has also carefully thought through a comprehensive process that will determine the key sci-ence and technology investments enabling it to achieve this vision. The process the Army has created to navi-gate into the future is working very well. The future Army and the United States will be the beneficiaries of this cooperative but challenging effort. Authors Note: The authors would like to acknowledge the contributions of Doug Lovelace of the Army War College and Dr. Tom Killion of the Army Research Laboratory in the preparation of this article.

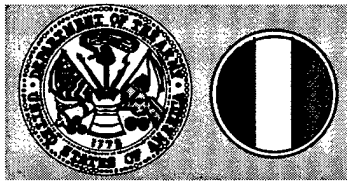

Advanced Fuel Cell Membranes for Non-conventional Fuels

Technology Opportunities

The Army After Next Project

LTC Kenneth L. Jones
Technology Integration Manager
Army Research Office
Presented 28 April 1998

The Path to AAN Begins With the AWE and Passes Through Army XXI

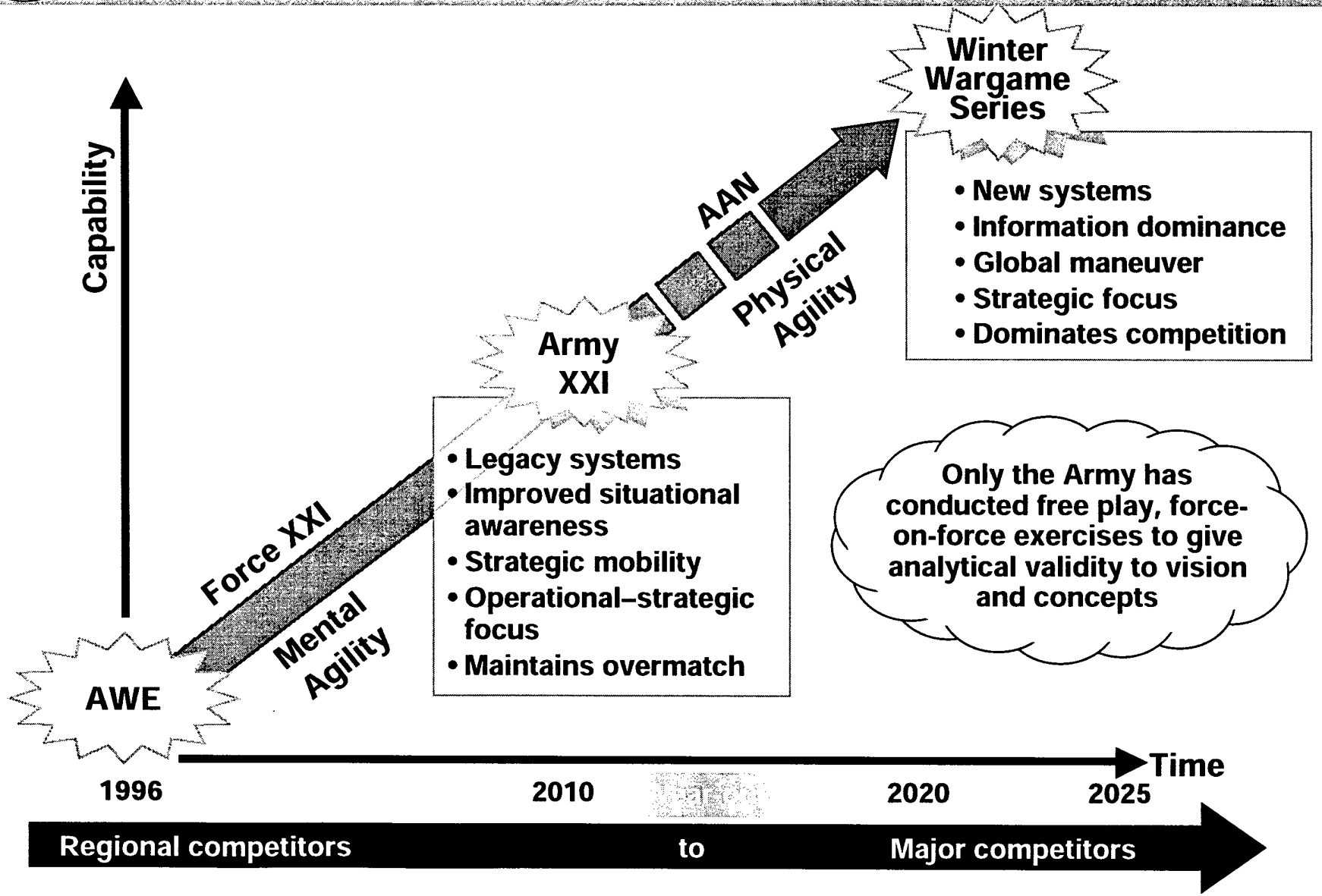

Nesting Technologies with Other Facets of Warfare

- Psychological Hardening
- Cohesion – Units, Staffs
- Emphasis on Maturity & Judgment
- Performance Enhancements
- Train – Rehearse – Execute Cycle Compressed

Human Behavior

Organizational Design

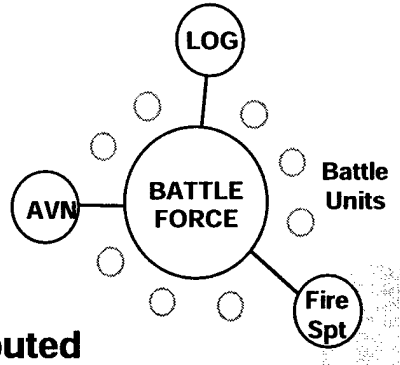

- Distributed
- Dispersed
- Small Teams to Joint Arms TF
- Efficiency – Effectiveness
- "CRAF"-like/Contract/Civilian

Technology

- Info Technologies
- Hybrid Propulsion
- Electromagnetic Gun
- Non-lethal Capabilities
- Electromagnetic Pulse Protection
- Robotic Companions (Ground & Aerial)

Military Art

- Speed – Mobility
- Global – Strategic Maneuver
- Unified Air-Ground Concept
- Cut Logistical Footprint
- Reduce Logistics Requirements

AAN Major Events

Summer Wargame
Sep 1997

Tactical War Games
(Oct - Dec 97)

Technology

Military Art

Human and
Organizational
Behavior

Geopolitics

Spring Wargame (Apr 98)

Resource Game (May 98)

Annual Report
to CSA
(Nov 98)

FY 98 Spring Wargame Schedule

Feb-Mar 1998

- Pol-Strat Preplay (23-24 Mar 98)
- Franchise Games

April

Sun	Monday	Tuesday	Wednesday	Thursday	Friday	Sat
19	20	21	22	23	24	25
Player Registration	•Opening Session •Player Training •Social	Move 1	Move 2	Move 3	Move 4	
26	27	28	29	30	1	2
	Move 5	•Sit Update •Team AAR •Prep for Plenary	•Plenary-AM •Preparation for SLS -- PM	Prep for SLS Senior Seminar	White Team Hot Wash	

May-Jun 1998

- Excursions
- Begin Analysis

Force XXI -- Transformation Process

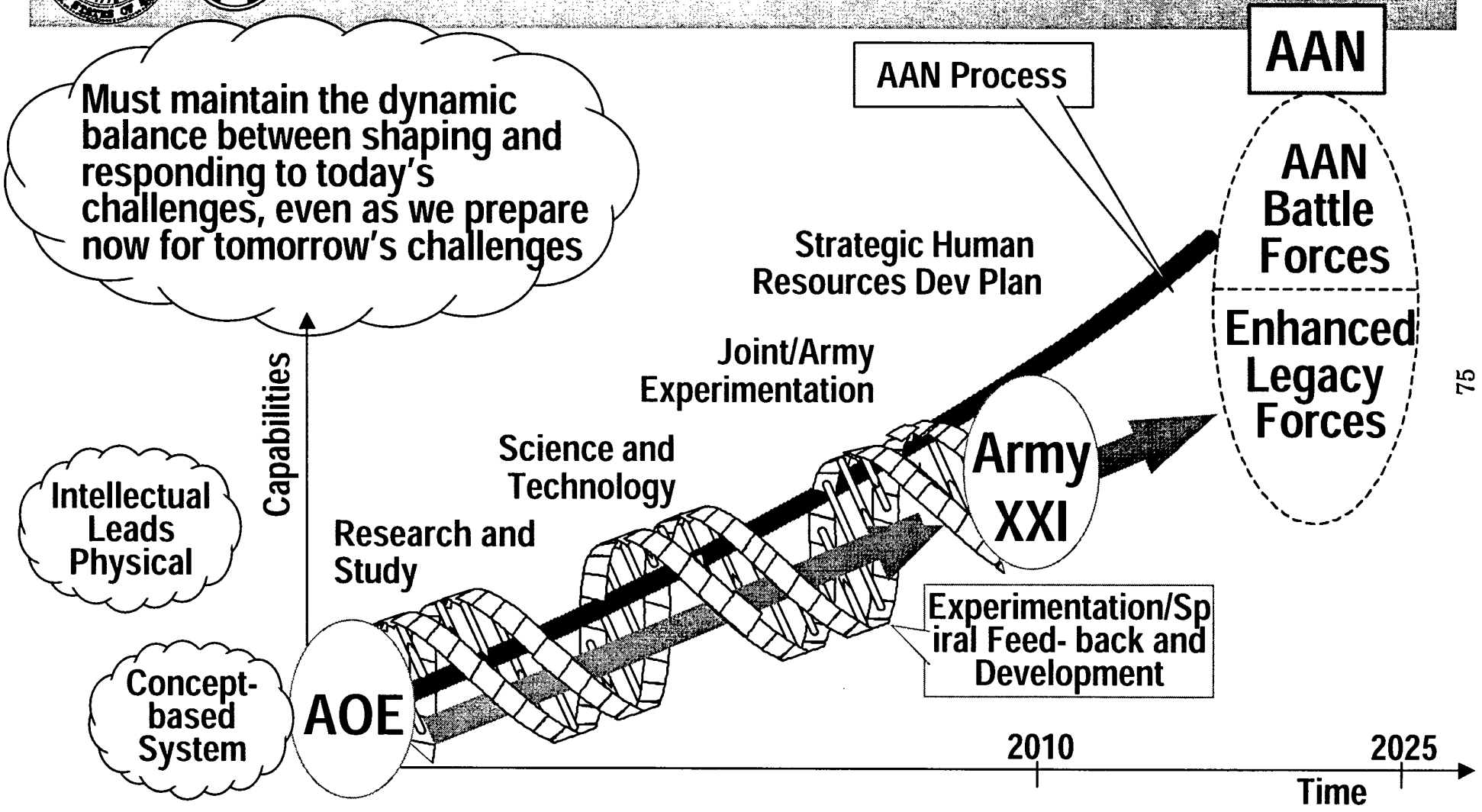

Transformation Enablers: • Revolution in Business Affairs • Strategic Mobility
• Revolution in Military Logistics • 2nd Training Revolution • AC-RC Integration

The AAN Cycle

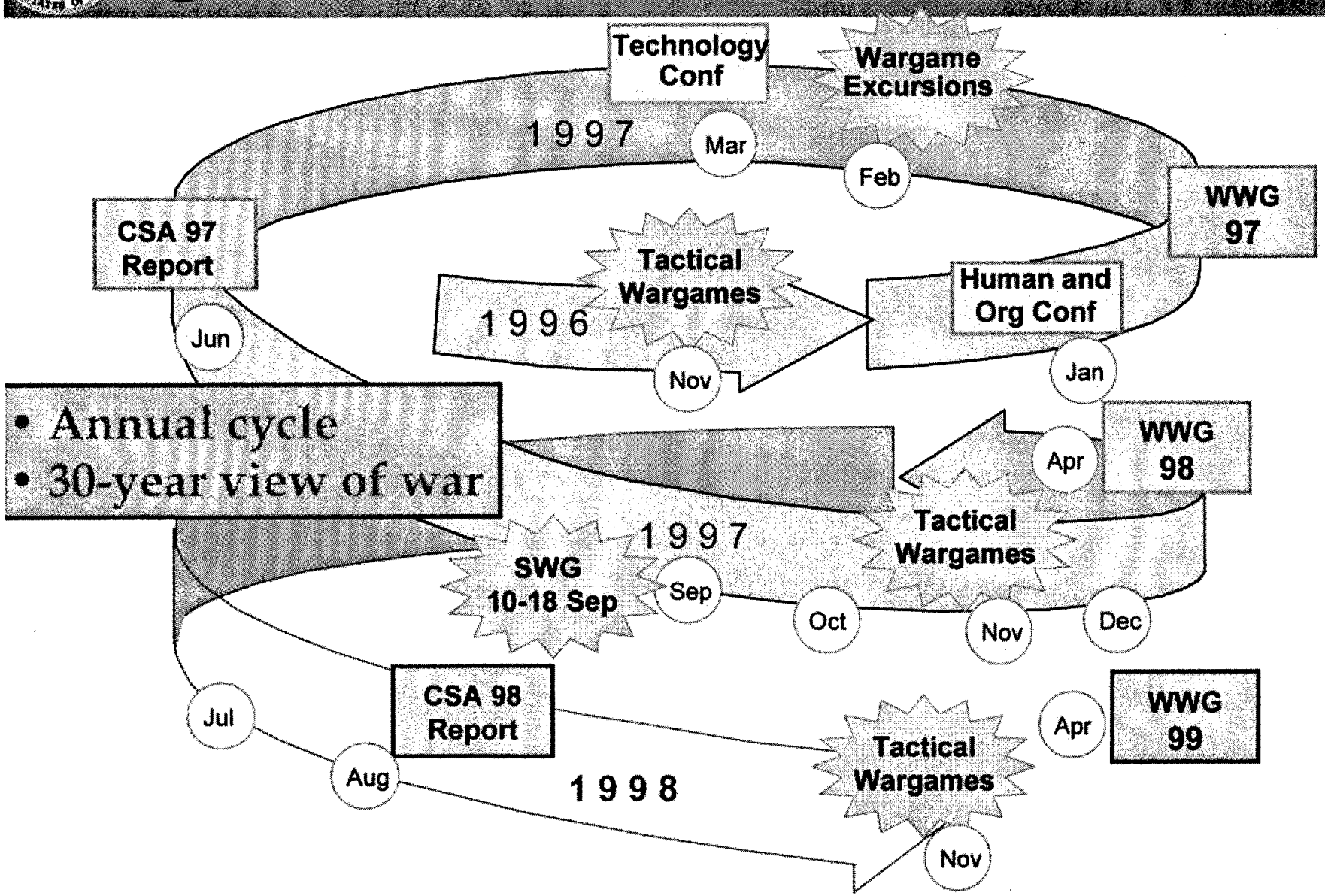

AAN FUTURES RESEARCH FOCUSES INITIALLY ON FOUR AREAS CIRCA 2025:

- Probable geopolitical realities: **Ensure stability across the spectrum**
- Evolving military art: **Balance Precision Engagement and Dominant Maneuver**
- Technology: **Speed to exploit Information Dominance**
- Human and organizational behavior: **Mature, cohesive force operating at the limits of human cognition**

The Process of Change

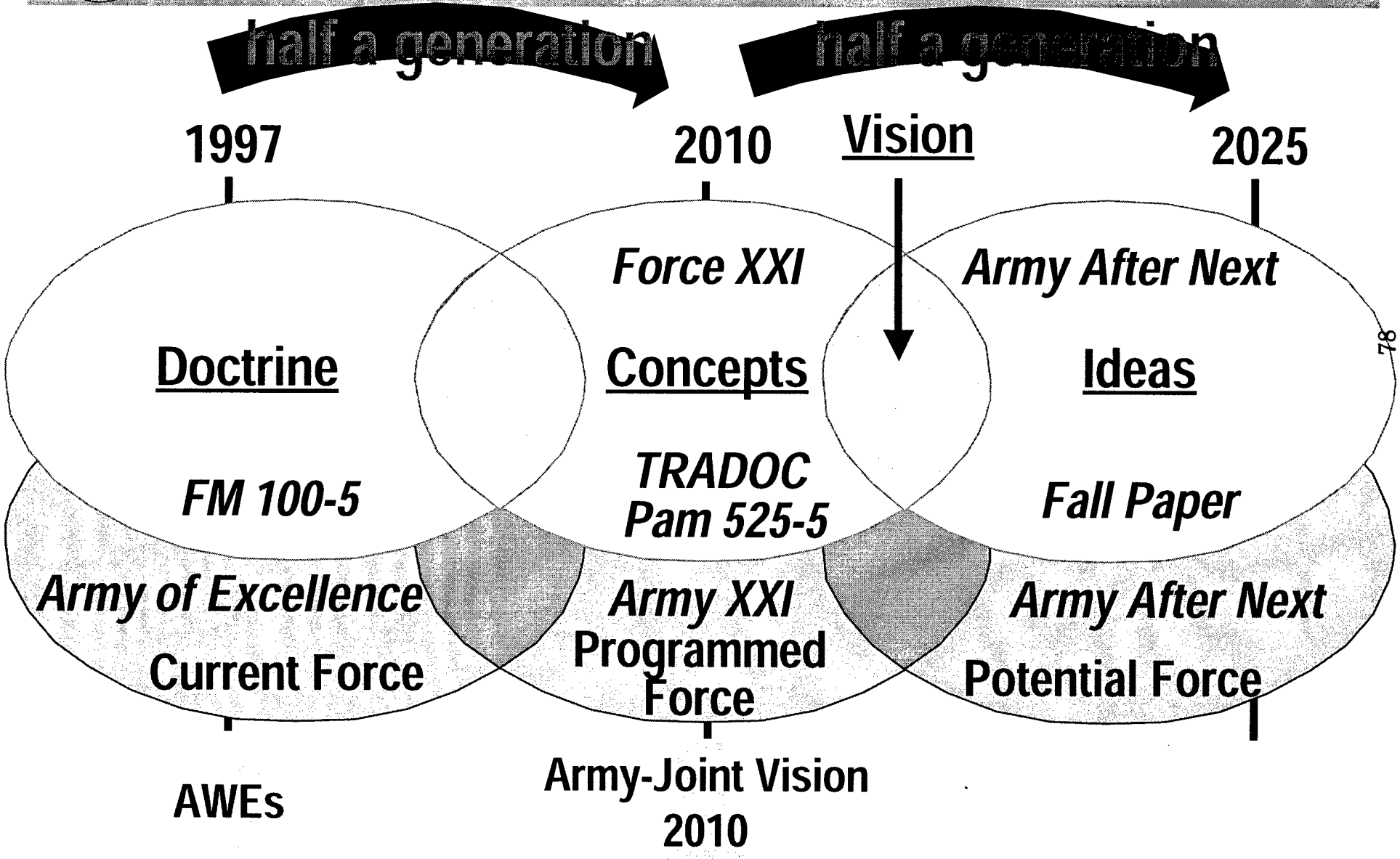

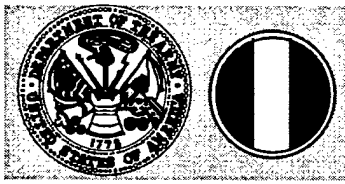

AAN Project Mission Statement

Conduct broad studies of warfare to about the year 2025 to frame issues vital to the development of the U.S. Army after about 2010 and provide those issues to senior Army leadership in a format suitable for integration into TRADOC combat development programs.

CSA Guidance

Define what we want in the Army After Next so that . . .

- Force XXI expands to link Army XXI and Army After Next
- Force XXI does not get disjointed from long term vision
- Also, we must
  - Focus our R&D efforts
    - Narrow the gap between heavy and light forces
    - Improve mobility, enhance firepower
  - Leverage the work already done in OSD's RMA studies
  - Identify organizational concepts that better integrate AC&RC
  - Revolutionize logistical concepts . . . continue developing total asset visibility and velocity management
  - Institutionalize AAN concepts and process
  - Think joint and involve other services in AAN process

AAN INFLUENCE ON S&T INVESTMENT STRATEGY

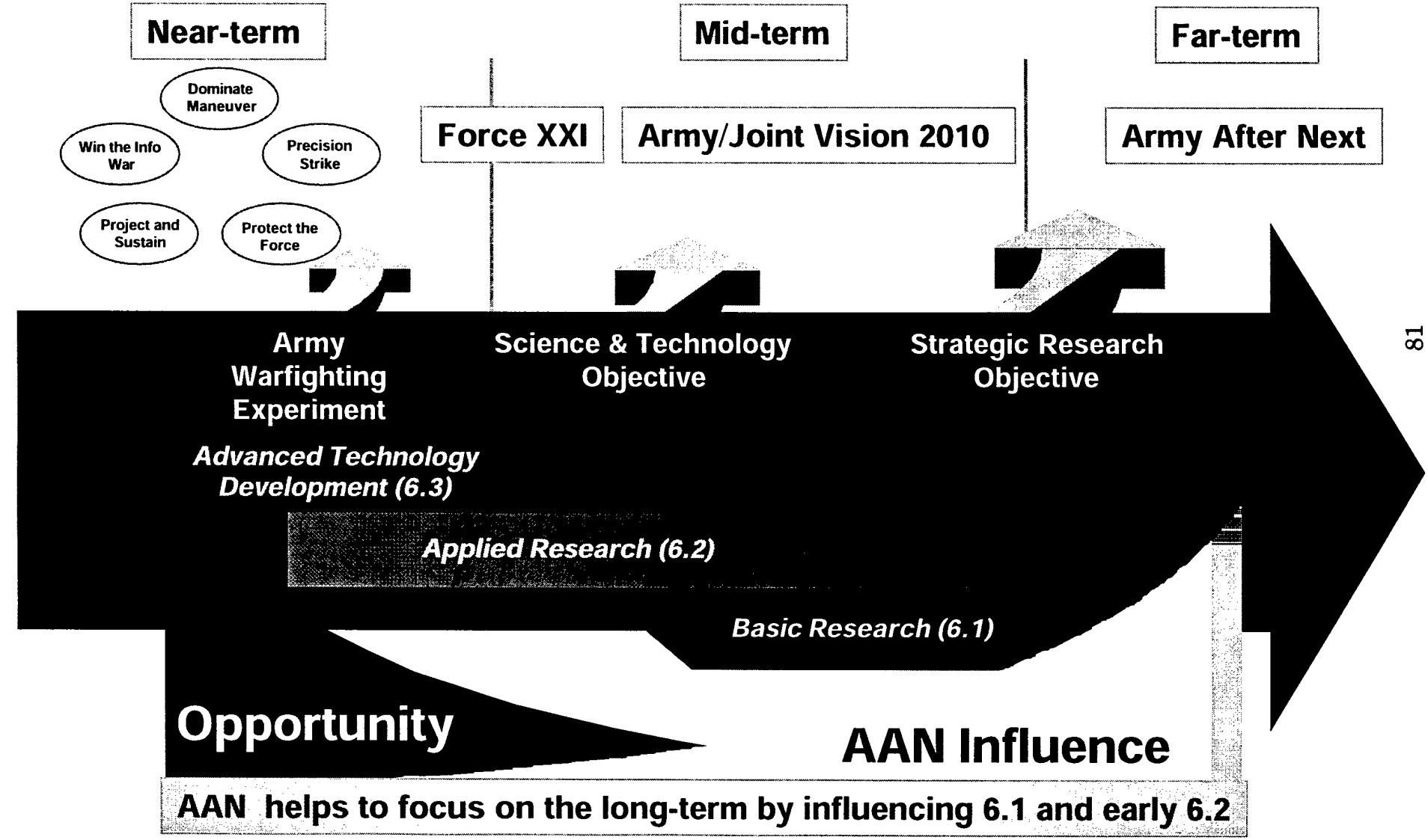

INFLUENCES ON THE ARMY'S FUTURE – GETTING TO AAN AND BEYOND

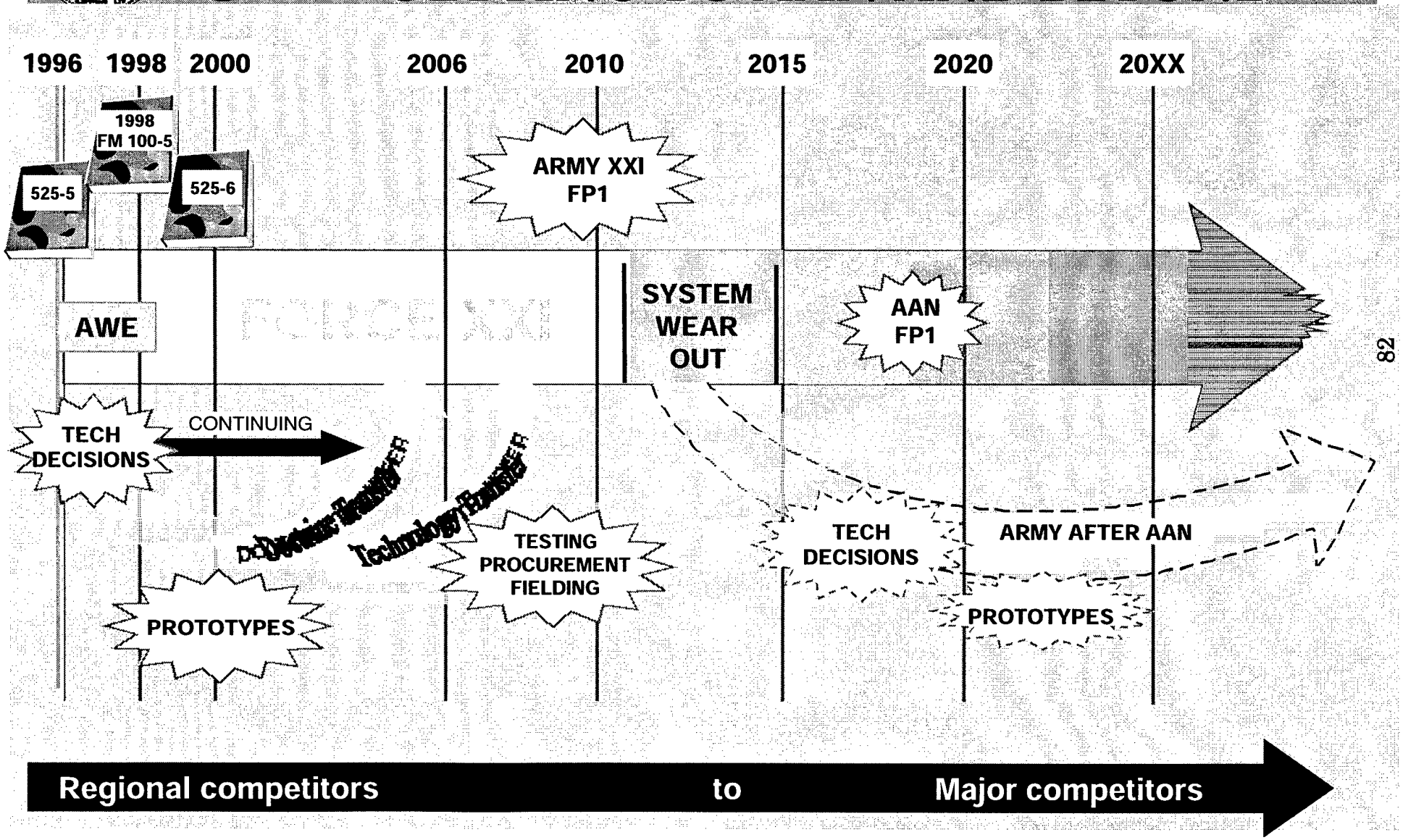

Firepower-Centered Approach: Unnecessary Risk. Firepower Effect Declines Over Time

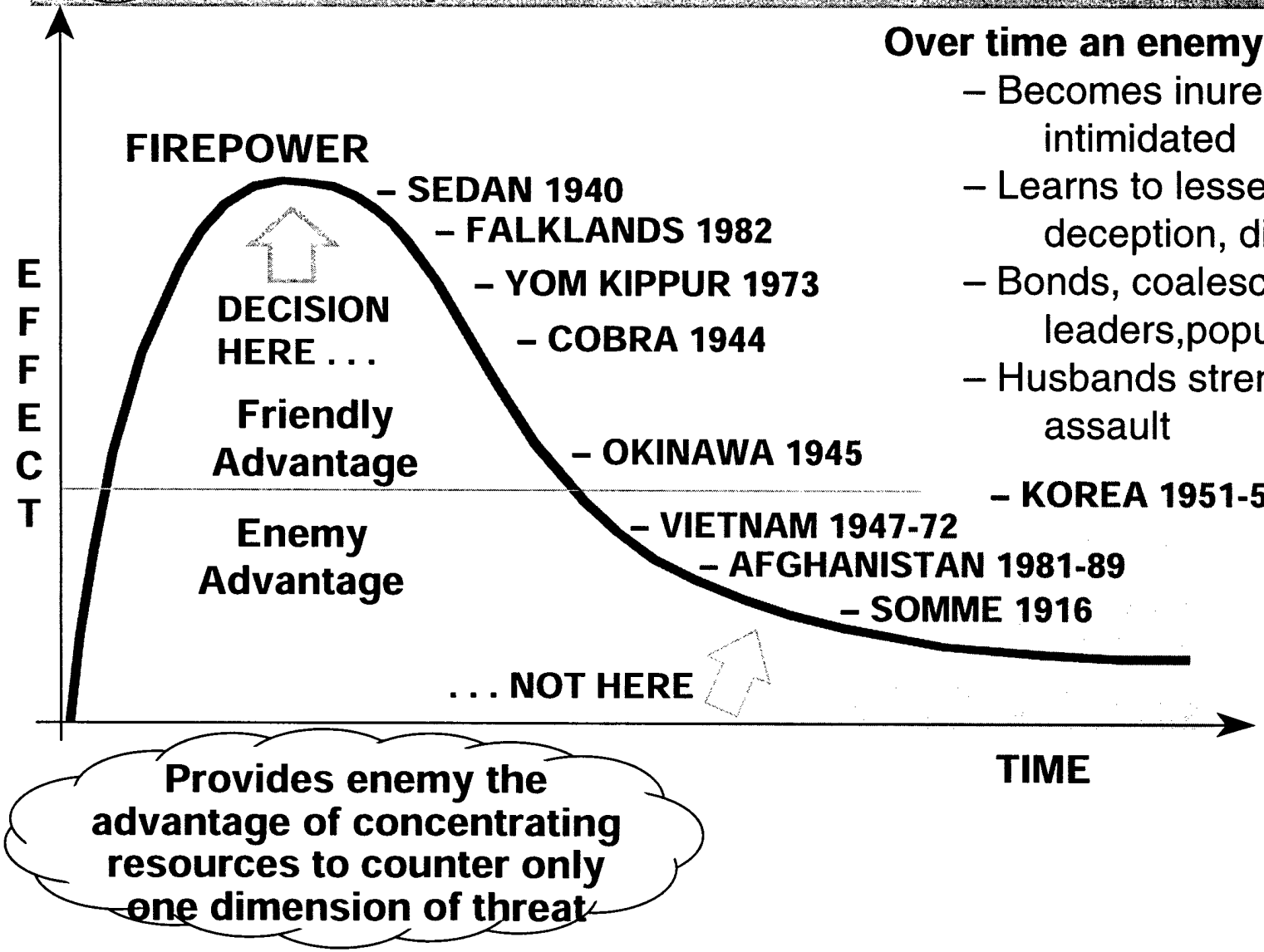

Over time an enemy:

- Becomes inured, less intimidated
- Learns to lessen effects through deception, dispersion
- Bonds, coalesces with leaders,population
- Husbands strength, prepares for assault

Provides enemy the advantage of concentrating resources to counter only one dimension of threat

Rate of Change Determined by Affordability and Acceptability

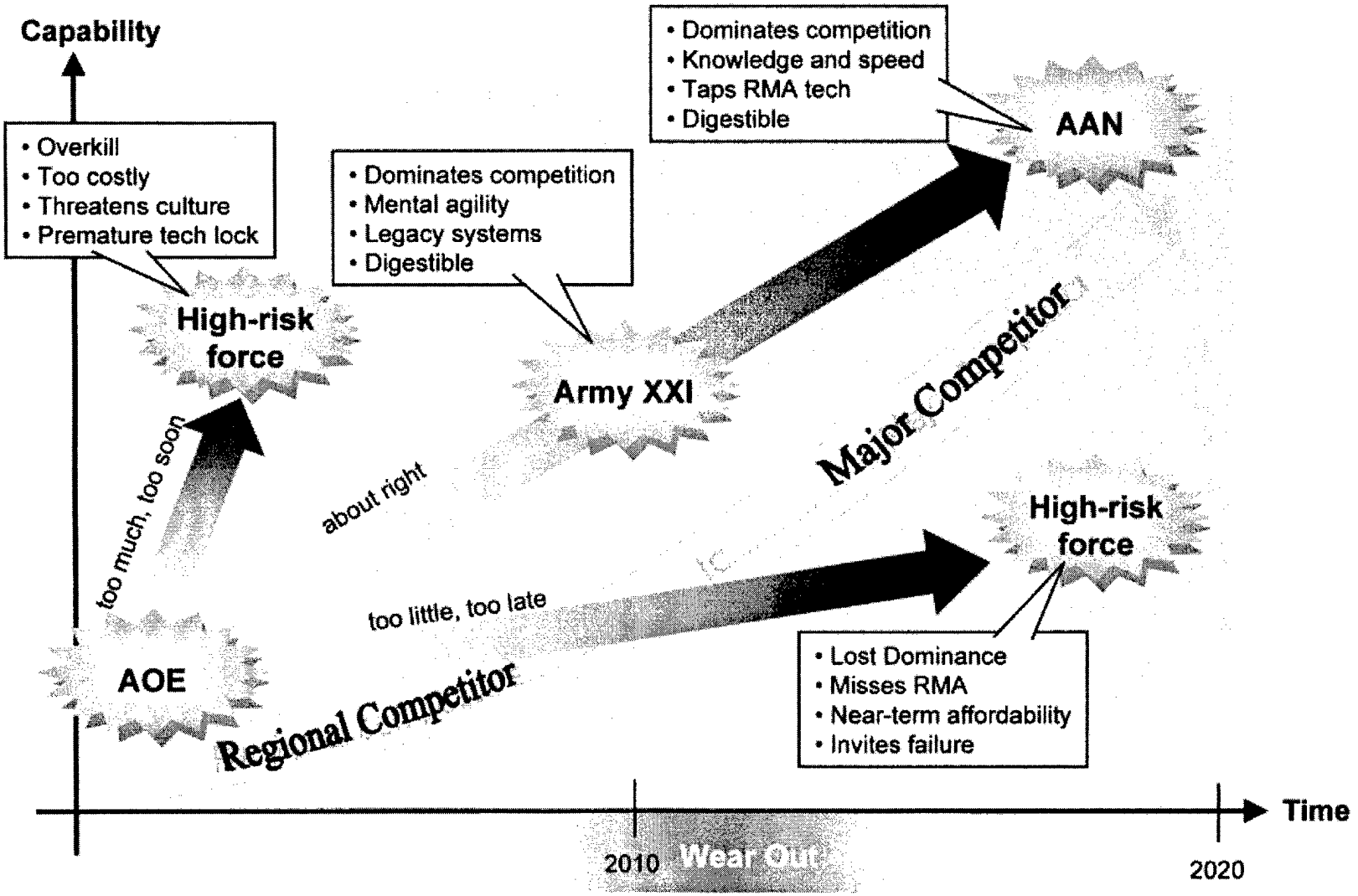

Looking Back from the Future

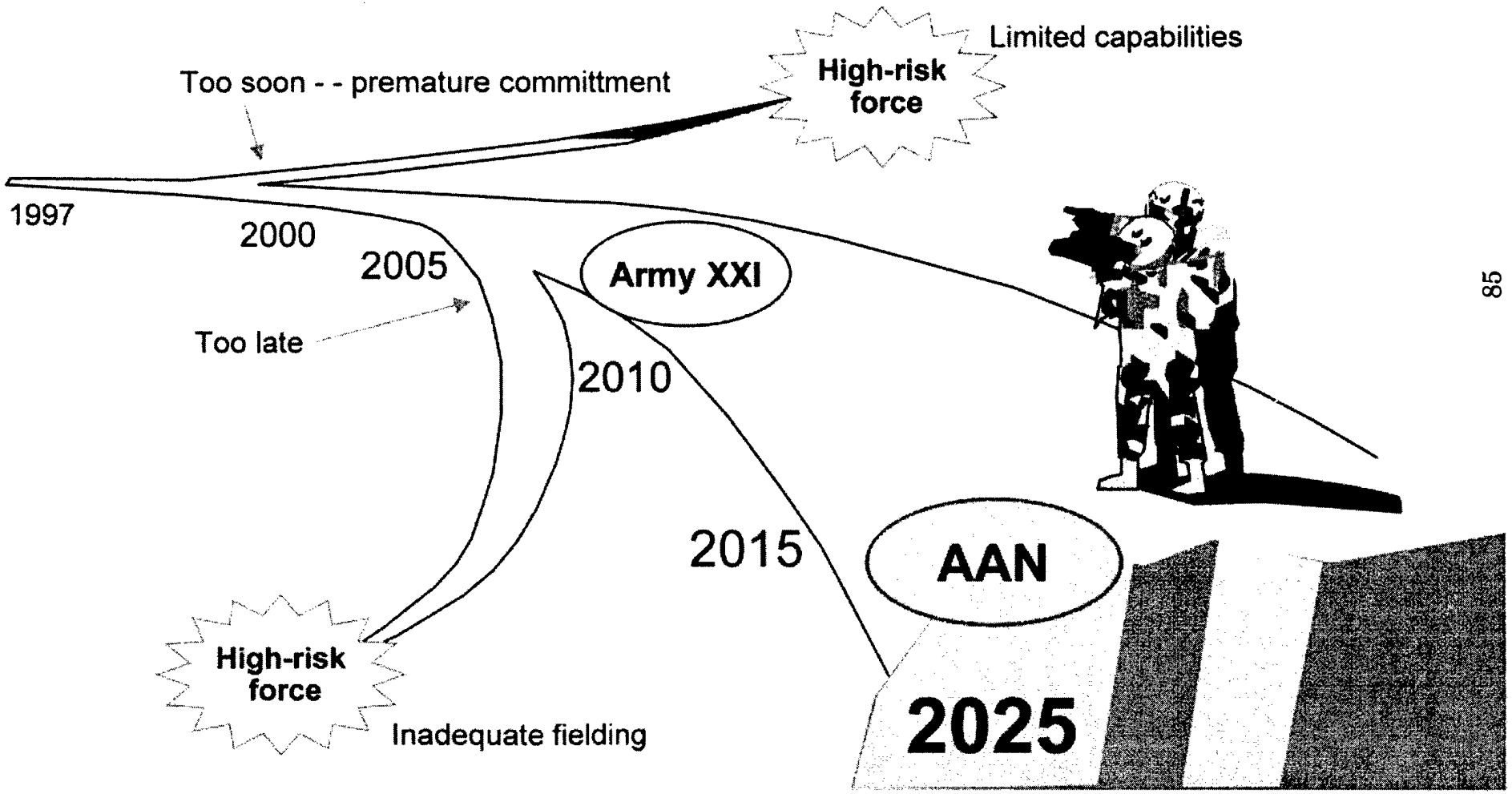

Annual Report on the AAN Project

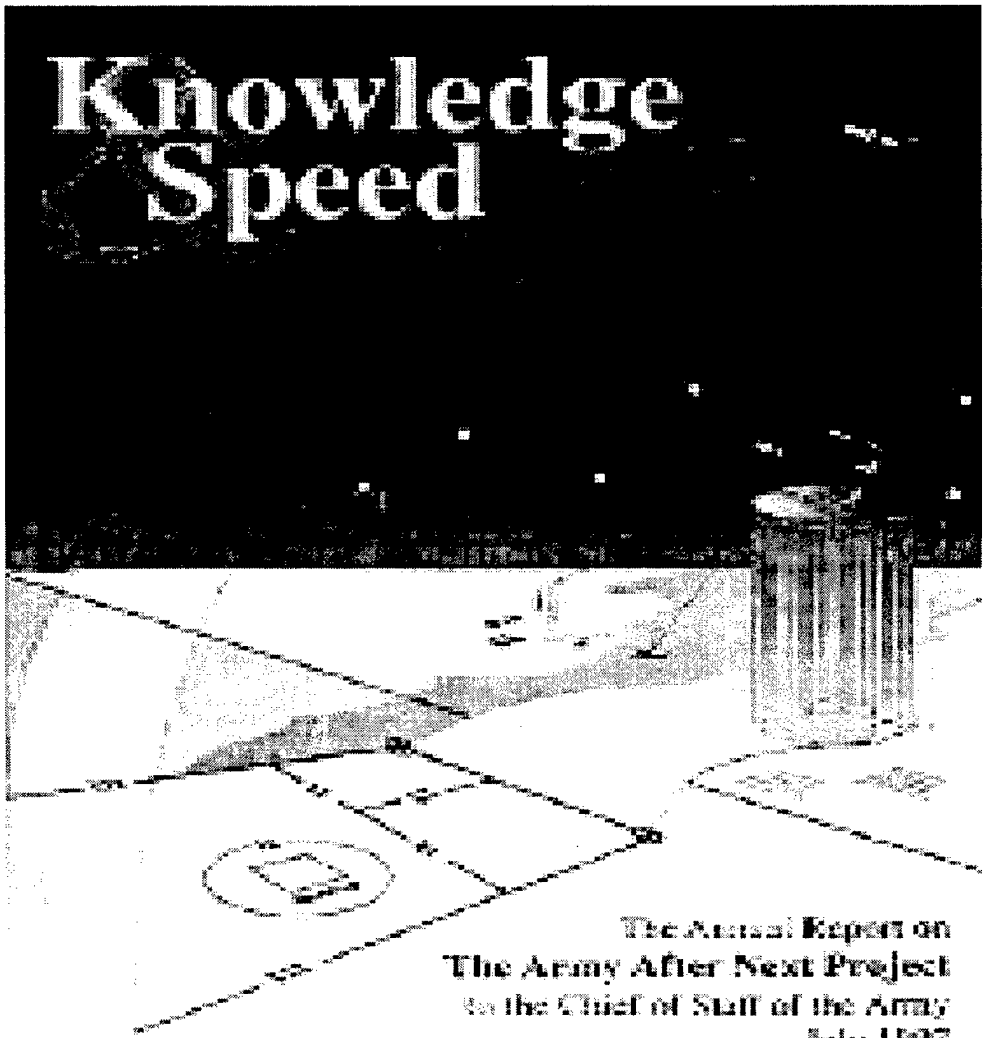

Operational Characteristics of AAN

AAN Goal:

- **An Army that is a *strategic* force option for the NCA**
  - **Strategically deployable**
  - **Highly mobile**
  - **Minimal logistic train**

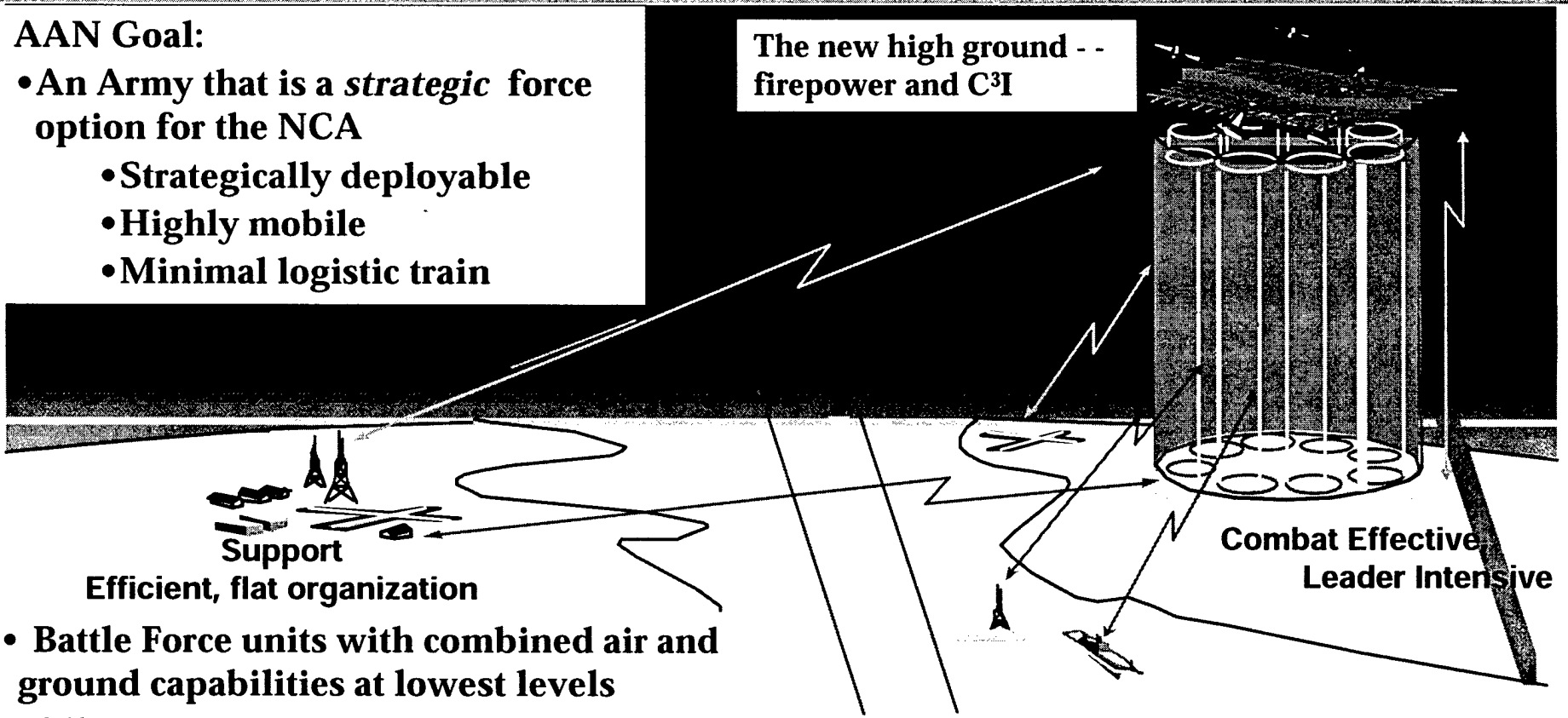

- **Battle Force units with combined air and ground capabilities at lowest levels**
- **All operating systems resident within battle force**
- **"Reach back" for combat functions (Fires, C^2, Logistics)**
- **Independent operations for 2 to 14 days without resupply / refuel**

- **Self-protection through movement, organic weapons, low-observables, and situational awareness**
- **Engage enemy with information, organic, and inorganic weapons**

AAN – FROM LINEAR TO VERTICAL

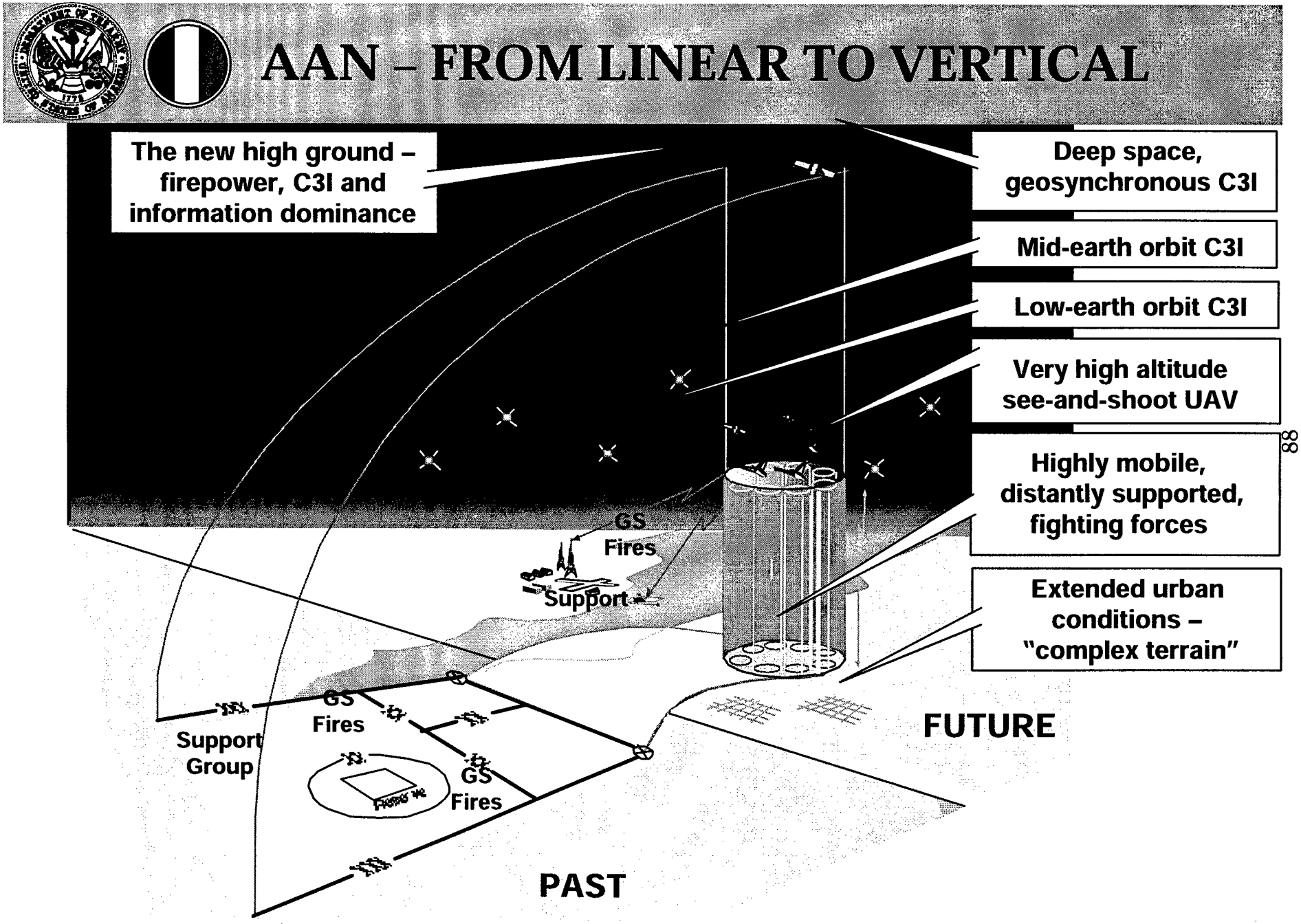

How Landpower Might Be Applied

- Operational offensive, tactical defensive
- Strikes directly at strategic and operational centers of gravity
- Speed, reach and overwhelming tempo = physical and psychological domination
- Merges heavy and light
- Establishes and assures control; long-term sustained staying power
- Hybrid force: mix of mature Force XXI units and AAN units
- Organic integration of air and ground capabilities at lowest level

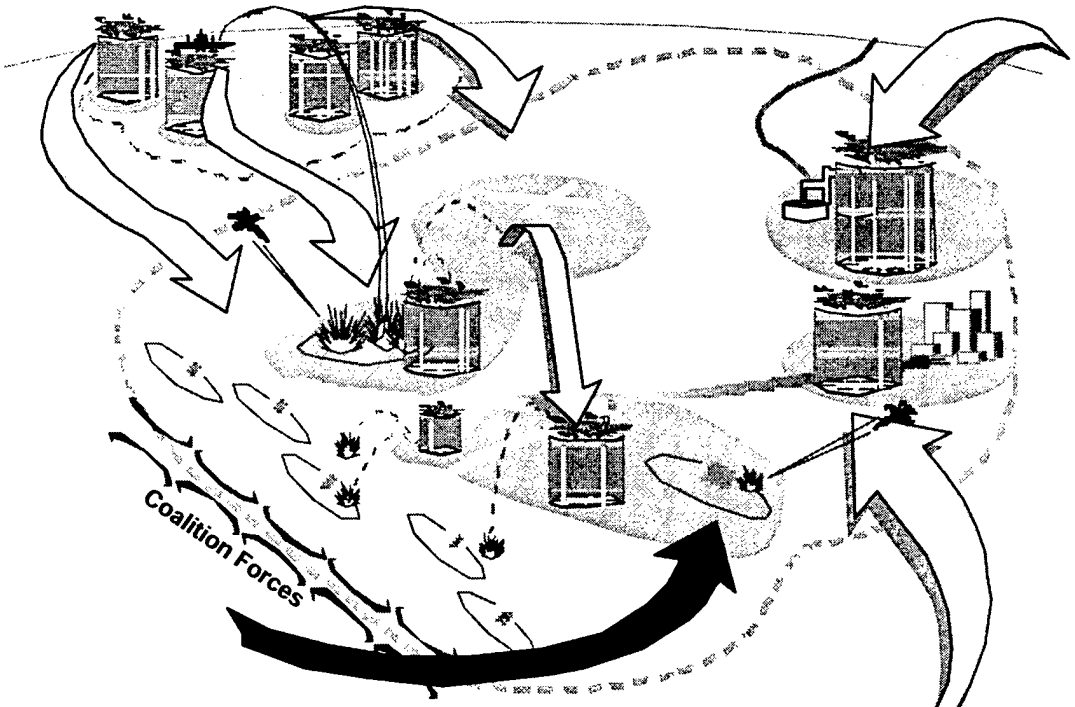

Controls center of gravity.
Forces enemy to come to us and either fight and lose, or abstain and concede.

BACK TO PATTERNS AND CYCLES . . . JUST CAUSE AS A WINDOW INTO THE FUTURE

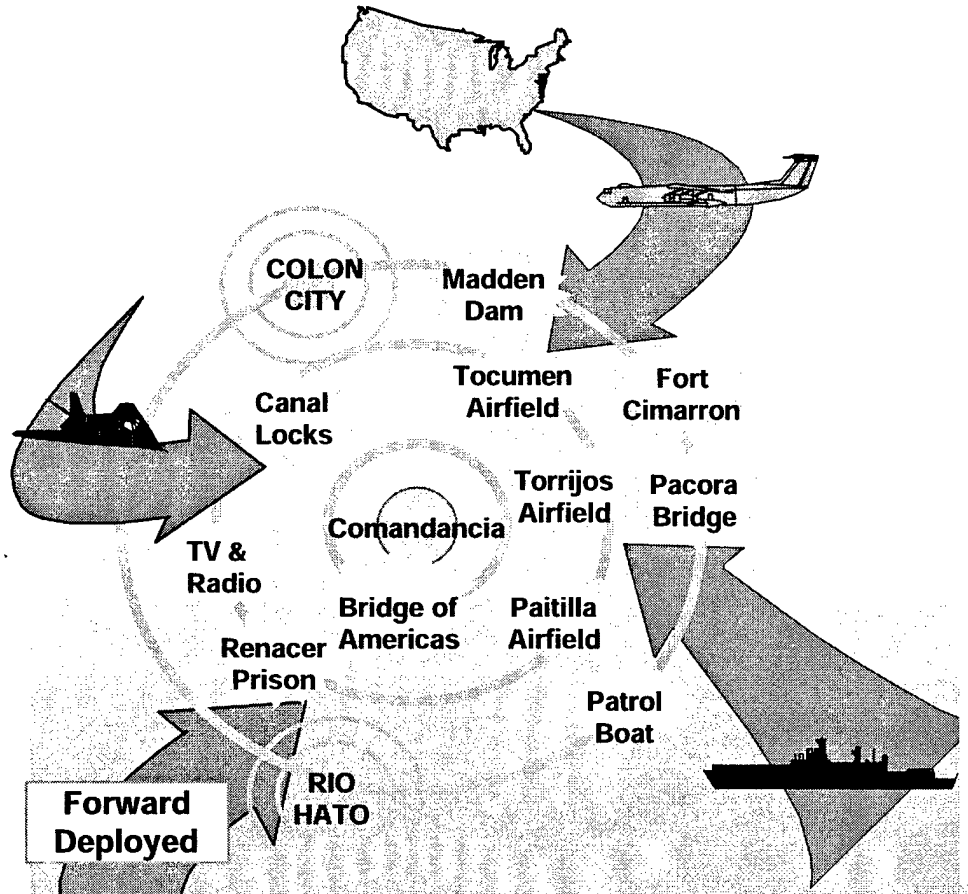

- Center of Gravity: Will of the Opponent
- Speed
- Overmatch
- Limited Killing, Damage
- Information Dominance
- Assured Land Control
- Assured Termination
- Strategic Reach
- Strategic Convergence
- Overseas Presence
- Dispersed Operations
- Urban Warfare
- Melding of Land, Air, Sea, and Space in Joint Operations

In a swift, overwhelming campaign the objective is the enemy's will – not overwhelming destruction

AAN - An Image of Operations In 2025

- A Strategic Maneuver Capability
  - Balanced capabilities for the NCA
    - Fully integrated with air, sea, and space
  - Strategically projects a multi-capable, fully integrated land force
  - Executes rapid global maneuver
  - Enhances deterrence (and coercion)
  - Strikes quickly at operational or strategic center of gravity
  - Composed of a variety of maneuver capabilities
    - Mature Force XXI and AAN units
  - Capable of sustained land operations
  - Speed, reach, lethality, and overwhelming tempo = physical and psychological disintegration

The Goal: A globally self-deploying force capable of striking directly at strategic and operational centers of gravity.

Enablers for the 2025 AAN

- **System Characteristics**
  - Hybrid power sources
  - Alternative propellants
  - Precision weapons
  - Redesigned organizations
  - Robotics
  - Signature control
  - Modular, tailored logistics packages
  - Mini - Micro - Nano scale
  - Planning, simulation, rehearsal capabilities
  - Multi-functional

AAN: Technologies and Systems for a Balanced Approach to Warfare

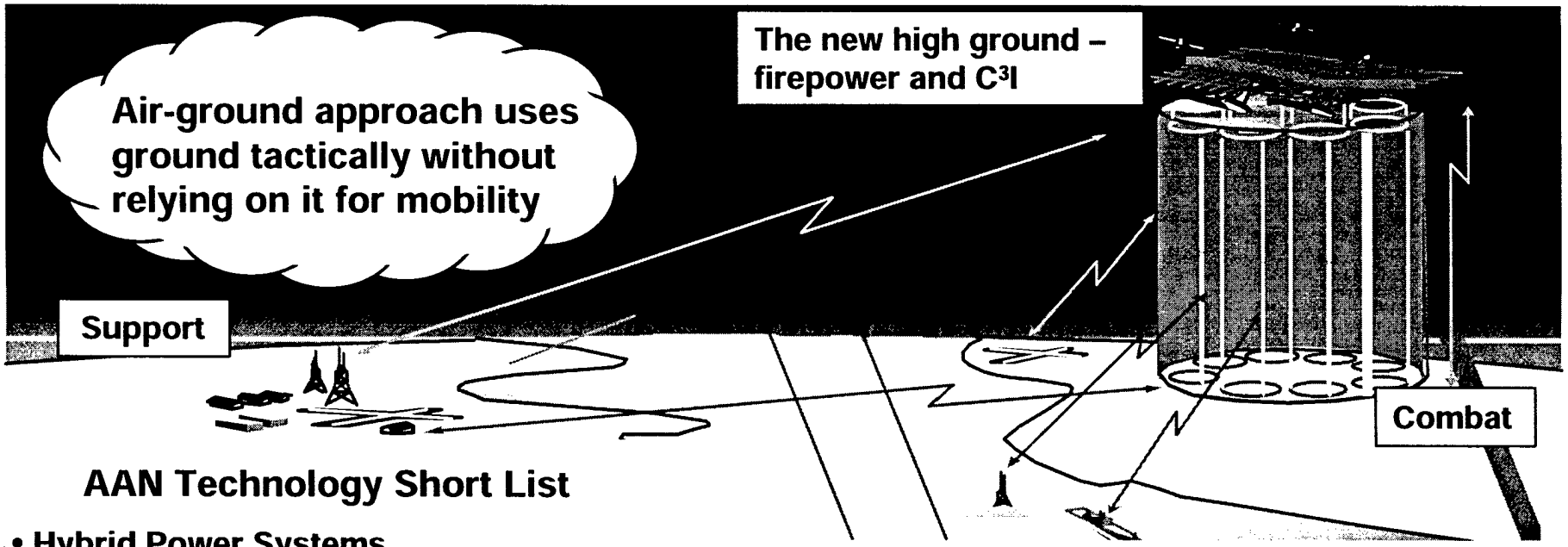

AAN Technology Short List

- Hybrid Power Systems
- Fuel Efficiency (reduce consumption by 75%)
- Human Engineering/Cognitive Engineering
- Signature Control (including counters)
- Protection Schemes for Land Systems (including active protection)
- Advanced Materials
- Alternative Propellants
- Biological and Chemical Protection, Antidotes, and Vaccines
- Logistics Efficiencies

AAN Systems Short List

- Future Ground Craft
- Advanced Airframe
  – Heavy Lift/Tactical Utility Lift
- Autonomous and Semiautonomous Unmanned Systems (air, ground, sensors)
- Advanced Fire Support System
- "Living Internet"
- Active Protection
- Soldier as a System

Connecting AAN to the S&T Process

Integrated Idea Teams (IIT)

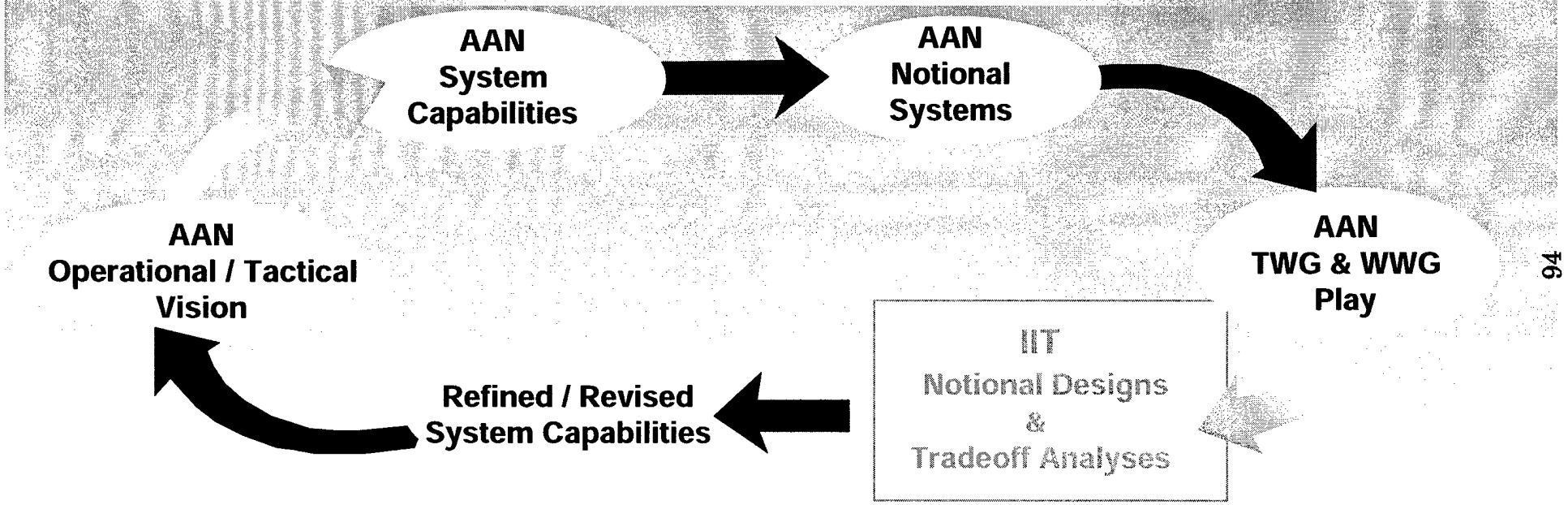

- Process for the national S&T community and the AAN/User community to collaborate.
- Patterned after the Integrated Concept Team (ICT).
- Helps focus Army 6.1 & 6.2 S&T Program.
- RAND to conduct system-of-systems effectiveness analysis
- Issues that mature are passed to the Combat Developer (ICT).

Mobility IIT

Boeing
Bell-Textron
Universities
Army Medical Research and Materiel Command
Army Research Institute
Army Research Lab
Army Research Office
Armaments RDEC
Aviation RDEC
Army Materiel Systems Analysis Agency
Combined Arms Support Command
Communications-Electronics RDEC
Corps of Engineers
DARPA
Edgewood RDEC
General Dynamics
Lockheed-Martin
Missile RDEC
NASA
Natick RDEC
SARDA
Sikorski
TRADOC
Tank Automotive RDEC
Test & Evaluation Command
USMA
UDLP

- **Focus: Tactical & Operational Mobility**
- **Accomplishments (May 97 - Sep 97)**
  - **Concepts for AAN notional mobility systems [Advanced Combat Vehicle and Advanced Airframe] put on sound technical footing**
  - **Alternative system concepts developed**
  - **Revised system concepts fed back to AAN Military Arts cell**
  - **Variations to be evaluated in '98 Tactical Wargame**

AAN Mobility IIT- Baseline Concepts

Walter Christie's M-1932

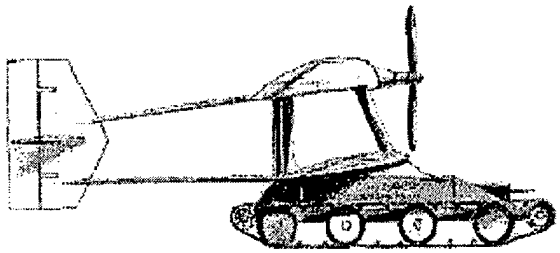

Back to the Future...

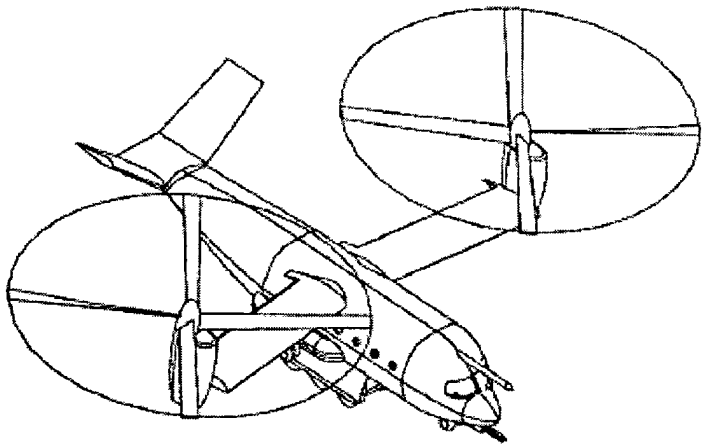

Advanced Air Frame

Designs Developed by IIT

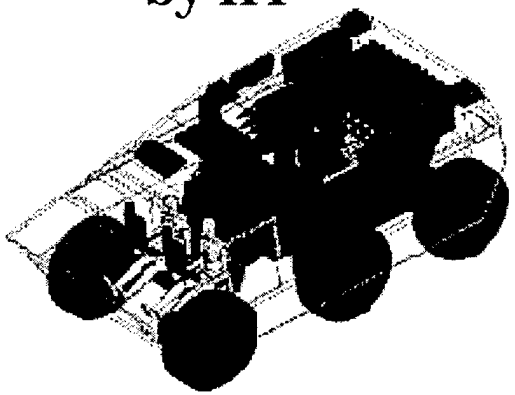

Advanced Fighting Vehicle

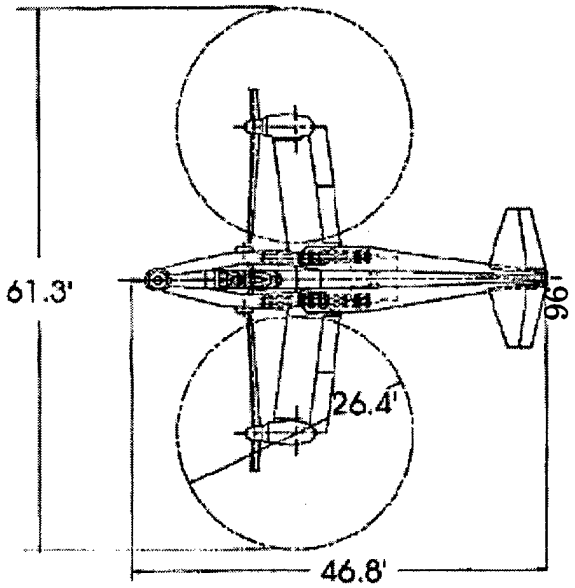

AAN Attack TR

AAN Mobility IIT - Modular Concept

Advanced Modular Fighting Vehicle

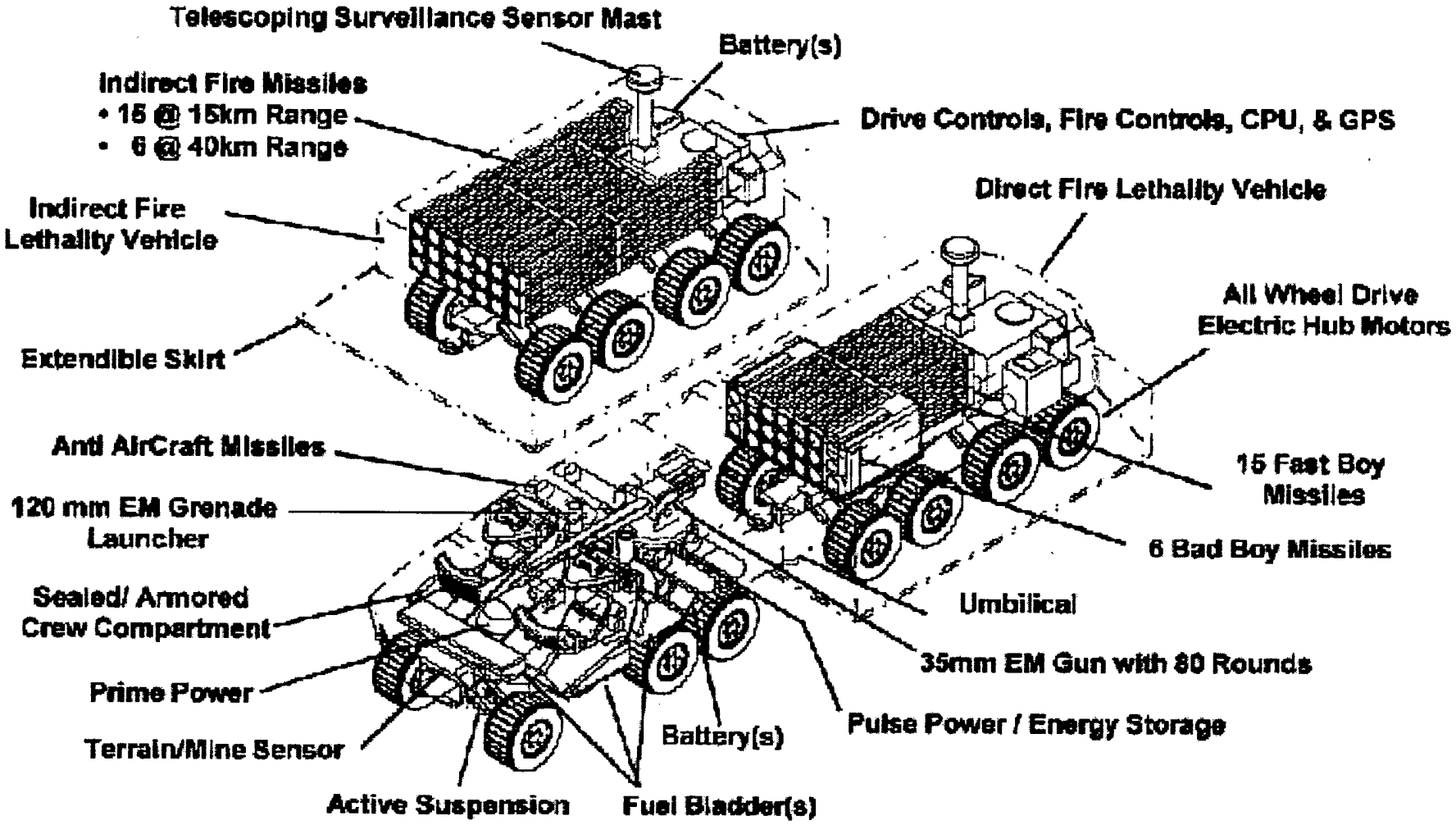

Nesting Technologies for Ground Maneuver - an Example

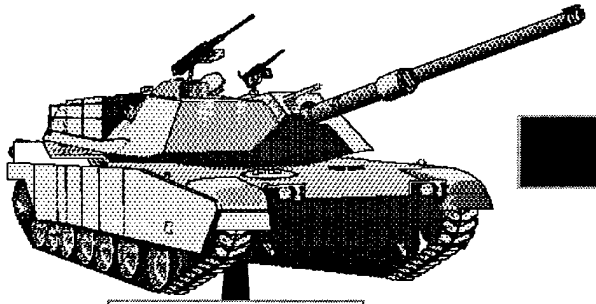

70+ Tons

Armor/ Protection

Armament & Propellants

Fuel Efficiency

C4I

Suspension

Crew

Future Fighting Vehicle
15 Tons
(?)

Trade-offs among technology advantages in all arms

Components:			
Protection –	Reactive Armor	Ceramics	Active Protection
Armament –	Gun	Missile	Electric or Directed Energy
Propulsion –	Gas Turbine	Hybrid	?
Suspension –	Tracks	Wheels	Air-Ground Capable
Crew –	3	2	(Robotic)
C4I –	Appliqué	Living Internet	Space-Based

Future IIT

- Additional IIT will be established in FY98
  - *Fires* ~Distributed Cooperative Engagement
    - Major Players: ARDEC / MRDEC / CERDEC
  - Other Candidates:
    - "Living Internet"
    - UAV Architecture for AAN
    - Less-than-lethal Weapons

Convergence of Technological Possibilities

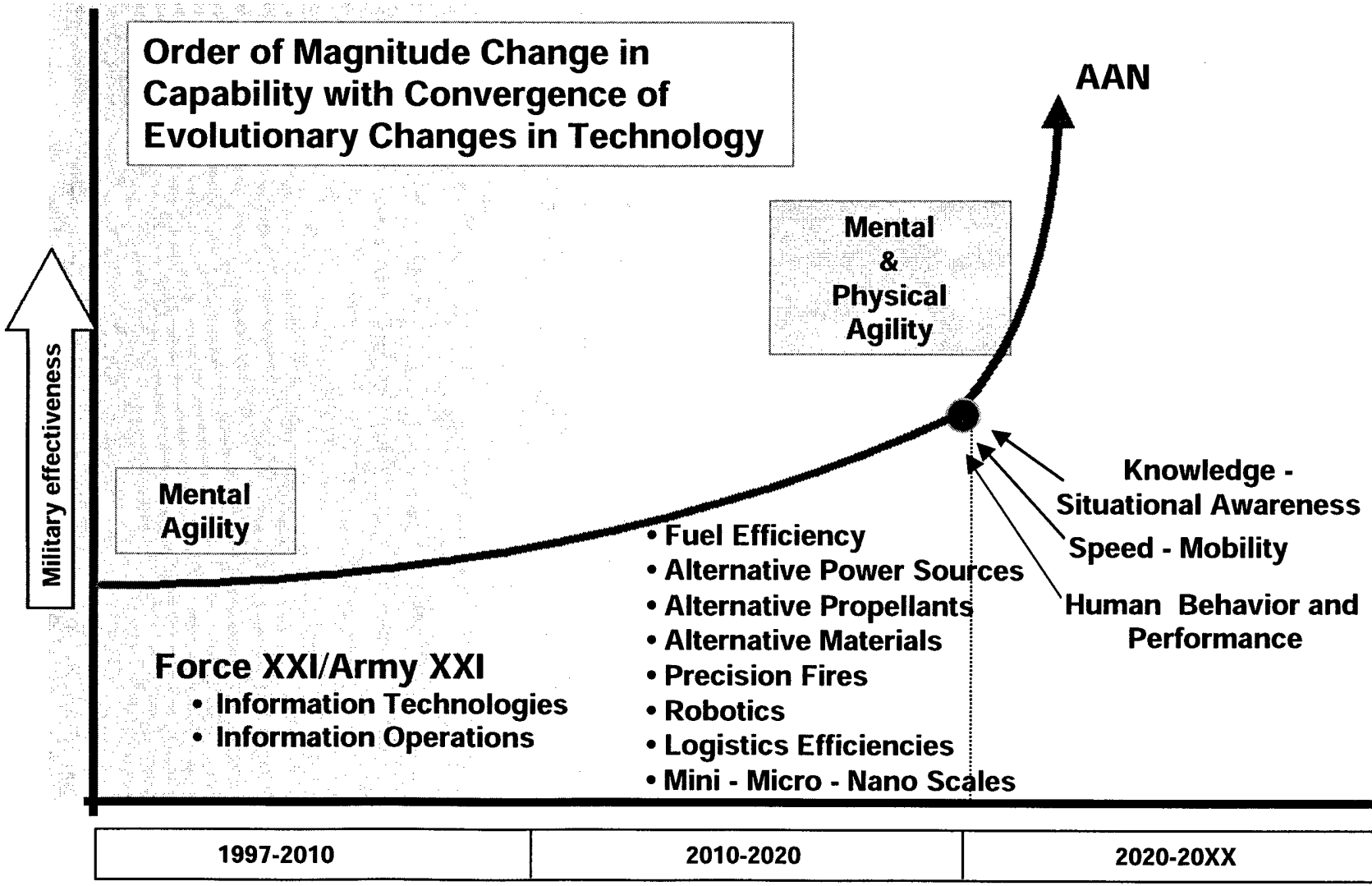

ARTAC-Net

The Army Technology and Concepts Network

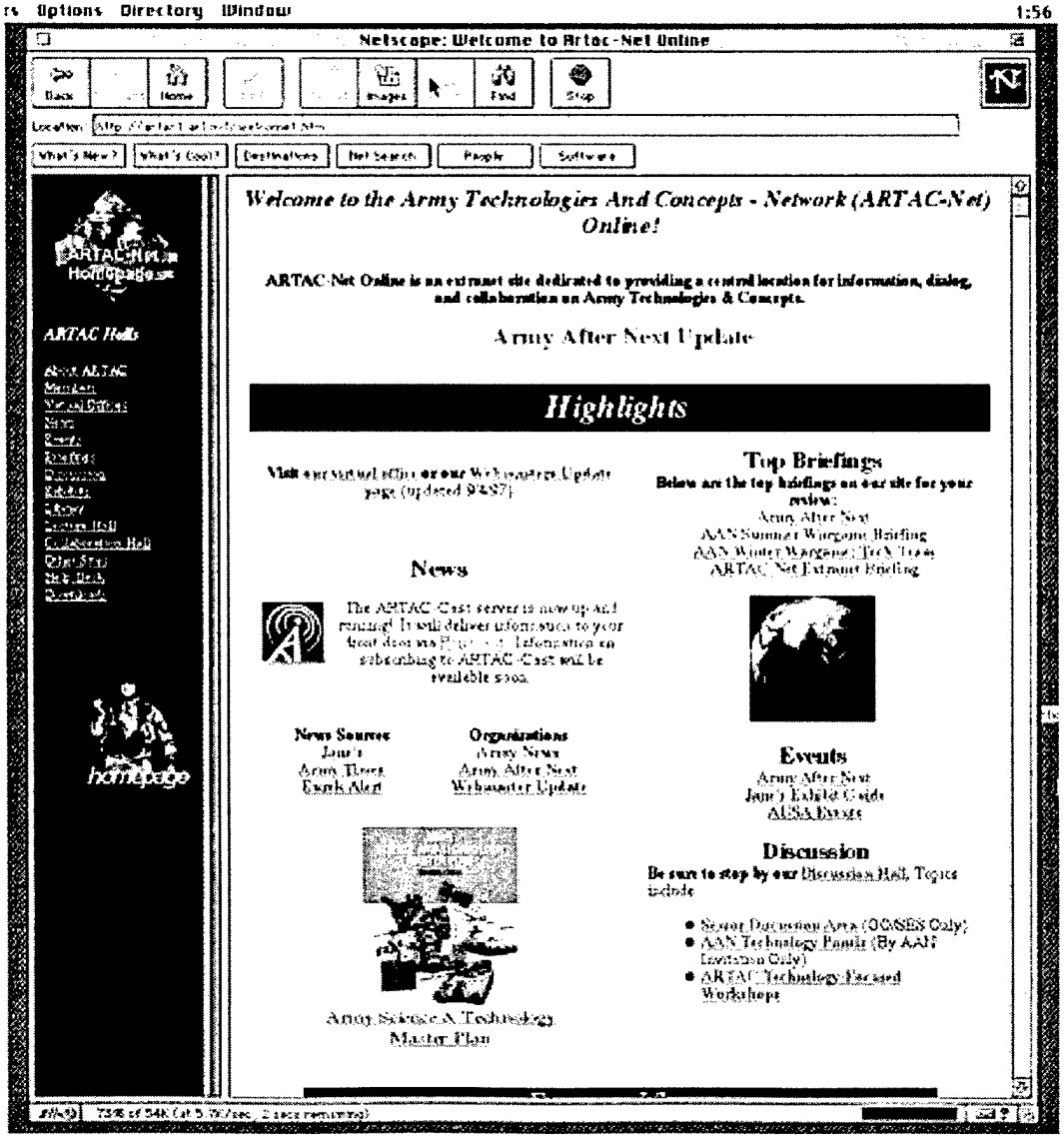

Goal:

- Information resource
- Collaboration tool
- Open & Password-protected sections

Benefits:

- Central location for information on Army Technologies and Concepts
- Enhance efficiency via on-line collaboration
- Reduce administrative costs
- Open channels for innovation
- Break down stovepipes
- Facilitate accesses to information and expertise

For more information and an online application to become an ARTAC-Net Member, go to http://artac1.arl.mil

Prospector X

"Soldier Portable Hybrid Electrical Power Systems"

Henry W. Brandhorst, Jr.
Space Power Institute - Auburn University

The purpose of this workshop, held March 31-April 3, 1998 in Park City, Utah, was to explore fully the technologies associated with hybrid energy sources and the systems implications of those technologies within systems concepts adapted to a military need. Specific objectives included a state-of-the-art assessment of relevant technologies, key issue identification, identification of barrier issues to introduction into the inventory, what power/energy regimes are suitable for hybrid systems and establishing parameters for consistent evaluations of hybrid systems.

Three working groups were established to analyze three different scenarios where hybrid power systems might be applicable: Soldier System/Dismounted Soldier, Sensors and Pulsed Communications and Tactical Operations Center. These working groups were to identify relevant technologies and the next steps that would support that specific application. However, in order to be successful, the groups had to use relevant power profiles of the intended mission. These were either obtained from the presentations or were created by the group.

The Soldier System/Dismounted Soldier group established baseline missions ranging from 12 hours to 10 days requiring 200 to 1500 Whr respectively (Land Warrior to Army After Next scenarios). Primary and intermediate storage options were developed and compared to the present Lithium battery (BA 5590) standard on a mass and volume basis. These included fuel cells, Alkalai Metal Thermoelectric Converters (AMTEC), microturbines and metal-air batteries (Zn and Al). The working group concluded that the Zn-air battery was superior to all other near term candidates for 12 and 72 hr missions and all technology options except Al-air and 3% efficient microturbines were superior for 7 and 10 day missions at least on a mass basis. Importantly, the group concluded that low risk, hybrid fueled systems competitive with batteries can be built in the near term.

The Sensors and Pulsed Communications group proposed three system concepts as well as a "Hybrid System Design Procedure". The three concepts were for various remote sensor and other communication applications covering a range of power and energy requirements from microwatts to watts. They identified suitable hybrid system options that would meet the three specific applications and also noted that the best performance and lowest cost come when power considerations are made early in the design cycle.

The Tactical Operations Center group developed and used a hybrid system design process that was essentially identical to that proposed by the second group. This procedure included requirements, power/energy profiles, candidate technologies and a ranking against the current power system (3 kW generator sets). Because no

power/energy profiles were readily available, the group developed one. Conclusions were that all competing systems (ThermoPhotoVoltaics, AMTEC, SOFC, PEMFC and Stirling engines) and appropriate hybrid peaking sources were superior in mass and volume to the existing gensets.

All groups reached similar conclusions: hybrid technologies appear to promise mass and volume reductions, but some are immature. Many strong competitors will emerge in the next four years. There is a need for a good design methodology, a good database, and real power/energy profiles in order to discriminate between competing technologies. Finally, system level tests are highly desirable.

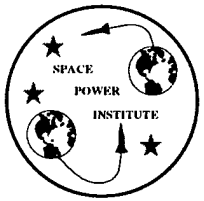

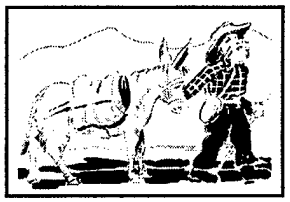

Prospector X:
"Soldier Portable Hybrid Electrical Power Systems"

Inn at Prospector Square

Park City, UT

March 31 - April 3, 1998

Henry W. Brandhorst, Jr.

Purpose and Approach

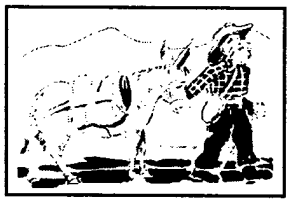

- **Background:**
  - With reduced energy demand and more energetic sources, it might be possible to simplify or eliminate some logistics items while providing the soldier with vastly improved autonomy and time in the field
- **Purpose:**
  - To explore fully the technologies associated with hybrid energy sources and the systems implications of those technologies within systems concepts adapted to a military need.
- **Approach:**
  - Plenary and overview sessions
  - Presentations on specific relevant technologies
  - Working group discussions
  - Plenary summary

Specific Objectives

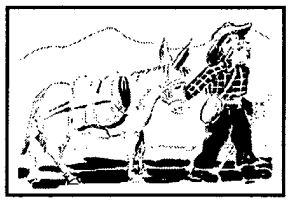

- Assess the state of the art in relevant technologies
- Characterize innovative emerging technologies
- Identify the key research issues pacing hybrid power system development
- Identify key barrier issues to introduction into the inventory
- Distinguish limitations imposed by technology from those imposed by nature
- Identify the power/energy regimes for which hybrids are applicable
- Identify the limits to hybrid systems for mission-specific energy/power profiles
- Establish the parameters for consistent evaluation of hybrid systems
- Identify power conditioning technologies within cost, weight and volume constraints

Working Groups

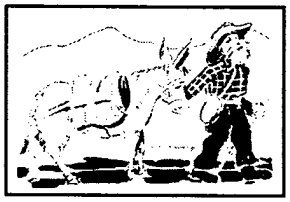

- Initially planned working groups were aimed at technology issues relevant to soldier portable hybrid electrical power systems. At the meeting, the following topics were chosen:
  - » Working Group I: Soldier System/Dismounted Soldier
  - » Working Group II: Sensors and Pulsed Communications
  - » Working Group III: Tactical Operations Center
- These working groups were to identify relevant technologies and next steps that would support that specific application
  - » Power profiles relevant to the application were either presented or created
  - » Technologies were based upon previous presentations

Working Group I: Soldier Systems/Dismounted Soldier

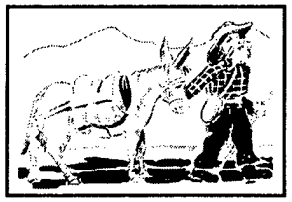

- Four baseline missions were considered for comparison with battery power:
  - 12 hr - 200 Whr (Land Warrior)
  - 72 hr - 500 Whr (Land Warrior)
  - 7 day - 1000 Whr (AAN)
  - 10 day - 1500 Whr (AAN)
- Primary and intermediate storage options were developed and compared to the present battery-only option (Li-based) on a mass and volume basis
  - Fuel cells (PEM and MEOH), Li batteries, AMTEC, Microturbines, and metal-air batteries
  - Zn-Air battery best option at 12 and 72 hrs, all options except Al-air and 3% eff. μturbines were better for 7 and 10 day missions (better in both mass and volume)
  - Research and other key issues were identified
- Bottom Line
  - Low risk hybrid fueled systems competitive with batteries can be built near-term
  - Special consideration must be taken for both the battery and PMAD in hybrid systems

Working Group II: Sensors and Pulsed Communications

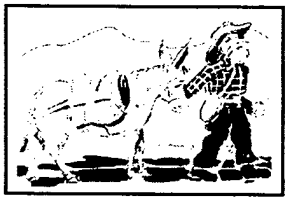

- Proposed three system concepts as well as a "Hybrid System Design Procedure"
- Conclusions
  - Use of a "smart, adaptive controller" is easiest way to optimize generic systems
  - Best performance and lowest cost come when power considerations are made early in the design cycle

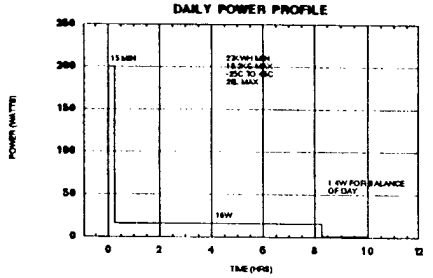

- Power Profile
  - 200 W for 0.25 hr/day
  - 16 W for 8 hr/day
  - 1.4 W for 15.75 hr/day
  - buried, 40 lb max, 6 mo life, -25° to 45° C
- Hybrid Solution: 32 W fuel cell + Li-ion battery
  - Weight constraint precludes desired lifetime

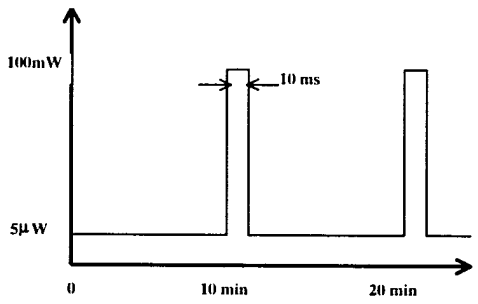

- Power Profile
  - Steady state: 5 μW
  - Transmit: 100 mW for 10 msec every 10 min
- Hybrid System: capacitor + thin film battery + scavenger

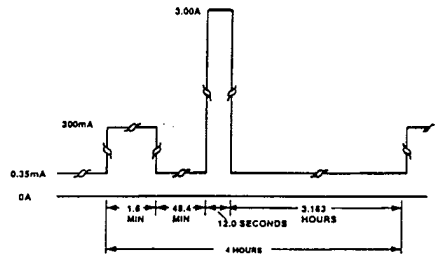

- Power Profile
  - 6x/day, 12 V, -30 ° to 70° C, packaging ≤ 0.5 in, 3-4 months
  - presently use Li/CFx battery
    - 600-800 Wh/kg
    - 1000-1200 Wh/l
- Hybrid solution: carbon capacitor + battery

Working Group III: Tactical Operations Center

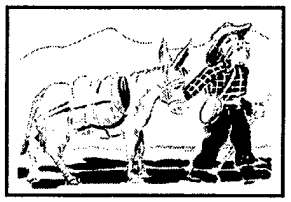

- Developed and used a design process (virtually same as that proposed by WG II)
  - » Requirements, power/energy profiles, system block diagram and candidate technologies
  - » Ranked candidates against requirements and existing gensets
- Final estimates (w/o fuel)
  - » Converters: TPV, AMTEC, SOFC, PEMFC (all ~7-12 kg goal) and Stirling
  - » Battery: Pb/TFM or Li:xxx (less than 5 kg)
  - » Capacitor and electronics: (less than 2 kg)
  - » Total mass: 14-19 kg vs gensets at ~50 kg
  - » With ruggedization, add ~5 kg to the mass
  - » Use photovoltaic augmentations as feasible
- System demonstrations are desirable

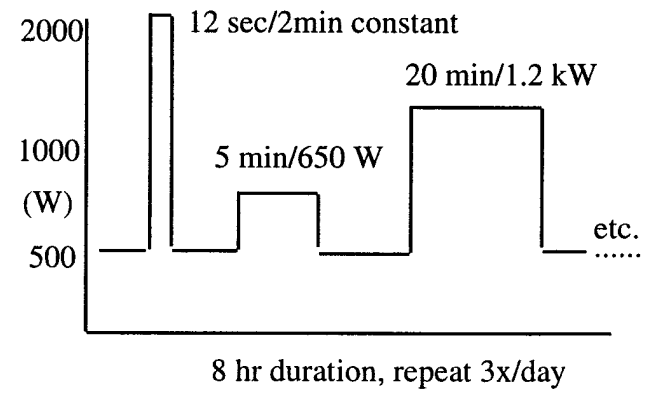

8 hr duration, repeat 3x/day

Loads/Technologies:

Comm.	Video	Fax (Sincgars)
12 sec/2 min	5 min	20 min
2kW peak	650 W peak	1/2 kW peak
7 Whr	55 Whr	400 Whr
720x/day	3x/day	3x/day

Power baseline: 500 W cont., 12 kWh/day

General Conclusions/Summary

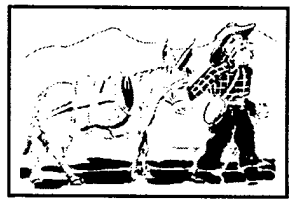

- All working groups came to similar conclusions:
  - Hybrid technologies appear beneficial, but some are immature:
    - System level mass and cost reductions appear likely
    - Many competing technologies appear feasible in the next 4 years
  - A design methodology is necessary for good system trades
    - As well as more performance information of emerging technologies
  - There is a need for a design database for competing systems:
    - Includes life, cost, durability and system constraints information
  - Real power/energy profiles in present applications are needed to discriminate between competing technologies
  - System level tests of some desirable systems are needed
- Overall, it was a very successful workshop
  - Proceedings will be out in about 2 months

Satisfying the Commercial Requirements for Alternative Energy Applications

Joan E. Bartelt
DuPont Nafion®
Fayetteville, NC

PEM (Proton Exchange Membrane) fuel cells have progressed rapidly in the past ten years and are now on the verge of commercial reality. DuPont Nafion(has been offering membrane products to researchers for the past 20+ years and is excited with the advances made by developers of the PEM fuel cell. Our message today is that DuPont Nafion(is committed to being the leading supplier of perfluorinated ionomer materials as the PEM fuel cell commercial market emerges and grows.

The discussion today is structured in three main areas: the growth in viable commercial applications, the need for improved cost and performance efficiencies and DuPont's programs for improved products and services.

The recent progress toward commercialization of PEM fuel cells has been dramatic. The number of companies seriously pursuing fuel cell development and the associated funding of fuel cell programs has risen tremendously. A wide variety of fuel cell applications including residential power, automotive, portable and stationary power are being pursued in the effort to increase fuel efficiency and reduce pollution. The convergence of gas and electricity is one area of specific interest to utility companies and fuel cell developers.

In order for fuel cells to reach the level of commercialization needed to impact a majority of the world population, there are many hurdles to overcome, the primary hurdle being cost of manufacture. Certainly mass production is needed to reduce costs. At the fuel cell system level, several aspects of design and assembly are being addressed by stack manufacturers. At the stack level, component cost and design are the main targets. The biggest impact that DuPont Nafion(can make towards these hurdles is improvements in ion-exchange membranes and reduction of their cost.

The benefits of commercial experience to reduce overall costs are great. As an illust ration, DuPont Nafion(has witnessed this benefit in the chloralkali business, a different application of our ion-exchange membrane. For the large scale production of chlorine and caustic soda, the primary variable cost is the power consumption in kWh per metric ton of caustic produced. Over the timeframe in which membrane plants became commercial, the power consumption has dropped to the point that today it is near the practical limit for electrolytic cells. This drop is a result of both cell manufacturers and membrane manufactures working together to improve the performance of these units. From our experience in the chloralkali market, we expect a similar type of improvement in the fuel cell industry in the coming years.

A chloralkali membrane produced by DuPont today is very different from their predecessors. Over the years, the structure has gone from a simple one layer/one polymer design to a sophisticated combination of two polymers, a fabric reinforcement, and surface modifications. Each change was made in an effort to solve specific technical problems, improve performance and reduce costs for the manufacture of chlorine and caustic soda.

In an analogous fashion, we can expect the structure of the fuel cell membranes to evolve with time. In the hydrogen and reformate fuel cells, the membrane and membrane electrode assembly (MEA) are the heart of the system. There are three distinct regions of the MEA that pose challenges. Improvements in the anode interface, the membrane itself and the cathode interface can impact the performance and cost of delivering power with a fuel cell. DuPont collaborates with stack manufacturers to understand and solve these challenges. Five years ago, the DuPont membrane Nafion(N-117 was the best fuel cell membrane available. Today, by manufacturing thinner and more sophisticated membranes, DuPont membranes continue to be the performance benchmark in the fuel cell industry. Current-voltage curves of several membranes show that our new experimental products will have better performance at higher current densities.

For the case of direct methanol fuel cells (DMFC), different challenges arise. The fuel crossover issue is a top concern, and Nafion(N-117 remains the performance standard. By tailoring the structure of the membrane, significant reduction in the fuel cross over has been achieved.

While these performance challenges are being recognized and met, the cost of the ion-exchange membranes is a major concern for stack manufacturers. The various app lications have a wide range of cost hurdles --portable power at the highest allowable cost and automotive the most demanding in cost --to achieve commercialization.

DuPont has projected the future cost of Nafion(materials with greatly increased volum es. Based on the membrane Nafion(N-112, the cost is projected to be near $10/kW at an annual installed fuel cell capacity of 10 million kW. The basis of this projection is that performance improvements will be made from an average of 3.0 kW/m2 today to a future 5.5 kW/m2, and that normal increased volume benefits will be realized.

To emphasis our commitment to the fuel cell industry, has expanded our product offering.. We offer two membrane lines, based on our standard ion-exchange capacity polymer and a higher ion-exchange capacity polymer. Similarly we offer both solutions and thermoplastic resins based on the same polymers. For specific customer needs we may provide other materials to meet their requirements.

With PEM fuel cells emerging on the global commercial market, DuPont Nafion(is committed to being the leading supplier of perfluorinated ionomer materials worldwide.

DuPont Fluoroproducts

Satisfying the Commercial Requirements for Alternative Energy Applications

114

NAFION® only by DuPont

Joan E. Bartelt, DuPont Fluoroproducts

Our Message

- Commercial Reality of PEM Fuel Cells

- Nafion® Products is Committed to being the Leading Supplier of Perfluorinated Ionomer Materials

NAFION® only by DuPont

Outline

DuPont Fluoroproducts

- Growth of Viable Commercial Applications in Global Alternative Energy Markets
- Need for Improved Cost and Performance Efficiencies, with a Focus on Components and Manufacturing Processes
- DuPont's Programs for Improved Products Designed for Cost-Efficient Utilization

Potential Market Growth

DuPont Fluoroproducts

- Evidence of PEMFCs Commercial Importance:
  - Deluge of press releases on PEMFC developments for transportation applications
  - Since 1985, ten-fold increase in the number of companies pursuing serious FC development
  - Since 1993, five-fold increase in European Commission funding in FC Framework Program (FP)
- Increasing Interest by Utilities to Employ PEMFC Systems (Gas-Electricity *convergence*)

Areas for Cost Improvements

DuPont Fluoroproducts

- System:
  - Fuel-Processing (reformer, clean-up) and Controls
  - Power Conditioning
  - Stack Design, Fabrication and Assembly
  - System Integration and Optimization
  - System Design, Assembly and Operation
- Stacks:
  - Overall Design and Manufacturing / Assembly Process
  - Bipolar Plates
  - Housing
  - ***Ion-Exchange Membranes***
  - Catalyst Selection and Gas Diffusion Barrier
  - Mass / Heat Flow Controls

NAFION® only by DuPont

Benefits of Commercial Experience

DuPont Fluoroproducts

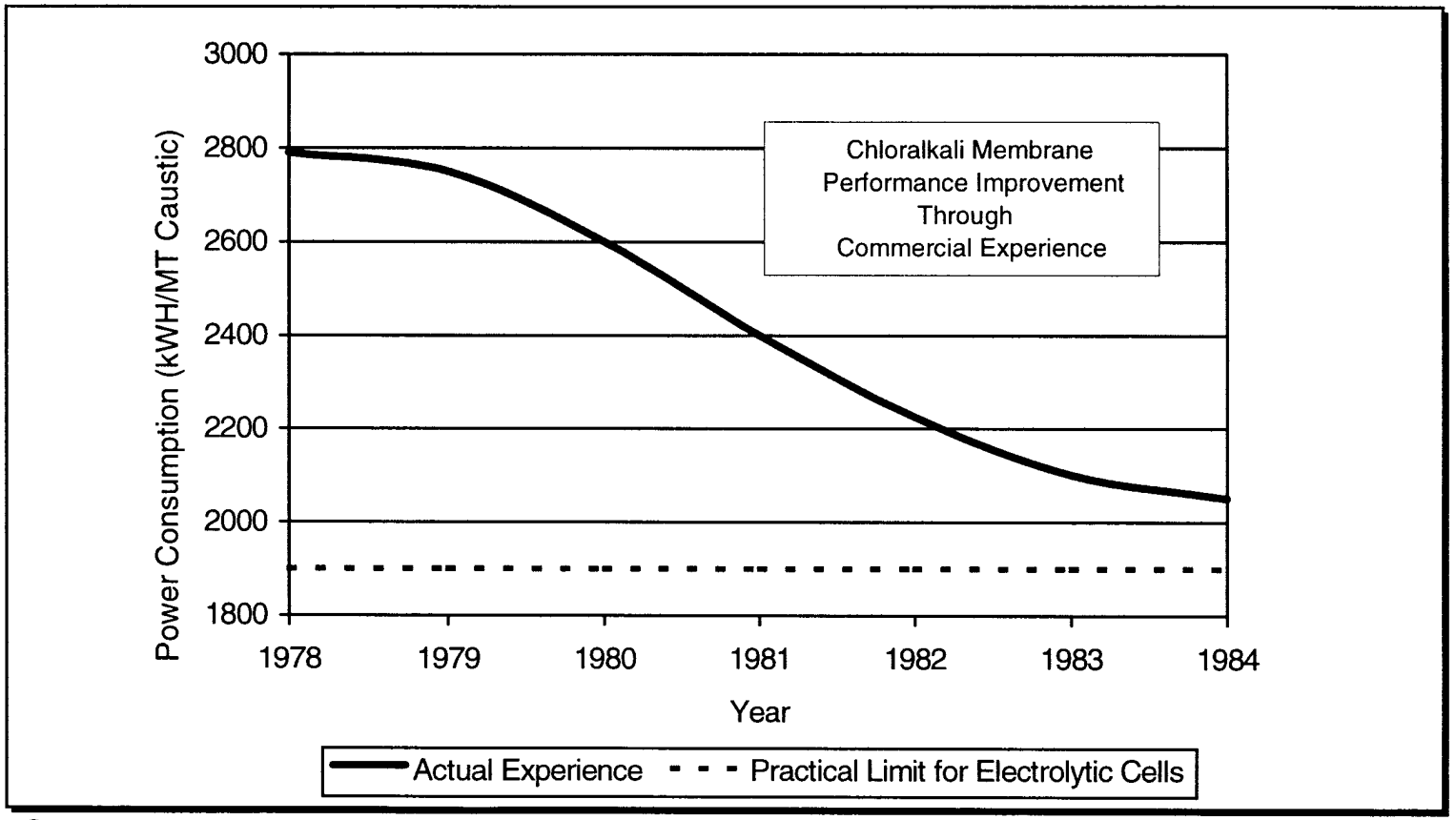

NAFION® only by DuPont

Nafion® Chloralkali Membrane Structure / Function

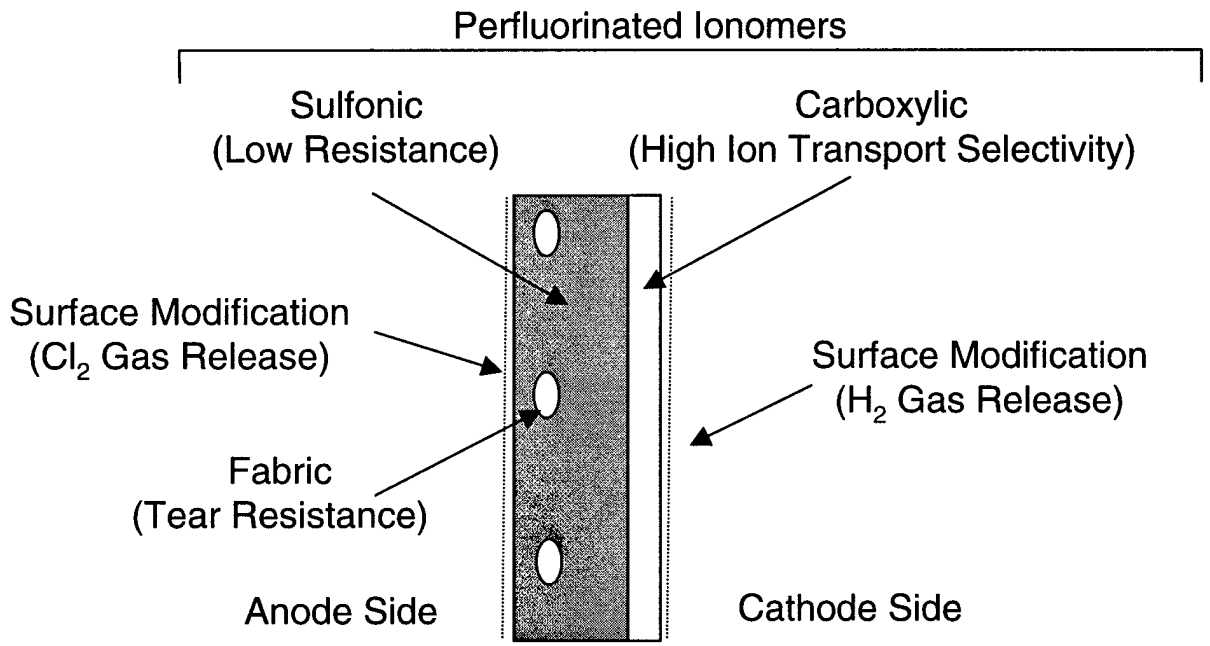

NAFION® only by DuPont

Membrane and MEA Architecture Challenges

DuPont Fluoroproducts

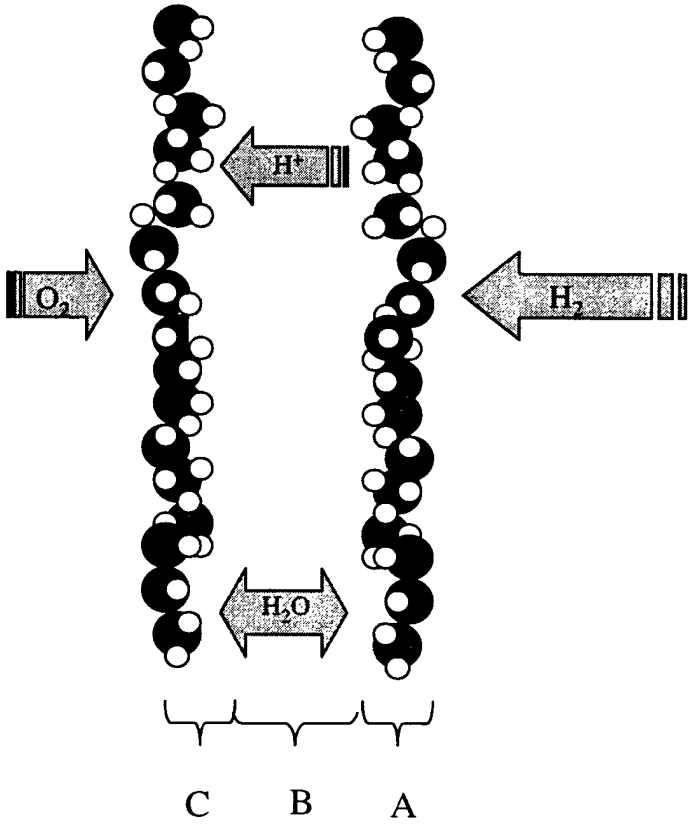

NAFION® only by DuPont

H_2 / Reformate Systems

Region A. Anode Interface
- resistance to dehydration
- improve 3 phase contact

Region B. Membrane
- higher conductivity
- better water management

Region C. Cathode Interface
- avoid flooding
- improve 3 phase contact
  (reaction kinetics / O_2 perm)

121

Commercial and Experimental Membranes for H_2 Fuel Cells

DuPont Fluoroproducts

Fuel Cell Membrane Performance

50 cm^2 cell, H_2/air - 30/30 psig, 1.8/7.0 SLPM, T = 85°C

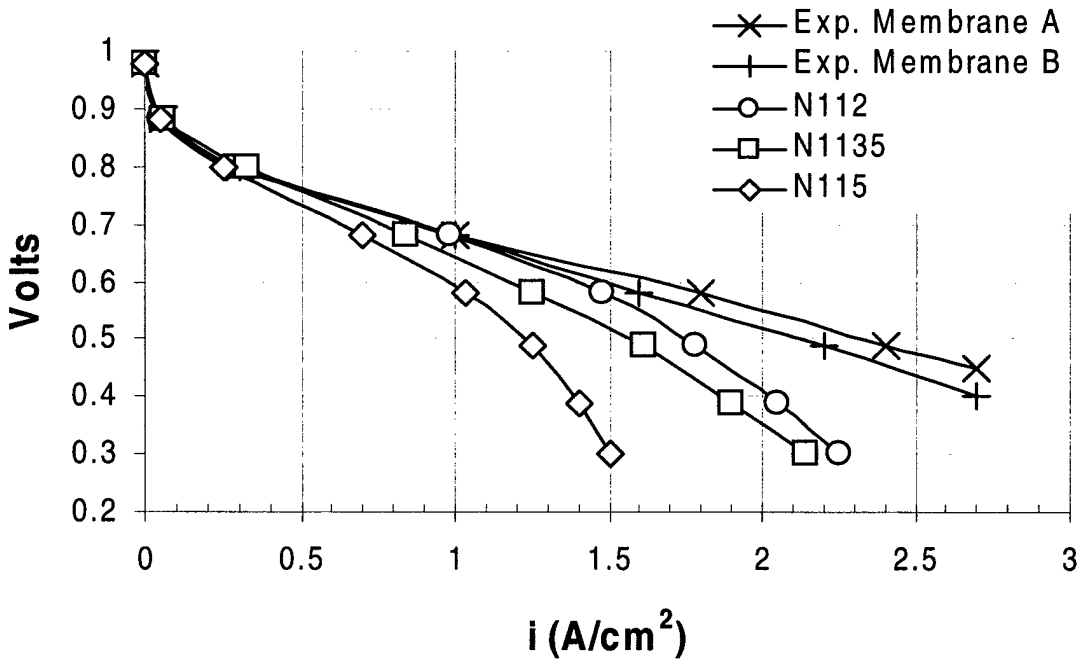

122

NAFION® only by DuPont

Membrane and MEA Architecture Challenges

DuPont Fluoroproducts

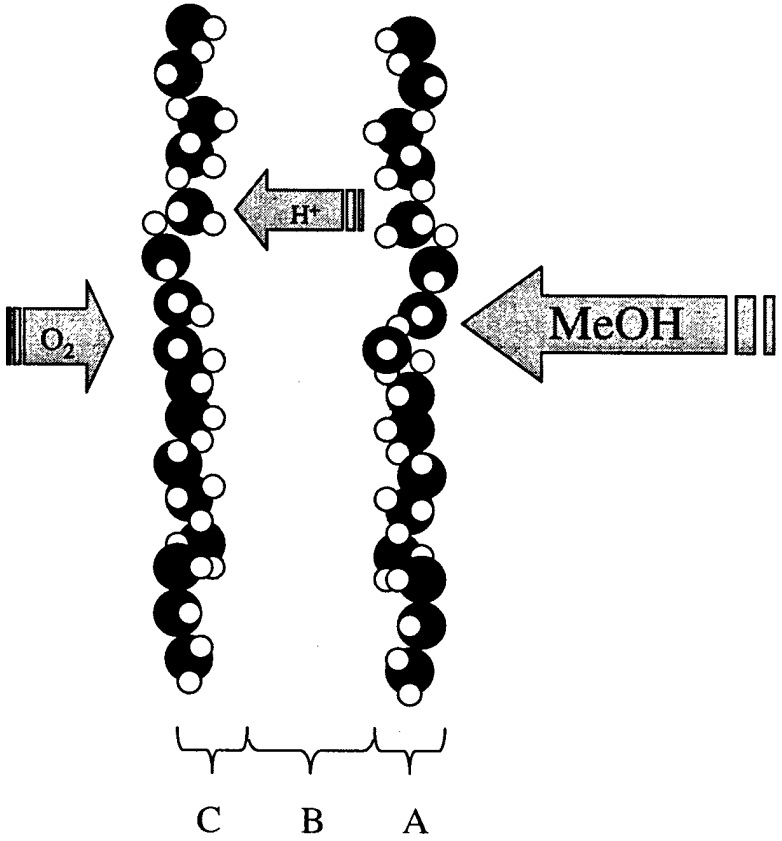

NAFION® only by DuPont

Direct Methanol Systems

Region A. Anode Interface
- improve reaction kinetics (or do no harm)
- gas release

Region B. Membrane
- reduce methanol permeation
- high T and P operation

Region C. Cathode Interface
- improve 3 phase contact (reaction kinetics / O_2 perm)

123

Commercial and Experimental Membranes for DMFC

DuPont Fluoroproducts

Nafion® Membrane Type	Cell Resistance (Ω cm^2)	Cross Over CD @ 150mA/cm^2 (mA/cm^2)	Cell Voltage (V)	Cross Over Reduction (%)
N117	0.225	1.5	0.41	----
EM2 (≈ 5 mil thickness)	0.250	63	0.42	40
EM3 (≈ 7 mil thickness)	0.375	48	0.38	54

1 M Methanol, 3 LPM Air, Ambient Pressure, 60°C, 25 cm^2 Cell

NAFION® only by DuPont

Market-back Estimates of Cost *Hurdles*

DuPont Fluoroproducts

	Portable Power	Distributed Stationary Power	General Automotive
System	~ $2,000/kW	$500 to $1,500/kW	$100/kW
Stack	$1,000/kW	$200 to $500/kW	$50/kW
Membrane (5 kW/sq.meter and 20% of Stack Cost)	$1,000/ m^2	$200 to $500/$m^2$	$50/$m^2$

NAFION® only by DuPont

Joan E. Bartelt, DuPont Fluoroproducts

Membrane Cost Improvements

DuPont Fluoroproducts

- Membrane cost projected to be near $10/kW at annual installed capacities of 10 - 12 million kW. Based on Nafion® 112.
- Includes System/Membrane Performance Improvements.
  (from 3.0 kW/m^2 to 5.5 kW/ m^2)
- Includes Process and Material Cost Improvements with Increased Production Volume

Product Offerings

- Nafion® Membranes:

  N-117, N-115, N-1135, N-112,
  NE-105, NE-1035

- Nafion® Solutions:

  SE-5112, SE-5012

- Nafion® Resin (Thermoplastic):

  R-1100, R-1000

- Custom Materials specific to Customer Needs

NAFION® only by DuPont

Conclusion

- Commercial Markets for Alternative Energy Sources (such as PEM fuel cells):
  - Emerging Globally
  - Large !
- Nafion® Products is Committed to being the Leading Supplier of Perfluorinated Ionomer Materials

Advanced Components for PEM Fuel Cells from W. L. Gore and Associates

*GORE-SELECT Ionomer Composite Membrane
*PRIMEA Series 5510 MEA
*CARBEL-CL Gas Diffusion Media

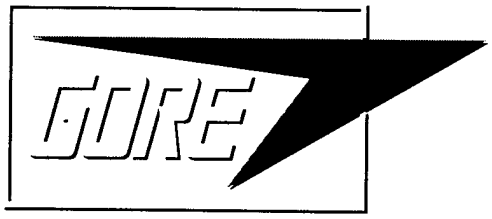

W. L. Gore and Associates, Inc.

GORE-SELECT, PRIMEA and CARBEL are trademarks of W. L. Gore & Associates, Inc.

PRIMEA MEA with CARBEL Gas Diffusion Media

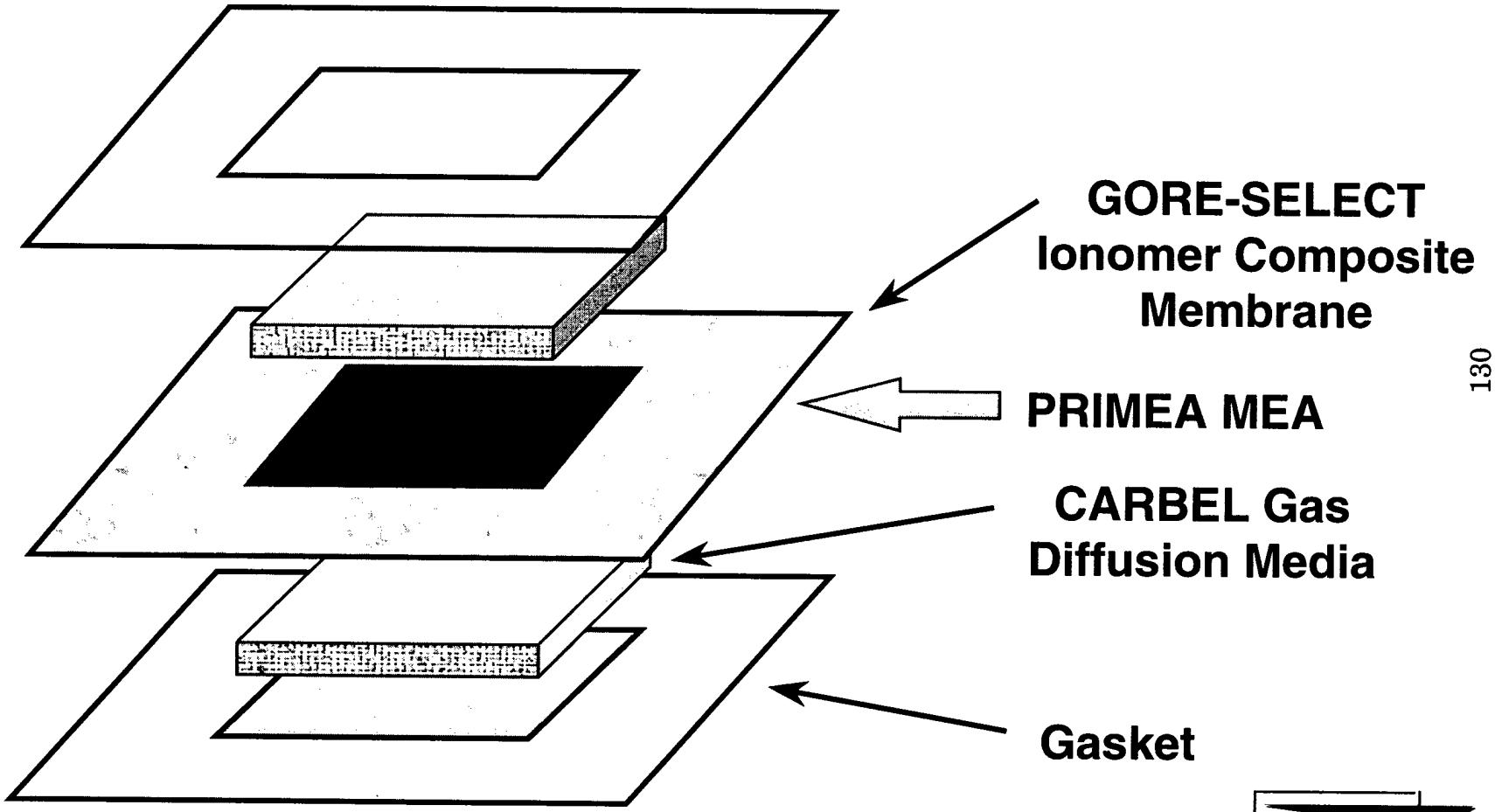

PRIMEA and CARBEL are trademarks of W. L. Gore & Associates, Inc.

GORE
Creative Technologies Worldwide

Micro-Reinforcement Has Unique Advantages Not Previously Achievable

- Low operating voltage drop across the membrane can now be combined with physical strength.
- Previously the strength and electrochemical properties were linked.
- Gore's technology allows the ionomer to be optimized for the electrochemical performance and the micro-reinforcement provides the physical strength.
- Adds dimensional stability.

GORE
Creative Technologies Worldwide

Decoupled Physical / Electrochemical Performance

By combining ionomers with micro reinforcement we now can optimize the membrane around the ionomers electrochemical performance without having to compromise to achieve the required strength.

The micro-reinforcement adds strength and controls dimensional stability allowing the use of ionomers not previously suitable for membranes.

GORE
Creative Technologies Worldwide

Ideal Reinforcement Properties

- Chemical Stability
- Thermal Stability
- Strength
- Dimensional Stability
- Low Ionic Resistance

GORE
Creative Technologies Worldwide

Gore reinforcement is ideal for advanced PEM Fuel Cells because:

- Chemical resistance not limited by the reinforcement
- Operating temperature not limited by the reinforcement
- High mechanical strength
- Outstanding dimensional stability during hydration/dehydration
- Minimal contribution to ionic resistance
- Allows a variety of ion exchange material

GORE
Creative Technologies Worldwide

Additional Degrees of Flexibility in Membrane Fabrication

- Reinforced micro-composites can use a variety of ionomers from fully fluoridated to non-fluoridated even ones that were unsuitable in the past due to extremely poor mechanical properties.
- Other ion exchange media
- Can be made with multiple layers

GORE
Creative Technologies Worldwide

GORE-SELECT Ionomer Composite Membrane

- Patented composite structure allows membranes to be made which are very thin and still extremely strong, and thus low resistance
- Beyond the mechanical strength, the GORE-SELECT membrane has excellent dimensional stability
- Improved water transport (ability to stay hydrated)
- Can utilize any ionomer, regardless of the ionomer's basic mechanical properties

GORE-SELECT is a trademark of W. L. Gore & Associates, Inc..

GORE
Creative Technologies Worldwide

Polarization Curve Interpretation

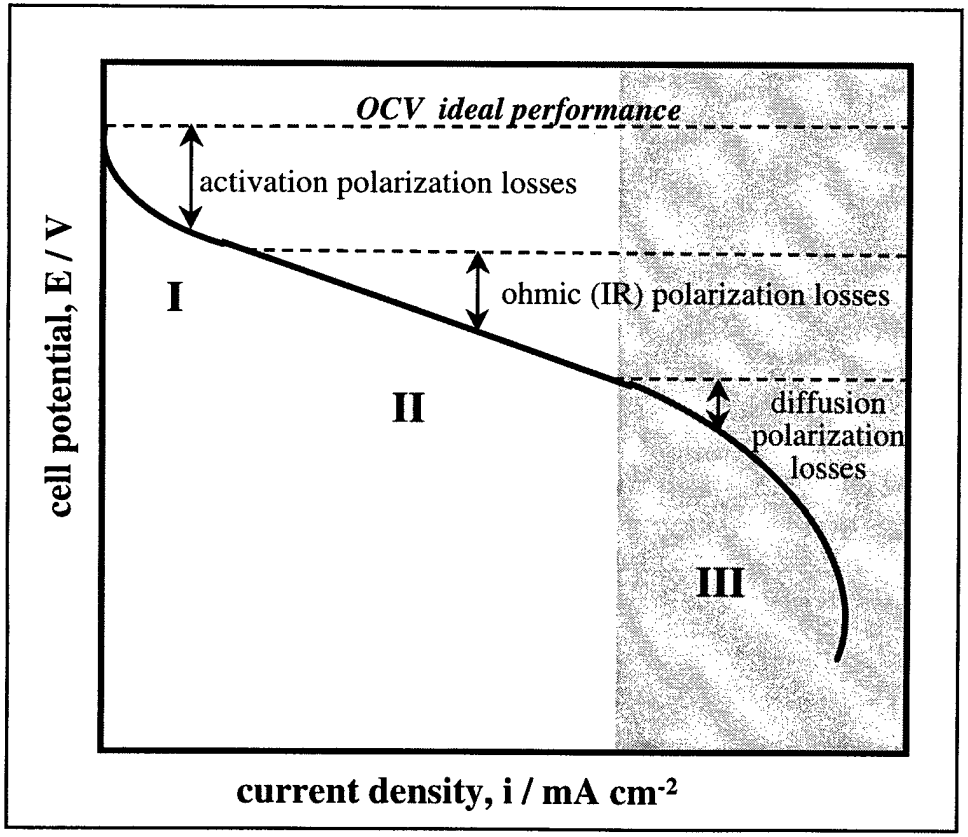

I. Activation (catalyst)

II. Ohmic (mostly membrane)

III. Mass Transport (electrode and gas diffusion media)

GORE
Creative Technologies Worldwide

PRIMEA Series 5000 MEA

- First Generation MEA from Gore
- Long life, high performance MEA (over 5000 hours demonstrated)
- Based on GORE-SELECT Ionomer Composite Membrane

PRIMEA and GORE-SELECT are trademarks of W. L. Gore & Associates, Inc..

GORE
Creative Technologies Worldwide

PRIMEA Series 5000 MEA

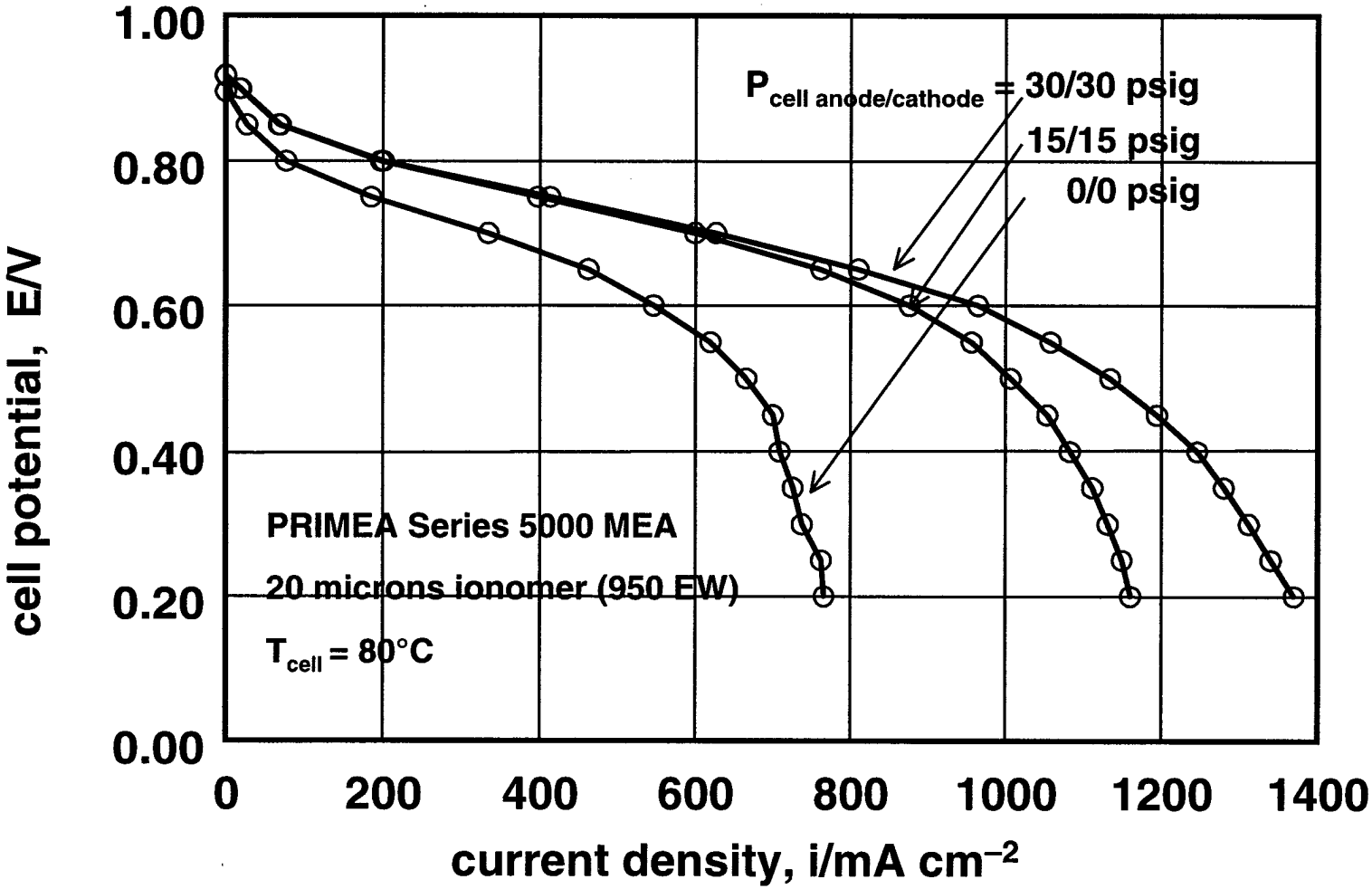

PRIMEA is a trademark of W. L. Gore & Associates, Inc..

GORE
Creative Technologies Worldwide

PRIMEA Series 5000 MEA

Long-Term Stable Performance

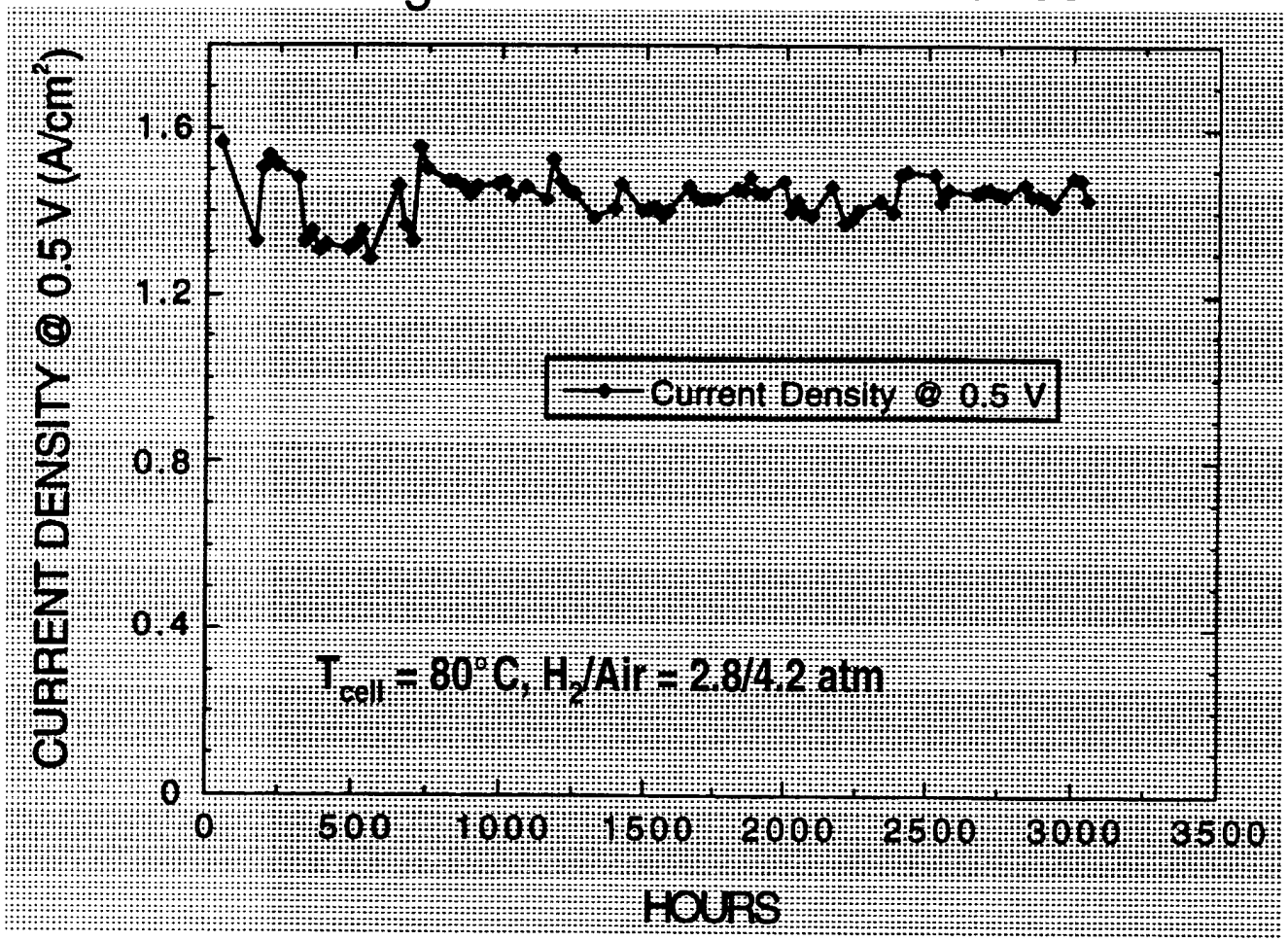

Source: Los Alamos National Laboratory

PRIMEA is a trademark of W. L. Gore & Associates, Inc..

GORE
Creative Technologies Worldwide

PRIMEA Series 5510 MEA

- All-around higher performance MEA
- **B**ased on GORE-SELECT membrane technology and Gore's proprietary advanced electrode technology
- Designed for high power density operation on H_2
- Unleashes the true potential of the GORE-SELECT membrane

PRIMEA and GORE-SELECT are trademarks of W. L. Gore & Associates, Inc..

GORE
Creative Technologies Worldwide

PRIMEA Series 5510 MEA

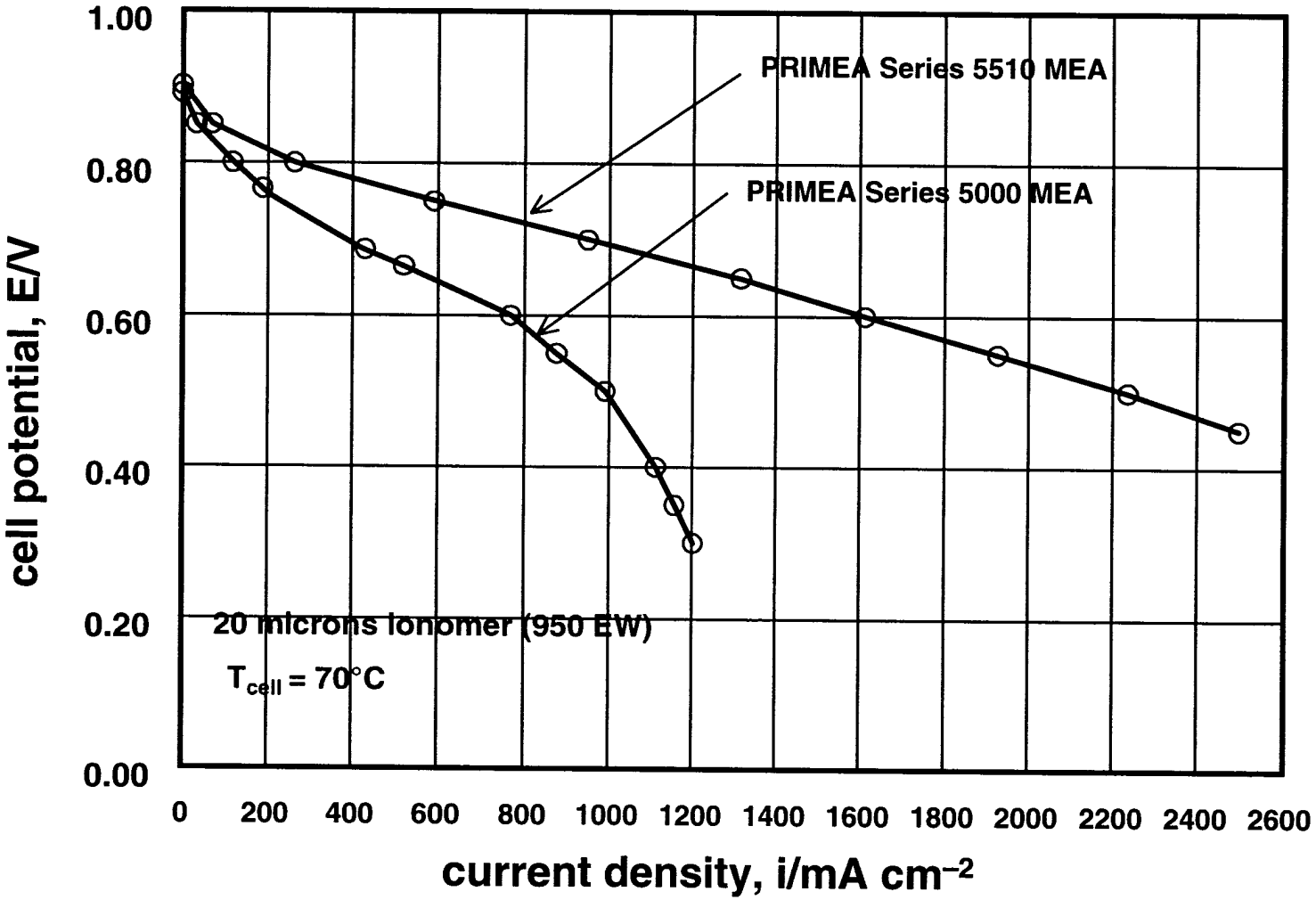

PRIMEA is a trademark of W. L. Gore & Associates, Inc..

GORE
Creative Technologies Worldwide

PRIMEA Series 5510 MEA

- Utilizes same proven chemistry (perfluorinated ionomers)
- Long-term stable performance under a broad range of operating conditions

PRIMEA is a trademark of W. L. Gore & Associates, Inc..

GORE
Creative Technologies Worldwide

PRIMEA Series 5510 MEA

Stability of Performance

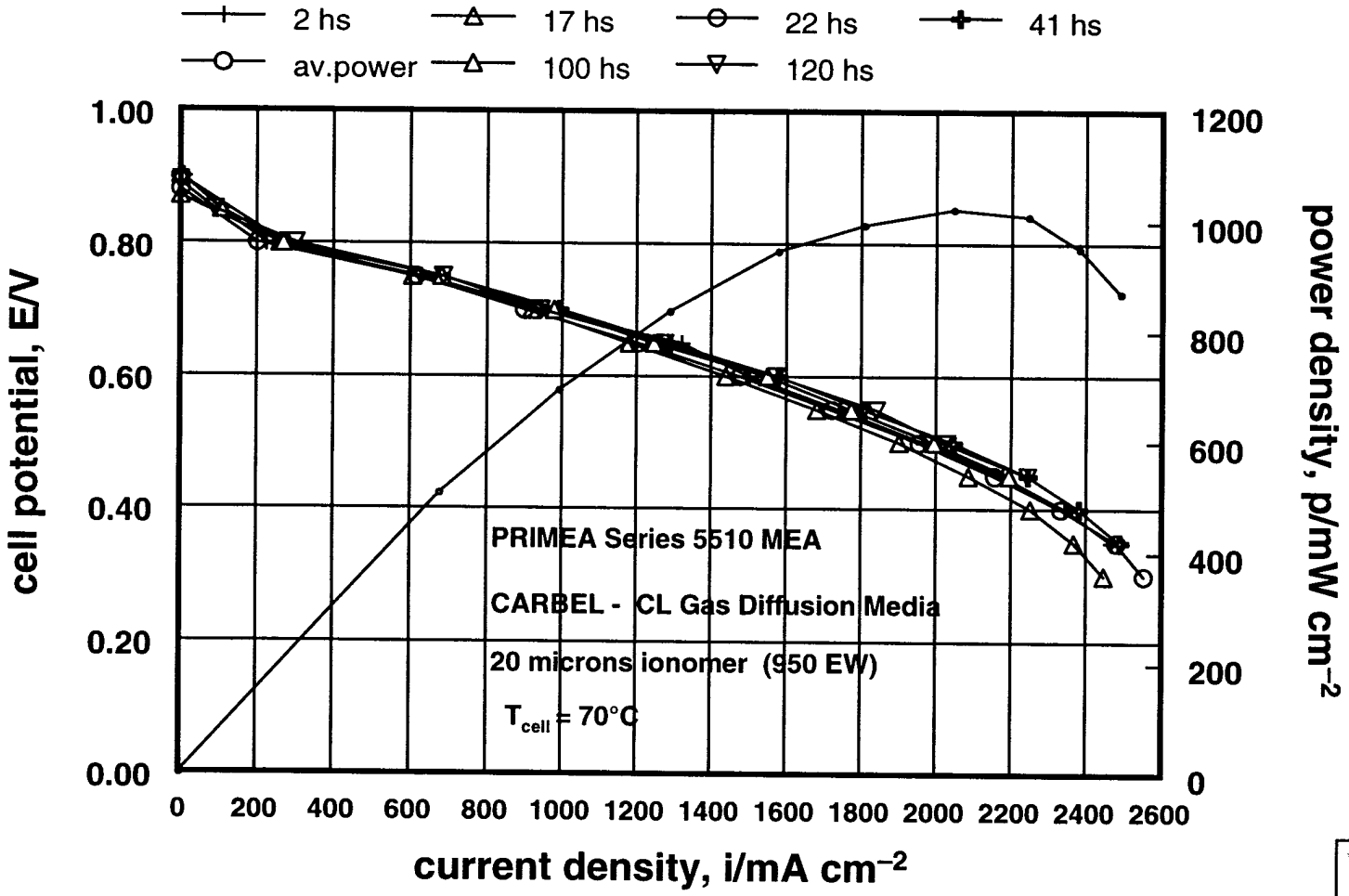

PRIMEA and CARBEL are trademarks of W. L. Gore & Associates, Inc.

PRIMEA Series 5510 MEA

Durability: Automotive Driving Cycle

Typical Power Density Profile for FUDS Testing

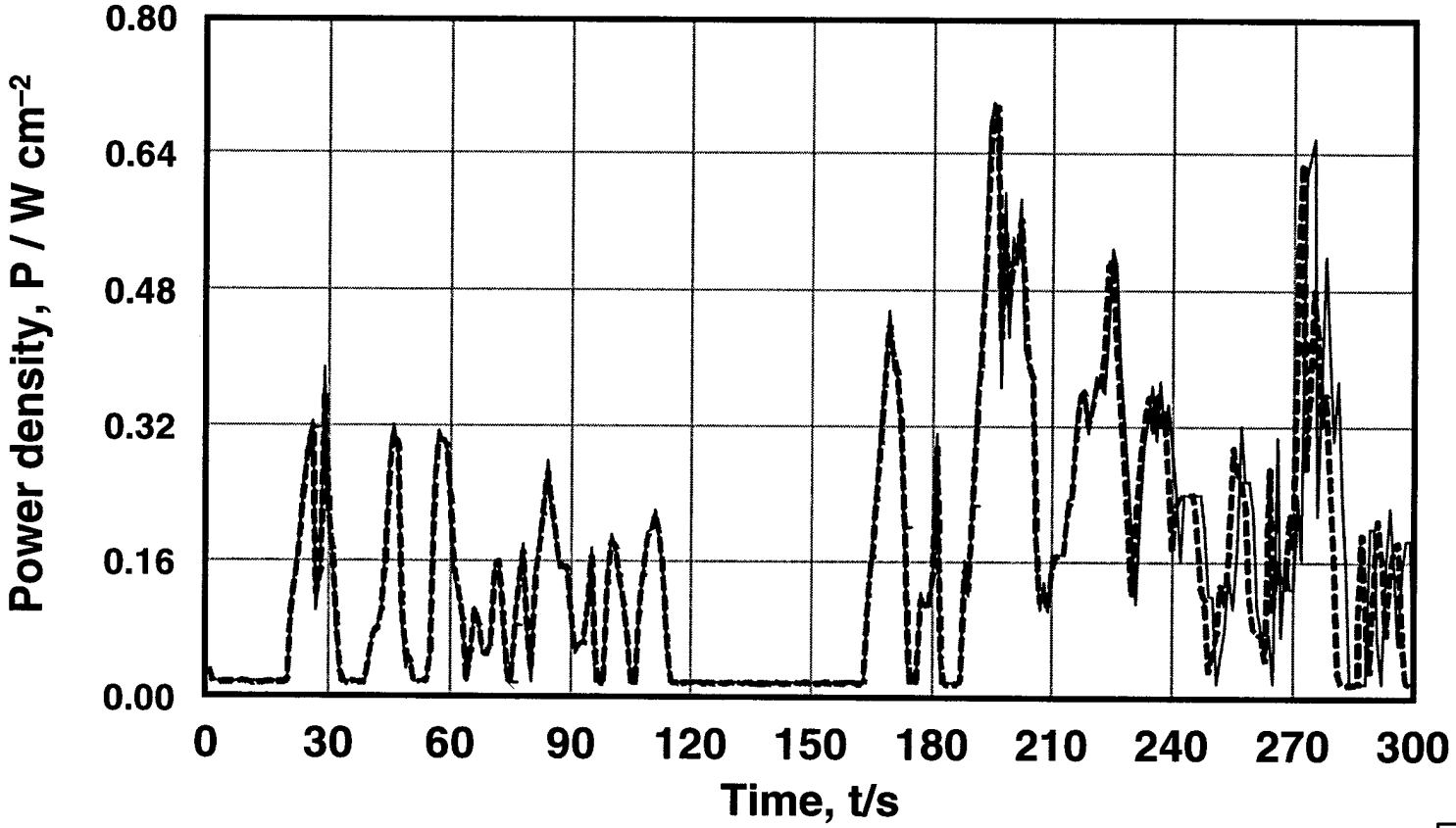

PRIMEA is a trademark of W. L. Gore & Associates, Inc.

GORE
Creative Technologies Worldwide

PRIMEA Series 5510 MEA

Durability: Automotive Driving Cycle

Effect of FUDS Testing on Polarization Performance

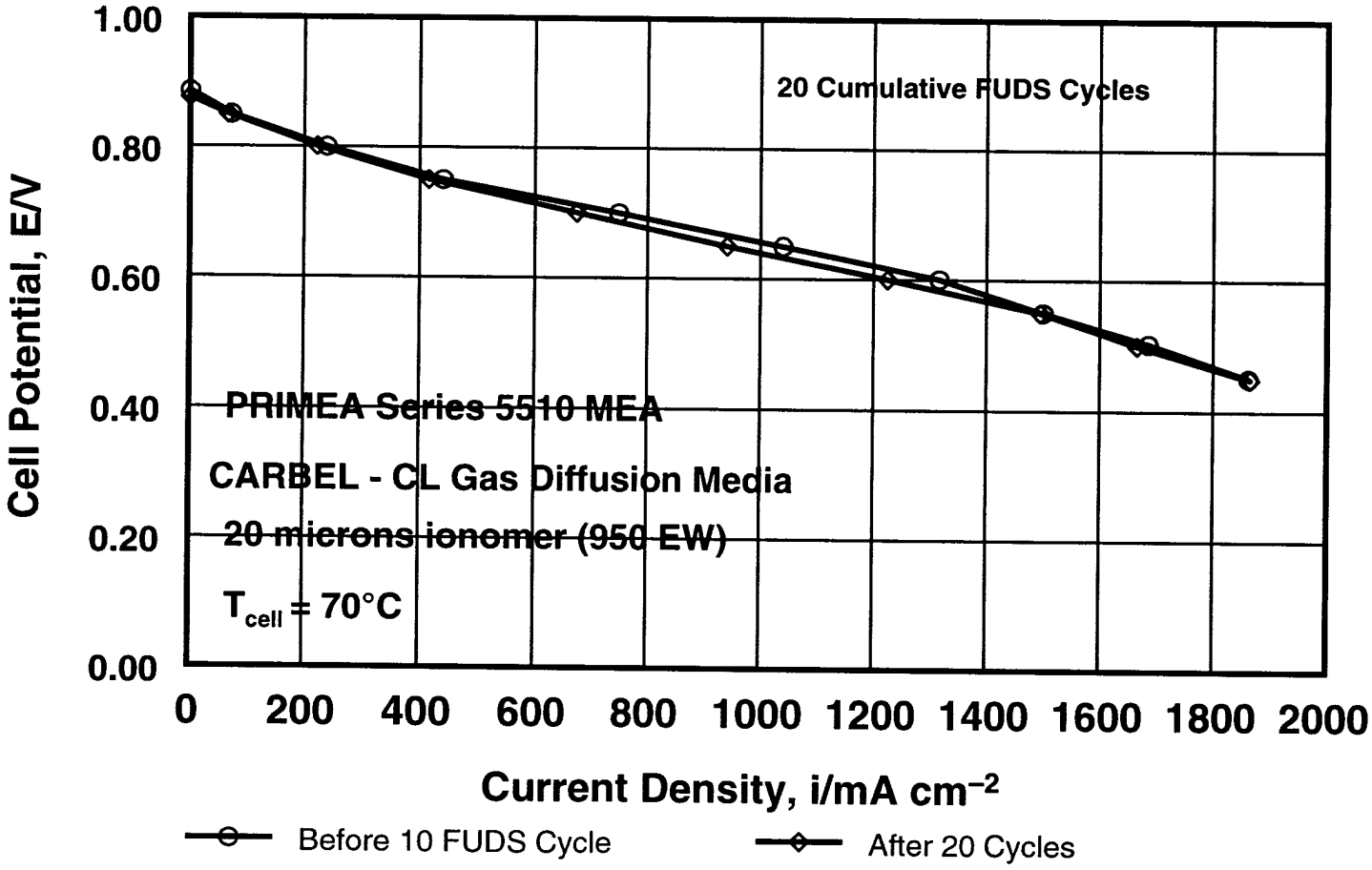

PRIMEA and CARBEL are trademarks of W. L. Gore & Associates, Inc.

GORE
Creative Technologies Worldwide

PRIMEA Series 5510 MEA

Durability: Start-up/Shut-down

PRIMEA Series 5510 MEA **CARBEL - CL Gas Diffusion Media**
20 microns ionomer (950 EW)

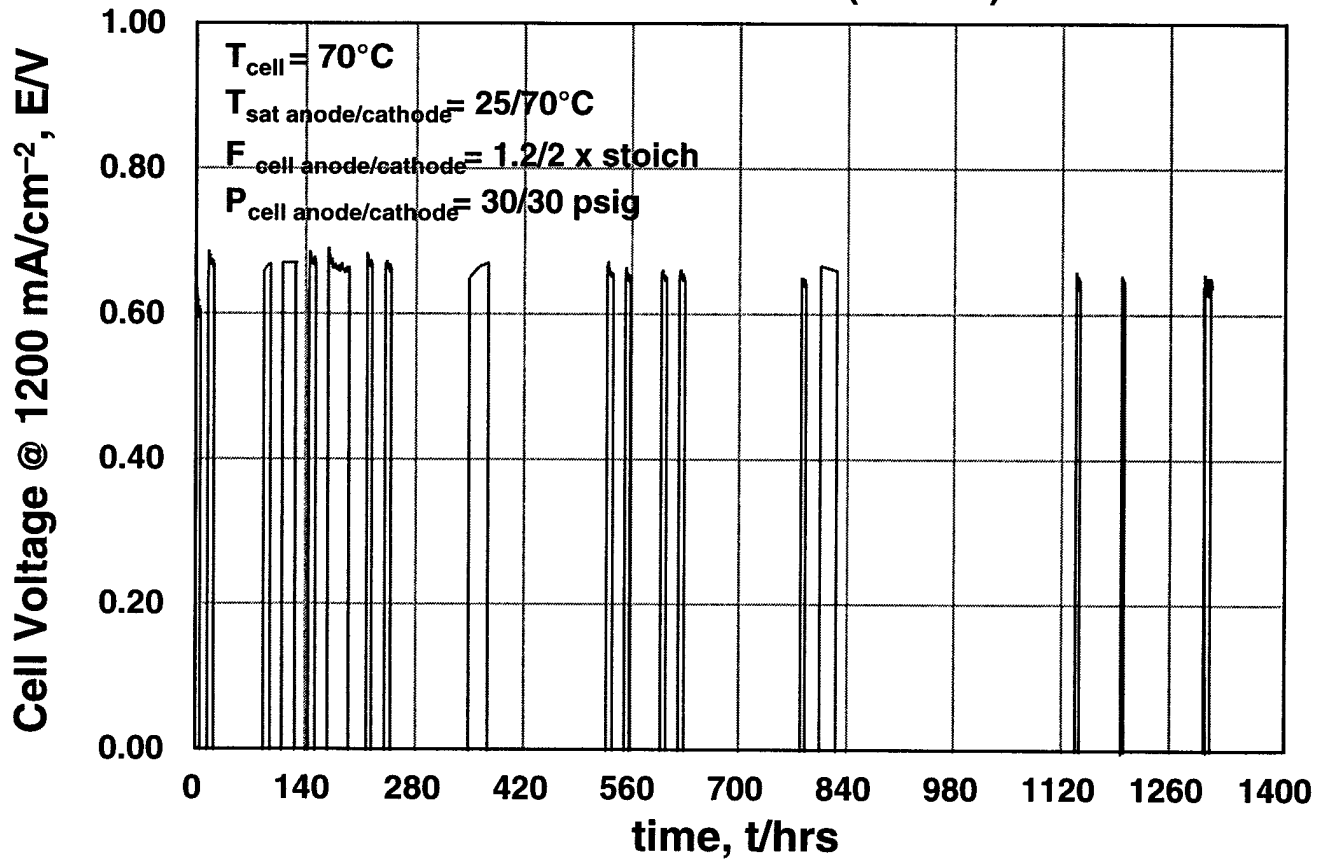

PRIMEA and CARBEL are trademarks of W. L. Gore & Associates, Inc..

GORE
Creative Technologies Worldwide

PRIMEA Series 5510 MEA

Schatz Energy Research Center

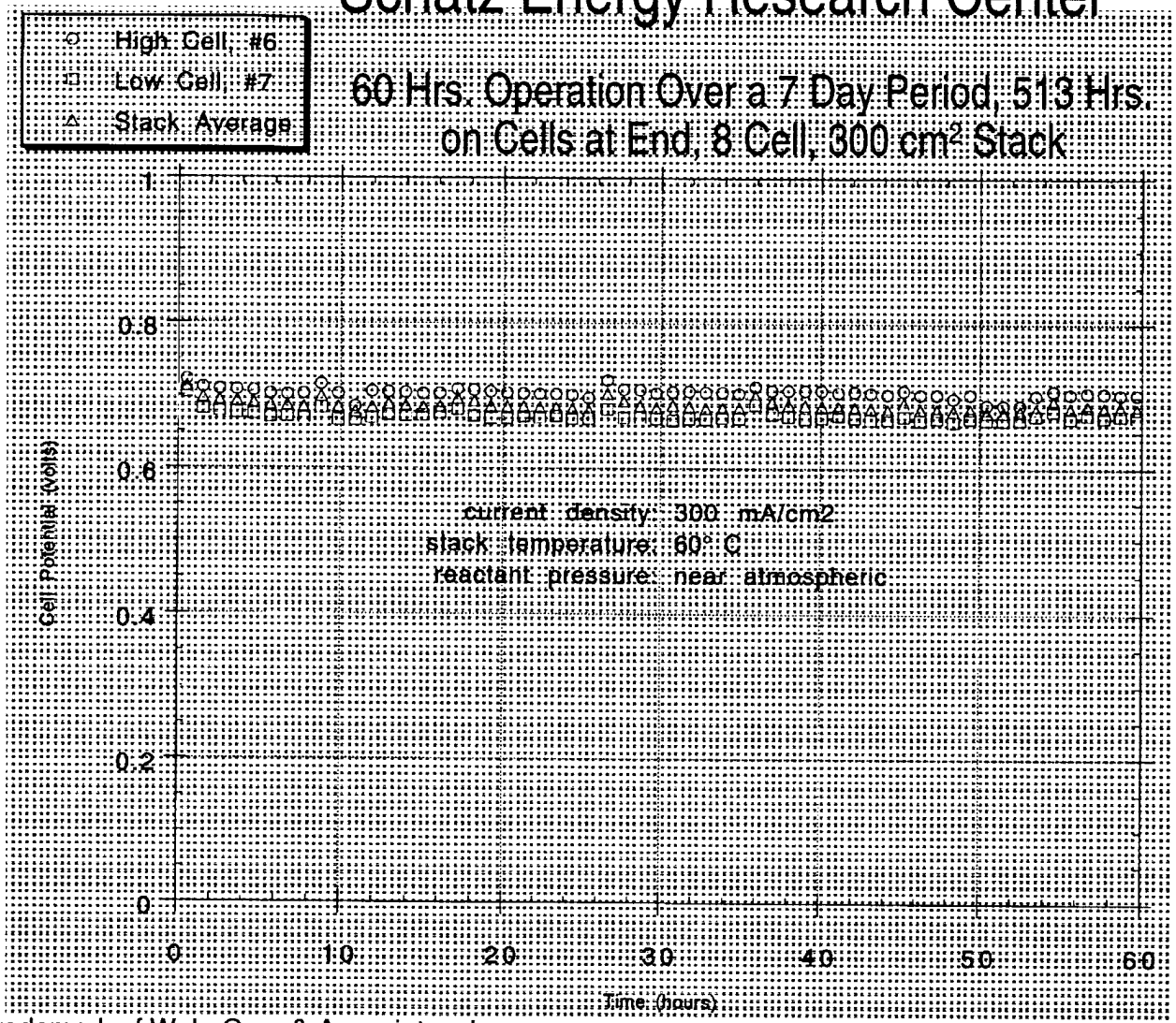

PRIMEA is a trademark of W. L. Gore & Associates, Inc.

GORE
Creative Technologies Worldwide

Endurance Testing of PRIMEA Series 5510 MEAs

Performed at Energy Partners 11"x11" Active Area

Two cell stack, 30 psi air exit, 45 psi H_2 exit, current density: 515 mA/cm^2 constant

PRIMEA 5510 MEA, 40 microns thick, 0.3 mg/cm^2 each electrode

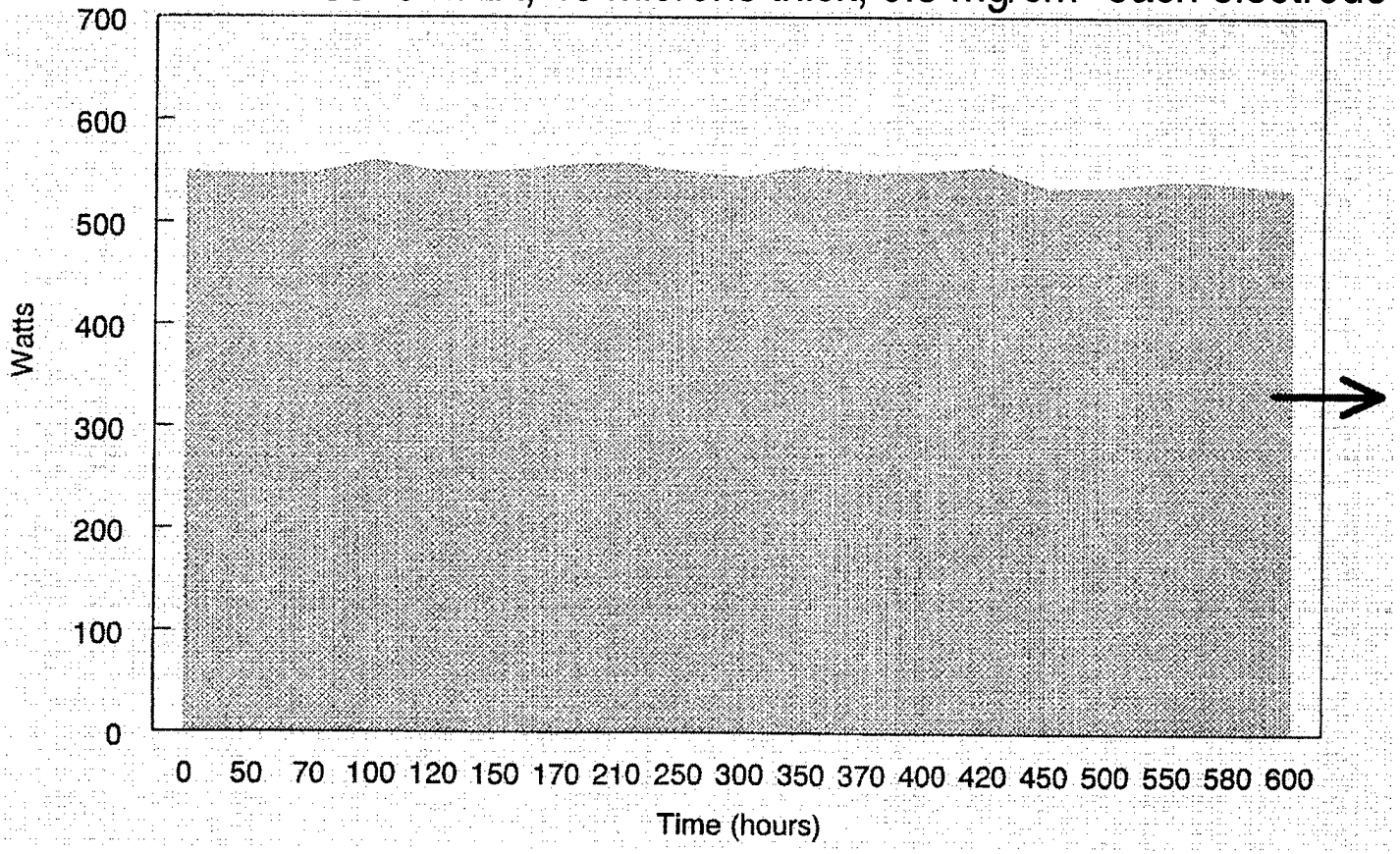

PRIMEA is a trademark of W. L. Gore & Associates, Inc..

GORE
Creative Technologies Worldwide

CARBEL-CL Gas Diffusion Media

- New high performance microporous / macroporous gas diffusion media
- Allows very high current density operation at low stoichiometric gas flow rates without significant mass transport limitations
- Low cost / high volume production capable

CARBEL is a trademark of W. L. Gore & Associates, Inc.

GORE
Creative Technologies Worldwide

CARBEL-CL Gas Diffusion Media

Low "Stoichiometric Sensitivity"

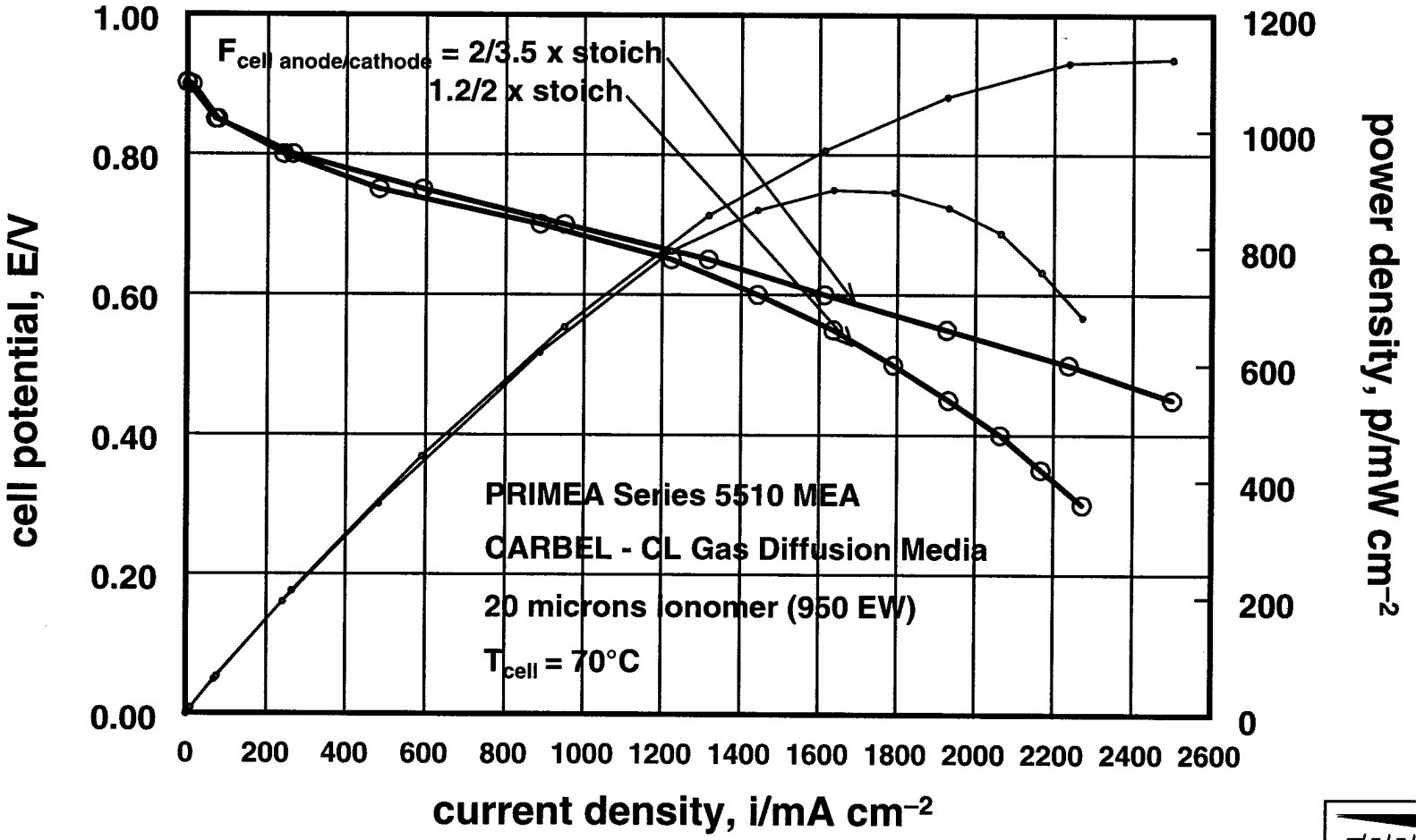

PRIMEA and CARBEL are trademarks of W. L. Gore & Associates, Inc.

GORE
Creative Technologies Worldwide

PRIMEA Series 5510 MEA with CARBEL-CL Gas Diffusion Media

Effect of Operating Pressure

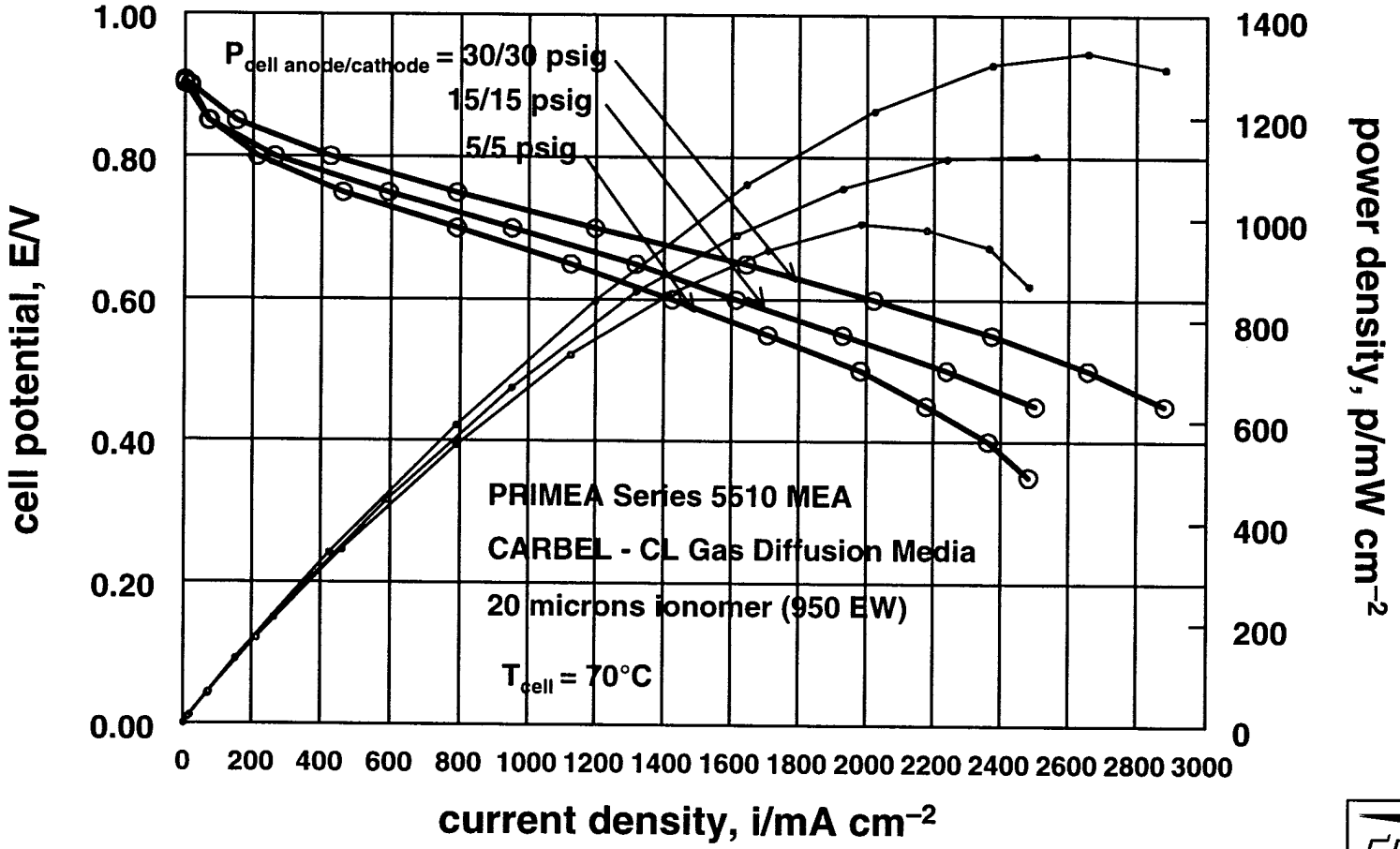

PRIMEA and CARBEL are trademarks of W. L. Gore & Associates, Inc.

GORE
Creative Technologies Worldwide

PRIMEA Series 5510 MEA with CARBEL-CL Gas Diffusion Media

Low Catalyst Loading

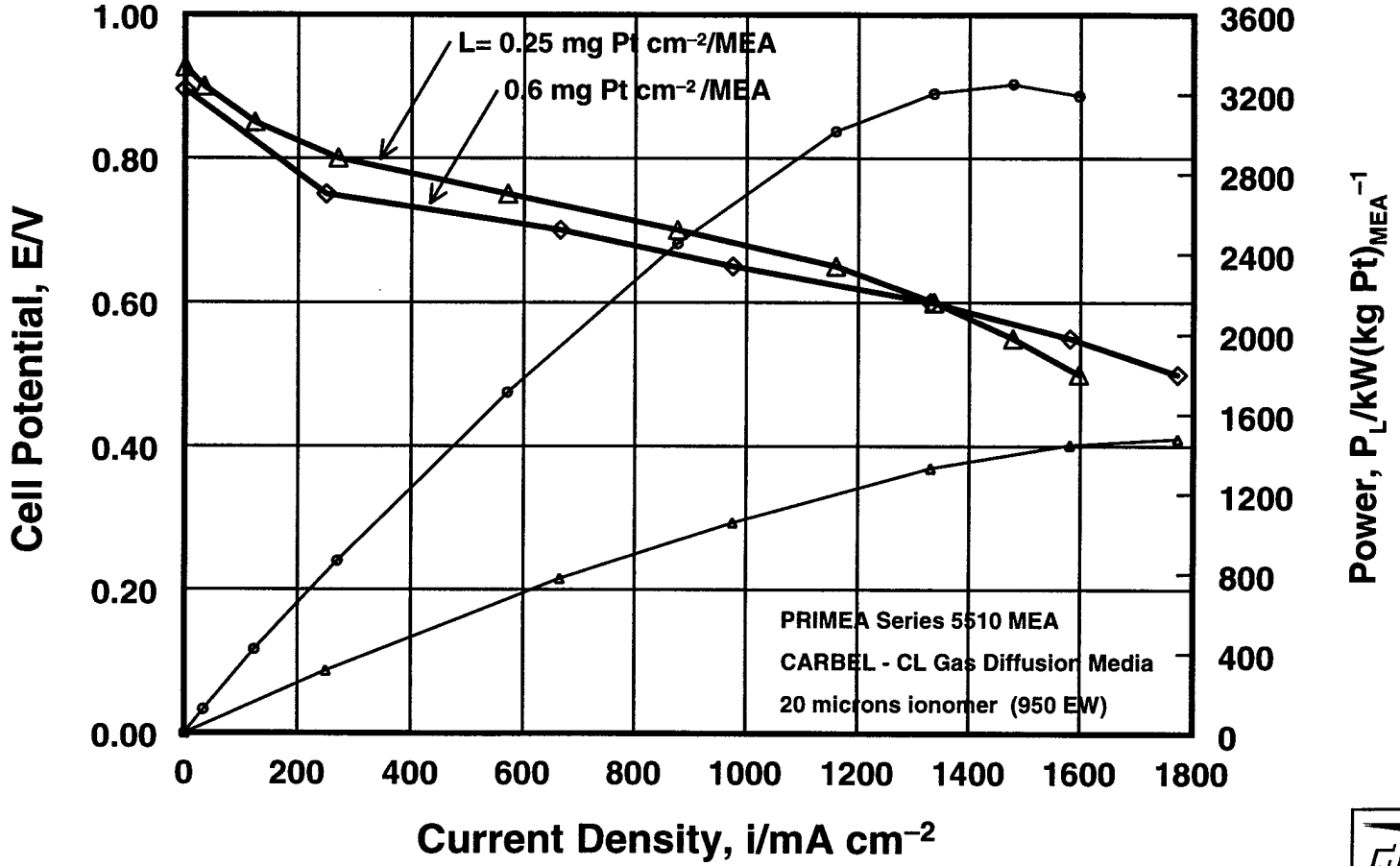

PRIMEA and CARBEL are trademarks of W. L. Gore & Associates, Inc..

GORE
Creative Technologies Worldwide

Continuous Development

- Gore is already developing the next generation(s) of MEA's, PRIMEA Series XXXX, YYYY, ...
- We are committed to continuous performance improvement, developing cutting edge technology

PRIMEA is a trademark of W. L. Gore & Associates, Inc..

GORE
Creative Technologies Worldwide

Membrane Electrode Assemblies

Shimshon Gottesfeld

Los Alamos National Laboratory

The Membrane

Nature/Properties

Thickness

MEA Fabrication Modes

Overall Catalyst Composition

Application to Membrane or C Paper

Catalyst Layer Properties

Robustness

Transport Properties

CROSS SECTION OF POLYMER ELECTROLYTE FUEL CELL

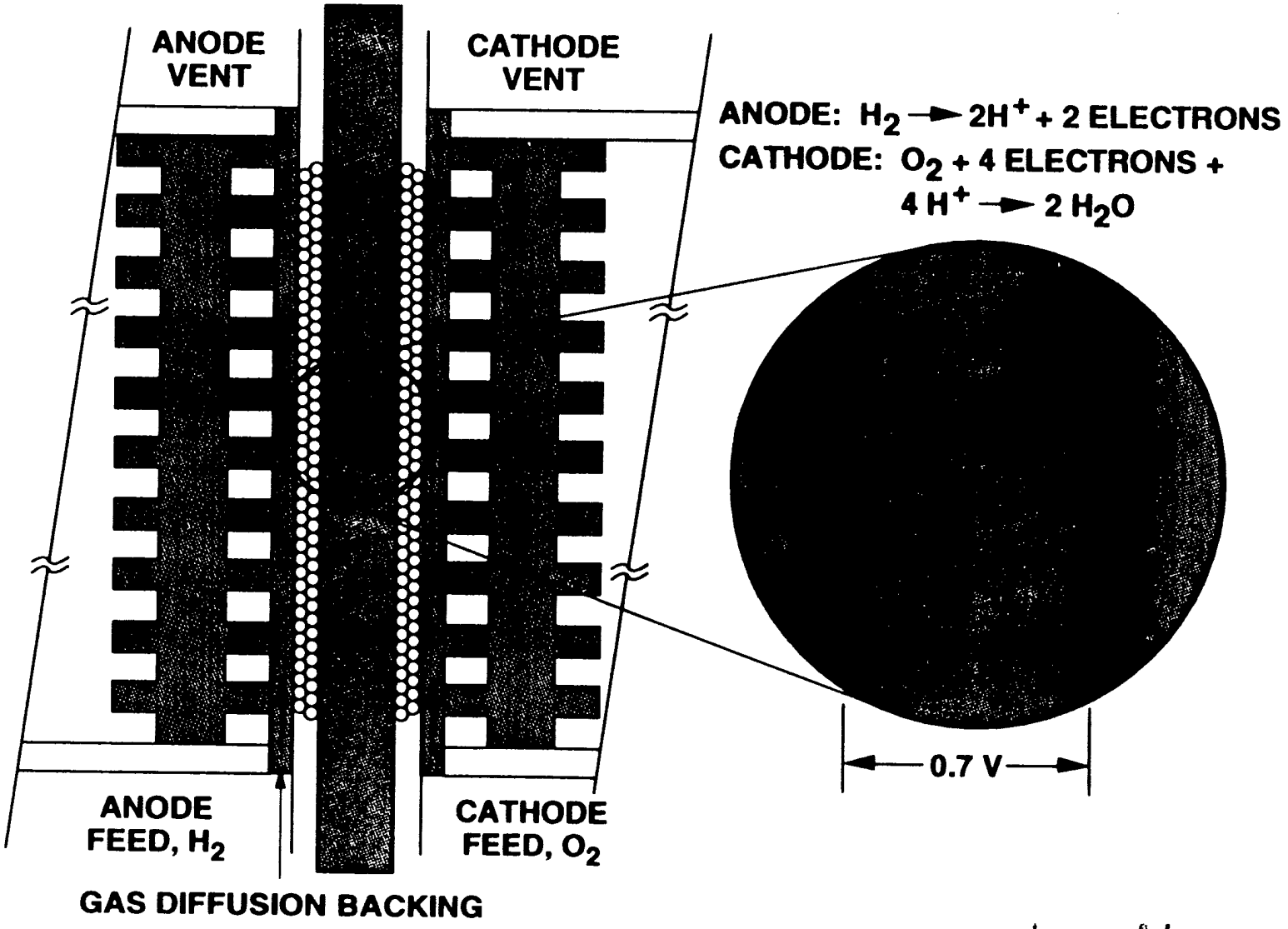

Membrane Electrode Assemblies

Conclusions

(1) Reformate/Air PEFCs

Membrane Thickness:

* In operation on hydrogen rich gas mixtures, thin ionomeric membranes (50 µm thick or less) provide highest performance and effective MEA hydration. Some further testing may be required to document any trade-off with robustnes and long-term stable performance, per given hardware under full range of conditions.

Membrane Chemistry:

* To date, no substantial proof has been provided for competitive position of a hydrated non-PFSA vs. hydrated PFSA membranes within the ordinary PEFC temperature domain.

Incentive to change membrane chemistry could come mainly from higher temperature objectives

Best DMFC Performance obtained with Decal Method to Form Thin Film Catalyst Layer on Ionomeric Membrane

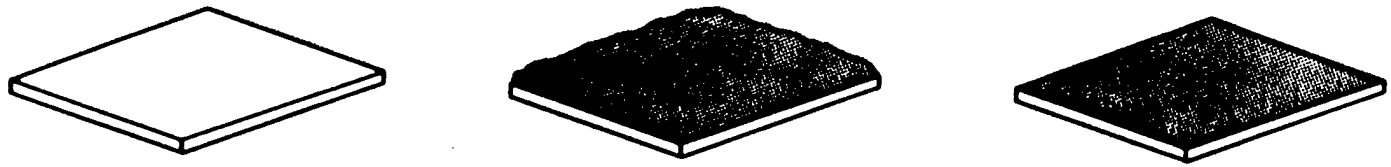

a) Teflon Blank → b) Painting Ink (Pt 92%, Nafion 8%) (Pt-Ru 85%, Nafion 15%) → c) Drying (120°C)

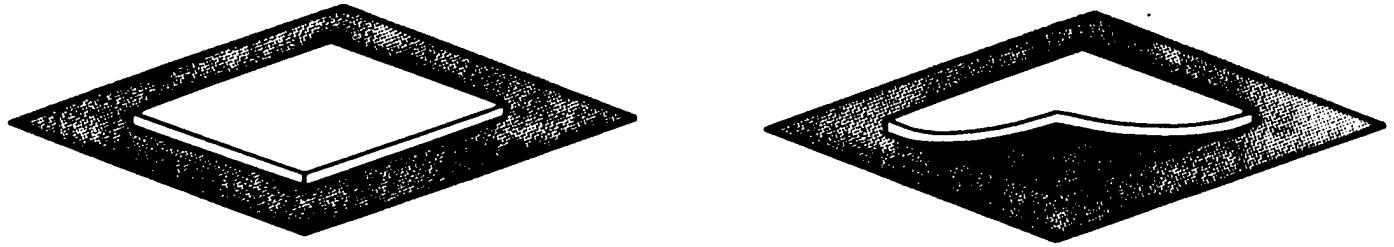

d) Hot-Pressing to Membrane (1200 pounds, 120°C) → e) Peeling Off Blank

Automated Printing of Catalyst on Membrane

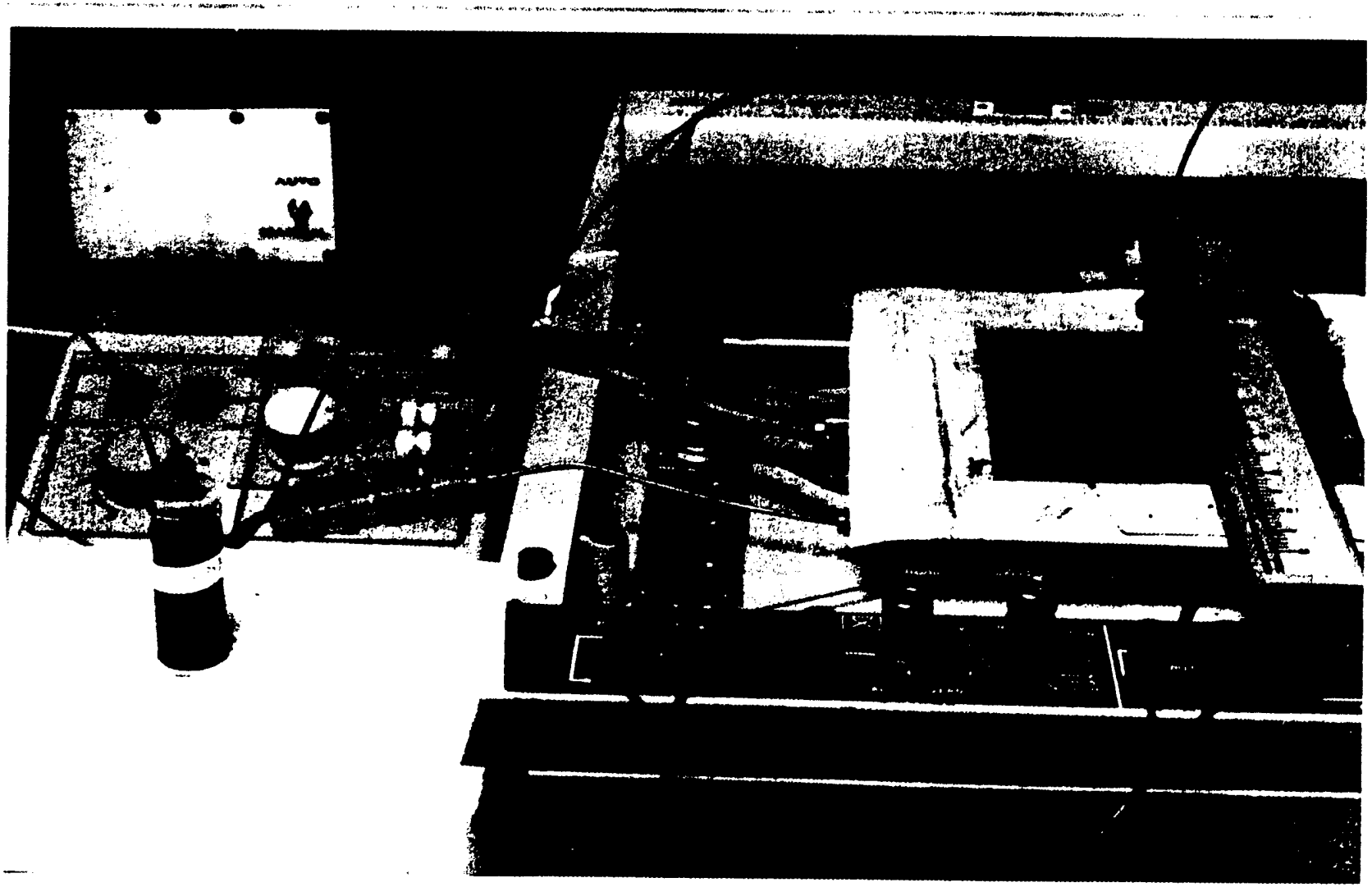

12.7mm
11.5mm

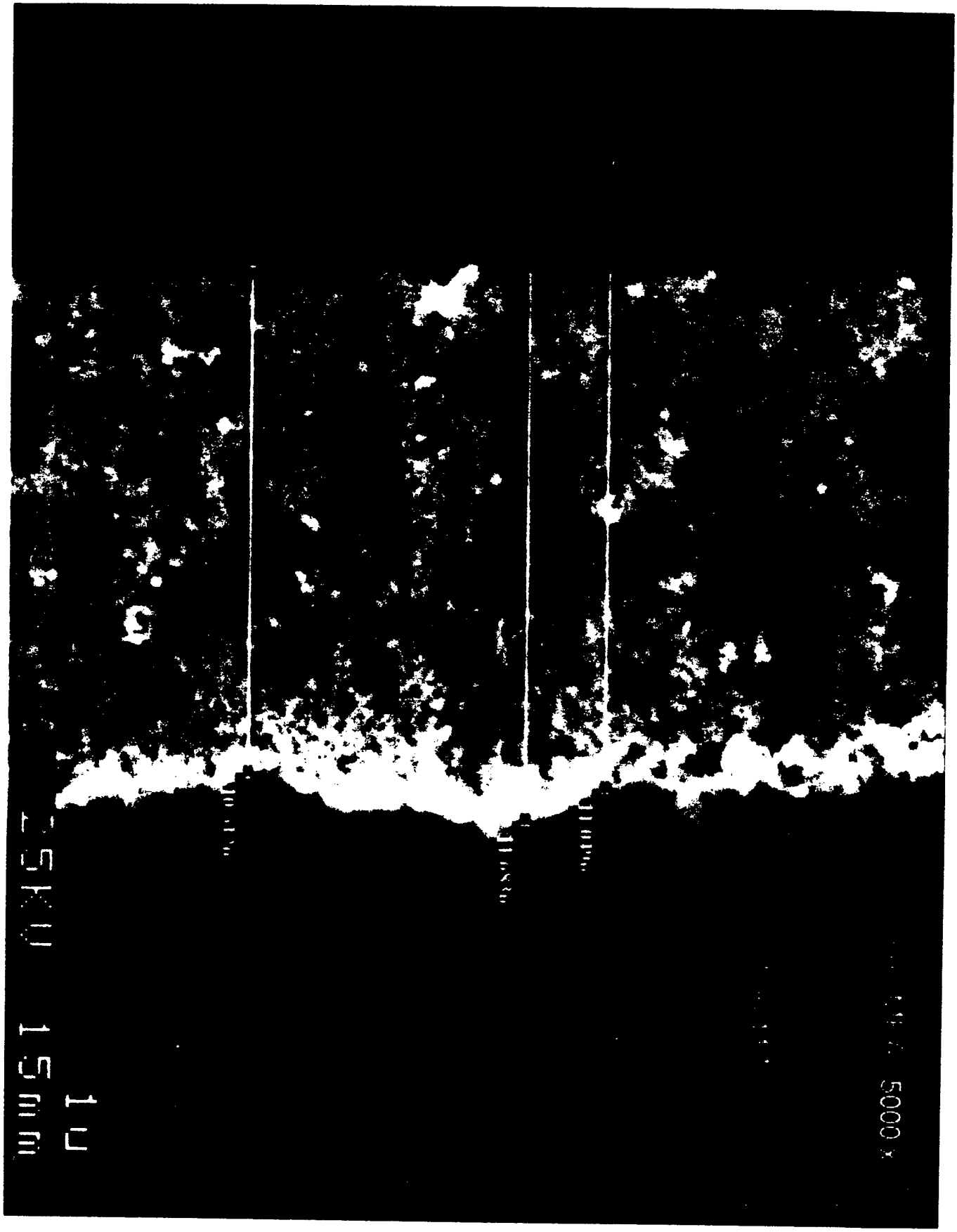
WD51 0457 15KV 15MM
10
X5000

Effect of Nafion Content on DMFC Anode Catalyst Activity: Catalyst A

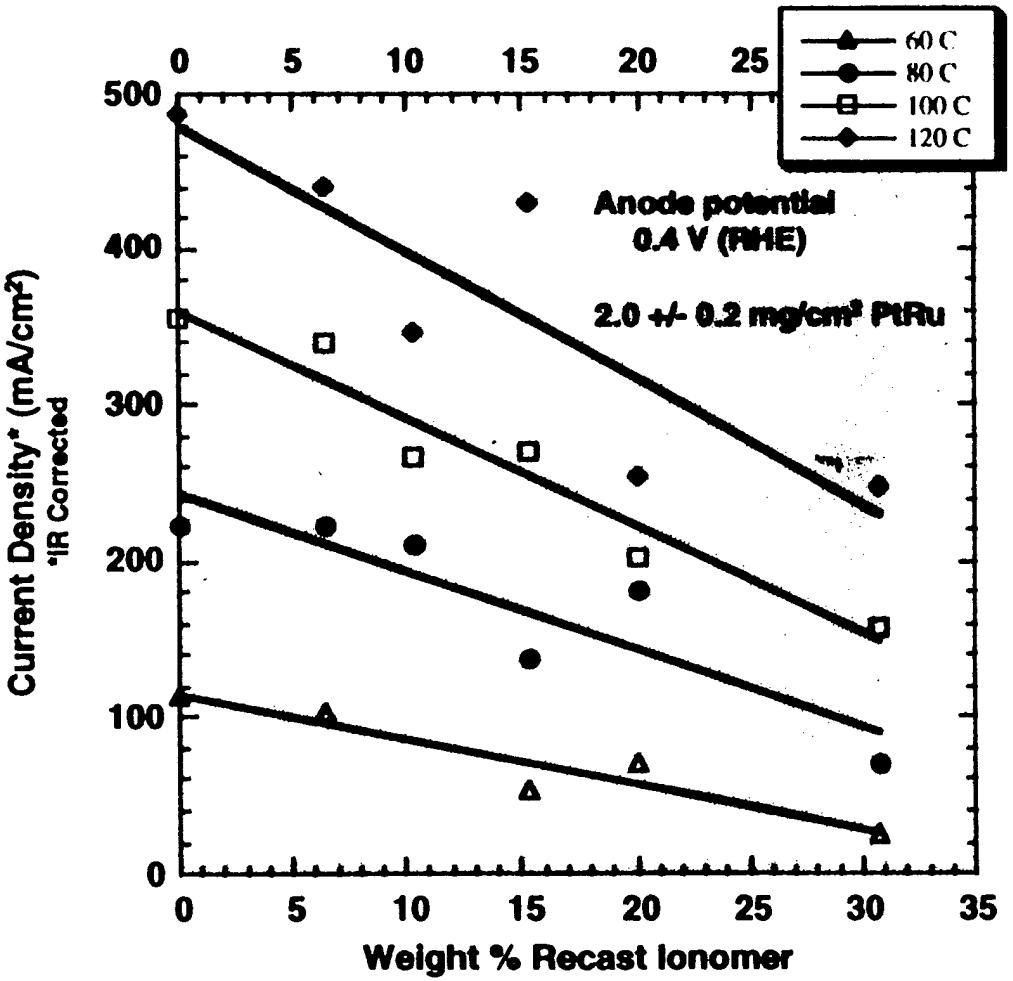

Anode: 1 M methanol at 2 ml min^{-1}, with 0, 0, 20, and 40 psi back pressures at cell temperatures of 60°C, 80°C, 100°C, and 120°C.

Cathode: H_2 at 300 ml min^{-1} and back pressure of 15 psi, humidified at 90°C, 105°C, 120°C, and 135°C.

Membrane Electrode Assemblies

Conclusions

(1) Reformate/Air PEFCs

MEA Fabrication:

* Several approaches are possible, including both wet and dry techniques.

* Optimization of catalyst layer preparation is function of PEFC application, *for example* : catalyst layers with enhanced transport properties are required for more dilute hydrogen feed streams containing impurities, vs. those required for operation on neat hydrogen.

* Optimization of catalyst layer preparation mode is sensitive function of nature of catalyst

Schematic of Various Regions Considered in Fuel Cell Modeling

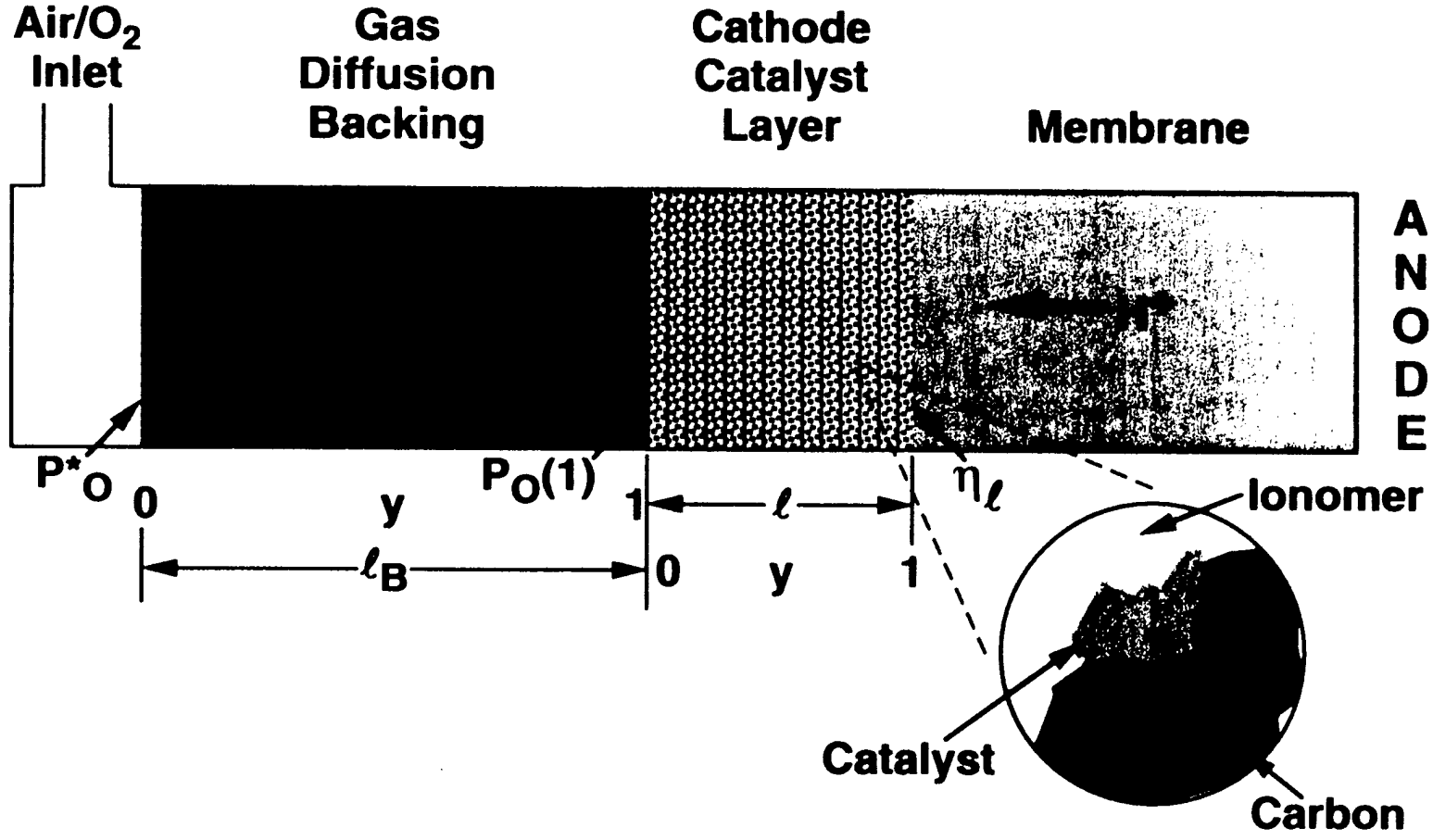

Simultaneous Fit to Four Polarization Curves for 5 cm^2 PEFC with 300 μm Backing Layer, 7.5 μm Catalyst Layer

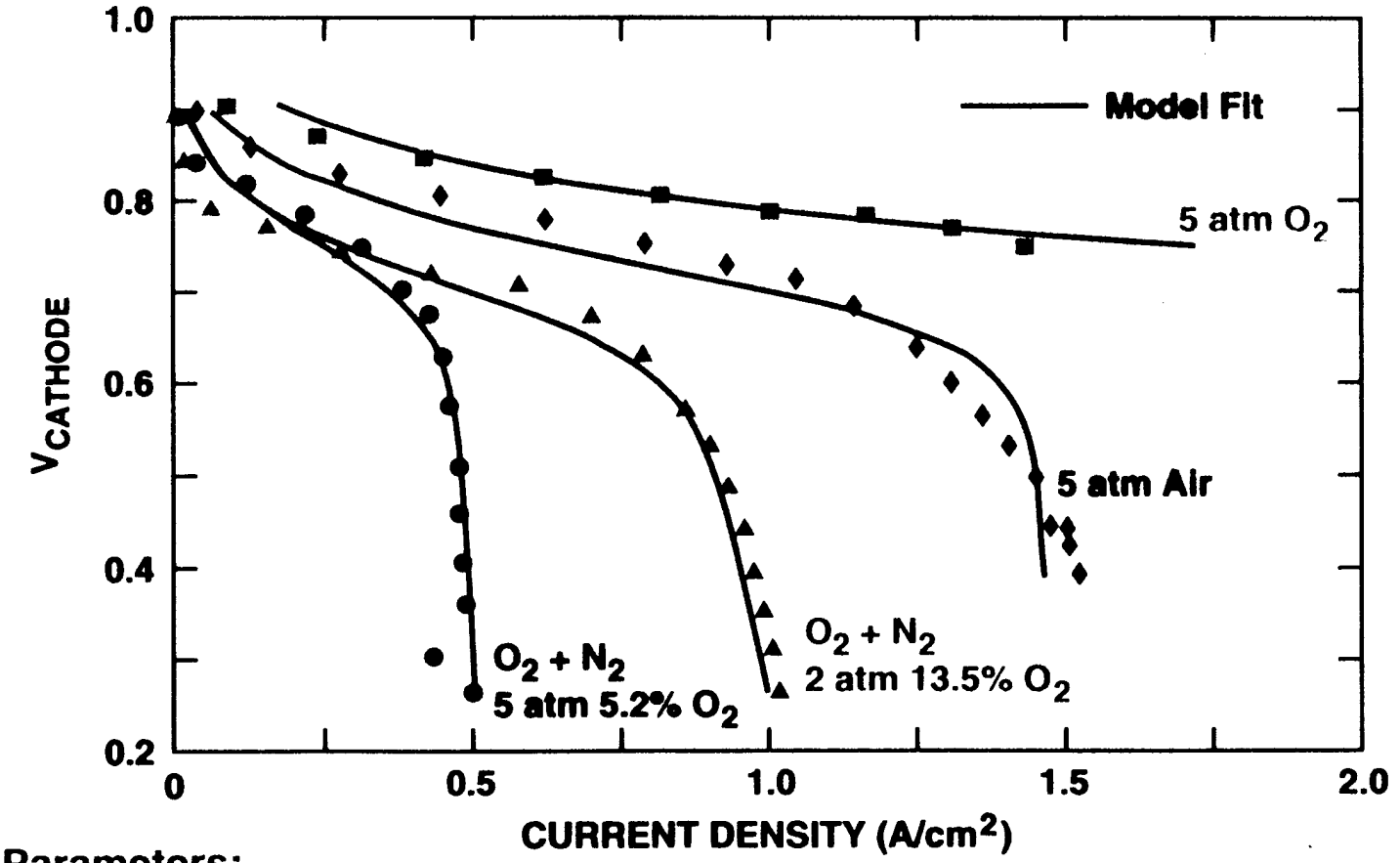

Fitted Parameters:

- Cathode catalytic activity @ 0.9 V: 90 mA/cm^2
- dV/dlogJ: 85 mV/decade
- σ = 0.0013 S/cm (protonic cond. in catalyst layer)
- DC* = 1.9 x 18^{-8} mol/cm-s-atm (gas perm. in catalyst layer)
- Backing porosity: 0.25 - 0.19 (assuming zero tortuosity)

Membrane Electrode Assemblies :

Catering for Fuels other than Pure Hydrogen

Impurity Tolerance in Hydrogen Rich Gas Mixtures

*Advanced Electrocatalysts

*MEAs operating at Higher Temperature

Direct Methanol Fuel Cells

* MEAs of Higher Fuel Efficiencies *and* High Performance

Generic Pattern of Polarization curve in Presence of CO\(Pt/C Anode Catalyst)

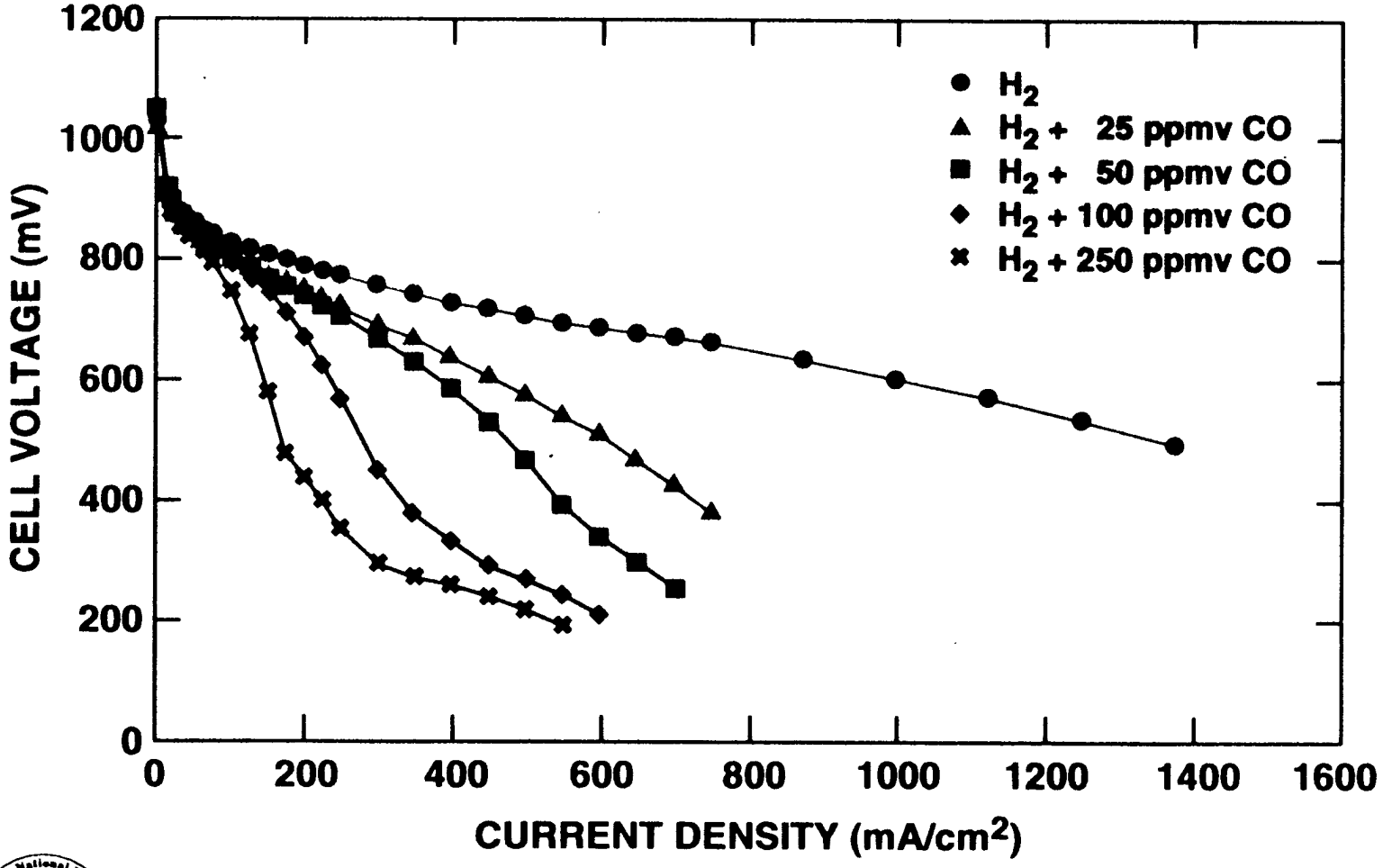

CO Tolerance in PEFCs: Full Tolerance to 100 ppm at 80°C with Air Bleeding

Reconfigured Anode enabled complete CO tolerance at 80°C
1% Air Bleeding, 0.6 mg/cm2 anode catalyst loading

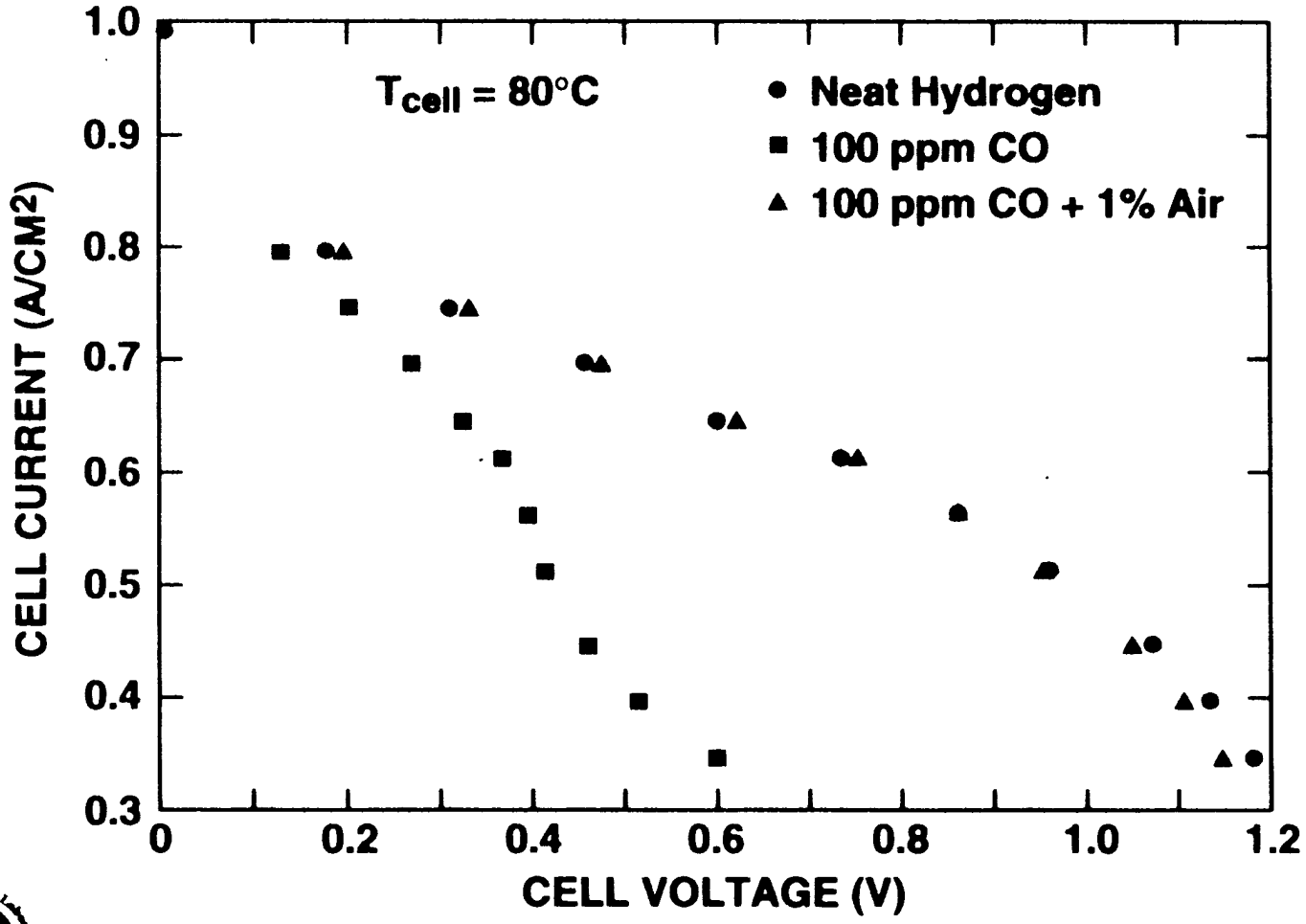

Tolerance to 100 ppm at 80°C: Life Test Demonstrates Viability of Air Bleed

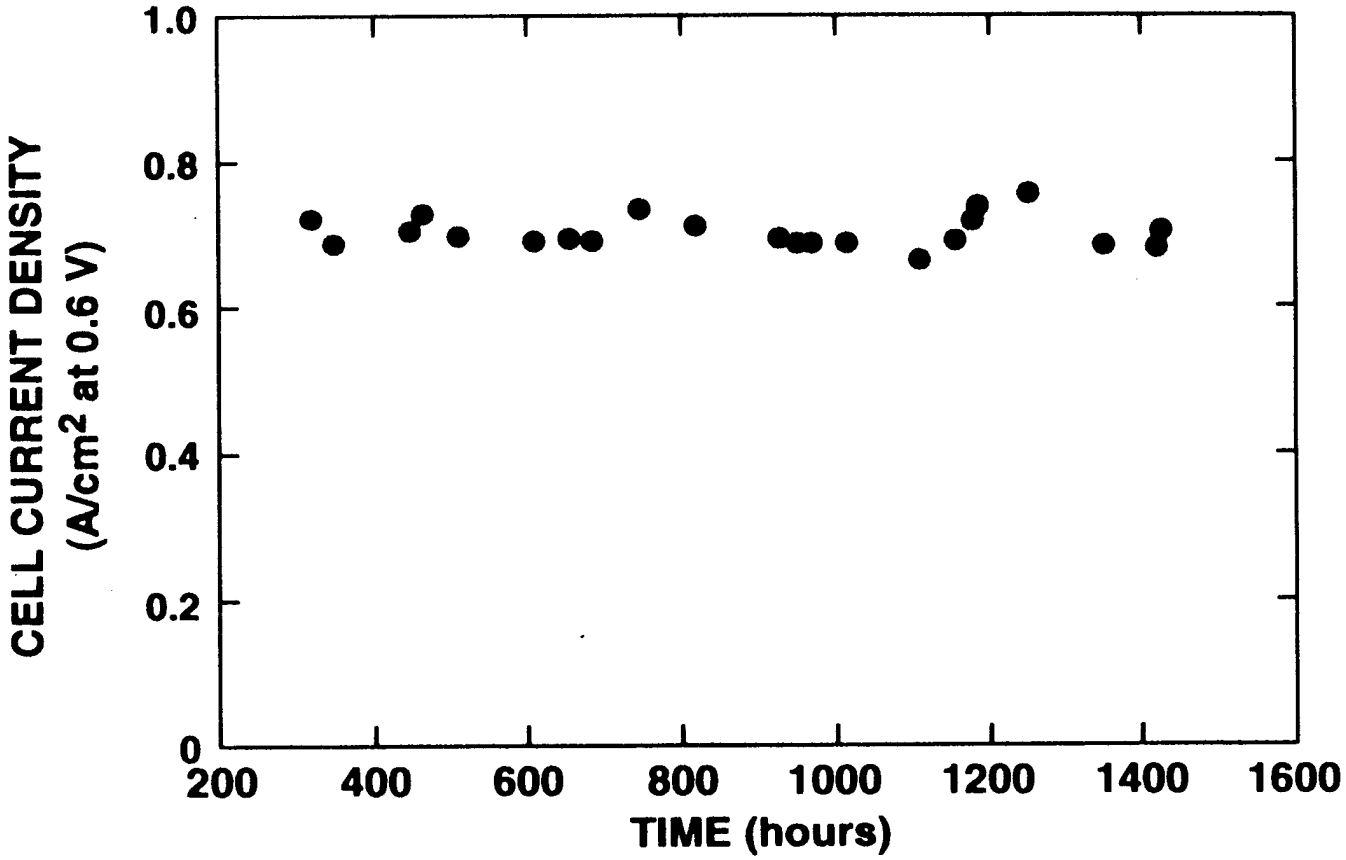

Life Test of Cell with Reconfigured Anode, 0.7 mg/cm^2 Precious Metal, Continuously Exposed to 100ppm CO

- **3% Air Bleed**
- **Last 1100 of 1400 Total Hours of Cell Life Shown**

CO Tolerance in PEFCs: Demonstration of Short TermTolerance to 1000 ppm C

- 120°C, 1.6 mg PtRu/cm^2
- Illustration of beneficial effects of higher cell operating temperature

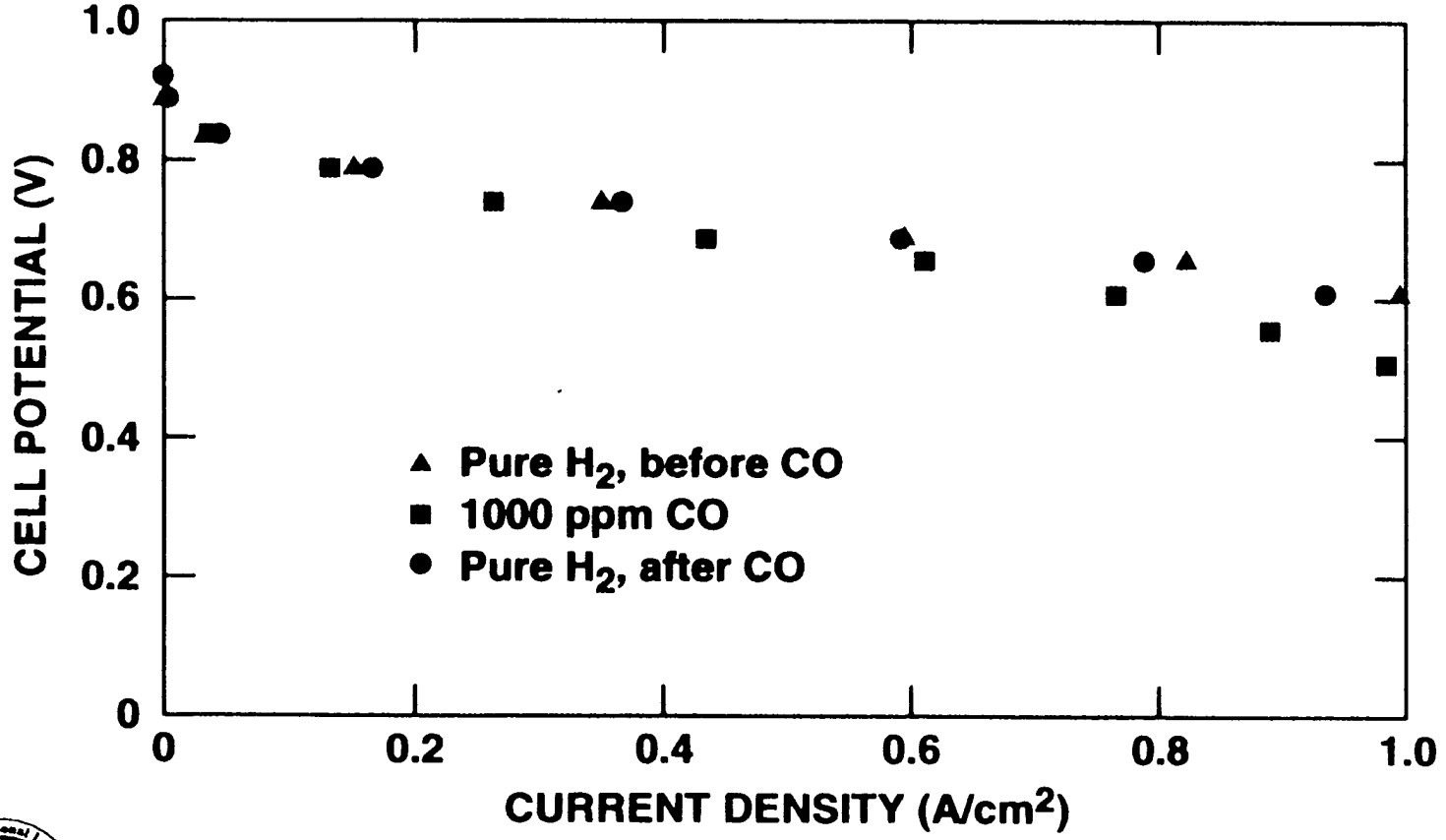

Electrocatalysis Model for PEFC Performance on Hydrogen containing CO at 100 ppm Level

(1) Adsorption and Electrochemical Reactivity at Pt Surface in Contact with Hydrogen/CO Mixtures

$$CO + Pt \underset{b_{fc}k_{fc}}{\overset{k_{fc}}{\rightleftharpoons}} (Pt - CO) \qquad [1]$$

$$H_2 + 2\,Pt \underset{b_{fh}k_{fh}}{\overset{k_{fh}}{\rightleftharpoons}} 2(Pt - H) \qquad [2]$$

$$(Pt - H) \xrightarrow{k_{eh}} H^+ + e^- + Pt \qquad [3]$$

$$H_2O + (Pt - CO) \xrightarrow{k_{ec}} Pt + CO_2 + 2H^+ + 2e^- \qquad [4]$$

Electrocatalysis Model for PEFC Performance on Hydrogen Containing CO at 100 ppm Level

Analytic Solution Found for Rate of Hydrogen Electrooxidation in presence of CO (Mathematica)

$$s_1 = k_{eh} \sinh\left(\frac{h}{b_h}\right)$$

$$a_1 = e^{\frac{h}{b_c}} k_{ec} + k_{fc}\,(b_{fc} + P_{co}),\quad a_2 = (e^{\frac{h}{b_c}} k_{ec} = b_{fc}k_{fc})^2,\quad a_3 = b_{fh}k_{fh} + 2s_1$$

$$j_h = \frac{2s_1\,(a_1\sqrt{a_2a_3k_{fh}P_h + a_1^2s_1^2} - a_1^2s_1 - a_2k_{fh}P_h)}{k_{fh}\,(b_{fh}a_1^2 - a_2P_h)} \qquad [8]$$

$$j_{co} = \frac{e^{\frac{h}{b_c}} k_{ec}k_{fc}P_{co}\,(a_1b_{fh}k_{fh} + a_1s_1 - \sqrt{a_2b_{fh}k_{fh}^2P_h + 2a_2k_{fh}P_hs_1 + a_1^2s_1^2})}{k_{fh}\,(b_{fh}a_1^2 - a_2P_h)} \qquad [9]$$

Base Case Parameters

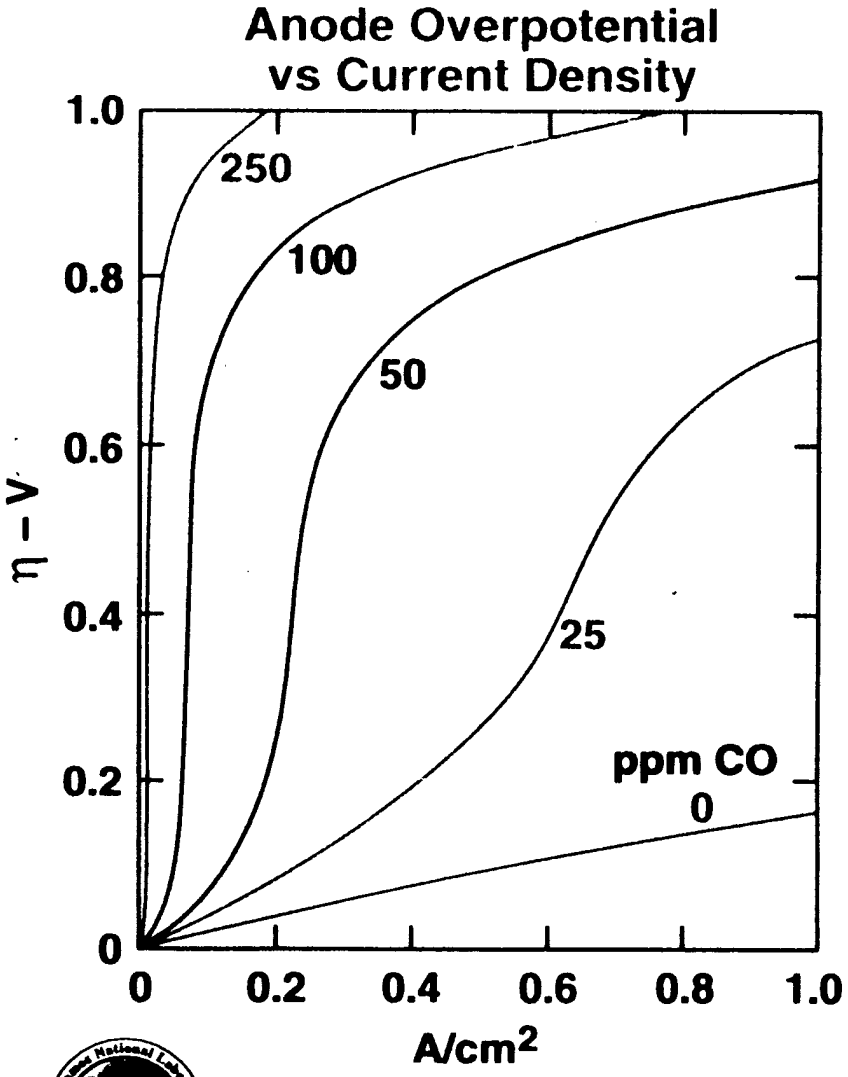

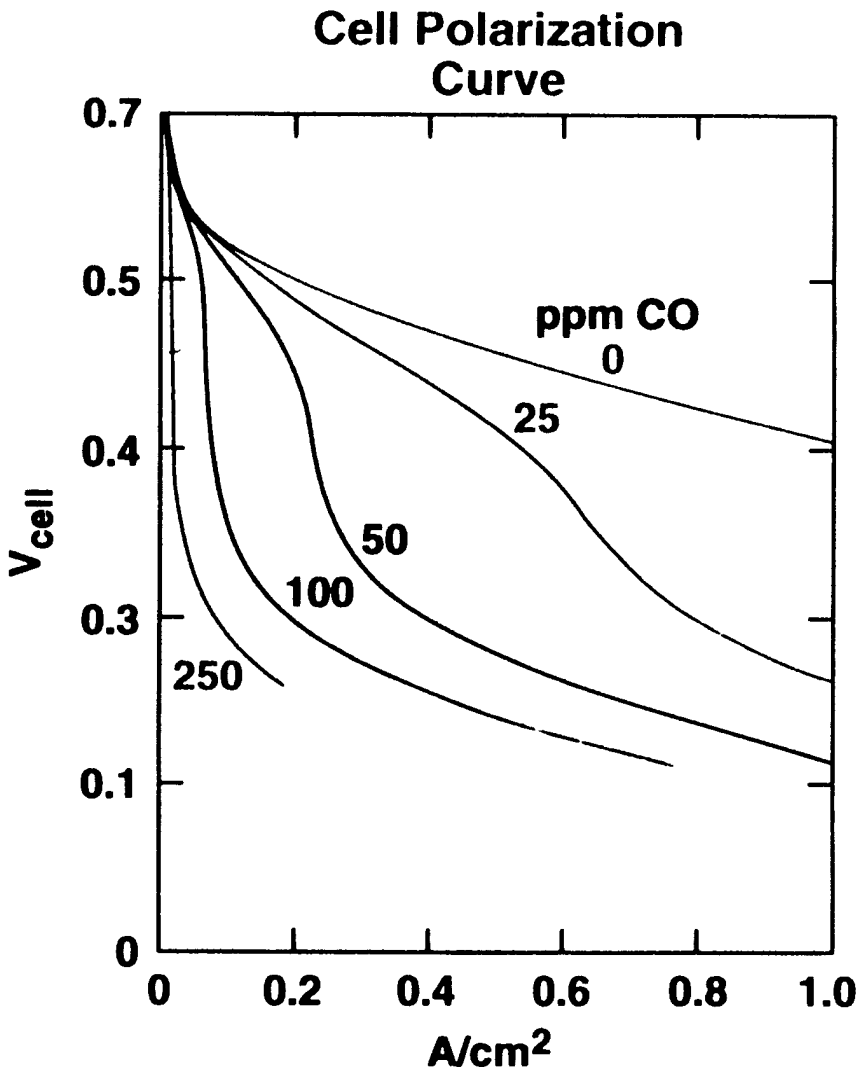

Electrocatalysis Model for PEFC Performance on Hydrogen containing CO at 100 ppm Level

Conclusions:

(b) Experimental

- **Raising cell temperature can achieve small but significant lowering in CO coverage through effect on equilibrium constant for CO adsorption. (This may be an important effect of Ru in the PtRu alloy catalyst).**

- **Very low CO electro-oxidation rates at 0.1 V could be sufficient, in principle, to achieve similar lowerings of CO steady state coverage. The CO electro-oxidation currents involved could be too low to be measurable, yet sufficient to have a significant beneficial effect.**

- **The most radical approach to eliminate effects of CO at a Pt catalyst at 80°C remains oxidative *removal of CO from the anode gas* by bleeding of air into the hydrogen feed stream.**

Membrane Electrode Assemblies

Conclusions

(1) Reformate/Air PEFCs

MEAs of Higher Impurity Tolerance:

* Other than PtRu, catalysts of higher CO tolerance may include other Pt-based binaries or ternaries, however: @ 80°C, air bleeding seems to be required to ensure long-term performance stability, even at 10 ppm CO

* Somewhat higher cell temperatures, e.g., 90 - 110 deg C, could provide signficantly better CO tolerance while maintaining humidified PFSA membranes

* Effective membrane for higher temperature operation, (150-200°C), is difficult to achieve because without water effective protonic conductivity is rare *and* electro-reduction of oxygen is sluggish

STRUCTURE OF THE PLATINUM/RUTHENIUM CATALYST FOR DMFC

G. Tremiliosi-Filho[†], H. Kim, and A. Wieckowski[*]

Department of Chemistry, University of Illinois, Urbana, IL 61801

ABSTRACT

The best anode catalyst in the direct oxidation methanol fuel cell (DMFC) consists of small platinum/ruthenium particles, either unsupported or supported on vulcanized carbon in contact with PEM membranes. However, figures of merit in heterogeneous catalysis demonstrate that the activity of this catalyst is far from desired. In search for higher activity we have combined a broad range of surface spectroscopies with electrochemistry for determining the details of surface structure and chemistry of platinum electrodes covered by controlled amounts of electrodeposited ruthenium. The focus is on establishing surface structure/reactivity relationships in methanol oxidation reaction on such well-defined catalytic surfaces, which is elaborated on in the report. This conclusion is that the most active phase of the Pt/Ru catalyst currently considered for use in the direct oxidation methanol fuel cell is Pt(111)/Ru. In contrast, Pt(100)/Ru is inactive, and Pt(110)/Ru and Pt(poly)/Ru are moderately active. Therefore, a structural optimization is needed to increase the representation of the (111) phase in the catalytic Pt/Ru materials at the expense of other surface phases. In order to investigate temperature effects in methanol oxidative reactivity, we have constructed Arrhenius plots for Pt(111)/Ru, Pt(100)/Ru and Pt(110)/Ru catalysts, and tabulated apparent activation energies from the plots. The data indicate that, again, the surface structure effect is the dominating effect in these activation energies, as well as in the Tafel slopes, see also: W. Chrzanowski and A. Wieckowski, *Langmuir*, 14, 1967 (1998). XPS spectra of ruthenium obtained by spontaneous deposition provide evidence that ruthenium oxides are present on the surface. After routine activation cycles, the reduced Ru deposit becomes catalytically active toward methanol oxidation. It is concluded that metal particle structure/crystallography should be considered as an effective variable in syntheses of more potent mixed metal catalysts for the DMFC use. With further efforts, this project may directly contribute to the development of small particle fuel cell catalysts having activity superior to the presently utilized catalysts.

I. INTRODUCTION

[†] permanent address: Instituto de Química de São Carlos/USP, 13560-970 - São Carlos, SP, Brazil

[*] author to whom correspondence should be sent

Of interest to the reported investigations is the backbone of methanol fuel cell catalysis, the anode catalysis, where the actual methanol oxidation occurs. As already well known, ruthenium[1-20] and, to a similar extent, osmium,[6,21-23] magnify the catalytic activity of platinum towards methanol which would otherwise be much lower due to surface poisoning by methanol oxidation side product(s). In this laboratory, we have investigated macroscopic single crystal surfaces covered by controlled amounts of ruthenium produced by electrodeposition[9] to simulate catalytic fuel cell behavior of individual crystal faces of nanoscale fuel cell catalysts.[1,10-14] Specifically in this report, the effect of ruthenium coverage (θ_{Ru}) on methanol oxidation current is investigated for four surfaces: Pt(111), Pt(100), Pt(110) and Pt(poly)[24] (see also: Refs. 25,26). The results of such structural studies, besides their basic science significance, may affect practical Pt/Ru electrocatalysis since surface crystallography of platinum/ruthenium particles can be adjusted through the particle size and thermal or electrochemical treatment[27,28] (and references therein). It is hoped that if the most catalytic crystal plane is identified using the *macroscopic* single crystal electrodes, the crystallographic adjustment of catalytic *nanoparticles* to the predetermined, high reactivity direction may add to the development of more potent catalysts.

Previously, we: (i) provided evidence for the spontaneous deposition of ruthenium on platinum[29], and determined the ruthenium coverage by the use of quantitative AES treatment under a variety of deposition conditions[30], (ii) showed that the spontaneously produced Ru deposits exhibited catalytic enhancement in the oxidation process,[30] (iii) analyzed surface structure effects in the voltammetric behavior of submonolayer amounts of ruthenium on the Pt(111)Ru, Pt(100)/Ru and Pt(110)/Ru surfaces in methanol containing solutions,[25] (iv) commented on the anion effect on the methanol oxidation rate on Pt/Ru surfaces,[25] and (v) identified the Pt(111)/Ru electrode as the best catalyst in the methanol oxidation process.[20,24,25] In parallel to our efforts, other investigators have produced scanning tunneling microscopy (STM) data about platinum single crystal electrodes covered by ruthenium.[31,32] These studies have demonstrated that in the coverage range of interest to this report, the ruthenium deposition process leads to formation of essentially two-dimensional, monoatomic islands of about 2-5 nm in diameter. This observation, together with the well-known result that ruthenium is inactive towards methanol at room temperature, and methanol creates CO on platinum easily, identifies the ruthenium island circumference as the site for methanol oxidation.

In this report, we will first examine *figures of merit* from heterogeneous catalysis in order to create a basis for referring the activity of fuel cell catalytic materials for DMFC to universal standards in catalytic activity for gas phase oxidation reactions. Following the FIGURES OF

MERIT and EXPERIMENTAL sections, we will demonstrate that the highest activity toward methanol is obtained with the Pt(111) surface covered by 0.20 monolayer (ML) of ruthenium, and comment on the extent to which such a Pt(111)/Ru catalyst outperforms the industrial Pt/Ru catalyst. Also, we will investigate the temperature effects involved in methanol oxidation on the low index Pt(hkl)/Ru electrodes. We will then focus on the issue: what is the nature of the "ruthenium enhancement"? Two mechanisms to account for such an enhancement have been proposed: a bifunctional mechanism, i.e., a ruthenium facilitated generation of oxygen-like species on the catalyst surface,[33,34] and a ligand-effect mechanism, i.e., the modification of electronic properties of platinum via a Pt/Ru orbital overlap.[9,17,35] To date, a clear-cut evidence to show which of these mechanisms accounts for the enhancement is not available. We believe that the data on the methanol oxidation reaction at Pt/Ru electrochemical interfaces collected in this report are adding meaningfully to the information previously obtained on these important mechanistic themes.

II. FIGURES OF MERIT IN HETEROGENEOUS CATALYSIS

The figure of merit for catalytic activity in heterogeneous catalysis and electrocatalysis is the turnover number (or turnover frequency) defined as the rate of the molecules converted per surface site per second.[36,37] In order to obtain turnover numbers (***tn***) from electric current densities (mA·cm^{-2}, per real surface area), it is convenient to use a simple formula[24]:

$$\boldsymbol{tn}\left(\frac{\text{molecules}}{\text{s}\cdot\text{site}}\right) = \frac{\text{i (mA}\cdot\text{cm}^{-2}) \cdot 6.02\times10^{20}}{\text{nF}\cdot1.3\times10^{15}} = 0.8\cdot\text{i (mA}\cdot\text{cm}^{-2}) \qquad (1)$$

since there is 1.3×10^{15} platinum sites per 1 cm^2 of the real platinum surface area, and n = 6, for methanol oxidation yielding CO_2. Therefore, provided that all sites are counted (which is the case when the real catalyst surface area is taken into consideration), a 1 mA·cm^{-2} current density roughly corresponds to a turnover number equal to 1 *tn* (in CH_3OH molec.·site^{-1}·s^{-1}). It is well known that for catalytic hydrogenation, dehydrogenation or cyclization of hydrocarbons, the turnover number vary from 10^{-4} to 100. It is also generally acknowledged that for oxidative heterogeneous catalysis, the turnover number should be in the range from 10 to 100, in order to make a given material an effective catalyst. How large, or small, are turnovers involved in the DMFC methanol oxidation reactions will be demonstrated in the RESULTS and DISCUSSION section.

III. EXPERIMENTAL

For methanol oxidation rate measurements, three platinum single crystals (of ca. 0.2 cm in diameter): Pt(111), Pt(110) and Pt(100), and polycrystalline platinum, Pt(poly), were used as templates for ruthenium adlayers. The crystals were flame annealed and cooled in argon/hydrogen atmosphere, as previously reported.[38-40] The real surface area of the electrodes was determined using hydrogen adsorption-desorption charges.[39,41] Before ruthenium electrodeposition, platinum surfaces were activated by several cyclic voltammograms (CV) at 50 $mV \cdot s^{-1}$ in the electrode potential range from 0.00 to 0.90 V vs. a reversible hydrogen electrode (RHE). Ruthenium adlayers to platinum at various coverage were deposited either by spontaneous deposition or by electrolysis.[24,29] After the deposition, the electrode was removed from the solution, rinsed with 0.1 M $HClO_4$ solution, "activated" by two voltammetric cycles in 0.1 M $HClO_4$ electrolyte[29], and transferred to the cell containing methanol solution (0.1 M $HClO_4$ + 0.6 M of CH_3OH). In the experiments with sulfuric acid/methanol solutions, the electrode was rinsed and "activated" in 0.1 M H_2SO_4 before transfer to solution of 0.1 M H_2SO_4 with 0.6 M of CH_3OH. Finally, methanol oxidation reaction was conducted using such prepared surfaces under mainly chronoamperometric conditions.

Once the Pt/Ru electrode was in the methanol containing solution, a single activating potential step was applied to the electrodes between 0.20 V and 0.87 V (vs. RHE). The waiting time at the low and high bias was 1 s. Immediately before recording the oxidation current, the electrode was potentiostated for 1 s at an electrode potential 40 mV more positive than the onset hydrogen evolution. The delay of 1 s was overwhelmingly sufficient to reduce remnants of adsorbed oxide/hydroxide on the surface formed at the upper potential, but short enough to avoid a noticeable methanolic CO formation. The chronoamperometric current for the methanol oxidation was measured between 0.2 and 0.4 V vs RHE for 30 min.

Design of the electrochemical cell in which methanol oxidation process is carried out was previously reported[42]. This cell had a built-in Luggin capillary and, after draining the methanol containing solution off, could easily be refilled with supporting electrolyte solution under an ultra-high purity argon blanket (argon purity was 99.999%). The auxiliary electrode was a platinum wire. A silver/silver chloride electrode in 0.1 M $HClO_4$ was used as a reference, but all potentials given in this paper were recalculated and are reported against RHE. Whenever needed, electrode potentials were corrected for the change in the reference electrode potential with temperature.

Auger Electron Spectroscopy (AES) was the primary characterization technique. The characterization was limited to Pt(111)/Ru, and it is believed that the data obtained with Pt(111) are representative to other surfaces examined. The Pt(111)/Ru surface was selected for the systematic analytical scrutiny because of its unique activity toward methanol.[20,24] The AES measurements were carried out at the primary beam energy of 3 keV using the combined ultra-high vacuum-electrochemistry (UHV-electrochemistry) instrument, Ref. 43, and references therein. Argon ion bombardment - oxygen annealing (at 800 °C) cycles were repeated until the appropriate order and cleanness of the Pt(111) surface (6 mm diameter, Aremco) were confirmed by Low Electron Energy Diffraction and AES. The clean and ordered Pt(111) sample was transferred, without exposure to air, to the system antechamber for electrochemical measurements using a conventional three-electrode, one-compartment cell[44].

Preliminary XPS spectra of ruthenium adlayers on Pt(111), obtained by spontaneous deposition, are also presented. Experiments were performed using an ESCA M-Probe system, manufactured by *Surface Science Instruments*, including a high-resolution multi-channel hemispherical electron analyzer (100 mm-radius) under constant pass energy of 25 eV. A monochromatic Al $K\alpha$ line ($h\nu$ = 1,486.6 eV) operating at 150 Watts was employed. The size of the incident X-ray beam was 800 μm. The Pt $4f_{7/2}$ line at 71.7 eV was used as an energy reference. As in the case of the AES measurements, neither the surfaces transferred from UHV to the electrochemical cell, nor those emersed from electrolytic media, were exposed to air before XPS characterization. Nonlinear least-square curve fitting and data analysis were carried out by the S-Probe version 1.36 ESCA software from *Fison Instruments*. Simulated spectra were produced from a mixed Gaussian-Lorentzian sum function[45,46] with Shirley-type baseline[47].

Chemicals were: Millipore water (18 MΩ×cm), perchloric and sulfuric acids double distilled from Vycor (GFS Chemicals), $RuCl_3 \cdot xH_2O$ and $Ru(NO)(NO_3)_3.xH_2O$ (Alfa Aesar) and ACS certified methanol (Fisher Scientific). The experiments were carried out at ambient temperature of 25 ± 1 °C, unless stated otherwise. A Haake model W10/C1 thermostat was used throughout the study. The electrode potential was controlled via a PAR 283 potentiostat interfaced to a PC. Data were collected by the use of HEADSTART (with our own setups) and M-270 programs (PAR-EG&G) and were processed using Sigma Plot (Jandel Scientific Software) on Gateway 2000, 486PC.

The reproducibility of cyclic voltammetric curves involving the Ru-covered surfaces was better than 5%. Integrated ruthenium deposition charges for a given electrolysis time displayed

the relative error of 2%. Ruthenium coverage data presented below were obtained out of the average of 3 points.

IV. RESULTS AND DISCUSSION

1. Surface characterization in UHV

The clean and ordered Pt(111) sample in ultra-high vacuum (see EXPERIMENTAL), was transferred to the electrochemical chamber for electrochemical deposition of ruthenium[48]. Spontaneous deposition of ruthenium[30] was carried out from $RuCl_3$ solution in 0.1 M $HClO_4$ (RuO^{2+}). A constant-potential potentiostatic ruthenium deposition (at 0.300 V[20,24,29]) was carried out either from $RuCl_3$ solution in 0.1 M $HClO_4$ (RuO^{2+}) or from $Ru(NO)(NO_3)_3$ solution in 0.5 M H_2SO_4. Deposition charges were collected and are presented as the charge vs. ruthenium coverage plots, with the coverage obtained from the Auger Electron Spectroscopy measurements.[24,25]

In Figure 1A, the AES peak at 274 eV, obtained after Pt(111) exposure to $RuCl_3$ solution (in 0.1 M $HClO_4$) for 2 min, is due to ruthenium spontaneously deposited on platinum. The peak increases by a factor of 2 when more concentrated solution (5×10^{-4} M $RuCl_3$ in 0.1 M $HClO_4$) are used (Figure 1B), and the coverage is: 0.12 ± 0.02 and 0.18 ± 0.03 ML from 5×10^{-5} M and 5×10^{-4} M solutions of $RuCl_3$, respectively. (The coverage in fractions of a monolayer, ML, is defined as the ratio of the number of ruthenium adatoms to the number of surface platinum atoms.) The AES spectra following the potentiostatic deposition are shown in Figures 1C and D.

Using the data such as those shown in Figures 1C and D, the AES coverage is plotted as a function of the deposition charge (Figures 2A and B). A straight line: AES coverage vs. charge is obtained. The contribution from the spontaneously deposited ruthenium when $RuCl_3$ is used appears as an intercept of the straight line (Figure 2A). At a threshold AES coverage of 0.2 and 0.3 ML, for $Ru(NO)(NO_3)_3$/0.5 M H_2SO_4 and $RuCl_3$/0.1 M $HClO_4$, respectively, the deviation from the straight line is found, indicating a significant drop in the electrolysis yield. This shows that ruthenium nucleates relatively fast and efficient at the electrolysis beginning, that is, on ruthenium free platinum, or on the surface sparsely populated by ruthenium, but the nucleation slows down at the higher coverage. This behavior can, in part, be related to the presence of ruthenium oxides in the spontaneous deposit, and to the difficulty in the Ru layer growth on a Ru/RuO_x covered electrode. In contrast, no spontaneous deposition of ruthenium was found when $Ru(NO)(NO_3)_3$ solution was used (Figure 2B), indicating a high stability of the Ru(III) nitrosyl complex precursor. Notably, previous Auger electron data provide evidence that

the destruction of the $Ru(NO)(NO_3)_3$ solution complex on the surface is complete, since no nitrogen is found by AES.[24,25]

Ruthenium deposits can also be added to platinum by the use of cyclic voltammetry[49]. The results of such a procedure are demonstrated in Figure 3, presenting graphical relationships between the Ru-coverage (obtained by AES) and the number of depositing cycles. The cycles were taken in the electrode potentials range from 0.00 to 0.88 V, in both $RuCl_3/HClO_4$ and $Ru(NO)(NO_3)_3/H_2SO_4$ solutions (see Figure 3 captions). Apparent is the same tendency of saturation in the amount of Ru uptake with the duration of the electrolysis, as discussed above for the potentiostatic ruthenium deposition. After a couple of cycles, the coverage as high as ca. 0.4 ML is obtained. This coverage is higher than that obtained under constant potential electrolysis conditions at 0.300 V, and at a comparable experiment time. This is as expected since upon the voltammetric treatment, the electrode is scanned through potentials more negative than 0.300 V, and ruthenium deposition process is facilitated. Indeed, if more negative potentials than 0.300 V are used for the potentiostatic depositions, higher ruthenium coverages are obtained on the same timescales as applied for the 0.300 V electrolysis. We therefore conclude that both potentiostatic[18,32] and voltammetric deposition[17,50] can be used for obtaining ruthenated platinum surfaces at any coverage desired, and in the both cases the Auger Electron Spectroscopy method provides quantitative Ru coverage data.

2. XPS of ruthenium adlayer obtained by spontaneous deposition

Ruthenium adlayers on Pt(111), obtained by spontaneous deposition of ruthenium from $RuCl_3$ solution in $HClO_4$, were analyzed using X-ray Photoelectron Spectroscopy with the goal to evaluate the extent of adlayer oxidation. Such an oxidation of ruthenium adlayers was concluded in our earlier electrochemical study discussing deposition of ruthenium on platinum single crystal electrodes[20]. Despite the overlap with the C *1s* band, the Ru *3d* band was chosen for analysis based on its intensity and the larger amount of reference data for this region. A Ru *3d* photoelectron spectrum representative of the Ru/Pt(111) system – with ruthenium obtained by spontaneous deposition -- is shown in Figure 4. Peak fitting of the Ru *3d* region reveals three spin-orbit split doublets, easily distinguishable from the C *1s* band. The $Ru3d_{5/2}$ feature at 281.3 eV shows that the surface is indeed oxidized[20], since metallic ruthenium would be indicated by spin-orbit features at 280.0 eV (Ru $3d_{5/2}$) and at 284.1 eV (Ru $3d_{3/2}$)[51-56]. The best fit for the Ru *3d* band was obtained by assuming that Ru^{3+} was the main oxidation state and the main component of the spectrum. Two other ruthenium oxidation states at 282.0 eV and 284.5

eV, Ru^{2+} and Ru^{6+}, were also identified. The platinum binding energy was stable and always indicated the metallic form. A more complete analysis of the XPS data will be given elsewhere.

3. Voltammetry at 50 $V \cdot s^{-1}$

In order to have an on-line control of the CO formation process when methanol decomposition proceeds, the oxidation experiments, carried out under chronoamperometric conditions with Pt(111) and Pt(111)/Ru electrodes, were combined with fast cyclic voltammetric sweeps.[57] When sufficiently high sweeps are used, Figure 5A (dashed line), for instance, 50 $V \cdot s^{-1}$, cyclic voltammograms in 0.6 M MeOH in 0.1 M $HClO_4$ solution indicate a CO free surface. (The degree of hydrogen adsorption/desorption modification due to MeOH presence in solution is found negligible vs. that in 0.1 M $HClO_4$ without methanol). As previously reported for clean platinum[57] (see also: Ref. 58), the peak at 0.6 V is due to bulk methanol oxidation leading to CO_2 formation. After the constant potential experiment is carried out for 10 min at 0.310 V in the MeOH containing solution, during which CO accumulates on the surface and is coadsorbed with ruthenium (as ruthenium islands[31,32]), a different curve is recorded, Figure 5A (solid line). Namely, a peak with the maximum at 0.8 V is found, and is assignable to CO stripping process.

The charge under the stripping peak (at 0.8 V) for clean Pt(111), and Pt(111)/Ru surfaces for three adsorption times: 1s, 10s and 10 min, are compared in Table 1. It is seen that there is no statistically significant difference in the oxidation charge between Pt(111) and Pt(111)/Ru. There is no any significant difference either in the oxidation charge when the oxidation time was varied from 1s to 10 min (except for the lowest electrode potential for Pt(111)/Ru), and the data for 10 and 30 min are very similar (not shown). For the discussion of the data, it is assumed that under the reported conditions, the chemisorbed CO is the sole methanol decomposition product, and that bulk methanol oxidation does not contribute to the CO stripping charge. While there are no reason why not to accept the first assumption, the second may not be strictly correct. However, if there is a contribution of bulk MeOH oxidation to the 0.8 V peak charge, it is probably a small constant term that may, for the sake of the current discussion, be ignored.

The results shown in Table 1 demonstrate that under the experimental conditions referred to above, a 0.5 ML of CO is formed (it is lower somewhat at 0.55 V, indicating the beginning of an accelerated CO oxidation from the surface). It is noticebly higher than obtained on Pt(111) after cell rinsing and a slow potential scan CO stripping into a clean electrolyte[59]. This behavior needs to be investigated more thoroughly, at present it may show a

presence of a weakly adsorbed methanol decomposition product, coadsorbed with surface CO, that does not survive the electrolyte exchange.

Why adding 20% of ruthenium to the surface is not changing the CO coverage may also deserve a more closer look (Table 1). For the present discussion it is important to point out that the drop in current by a factor of 3.3 between the 1s and 10 min experiment (Figure 5B, inset) is not associated with a meaningful uptake increase in CO. Evidently, the drop is due to an internal rearrangement in the Pt(111)-Ru-CO mixed adlattice removing active sites, such as, for instance, Ru islands coalescence as a function of the two-dimensional CO surface pressure. This is a stimulating observation that will be addressed by future research. On the other hand, the drop in the oxidation current at the experiment beginning, that is, on the millisecond timescale (Figure 5B), is associated with methanol decomposition/CO poisoning processes on clean platinum sites, as reported previously[38,39].

4. Methanol oxidation current under chronoamperometric conditions

Using chronoamperometric measurements of methanol oxidation on the Pt(hkl)/Ru surfaces[20], a ruthenium coverage corresponding to the maximum methanol oxidation rate was found for each surface. Such an "optimized coverage" was 0.20, 0.15 and 0.30 ML for Pt(111), Pt(110) and Pt(100), respectively. All data presented below were obtained with the coverage-optimized, Pt(hkl)/Ru surfaces.

Representative, high-temperature current density data for methanol oxidation as a function of reaction time, at 65 °C and 0.310 V for Pt(100)/Ru, Pt(110)/Ru and Pt(111)/Ru, are shown in Figure 6 (in 0.1 M H_2SO_4/0.6 M CH_3OH). The electrode potential, E = 0.310 V, was selected for this research since this is an ideal "fuel cell potential" which may be chosen to operate the direct oxidation methanol fuel cell (DMFC) devices[14]. As shown in Figure 6, see also: Ref. 20, the rate of the current decay is very low at longer times, indicating that *pseudo steady-state* kinetic conditions were obtained. It is also shown that the rate of current decay, and the values of the current densities measured at 30 min, are surface structure sensitive. In particular, the 30 min current is the smallest for Pt(100)/Ru and the highest for Pt(111)/Ru.

Arrhenius plots (straight lines, not shown) were taken for the three low index Pt surfaces covered by ruthenium in the temperature range from 0 to 65 °C, and the apparent activation energies were measured at 0.250, 0.310 and 0.370 V (Table 2), Ref. 42. The data indicate that there is a weak dependence of the activation energy on the electrode potential, and on the type of the deposit precursor. The effect by the surface structure of a Pt(hkl) substrate is, however, quite significant, and doubles in the most extreme case: at E = 0.250 V, from 38 $kJ \cdot mol^{-1}$ for

Pt(110)/Ru to 84 kJ·mol^{-1} for Pt(111)/Ru, Table 2. Even if the values averaged over the potentials are used, 45 kJ·mol^{-1} for Pt(110)/Ru and 69 kJ·mol^{-1} for Pt(111)/Ru, the effect is still quite pronounced. Notably, it shows that the temperature rise is the most beneficial for methanol oxidation catalysis at the Pt(111)/Ru surface. The activation energy values obtained from this series compare favorably with the previous, already published values from this laboratory[20], 72, 65, and 50 kJ/mol, for 0.25 V, 0.31 V, and 0.49 V, respectively. Moreover, the average activation energy value thorough the three potentials is 58 kJ·mol^{-1}, a near perfect replicate of the value obtained by Markovic et al. (60 kJ·mol^{-1}) under similar experimental conditions to ours, but with polycrystalline Pt/Ru alloys; with the Pt : Ru ratio also optimized to the highest methanol reactivity[34].

At room temperature, the (formal) Tafel slopes, d(logi)/dE, can be compared with the previous data in the electrode potential range examined in this paper, from 0.250 to 0.370 V (Figure 7). All Tafel slopes are distributed around 60 mV·dec^{-1}, in an excellent agreement with the results of the previous study.[20] It is essential to recall that for Pt(100)/Ru and Pt(110)/Ru (and for polycrystalline Pt/Ru), the formal Tafel slope of 60 millivolts per decade extends over a broad electrode potential range. In contrast, the linearity with Pt(111)/Ru breaks at around 0.30 V to give two slopes: a 60 mV·dec^{-1} between 0.220 - 0.310 V and ca. 200 mV·dec^{-1}, between 0. 310 - 0.490 V (Figure 7). The fact that one Tafel slope is found for Pt(100)/Ru, Pt(110)/Ru and polycrystalline Pt/Ru, and two slopes for Pt(111)/Ru, underscores a major mechanistic difference in the methanol oxidation process between these two specific sets of surface structures. Also it is important to indicate that the Tafel slopes do not have an usual quantitative meaning assigned to them by the Butler-Volmer formalism. This is because the Pt/Ru surface does not make a stable electrode, its composition changes as a function of the electrode potential, definitely in terms of the ruthenium oxidation state and also, most likely, in terms of surface morphology (in response to the ruthenium valency change). Therefore, only the <u>difference</u> in the Tafel slopes can be put forward and interpreted within the realm of the surface structure effects in methanol oxidative catalysis on the Pt/Ru electrodes, but still in a very phenomenological manner.

Overall, as shown in Figure 8 for 25 and 65 °C, the currents measured at 30 min (*the pseudo steady-state currents*[20]) at Pt(111)/Ru are by 2 orders of magnitude higher than those at Pt(100)/Ru. They are also by ca. one order of magnitude, higher than with Pt(110)/Ru and with polycrystalline Pt(poly)/Ru. The diagrams are comprehensive enough to demonstrate simultaneously the effect of substrate surface crystallography and the change in solution anion

from perchlorate to bisulfate. Clearly, the anion effect is minor compared with the surface structure effect. From the practical perspective, we conclude that the most active phase of the catalysts currently considered for use in the direct oxidation methanol fuel cell is Pt(111)/Ru, and that the Pt(100)/Ru phase is inactive. Structural optimization of catalytic Pt/Ru materials is needed to increase the representation of the (111) phase at the expense of other surface phases in these industrial materials.

At room temperature[20], typical numerical data obtained are demonstrated in Table 3. The value of the electrode potential E = 370 mV is chosen since at 370 mV, all the tendencies observed at other potentials are well represented. The r*uthenium enhancement* term is defined as the ratio of the current density corresponding to methanol oxidation with and without ruthenium on the surface.[20,25] Above 1 s, all Ru covered Pt single crystal surfaces, and the polycrystalline Pt/Ru surface, are more active than the clean Pt catalyst. The enhancement is very large at the experiment end, approaching infinity at 30 min, since clean Pt(111) at 370 mV is incapable of producing any measurable oxidation current due to the CO poisoning.[39] Finally, data in Table 4 show that in each of the demonstrated examples more than a monolayer of methanol reacted to CO_2 in 30 min (e.g., 4 and 377 monolayers for 250 and 490 mV, respectively), and that the rate of the current decay (2nd column of Table 4) is electrode potential dependent.

5. Polarization curves and turnover considerations

Applied opportunities to be derived from our structural observations have been pointed out above and in Refs. 20,24 In order to highlight the advantage of conducting methanol oxidation reactions on preoriented Pt/Ru catalysts toward the Pt(111)/Ru plane, we have measured the polarization curve: electrode potential readings at fixed currents, all at 30 min, and compared the polarization curve with data in literature (Figure 9). We have examined Hogarth and Hards' reactivity data[60] for a catalyst prepared from 20 wt. % platinum-10 wt. % ruthenium (Type II) supported on carbon black, comprising a soluble form of the polymer electrolyte, bound as a thin layer between a Nafion®-117 membrane and the current collecting substrate. These data,[60] obtained at 80°C, are given not in terms of the current density per catalyst load (or per apparent surface area), as usually done in fuel cell literature, but in terms of current density standardized to the real surface area. Only such data, as directly proportional to reaction turnovers, see below, have an objective meaning on the reactivity scale in heterogeneous catalysis.

Using the equation 1 in the FIGURES OF MERIT section, the quasi steady-state current densities in Figure 9 (at 30 min) were converted to turnover numbers (see the top axis in Figure 9). The data in Figure 9 show that at 0.310 V the turnover for the Pt(111)/Ru catalyst for 65 °C is already higher by a factor of 2 than that of the industrial catalyst at 80 °C. When this advantage is multiplied by the activation energy term ratio between 65 and 80 °C, we obtain an overall advantage close to one order of magnitude vs. the industrial Pt/Ru catalysts [20,24], and a reaction turnover approaching 1 *tn.*[20,24] We may therefore conclude that at 80 °C, the crystallographically optimized, Pt(111)/Ru catalyst has the activity that is higher than that extrapolated from the industrial data but still lower than the expected performance level in heterogeneous catalyst for oxidation reactions (turnover = 10 *tn*). Nevertheless, the attempts to morphologically optimize the catalytic materials dedicated to DMFC fuel cell systems have a strong practical merit. Realistically however, to fulfill the demands by the advanced reactivity criteria from heterogeneous catalysis, yet another order of magnitude improvement should be sought via further, DMFC-oriented research in electrochemistry and surface science.

6. Mechanisms involved in enhanced methanol oxidation on Pt/Ru electrodes

Enhanced methanol oxidation on Pt/Ru electrodes is a typical case of a heterogeneous catalytic reaction occurring in an electrochemical cell. Such catalytic reactions involve a chemical activation and excitations of multielectron systems at a metal surface, and are very complex.[61-63] It is therefore difficult to define an universal response function to determine the activity of the metal surface vs. the incoming reactants. Nevertheless, the electronic distribution at the surface, adapting to the change in the relaxation or reconstruction on both clean and adsorbate-covered surfaces, and to the atomic scale structural diversity, like terraces, steps, and kinks, is underlying all surface events of interest to heterogeneous catalysis[64]. As shown recently, local, Fermi level densities of states (E_f-LDOS) epitomize the catalytic activity of metal surfaces quite effectively[62,64-66]. Whether indeed this is the most appropriate and universal surface reactivity qualifier will become more evident in further research. Nuclear magnetic resonance (NMR-electrochemistry) strategy was unveiled in this laboratory to address such issues quantitatively[67]. Before such NMR data become interpreted on the quantitative level, individual classes of reactions involved in heterogeneous electrocatalysis need to be dealt with separately.

In view of the above, a pertinent question in enhanced methanol oxidation on Pt/Ru electrodes is what is the active site? The key finding here (see also: Refs. 20 and 24) is that

the most active catalyst in the oxidation process in acidic media is Pt(111)/Ru. As we have already indicated before, the (111) site on a fcc cubic surface is not a typical "active site" since it is generally known that structurally defected, or rough (stepped, kinked) surfaces[63] are better candidates for effective catalysis. The advantage in the reactivity on rough surfaces results from the decrease in work function, and a concomitant increase in the electron density in the region outside the metal surface, which occurs when terrace-like surfaces are perturbed by defects[62b,66,68,69]. Notably, since the electronic tail outside the surfaces comprises mainly electrons at the Fermi energy level[66], the spill-over argument is not in disagreement with conclusions from the "frontier orbital" picture[70], postulating that the reactivity enhancement at metal surfaces results from weakening the molecular bonds of the reactants via filling electrons into their anti-bonding orbitals. The purely electronic effects usually dominate over a yet another effect characteristic of imperfect surface, namely, the higher heat of chemisorption (bond energy, see below) which increases the adsorbate residence times[71], and reduces catalytic reaction rates. Specifically however, the enhanced stability of surface oxygen on Pt(111)/Ru surfaces at low potentials has a yet another beneficial effect in methanol oxidation, as already discussed in Refs. 24 and 29.

Phenomenologically, without invoking the electronic arguments, a bimolecular reaction between surface CO and RuO_x leading to CO_2 and electrons formation, can occur faster on a smooth surface rather than on a stepped surface, because of several factors[24]: (i) less "O_x" chemisorption on Pt/Ru terraces increasing the "oxygen" site-to-site mobility and reactivity, (ii) smaller CO bonding energy, or heat of CO adsorption (as the magnitude proportional to the Pt-CO bond energy[72-74]), on Pt(111) than on Pt(110) and even more so, on Pt(100)[42] and, possibly, (iii) the more favorable active site geometry allowing surface oxygen (O_x) to be closer to CO. The latter would facilitate the surface activation state formation. Notably, the data in this article indicate that the steady-state oxidation of methanolic CO occurs on the surface crowded by high-coverage carbon monoxide and ruthenium. This adds a new credibility to the bifunctional mechanism of the enhanced methanol oxidation on Pt/Ru electrodes (Ref. 33, see INTRODUCTION) since: (i) CO and RuO_x are close together facilitating the oxygen transfer without the need for a long-range surface diffusion, (ii) not too many "clean" Pt sites exist to be available to activate water as the CO oxidant, all are probably engaged in CO chemisorption and Ru deposition, (iii) and the option for CO to use bulk water on its way to CO_2 seems unlikely. The fact that we deal with a crowded surface also explains the lack of the anion effect in the reactivity, in a clear contrast to the data on methanol oxidation on clean platinum electrodes[39]. However, what would not be contradictory to the essence of this mechanism is

that "oxygen" shared between Pt and Ru site is transferred to CO, rather than "oxygen" specifically associated with Ru. It is neither contradictory to assume that such an oxygen is transferred to an electronically modified Pt-CO site due to the ruthenium (or ruthenium oxide) addition. Ruthenium, for instance, may perturb platinum electron polarizabilities and orbital symmetries, thus affecting the orbital spatial distribution and the reaction rate[75].

The above conclusions do not contradict the electronic (ligand) mechanism, understood as the modification of electronic properties of platinum via a Pt/Ru orbital overlap as a component of the overall mechanistic considerations. Theory strongly suggests that the formation of an alloy and its interaction with oxygen significantly affects the local density of states around each of the individual metal site[76,77]. Synchrotron X-ray Absorption Spectroscopy data[78] under *in situ* conditions, have demonstrated that alloying platinum with ruthenium increases Pt *d* band vacancies and decreases the Pt-Pt bond distance and, indirectly, the infrared data with carbon monoxide may be interpreted to demonstrate a higher availability of the antibonding $2\pi^*$ electrons on Pt/Ru than on clean Pt[32]. In fact, from the above discussion we believe that Pt/Ru catalytic enhancement may be explained in terms of both electronic and bifunctional effects. Such a complete mechanism would support a dual role of ruthenium in attracting oxygen to the catalytic surface at ca. 0.30 V more negative potentials than without Ru[34] and, simultaneously, in affecting the electron density on the neighboring Pt site to make adsorbed CO more susceptible to the oxygen attack. Since the discrimination between these two mechanistic pathways, or ranking the significance of their contribution is not, at present possible, more research is needed to address these issues both theoretically and experimentally.

V. CONCLUSIONS

We have demonstrated that methanol oxidation is remarkably sensitive to the Pt/Ru electrode surface structure. The highest oxidation rate was found for Pt(111)/Ru and, in contrast, Pt(100)/Ru is inactive, and Pt(110)/Ru is moderately active. While the Pt(111)/Ru surfaces will never make practical catalysts, the results of such studies may affect the future development in Pt/Ru electrocatalysis since surface crystallography of catalytic platinum/ruthenium particles can be adjusted through the particle size and thermal or electrochemical treatment[27,28]. Therefore, if the most catalytic crystal plane is identified using macroscopic single crystal electrodes, a crystallographic refining of the catalytic nanoparticles toward the highest reactivity may add to the development of more potent catalysts (INTRODUCTION).

A great deal of effort in the report was put forth in an attempt to capture the origin of this structural effect, albeit still on the qualitative level. It has been noticed that the enhanced oxidation of methanol on Pt/Ru electrodes is a bimolecular reaction that occurs between methanolic CO and oxygenated ruthenium site (that closely resembles the well-know *Langmuir-Hinshelwood* surface reaction, but which is termed in electrochemical literature as a bifunctional mechanism):

$$Pt\text{-}CO + Pt/RuO_x \rightarrow Pt + Pt/RuO_{x-1} + CO_2$$

The active site, that is one where CO_2 is formed, is the site at a perimeter of the ruthenium island on the Pt substrate. The crucial issue is therefore: why is the Pt(111)/Ru site more active than any other site? We have concluded that three possible reasons, collectively or alternatively, may be involved: (i) less "O_x" chemisorption on Pt/Ru terraces increasing the "oxygen" site-to-site mobility and reactivity, (ii) smaller heat of adsorption of CO on Pt(111) than on Pt(110) and even more so, on Pt(100)[42], and, (iii) the more favorable active site geometry allowing surface oxygen (O_x) to be closer to CO. The latter would facilitate the surface activation state formation.

The data also indicate that the steady-state oxidation methanolic CO occurs on the surface crowded by high coverage by carbon monoxide and ruthenium. This adds a new credibility to the bifunctional mechanism since: (i) CO and RuO_x are close together facilitating the oxygen transfer without the need for a long-range surface diffusion, (ii) not too many "clean" Pt sites exist to activate water which may next be used to oxidize CO, all are probably engaged in CO chemisorption and Ru deposition, (iii) and the option for CO to use bulk water on its way to CO_2 seems unlikely. The fact that we deal with a crowded surface also explains the lack of the anion effect in the reactivity[25]. However, what would not be contradictory to the general spirit of this mechanism is that the oxygen shared between Pt and Ru site is transferred to CO, rather than that specifically associated with Ru. It is neither contradictory to assume that the oxygen is transferred to an electronically modified Pt-CO site due to the ruthenium addition to the surface. Ruthenium, for instance, may perturb platinum electron polarizabilities and orbital symmetries, thus affecting the orbital spatial distribution and the reaction rate.

The grand conclusion from this study is that there may not be a contradiction between the electronic (ligand) mechanism, and the bifunctional mechanism in accounting for the overall methanol oxidation mechanism. In particular, we may refer to the Synchrotron X-ray Absorption Spectroscopy data by McBreen et al,[78] showing that alloying platinum with ruthenium increases

Pt *d* band vacancies and decreases the Pt-Pt bond distance which, *per se*, would support of the ligand mechanism. We therefore believe that the Pt/Ru catalytic enhancement effect may be explained in terms of the combined electronic and "bifunctional" effects. Such a complete mechanism would assume a dual role of ruthenium in attracting oxygen to the catalytic surface at ca. 0.3 V more negative potentials than without Ru and, simultaneously, in affecting the electron density on the neighboring Pt site to make adsorbed CO more susceptible to the oxygen attack.

Acknowledgments

This work is supported by the National Science Foundation under grant No. CHE 97-000963, and by the Department of Energy grant DEFG02-96ER45439 administered by the Frederick Seitz Materials Research Laboratory at the University of Illinois. Dr. Tremiliosi-Filho greatly acknowledges FAPESP-Brazil for the sabbatical fellowship. AW appreciates helpful discussion with Dr. Y. Tong about the mechanistic issues presented in this report.

References

1. J. O'M. Bockris and H. Wroblowa, J. Electroanal. Chem., 7 (1964) 428.

2. O. A. Petry, B. I. Podlovchenko, A.N. Frumkin and Hira Lal, J. Electroanal. Chem., 10 (1965) 253.

3. H. Binder, A. Kohling and G. Sandstede, in: B. S. Baker (Ed.), Hydrocarbon Fuel Cell Technology, Academic Press, New York, 1965, pp. 91-102.

4. H. Binder, A. Kohling and G. Sandstede, in: G. Sandstede (Ed.), From Electrocatalysis to Fuel Cells, University of Washington Press, Seattle, 1972, pp. 43-58.

5. M. Watanabe and S. Motoo, J. Electroanal. Chem., 60 (1975) 267.

6. M. M. P. Janssen and J. Moolhuysen, Electrochim. Acta, 21 (1976) 869.

7. B. D. McNicol and R. T. Short, J. Electroanal. Chem., 81 (1977) 249.

8. B. Beden, F. Kadirgan, C. Lamy and J.-M. Leger, J. Electroanal. Chem., 127 (1981) 75.

9. T. Iwasita, F. C. Nart and W. Vielstich, Ber. Bunsenges. Phys. Chem., 94 (1990) 1030.

10. K. Franaszczuk and J. Sobkowski, J. Electroanal. Chem., 327 (1992) 235.

11. C. T. Hable and M. S. Wrighton, Langmuir, 9 (1993) 3284.

12. M. Krauza and W. Vielstich, J. Electroanal. Chem., 379 (1994) 307.

13. N. M. Markovic, H. A. Gasteiger, P. N. Ross Jr., X. Jiang, I. Villegas and M. J. Weaver, Electrochim. Acta, 40 (1995) 91.

14. X. Ren, M. S. Wilson and S. Gottesfeld, J. Electrochem. Soc., 143 (1996) L12.

15. J. Munk, P. A. Christensen, A. Hamnett and E. Skou, J. Electroanal. Chem., 401 (1996) 215.

16. D. Chu and S. Gilman, J. Electrochem. Soc., 143 (1996) 1685.

17. T. Frelink, W. Visscher and J. A. R. van Veen, Langmuir, 12 (1996) 3702.

18. D. Aberdam, F. Razafimaharo, R. Faure, A. Kabbabi and R. Durand, in: A. Wieckowski and K. Itaya (Eds.), Electrode Processes VI, The ECS Proceedings, vol. 96-8, The Electrochemical Society, Pennington, 1996, pp. 280-290.

19. C. E. Lee and S. H. Bergens, J. Phys. Chem. B, 102 (1998) 193.

20. W. Chrzanowski and A. Wieckowski, Langmuir, 14 (1998) 1967.

21. A. Hamnett and B. J. Kennedy, Electrochim. Acta, 33 (1988) 1613.

22. R. Liu, K. L. Ley, C. Pu, Q. Fan, N. Leyarovska, C. Segre and E. S. Smotkin, in: A. Wieckowski and K. Itaya (Eds.), Electrode Processes VI, The ECS Proceedings, vol. 96-8, The Electrochemical Society, Pennington, 1996, pp. 341-355.

23. K. L. Ley, R. Liu, C. Pu, Q. Fan, N. Leyarovska, C. Segres and E. S. Smotkin, J. Electrochem. Soc., 144 (1997) 1543.

24. W. Chrzanowski and A. Wieckowski, in: A. Wieckowski (Ed.); Interfacial Electrochemistry: Experimental, Theory and Applications, Marcel Dekker, New York, in press.

25. W. Chrzanowski, H. Kim, G. Tremiliosi-Filho, A. Wieckowski, B. Grzybowska and P. Kulesza, J. New Mat. Electrochem. Systems, 1 (1998) 31.

26. A. Hamnett, in: A. Wieckowski (Ed.); Interfacial Electrochemistry: Experimental, Theory and Applications, Marcel Dekker, New York, in press.

27. W. H. Lee, K. R. Vanloon, V. Petrova, J. B. Woodhouse, C. M. Loxton and R. I. Masel, J. Catal., 126 (1990) 658.

28. L. Palaikis and A. Wieckowski, Catal. Lett., 3 (1989) 143.

29. W. Chrzanowski and A. Wieckowski, Langmuir, 13 (1997) 5974.

30. W. Chrzanowski, H. Kim and A. Wieckowski, Cat. Lett., 50 (1998) 69.

31. S. Cramm, K. A. Friedrich, K.-P. Geyzers, U. Stimming and R. Vogel, Fresenius J. Anal. Chem., 358 (1997) 189.

32. K. A. Friedrich, K.-P. Geyzers, F. Henglein, A. Marmann, U. Stimming, W. Unkauf and R. Vogel, in: A. Wieckowski and K. Itaya (Eds.), Electrode Processes VI, The ECS Proceedings, vol. 96-8, The Electrochemical Society, Pennington, 1996, pp. 119-135.

33. M. Watanabe and S. Mooto, J. Electroanal. Chem., 60 (1975) 275.

34. H. A. Gasteiger, N. Markovic, P. N. Ross Jr. and E. J. Cairns, J. Electrochem. Soc., 141 (1994) 1795.

35. T. Frelink, W. Visscher and J. R. A. van Veen, Surf. Sci., 335 (1995) 353.

36. G. A. Somorjai, Introduction to Surface Chemistry and Catalysis, Wiley-Interscience Publication, New York, 1994, pp. 446, 447.

37. R. I. Masel, Principles of Adsorption and Reaction on Solid Surfaces, Wiley-Interscience Publication, New York, 1996, pp. 483, 484.

38. K. Franaszczuk, E. Herrero, P. Zelenay, A. Wieckowski, J. Wang and R. I. Masel, J. Phys. Chem., 96 (1992) 8508.

39. E. Herrero, K. Franaszczuk and A. Wieckowski, J. Phys. Chem., 98 (1994) 5074.

40. J. Clavilier, J. Electroanal. Chem., 107 (1980) 211.

41. E. Herrero, W. Chrzanowski and A. Wieckowski, J. Phys. Chem., 99 (1995) 10423.

42. G. Tremiliosi-Filho, H. Kim, W. Chrzanowski, A. Wieckowski, B. Grzybowska and P. Kulesza, J. Electroanal.Chem., submitted.

43. Y.-E. Sung, W. Chrzanowski, A. Zolfaghari, G. Jerkiewicz and A. Wieckowski, J. Am. Chem. Soc., 119 (1997) 194.

44. Y.-E. Sung, S. Thomas and A. Wieckowski, J. Phys. Chem., 99 (1995) 13513.

45. S. Doniach and M. Sunjic, J. Phys. C: Solid St. Phys., 3 (1970) 285.

46. E. Desimoni, G. I. Casella, T. R. I. Cataldi and C. Malitesta, J. Electron Spectrosc. Relat. Phenom., 49 (1989) 247.

47. D. A. Shirley, Phys. Rev., B 5 (1972) 4709.

48. S. Thomas, Y.-E. Sung, H. Kim and A. Wieckowski, J. Phys. Chem., 100 (1996) 11726.

49. E. Herrero, K. Franaszczuk and A. Wiekowski, J. Electroanal. Chem., 361 (1993) 269.

50. T. Frelink, W. Visscher, A.P. Cox and J.A.R. van Veen, Ber. Bunsenges. Phys. Chem., 100 (1996) 599.

51. H. J. Lewerenz, S. Stucki and R. Kötz, Surf. Sci., 126 (1983) 463.

52. R. Kötz, H. J. Lewerenz and S. Stucki, J. Electrochem. Soc., 130 (1983) 825.

53. J. B. Goodenough, A. Hamnett, B. J. Kennedy, R. Manoharan and S. A. Weeks, J. Electroanal. Chem., 240 (1988) 133.

54. E. Ticanelli, J. G. Beery, M. T. Paffett and S. Gottesfeld, J. Electroanal. Chem., 258 (1989) 61.

55. J. P. Moulder, W. F. Stickel, P. E. Sobol and K. D. Bomben, Handbook of X-ray Photoelectron Spectroscopy, Perkin-Elmer Corporation, Physical Electctronics Division, Eden Prairie, MN, 1992, p. 235.

56. M. Vukovic, T. Valla, and M. Milun, J. Electroanal. Chem., 356 (1993) 81.

57. A. Wieckowski, W. Chrzanowski and E. Herrero, in: O. Savadogo, P.R. Roberge and T.N. Veziroglu (eds.), Proceedings of the First International Symposium on New Materials for Fuel Cells Systems, Editions de L'Ecole Polytechnique de Montreal, Montreal, 1995, pp. 326-336.
58. A. Papoutsis, J.-M. Leger and C. Lamy, J. Electroanal. Chem., 234 (1987) 315.
59. S. G. Sun and J. Clavilier, J. Electroanal. Chem., 236 (1987) 95.
60. M. P. Hogarth and G. A. Hards, Plat. Met. Rev., 40 (1996) 150.
61. J. E. Inglesfield, Rep. Prog. Phys., 45 (1982) 223.
62. P. J. Feibelman and D. R. Hamann, a) Phys. Rev. Letters, 52 (1984) 61; b) Surf. Sci., 149 (1985) 48.
63. G. A. Somorjai, J. Phys. Chem., 94 (1990) 1013.
64. Y. Tong, Ph. D thesis, "Metal-Adsorbate and Metal-Matrix Interactions in Platinum Catalysts Studied by ^{195}Pt NMR", EPFL, Lausanne, Switzerland, 1994.
65. J. P. Bucher and J. J. van der Klink, Phys. Rev. B, 38 (1988) 11038.
66. Y. Tong, A. J. Renouprez, G. A. Martin and J. J. van der Klink, Studies in Surf. and Catal., 101 (1996) 901.
67. Y. Y. Tong, E. Oldfield and A. Wieckowski, Anal. Chem., 70 (1998) 518A.
68. M. D. Thompson and H. B. Huntington, Surf. Sci., 116 (1982) 522.
69. K. Besocke, B. Krahl-Urban and H. Wagner, Surf. Sci., 68 (1977) 39.
70. R. Hoffmann, Rev. of Mod. Phys., 60 (1988) 601, S. Sung and R. Hoffmann, J. Am. Chem. Soc., 107 (1985) 578.
71. G. A. Somorjai, Surf. Sci., 242 (1991) 481.
72. I. Toyoshima and G. A. Somorjai, Catal. Rev.-Sci. Eng., 19 (1979) 105.
73. R. W. McCabe and L. D. Schmidt, Surf. Sci., 66 (1977) 101.
74. E. Shustorovich and A. T. Bell, Surf. Sci., 289 (1993) 127.
75. R. B. Woodward and R. Hoffman, J. Am. Chem. Soc., 87 (1965) 395.
76. A. Ruban, B. Hammer, P. Stoltze, H. L. Skriver and J. K. Norskov, J. Molecular Catal. A: Chemical, 115 (1997) 421.
77. J. K. Norskov, Rep. Prog. Phys., 53 (1990) 1253.
78. J. McBreen and S. Mukerjee, J. Electrochem. Soc., 142 (1995) 3399.

Figure Captions

Figure 1. Secondary Auger electron spectra of the Pt(111) electrode for[30]: (A) Pt(111) surface covered by the Ru spontaneous deposit obtained in $5x10^{-5}$ M $RuCl_3$ + 0.1 M $HClO_4$ after 2 min of deposition, (B) Pt(111) surface covered by the Ru spontaneous deposit in $5x10^{-4}$ M $RuCl_3$ + 0.1 M $HClO_4$ (during 2 min), (C) Pt(111) surface covered by the Ru deposit obtained at 0.3 V (*vs.* RHE) for 10 s in $5x10^{-4}$ M $RuCl_3$ + 0.1 M $HClO_4$, and (D) Pt(111) surface covered by the deposit obtained at 0.3 V for 10 s in $2x10^{-3}$ M $Ru(NO))(NO_3)_3$ + 0.5 M H_2SO_4. AES measurements were carried out in a differential mode with a 2 eV modulation amplitude, at 3.5 keV of primary electron energy, and 0.5 μA sample current, lock-in amplifier time constant 3 ms, using a Perkin Elmer (PHI) 10-155 cylindrical mirror analyzer (CMA). Spectra were acquired using a digital data acquisition system, and smoothed one time using a 11 points averaging technique. The p/p amplitudes were measured for a number of scans, extending over several seconds, and then extrapolated to zero time to obtain signal intensities not perturbed by the beam damage.

Figure 2. (A) Deposition of ruthenium at 0.300 V from $5x10^{-4}$ M $RuCl_3$ solution in 0.1 M $HClO_4$: the dependence of ruthenium coverage (in ML) on the deposition charge[24]. (Note that the deposition process is severely retarded above the ruthenium coverage of 0.28 ML.) The coverage due to spontaneous deposition is indicated by the arrow. (B) Deposition of ruthenium at 0.300 V from $2x10^{-4}$ M $Ru(NO)(NO_3)_3$ solutions in 0.5 M H_2SO_4: dependence of ruthenium coverage (in ML) on the deposition charge. (Note that the deposition process is retarded above the ruthenium coverage of 0.18 ML.) On Figures 2 A and 2 B, the data for the top axis: "surface coverage" were obtained from the deposition charge using the number of electrons involved in the electrolysis, 4 and 3, respectively[24].

Figure 3. Deposition of ruthenium under cyclic voltammetric conditions: the dependence of ruthenium coverage (in ML) on the number of voltammetric cycles in the range from 0.00 to 0.88 V in two solutions: (•) $5x10^{-4}$ M $RuCl_3$ + 0.1 M $HClO_4$, (O) $2x10^{-3}$ M $Ru(NO)(NO_3)_3$ + 0.5 M H_2SO_4.

Figure 4. XPS spectra of the Pt(111)/Ru electrode obtained by spontaneous deposition of ruthenium on clean Pt(111) from $5x10^{-4}$ M $RuCl_3$ solution in 0.1 M $HClO_4$. Experiments were performed using ESCA M-Probe system equipped with a monochromatic Al *K* α line (hν = 1486.6 eV) operating at 150 Watts, and a multi-channel hemispherical electron analyzer, 100 mm-radius (*Surface Science Instruments*). The X-ray spot size was 800 μm. (See text.)

Figure 5. (A) High sweep rate cyclic voltammetric curves for the Pt(111)/Ru electrode in 0.1 M $HClO_4$ + 0.6 M CH_3OH solution. Solid line, CO stripping voltammogram after CO accumulation for 10 min at 0.310 V. Dashed line, the cyclic voltammogram obtained after CO stripping in the same 0.1 M $HClO_4$ + 0.6 M CH_3OH solution. Sweep rate: 50 $V \cdot s^{-1}$. (B) Chronoamperometric curve for the Pt(111)/Ru electrode at 0.310 V (*vs.* RHE) in 0.1 M $HClO_4$ + 0.6 M CH_3OH solution. Inset shows the time window from 1 to 10 s (see text).

Figure 6. Current density - time plots for methanol oxidation at 65 °C (left axis), and reaction turnovers corresponding to the current densities (right axis), at the Pt(111)/Ru, Pt(110)/Ru and Pt(100)/Ru electrodes (at the optimum Ru coverage of 0.20, 0.15 and 0.30 ML respectively), all in 0.1 M H_2SO_4 + 0.6 M CH_3OH. The applied electrode potential was 0.310 V. Data were smoothed using a low-pass numeric filter.

Figure 7. Log i vs. E (the Tafel) plots for: (●) Pt(111), (↑) Pt(110), and (◀◀) Pt(100).

Figure 8. Methanol oxidation on the Pt(hkl)/Ru electrodes under steady-state conditions. Oxidation efficiency diagrams as a function of surface crystallography of the platinum substrate. All ruthenium coverages were optimized to the maximum methanol oxidation reactivity. The *pseudo steady-state* currents were measured at 0.310 V after 30 min of polarization. Solution temperature was A: 25 °C[24] and B: 65 °C.

Figure 9. A polarization current - potential curve for Pt(111)/Ru obtained at 65 °C in 1 M H_2SO_4 + 2 M CH_3OH, under optimum Ru coverage conditions (■). For comparison, polarization data for the industrial catalyst (●) are included[60].

Table 1. CO stripping charges (obtained from cyclic voltammetry at 50 $V \cdot s^{-1}$, Figure 5) on Pt (111) after adsorption from 0.1 M $HClO_4$ + 0.6 M CH_3OH solution at selected potentials and for different methanol decomposition times (at 25°C).

Potential (V *vs* RHE)	Q ($mC\ cm^{-2}$)					
	clean Pt(111)			$Pt(111)/Ru_{opt}$		
	1 s	10 s	10 min	1 s	10 s	10 min
0.55	140 ± 3*	170 ± 10	155 ± 15	190 ± 25	180 ± 9	160 ± 36
0.43	190 ± 25	203 ± 3	206 ± 5	239 ± 3	236 ± 4	228 ± 6
0.31	230 ± 8	250 ± 15	220 ± 12	230 ± 1	260 ± 15	260 ± 4
0.25	231 ± 5	240 ± 12	223 ± 8	170 ± 12	224 ± 4	244 ± 5

*error is the standard deviation of the mean.

Table 2. Activation energy for methanol oxidation on Pt(hkl)/Ru electrodes at selected potentials in 0.1 M sulfuric acid.

Potential (V *vs* RHE)	Activation Energy (kJ mol^{-1})			
	Pt(100)/Ru[a]	Pt(110)/Ru[a]	Pt(111)/Ru[a]	Pt(111)/Ru[b,]
0.25	61 ± 11[c]	38 ± 4	84 ± 10	70 ± 7
0.31	53 ± 7	50 ± 5	66 ± 7	56 ± 5
0.37	65 ± 4	47 ± 8	56 ± 5	54 ± 4

[a]Ruthenium deposited from $2x10^{-4}$ M $Ru(NO)(NO_3)_3$ in 0.5 M H_2SO_4.

[b]Ruthenium deposited from $5x10^{-5}$ M $RuCl_3$ in 0.1 M $HClO_4$.

[c]Error is the standard deviation of the mean.

Table 3. Ruthenium enhancement of methanol electrooxidation at Pt(hkl)/Ru electrodes at +370 mV vs. RHE at room temperature[20].

Time (s)	Ruthenium enhancement[a]		
	Pt(100)	Pt(110)	Pt(111)
0.5	1.0	1.5	1.8
1	1.0	1.4	1.4
10	1.3	3.0	7.7
300	14	34	240
600	$\Rightarrow \infty$[b]	58	$\Rightarrow \infty$
1800	$\Rightarrow \infty$	$\Rightarrow \infty$	$\Rightarrow \infty$

[a] ratio of oxidation current with and without ruthenium on Pt.

[b] enhancement approaching infinity is due to clean platinum inability to produce measurable oxidation current (see text).

Table 4. Quantitative data on the rate of methanol oxidation current decay, and the progress of reaction at several electrode potentials at the Pt(111)/Ru electrode at room temperature[20].

Potential (V vs. RHE)	$\partial(\log i)/\partial t$[a] ($min^{-1}$)	Charge[b] ($mC \cdot cm^{-2}$)	CH_3OH monolayers reacted in 30 min[c] (monolayers)
0.49	-0.014	194	377
0.37	-0.006	36	72
0.28	-0.001	5.8	11
0.25	0.000	2.1	4

[a] rate of current decay during the last 3 minutes of the experiment.

[b] the charge involved in methanol oxidation during 30 minutes of oxidation.

[c] assuming realistically 3 Pt sites per one methanol molecule and 1.5×10^{15} catalytic sites$\cdot cm^{-2}$.

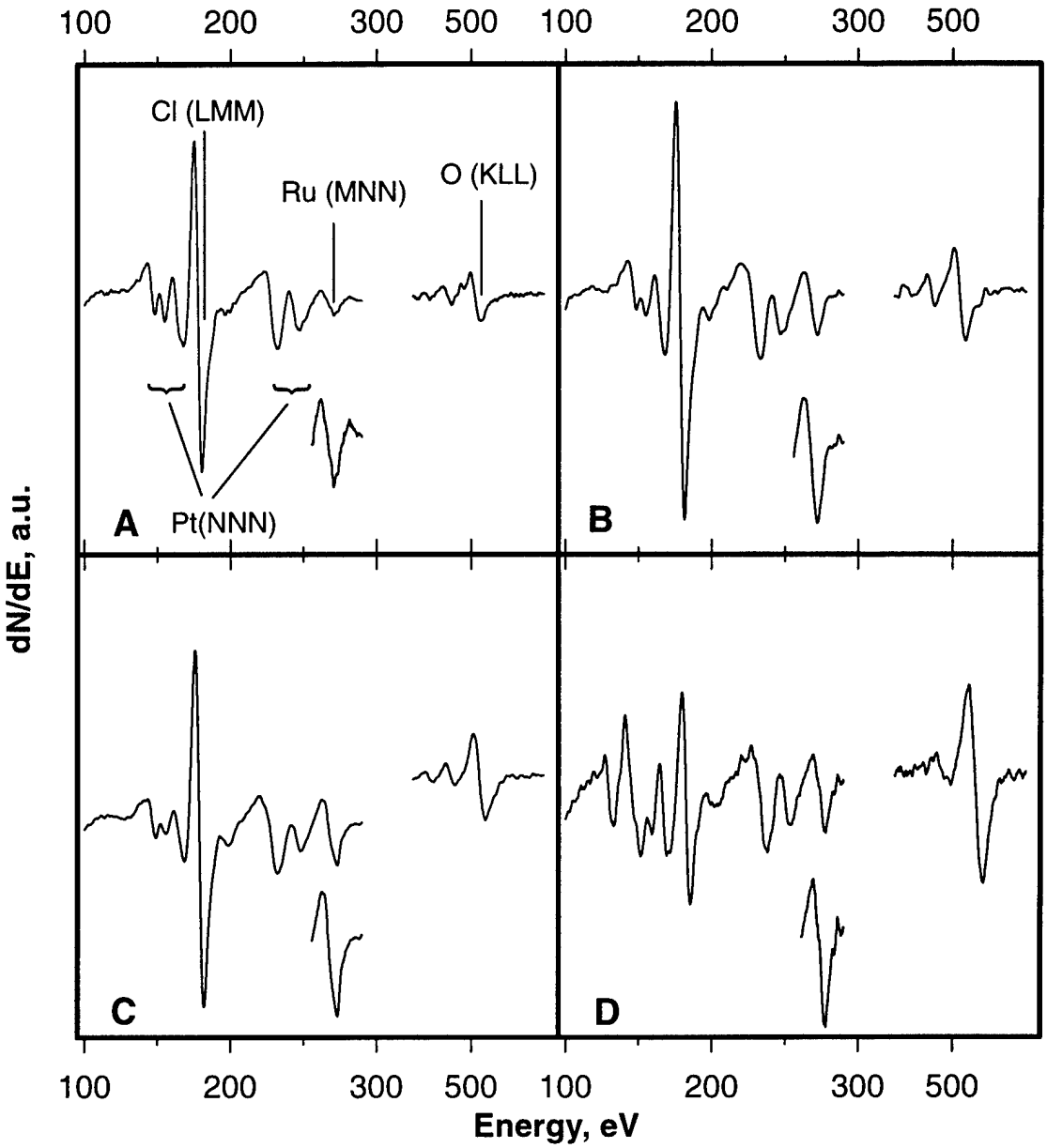
100
200
300
500
100
200
300
500
Cl (LMM)
Ru (MNN)
O (KLL)
Pt(NNN)
A
B
C
D
dN/dE, a.u.
Energy, eV

Figure 1

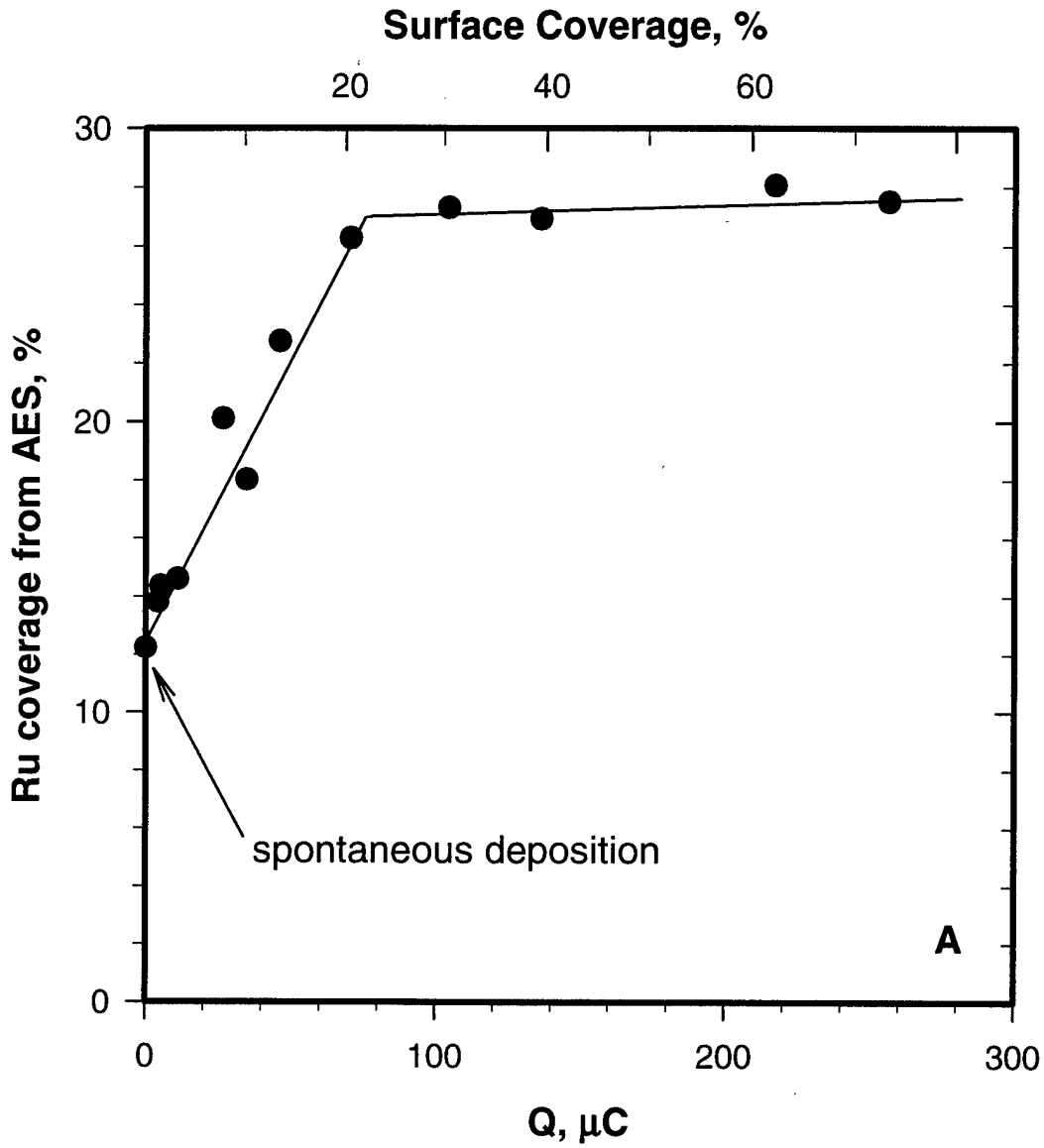
Surface Coverage, %
20
40
60
30
20
10
0
Ru coverage from AES, %
spontaneous deposition
A
0
100
200
300
Q, μC

Figure 2A

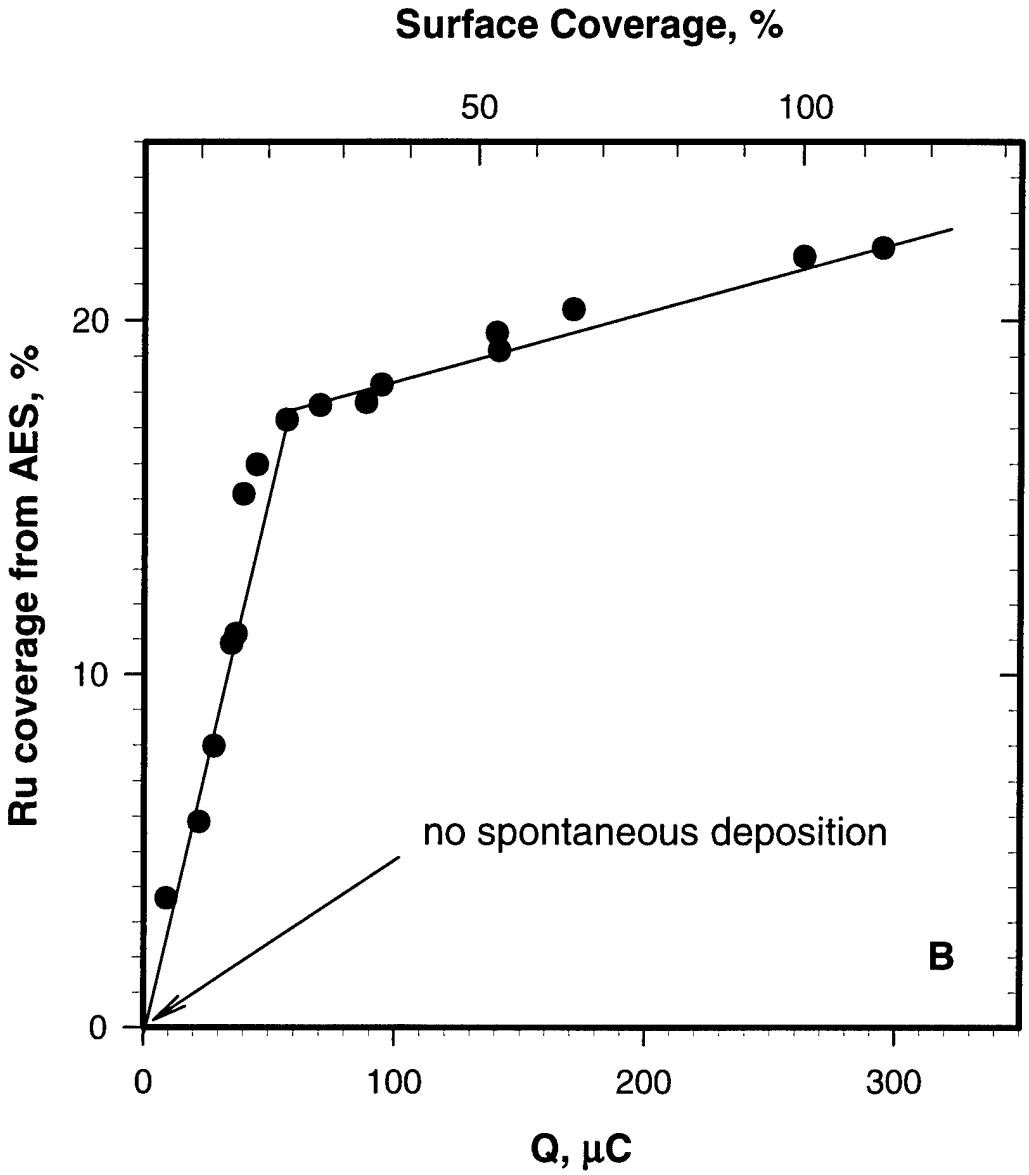
Surface Coverage, %
50
100
20
10
0
Ru coverage from AES, %
no spontaneous deposition
B
0
100
200
300
Q, μC

Figure 2B

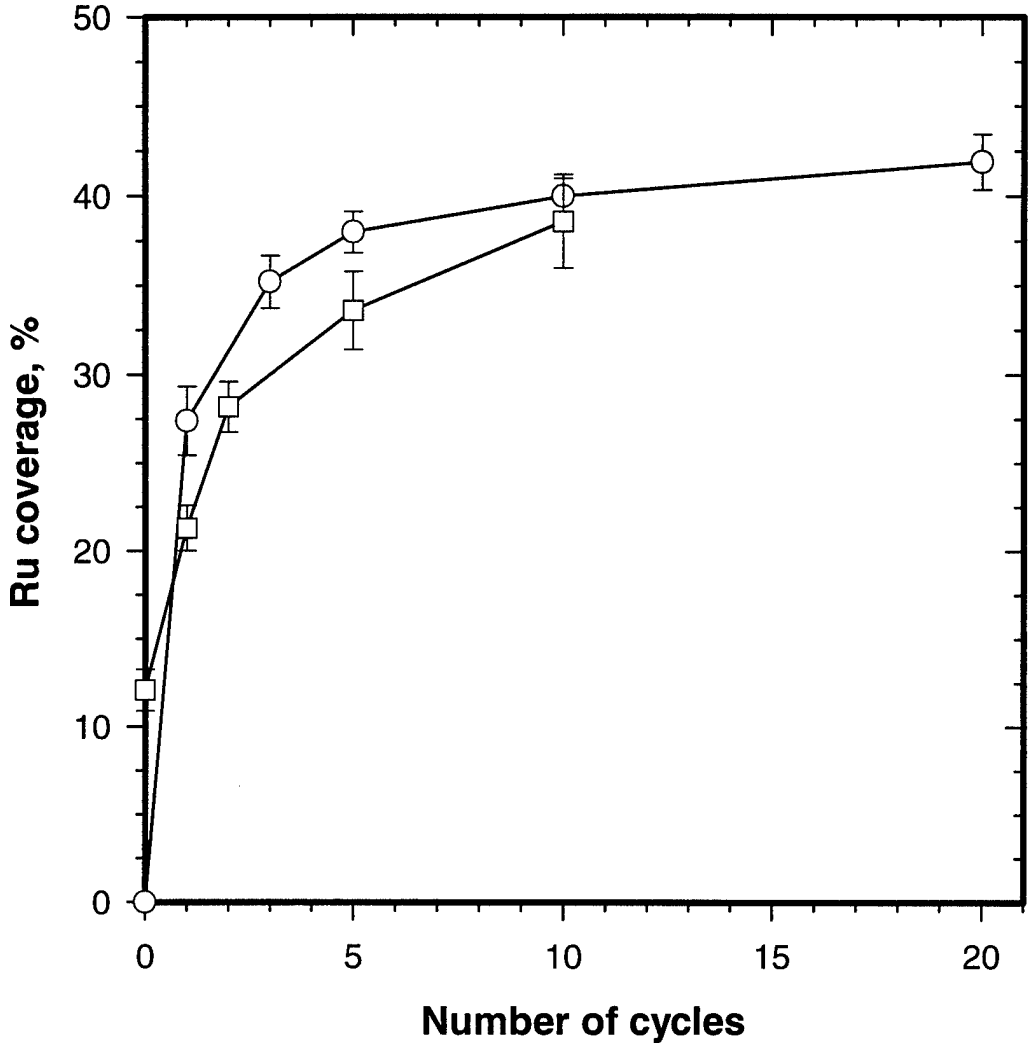

Figure 3

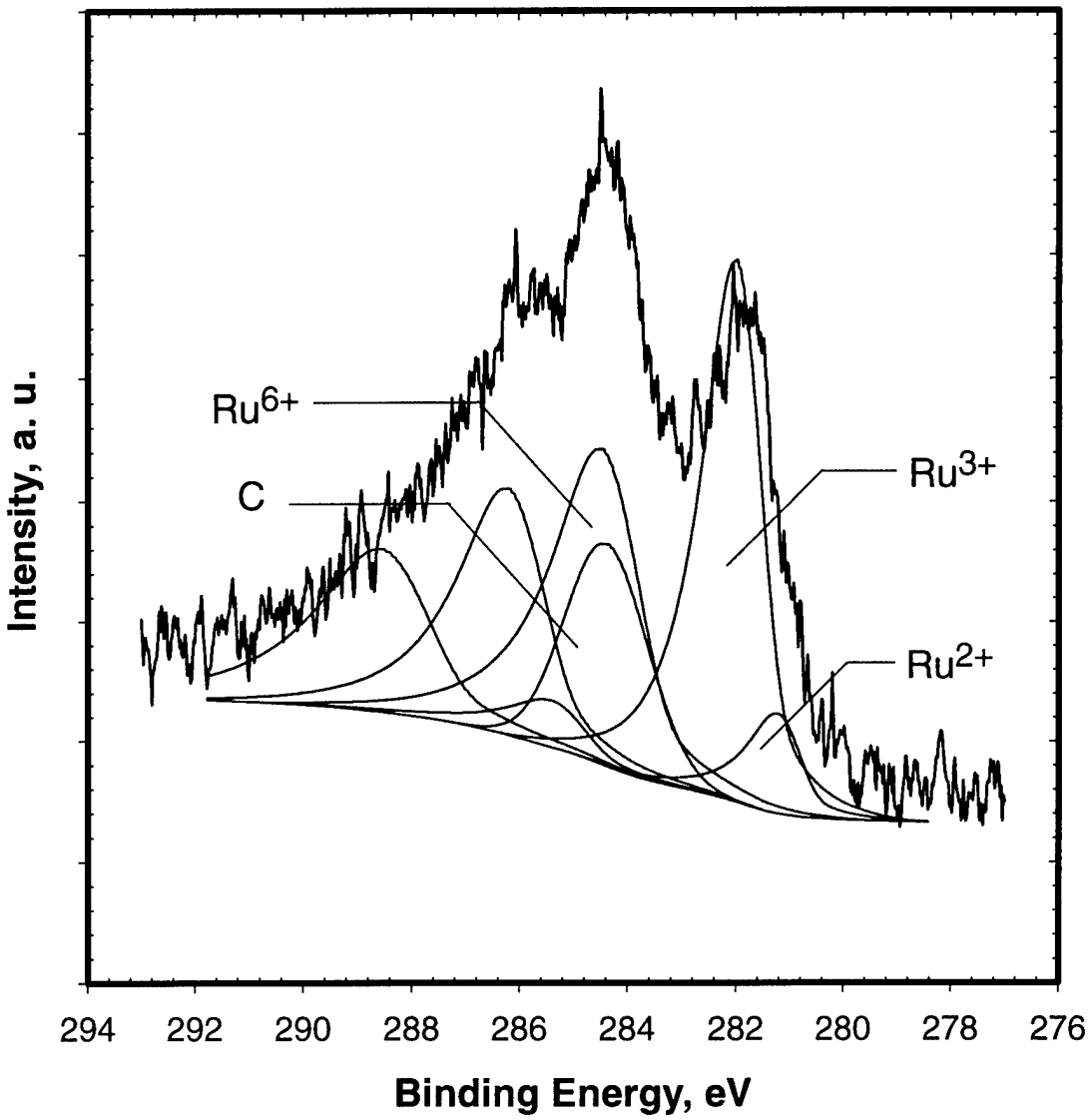
Intensity, a. u.
Ru6+
C
Ru3+
Ru2+
294
292
290
288
286
284
282
280
278
276
Binding Energy, eV

Figure 4

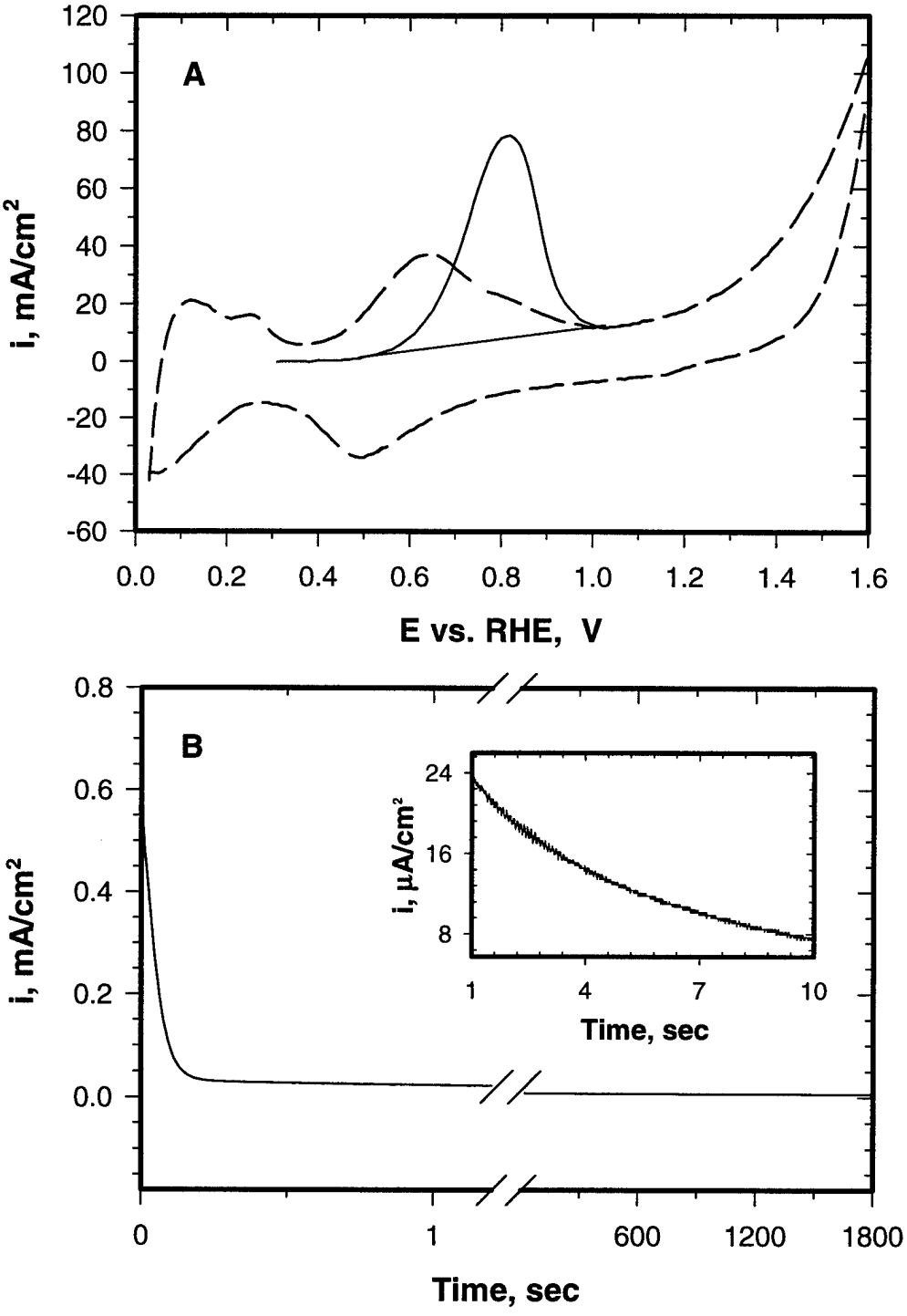

Figure 5

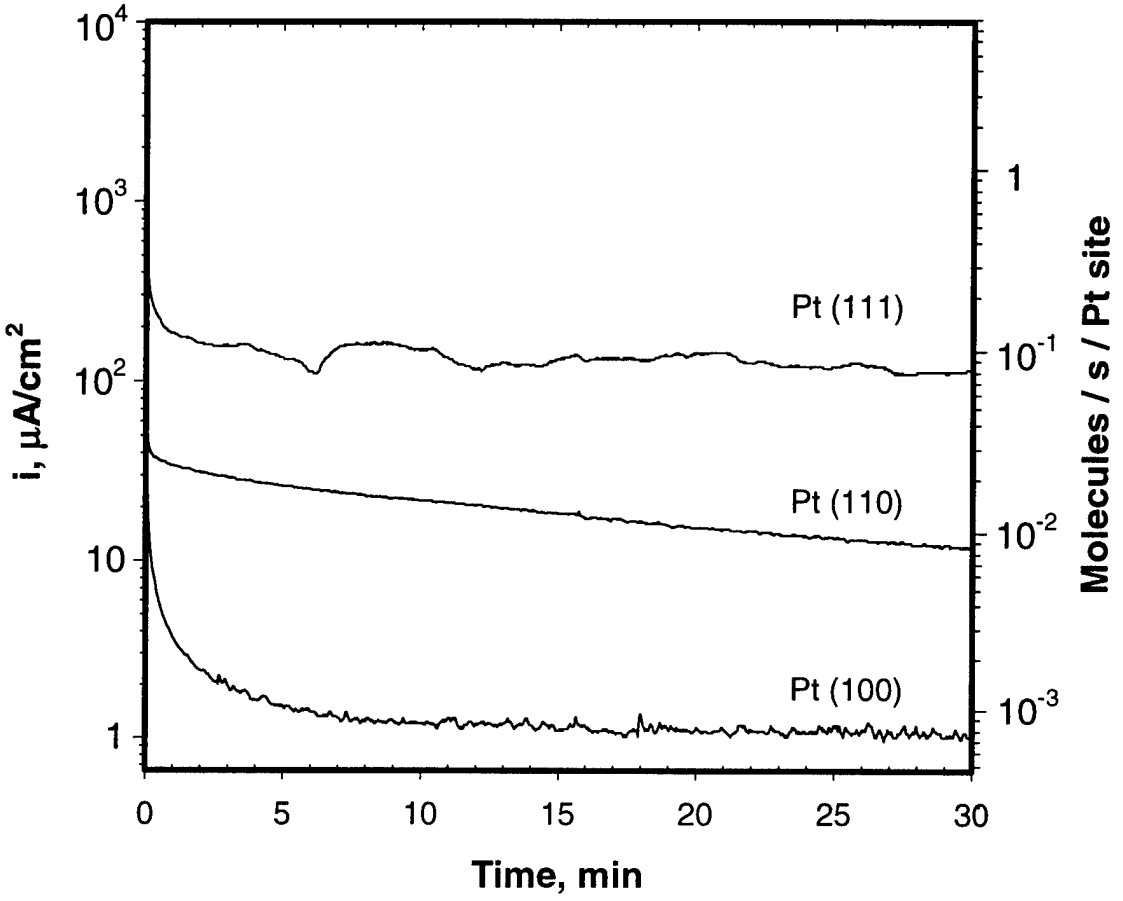
10^4
10^3
10^2
10
1
i, μA/cm²
Pt (111)
Pt (110)
Pt (100)
1
10^{-1}
10^{-2}
10^{-3}
Molecules / s / Pt site
0
5
10
15
20
25
30
Time, min

Figure 6

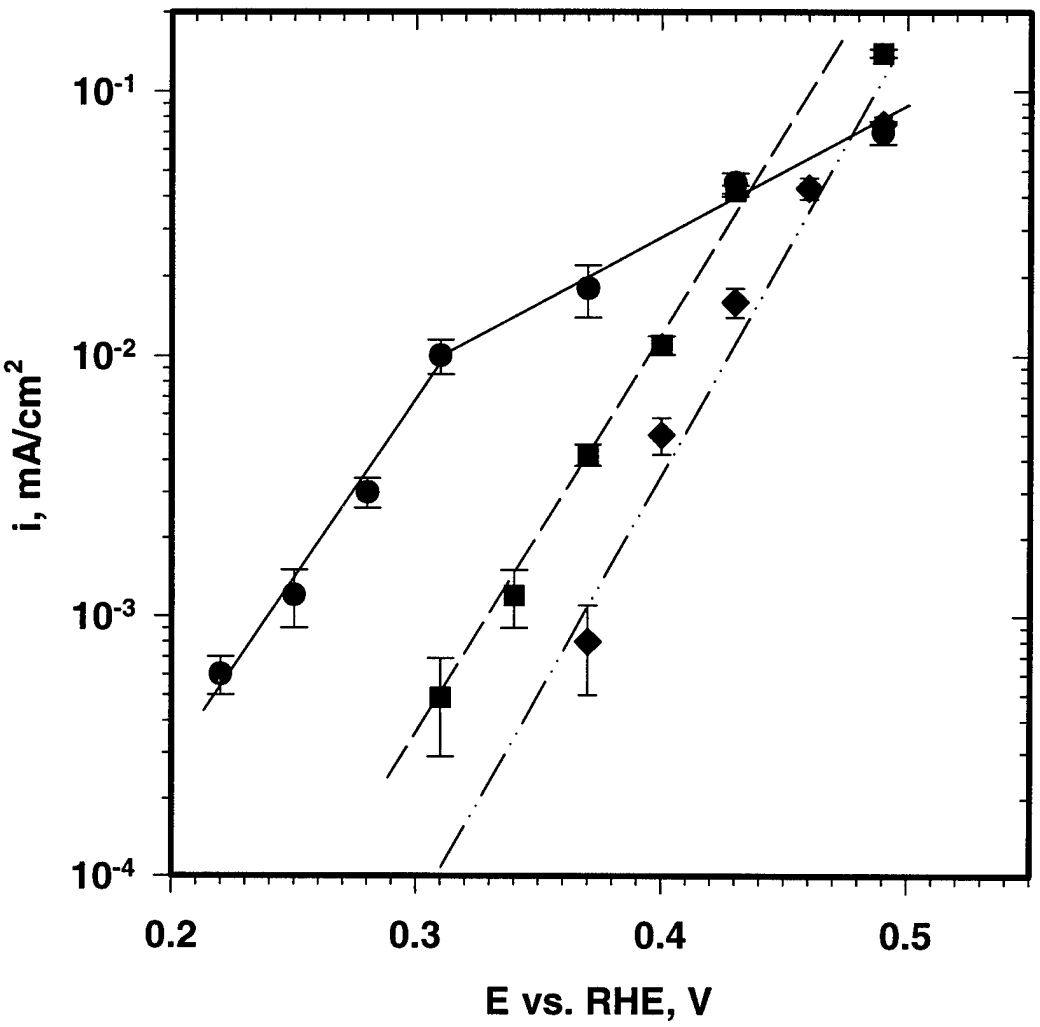

Figure 7

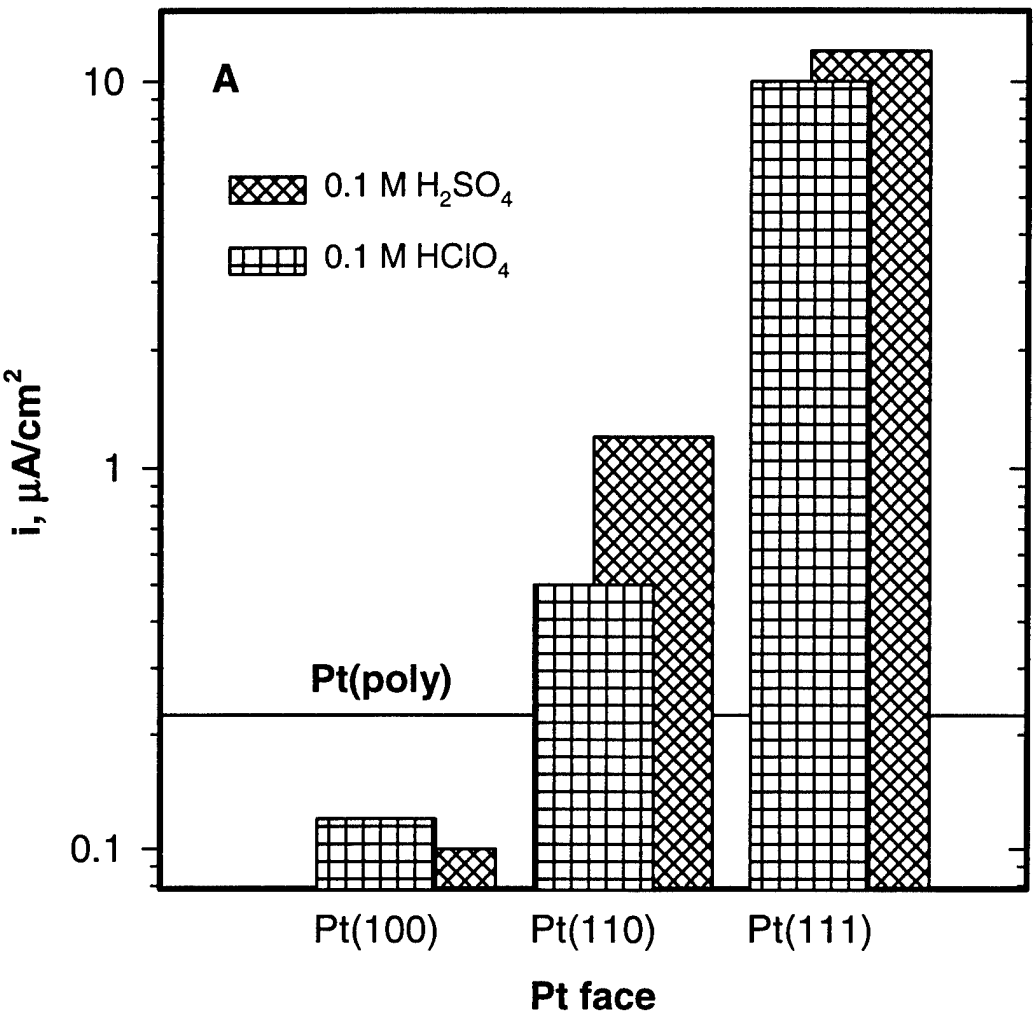
A
10
1
0.1
i, μA/cm²
0.1 M H₂SO₄
0.1 M HClO₄
Pt(poly)
Pt(100)
Pt(110)
Pt(111)
Pt face

Figure 8A

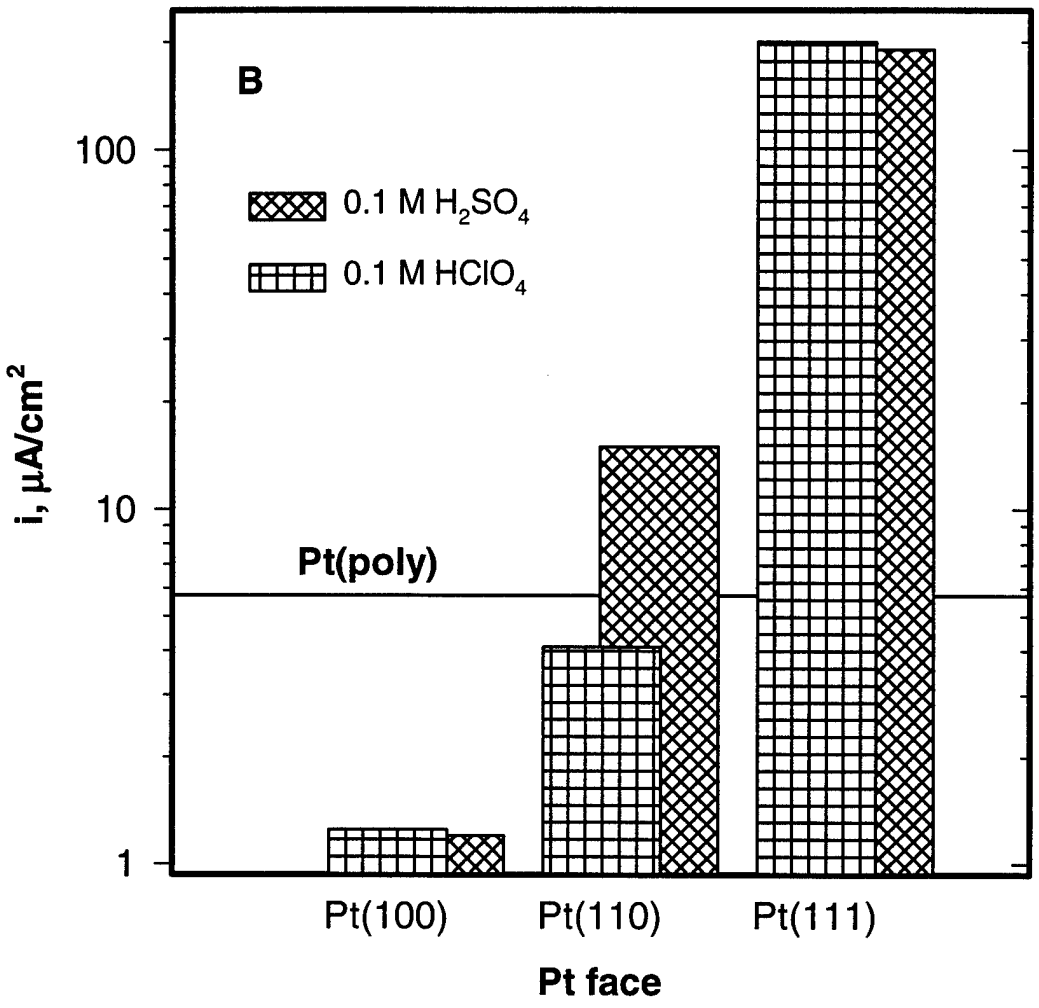
B
100
10
1
i, μA/cm²
0.1 M H₂SO₄
0.1 M HClO₄
Pt(poly)
Pt(100)
Pt(110)
Pt(111)
Pt face

Figure 8B

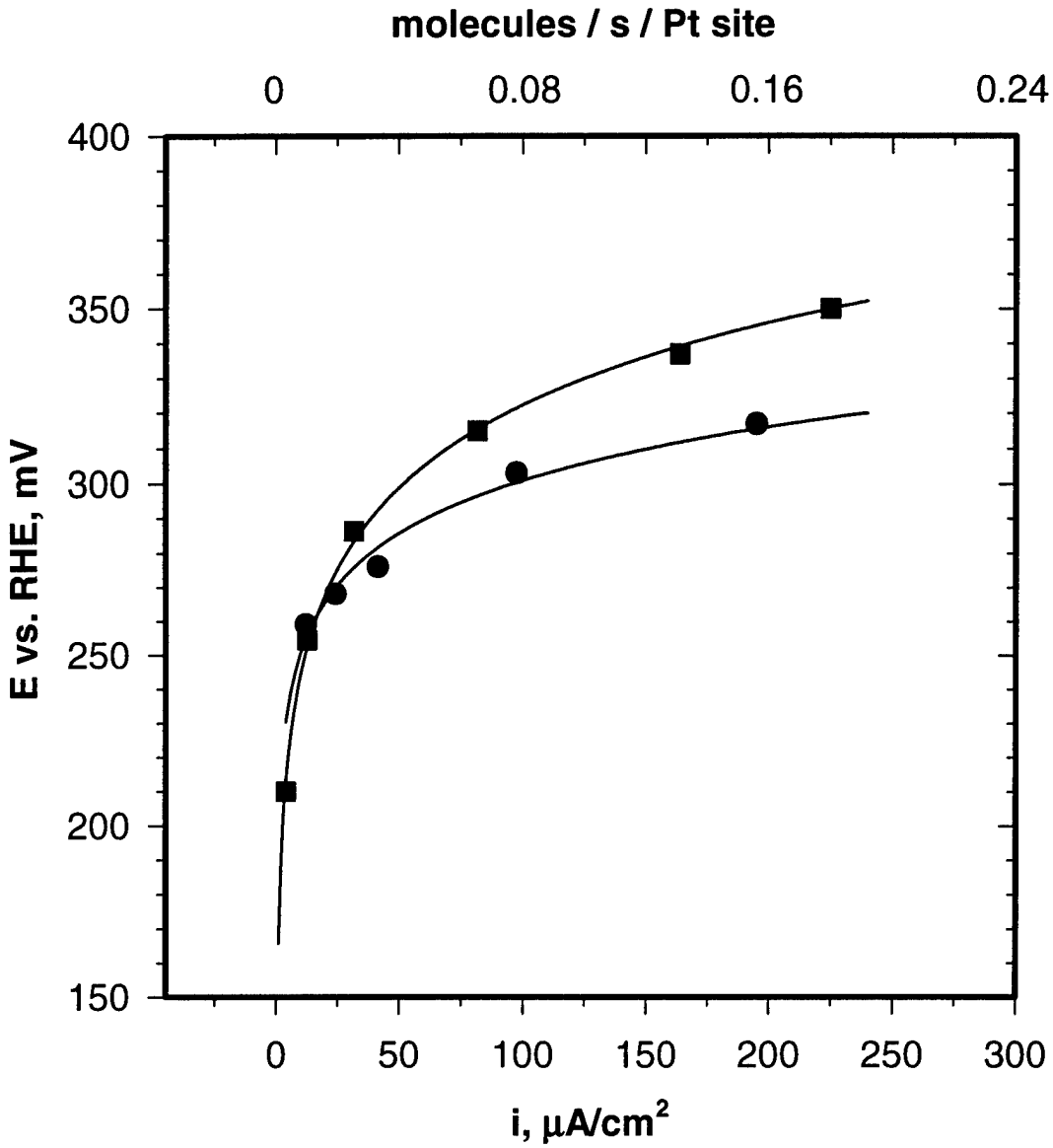
molecules / s / Pt site
0
0.08
0.16
0.24
400
350
300
250
200
150
E vs. RHE, mV
0
50
100
150
200
250
300
i, μA/cm²

Figure 9

Stucture of perfluorinated ionomer solutions.

M. Pineri (CEA/CEREM)

Summary
In this lecture, we will first recall the different procedures to get solutions of perfluorinated iomers. The structure of these solutions will then be analyzed from small angle scattering results obtained with X rays and neutrons. Evidence of rod like particles in these solutions will be given from scattering data analysis by geometrical considerations, Guinier analysis of the diluted solutions and from Porod laws. Chemical composition of these scattering objects will be given from contrast isotopic variation experiments in neutron scattering experiments. Relevant parameters defining the rod diameter will be then considered. Finally viscosity measurements will show a so-called "polyelectrolyte behavior", consistent with the vision of the rods as super polyelectrolytes.

In ionomers (1), the percentage of charged groups along the polymer backbone is generally smaller than 15 %. Because of intermolecular associations of both hydrophobic sequences and ionic groups, most of these polymers present some phase separation with the presence of ionic "clusters" . It is difficult to get solutions from the polymers because of these different physical crosslinks. One possibility is to use mixtures of non polar solvents and polar solvents for breaking the ionic associations. Another possibility is to drastically improve the swelling of the ionic domains by increasing the temperature and therefore the absolute pressure of the polar solvents. The solutions so-obtained may not be true solutions but may contain some micellar structures . The aim of this presentation is to summarize the results which have been obtained identifying the presence of micelles in these perfluorinated solutions.

Sulfonated perfluorinated ionomer solutions are used for casting thin membrane layers onto the catalyst particles in low temperature fuel cell applications (2). It is therefore very important to know the solutions "structure", the conditions of casting and the structure of the recast membranes for optimising the membrane-electrode assemblies. Annealing of the recast membranes changes the mechanical properties and the swelling properties because of a partial recrystallisation (3).
The results summarized in this lecture correspond to experiments and publications of " Molecular Physico Chemistry" group at CEA Grenoble (4-9) .

Materials:

Three different kinds of perfluorinated materials have been studied whose chemical structures are given below:

Type 1: Nafion® 117 from Du Pont de Nemours

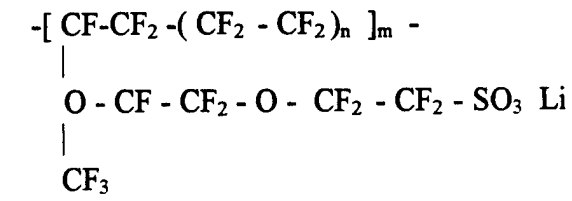

Type 2: Dow Chemical material

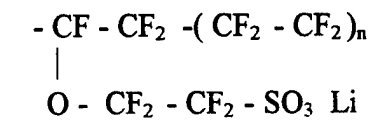

Type 3: Hoescht material

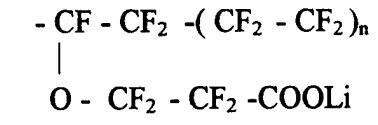

Polymer solutions have been obtained by dissolving small pieces of membrane in a 50/50 water/ethanol mixture for one hour in an autoclave heated at 250° C (10, 11). Solutions in different solvents were then obtained according two different procedures. The so obtained solution is concentrated by slow evaporation at 80° C and then dried. A fine powder is obtained, by milling at room temperature in an agate mortar, which dissolves at room temperature in many polar solvents. Another process consists in dialyzing the starting solution with pure solvents and adjusting the concentration.

Small angle experiments have been performed at Leon Brillion Laboratory with the SANS spectrometer PACE for the neutrons experiments and at LURE in Orsay with the D22 synchrotron radiation spectrometer for the X rays experiments.

Rod like structure of the perfluorinated ionomers solutions in polar solvents.

In small angle scattering experiments, existence of a well defined maximum whose position varies with concentration gives evidence of scattering particles in the solutions. The peak position, associated with an interfernce peak between the scattering particles, varies with the square root of the concentration involving a rod like structure for the particles. Diameters of the rods were first obtained from geometrical considerations with simple hexagonal or cubic two dimensional geometric arrangements of these rods. Further experiments on diluted solutions permitted to analyze the form factor of the scattering particles and to confirm the rod like shape and also to get the diameter of the rods from Guinier analysis.

Radii of 20/25 Å have been obtained for the type 1 polymers with long side chain groups in methanol or water. Smaller values (15/17 Å) have been obtained for the carboxylated and sulfonated polymers with shorter side chain groups (Types 2 and 3). Such results show that this side chain length is a key parameter for defining the diameter of the rods rather than the molecular weigth, nature of the charged groups and counterions, solvent characteristics. Solvent contrast variation studies have shown that the coherent scattering length value of the scattering particles was consistent with a perfluorinated chemical structure.

Addition of salts in the solutions induces the disappearing of the interference peak and an increase of the intensity scattered at low Q values. The Guinier plot remains unchanged except for an increase in intensity at very low Q values. Such results have been interpreted as corresponding to a decrease in the electrostatic repulsions between rods inducing a loss of order and a beginning of agregation.
A model for these rods is given below, model including the above mentionned results, in which most of the charged groups lie on the surface of the particles in contact with the polar solvent.

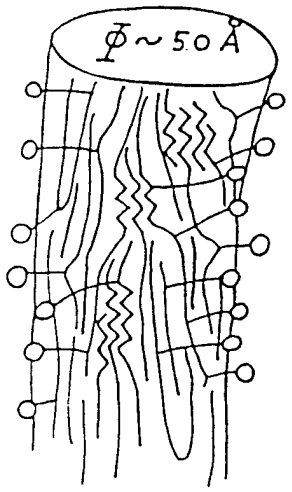

o : SO_3^-
— : CF_2-CF_2 backbone
≈≈: "Crystalline" CF_2-CF_2 structures in the center of the rods

Polyelectrolyte effect in perfluorosulfonated ionomer solutions (12).

Polyelectrolyte effect corresponding to an increase in viscosity at high dilutions has been evidenced in solutions with most of the polar solvents. Dielectric constant of the solvent seems to be a key parameter since for low values of this parameter the polyelectrolyte effect increases with the ε value while it disappears at high values. These rod like particles behave as "superelectrolytes" with an increase of the persistence length at high dilutions because of decondensation of counterions therefore inducing a transition from a "worm like rod" to a "rigid " one.

Ionic conductivity (6, 13).

Nafion® solutions or gels of 1100 EW Li salts were obtained according to the process previously described. N-methyl formamide, propylene carbonate and triethyl phosphate have been considered as solvents. Conductivity measurement have been done over a large frequency range. Larger conductivities have been obtained for N-methylformamide solutions with values of 4 10^{-3} S/cm at 25 C° and 7 10^{-3} S/cm at 80 C° for a concentration of 0.25 mol/l. Down to -40° C, there are only small changes of conductivity mainly because of viscosity modifications of the solvent as evidenced from the calculated activation energies.

Conclusions.

In polar solvents perfluorosulfonated ionomers form rod like particles which reorganize after casting and annealing. High conductivities are obtained in the presence of polar solvents mainly because of this rod like structure with the charges on the surface.

(1) Ionomers: Characterization, Theory and Applications; Schlick, S., Ed.; CRC Press: Boca Raton, Fl, 1996.

(2) Polymer electrolyte fuel cells. Electrochimi. Acta 1995, 40, 283

(3)G. Gebel, P. Aldebert, M. Pineri: Structure and related properties of solution cast perfluorosulfonated ionomer films, Macromolecules, 20, 1425 1987.

(4) P. Aldebert, B. Dreyfus, M. Pineri: Small-angle neutron scattering of perfluorosulfonated ionomers in solution, Macromolecules, 1986, 19, 2651.

(5) P. Aldebert, B. Dreyfus, G. Gebel, N. Nakamura, M. Pineri, F. Volino: Rod like micellar structures in perfluorinated ionomer solutions; J. Phys. France 49 (1988) 2101-2109.

(6) M. Guglielmi, P. Aldebert, M. Pineri: Ionic conductivity of perfluorinated ionomer solutions, Journal of applied electrochemistry 19 (1989) 167-173.

(7) G. Gebel: Ionomer solutions: Polyelectrolyte or ionomer behavior? Macromolecular complexes in chemistry and biology, Eds: Dubin/Bock/Davis/Schulz/Thies, Springer -Verlag Berlin Heidelberg 1994.

(8) G. Gebel, B. Loppinet: Colloidal structure of ionomer solutions in polar solvents. Journal of Molecular Structure 383 (1996) 43-49.

(9) B. Loppinet, G. Gebel: Rodlike colloidal structure of short pendant chain perfluorinated ionome solutions. to be published

(10) Grot, W. G. , Chadds. F.; European patent 0066369, 1982.

(11) Martin C. R., Rhoades T. A., Ferguson J. A; , Anal. Chem. 54 (1982) 1639

(12) P. Aldebert, G. Gebel, B. Loppinet, N. Nakamura: Polyelectrolyte effect in perfluorosulfonated ionomer solutions, Polymer, Volume 36, 2, 431-434 (1995).

(13) P. Aldebert, M. Guglielmi, M. Pineri: Ionic conductivity of bulk, gels and solutions of perfluorinated ionomer membranes. Polymer Journal, Vol. 23, No 399-406 (1991).

Dissolution

water/ethanol (50/50) autoclave 1h/250 C

↓

homogeneous and stable solution (10% w/w)

Solutions in pure solvents :

- dialysis
- powder

SMALL ANGLE SCATTERING STUDY

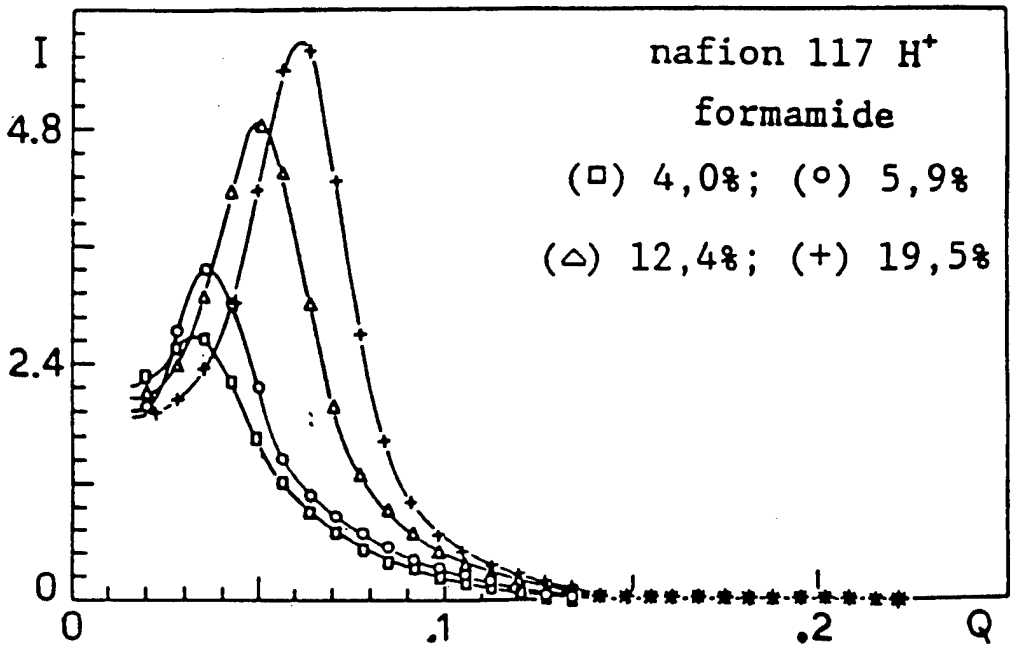

$d_{max} = 2\pi/q_{max}$

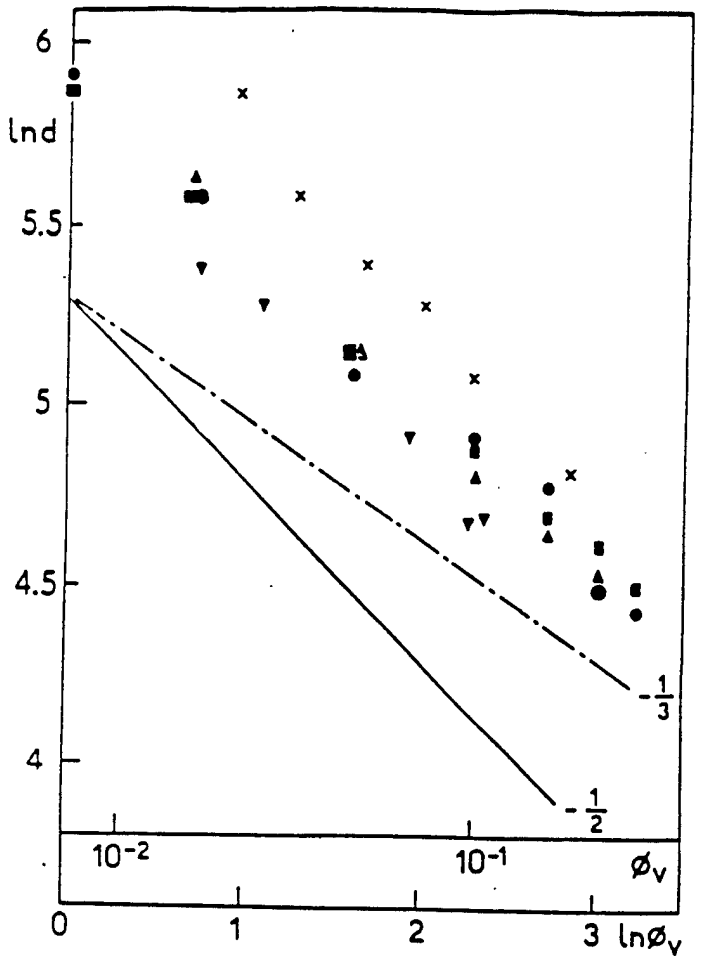

(×) 1100 H^+ eau

(▼) 1100 H^+ éthanol

(●) 1100 H^+ NMF

(■) 1200 H^+ NMF

(▲) 1200 Li^+ NMF

Slope −1/2 ⟶ rods

geometrical considerations

$$r = \left(\frac{2}{\pi\sqrt{3}}\right)^{1/2} \cdot d_{max} \cdot \Phi^{1/2} = 0.606 \cdot d_{max} \cdot \Phi^{1/2} \simeq 18\text{-}30\,\text{Å}$$

$$\sigma = \frac{2\pi r L \cdot v_0}{\pi r^2 L} = \frac{2 \cdot v_0}{r} \simeq 80\,\text{Å}^2$$

DILUTED SOLUTIONS

$I(q) = k\,|F(q)|^2\,S(q)$

$S(q) \longrightarrow 1$

$$I(q) \simeq k' \frac{\pi}{2qH} \cdot \frac{4J_1^2(qR)}{(qR)^2} \simeq \frac{k''}{q} \cdot e^{-\frac{q^2R^2}{4}}$$

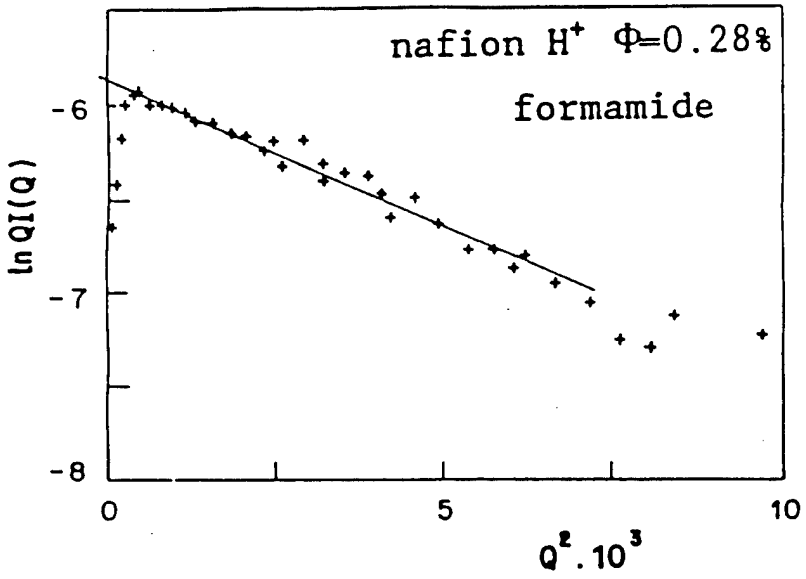

Linear behavior ⟶ rods

Slope ⟶ radius

	σ Å²	r Å	R Å
1100 H éthanol	88	21	18
1100 H NMF	84	22	26
1100 H formamide	71	26	27
1100 H eau	59	31	25
1100 Li méthanol	73	25	20
1100 Li éthanol	96	19	21
1100 Li DMA	82	22	19
1100 Li DMF	88	21	22
1100 Li NMF	82	22	
1200 Li NMF	78	26	
1200 Li NMF	83	24	

POLYMER/SOLVENT CONTRAST VARIATION

CH_3OH / CD_3OD

$$\rho_M = (1-\chi)\cdot\rho_H + \chi\cdot\rho_D$$

$$\sqrt{K} = \left| 1 - \chi\cdot\frac{\rho_D - \rho_H}{\rho_p - \rho_H} \right|$$

$$K = \frac{(\rho_p - \rho_M)^2}{(\rho_p - \rho_H)^2}$$

$$\begin{cases} \rho_H = -0.371\cdot10^{-10}\ \text{cm}\text{Å}^{-3} \\ \text{et} \\ \rho_D = +5.827\cdot10^{-10}\ \text{cm}\text{Å}^{-3} \end{cases}$$

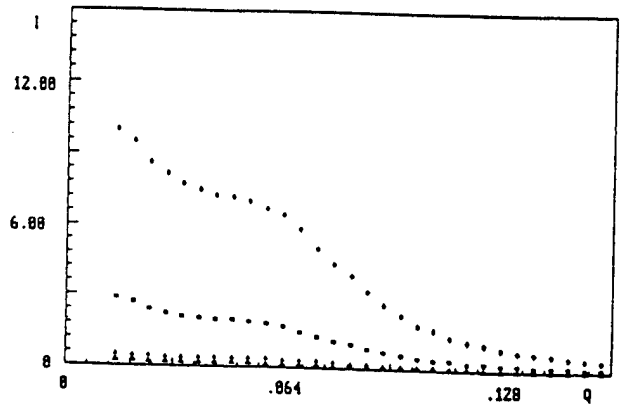

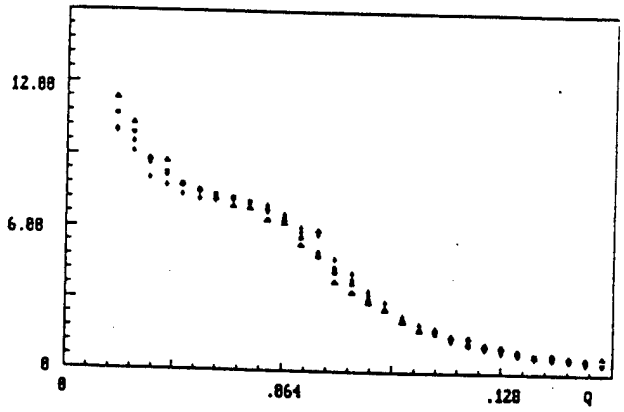

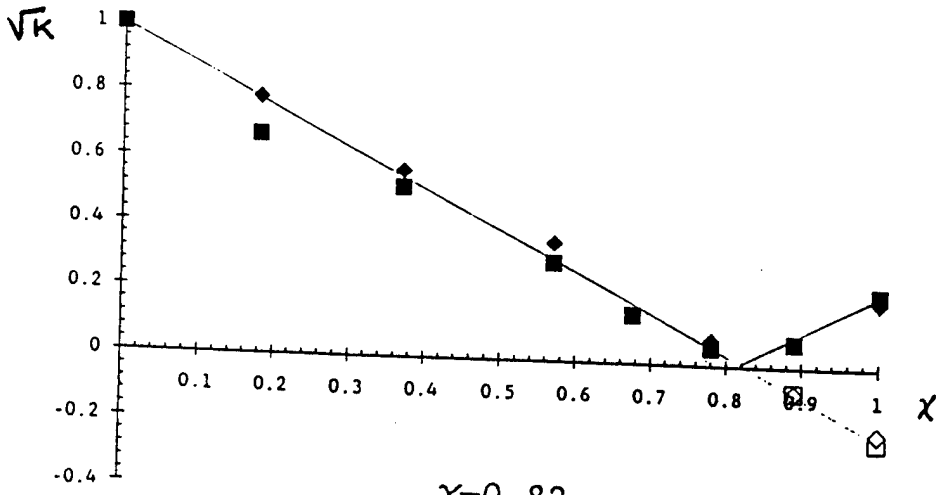

$\chi = 0.82$

$$\rho_p = 4,71\cdot10^{-10}\ \text{cm}\text{Å}^{-3}$$

$$\rho_{crist} = 5,08\cdot10^{-10}\ \text{cm}\text{Å}^{-3} \text{ et } \rho_{am} = 4,21\cdot10^{-10}\ \text{cm}\text{Å}^{-3}$$

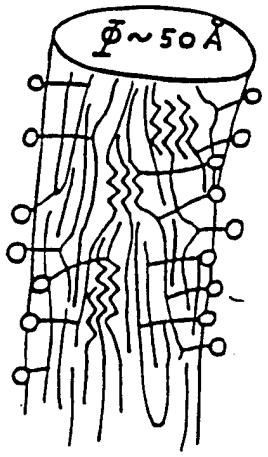

o: SO_3^-

—: chaines CF_2-CF_2

≈: "cristallites"

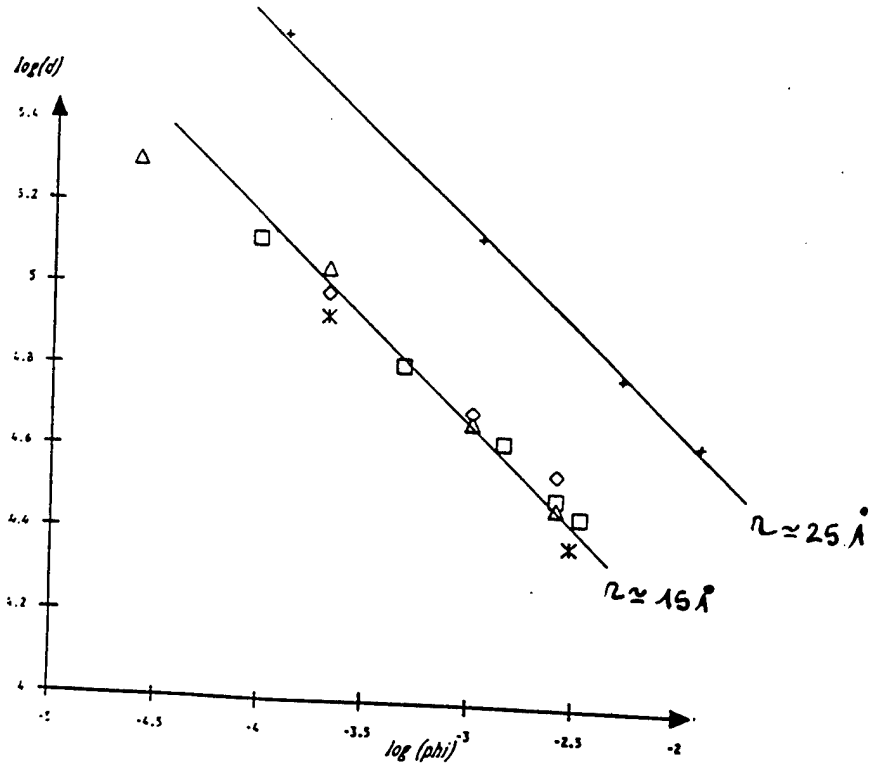

NAFION 117

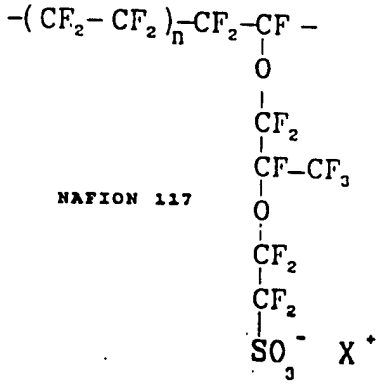

HOECHST

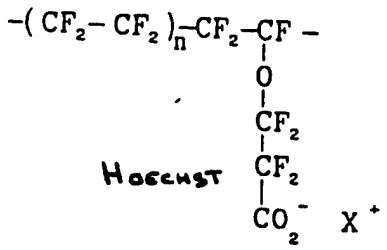

Investigations of Electrocatalyst Membrane Interface in Proton Exchange Membrane Fuel Cells using Synchrotron Based X-ray Absorption Techniques

Sanjeev Mukerjee and James McBreen
Department of Applied Science, Brookhaven National Laboratory
Upton, NY 11973

The need to adequately understand the electrocatalyst membrane interface is paramount for better design of membrane-electrode assemblies such as those with higher anode CO tolerance, better stability at higher temperatures and cathodes with lower sensitivity for methanol crossover. The use synchrotron based x-ray probes, specially the x-ray absorption spectroscopy offer new insights and direct spectroscopic evidence of various processes occurring at these interfaces. The principal advantage, this technique offers is the ability to study electrocatalyst interface under *in situ* electrochemical conditions with element specificity. The two complimentary parts of the spectra, the near edge (x-ray absorption near edge structure, XANES) and the extended part (extended x-ray absorption fine structure, EXAFS) offer information on changes in the chemical-state and short-range atomic structure around the individual elements. Further, the ability to probe the short-range atomic structure allows the study of both nanocrystalline and amorphous materials akin to actual supported electrocatalysts, eliminating the need to extrapolate evidence from model systems. This presentation will attempt to provide new insights into the different behavior exhibited by various electrocatalyst interfaces brought about by variations in particle size, alloying and under-potential depositions *etc.* The ability to characterize changes in the electrocatalyst in terms of variations in the electronic and short-range atomic structures during conditions of CO adsorption and methanol oxidation on carbon supported commercial electrocatalysts such as Pt, PtRu, PtSn *etc* and their implications on the overall fuel cell performance will be described.

Investigation of Electrocatalyst-Proton Exchange Membrane Interface using Synchrotron based In situ X-ray Absorption Spectroscopy

Sanjeev Mukerjee
Department of Applied Science
Material Science Division, Brookhaven National Laboratory
Upton, NY 11973

Presentation at the Workshop on
'Advanced Fuel Cell Membranes for Non Conventional Fuels'
Las Vegas, NV, April 28th-May 1st, 1998

OUTLINE

- ***Interfacial Structure:***
  -Factors Relevant to the Performance of the Membrane-Electrode Assemblies
- ***Synchrotron XAS:***
  -A Tool for In situ Characterization of the Membrane-Electrode Interface
- ***Experimental Aspects:***
  -Spectro-electrochemical Cells
  -Relevant Detectors and Techniques
- ***Some Recent Results:***
- ***Summary***
- ***Acknowledgements***

Interfacial Structure: The Effect of Electrolyte

The Structure:

- *Low Dielectric Constant region:*
  -[Hydrophobic fluorocarbon polymer matrix]
- *High dielectric Constant region:*
  -[Ion clusters including sulfonate exchange sites, counter ions, sorbed H_20]
- *Interfacial region:*

-[Pendant side chains of sulfonate groups]

Important Parameters:

- *Stability: Thermal and Electrochemical*
- *Proton Conduction:*
- *Reactant Solubility and Permeability*
- *Non Reactive:*
- *Anionic Adsorption:*

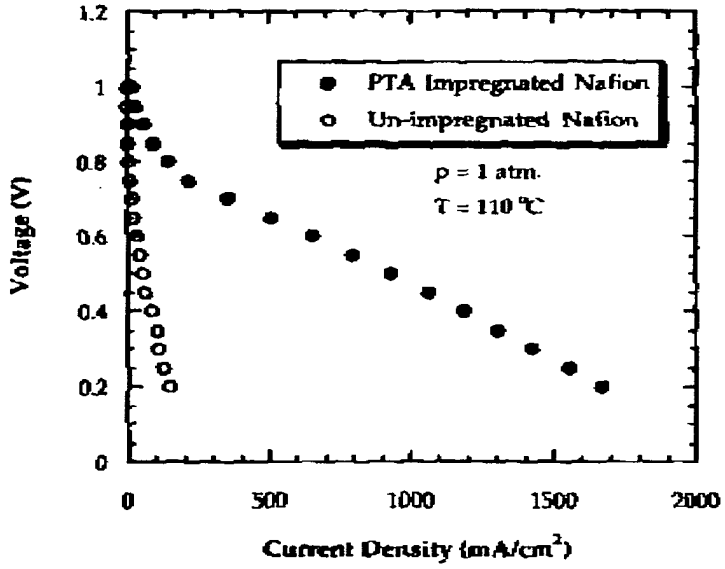

S. Malhotra and R. Datta, *JES*, **144**, L23 (1997)

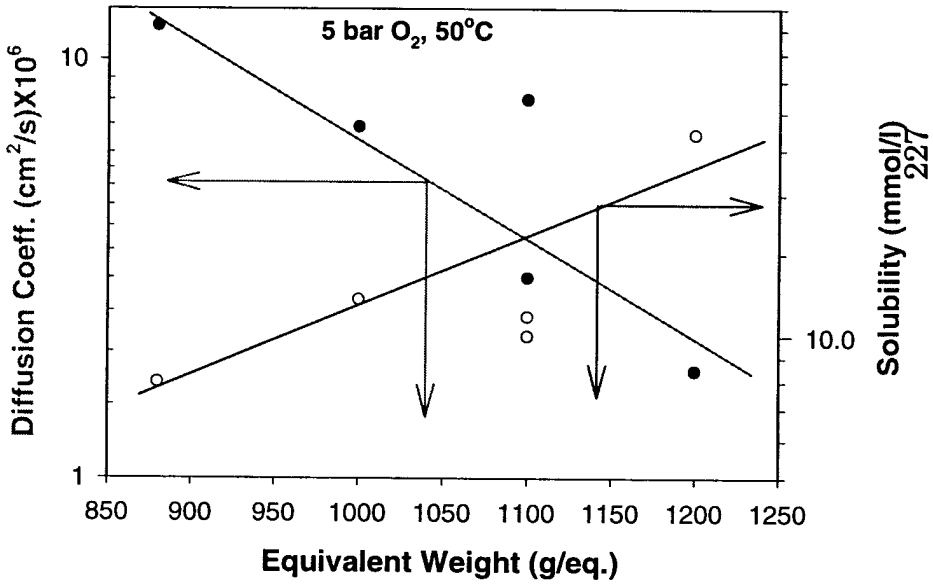

F. N. Buchi, M. Wakizoe and S. Srinivasan, *JES*, **143**, 927 (1996)

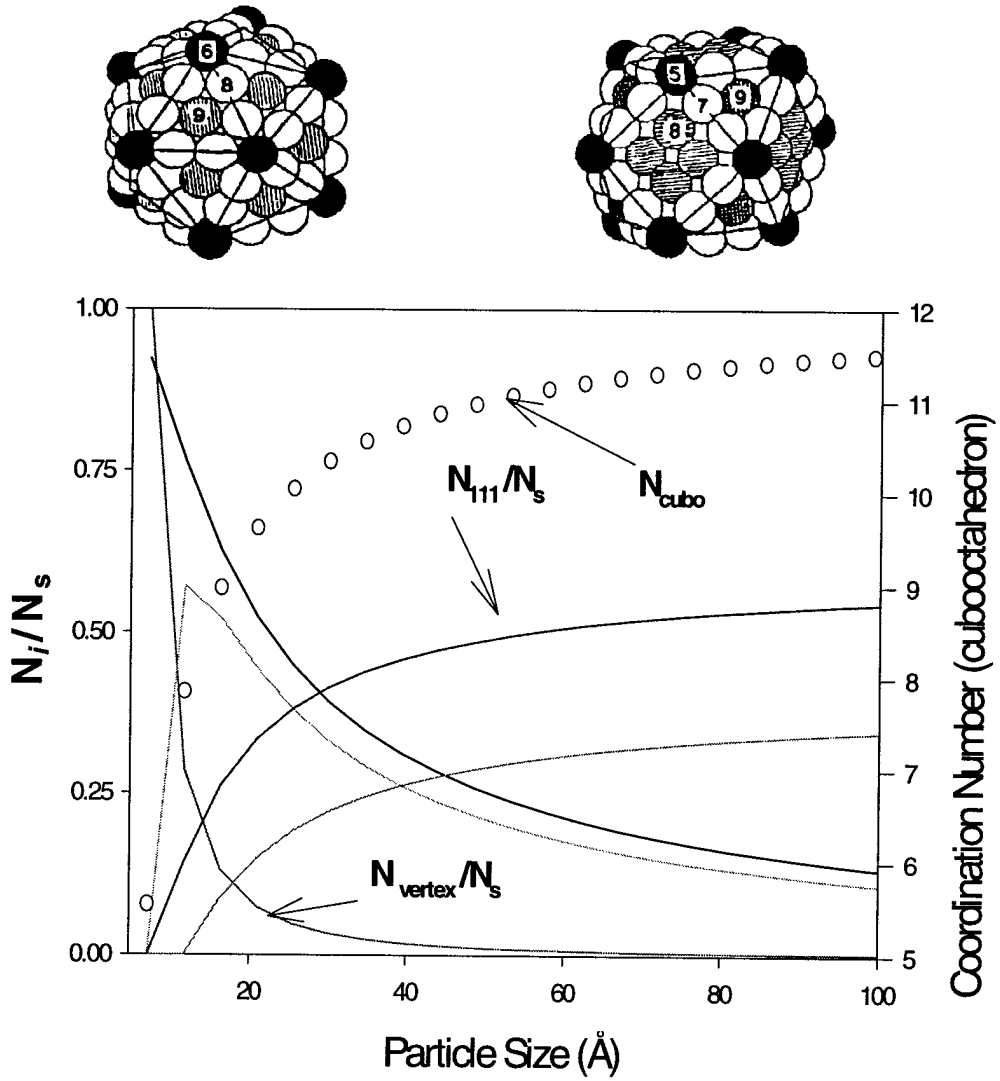
6
8
9
5
7
9
8
1.00
0.75
0.50
0.25
0.00
N_i/N_s
N_{111}/N_s
N_{cubo}
N_{vertex}/N_s
20
40
60
80
100
Particle Size (Å)
12
11
10
9
8
7
6
5
Coordination Number (cuboctahedron)

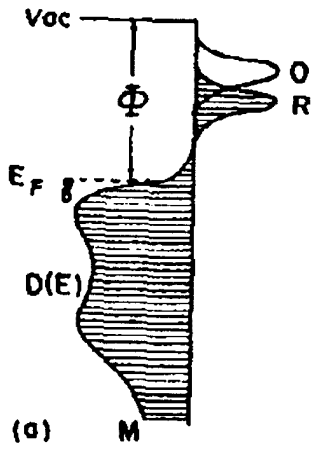

Redox reaction

$O + e(M) \not\rightleftharpoons R$

(non – matching energy levels)

3 coordination site requirement for methanol

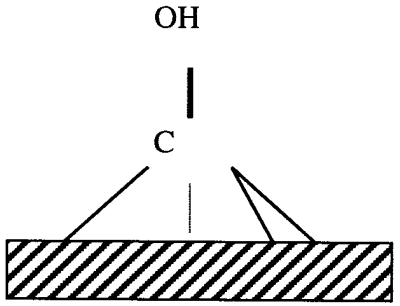

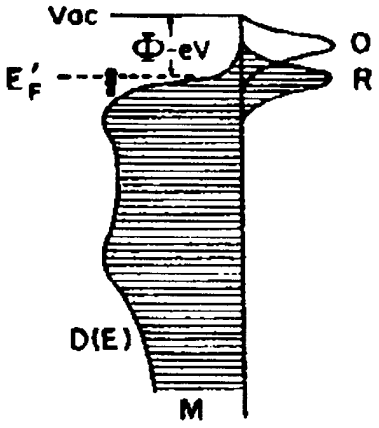

$O + e(M) \rightleftharpoons R$

at electrode potential V (matching energy levels)

$$\Phi_V = \Phi_{V=0} \pm eV$$

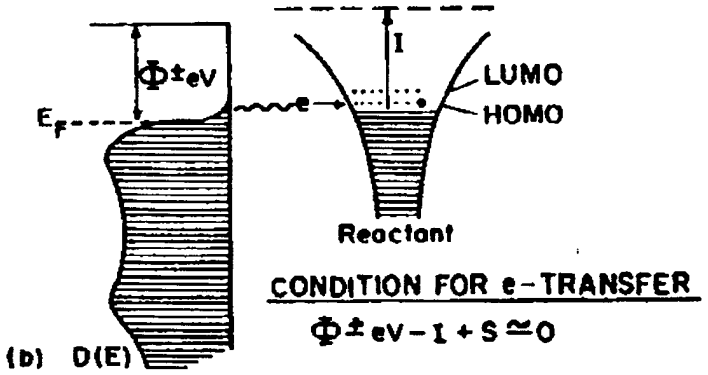

CONDITION FOR e-TRANSFER

$$\Phi \pm eV - I + S \simeq 0$$

Effect of Alloying

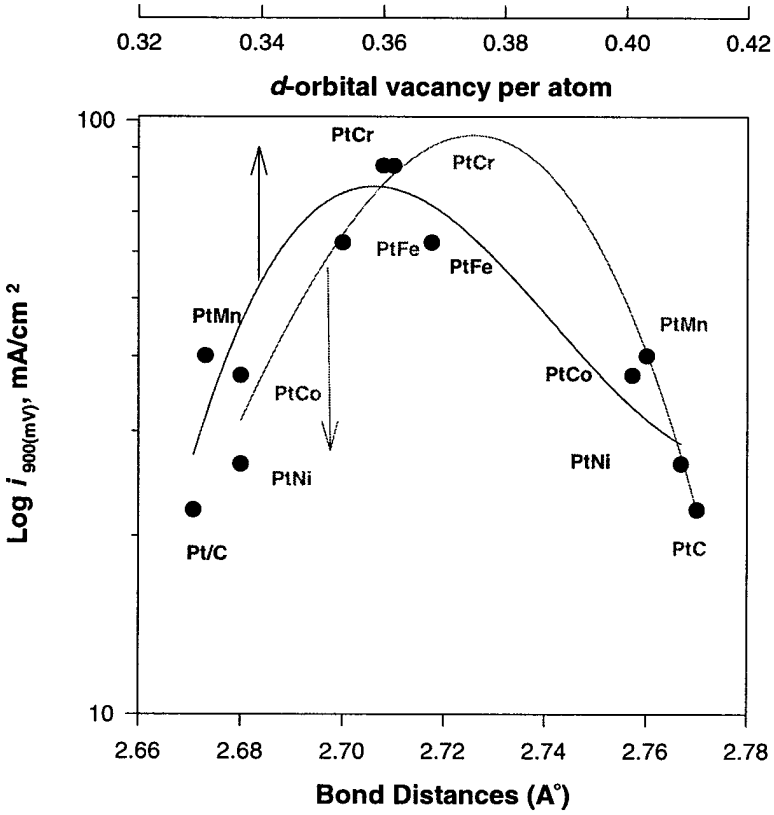

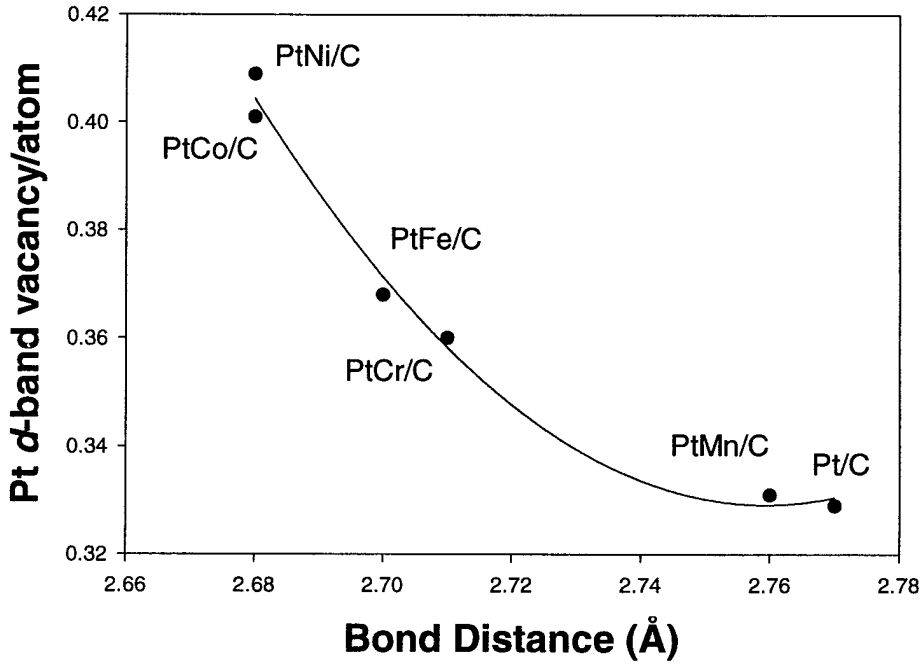

CO Tolerance by Pt and Pt Alloy Electrocatalysts

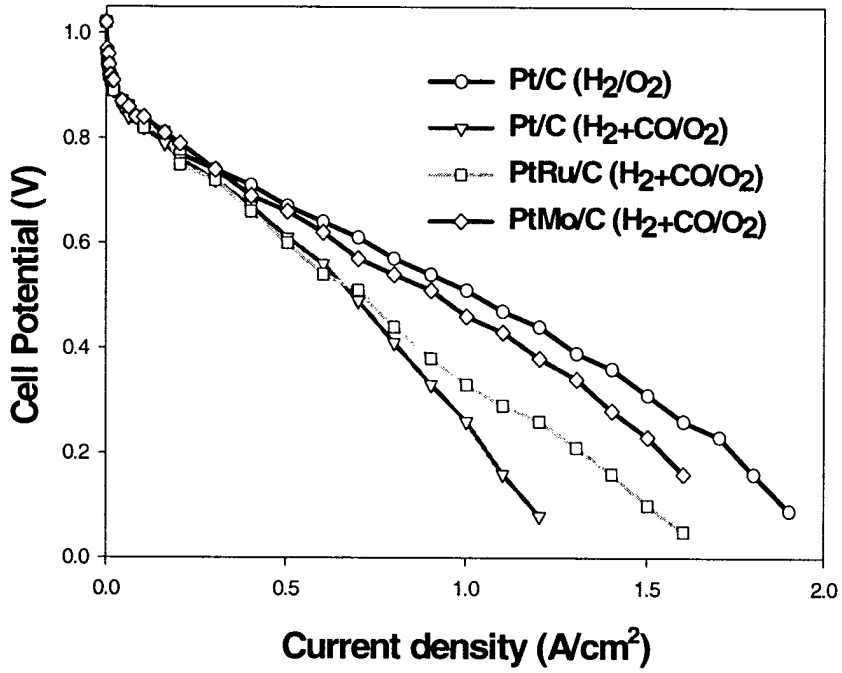

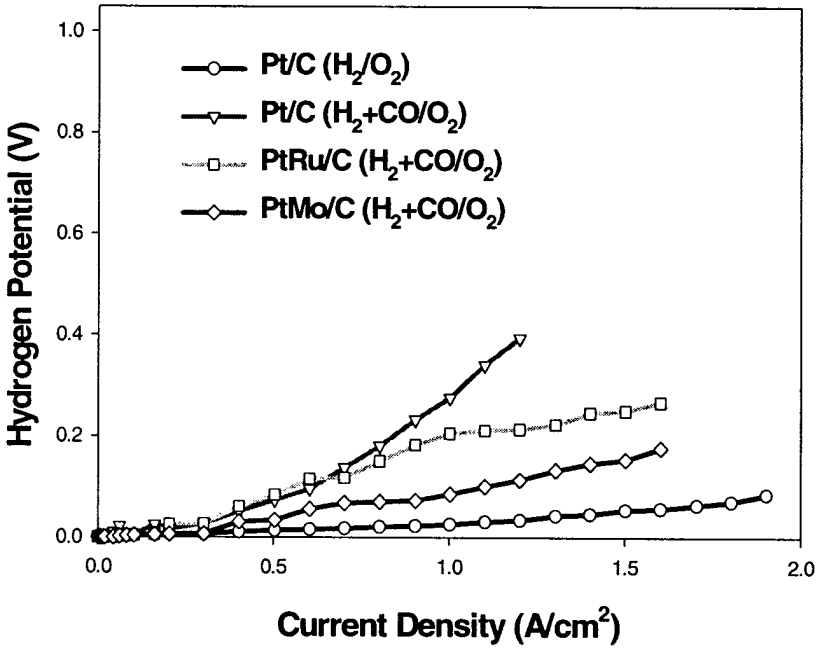

CO Concentration: 20 ppm, Operating temperature: 85°C, Electrode Loading: 0.4 mg/cm², Electrocatalyst Loading: 20% metal/C

Role of *In-situ* XAS as a Tool to Study Electrocatalysis

- In situ capability and Element Specificity
- Simultaneous Probe for Electronic and Structural Parameters

XANES Spectra

Physical Basis

Multiple scattering by low energy photo-electrons

Information

- **Determination of oxidation state and coordination symmetry**
- **Electronic Structure**
- **Extent of Corrosion**

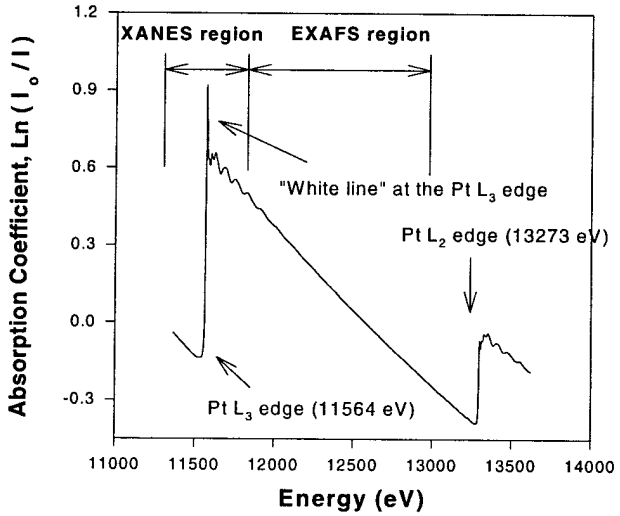

EXAFS Spectra

Physical Basis

Modulation of X-ray absorption by back scattered photo-electrons

Information

- **Determination of short range atomic order (bond distance, coordination number, Debye Waller factor *etc.*,)**

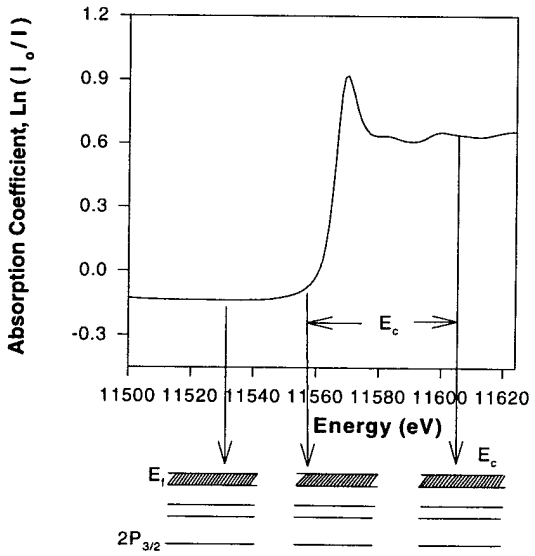

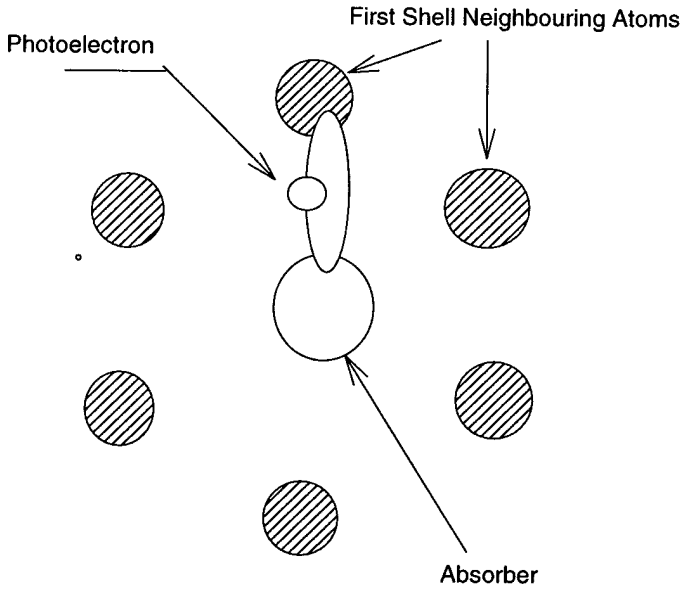

X-RAY ABSORPTION NEAR EDGE STRUCTURE

Calculation of *d* band vacancy of Pt from the Pt L_3 and L_2 absorption edges

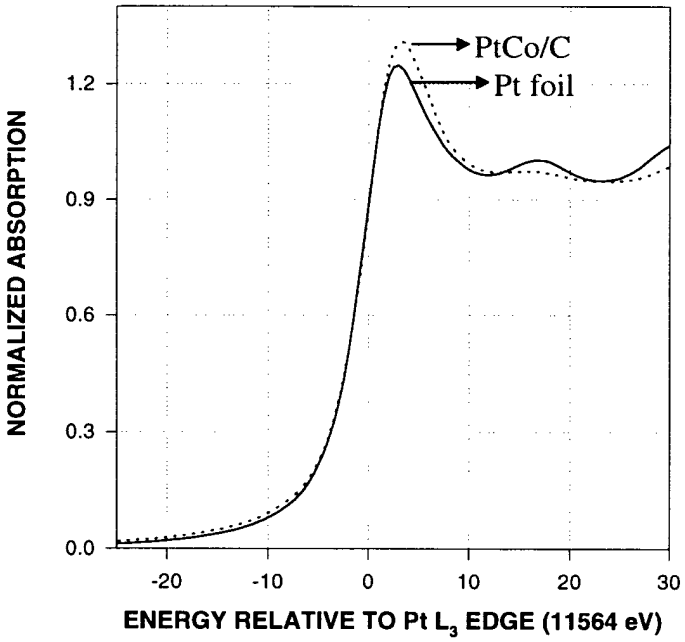

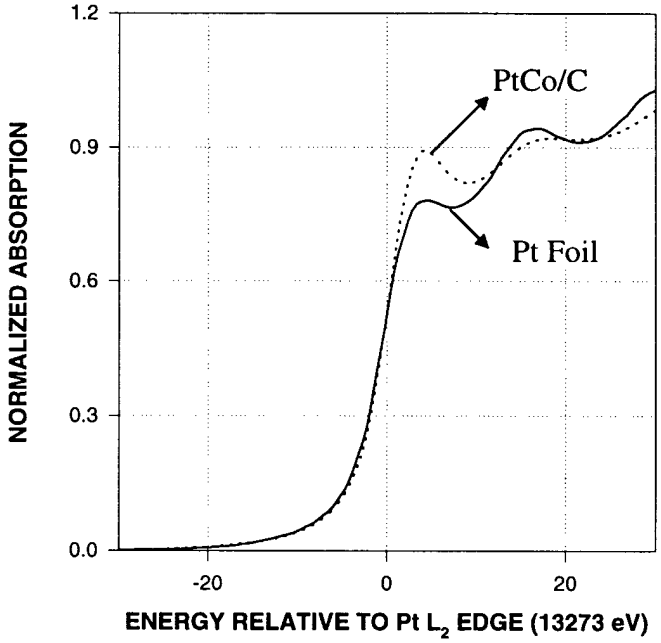

$$f_d = \frac{(\Delta A_3 + 1.11\Delta A_2)}{(A_3' + 1.11A_2')_r}$$

$$(h_J)_{t,s} = [1 + f_d]\,(h_J)_r$$

where $(h_J)_r = 0.3$ for pure Pt metal

EXAFS Analysis

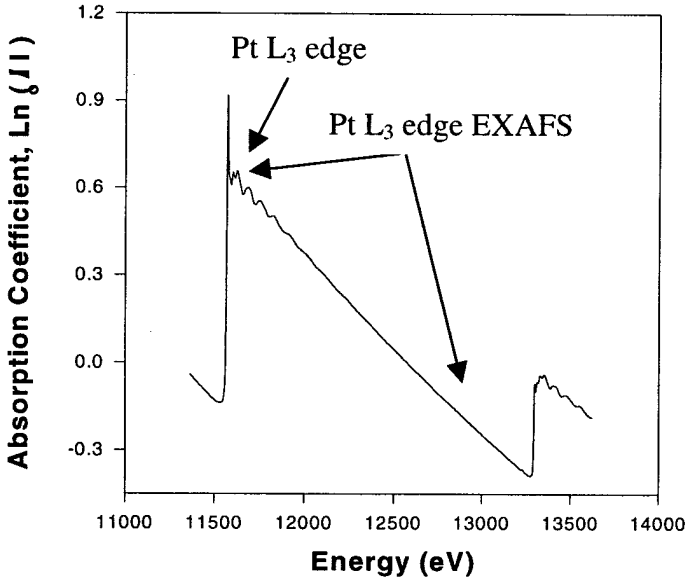

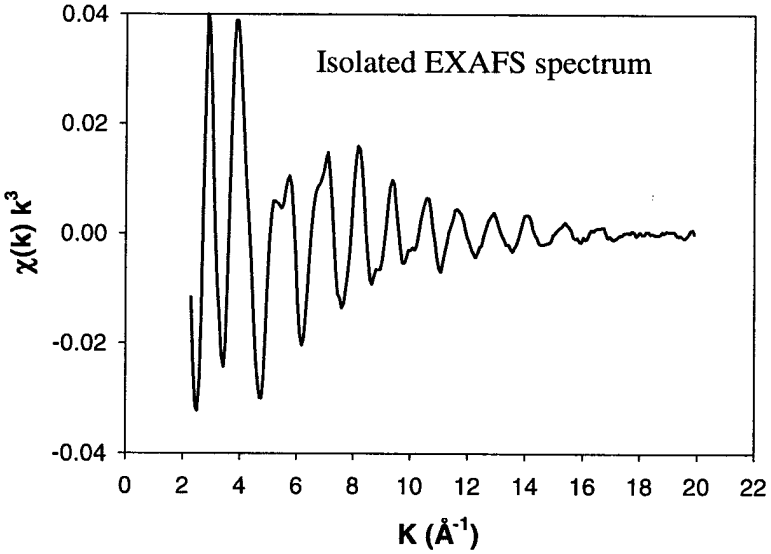

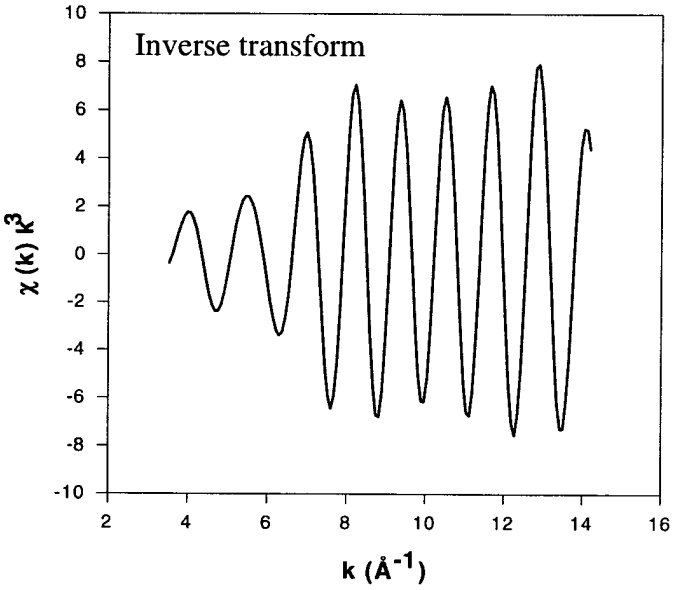

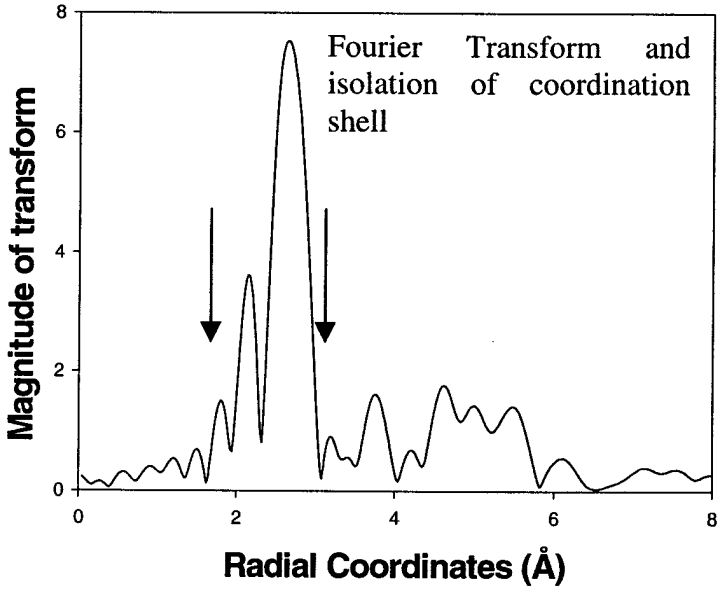

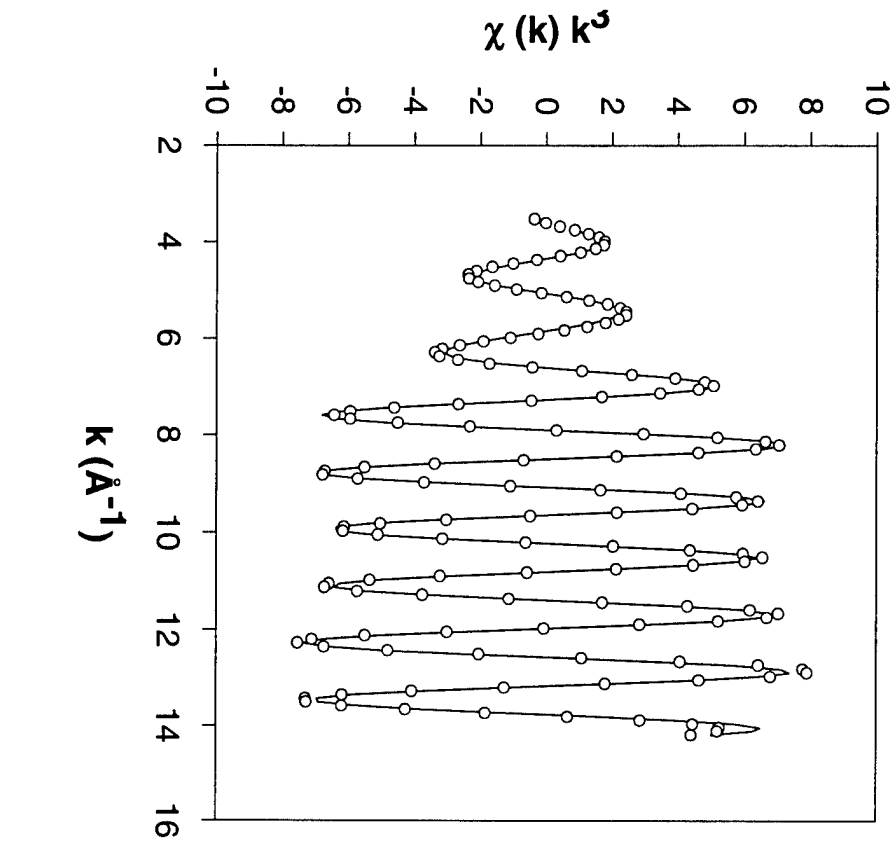
χ (k) k³
k (Å⁻¹)

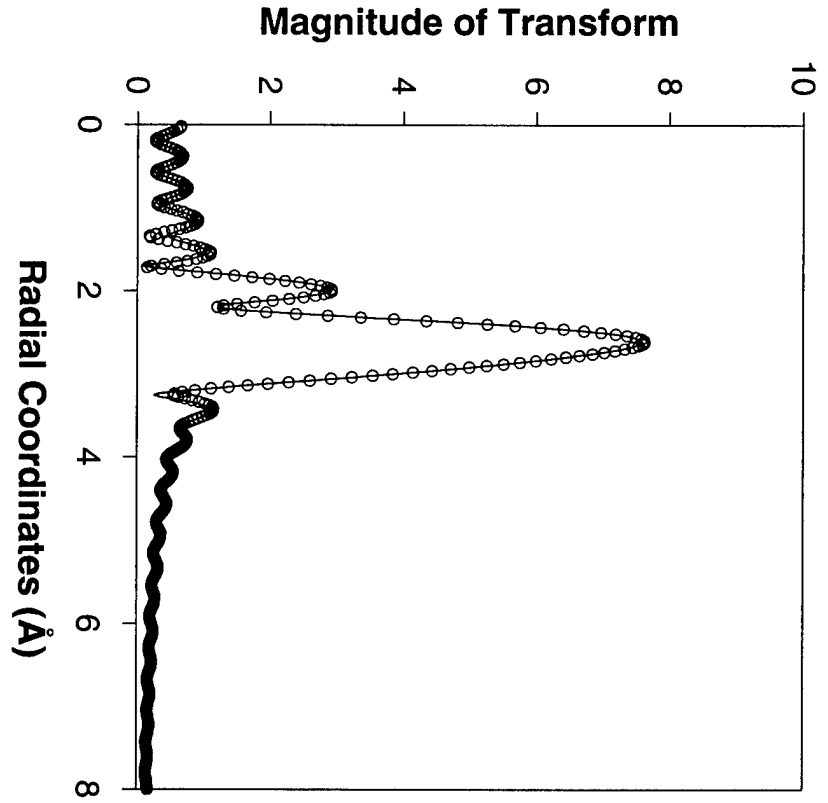
Magnitude of Transform
Radial Coordinates (Å)

Why Synchrotron?

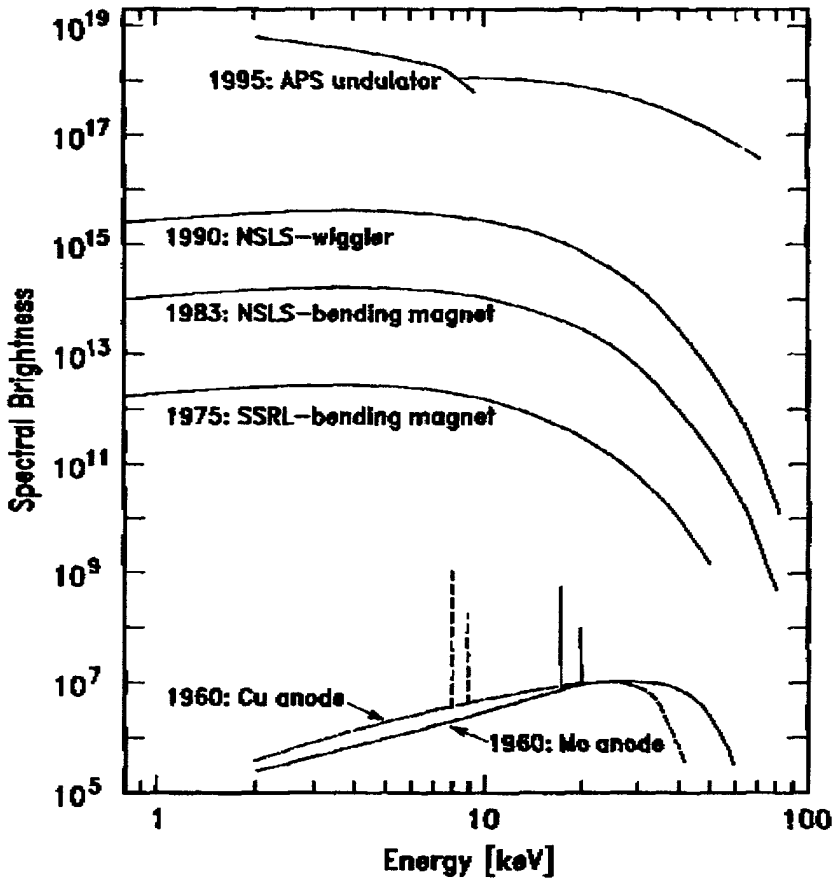

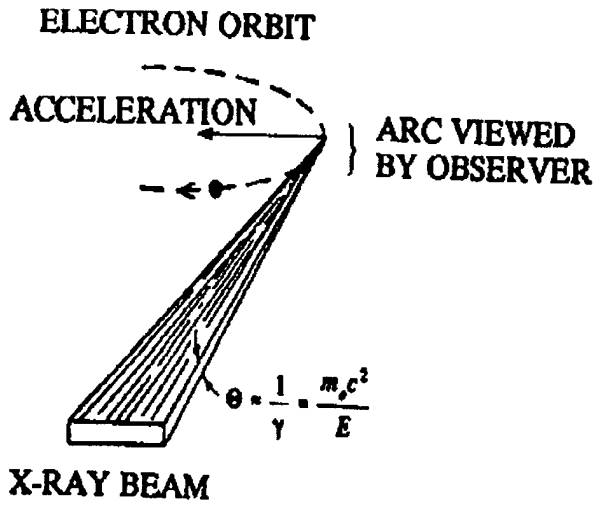

Advantages

- *High Intensity*
- *Broad Spectral Range*
- *High Polarization*
- *Pulsed Time Structure*
- *Natural Collimation*

Spectro-electrochemical Cell and XAS Data Acquisition Setup

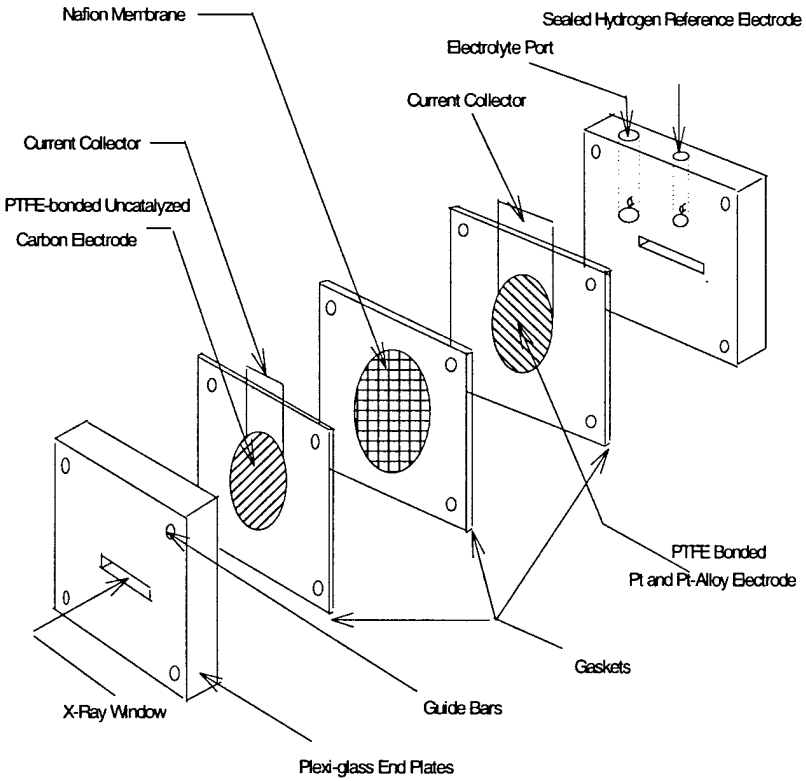

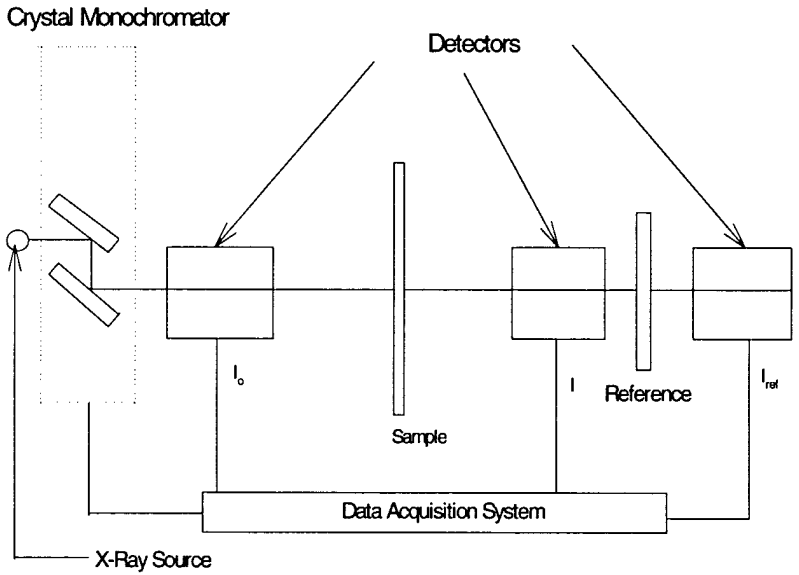

The Methanol Oxidation Reaction : Bifunctional Mechanism

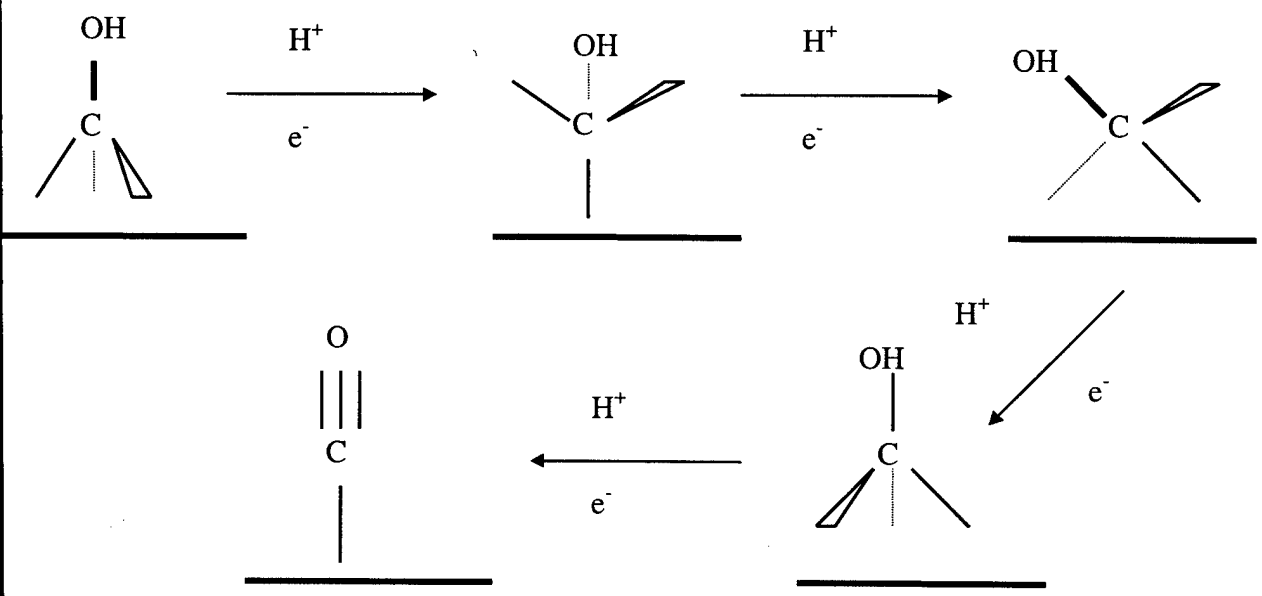

$$Pt + H_2O \rightarrow Pt - OH_{ads} + H^+ + e^-$$

$$M + H_2O \rightarrow M - OH_{ads} + H^+ + e^-$$

$$CO_{ads} + OH_{ads} \rightarrow CO_2 + H^+ + e^-$$

Motivation

- ***PtRu/C exhibits enhancement for both methanol and CO electro-oxidation irrespective of the nature of interaction between Ru and Pt.***
- ***PtSn/C alloy is a good catalyst for electro-oxidation of CO but not for methanol.***
- ***UPD Sn on Pt/C shows better performance for methanol oxidation as compared to Pt/C and PtSn/C alloy.***

EXPERIMENTAL

Electrocatalyst and Electrode Specifications (Pt and Pt Alloys)

- **Electrocatalysts:** **Pt/C, PtSn/C and PtRu/C**
- **Source:** **ETEK Inc., (Natick, MA)**
- **Alloy Composition:** **50/50 weight percent, Pt/Ru (~71 atom % Pt)**
- **Metal Loading on carbon:** **20 percent on Vulcan XC 72**
- **Pt loading:** **10 mg/cm^2**
- **PTFE loading:** **15 - 20 %**

X-ray Powder Diffraction Analysis

Electrocatalyst	Lattice Parameter (Å)	Particle Size (Å)
Pt/C	3.9271 (2.774)	32
PtRu/C	3.8907 (2.751)	35
PtSn/C	4.0015 (2.829)	34

UPD Sn on Pt/C

Deposited from 2mMol $SnCl_4$ in 1 M $HClO_4$ at 330 mV vs. RHE onto Pt/C (ETEK) for 3.75 hrs (θ_{Sn} = 0.6)

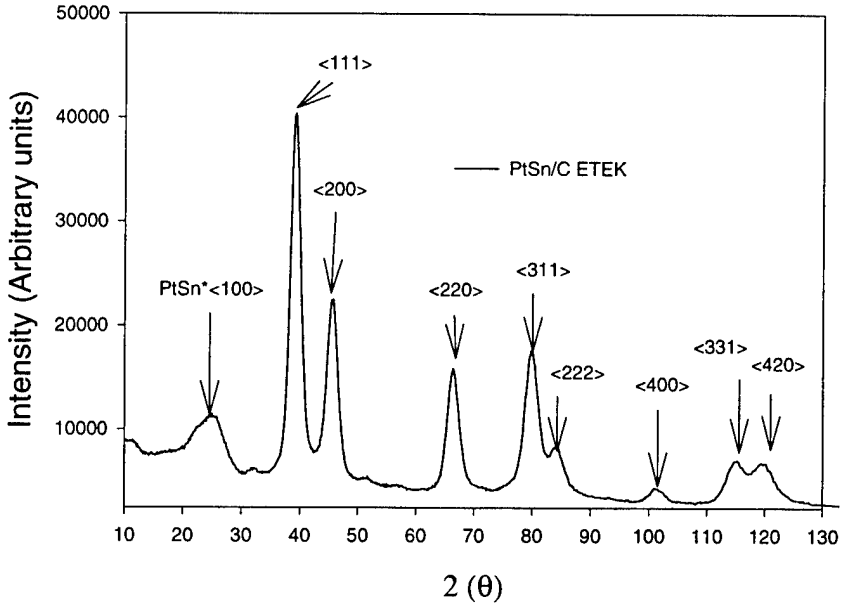

Powder x-ray diffraction pattern for the as received PtSn/C (ETEK) electrocatalyst

Voltammograms in 1 M $HClO_4$ with and without MeOH

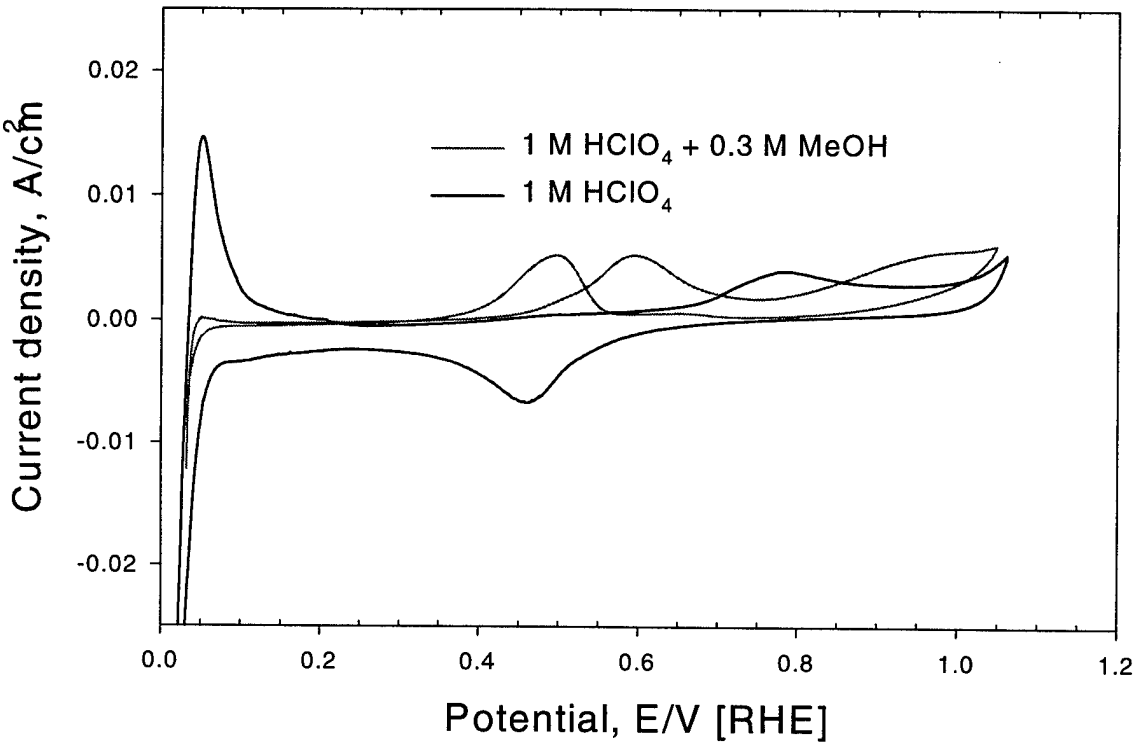

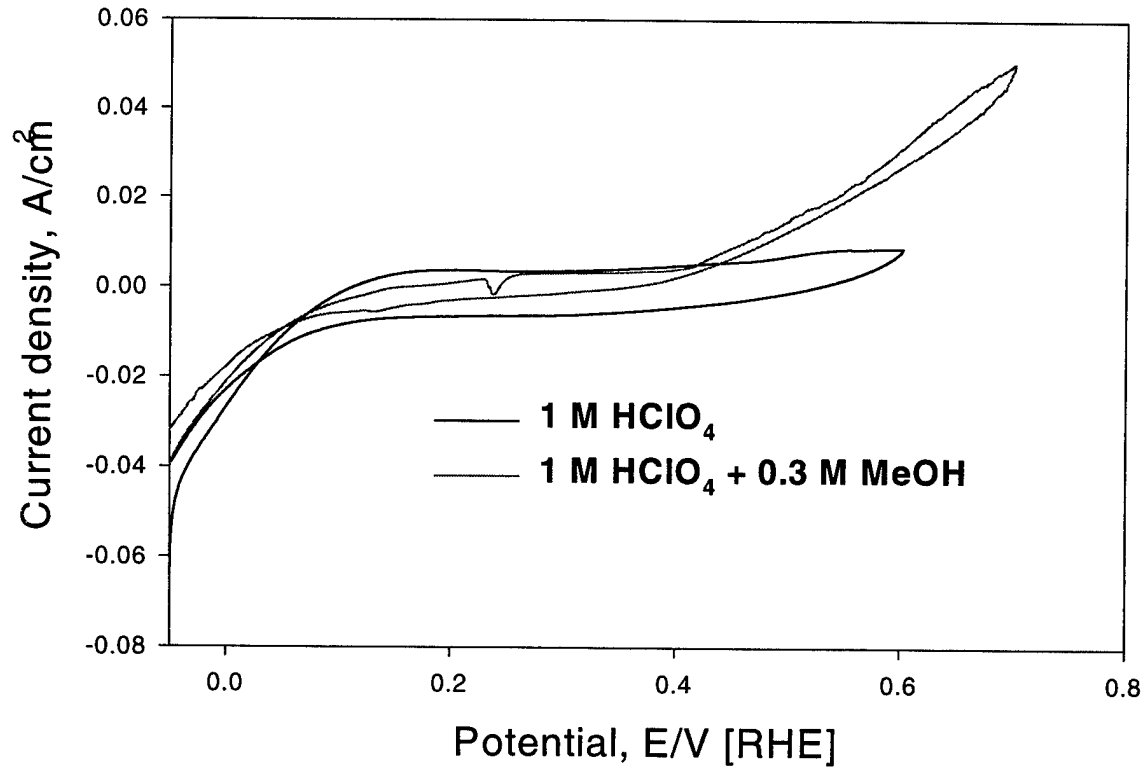

Voltammograms in 1 M $HClO_4$ with and without MeOH

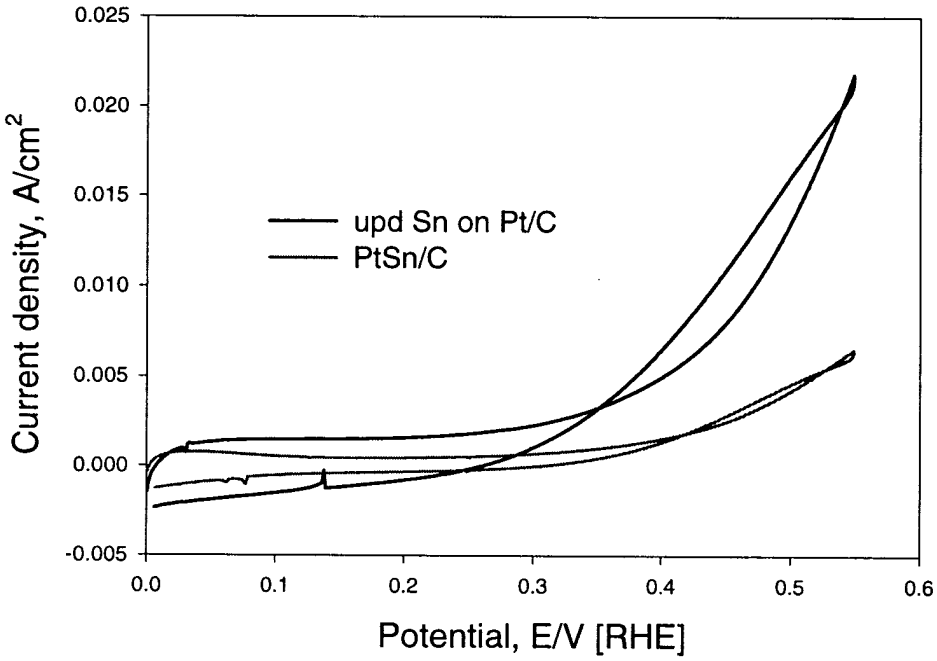

Comparison of PtSn/C (ETEK) and upd Sn on Pt/C ($\theta = 0.75$) in 1 M $HClO_4$ + 0.3 M MeOH.

In situ XAS at the Pt L_3 edge for Pt/C in 1 M $HClO_4$ + 0.3 M MeOH

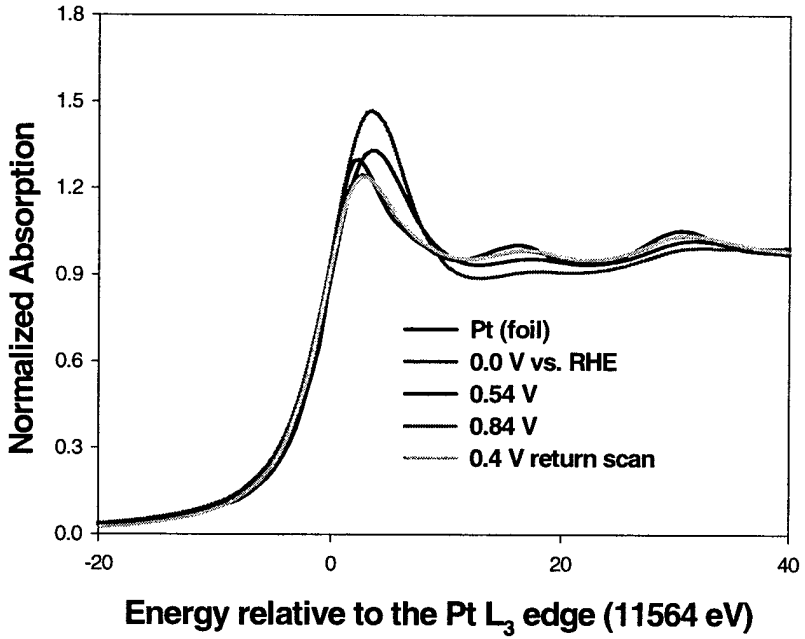

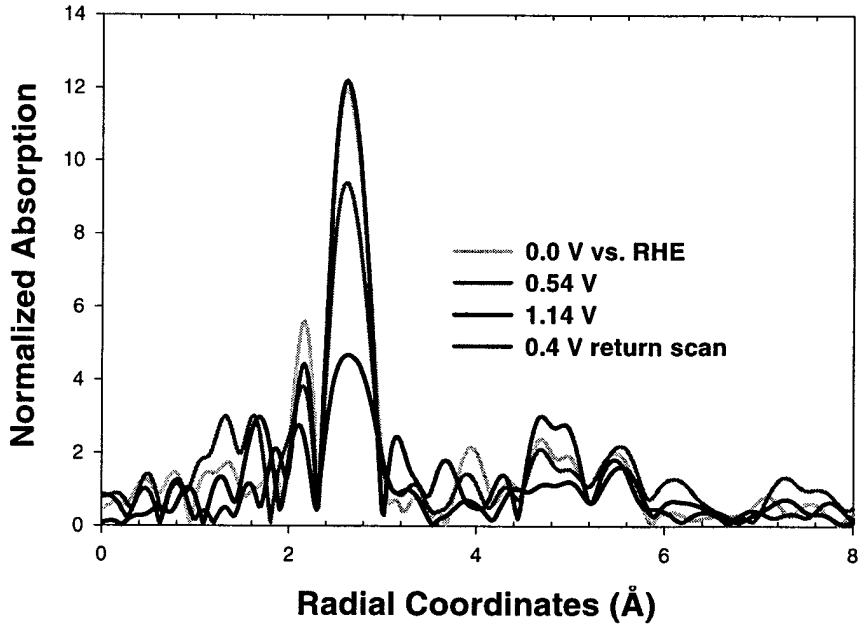

In situ XAS Study on the Effect of CO on Pt/C Electrocatalyst

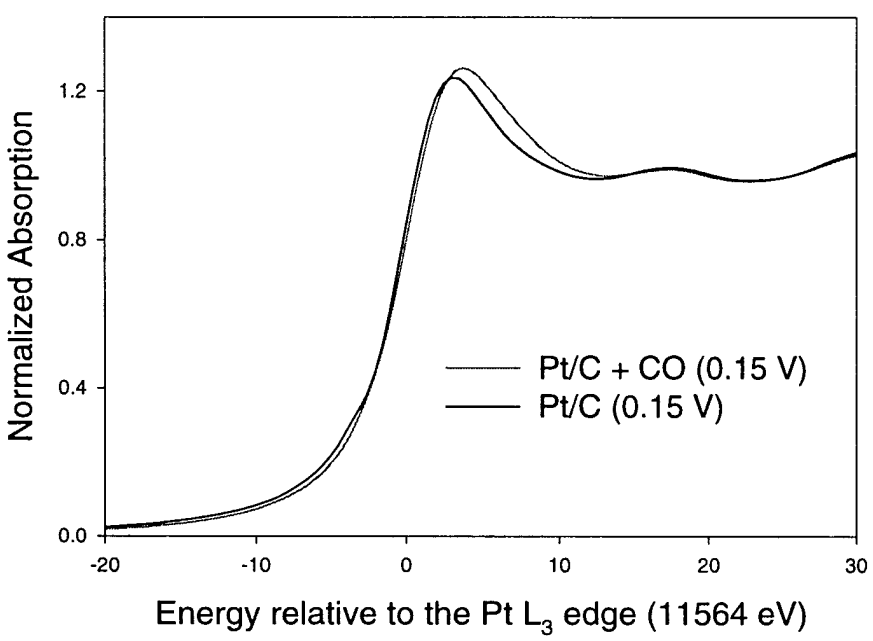

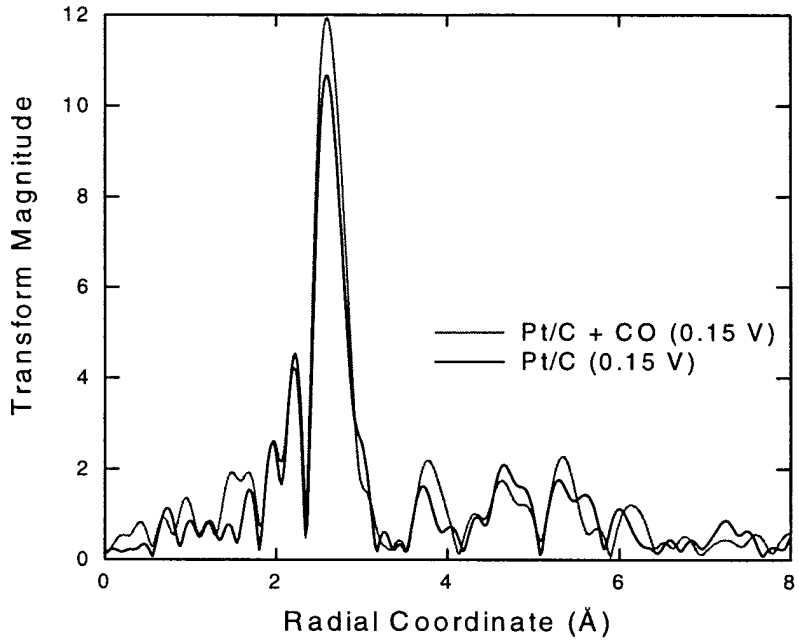

Coordination Shell	Coordination Number	Bond Distance (Å)
Pt-Pt	**10.19**	**2.77**
Pt-C	**0.5**	**1.92**

Pt L_3 XANES for PtRu/C and PtSn/C alloy at 0.54 V in 1 M $HClO_4$ with and without 0.3 M CH_3OH

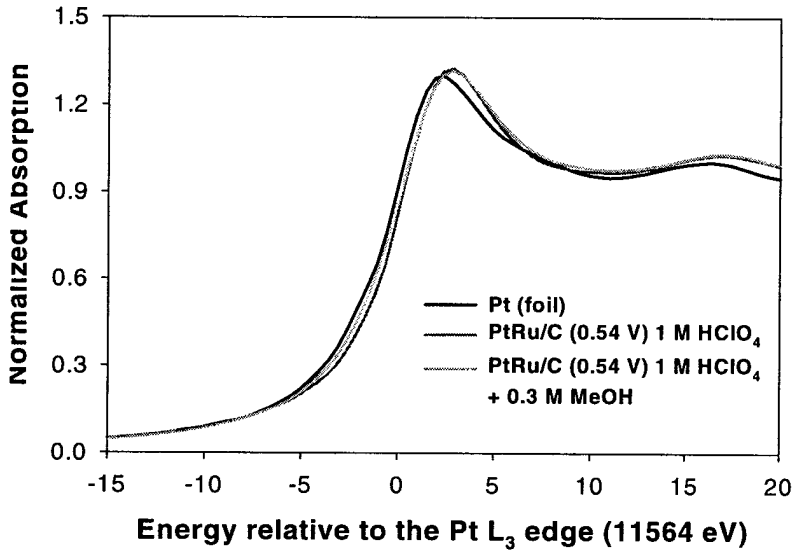

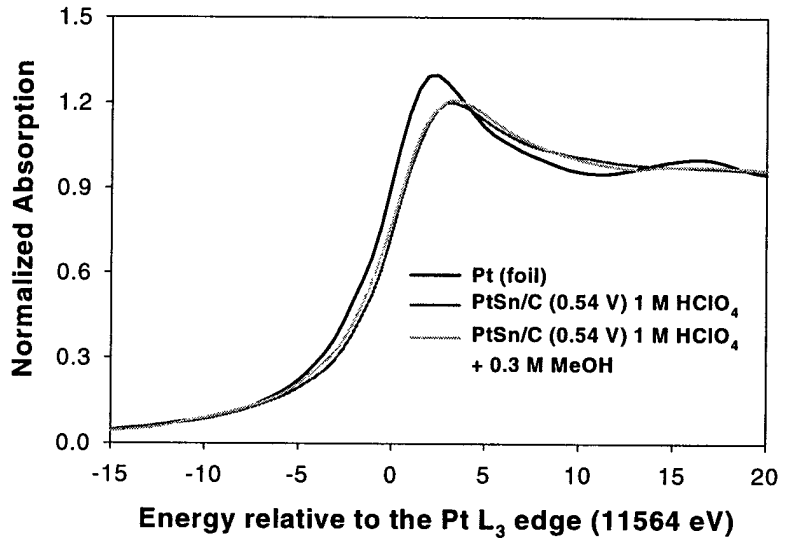

Results of XAS Analysis at Pt L3 edge in 1 M $HClO_4$ at 0.54 V vs. RHE for Pt/C, PtRu/C and PtSn/C

Electrocatalyst	Pt *d-band* Vacancy/atom	*EXAFS Parameters*				
		Coord. Shell	*N*	*R (Å)*	$\Delta\sigma^2$ (Å^2)	ΔE_o (eV)
Pt/C	0.329	Pt-Pt	8.66	2.773	0.0044	-0.88
PtSn/C	0.296	Pt-Pt	7.89	2.801	0.0051	3.55
		Pt-Sn	2.83	2.800	0.0097	-5.63
PtRu/C	0.382	Pt-Pt	7.52	2.73	0.0052	2.07
		Pt-Ru	2.61	2.69	0.0028	-6.24

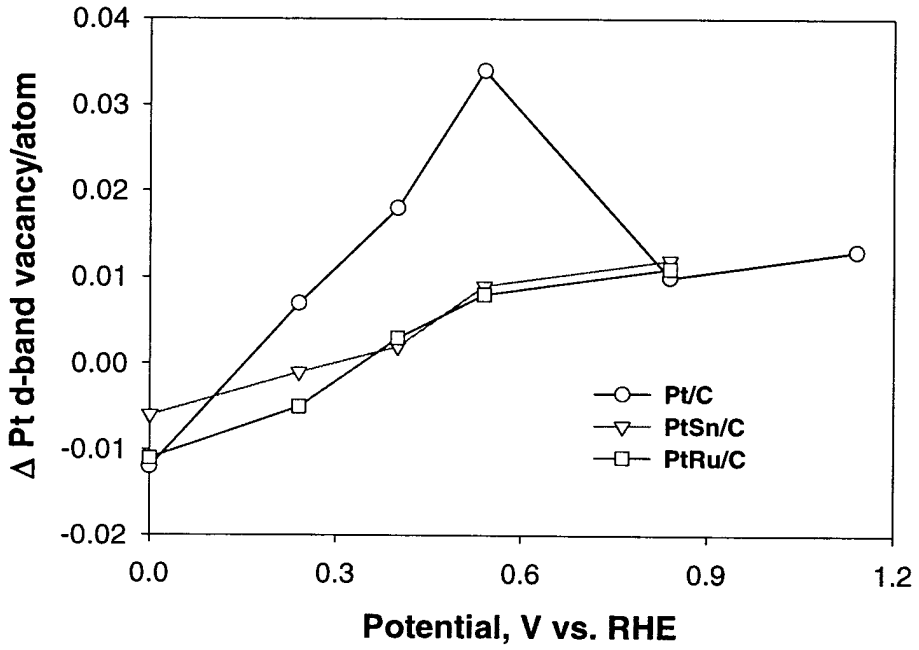

XANES at Sn and Ru K edge for PtSn/C and PtRu/C in 1 N $HClO_4$

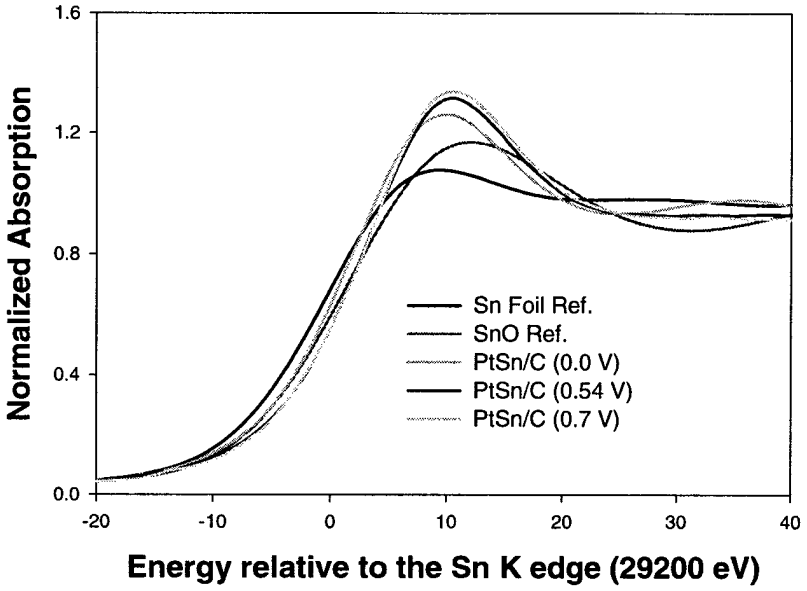

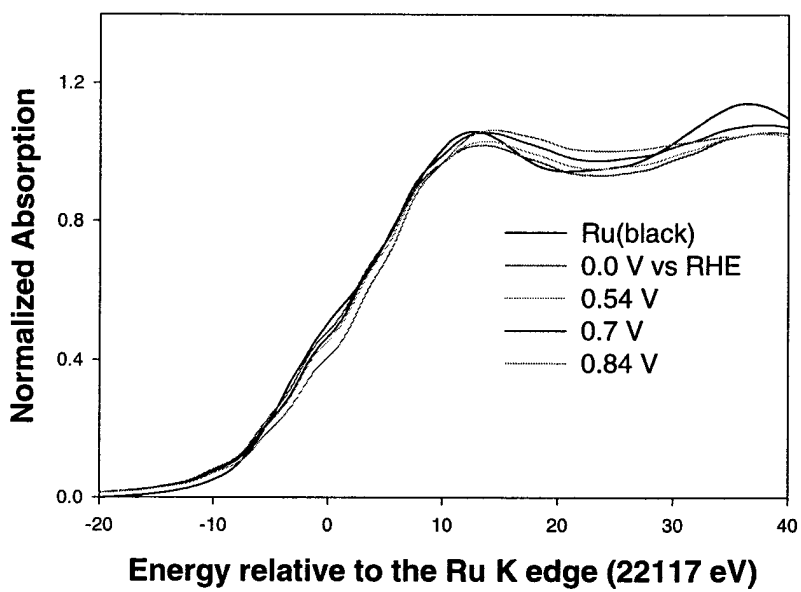

In situ XAS at the Sn K edge for upd Sn on Pt/C

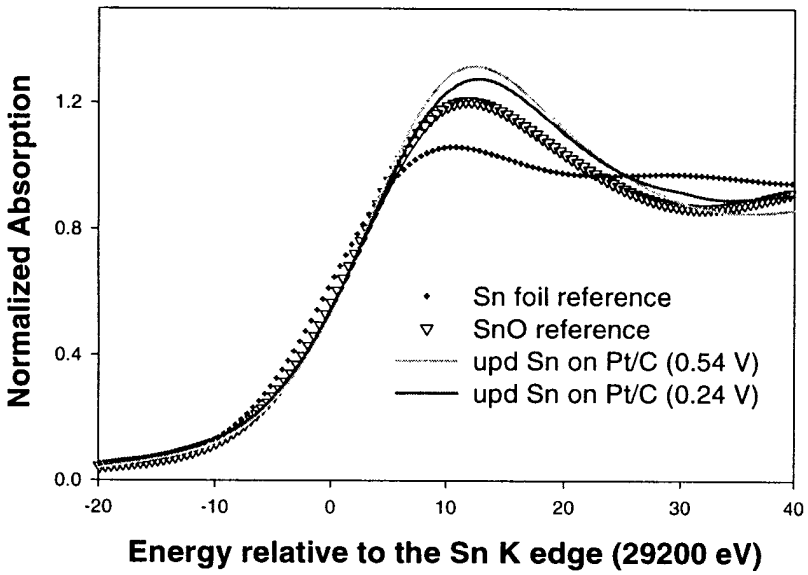

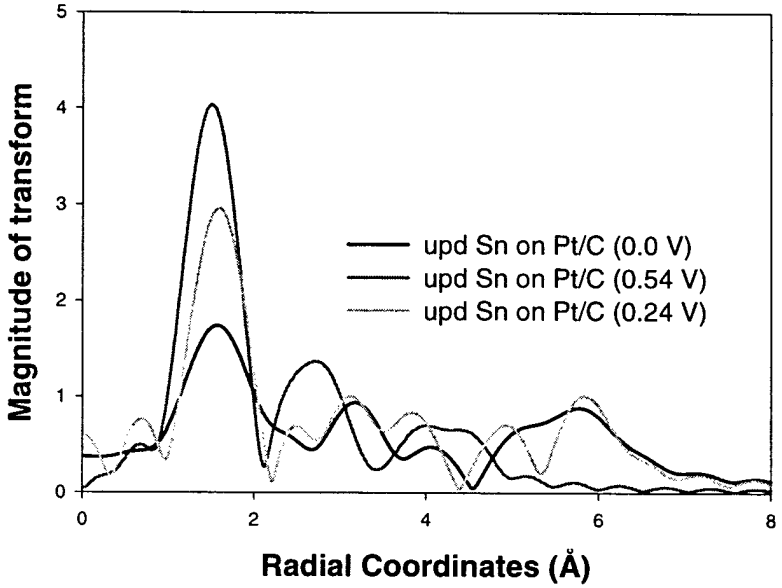

Electrode Potential V vs. RHE	EXAFS Parameters for Sn - O shell			
	N	R (Å)	$\Delta\sigma^2$ (Å^2)	ΔE_0 (mV)
0.54	6.0	2.05	-0.0004	5.1
0.24	3.5	2.10	-0.070	0.0
0.0	4.8	2.10	0.0080	0.5

XANES at Sn K edge for PtSn/C In 1 N $HClO_4$ + 0.3 N MeOH

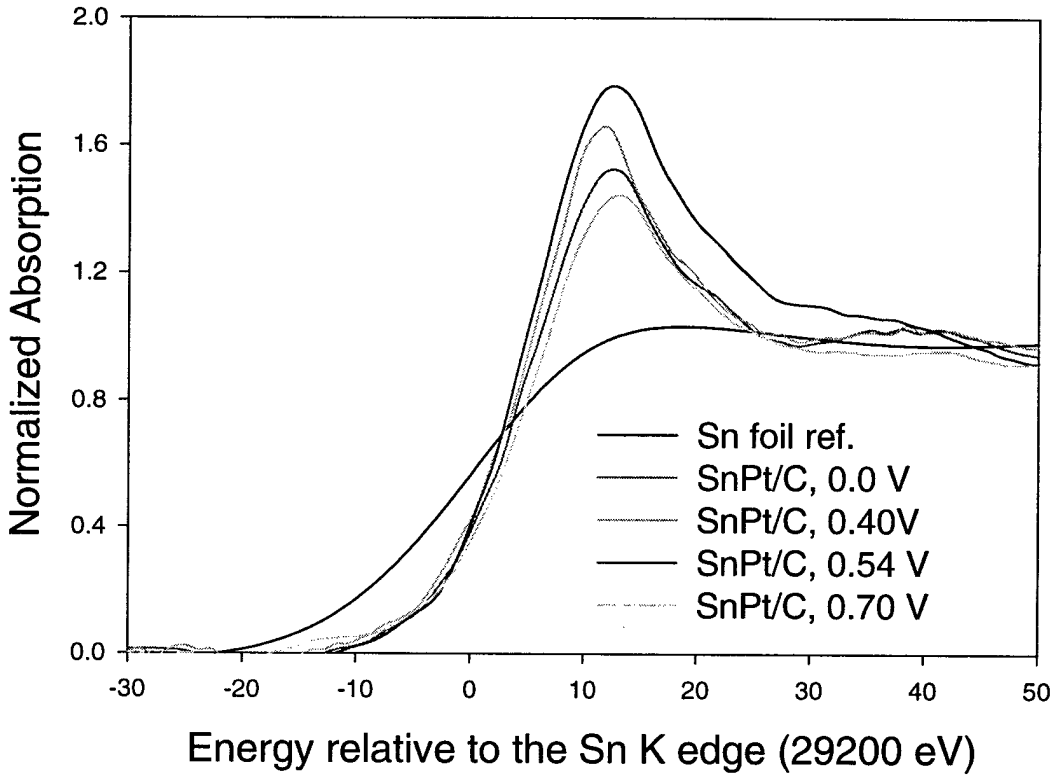

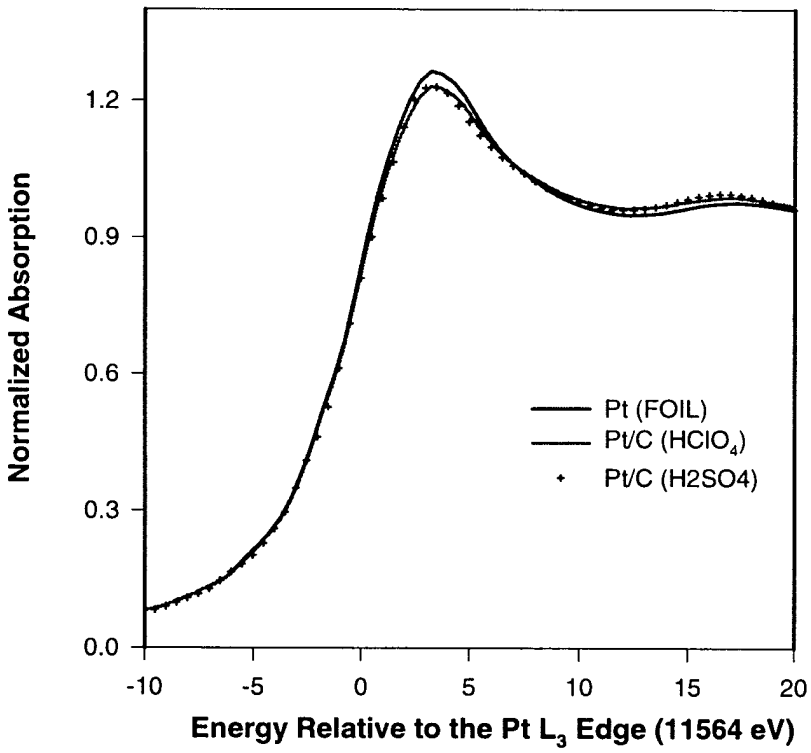
Normalized Absorption
1.2
0.9
0.6
0.3
0.0
-10
-5
0
5
10
15
20
Energy Relative to the Pt L3 Edge (11564 eV)
Pt (FOIL)
Pt/C (HClO4)
Pt/C (H2SO4)

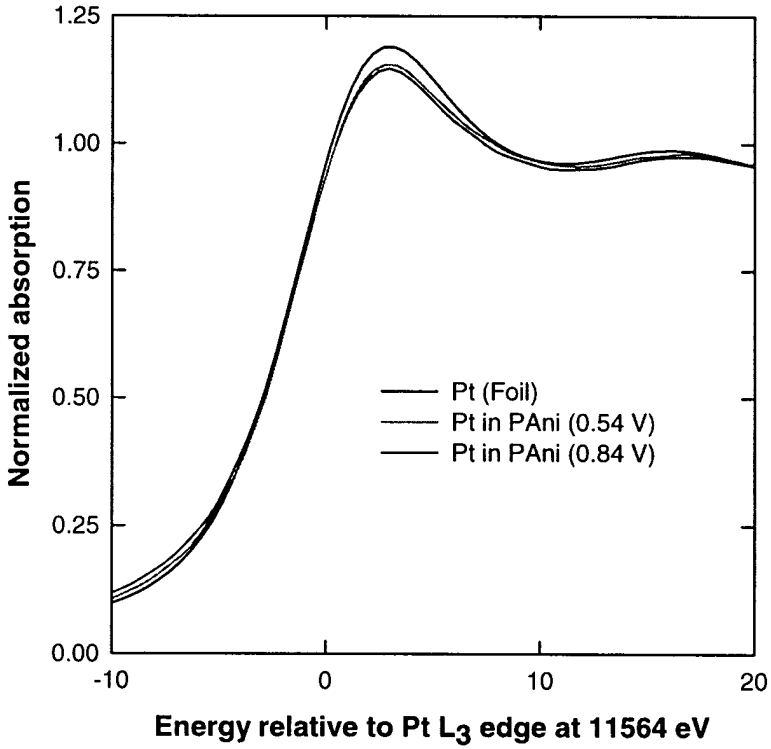
Normalized absorption
1.25
1.00
0.75
0.50
0.25
0.00
-10
0
10
20
Energy relative to Pt L3 edge at 11564 eV
Pt (Foil)
Pt in PAni (0.54 V)
Pt in PAni (0.84 V)

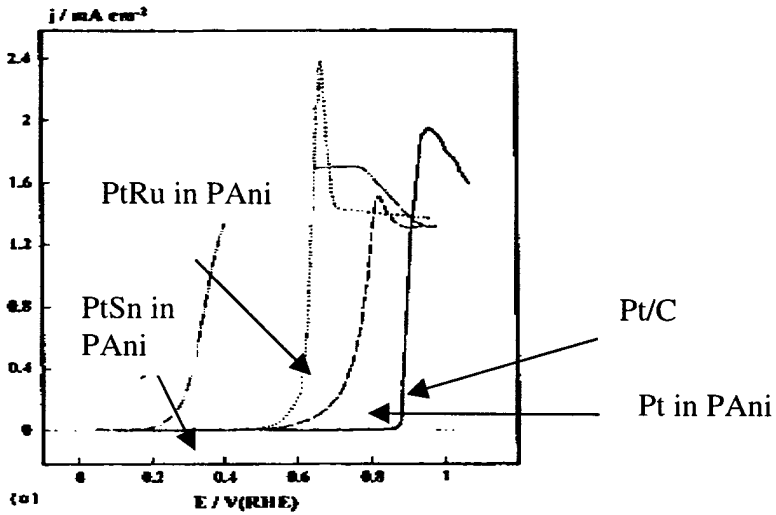
j / mA cm-2
2.4
2
1.6
1.2
0.8
0.4
0
0.2
0.4
0.6
0.8
1
E / V(RHE)
PtRu in PAni
PtSn in PAni
Pt/C
Pt in PAni

CONCLUSIONS

- *CO and methanol oxidation products induce major changes in the Pt L edge XAS in Pt/C.*
- *These effects are significantly lower for Pt alloyed with Ru and Sn.*
- *Alloying with Sn lowers the Pt d-band vacancies and increases the Pt-Pt bond distance, which could have adverse effect on the initial MeOH adsorption step (r.d.s). In case of alloying with Ru this case is opposite.*
- *In upd Sn on Pt/C, free Pt sites are available for the initial adsorption by methanolic species.*
- *Sn and Ru are readily oxidized at potentials significantly lower than Pt, Sn being present as an oxidized species even at 0.0V vs. RHE.*
- *Methanol oxidation induces major changes in the Ru and Sn K edge XAS which agrees with the 'bifunctional mechanism'.*

ACKNOWLEDGMENTS

U. S. Department of Energy
Brookhaven National Laboratory
Department of Applied Science
Material Science Division
(Contract # DE-AC02-76CH00016)

U. S. Department of Energy
Office of Transportation Technologies
Electric and Hybrid Vehicles

Water Uptake by Nafion Membranes

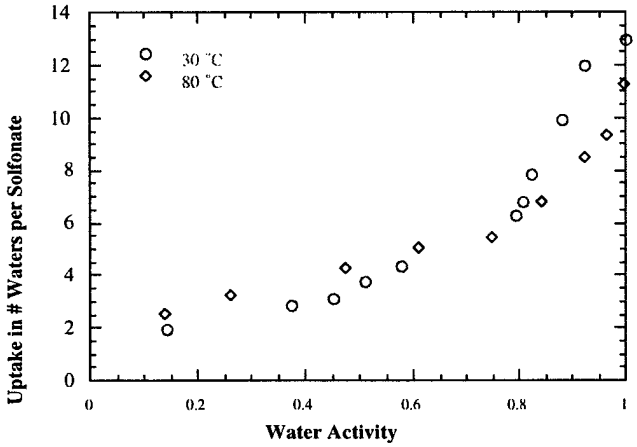

Low water activity ($\lambda < 0.7$):

- high enthalpy of water uptake
- water primarily solvates sulfonates and protons

High water activity ($\lambda > 0.7$):

- low enthalpy of water uptake
- low free energy of water uptake
- water primarily swells the polymer
- Water upake from unit activity vapor is less than uptake from unit activity liquid------>energetics of condensation of vapor on hydrophobic membrane surface.....

252

Diffusion Coefficient of Water vs. Hydration Level

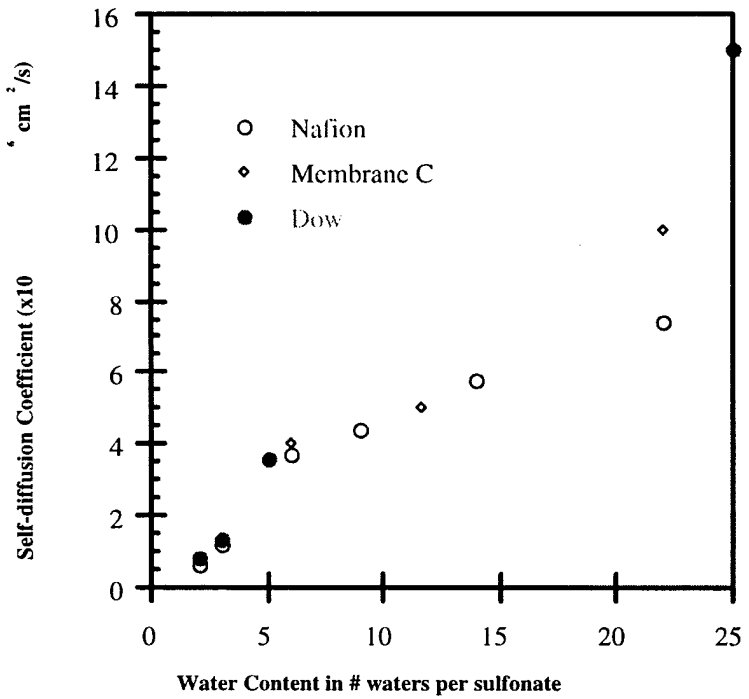

Protonic Conductivity vs. Hydration Level

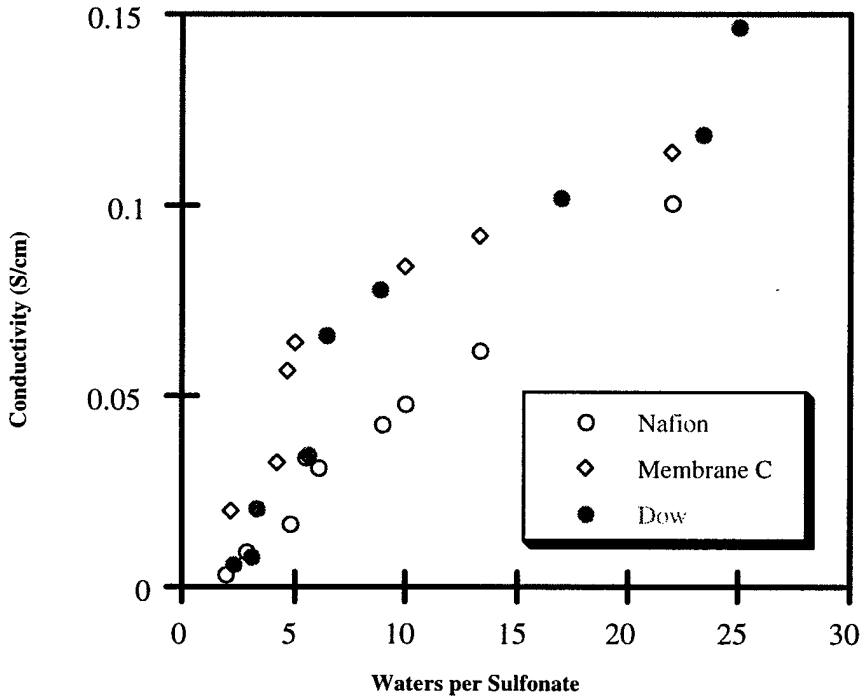

Deuterium Relaxation Time vs. Hydration Level

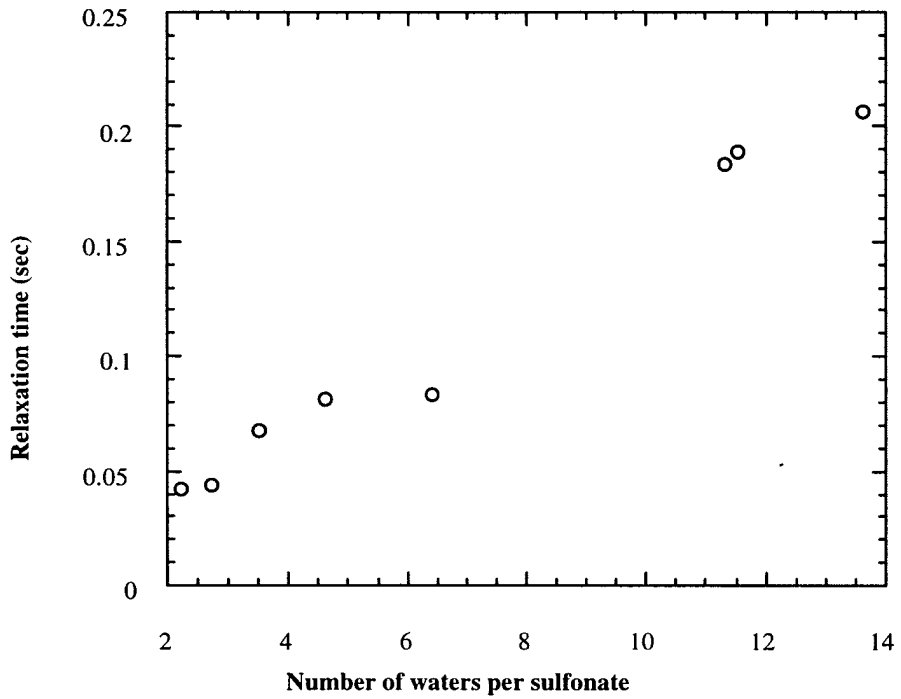

Free Energy of Water Uptake

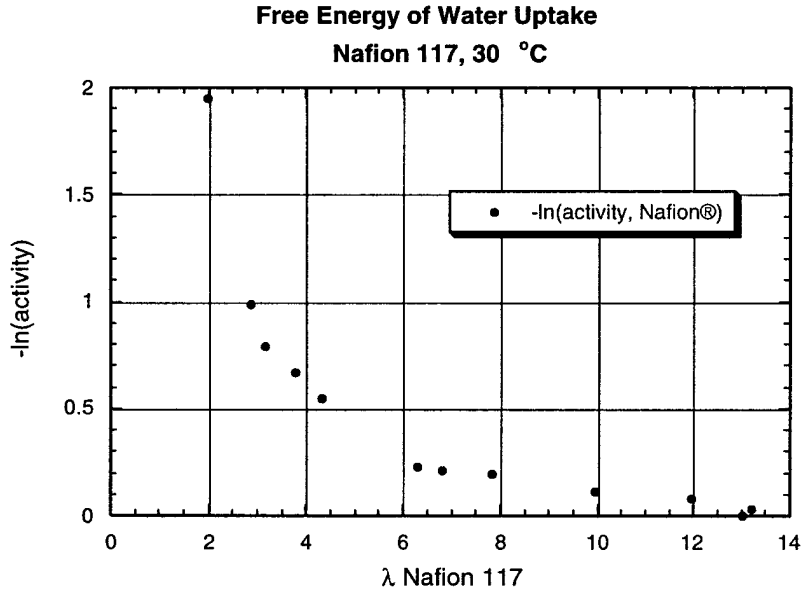

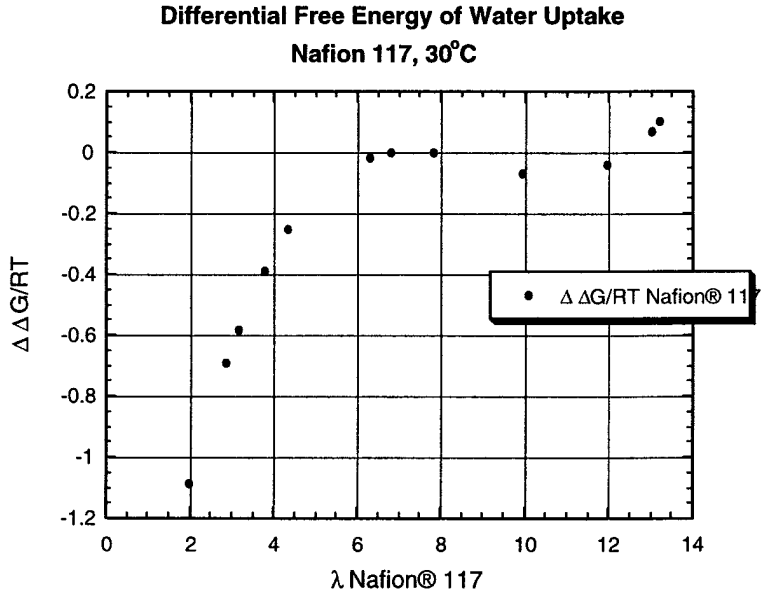

Driving force for water uptake decreases with increasing water activity
Close to zero ΔG for uptake of liquid water from λ=14 to 22
Similar for all ion exchange polymers

Temperature Dependence of Water Diffusion in PFSA Membranes

Activation energy for 1H self-diffusion coefficient in various membranes at various water contents. (activation energies in kcal/mol)

λ	Dow	Nafion 105	Nafion 117
30.5		3.3	
16.0		3.7	
14.0	3.1		3.7
9.8	3.0		3.7
5.5		4.1	
3.3	3.3		4.0
2.0	6.8		6.7

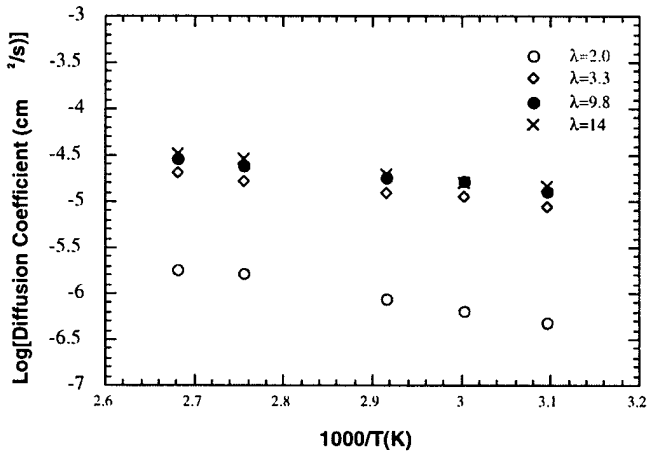

Electroosmotic Drag: Effect of Water Content, Temperature

- At 30°C, drag coefficient roughly 1 for all membranes for $\lambda<14$; for $\lambda>14$, drag coefficient is in the range 2-3.
- At higher temperatures:
  - Vapor equilibrated membranes: drag coefficient is 1
  - Liquid equilibrated membranes: drag coefficient increases with temperature
- Other membranes: drag coefficient for immersed membranes at 30°C is also in the range 2-3.

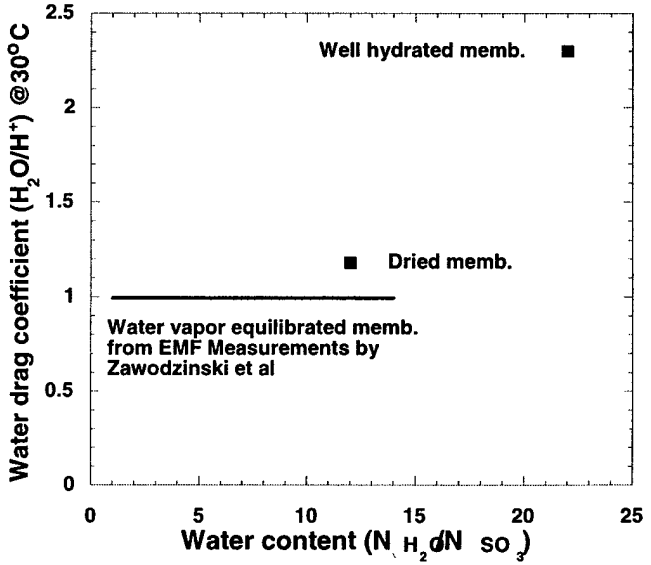

Next Steps Forward

- Model with periodic potential for transport---> incorporation of molecular information
  - Solution of Liouville equation to obtain a measure of frictional effects due to the presence of fixed anionic sites in a pore as a function of water content

- 'Transport' model using brownian dynamics to solve for transport of water and ions down pores of arbitrary shapes
  - molecular information incorporated into descriptions of localized 'ion traps'

- Different anionic groups

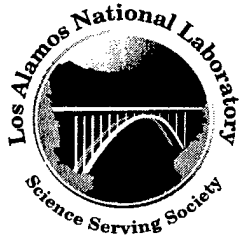

Conclusions, Opinions, Prejudices

- Likelihood of Water-free Proton Conduction
  - 'the medium is the message'
  - proton dissociation is <u>difficult</u>

- What other types of polymer electrolytes will make good protonic conductors?
  - anion basicity is the key factor

Transport in PFSA Membranes: Computational Studies

T.A. Zawodzinski Jr.

261

Electronics and Electrochemistry Group
Materials Science and Technology Division
Los Alamos National Laboratory

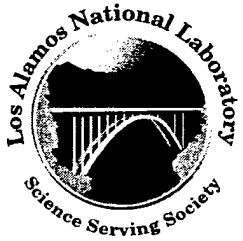

Outline

- Goal and Approach
- Experimental Observations
- Qualitative Picture Explaining Diffusion, Electroosmosis
- Quantum Mechanical Calculation Results
  - Minimum Energy Structures
  - Electrostatic Potentials
  - Free Energy Surfaces
- Quasichemical Models of Solvation
- Extensions to Complete Systems
- Cnclusions, Observations and Prejudices
- Acknowledgments

Goal and Approach

To describe ion solvent transport through hydrated polymer electrolyte membranes.

Starting Point: Nafion®

Approach: Molecular Level Comp. Chem. wedded to Chem. Eng.

- What is the charge and water distribution in the hydrated membrane?
- What is the overall conformation and dynamics of the fixed charge sites and side-chain?
- How are ions transported through this heterogeneous medium?
- Apply theory to learn about different local structures, i.e different materials--->predictive power for guided synthesis

Structure of Membranes

Nafion 117 (EW=1100)
Nafion 105 (EW=1000)
Membrane C (EW=900)

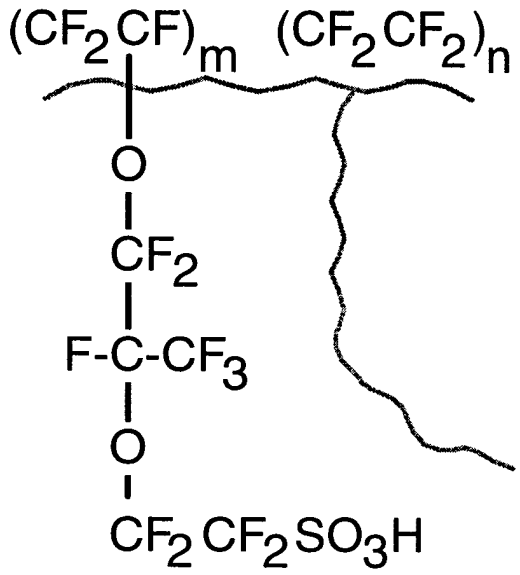

Dow Membrane
(EW=800)

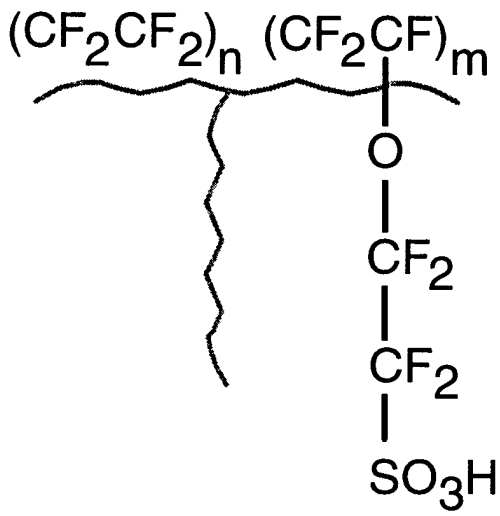

Proton and Water Diffusion

- hydronium ions move via vehicle mechanism

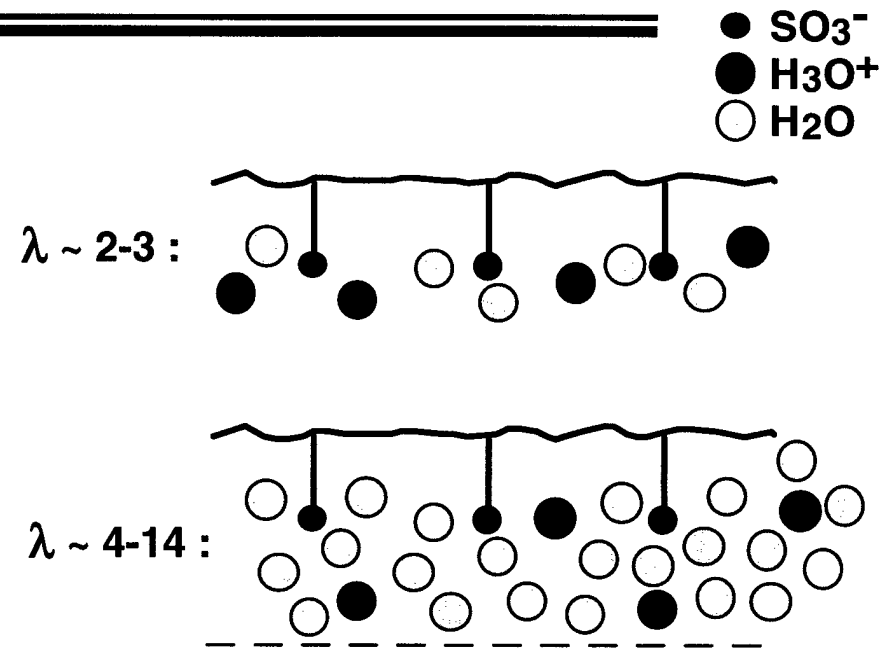

- water in interfacial region screens weakly bound water from ion-dipole interactions
- water and protons move more freely

Electroosmotic Drag

- **Key Factor: Tightness of water binding (water/water, water/ion interactions)**

- **Low water content**:

waters strongly bound in interfacial region; hydronium ion cannot overcome these strong interactions at ordinary temperatures

$\lambda < 14$:

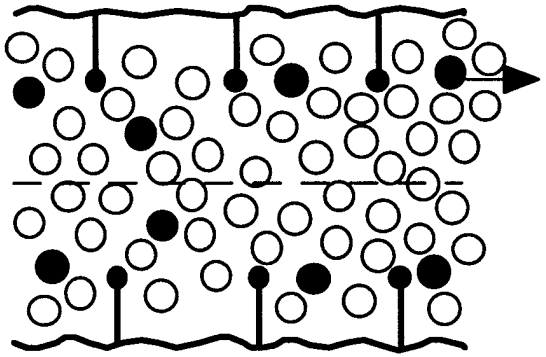

- **High water content**:

weakly bound water feels strong force from migrating hydronium; increasing kT further 'loosens' water/water interactions leading to higher drag

$\lambda > 14$:

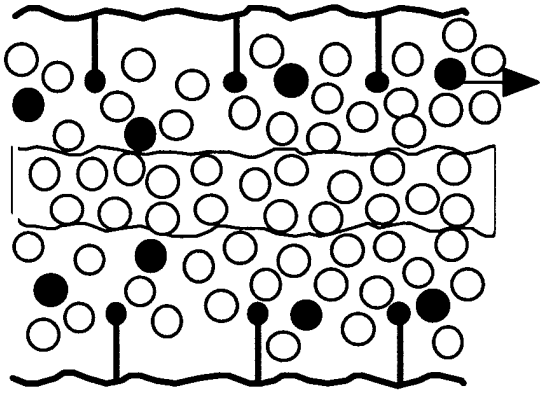

Electronic Structure Calculations

GAUSSIAN 94

- Geometry Optimizations:

HF/6-31G**, MP2/6-31G**, B3LYP/ 6-31G**

$CF_3SO_3H + H_2O$ $CF_3OCF_3 + H_2O$ $CF_3SO_3^- + nH_2O$

$CF_3–OCF_2CF(CF_3)\ OCF_2CF_2SO_3H\ (+ H_2O)$

$(CF_3CF_2)_2C–OCF_2CF(CF_3)\ OCF_2CF_2SO_3H$

- Potential Energy Surfaces
- Atom Centered Partial Charges

CHelpG

Dielectric Model of the Solvent

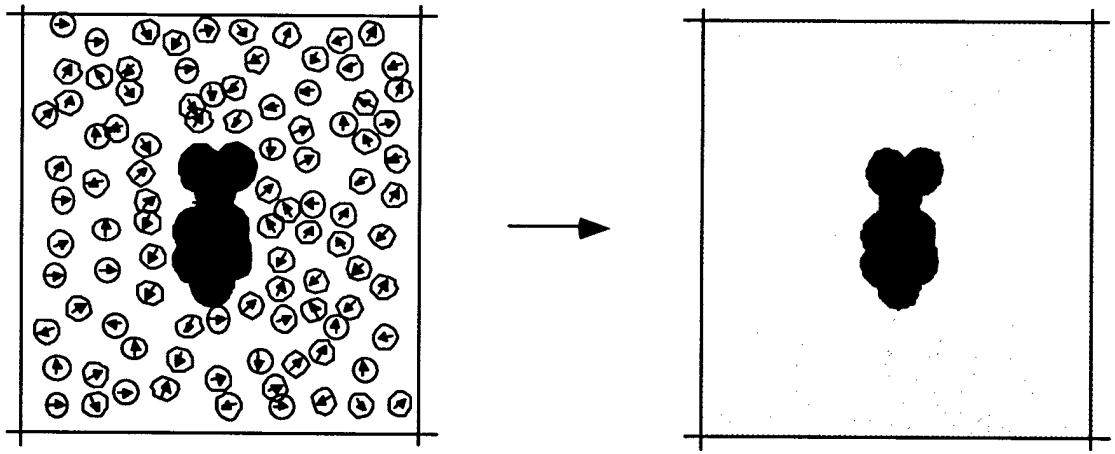

- use electronic structure information to calculate ACPCs
- immerse molcule in dielectric continuum
- solve Poisson's eqn.

Triflic Acid + H_2O

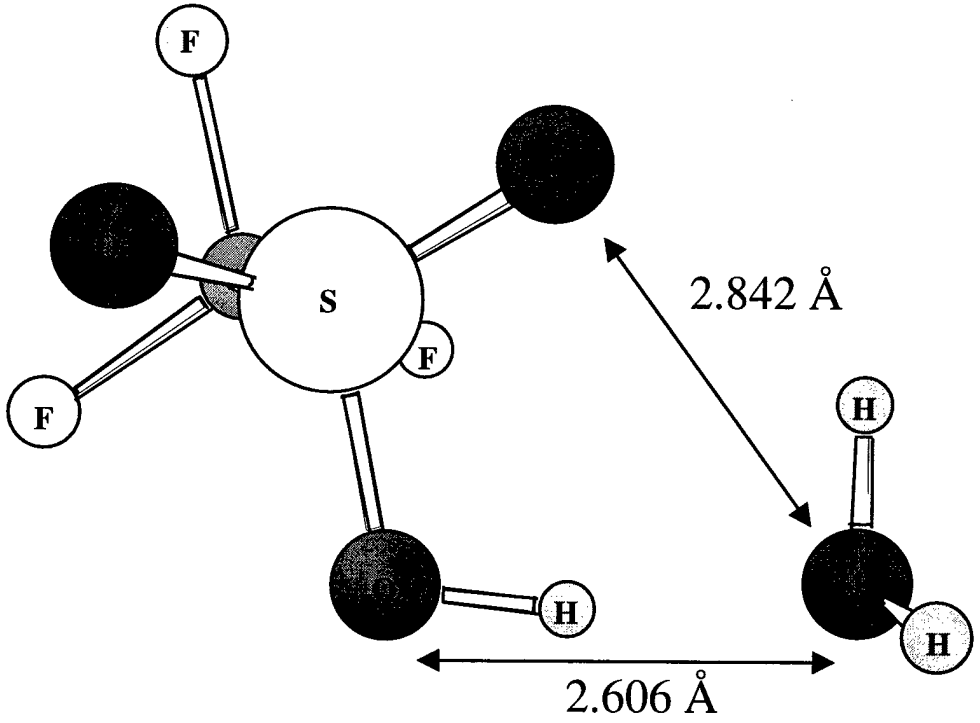

MP2/6-31G**

Energy Surfaces

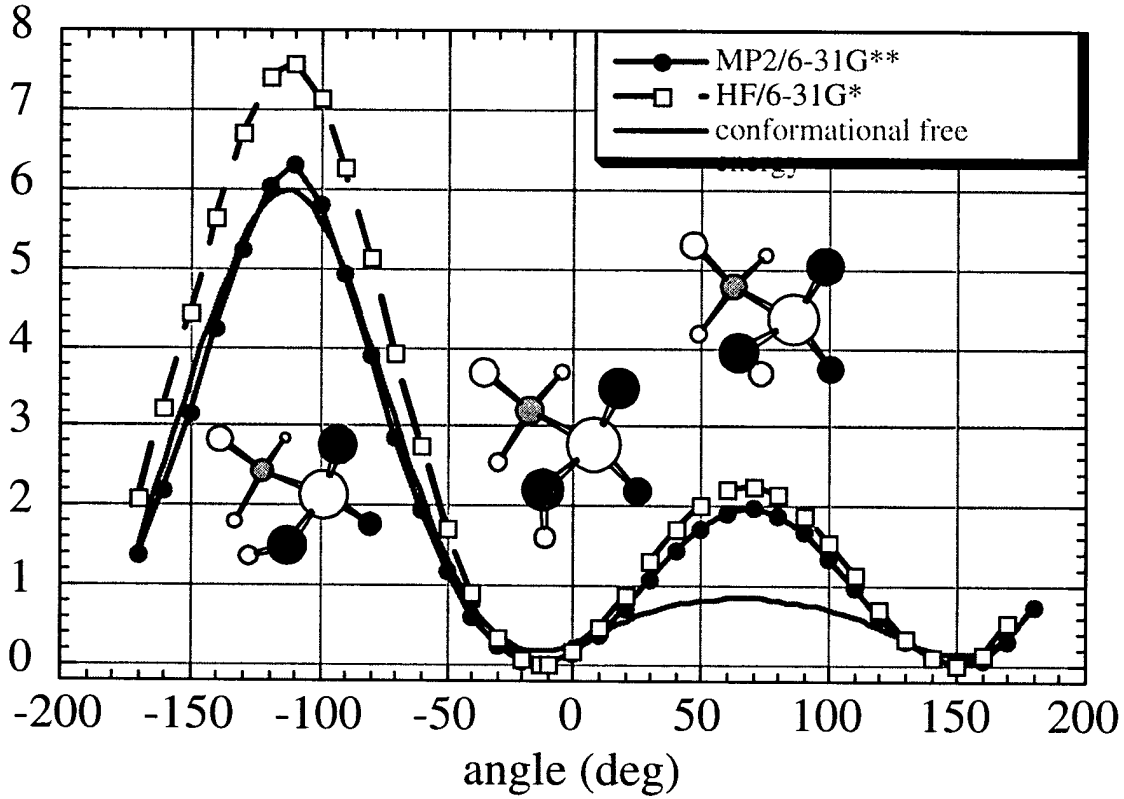

$CF_3OCF_3 + H_2O$

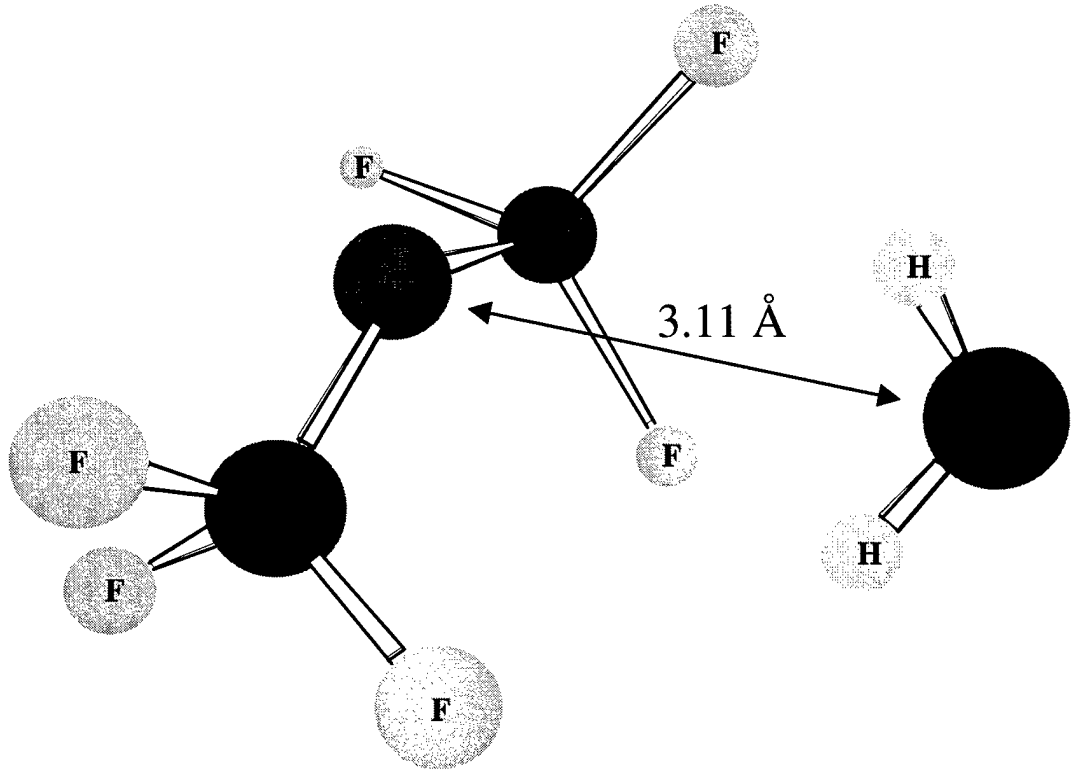

Pendant Chain

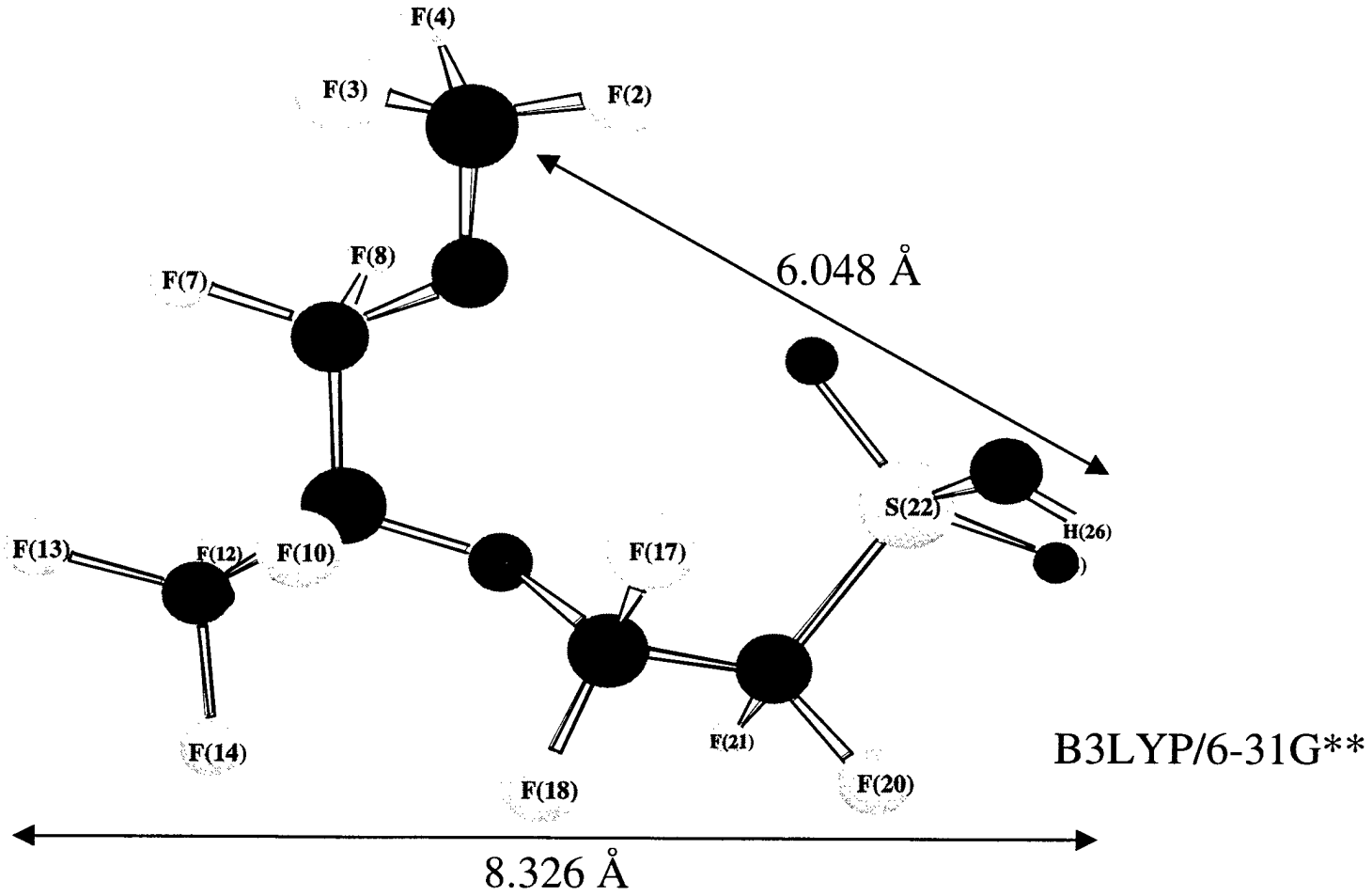

B3LYP/6-31G**

272

Optimized Geometries for Anion/Water Complexes: $CF_3SO_3^- + nH_2O$

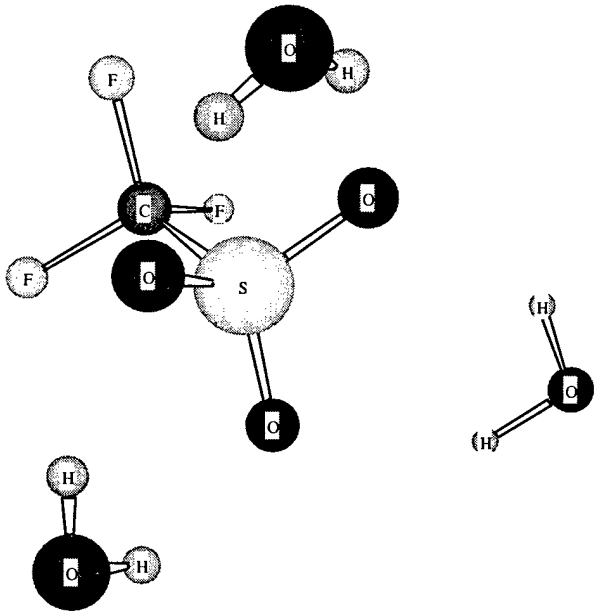

■ n =3

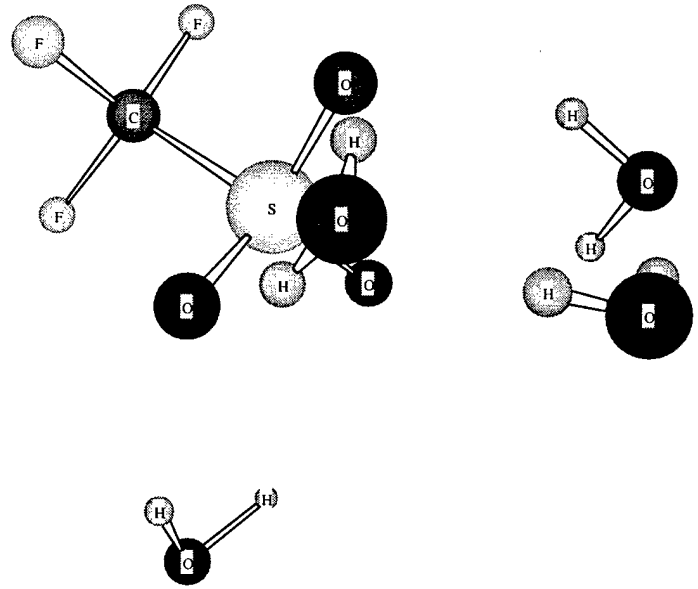

■ n=4

B3LYP/6-31G**

MD SIMULATION

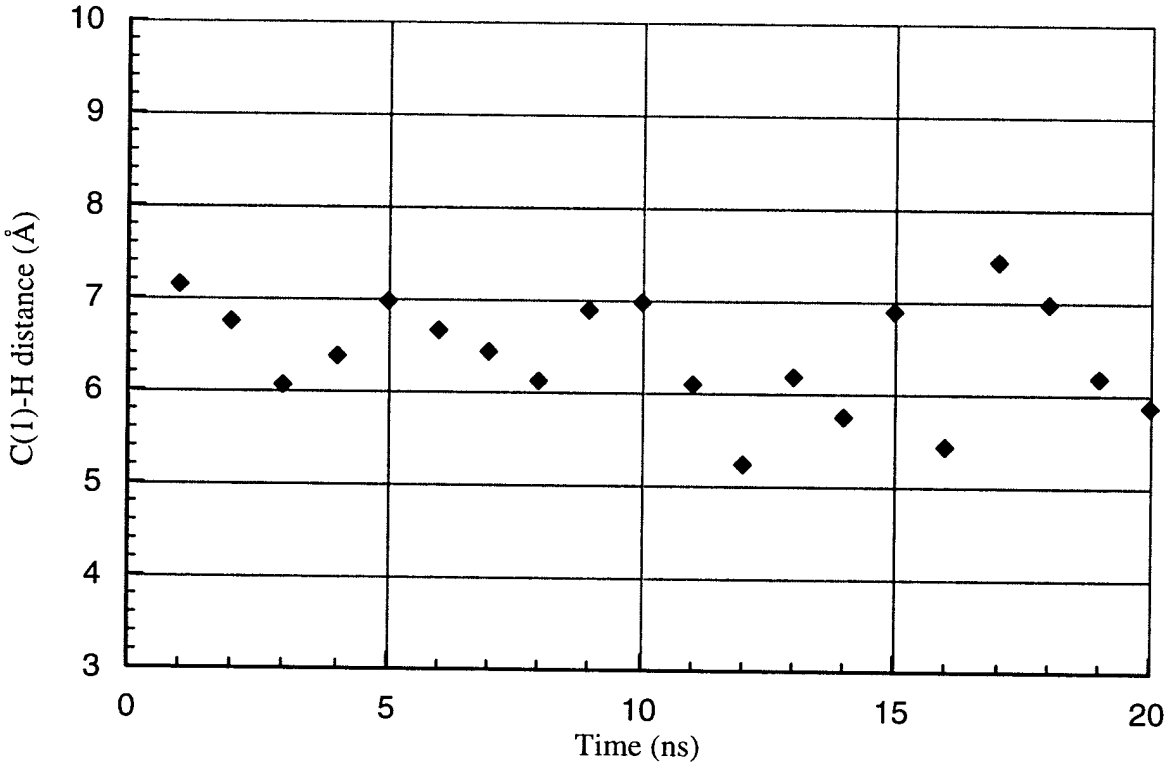

MD SIMULATION

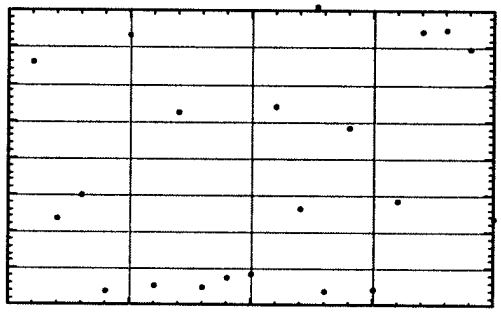

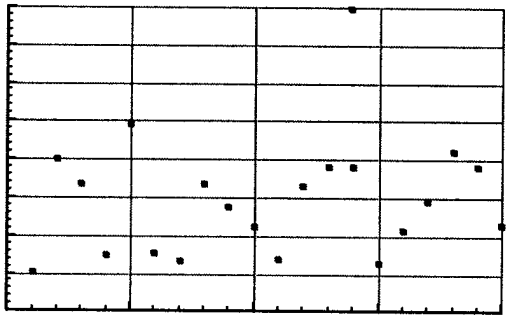

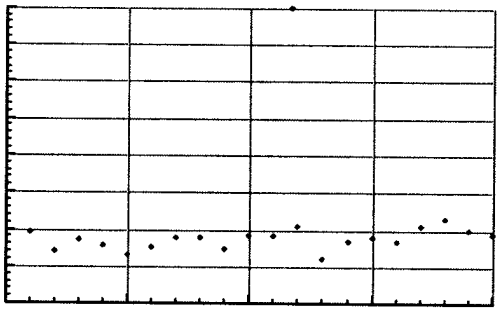

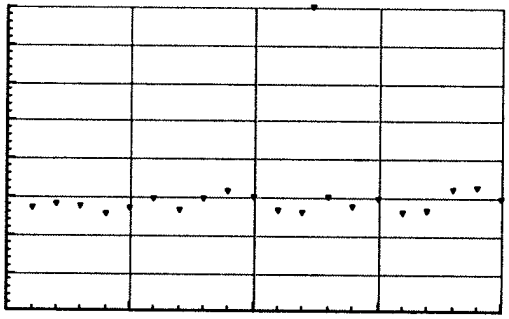

Potential Energy Surface

Rotation about the C(9)—O(15) bond in the Pendant Chain

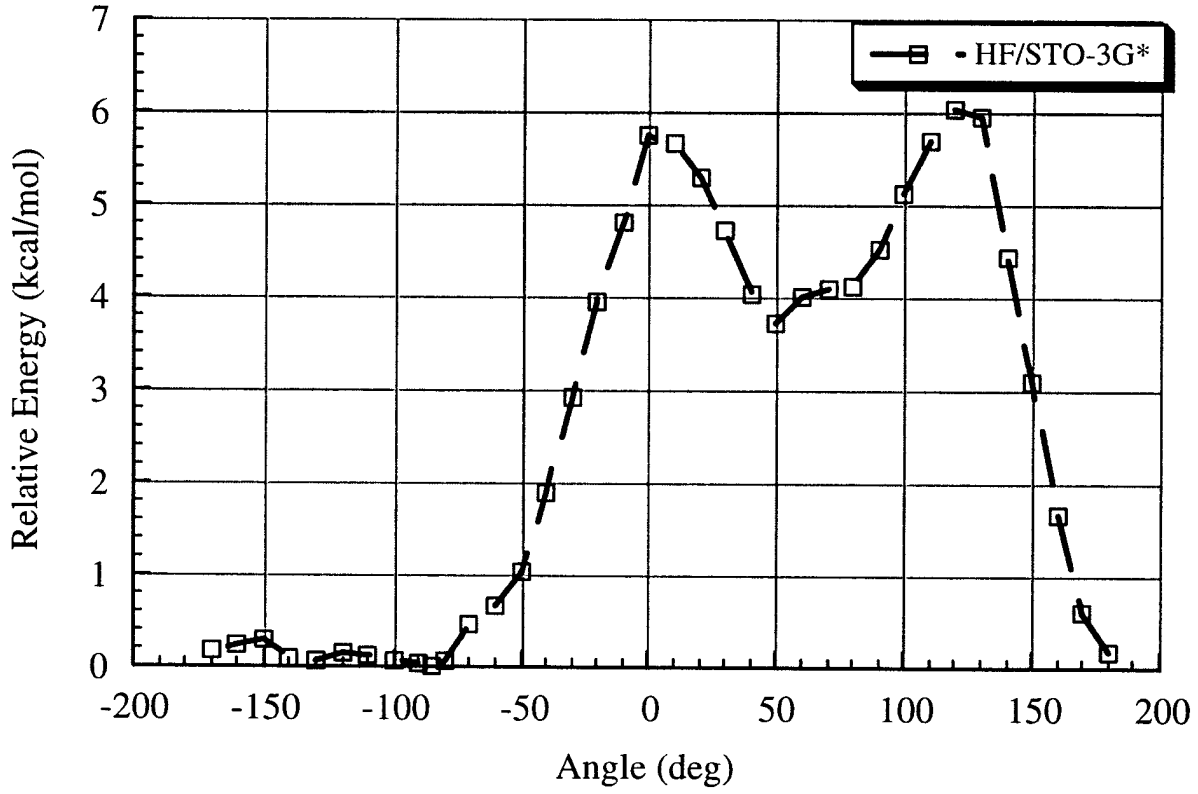

Acknowledgments

- the financial support by the Los Alamos National Laboratory LDRD program is gratefully acknowledged

  - L.R. Pratt - statistical mechanics, theory of liquids

    - Stephen Paddison - post-doc

SLIDE COMMENTARY FOR FUEL CELL MEETING

Held in Las Vegas, NV (April 28-May 1, 1998)

TITLE SLIDE: Nothing needed for that.

FIGURE 1: PERVAPORATION

In pervaporation, a liquid feed is evaporated across a membrane. The vapor that crosses, the permeate, is then condensed. The process has a selectivity which depends both on permeability and on volatility.

FIGURE 2: DISTILLATION VS. PERVAPORATION

The data sketched here are for ethanol-water. For a feed containing 20% ethanol, the equilibrium concentration in the vapor is above 60% ethanol. For pervaporation, the vapor permeate has about the same composition as the liquid. Thus for this feed, distillation is superior to pervaporation. For a feed containing 90% ethanol, distillation is compromised by the familiar azetrope, but the vapor permeate in pervaporation contains only about 5% ethanol.

FIGURE 3: TITLE is at the top of figure.

Pervaporation membranes have much lower conductivities than those used in existing fuel cells. As a result, one might expect that they would not be suitable. However, because pervaporation membranes can be made thin—one micrometer or less—their conductance can be sustained by making the membrane very thin. What is important is less the absolute value of conductance than the selectivity, i.e. the ratio of conductive flux of protons to diffusive flux of methanol.

FIGURE 4: CONDUCTIVITY VS. PERMEABILITY

We seek membranes with both a high conductivity and a low methanol permeability. Such membranes would fall in the upper right hand corner of this figure. Membranes with constant selectivity but varying permeabilities would fall along straight lines with a slope of (-1), like the solid line shown. As the data show, Nafion has a high conductivity, but a high methanol permeability. PBI has a greater selectivity even though its conductivity is significantly smaller than Nafion.

FIGURE 5: FUTURE DIRECTIONS

Go with the text.

Fig 1

Methanol Barrier Membranes

Ed Cussler

University of Minnesota

Two Strategies

(1) Good Proton Conductors

(2) Good Methanol Barriers

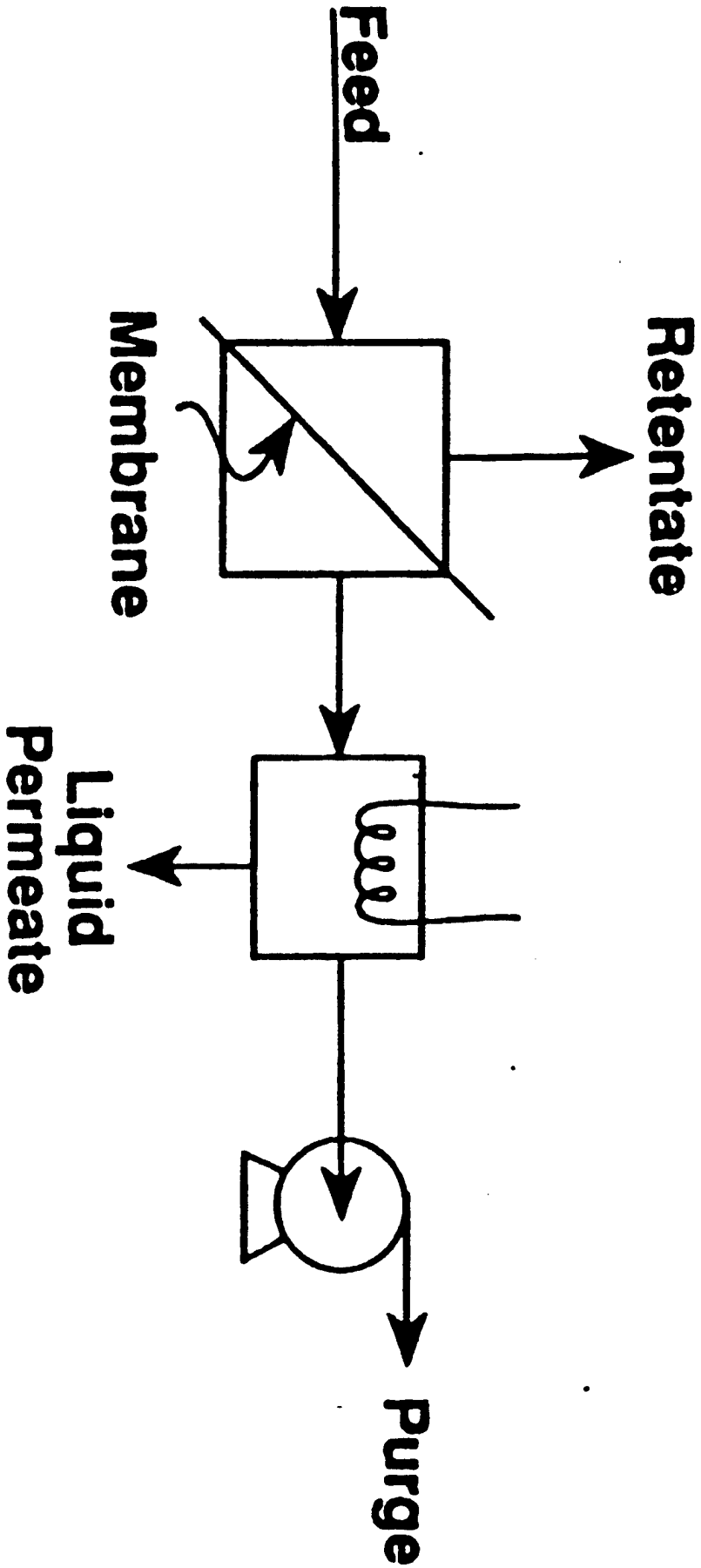
Feed
Membrane
Retentate
Liquid
Permeate
Purge

Fig 8.

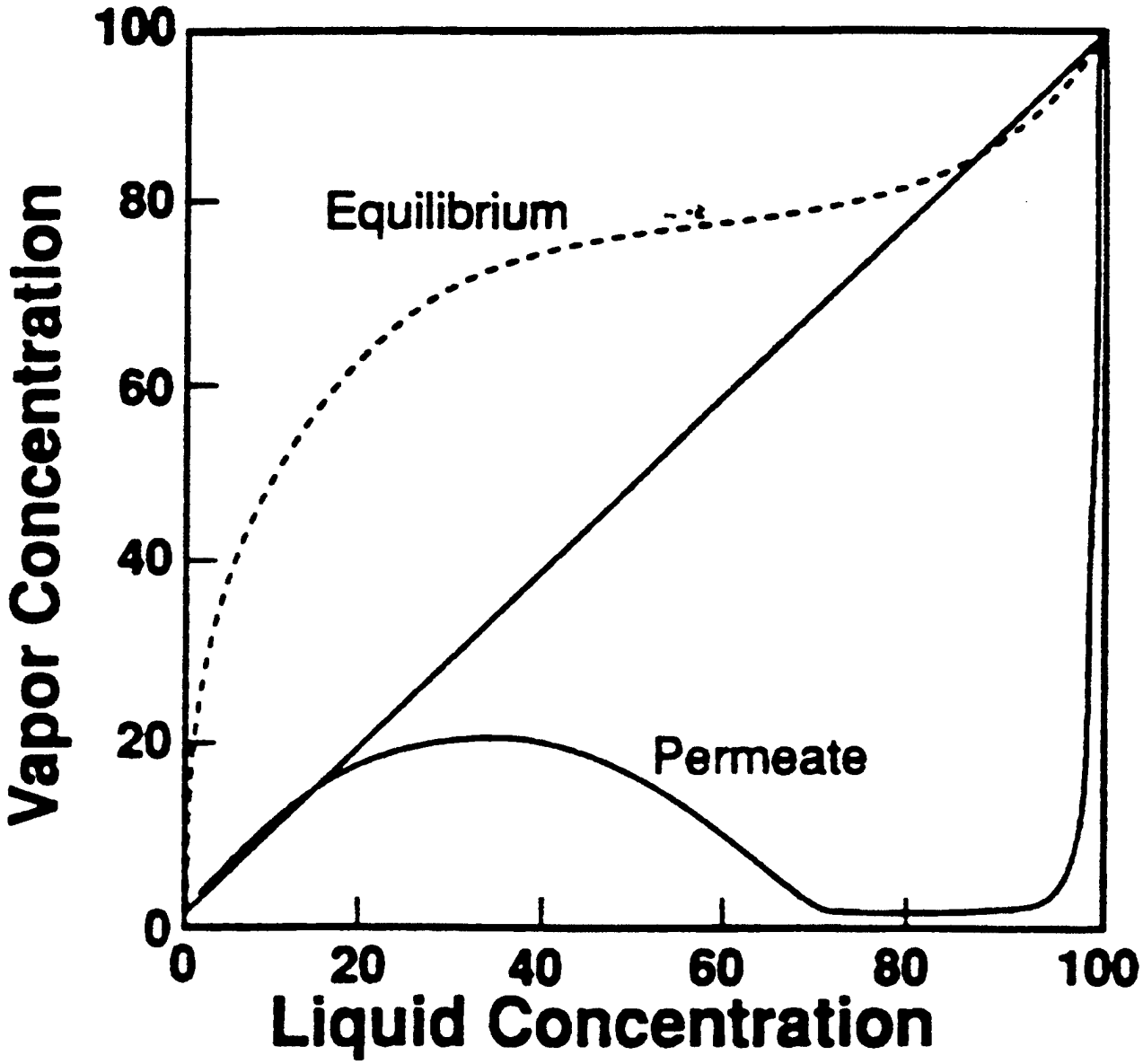
100
80
60
40
20
0
Vapor Concentration
Equilibrium
Permeate
0
20
40
60
80
100
Liquid Concentration

Fig 4

Isn't Low Conductance a Problem?

Conductance $\propto \sigma \Delta \varphi/(\text{thickness})$

Selectivity = proton flux/CH_3OH flux

$$\propto \frac{(D_H[H^+])}{(DK)_{CH_3OH}[CH_3OH]}$$

$\neq$ f(thickness)

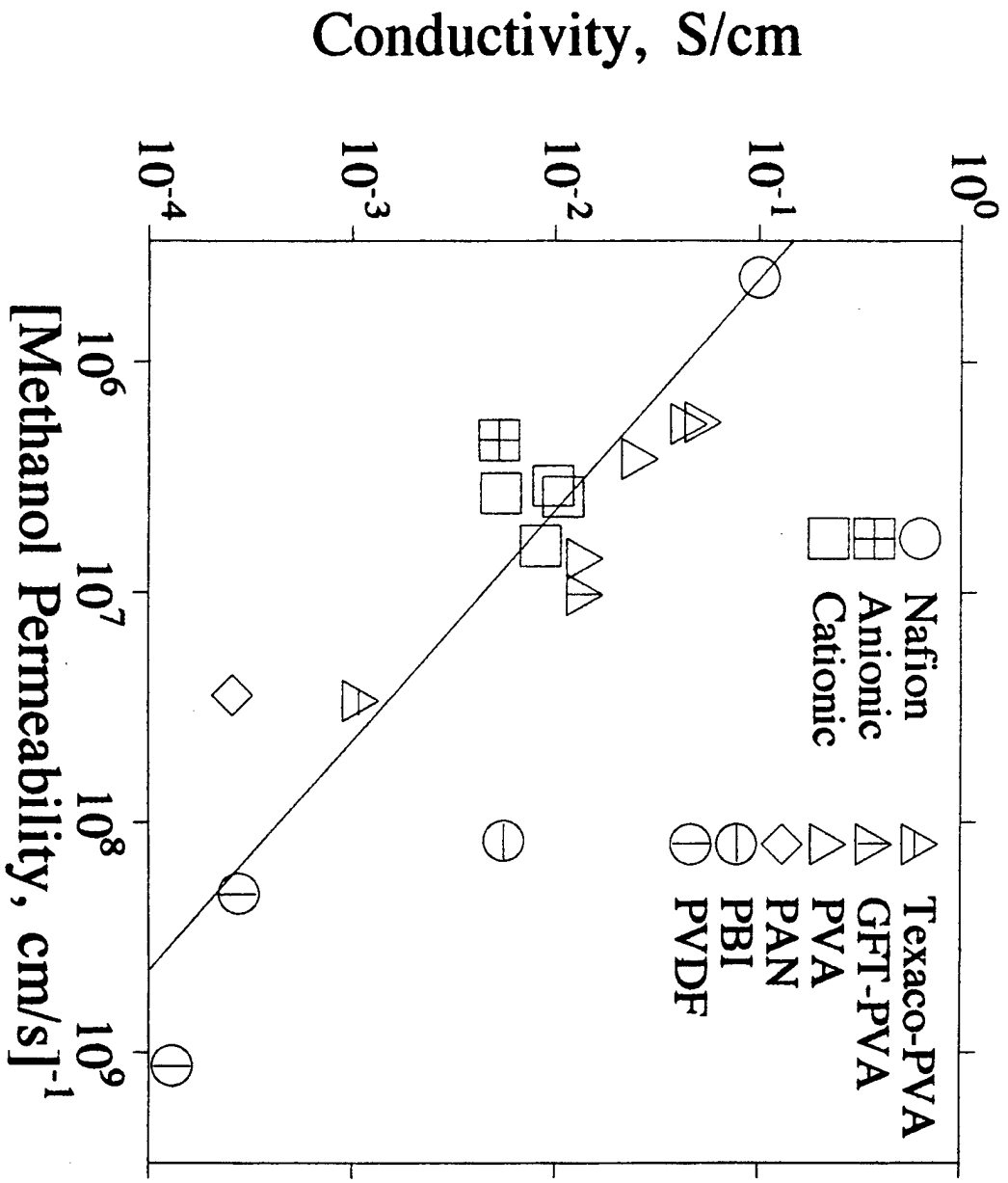
Conductivity, S/cm
10^{0}
10^{-1}
10^{-2}
10^{-3}
10^{-4}
10^{6}
10^{7}
10^{8}
10^{9}
[Methanol Permeability, cm/s]$^{-1}$
Nafion
Anionic
Cationic
Texaco-PVA
GFT-PVA
PVA
PAN
PBI
PVDF

Fig 6

To Improve Selectivity,

$$\beta = \frac{(D_H[H^+])}{(DK)_{CH_3OH}[CH_3OH]}$$

Use

(1) Small Electroosmosis

(2) Small Cation Mobility

(3) Small K

Direct Methanol Fuel Cells:

Recent Advancements at LANL

Shimshon Gottesfeld

Los Alamos National Laboratory

Direct Methanol Fuel Cell

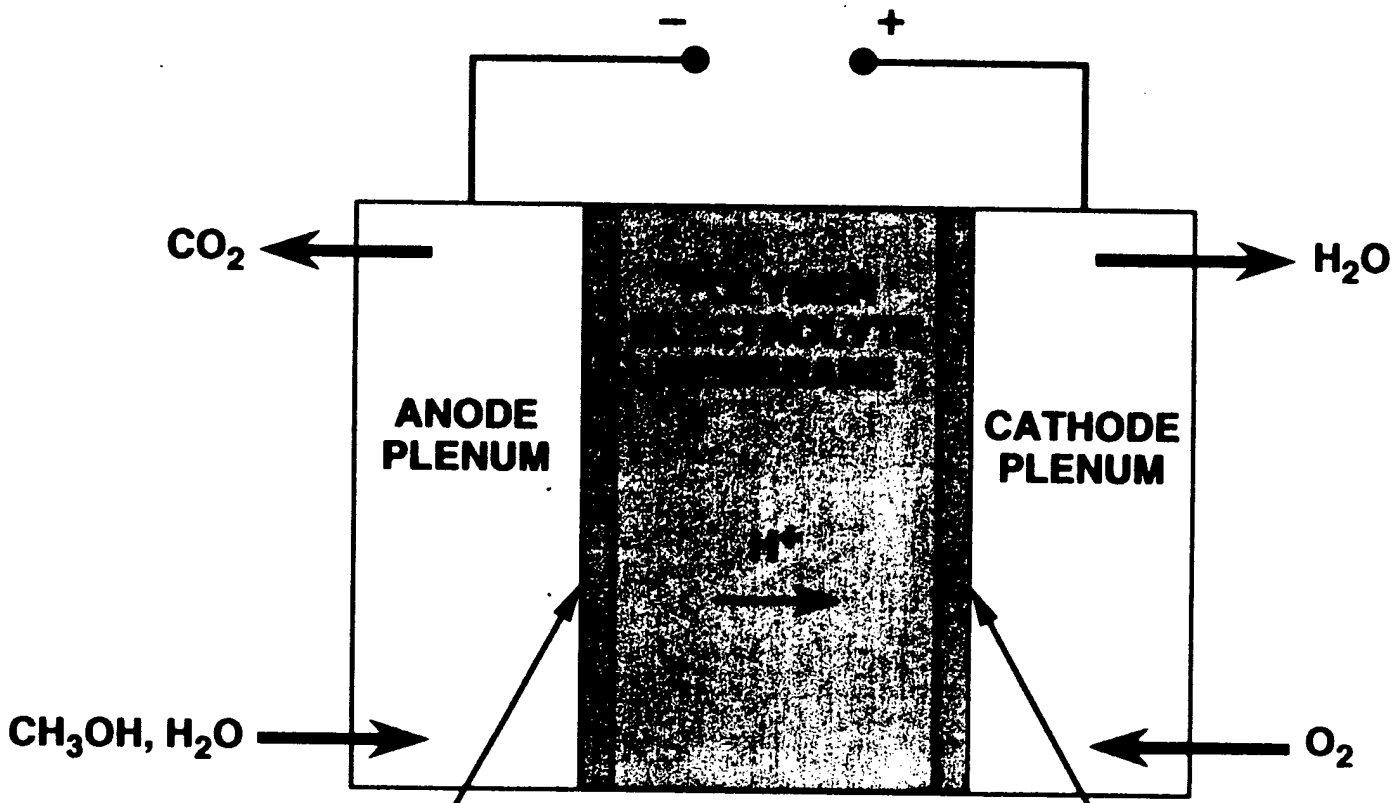

DMFC Cell and Stack R&D For DARPA

A **Optimizing cell components and MEA preparation by single cell tests to reach *best cell performance.***

B **Innovative stack design to achieve *highest cell package density.***

DMFC Anode Catalyst Evaluation, 80 °C

Catalyst	Pt/Ru Ratio	Particle Size (nm)	Calculated Area (m^2/g)	BET Area (m^2/g)	Anode Loading (mg/cm^2)	Cathode Loading (mg/cm^2)	i (mA/cm^2) @ 80 °C 0.35 V (Anode)	i (mA/cm^2) @ 80 °C 0.5 V (Cell)
	50/50	4.2	83	69	5.0	5.5	330	250
	70/30	5.3	59	60	4.5	3.8	160	90
	48/52	3.5	100	75	5.2	4.7	360	265
	—	4.6	76	—	4.0	4.6	245	245
	59/41	8.2	43	43	5.0	4.2	90	50
	46/54	8.4	42	29	4.9	4.2	30	20
	49/51	5.4	65	70	5.0	3.7	310	175
	54/46	3.3	105	78	5.0	4.2	340	235
	46/54	3.2	109	78	5.6	3.5	310	250
	43/57	3.2	109	—	5.1	5.0	250	280
	49/51	3.6	143	—	5.3	4.6	225	155
	50/50	3.2	161	—	5.6	4.7	235	140
	52/48	6.0	58	—	5.2	4.3	40	75
	44/56	3.1	112	—	4.1	4.3	280	240

289

Supplier A

Supplier B

LANL sample

Voltammograms for Methanol Flux Measurements at 80°C

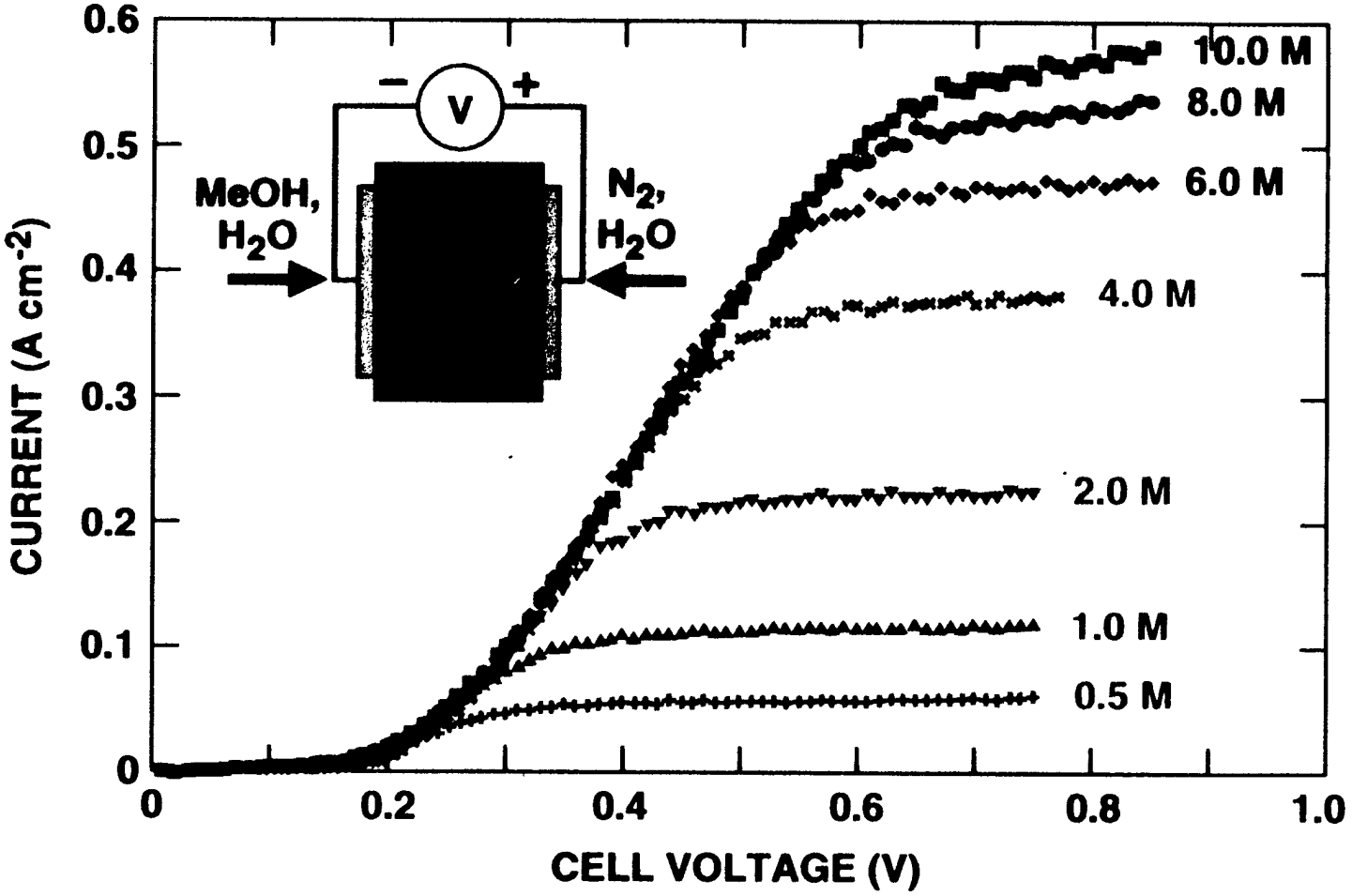

Evaluation of $D^{1/2}$ for Methanol (0.1-1 M) in Nafion 117

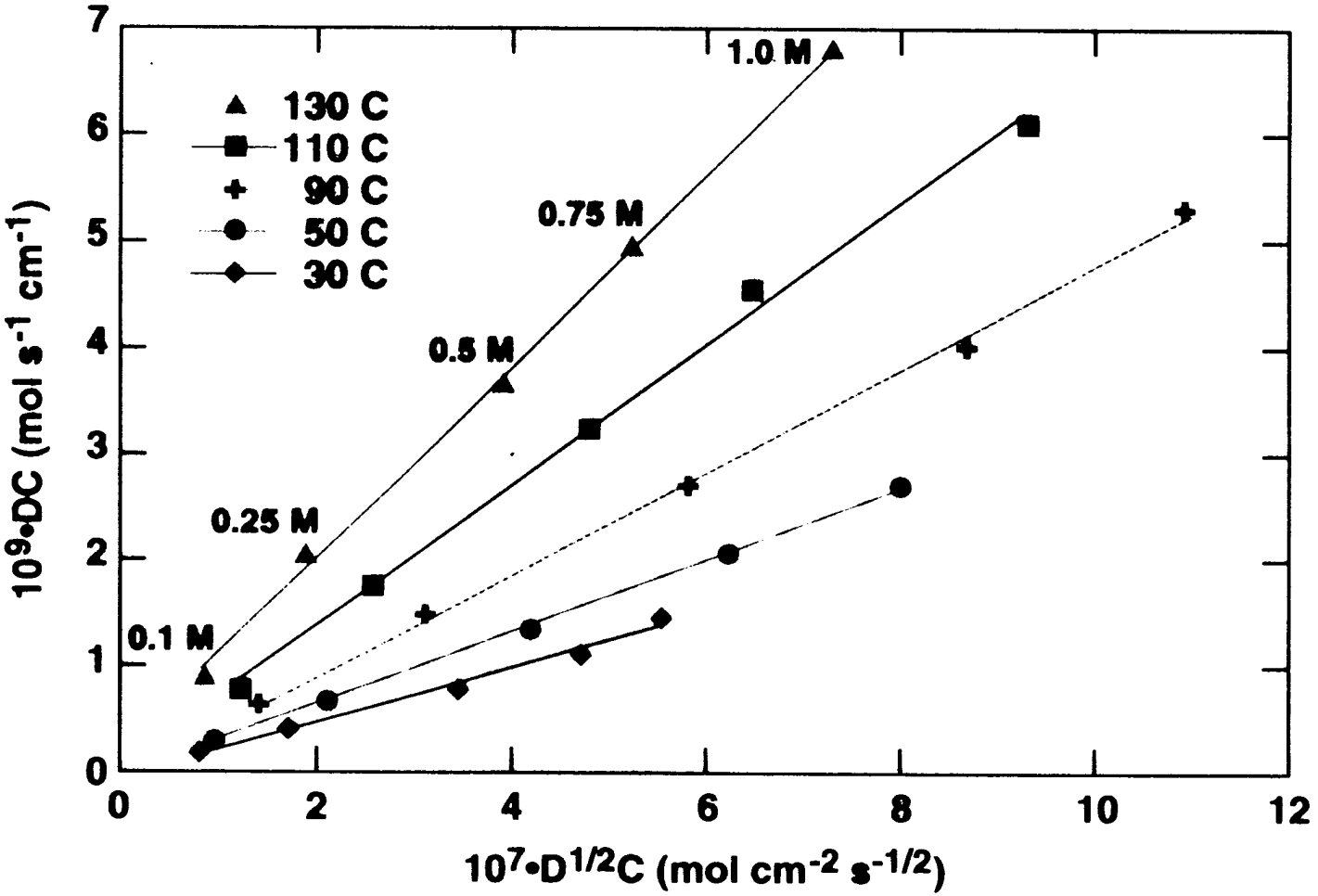

Methanol Cross-Over in Operating DMFCs

Determination by measurement of CO_2 in cathode effluent

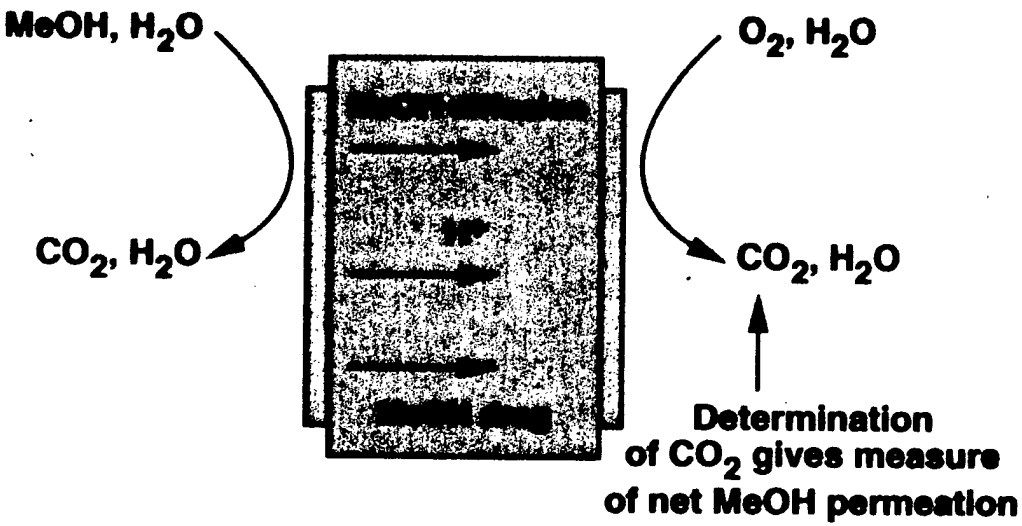

MeOH diffusion and drag flux are concurrent

LANL Results

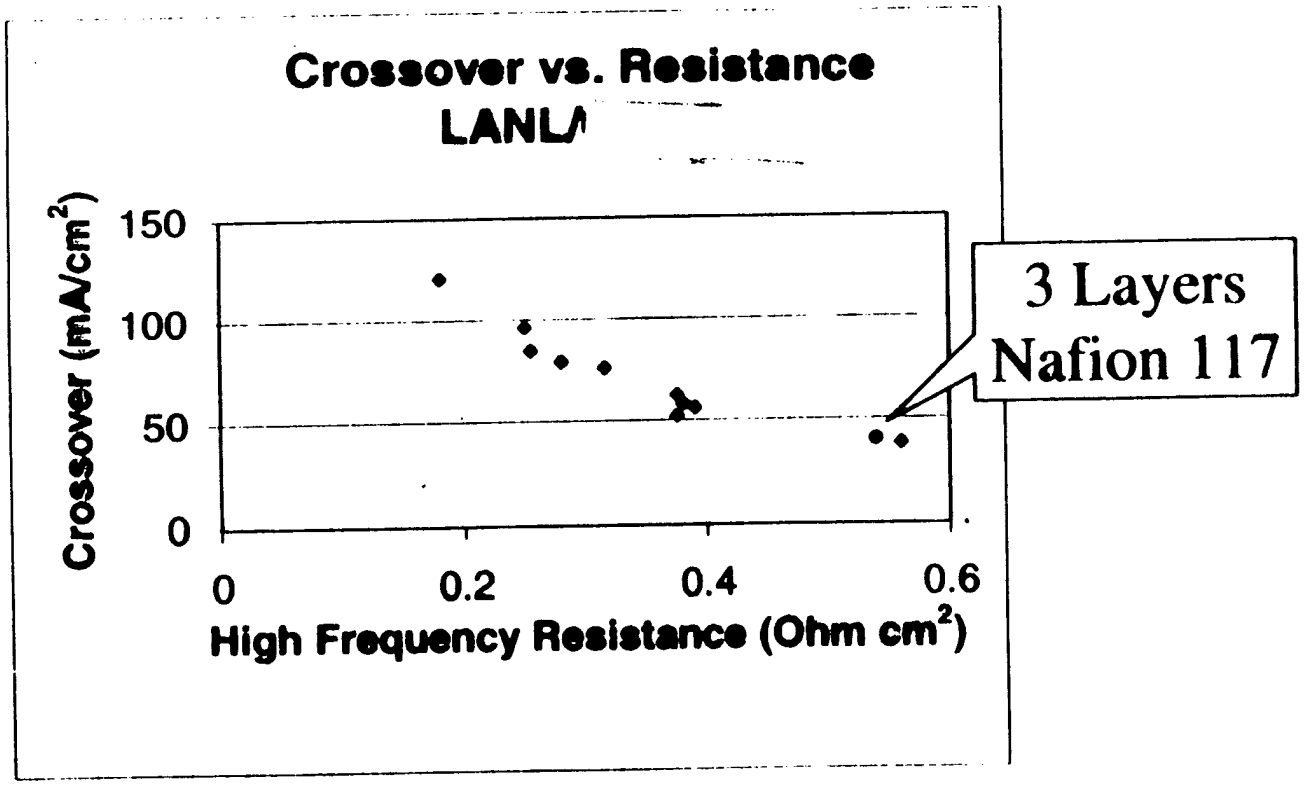

Membranes

Experimental Membranes of Lowered Methanol Permeability

- 10 new membranes supplied, made into MEAs and tested, including:
  - Membranes with modified cathodes
  - Membranes with methanol blocking components
  - Membranes of variable composition along thickness
  - Combinations of the above

- Conclusions:
  - Cross-over rate lowered to 30-50% of Nafion 117 with acceptable membranes, with slight performance loss at 0.5 V still observed
  - To date: fuel efficiencies of 75% achievable with these membranes at 1 M MeOH - could be improved at lower MeOH concentration

Methanol Cross-Over in DMFC's Using Two Different Anode Backings

(0.25, 0.5 and 1 M feeding Methanol solutions, cell at 80°C)

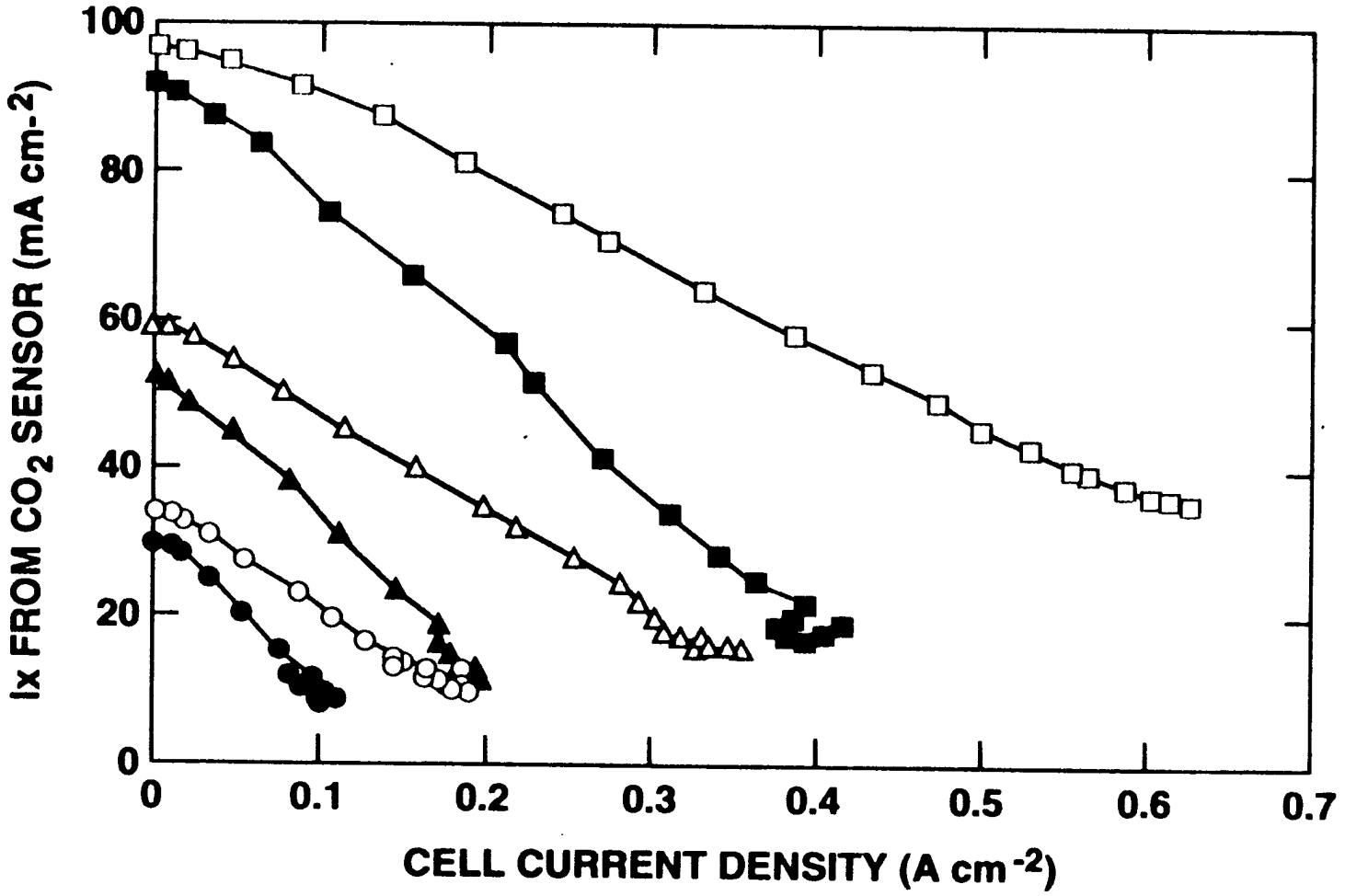

Fuel efficiency:
5 cm² cell with Nafion® 117 membrane
(0.50 V, 470 sccm, 30 psig air)

C_{MeOH} mole l^{-1}	Flow rate ml min^{-1}	i_{cell} A cm^{-2}	i_{cross} A cm^{-2}	Fuel efficiency %
6.0	0.50	0.070	0.560	11
	0.10	0.104	0.380	21
	0.05	0.122	0.210	37
	0.02	*unstable*		
1.0	0.50	0.186	0.102	65
	0.25	0.194	0.085	70
	0.20	0.200	0.063	76
	0.15	*unstable*		
0.5	1.00	0.186	0.036	84
	0.50	0.188	0.026	88
	0.35	0.186	0.021	90
	0.25	*unstable*		
0.25	2.00	0.174	0.020	90
	1.00	0.170	0.011	94
	0.50	0.150	0.005	97
	0.30	*unstable*		

Conclusion: Efficiencies in excess of 80% are obtainable with Nafion® 117 membranes in small single cells at $c_{MeOH} < 1$ M.

Air Cathode Performance in DMFC - Improved MEA (5 cm²)

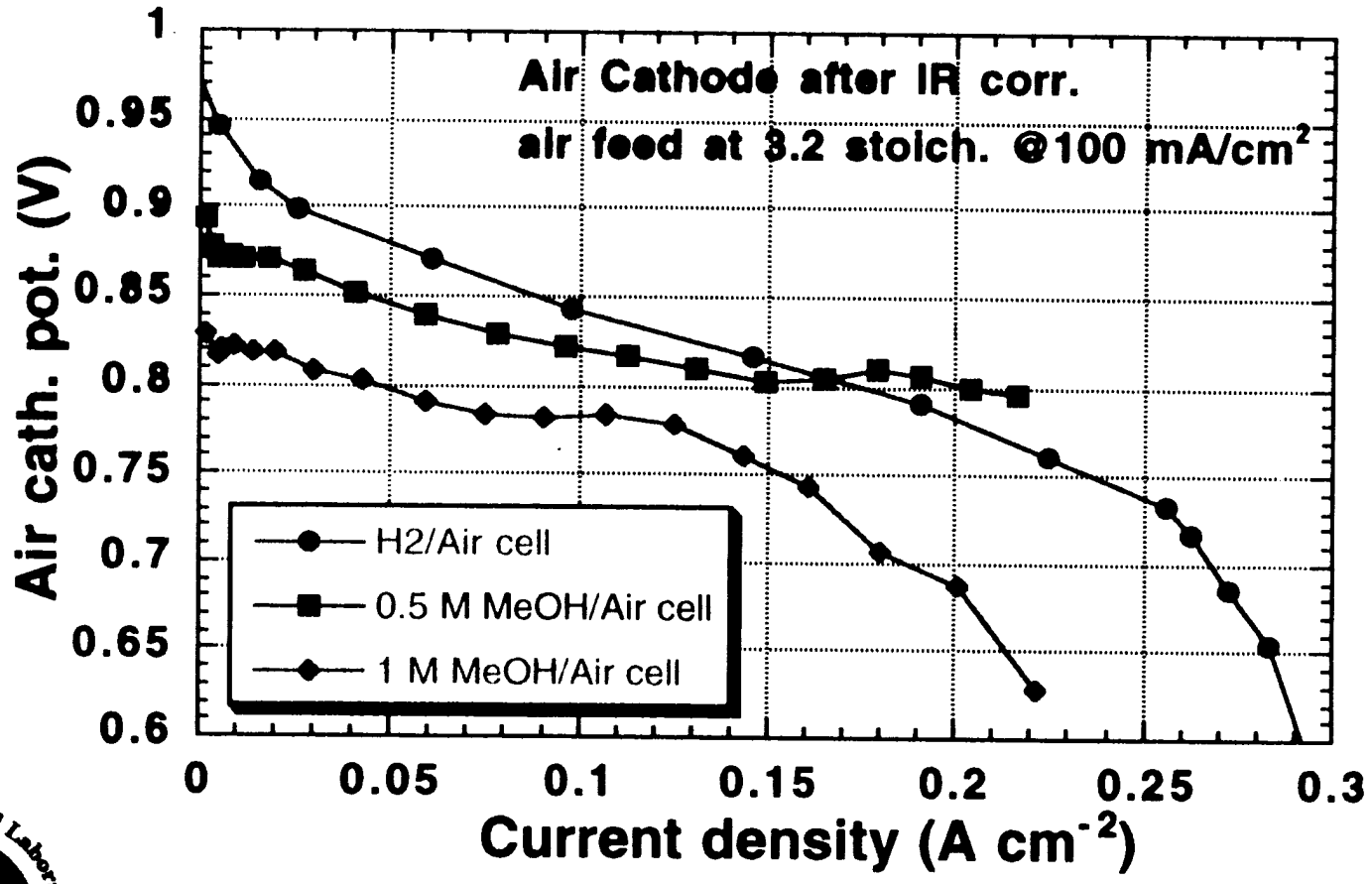

1.0 M MeOH/Air Cell Performance- Improved MEA (5 cm^2)

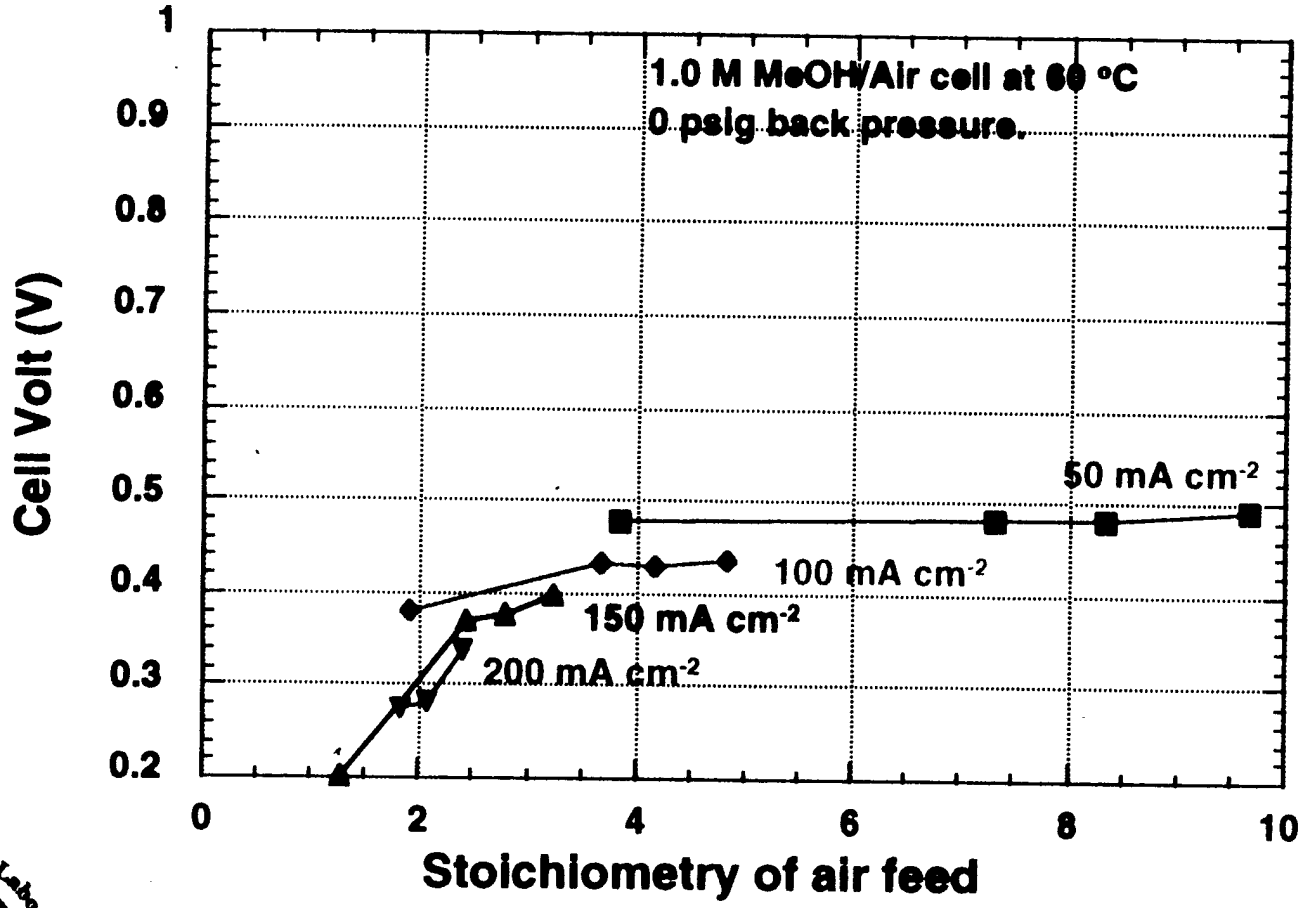

0.5 M MeOH/Air Cell Performance- Improved MEA (5 cm^2)

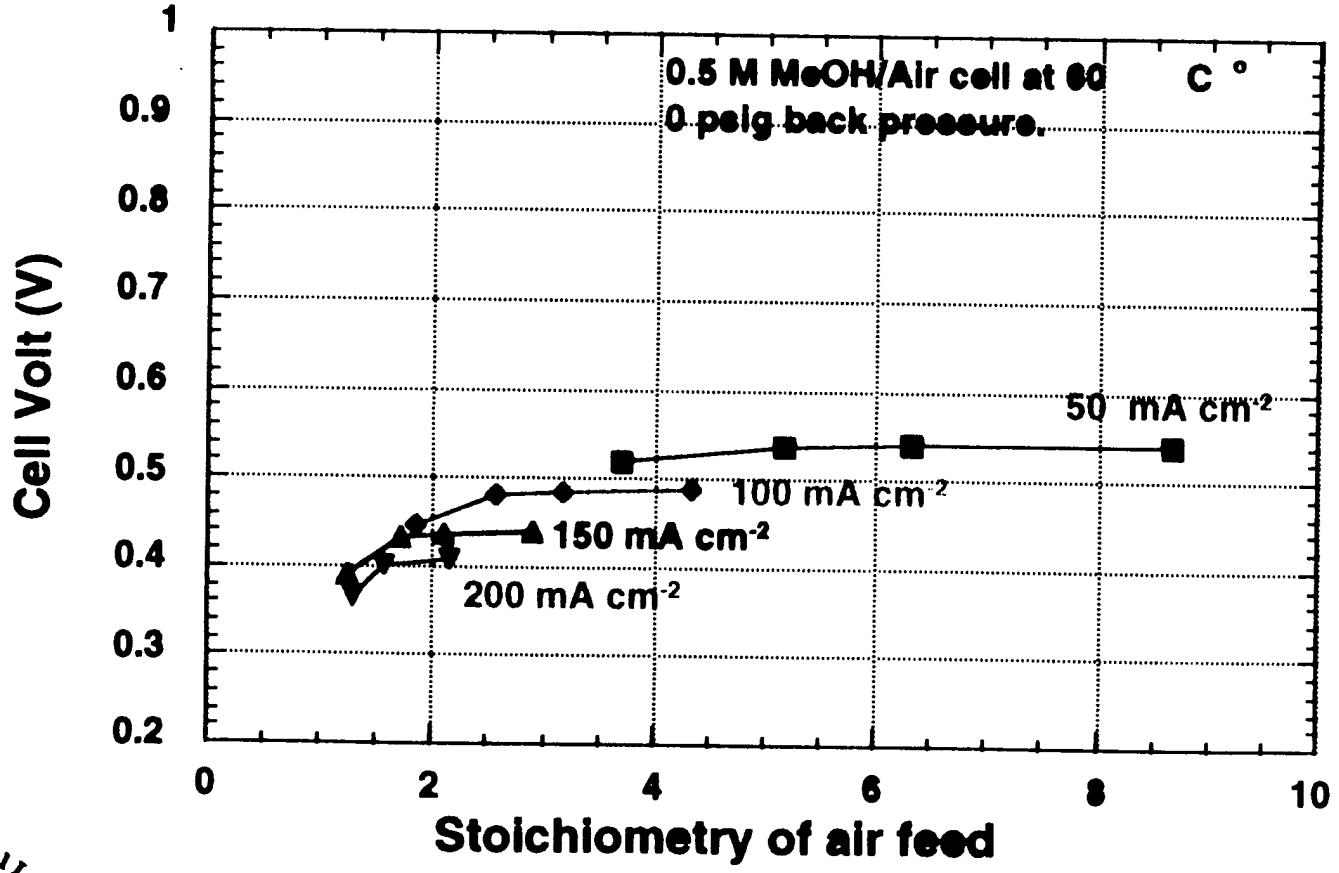

Record DMFC Performance - Improved MEA (5 cm^2)

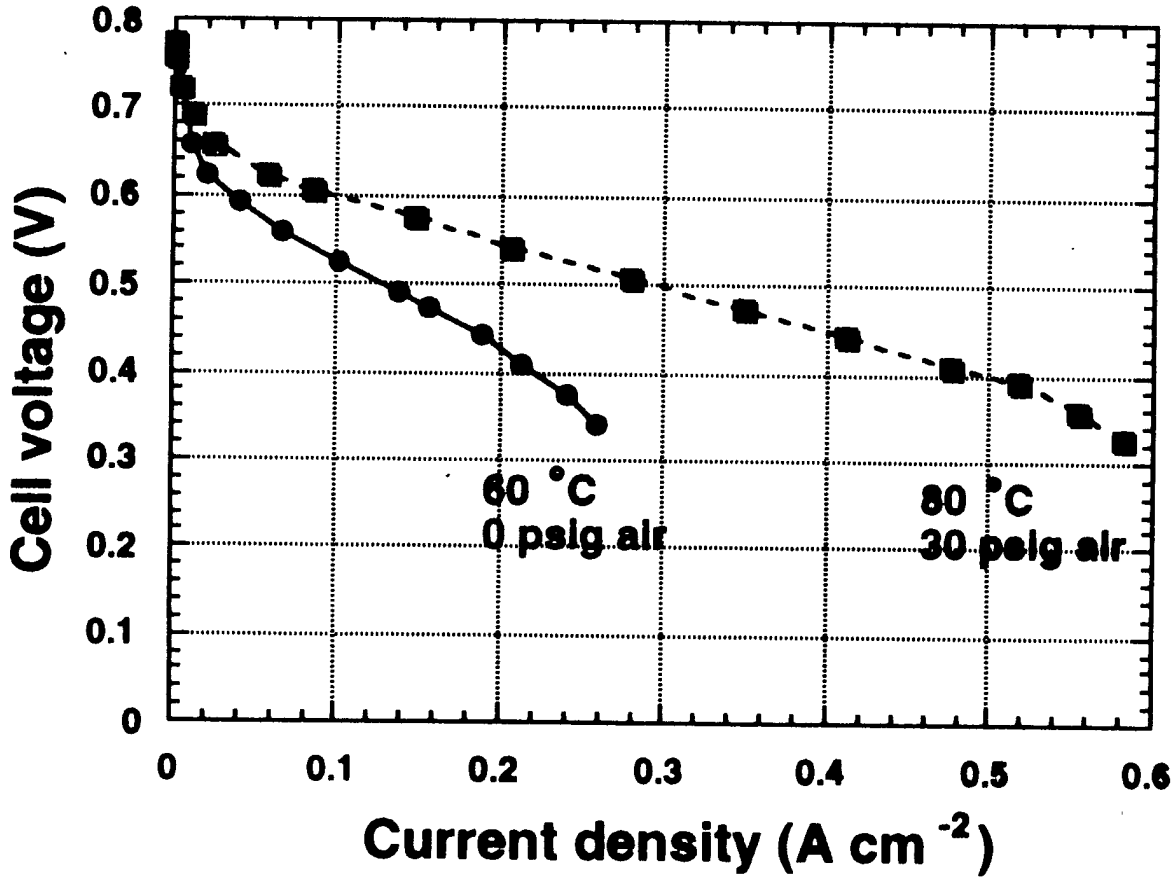

Test of DMFC anode stability

80 °C, 0.35 V (RHE)

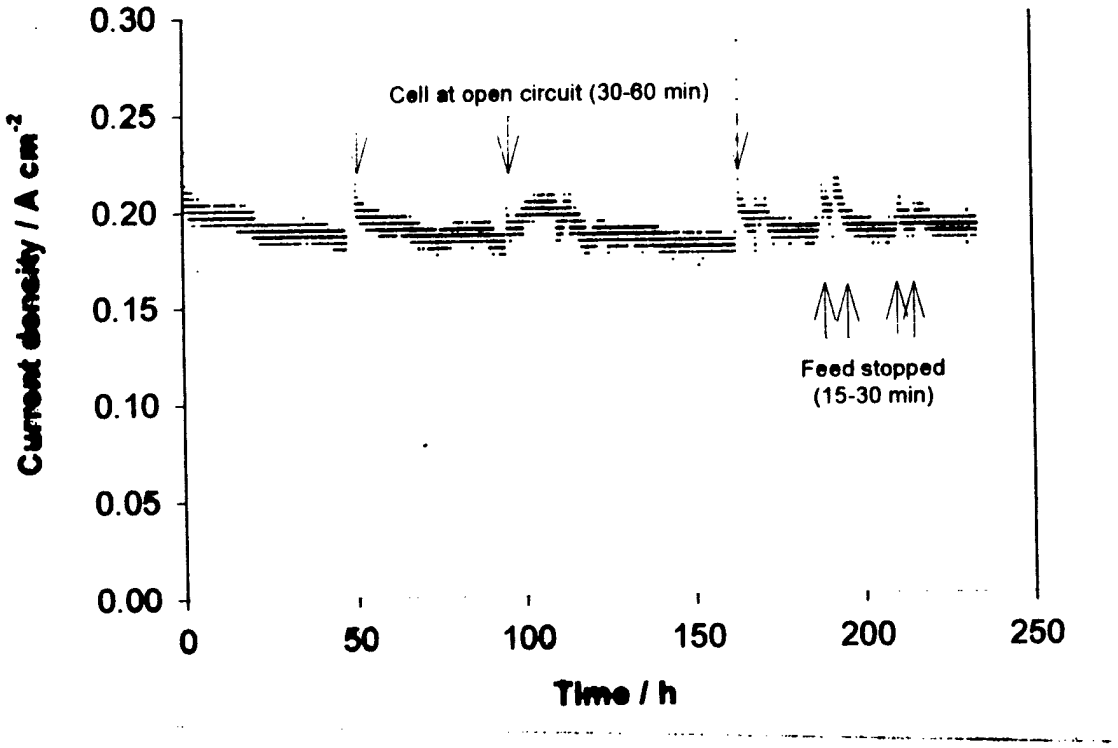

Direct Methanol Fuel Cells

Conclusions

The Anode Electrocatalyst

* Furhter optimization of both PtRu catalyst and PtRu-based catalyst layer are possible

* Is there an electro-catalyst better than PtRu ?

Cross-Over/Fuel Efficiency

* Any new membrane development should focus on overall fuel efficiency and overall cell performance, not just on "lowering methanol cross-over"

* Optimized overall cell structure and operation conditions could enable to achieve high fuel efficiencies in cells of high performance employing quite ordinary PFSA membranes

Direct Methanol Fuel Cells

Conclusions

The DMFC Cathode

* How to operate at low stoichiometric flows of ambient pressure air may be the remaining important challenge for simple portable power systems based on DMFCs

Technical issues **:**

* Maintaining a hydrophobic surface in face of H_2O/MeOH

*Effective overall cathode geometry

Organic/Inorganic Nanocomposites as Potential Fuel Cell Membranes

K.A. Mauritz, D. Mountz, D. Reuschle, R. F. Storey
Department of Polymer Science
University of Southern Mississippi
Hattiesburg, MS 39406-0076

1. Introduction

Organic/inorganic hybrid formulation *via* sol-gel reactions in polymers is occurring in a diverse, multidisciplinary arena in efforts to create advanced heterogeneous materials[1]. These hybrids are often tailored on a nanoscopic scale, *i.e.*, each of two or more phases has at least one dimension < ~100 nm, although scales < 100 Angstroms are encountered. Here, we discuss the work of Mauritz *et al.* with regard to potential applications in the arena of PEMs.

In sol-gel processes, acid or base-catalyzed hydrolysis → condensation reactions of inorganic alkoxides occur in a solvent containing water. Proper drying of the swollen gel can produce an inorganic oxide glass. Reaction variables include water:alkoxide ratio, solvent, pH, temperature, and drying method. The ability to conduct sol-gel processes at low temperatures allows for production of organic/inorganic hybrids via polymer-*in situ* sol-gel chemistry. In one scheme, alkoxide + water + solvent + pH factors, are imbibed by a pre-formed polymer film. Nature of polymer functional groups, T_g, and polymer morphology (crystallinity, phase separation) can influence the *in situ*-grown morphology of an inorganic oxide phase.

Mauritz *et al.* discovered that phase-separated morphologies of copolymer ionomers can act as templates for *in situ* sol-gel polymerizations so that inorganic, or organically-modified silicate (ORMOSIL) nanophases can be tailored within ionic domains. A polymer exploited in this regard is Nafion®. Recently, hard/soft block domain morphologies of elastomeric, sulfonated polystyrene-polyisobutylene-polystyrene block copolymers were employed in this capacity.

1. Perfluorinated Ionomers as Sol-Gel Reaction Templates

a. *Nafion®/[Silicate] Hybrids*

The morphology of Nafion® consists of clusters of sulfonate-terminated sidechains in a semicrystalline perfluorocarbon matrix[2]. Our work[3] was initiated assuming that this morphology would act as a *template* that catalyzes the sol-gel reaction and influences the geometry of the ultimate inorganic oxide phase. On exposure of Nafion® to a solution containing water, alcohol and hydrolyzed alkoxides, these polar molecules will preferentially migrate to the polar clusters. Subsequent polymerization of sorbed alkoxides is confined to these clusters which are viewed as nanometers-in-scale reaction vessels.

1100 EW, $-SO_3H$ membranes were pre-swollen in MeOH/water solutions. Alcohol enhances permeation of tetraethylorthosilicate (TEOS) monomer and hydrolyzed variants and incorporated water (H_2O:TEOS = 1:1 mol/mol) initiates sol-gel reactions.

Having removed the membranes from TEOS solutions, they were dried to remove volatiles and further drive SiOH condensation.

SAXS analyses of these hybrids established that the phase separated morphology of Nafion® persists despite invasion by the silicate phase[4], reinforcing our hypothesis of a 3-D template in which reactants are sequestered in clusters and the morphology directs silicon oxide phase geometry. Mechanical tensile studies indicated silicate phase percolation in that isolated clusters ultimately become inter-knitted by polycondensation reactions. FTIR spectroscopy uncovered a silicate network that grows to be increasingly less interconnected and that there is a large fraction of SiOH groups in/on these nanoparticles [5].

b. *Nafion®/[Organically-Modified Silicate] Nanocomposites: Organic Modification of Surfaces of Silicon Oxide Nanoparticles*[6]

$SiO_{2[1-x/4]}(OH)_x$ nanoparticles were generated via sol-gel reactions for TEOS within Nafion®-H membranes. SiOH groups were post-reacted with diethoxy-dimethylsilane (DEDMS), resulting in organically-shelled and interknitted nanoparticles. FTIR and ^{29}Si solid state NMR spectroscopies established structural incorporation of dimethylsilane groups onto silicon oxide cores and established degree of molecular connectivity within the silicate phase. Mechanical tensile experiments suggested linking of silicon oxide nanoparticles upon DEDMS post-reaction.

2.3 Nafion®/ORMOSIL Hybrids

Nafion®/ORMOSIL hybrids were formulated via sol-gel processes for TEOS and DEDMS mixtures, $Q = Si(O_{1/2})_4$ and $D = (CH_3)_2Si(O_{1/2})_2$ being network building blocks. FTIR spectroscopy quantified condensation extent by analyzing Si-O-Si and Si-OH bands, the former having components corresponding to Si-O-Si groups in cyclic and the other in linear substructures[7]. Shifting of the Si-C stretching band and shifting of the angular deformation band for Si-O-Si groups with variable D:Q implied random co-condensation between Q and D units, rather than Q and/or D block formation. ^{29}Si NMR investigations established that *in situ* D:Q is identical to that of the external monomer solution and provided more evidence of random co-condensation between TEOS and DEDMS[8]. As D:Q increases, ORMOSIL nanostructures are more hydrophobic and flexible. SAXS studies reinforced the morphological template concept for silicate, ORMOSIL and dimethylsiloxane phases in that scattered intensity vs. scattering vector magnitude plots retain the "ionomer peak"[9].

Pyrene (Py) photoprobes interrogated nanostructural polarity within (1) Nafion®/silicate and (2) Nafion®/ORMOSIL membranes[10]. In Py emission spectra having 5 vibronic peaks, peak 3 (383 nm) to peak 1 (372 nm) intensity ratio (I_3/I_1) decreases with increase in environmental polarity around Py. The interior of a pure silicate phase in which SO_3^- groups are embedded (1) is most polar. Polar/nonpolar interphases in (1) are next in decreasing polarity. The interior of the ORMOSIL phase in (2) has lowest polarity, reflecting presence of CH_3 groups and the interphase in (2) ranks higher in polarity. Equilibrium water uptake is ordered: Nafion®/ORMOSIL < unfilled

Nafion®-H < Nafion®/silicate. Significant, within the context of PEMs, is that the hydrophilicity of unfilled Nafion®-H can be tailored to be greater/lesser, as I_3/I_1 and water uptake correlate inversely. Hydrophilicity of clusters in Nafion®-H was enhanced by inserting silicate nanoparticles, attributed to the presence of many ≡SiOH groups to which numerous H_2O molecules can H-bond, as depicted below.

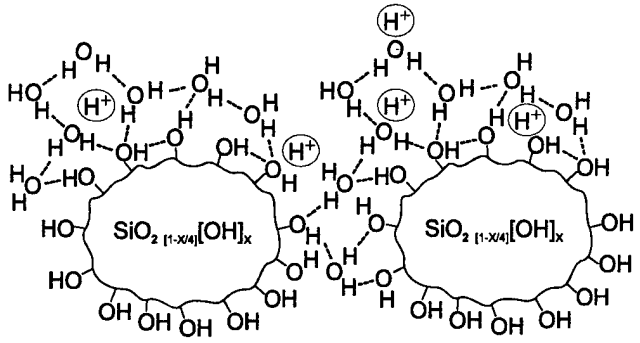

DSC and DMA studies suggest sidechain entrapment in silicate nanoparticles. The following figure shows that Nafion®/silicate has the greater affinity of H_2O over MeOH whereas the order is reversed for unfilled Nafion®-H in the sorption studies illustrated below[11]. The potential for tailoring membranes for use in direct methanol fuel cells is evident. Moreover, the fact that H_2O molecules strongly hydrate silicate nanoparticles has implications regarding membrane water management problems encountered in high temperature fuel cell operation.

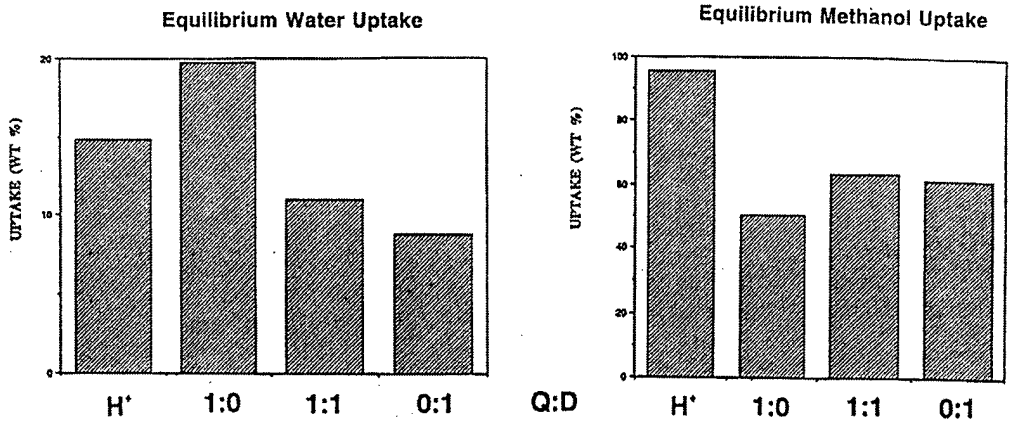

Dielectric loss (ε") vs. frequency (f) for the Q:D = 1:0 hybrid exhibits $\varepsilon'' \sim f^{-n}$ behavior over a broad range, suggestive of intercluster proton hopping[11]. The large hydrative capacity of this hybrid coupled with facile proton migration has implications within the realm of PEMs.

The integrated TGA-FTIR technique probed thermal degradation by identifying gas products vs. temperature[12]. The H-form formulated by first incorporating $SiO_{2[1-x/4]}(OH)_x$ cores, then organically modifying cores via post-reaction with DEDMS, has

greatest stability; SO_2 evolution retardation was rationalized in terms of sidechains immobilized within silicate cages.

Asymmetric silicate composition gradients were created along the thickness direction for 1-sided TEOS permeation[13]. Sol-gel reactions of TEOS were also conducted within Nafion® (COO^-/SO_3^-) bilayer membranes[14]. Silicate composition gradients can generate gradients in membrane hydration across the thickness for purposes of water management owing to membrane dehydration encountered at high temperatures.

2. Poly(Styrene-*b*-Isobutylene-*b*-Styrene) (PS-PIB-PS) Ionomers as Sol-Gel Reaction Templates

It was demonstrated that the phase separated morphologies of linear, sulfonated PS-PIB-PS block copolymer membranes that were ion exchanged to the benzyltrimethylammonium form also act as sol-gel polymerization templates for TEOS. Organic synthesis methods, including living cationic polymerization of PIB and the use of a real time, remote, *in situ* FTIR reaction probe, have permitted the tailoring copolymers having low polydispersity and precise block lengths. Hydrolyzed TEOS sorbed from external solutions migrates to, and assembles into bonded silicate nanostructures within the ionically-modified PS domains when DMAc is the carrier solvent. This cation-solvent combination is critical. Given sufficient hydration arising from numerous ≡SiOH groups, as illustrated in the first figure, as well as the presence of contiguous hydrogen bonding pathways along which protons can migrate, these hydrocarbon-based membranes may be PEM candidates for low cost, portable fuel cells for which long lifetimes are not critical. A key element in this strategy is the structuring of water by the silicate nanostructures. The silicate nanostructures, in turn, are organized by the natural phase separated morphology of the block copolymer ionomer template.

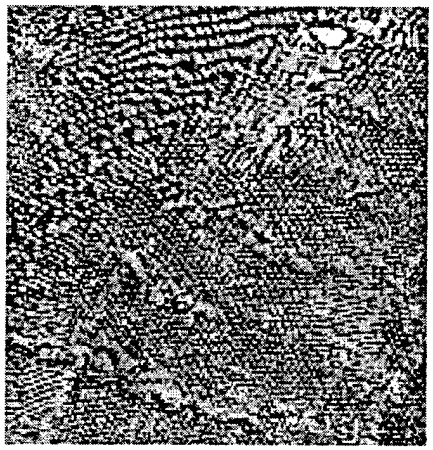

The figure above is an AFM micrograph (tapping mode, phase) for a PS-PIB-PS based hybrid having 18 mol% PS outer blocks that are sulfonated 16 mol% and there is 6.5% silicate uptake. A very well-defined morphology consisting of PS rods whose inter-axial spacings are *ca.* hundreds of Angstroms is seen. This is reasonable for this type of block copolymer at this composition. The entire field-of-view is 4 μm X 4μm.

Acknowledgements

This material is based partly upon work supported by a grant from the National Science Foundation/Electric Power Research Institute (Advanced Polymeric Materials: DMR-9211963). This work was also sponsored in part by the Air Force Office of Scientific Research, Air Force Systems Command, USAF, under grant number AFOSR F49620-93-1-0189. Partial support was also provided by the Mississippi NSF-EPSCoR program.

References

[1] Sanchez, C.; Ribot, F., Ed. *Proceedings of the First European Workshop on Hybrid Organic-Inorganic Materials*, **1993**, Paris; p. 9.

[2] T.D. Gierke, G.E. Munn and F.C. Wilson, *J. Polym. Sci.: Polym. Phys. Ed.* **1981**, *19*, 1687.

[3] Mauritz, K.A.; Storey, R.F.; Jones, C.K. in *Multiphase Polymer Materials: Blends, Ionomers and Interpenetrating Networks;* ACS Symp. Ser. No. 395, Ch 16.; Utracki, L.A., Weiss, R.A., Eds.; American Chemical Society: Washington, DC, 1989.

[4] K.A. Mauritz, I.D. Stefanithis, S.V. Davis, R.W. Scheetz, R.K. Pope, G.L. Wilkes, H. H. Huang, *J. Appl. Polym. Sci., 55*(1) (1995) 181.

[5] K.A. Mauritz and R.M. Warren, *Macromolecules*, *22* (1989) 1730.

[6] Deng, Q.; Mauritz, K.A.; Moore, R.B. in *Hybrid Organic-Inorganic Composites, ACS Symp. Ser. 585*, J.E. Mark, P.A. Bianconi and C.Y-C. Lee, Eds., **1995**, Ch.7.

[7] Deng, Q.; Moore, R.B.; Mauritz, K.A. *Chem. Mater.* **1995**, *7*, 2259.

[8] Deng, Q.; Jarrett, W.; Moore, R.B.;. Mauritz, K.A. *J. Sol-Gel Sci. Technol.* **1996**, *7*, 185.

[9] Deng, Q.; Cable, K.M.; Moore, R.B.; Mauritz, K.A. *J. Polym. Sci. B: Polym. Phys. Ed.* **1996**, *34*, 1917.

[10] Deng, Q.; Hu, Y.; Moore, R.B.; McCormick, C.L.; Mauritz, K.A. *Chem. Mater.* **1997**, *9*, 36.

[11] Deng, Q.; Moore, R.B.; Mauritz, K.A. *J. Appl. Polym. Sci.* **1998**, *68*, 747.

[12] Deng, Q.; Wilkie, C.A.; Moore, R.B; Mauritz, K.A. *Polymer* **1998**, in press.

[13] Gummaraju, R.V.; Moore, R.V.; Mauritz, K.A. *J. Polym. Sci.: B: Polym. Phys.* **1996**, *34*, 2383.

[14] Robertson, M.A.F.; Mauritz, K.A. *J. Polym. Sci.: B: Polym. Phys.* **1998**, *36*, 595.

Organic/Inorganic Membranes Nanostructured for Molecular Transport Applications

K.A. Mauritz
Department of Polymer Science
University of Southern Mississippi

Membrane Applications

- Gas Permselectivity
- Liquid Pervaporation
- Fuel Cells

Sol-Gel Chemistry

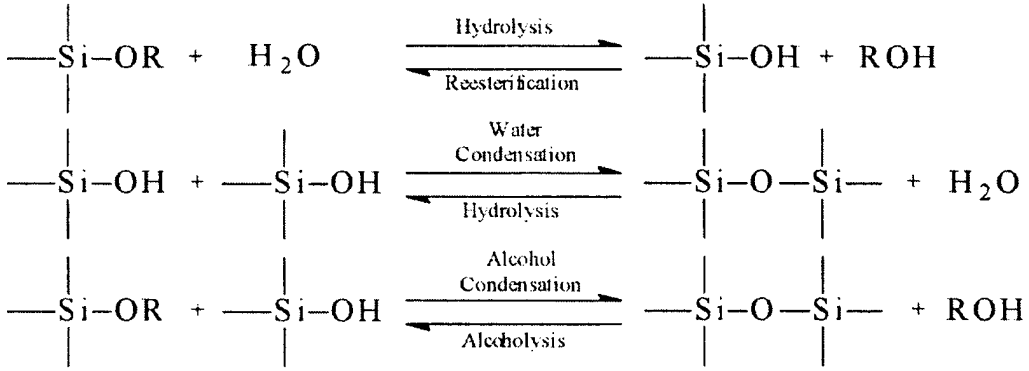

- Sol-gel precursors have a high affinity for the ionic domains
- Inorganic particle formation hypothesized to occur near the ionic domains

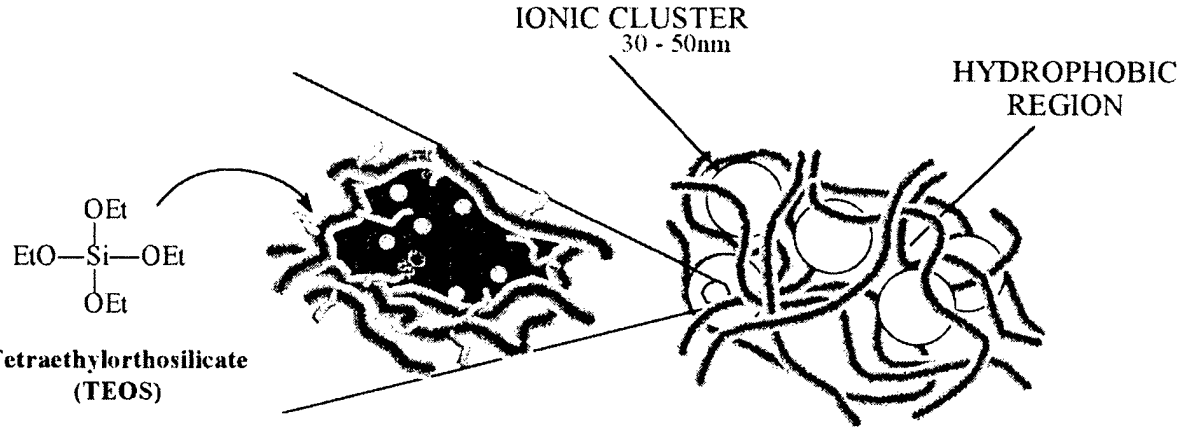

Benefits of Incorporating an Inorganic Domain into a BCPI

- Mechanical reinforcement and enhanced thermal properties
- Increase in T_g
- Tailored composition which can be used to alter the diffusion properties of the material

Nafion®/[SiO_2] Hybrids via *in-situ* Sol-Gel Reactions

- Sol-gel solutions incorporated preferentially into ionic clusters in Nafion®
- Sol-gel reactions catalyzed by the fixed SO_3H groups in the nanoclusters
- Nafion® nanophase separated morphology directs final morphology of the *in-situ* sol-gel derived phase

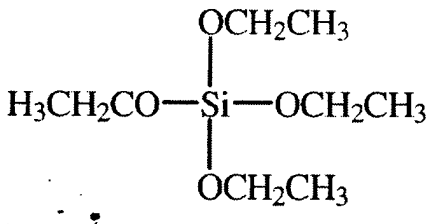

Tetraethoxysilane
(TEOS)

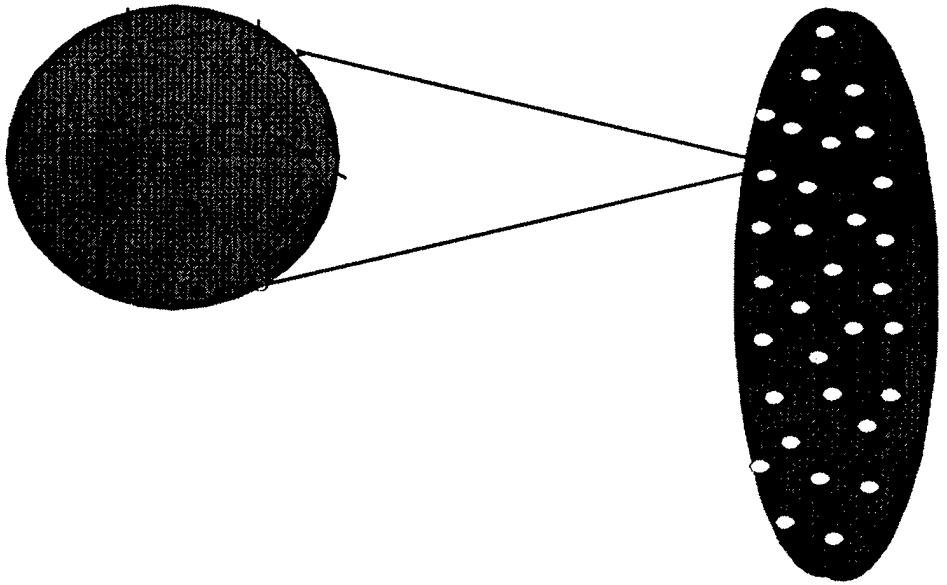

312

CHEMICAL/MORPHOLOGICAL TAILORING OF INORGANIC OXIDE PHASE

Inorganic Oxide Molecular Interconnectivity:

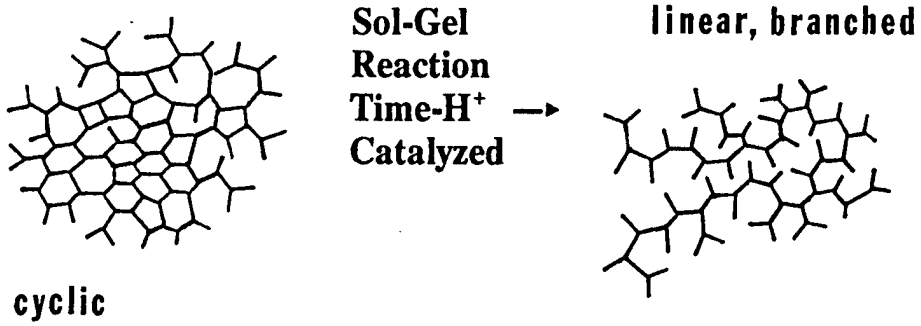

Percolation of Inorganic Nanoparticles:

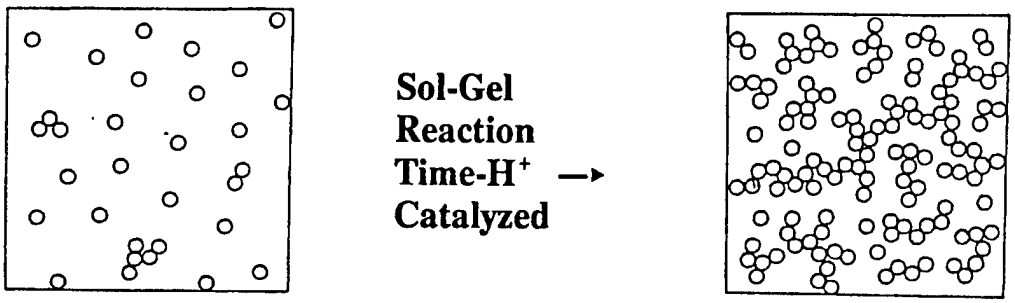

Post-Chemistry/ "Shelled Inorganic Oxide Nanoparticles:

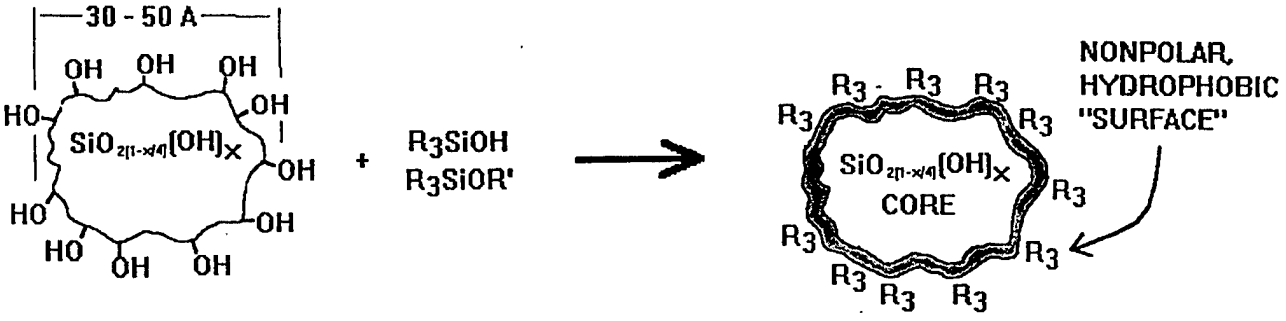

PFSI/ORMOSIL Systems

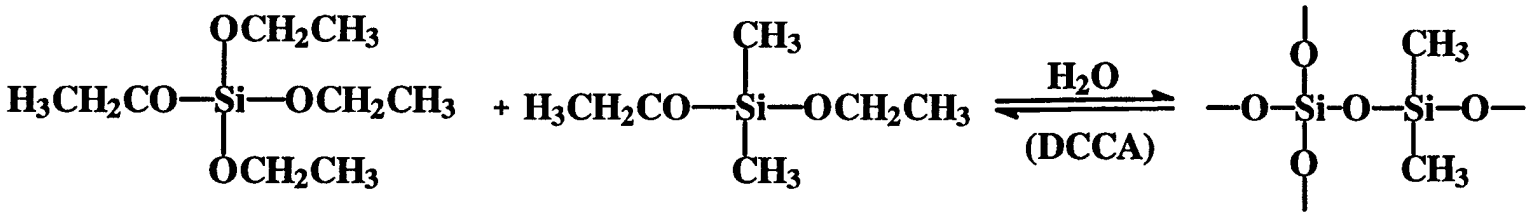

TEOS DEDMS

Organically Modified Silicates Used in Experiments:

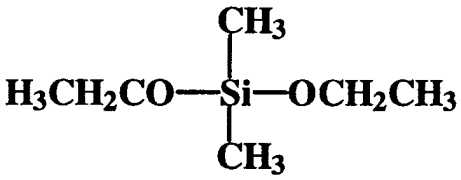

DiEthoxyDiMethylSilane (DEDMS)

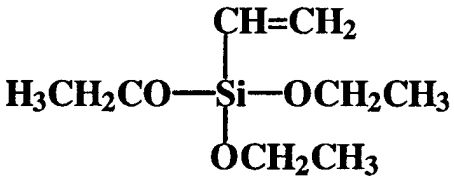

TriEthoxyVinylSilane (TEVS)

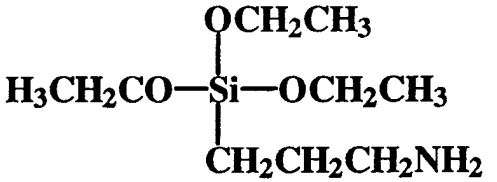

3-AminoPropylTriEthoxySilane (APTES)
****Too reactive to be useful for incorporation into membrane ****

Also:

Hydroquinone

Depiction of Formulation

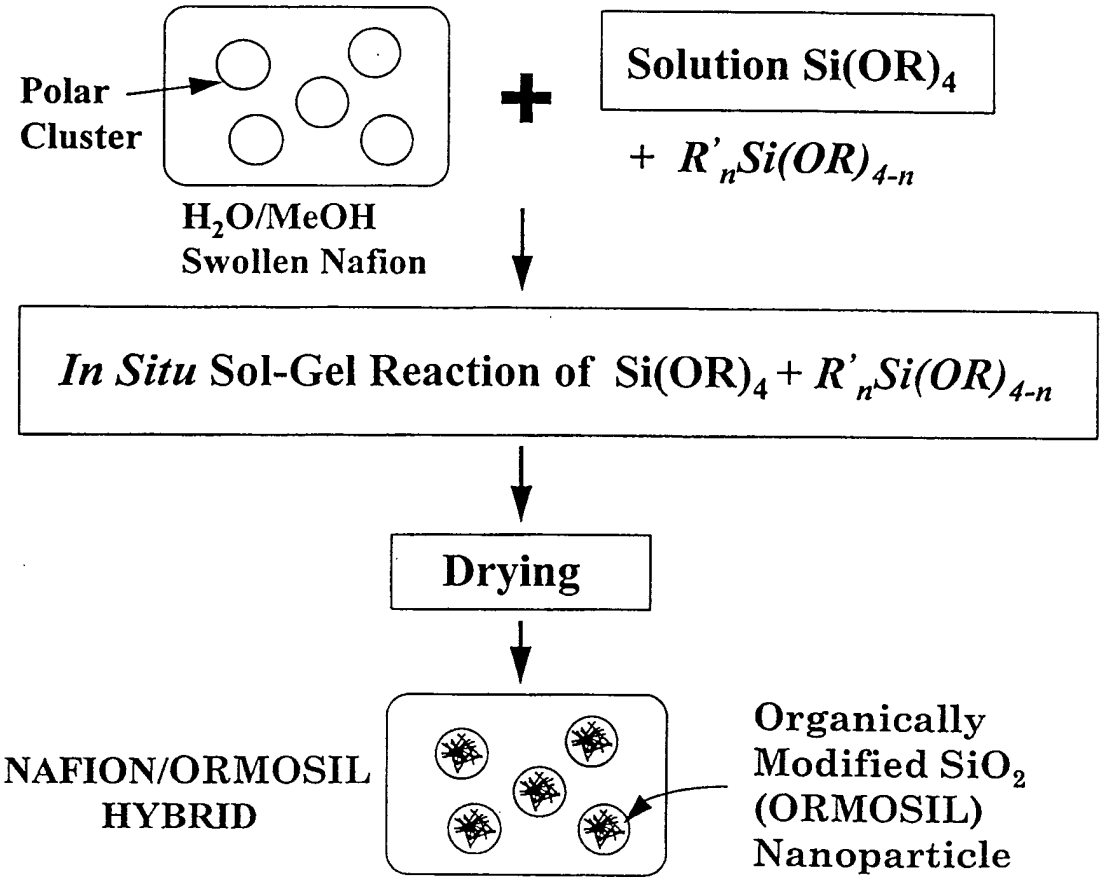

Linear and Cyclic Subunits of $SiO_{2[1-x/4]}(OH)_x$ Structures

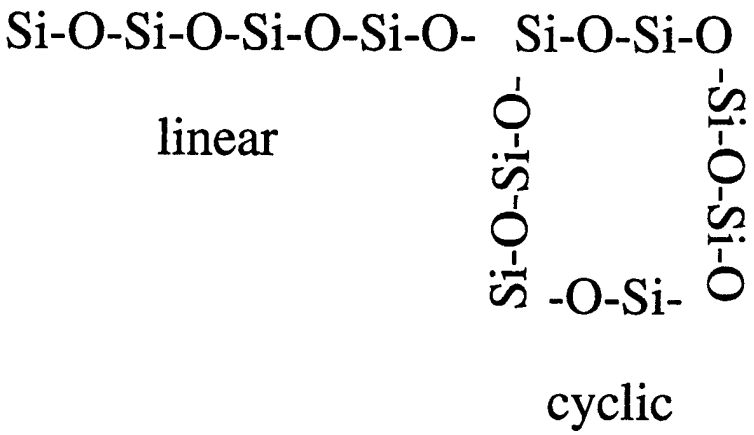

FTIR (ATR) Difference Spectra

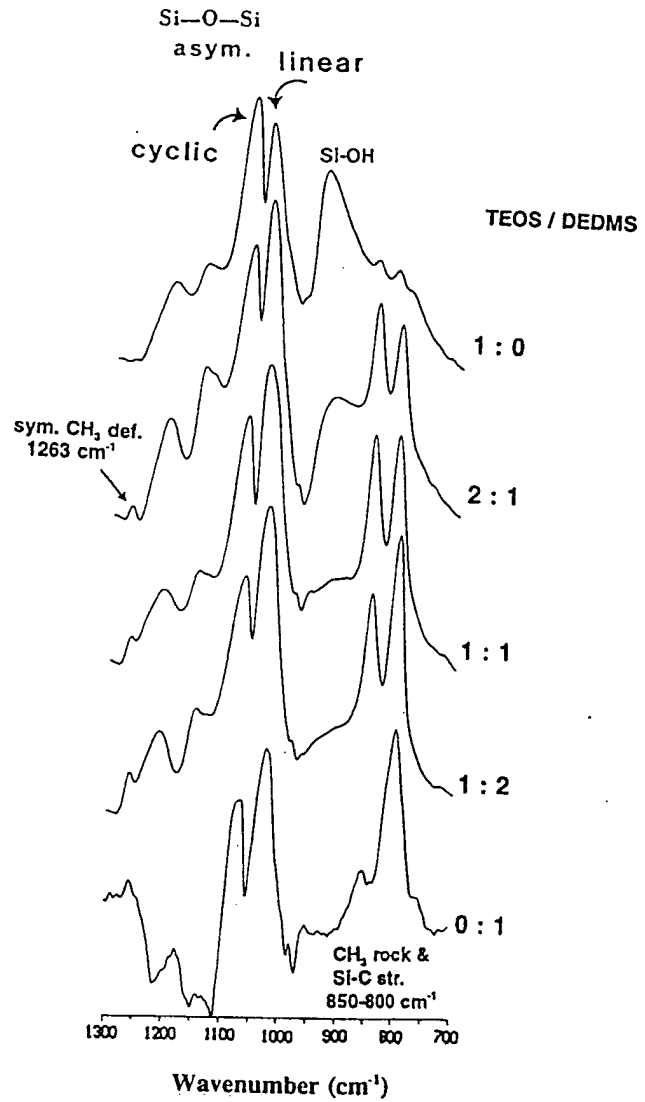

NANOPARTICLE "POROSITY"

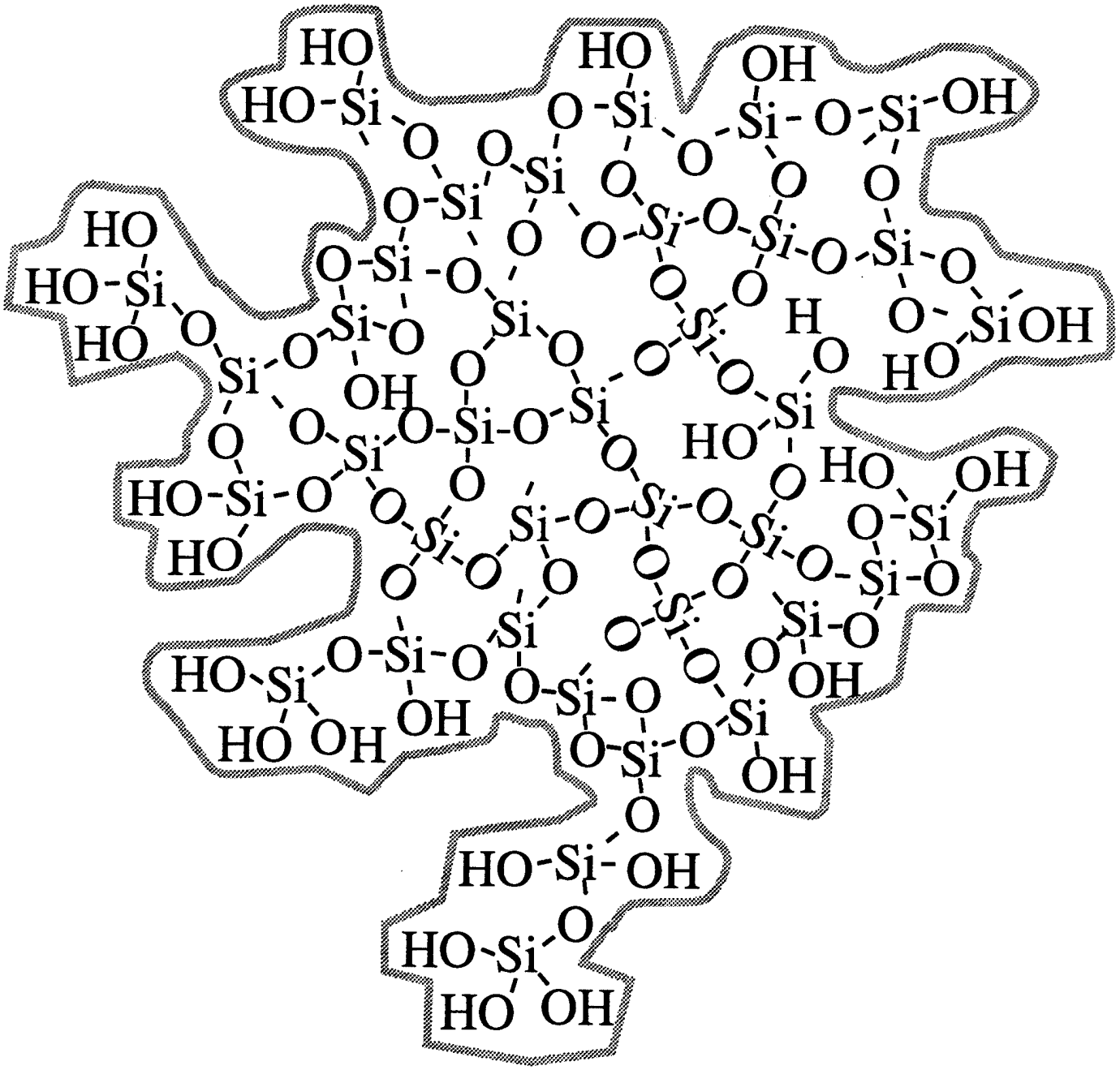

^{29}Si Solid State NMR Spectroscopy

$$Q_n = (SiO)_nSi(OR)_{4-n}$$

e.g., Q_3 =

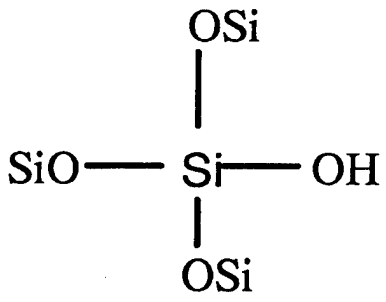

Solid State ^{29}Si NMR Spectra

(weight uptake around 10 %)
(TEOS / DEDMS molar ratio as indicated)

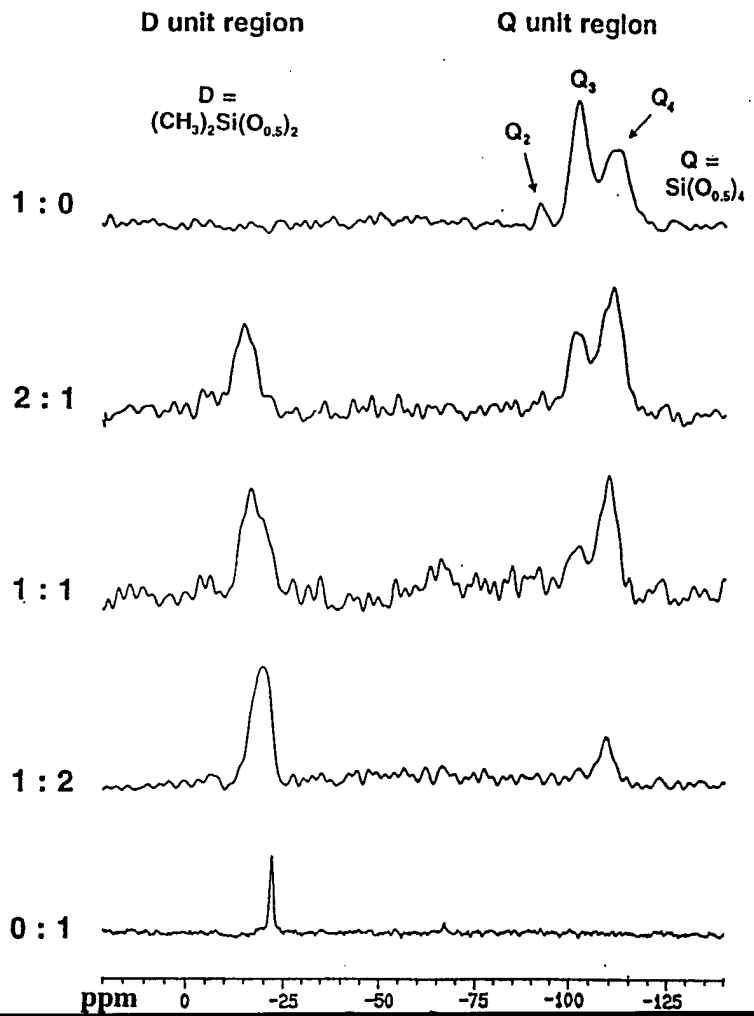

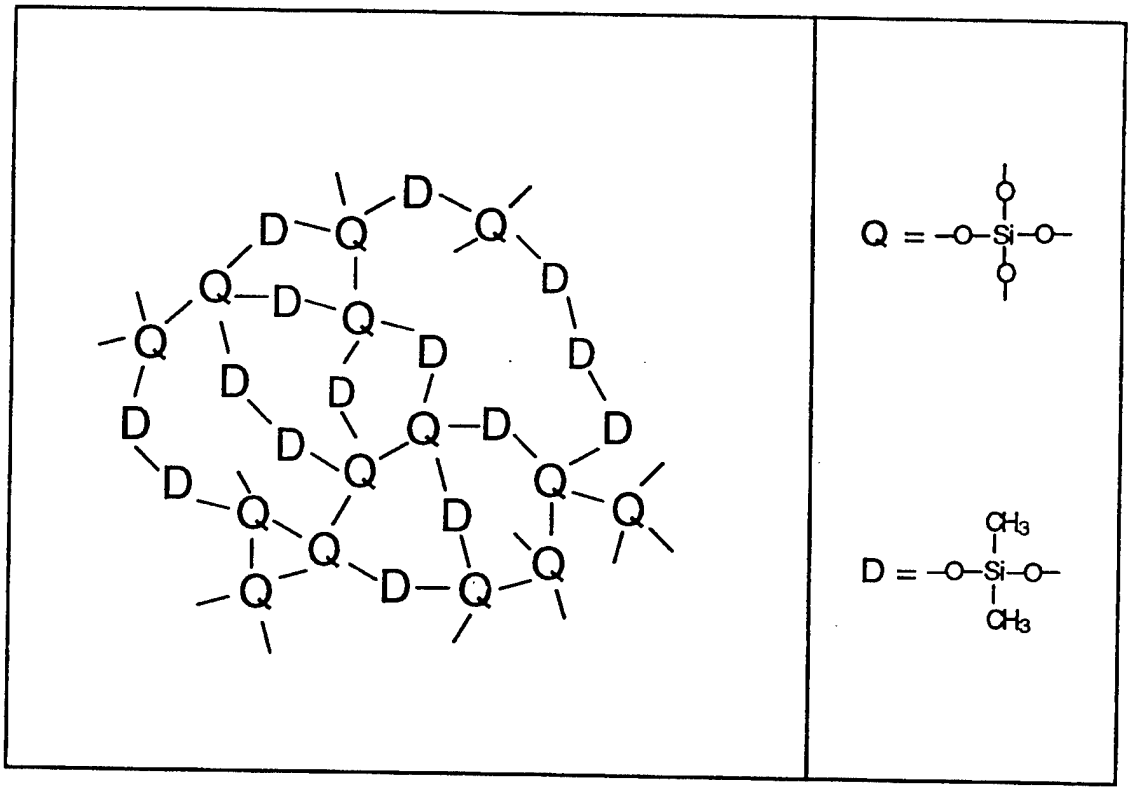
Q = –O–Si–O–
D = –O–Si–O–
CH3
CH3

Nafion®/[SiO_2] Hybrids via *in-situ* Sol-Gel Reactions

- Sol-gel solutions incorporated preferentially into ionic clusters in Nafion®
- Sol-gel reactions catalyzed by the fixed SO_3H groups in the nanoclusters
- Nafion® nanophase separated morphology directs final morphology of the *in-situ* sol-gel derived phase

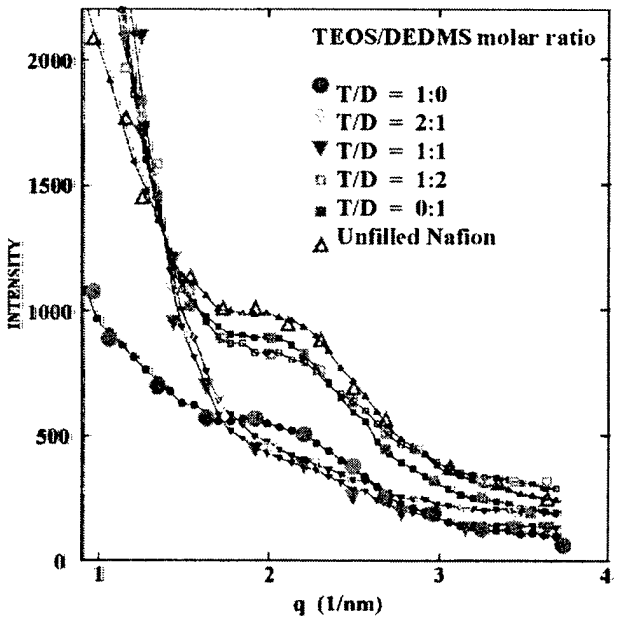

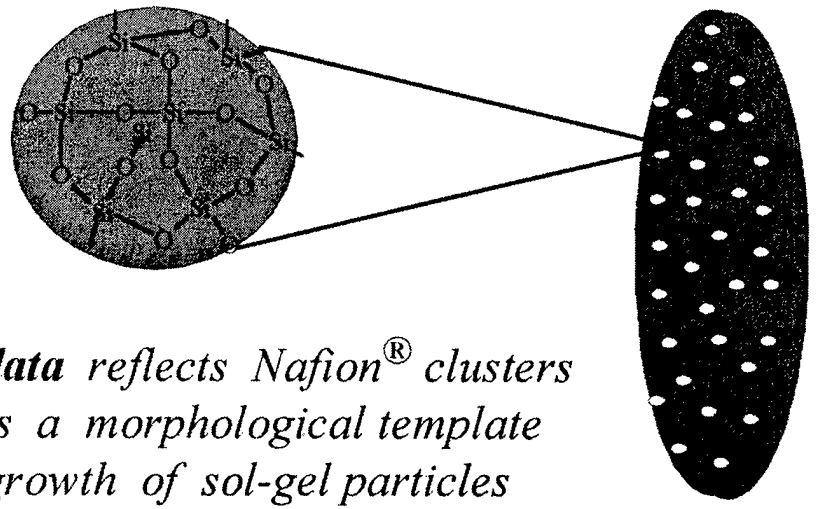

SAXS data *reflects Nafion® clusters acts as a morphological template for growth of sol-gel particles*

* *Peak in data &* * *Electron density changes*

322

Deng, Q.; Cable, K. M.; Moore, R. B.; Mauritz, K. A. J. Poly. Sci. Part B Poly. Phy., 34, 1917, **1996**

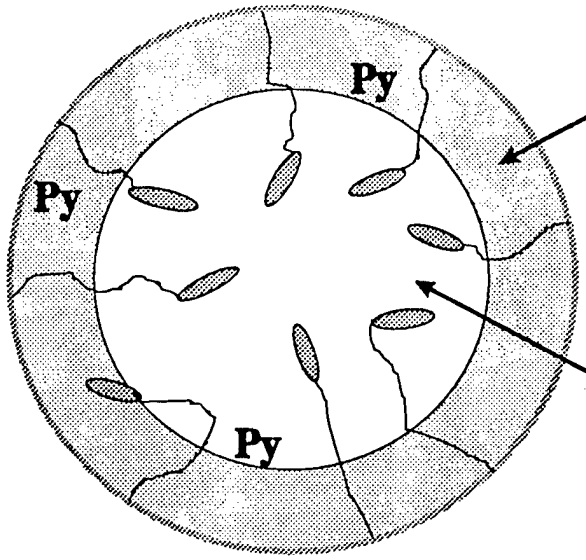

(a)

Unfilled Nafion

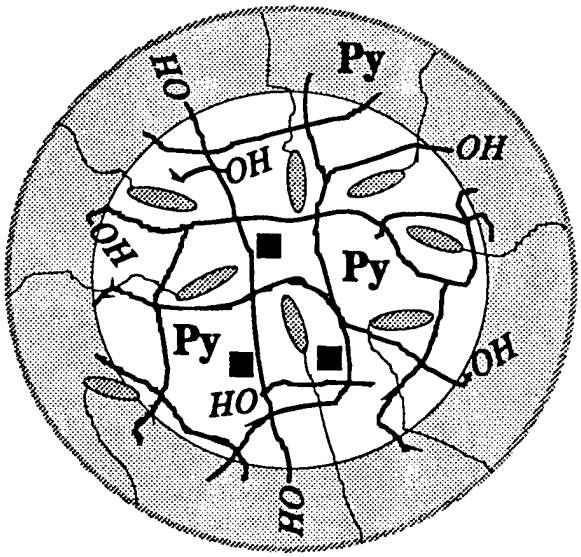

(b)

Nafion/SiO_2 Hybrid

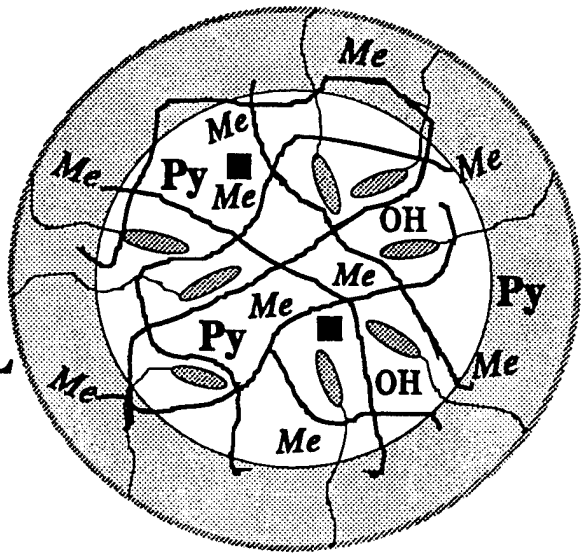

(c)

Nafion/ORMOSIL Hybrid

Py = *PYRENE*

$= SO_3^- H^+$

■ = *RESIDUAL H_2O, MeOH*

= *Si-O-Si NETWORK*

-OH = *Si-OH*

-Me = *Si-Me*

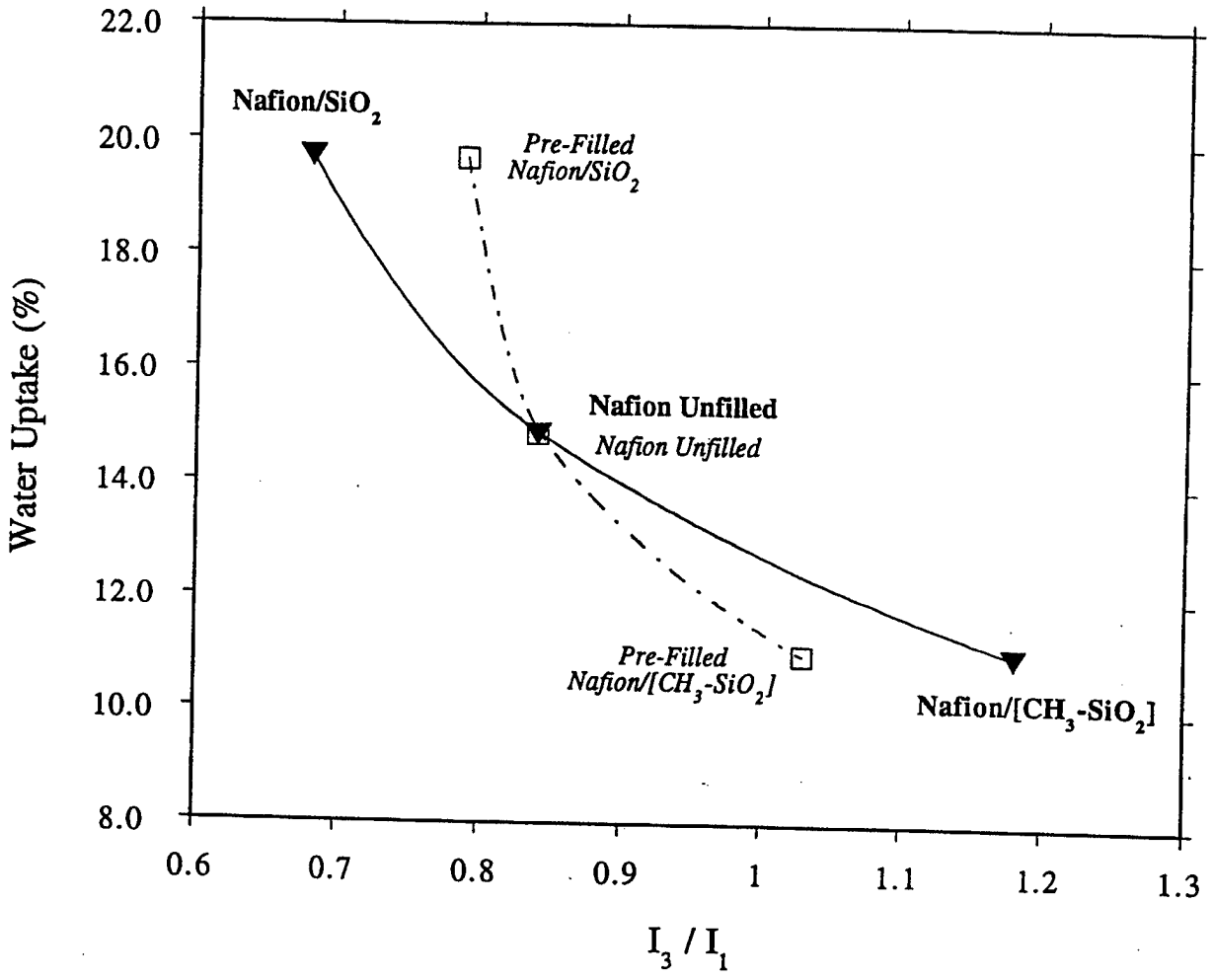
22.0
20.0
18.0
16.0
14.0
12.0
10.0
8.0
Water Uptake (%)
0.6
0.7
0.8
0.9
1
1.1
1.2
1.3
I_3 / I_1
Nafion/SiO_2
Pre-Filled Nafion/SiO_2
Nafion Unfilled
Nafion Unfilled
Pre-Filled Nafion/[CH_3-SiO_2]
Nafion/[CH_3-SiO_2]

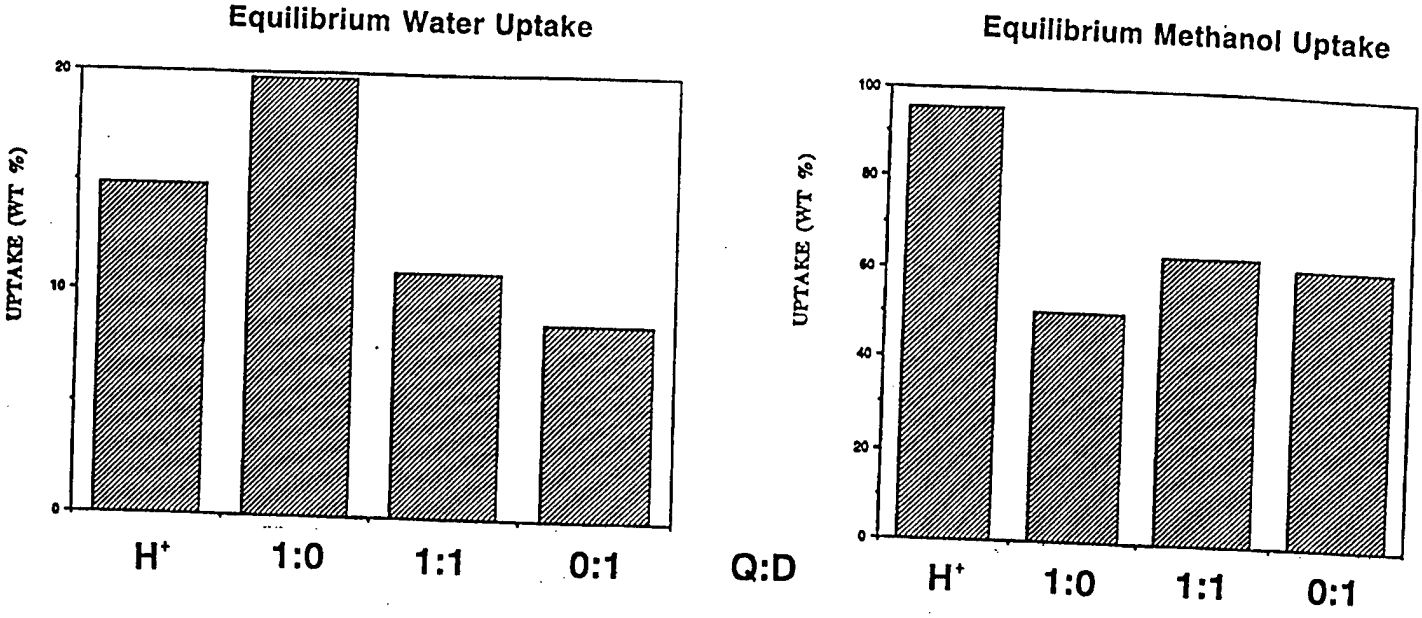
Equilibrium Water Uptake
UPTAKE (WT %)
20
10
0
H+
1:0
1:1
0:1
Q:D
Equilibrium Methanol Uptake
UPTAKE (WT %)
100
80
60
40
20
0
H+
1:0
1:1
0:1

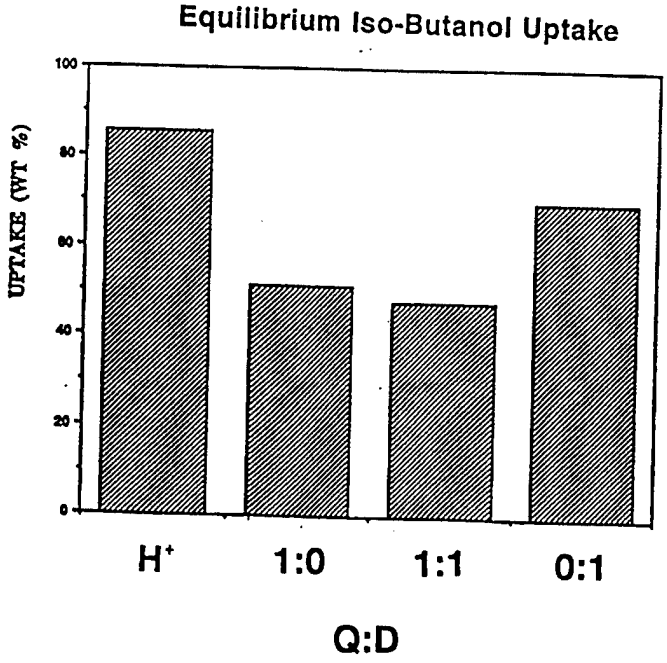
Equilibrium Iso-Butanol Uptake
UPTAKE (WT %)
100
80
60
40
20
0
H+
1:0
1:1
0:1
Q:D

HYDRATION MICROSTRUCTURE AROUND SILICATE NANOSTRUCTURES

ISSUES RELATING TO LONG RANGE PROTON CONDUCTION

(1) *Nafion®/SiO_2 membranes have greater hydrative capacity than Nafion®-H^+ membranes*

- ≡SiOH group interactions

(2) Hydration Microstructure

- H-bonded vs non-H-bonded H_2O
- ≡SiOH ---H_2O interactions
- Requirement: Structure long H-bonding pathways - contiguous silicate nanostructures

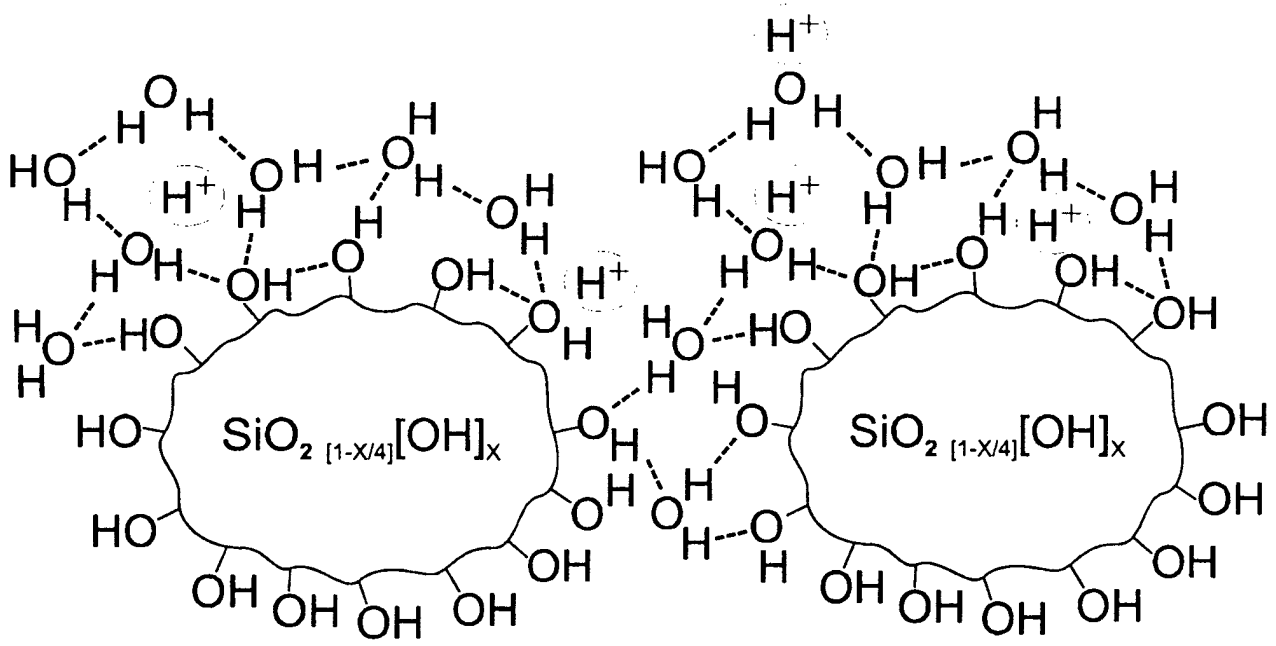

Concept of H^+ Hopping along Structured Hydrogen Bonded Pathways

The Case for Hydrocarbon Membranes

- **Scientific/Technical Issues**
- **COST - the real driver!**
- **G.E. Wnek, in C&EN, April 13, 1998, p. 41**

MORPHOLOGICAL TEMPLATES FOR *in Situ* SOL-GEL POLYMERIZATIONS

Phase Separated Block Copolymers:

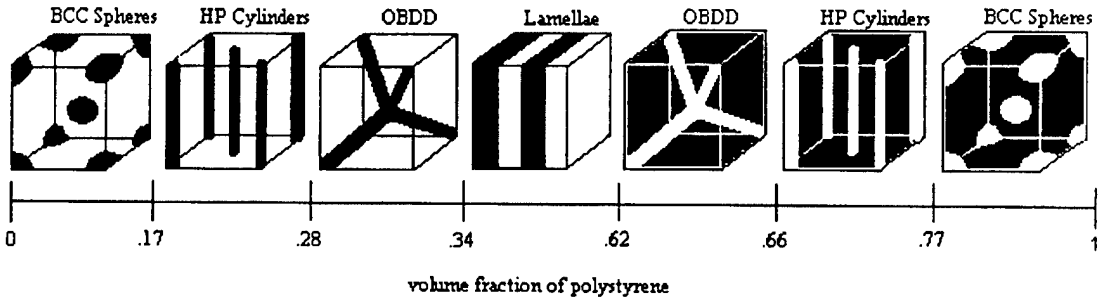

Template Hypothesis: Alkoxide monomers preferentially migrate to, polymerize and form nanostructures within only one domain.

e.g. PS-PIB-PS:

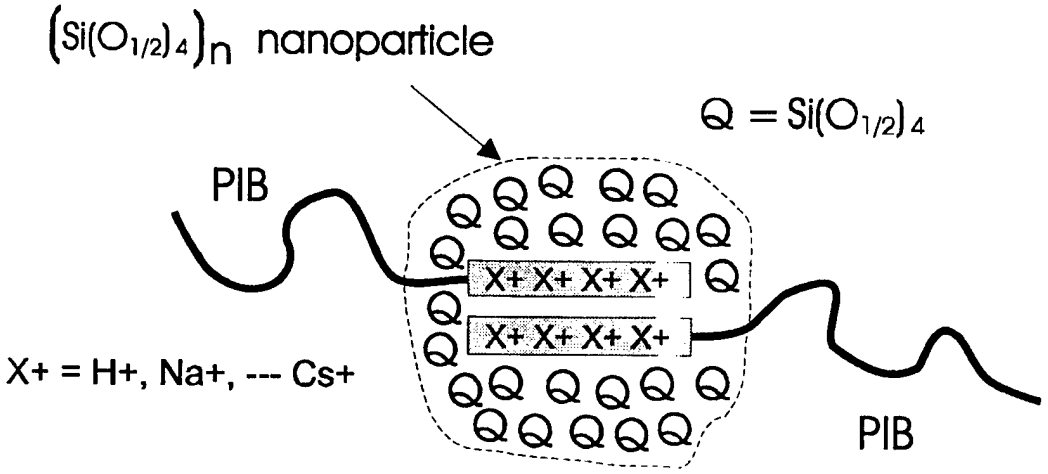

Various PIB-Based Elastomeric Matrix Materials

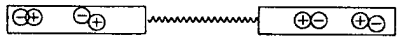

L-1

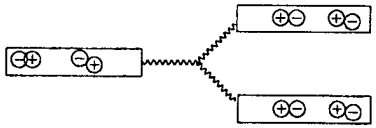

T-1

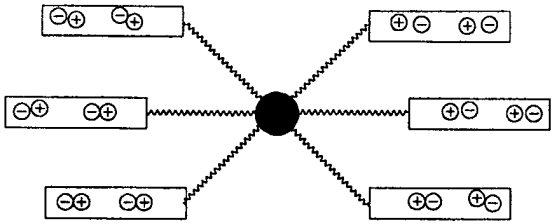

S-1

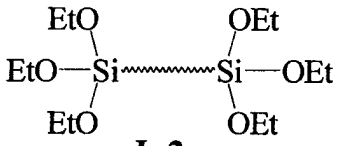

L-2

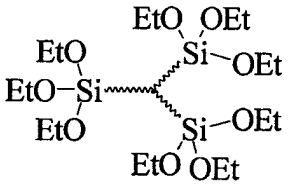

T-2

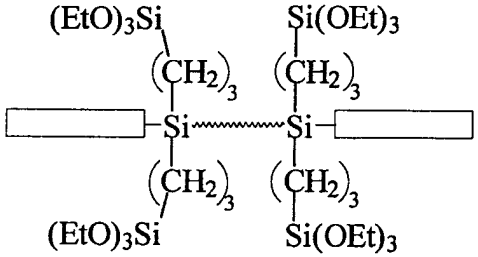

L-3

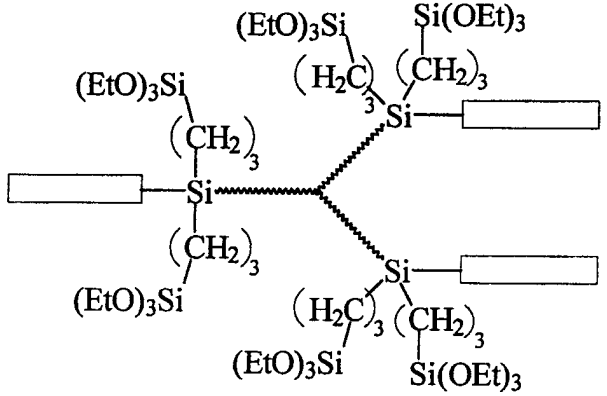

T-3

Synthesis of Block Copolymer

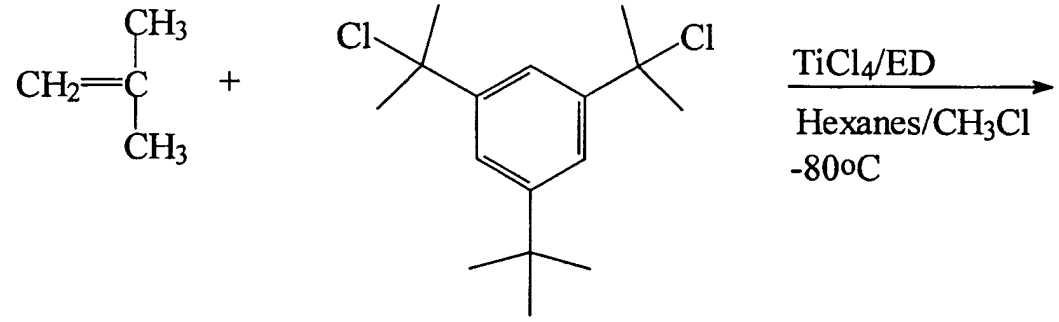

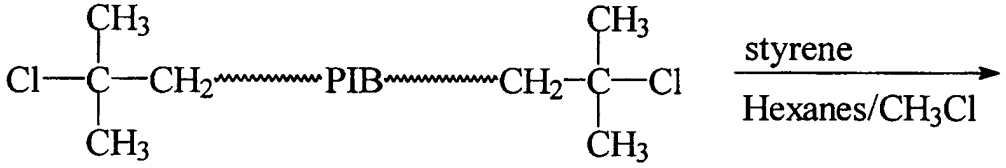

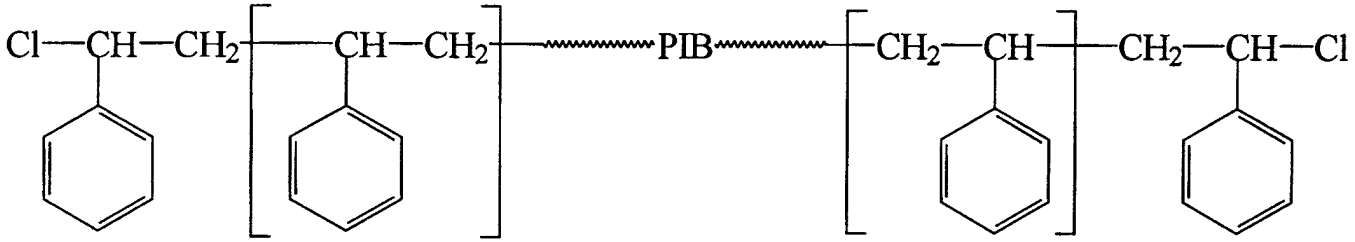

Styrene-Isobutylene-Styrene Ionomers

PS-PIB-PS $\xrightarrow[\text{dichloroethane}]{\text{acetyl sulfate}}$ Sulfonated BCP $\xrightarrow{\text{base}}$ BCPI

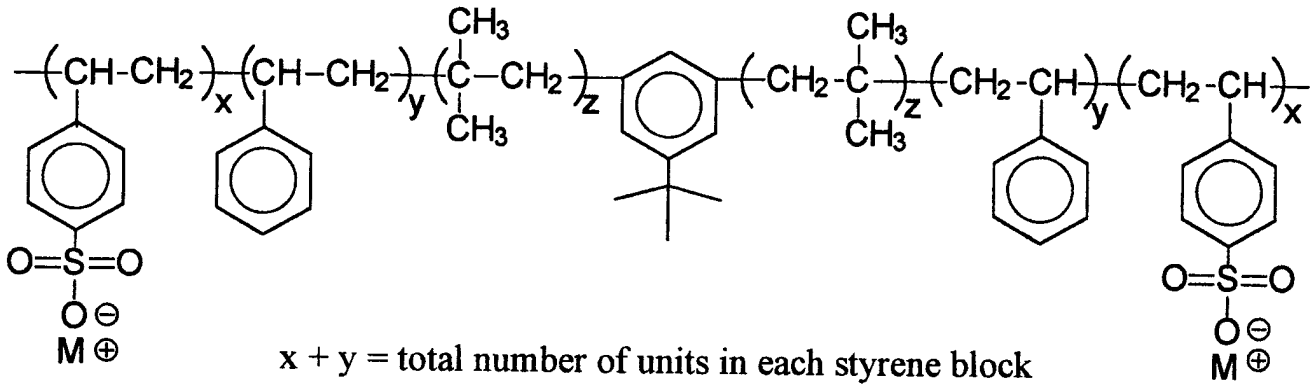

Effects of Sulfonate Ions on PS Regions

- Increase in the T_g
- Higher affinity for polar solvents

Experimental Scheme

Initial Preparation

Make BCPI films by Solution Casting

Sol-Gel Polymerization:

- Film Swollen in Solvent System
- ***In-situ*** Sol-Gel Reaction
- Dry the Film under Heat and Vacuum to Drive the Sol-Gel Reaction

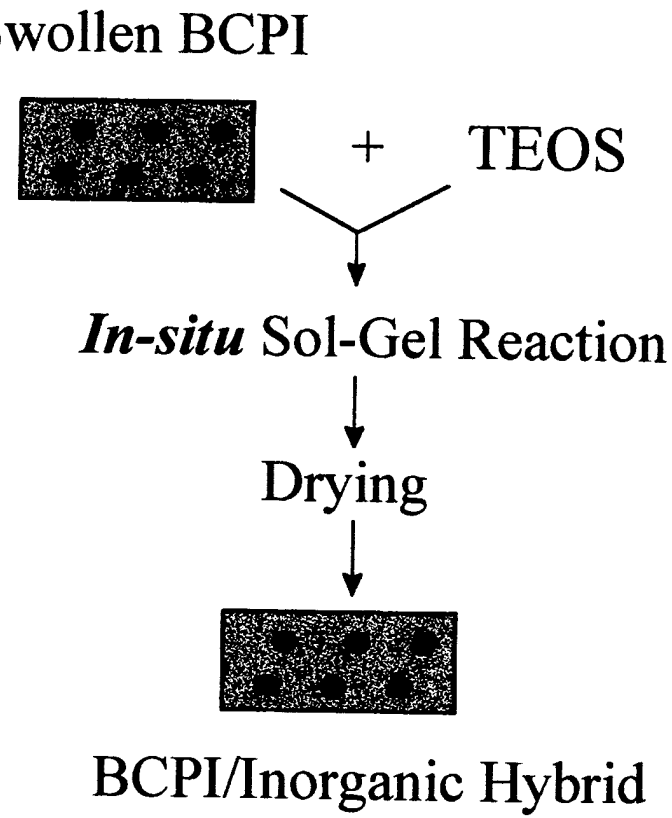

BCPI Solvent Swelling Profiles

(*Benzyltrimethylammonium* Form)

in

Dioxane (O)

DMAc (X)

1-PrOH/TEOS (▲)

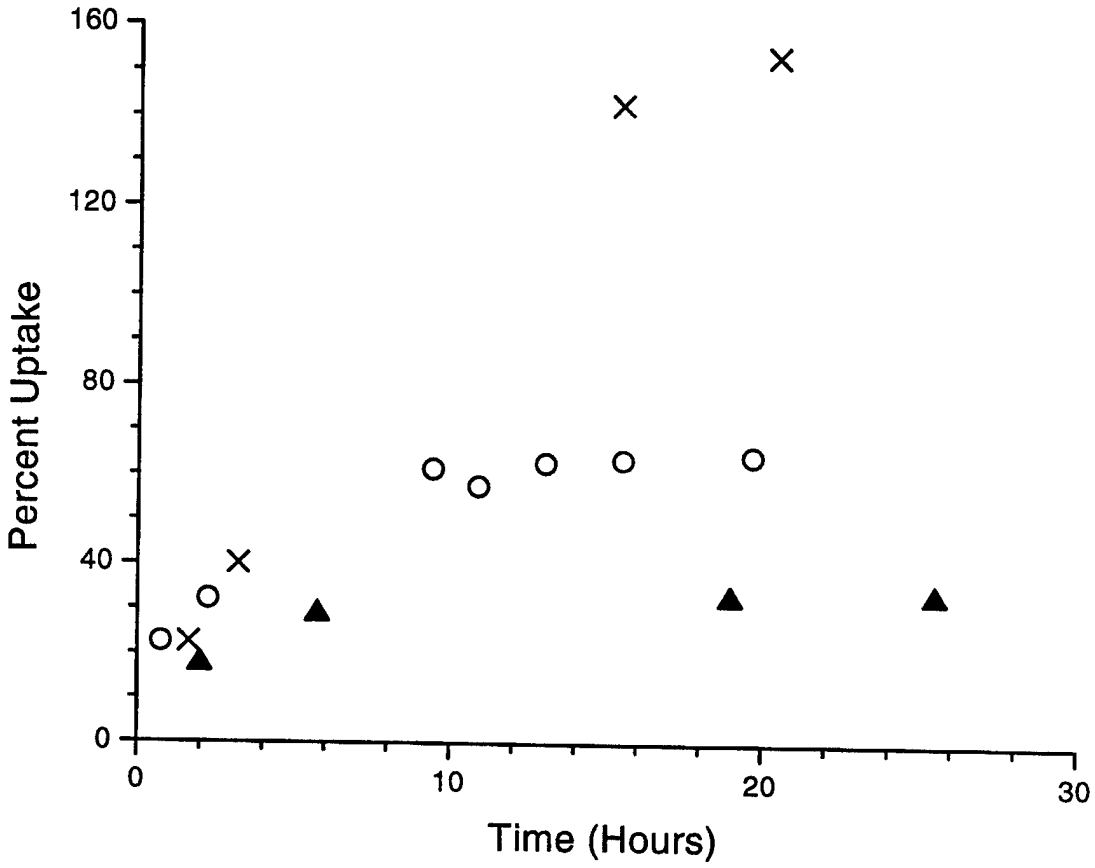

⇒ DMAc is superior swelling agent

DMAc molecules attack only hard block domains

ESEM/EDS Profile

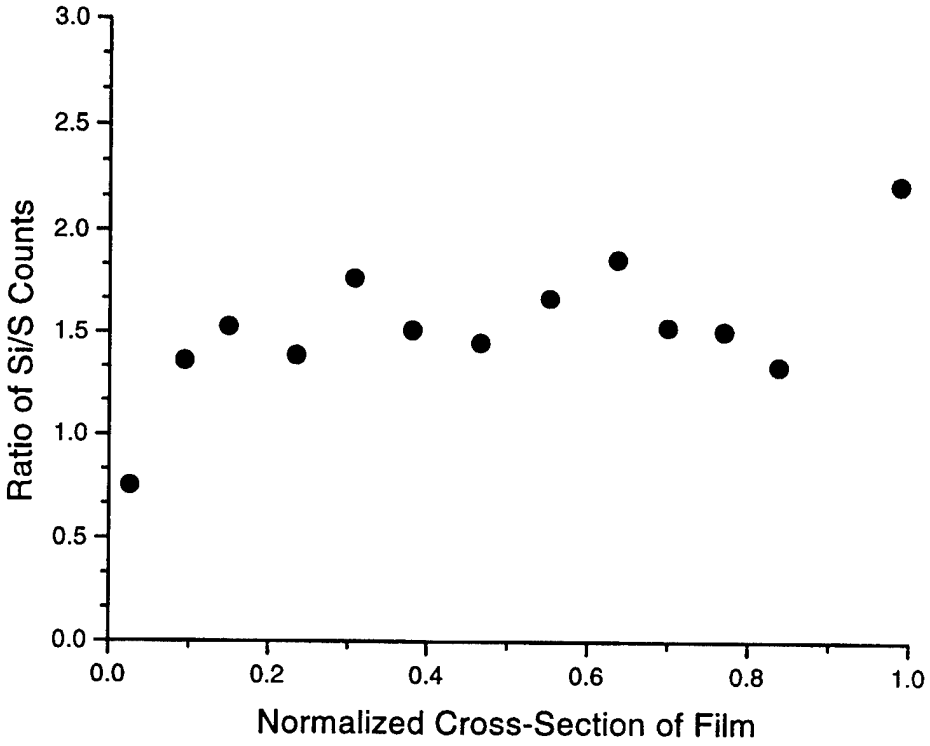

Block Copolymer Ionomer (*benzyltrimethylammonium* form)/[silicon oxide (6.5%)] hybrid

Pre-swollen in DMAc → soaked in TEOS for 1h

⇒ It is possible to grow a silicon oxide component within these polymers via *in situ* sol-gel chemistry.

TEM Showing Morphology of BCPI Hybrid

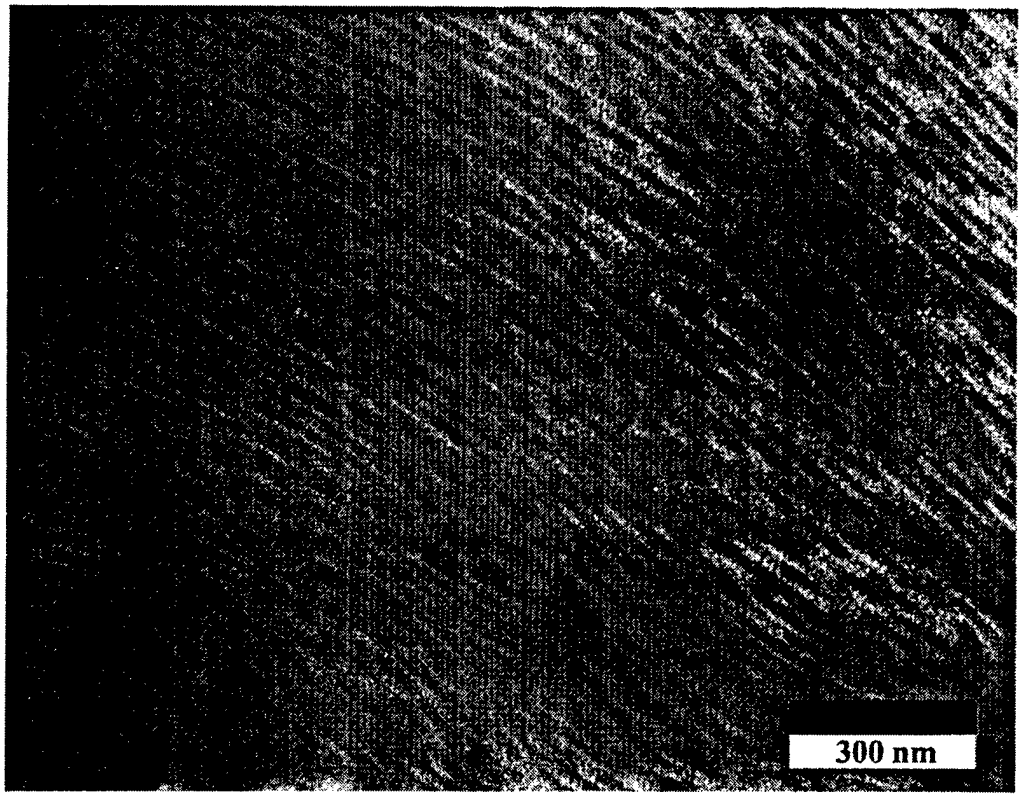

M_w=76,900; M_n=62,200; PDI = 1.24; 17.3 mole % styrene; 28.7 wt. % styrene;
15 mole % sulfonation of styrene blocks; BTMA neutralized; 8.5% Inorganic uptake.

[PS-PIB-PS *ionomer*]/SiO_2

cryo-microtomed/tapping mode (phase) image

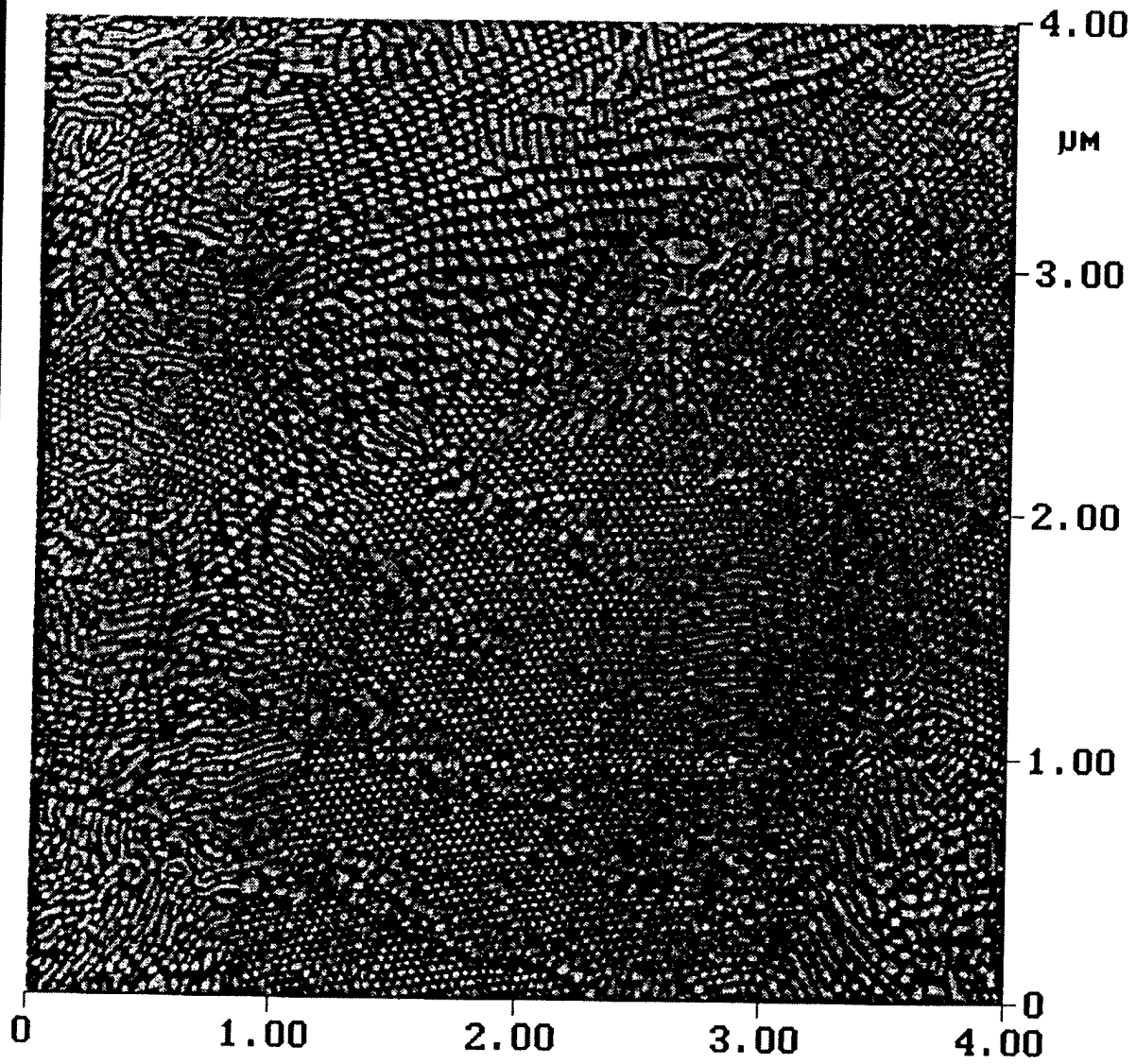

M_w = 76,900 / 18 mol% PS - sulfonated 16 mol% - benzyltrimethylammonium - exchanged sol-gel reaction using DMAc solvent - 6.5% SiO_2 uptake

RELATIONSHIP BETWEEN PROTON CONDUCTIVITY AND INFRARED CONTINUOUS ABSORPTION

"Easily Polarizable Hydrogen Bonds - Their Interactions with the Environment-IR Continuum and Anomalous Large Proton Conductivity"

The Hydrogen Bond, Recent Developments in Theory and Experiments, Vol. II. **1976**

P. Schuster, **G. Zundel** and C. Sandorfy, Eds.

Easily-polarizable H-bonds perturbed by:

- proton dispersion forces
- ions
- polarity of environment (reaction field)
- thermal rearrangements in environment

Consequence:

IR continuous absorption beginning at O-H stretch and extending to lower wavenumbers

Proton Transfer and "Structural Diffusion"

(*G. Zundel*)

Dynamic equilibrium between proton boundary structures:

(**I**) H_2OH^+---OH_2 $\leftrightarrow$ H_2O--- H^+OH_2 (**II**)

Rapid H^+ transfer within H_3O^+ to outer H atom in II:

$\underline{\mathbf{H}}^+OH_2 \rightarrow HOH\underline{\mathbf{H}}^+$

↓

Another H^+ transfer with 3rd H_2O molecule, etc.

↓

Thermal rearrangement redefines $H_5O_2^+$ groupings.

Proton Transfer within Hydration Structure of OH^--Containing Nafion® Membranes

Signature: Infrared Continuous Absorption

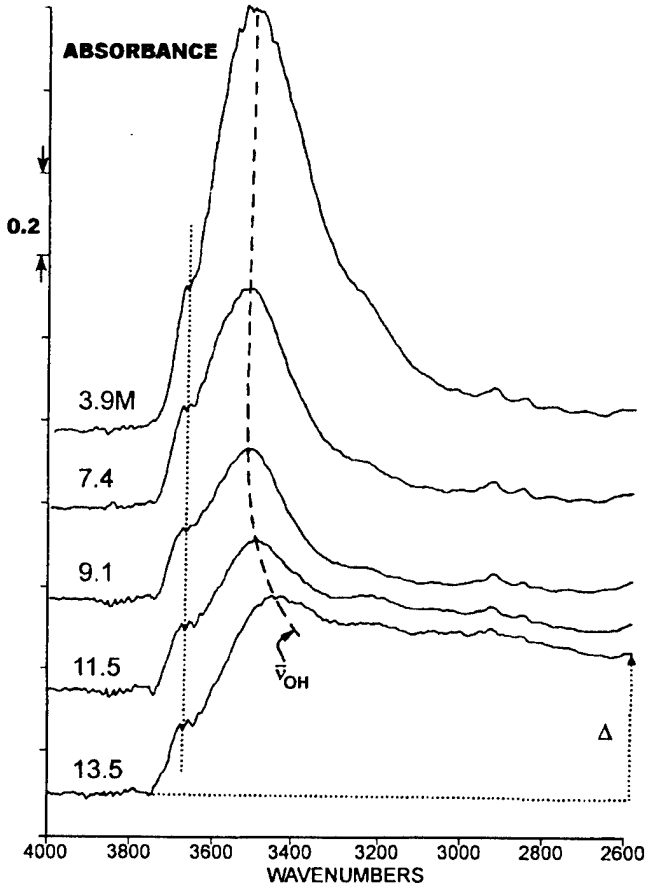

E (due to cation)

$$K^+ \; HO\underline{H} \; \text{---} \; OH^- \leftrightarrow HO^- \; \text{---} \; \underline{H}OH$$

K.A. Mauritz and C.L. Gray, *Macromolecules*, 16, 1279 (1983).

Financial Support

NSF-EPSCoR
NSF-EPRI
AFOSR
ARO-DOD-EPSCoR
ARO-DURIP
ICI
PRF-AC
E.I. DuPont Co.

Hydrocarbon PEMs Revisited

Gary E. Wnek
Department of Chemical Engineering, Virginia Commonwealth University, Richmond, Virginia 23284-3028

Joseph M. Serpico, Scott G. Ehrenberg, Timothy N. Tangredi and Eugene Zador
DAIS Corporation
2415-2 Destiny Way
Odessa, FL 33556
http://dais.net

Introduction

Ion-conducting polymers, or polymer electrolytes, are being utilized in an increasing base of applications which encompasses batteries,[1] fuel cells,[2] capacitors,[3] and electroluminescent devices.[4] We review here our collective efforts to design simple and inexpensive polymer electrolytes based on block polymers that have a wide array of useful characteristics, including excellent ion (especially proton) conduction, ion-exchange capability, modification of with redox-active ions for use as coatings for polymer-modified electrodes, and electromechanical responses in relatively small electric fields. Our work was initiated with the goal of developing low-cost proton conductors for use in hydrogen fuel cells which as an alternative to Nafion membranes. However, the rich array of morphologies and properties afforded by block copolymers[5] offered interesting opportunities for the design of materials exhibiting all of these characteristics.

Nafion is the most widely studied ionomer for use as a PEM due to its high conductivity and excellent chemical stability. The material consists on microdomains with phase segregation being driven by the chemical dissimilarity between the non-polar fluorinated backbone and the highly polar acid terminus of the side chains. It has been proposed that Nafion possesses an inverted micellar structure, with spherical (ca. 40-50 Å diameter) clusters lined with sulfonic acid groups, which are interconnected via ca., 10Å channels.[6-8] However, a recent re-evaluation of existing data has led to the proposal of lamellar domains that are locally planar.[9] The conductivity of H^+ form of Nafion when fully hydrated approaches 0.075 S/cm, making it an attractive material for a PEM.[10]

Our approach for a low-cost polymer electrolyte with comparable ion-conducting properties was to attempt to exploit inexpensive, hydrocarbon-based block polymers as a new class of PEMs which would have interconnected domains of sulfonated polymer chains, affording a high conductivity and good mechanical integrity derived from the remaining block(s). We elected to heavily[11] sulfonate selected commercially available styrene/ethylene-butylene/styrene (SEBS) triblock polymers (Kratons G1650 and G1652 from Shell), as these contain a saturated carbon center block which should be inert to the sulfonation reaction.[12,13] The general structure of the sulfonated polymer, manufactured by the Dais Corp., is shown in

Figure 1, which we will simply refer to as sulfonated, or S-, SEBS. Transmission electron microscopy of cast films of the sulfonated polymer (ca. 60 mole% of the styrene units sulfonated, stained with RuO_4) reveals distinct, phase-separated structures which indicate a lamellar structure with thicknesses of approximately 250Å. Much of the work reviewed here has focused on S-SEBS with sulfonation levels of 50-60% of the total styrene units.

Proton Exchange Membranes and Fuel Cells

The proton conductivity of S-SEBS, measured using a.c. impedance techniques on fully hydrated samples, reveals an expected sulfonation-dependent conductivity,[12] which approaches 0.08 S/cm at sulfonation levels of ca. 60%. This high conductivity renders S-SEBS a desirable material for use as a proton exchange membrane, and hydrogen fuel cells have been successfully constructed using such membranes.[14] The hydrocarbon nature of these materials necessitated the parallel development of electrodes with requisite catalytic activity and good interfacial bonding to the membranes.[15] Single fuel cells derived from these electrode/membrane assemblies can exhibit a current density of about 400 mA/cm^2 at 0.5V (ca. 200 mW/cm^2) using air at atmospheric pressure without humidification.[14]

Electrochemistry of Immobilized Species

Ion-exchange polymers such as Nafion have been extensively studied as electrode coatings for the design of chemically-modified electrodes.[16] We have found that S-SEBS can serve as an ion-exchange membrane and that it can be employed in a similar capacity as an electrode coating. For example, cationic, redox-active molecules such as trimethylammoniummethyl ferrocene, methyl viologen and ruthenium tris(bipyridyl) are readily exchanged for sodium ions in neutralized S-SEBS films, and the electrochemistry of these immobilized species has been studied in some detail.[17,18] The S-SEBS films appear to be good blockers of polyanionic species such as $Fe(CN)_6^{4-}$, which might be important in biosensor applications. The ability to control the block lengths and extent of sulfonation in our materials can dictate the morphology of the electrode coating, which may effect ion transport, electron exchange kinetics, and binding constants of electroactive species. We therefore have a unique opportunity to explore the effect of supermolecular structure of the redox molecule-loaded polymer films on these basic issues which are of great importance in applied electrochemistry.

Electromechanical Response

Many hydrogels immersed in an electrolyte solution deform in the presence of an electric field, and therefore they are capable of transducing an electrical stimulus, sometimes via a concomitant chemical change (e.g., pH), into mechanical energy.[19] We found that S-SEBS bends rather rapidly (ca. 2-3 sec) toward the cathode when immersed in aqueous salt solutions such as Na_2SO_4 and that the bending tracks field reversal for many cycles. Typical field strengths are in the range of 8-10 V/cm. The maximum extent and kinetics of bending are dependent upon the Na_2SO_4 concentration, field strength, and degree of sulfonation of

the polymer.[20,21] S-SEBS is to our knowledge the first example of a multiphase block copolymer with electromechanical activity, and further work will seek to establish relationships between electromechanical response and microphase morphology, block length and block composition. Possible applications of such materials include actuators, 'artificial muscles,' and electric field-stimulated drug delivery.

Conclusions

S-SEBS at sulfonation levels of 50-60% is a versatile ion-conducting, ion-exchange hydrogel with several potential applications. Studies are underway to further understand the morphology and properties of this interesting class of materials. Also, additional applications continue to be explored, including the use of S-SEBS as a matrix for dye immobilization for the quantitative analysis of metal ions.[22]

Acknowledgments

We are grateful to the Wright-Malta Co. and the New York State Energy Research and Development Authority for support of much of this work. We thank the Office of Naval Research for partial support for electromechanical studies, and Louis Raboin of UMass Amherst for the TEM of Figure 2.

References

1. F. M. Gray, Solid Polymer Electrolytes: Fundamentals and Technological Applications, VCH Publishers, Inc., New York (1991).
2. J. Leslie, *Wired*, p. 138, October 1997.
3. X. Liu and T. Osaka, *J. Electrochem. Soc.*, 3066 (1997).
4. Q. Pei, G. Yu, C. Zhang, Y. Yang, A.J. Heeger, *Science*, **269**, 1086 (1995).
5. F. S. Bates and G. H. Fredrickson, *Ann. Rev. Phys. Chem.*, **41**, 525 (1990).
6. T. D. Gierke and W. Y. Hsu, in Perfluorinated Ionomer Membranes, A. Eisenberg and H. L. Yeager, eds, Ch. 13, ACS Symposium Series 180, American Chemical Society, Washington, DC (1982).
7. E. J. Roche, M. Pineri, R. Duplessix and A. M. Levelut, *J. Polym. Sci. Polym. Phys. Ed.*, **19**, 1687 (1981).
8. T. D. Gierke, G. E. Munn, and F. C. Wilson, *J. Polym. Sci. Polym. Phys. Ed.*, **19**, 1 (1981).
9. M. H. Litt, *Polym. Prepr.*, **38**(1), 80 (1997).
10. T. A. Zawodzinski, M. Neeman, L. O. Sillerud, L. O and S. Gottesfeld, *J. Phys. Chem.*, **95**, 6040 (1991).
11. Lightly sulfonated SEBS has been studied in some detail, especially with respect to mechanical properties. See: A. Weiss, A. Sen, L. A. Pottick and C. L. Willis, *Polymer*, **32**, 2785 (1991).
    R. A. Weiss, A. Sen, L. A. Pottick and C. L. Willis, *Polym. Commun.*, **31**, 220 (1990).
12. G. E. Wnek, J. N. Rider, J. M. Serpico, A. G. Einset, S. G. Ehrenberg and L. Raboin, *Proc. First Intl. Symposium on Proton Conducting Membrane Fuel Cells*, Electrochem. Soc. Proc. Vol. 95-23, 247 (1995).

13. S. G. Ehrenberg, J. M. Serpico, G. E. Wnek and J. N. Rider, U.S. Patent 5, 468, 574 (1995).
14. S. G. Ehrenberg, J. M. Serpico, B. M. Sheikh-Ali, T. N. Tangredi,
15. E. Zador and G. E. Wnek, *Proc. Second Intl. Symp. on New Materials for Fuel Cell and Modern Battery Systems*, Montreal, July 1997, in press.
16. J. M. Serpico, S. G. Ehrenberg, G. E. Wnek and T. N. Tangredi, U. S. Patent 5, 677, 074 (1997).
17. R. W. Murray, in Molecular Design of Electrode Surfaces, R. W. Murray, ed., John Wiley & Sons, NY (1992), 1.
18. C. Karuppaiah, J. N. Rider and G. E. Wnek, *Polym. Prepr.*, **37** (1), 428 (1996).
19. C. Karuppaiah, G. E. Wnek, N. Tunoglu and T. A Zawodzinski, in preparation.
20. See, for example, T. Kurauchi, T. Shiga, Y. Hirose, and A. Okada, in D. DeRossi, K. Kajiwara, Y. Osada, and A. Yamauchi, eds. Polymer Gels. Fundamentals and Biomedical Applications, Plenum (1991).
21. Y. Ye, J. N. Rider, A. Sekhar, G. Wong, K. Trout, K. Graczyk, W. Brown, J. Gross, M. Stewart, M. Kamler and G. E. Wnek, *Polym. Prepr.*, **37** (1), 394 (1996).
22. Y. Ye and G. E. Wnek, in preparation.
23. N. Tunoglu, P. Cagler and G. E. Wnek, *J. Macromol. Sci., Pure Appl. Chem.*, **A35**(4), 637 (1998).

FIGURE 1: Structure of S-SEBS

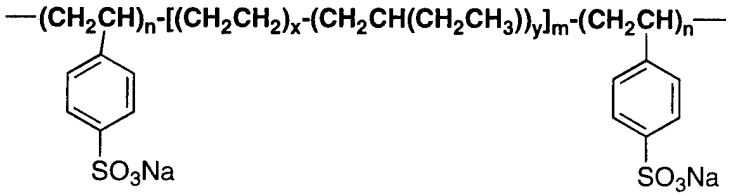

Hydrocarbon-Based PEMs Revisited

Gary E. Wnek
Department of Chemical Engineering
Virginia Commonwealth University
Richmond, Virginia 23284
gewnek@saturn.vcu.edu

Joseph M. Serpico, Scott G. Ehrenberg,
Timothy N. Tangredi, Eugene Zador
Dais Corporation
2415-2 Destiny Way
Odessa, FL 33556
http://dais.net

Electrochemical Devices

'Anode-Electrolyte-Cathode' Sandwich

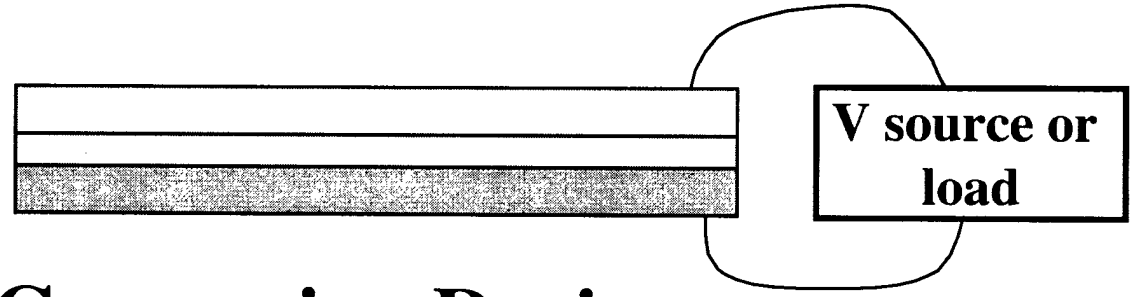

Energy-Consuming Devices:

electrolyzers, LEDs, electrochromics

Energy-Producing Devices:

batteries, fuel cells, electrolytic capacitors

Early PEM Materials from NASA Gemini Missions

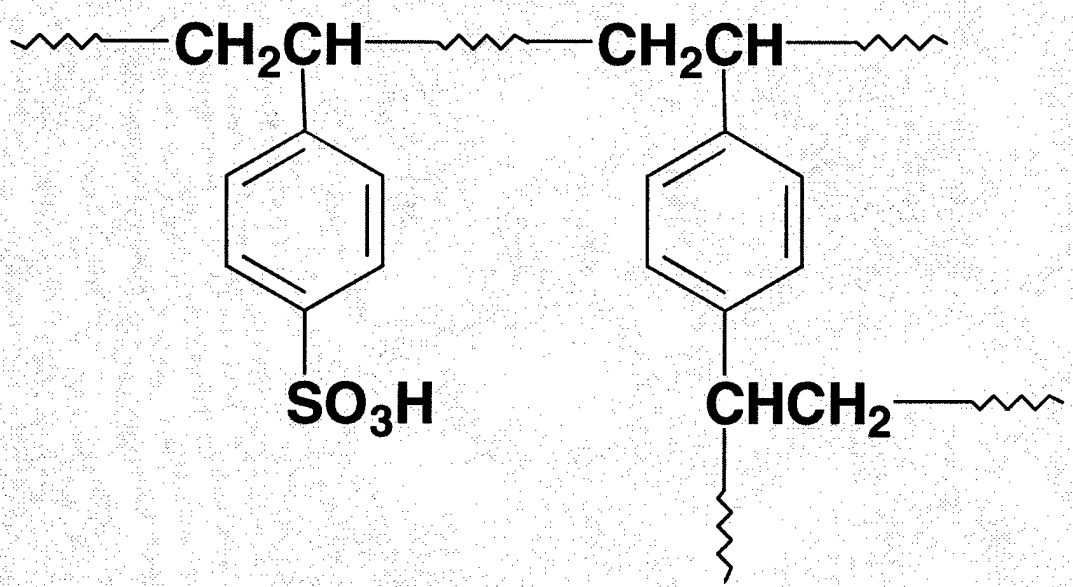

Sulfonated Styrene/DVB (+ inert support)

Nafion

Dais PEM Requirements

- Cheap
- Cheap
- Cheap
- Cheap
- Cheap
- Excellent Proton Conductivity
- Good Mechanical Properties
- Low Gas Transport Rate

Some Possible Degradation Pathways for Hydrocarbon PEMs

At cathode:

$$O_2 + e^- \rightarrow O_2^{-}\cdot$$
$$O_2^{-}\cdot + H^+ \rightarrow HOO\cdot$$
$$HOO\cdot + e^- \rightarrow HOO^-$$
$$HOO^- + H^+ \rightarrow HOOH$$
$$HOOH + 2e^- + 2H^+ \rightarrow 2H_2O$$

At anode:

$$O_2 + \text{"Pt-H"} \rightarrow Pt + HOO\cdot$$
$$HOO\cdot + R\text{-}H \rightarrow HOOH + R\cdot$$
$$R\cdot + O_2 \rightarrow ROO\cdot$$
$$ROO\cdot + RH \rightarrow ROOH$$
$$ROOH + M^{2+} \rightarrow RO\cdot + OH^- + M^{3+}$$

(M^{2+} or M^{3+} = transition metal ion such as Fe^{2+} or Fe^{3+})

$$RO\cdot + RH \rightarrow ROH + R\cdot$$
$$HOOH + M^{2+} \rightarrow HO\cdot + OH^- + M^{3+}$$
$$HO\cdot + RH \rightarrow H_2O + R\cdot$$
$$RO\cdot \rightarrow \text{chain cleavage}$$

Here R-H =

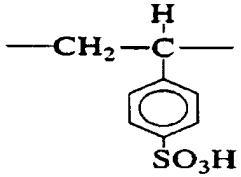

Block Copolymers: Examples of Self-Assembling Systems

Some types of block copolymers:

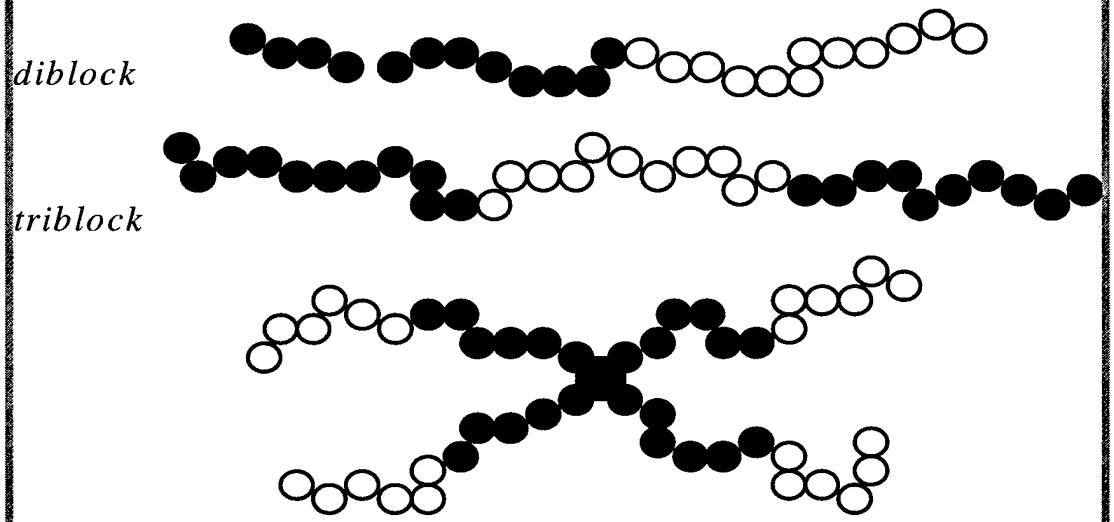

Gross phase separation is precluded since chains are connected, but microphase separation will occur

Possible morphologies depend upon relative block lengths, and include spheres and cylinders in a continuous phase, and lamellae

Examples of Block Polymer Morphologies

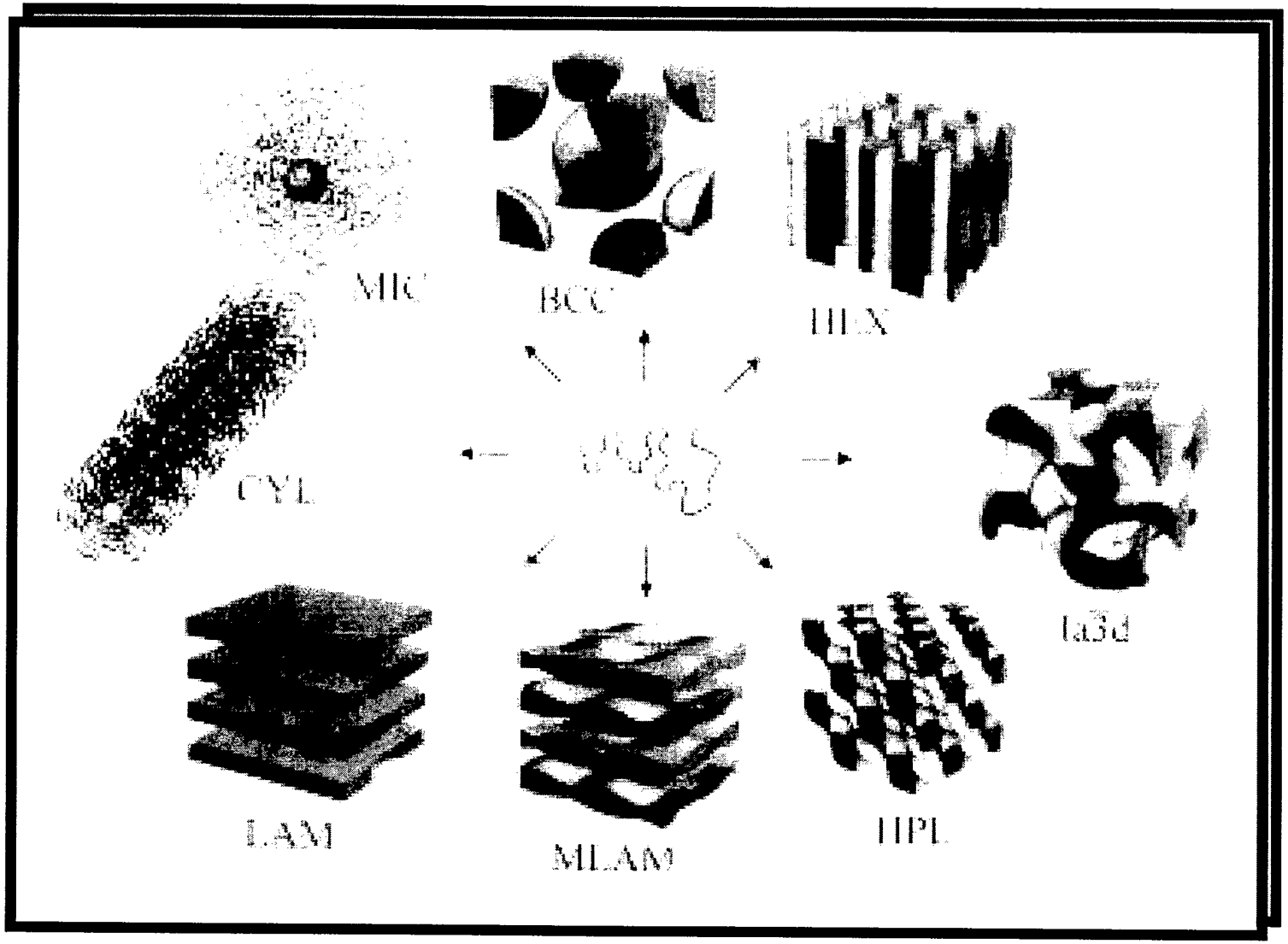

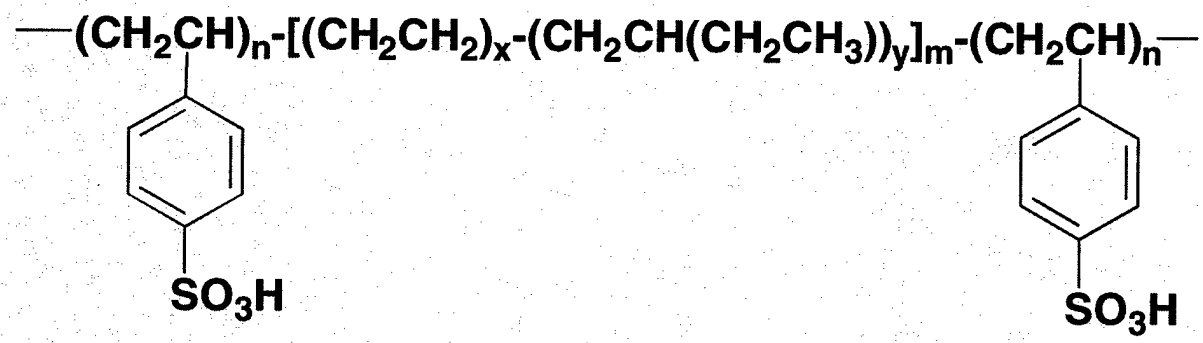

Sulfonated Styrene-Ethylene/Butylene-Styrene Triblock Polymer

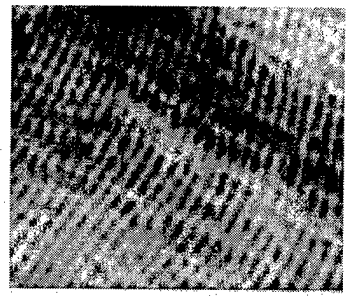

Transmission electron micrograph of triblock shown above, 29 mol% styrene with 55% sulfonation of styrene blocks. Sample was microtomed at –100°C and stained with RuO_4. Thicknesses of lamellae are ca. 25-30 nm

Conductivities of Sulfonated Block Polymers as a Function of Sulfonation Level

Percentage Sulfonation[a]	mmol/g[b]	Conductivity[c] (S/cm)
35	0.96	0.068
43	1.16	0.075
50	1.33	0.080
65	1.72	0.089

[a]Mole % based on styrene units, determined by titration. Data are averages of triplicate determinations.
[b]Millimol sulfonic acid per gram of total polymer
[c]Immersed in water, room temperature.

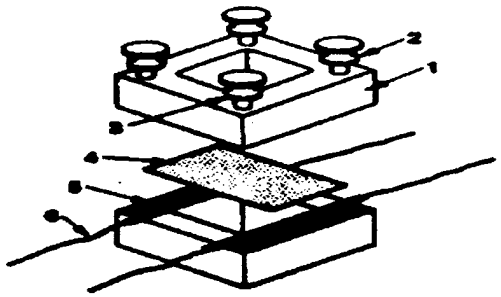

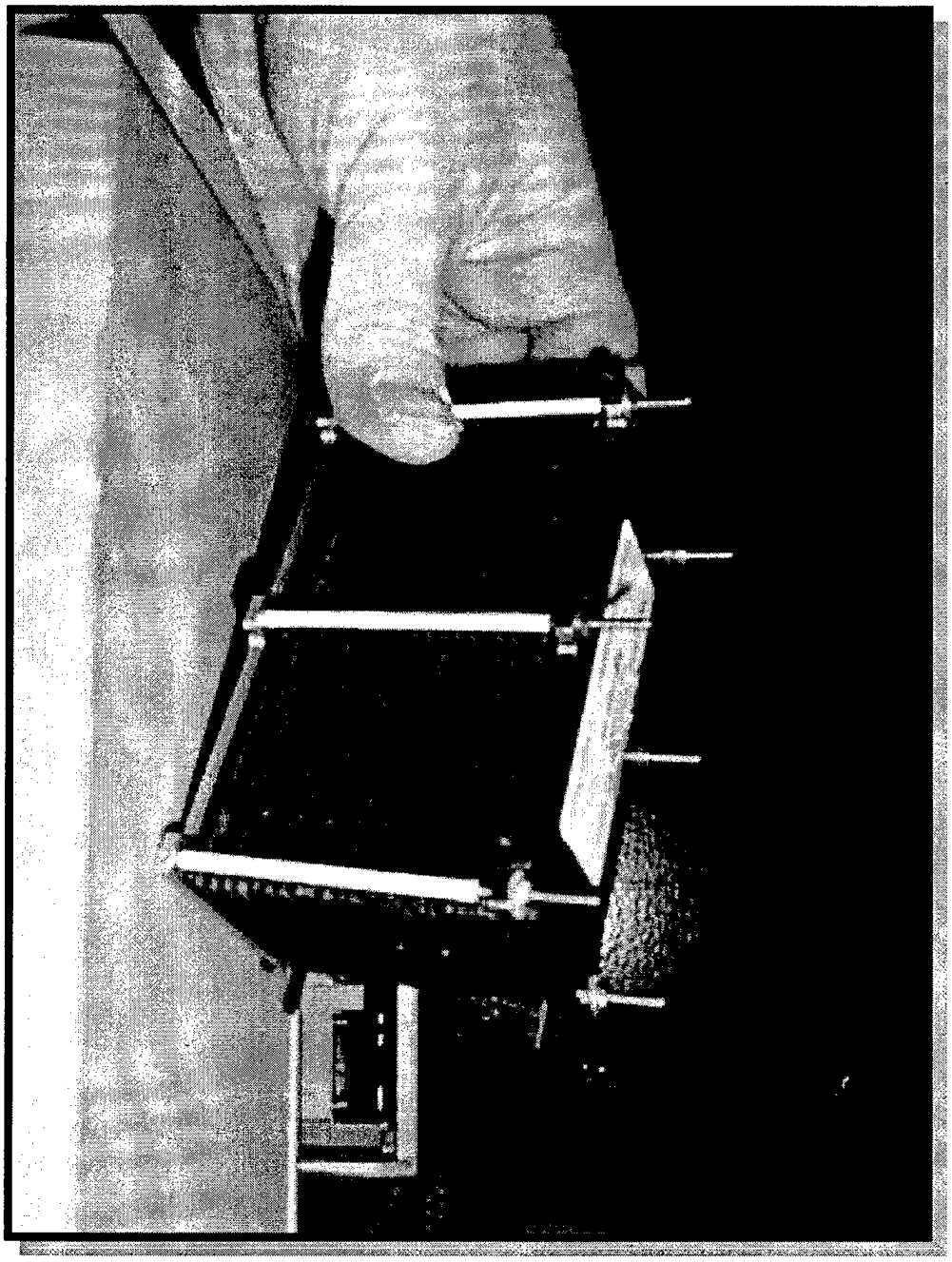

Other Interesting Characteristics of the Sulfonated Triblock Polymer Membrane

- Cation exchanger
- Electrochemistry from immobilized, redox-active cations (chemically modified electrodes)
- Electromechanical response (deflection of films towards cathode)
- Good biocompatibility

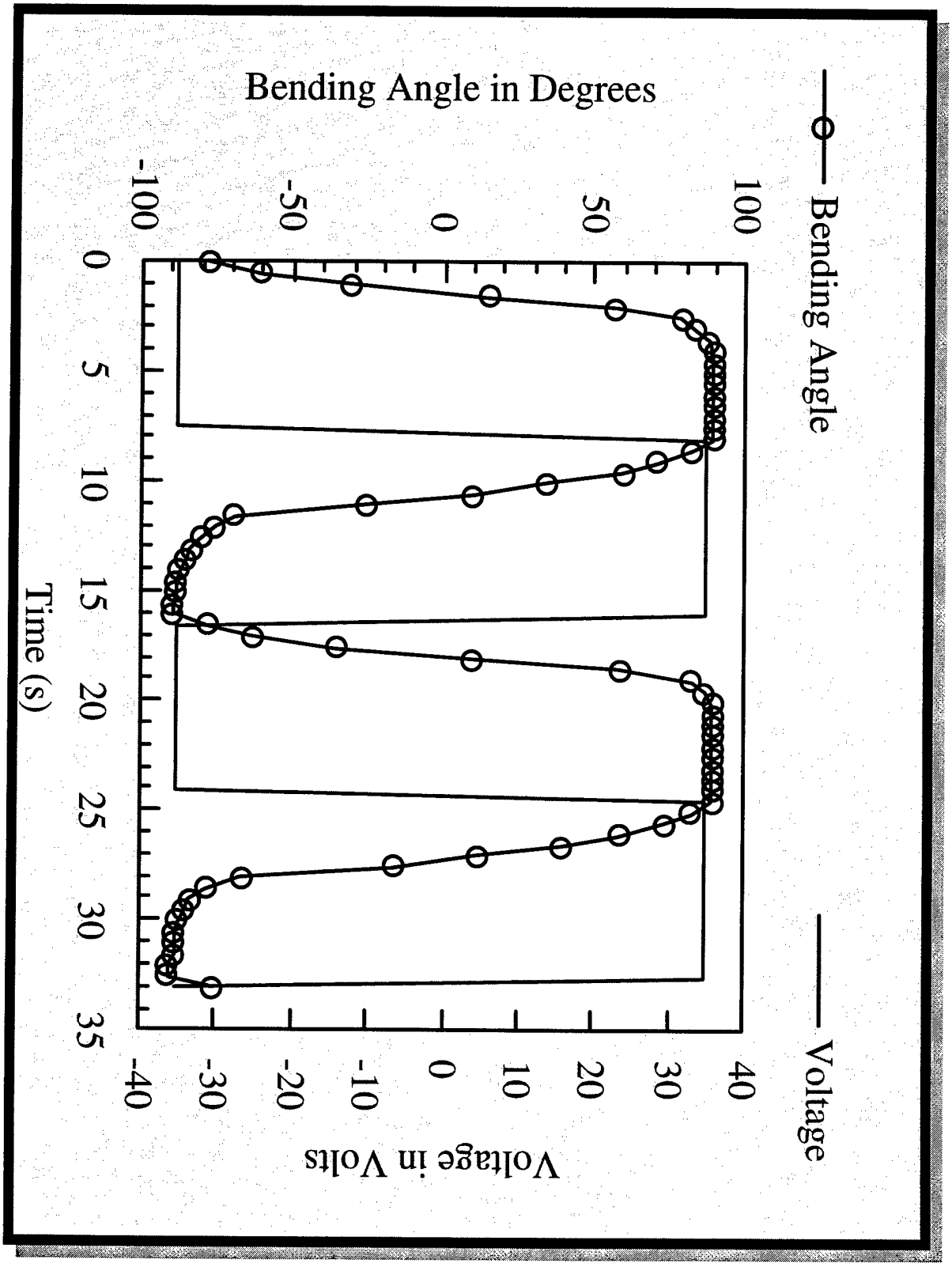
Bending Angle in Degrees
Bending Angle
Voltage
Voltage in Volts
Time (s)
-100
-50
0
50
100
-40
-30
-20
-10
0
10
20
30
40
0
5
10
15
20
25
30
35

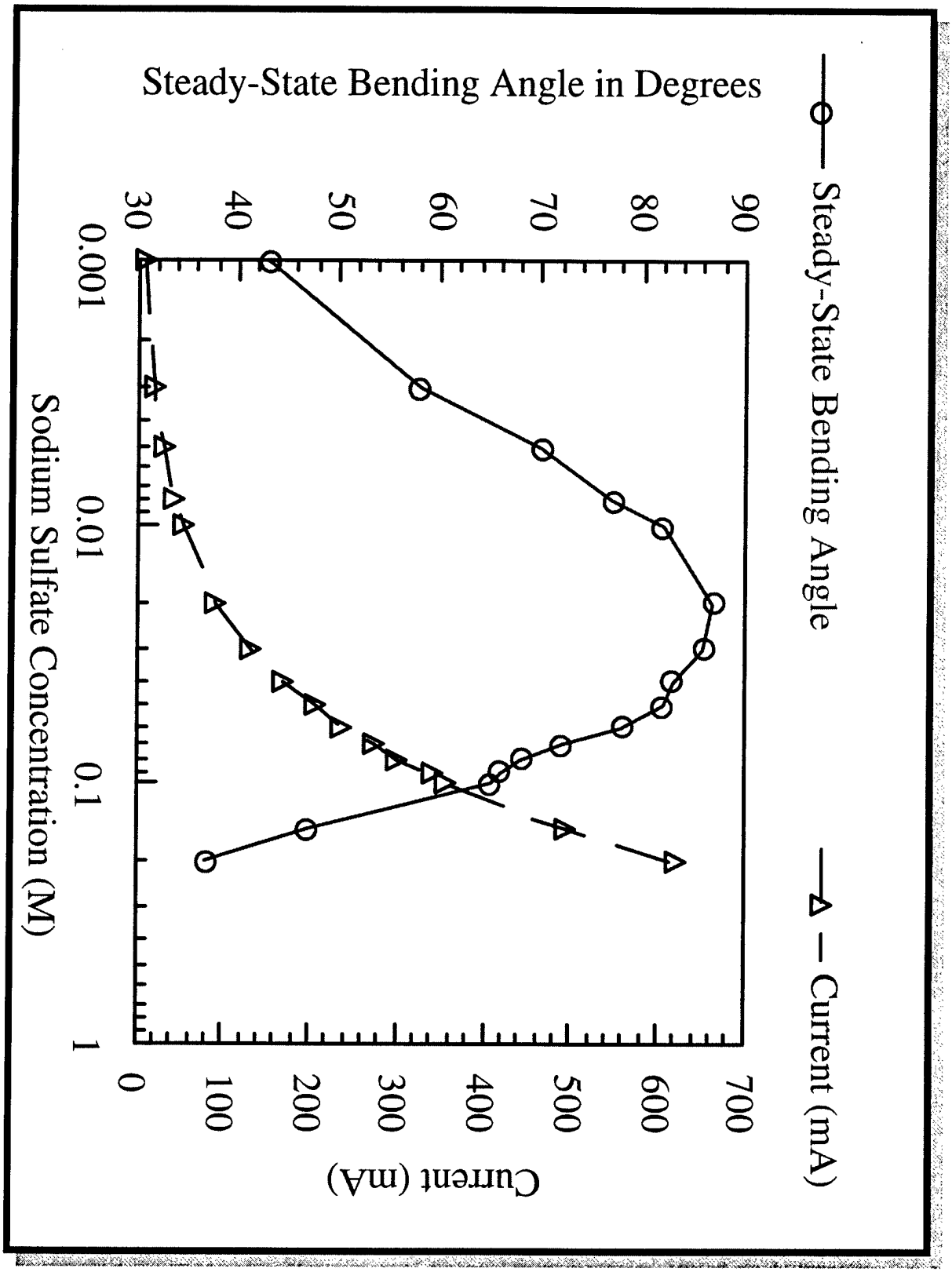
Steady-State Bending Angle in Degrees
Steady-State Bending Angle
Current (mA)
Sodium Sulfate Concentration (M)
Current (mA)
30
40
50
60
70
80
90
0
100
200
300
400
500
600
700
0.001
0.01
0.1
1

New Class of PEM: Sulfonated, Hydrogenated SBR (S-HSBR)

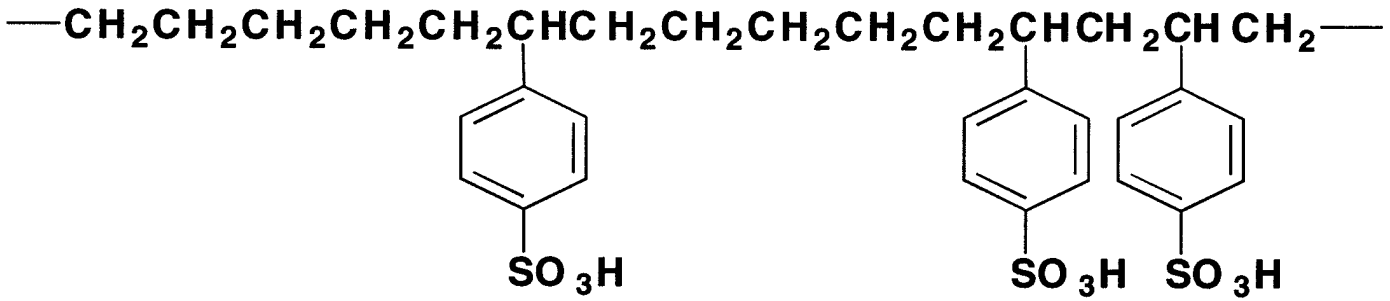

Sulfonated, Hydrogenated SBR Random Copolymer

S-HSBR compared with S-SEBS:

Better mechanical properties

Better high-temperature stability

Equivalent conductivity (?)

Acknowledgments

- Wright-Malta Company
- New York State Energy Research and Development Authority

Thanks to Tom Zawodzinski of LANL for many helpful discussions

SULFONATED POLYIMIDES AS NOVEL PROTON EXCHANGE MEMBRANES FOR H_2/O_2 FUEL CELLS

Michel PINERI
Département d'Etude des Matériaux, SCPM, CEA/Grenoble, 17, rue des Martyrs
38054 GRENOBLE cedex 9, France

Solid polymer H_2/O_2 fuel cells are considered as a promising technology for the production of electricity.[i,ii] Powerful and long lifetime fuel cells are now developped using perfluorinated ionomer (PFI) membranes as solid polymer electrolyte.[iii] However, in spite of outstanding properties such as high proton conductivity and high chemical inerty, these PFI membranes are costly to manufacture as thin films ($\approx$600\$/m^2) which is a major drawback for the development of such technology for the electric vehicle application, where around 10 square meters of membranes are necessary. The main requirements for a membrane to be used in solid polymer electrolyte fuel cells are : i) an ionic conductivity larger than 10^{-1} S/cm at 80°C, ii) good mechanical properties and a low permeability for oxygen and hydrogen in order to be able to use thin membranes, iii) an excellent chemical resistance which allows a lifetime larger than 3000 hours in the fuel cell operating conditions, iv) a cost in agreement with the commercial requirements for the fuel cell market. Over the last few years, several approaches to develop new proton conducting and low cost membranes for fuel cells have emerged. For example, Ballard Corp., which is very active in the field, has proposed a new less expensive polymer named BAM3G [iv]. The synthesis of proton exchange membranes via the sulfonation of polymers such as the poly(ethersulfone) [v] or the poly(arylether ketones) [vi] has been also investigated. Most of the protonated polymers investigated in order to prepare low cost membranes to replace the PFI membranes exhibit a lifetime which does not exceed 1500 hours in fuel cell operating conditions as observed for membranes prepared by radiation grafting and sulfonation.[vii] Since the polymers presenting aliphatic chains seems to be sensible to oxidation, we expected that polyaromatic polymers could be a good compromise to obtain low cost membranes presenting the required lifetime. The polyimide polymers are known for their good thermal and chemical stability and appears as a good candidate for proton exchange membranes when sulfonated. In this paper, we present first results about the synthesis, the structural characterization and the fuel cell tests of these novel membranes in comparison with the classical PFI membranes. The molecular structure of polyimides are represented in table I.

Acronym	Structure
phthalic SPI BDSA/OPDA/ODA	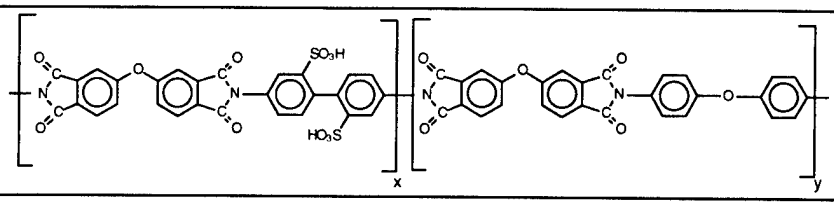
naphthalenic SPI BDSA/DNTA/ODA	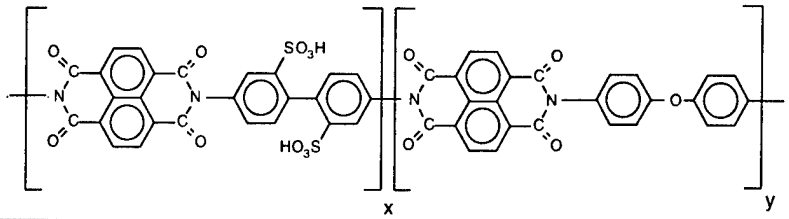

TABLE I - STRUCTURAL VARIATIONS IN SULFONATED POLYIMIDES

Sulfonated polyimide synthesis.

Numerous experiments were run to determine the proper reaction conditions, including reagent concentration, addition sequence, solvents and temperature. For both phthalic and naphthalenic polyimides, the synthesis in one-pot/two-stage procedure in phenolic solvents was found to be the most effective for producing imidized materials. First the sulfonated sequence was prepared by offsetting the monomer stochiometry BdSA/OPDA or BdSA/DNTA in favor of BdSA monomer. In a second stage, ODA and OPDA or DNTA monomers were added to extent the polymer chain. The molar ratio of BdSA over ODA for each polymer was fixed at 30/70.

The copolyimide BdSA/ODA/OPDA soluble in DMSO d_6 was structurally characterized by ^{1}H and ^{13}C NMR. The spectra were consistent with the expected structure. For the naphthalenic polyimide, the structure was confirmed by FTIR. Although we are not able to correctly determine the molecular weight of these polymers, the question of whether high molecular weight polymers were prepared was answered by several observations. All these polymers were highly fibrous materials. Films could be produced by casting solution which are tough and finger-nail creasable indicative of substantial molecular weight.

Physical characterization.

The **water uptake** of membranes is usually defined in weight percent with respect to the weight of the dry membrane. The water uptake at 25°C for the phthalic and naphthalenic SPI membranes are 26% and 30%, respectively. The water uptake observed for PFI in the same conditions is 20%. The water uptake obtained for the different membranes can not be compared due to the large value of the perfluorinated matrix density (2.1g/cm^3), and should be replaced by the water uptake by volume.

Since the polymer density is not known precisely for the SPI ionomers, the solvent uptakes have been expressed as the number of water molecules per ionic group, λ. The λ values for the phthalic and naphthalenic SPI and PFI membranes are 12.5, 13.2, and 12, respectively. These values appear to be similar and allow to consider the PFI membranes as a good reference for the conduction properties. However, the effect of temperature is strongly different between SPI and PFI membranes. For PFI membranes, the solvent uptake increases exponentially with the temperature,[viii] while the solvent uptake is almost constant varying the temperature for SPI membrane .

The **hydrogen gas permeation** experiments performed on dry films showed that these polyimides are less permeable than Nafion membranes by a factor of 3.[ix] Nevertheless, the permeation experiments should be performed on swollen membranes since it is well known that the gas permeation is considerably larger in the ionic domains compared to that in the polymer matrix.

The **ion-exchange capacity** was determined by the usual titration method. For the phthalic SPI membrane which is soluble in DMSO-d_6, the ion-exchange capacity was also determined by the analysis of the NMR lines areas for both ^{1}H and ^{13}C atoms. All determinations are in good agreement with the theoretical values 1.16meq/g and 1.26meq/g for the phthalic or naphthalenic SPI, respectively.

A preliminary small-angle neutron scattering (SANS) study of the membranes was performed in order to evidence the **phase separation** between the ionic domains and the polymer matrix. The first observation is that the spectra obtained for the PFI and phthalic SPI membranes present a well defined scattering maximum, called ionomer peak, which indicates the presence of ionic domains. The intensity of the ionomer peak is larger by a factor of 100 and is located at a q value lower by a factor of 10 for the phthalic SPI compared to the PFI membrane indicating that the ionic domain are roughly ten times larger. This result is confirmed by the analysis of the intensity scattered at large q values which is related to the dimension of the scattering particles through their surface over volume ratio. These results can be understood as an effect of the block character of the SPI polymers. The ionic groups are gathered in blocks along the polymer chain and the ionic blocks are separated by long hydrophobic sequences which allow to form large ionic domains which is not oberved in statistical polymers such as PFI membranes.

The SANS spectrum obtained for the naphthalenic SPI membrane presents a high level of scattered intensity at low q values indicating also the existence of large ionic domains embedded in the polymer matrix but the fact that no ionomer peak can be observed shows that the distribution (or the shape) of the ionic domains strongly differs compared to the phthalic SPI membranes. The effect is due to the rigidity of the polymer chain which is considerably larger for the naphthalenic SPI polymer compared to the phthalic one and not due to the number of atoms in the heterocycle but to the absence of ether bridge in the naphthalenic dianhydride monomer.

Fuel cell experiments.

At the beginning of each fuel cell test, the performances of the fuel cell increased up to a plateau. The polarization curves were recorded when the steady state condition were achieved (≈24h). The polarization curves are presented on Figure 1 for the two SPI membranes studied in this work along with the PFI membrane one as reference. In these experiments, the thickness of the membranes was identical in order to compare the cell performances. The three curves present the typical behavior obtained in fuel cells. The first part, at current densities lower than 0.05 A/cm^2, the drop in potential is usually attributed to the electrode kinetics of catalysis. The fact that the results are different for the three membranes is surprising because the electrodes are identical. The second part is almost linear and is due to ohmic losses in the system and mainly in the membrane electrode assembly. For the PFI membrane, the ohmic losses observed are significantly larger than the one usually observed with such membranes and can be connected to the fact that the electrodes are not hot pressed. The performances obtained for the naphthalenic SPI membrane are very close to those obtained with the PFI membrane. This result can be consider as encouraging since the electrodes were not optimized for such membrane. The third part of the curve is associated with the gas diffusion through the activation layers and was expected to be identical for the three membranes since the same electrodes are used. For the PFI membrane, a partial dehydration of the PFI membrane at high current densities due to electroosmosis can induce a dehydration of the impregnation layer which become less permeable to gases while, for the SPI membrane, the swelling of the activation layer made of PFI material can remain if the swelling of the PFI layer is favored at the expense of the SPI membrane.

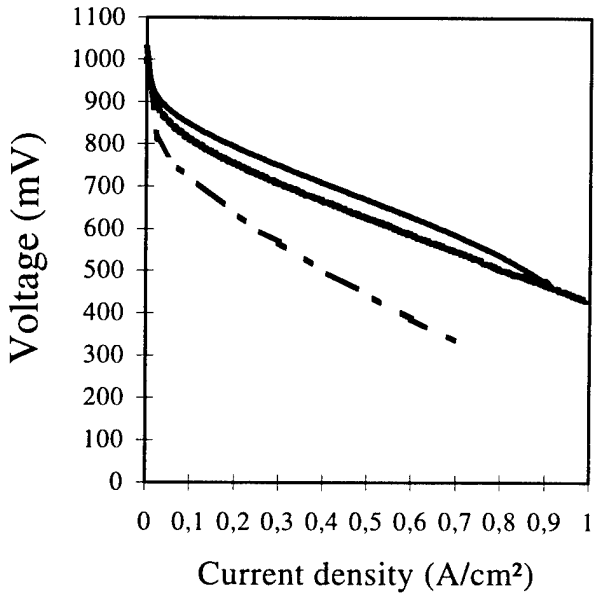

Fig.1 - POLARIZATION CURVES RECORDED AT 70°C AND P(H_2) = P(O_2) =4 BAR FOR THE PHTHALIC (— - —) AND NAPHTHALENIC (-----) SPI MEMBRANES AND THE PFI MEMBRANE AS REFERENCE (——)

Lifetime experiments were performed with the phtalic polyimide and PFI membranes presenting the same thickness (175 µm) while a 70µm naphthalenic SPI membrane was used. The tests were performed at 60°C, at a 3 bar pressure for H_2 and O_2 and under a constant current density of **250 mA/cm²**. Different stability behaviors were observed as illustrated in the figure 2.

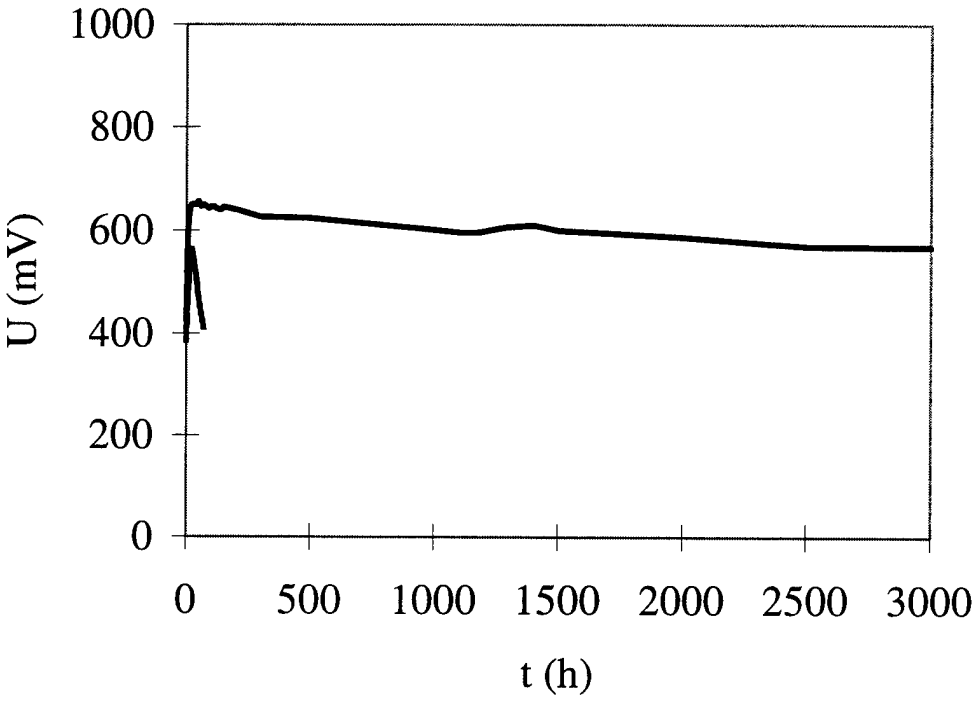

Fig.2 - LONG TIME EXPERIMENTS IN FUEL CELLS CONDITIONS $P(H_2)=P(O_2)=3$ BAR, T=60°C, I=250 MA/CM^2 FOR THE PHTHALIC (DASHED LINE) AND NAPHTHALENIC (SOLID LINE) SPI

The phthalic structure quickly degrade and become brittle in a few days. Generally the membrane breaks after 70 hours leading to a local combustion of the membrane. On the other hand, naphthalenic polyimides are stable and life time larger than 3000 hours were obtained. The decrease of the fuel cell performances can be attributed either to a incipient degradation of the membrane structure as observed for the phthalic structure and which could be kinetically delayed or to a partial dehydration of the membrane due to a problem of water management.

One speculative explanation to account for the degradation of the phthalic SPI membrane is the hydrolysis of the imide ring of the sulfonated imide sequence leading to chain scissions. Such decrease of the molecular weight could explain the loss of the mechanical properties, and consistently the brittleness of the membrane. This phenomenon was not observed for naphthalenic SPI membranes confirming that the

stability of the naphthalenic polyimides is better than phthalic polyimides, as reported by A. Rusanov[x].

The structure and the conduction properties of proton exchange membranes and especially PFI membranes have been the object of numerous studies over the last decades due to the increasing industrial interest in electrochemical applications.[ii,xi,xii] There is no theoretical approach to describe the structure-properties relationships in these systems, and consequently to define the best polymer for a given application. The ionomer membranes are characterized by a microphase separation between the ionic domains and the polymer matrix. The hydrophobic polymer matrix sustains the mechanical properties while the presence of percolated swollen ionic domains allows an ionic conduction close to one encountered in ionic solutions.[xiii] The SPI polymers represent a class of ionomer and allow to vary continuously the block character, the ionic content and the flexibility of the polymer chain. The study of the effect of the structural modification on the conduction properties is now under progress.

CONCLUSION

Polymers based on sulfonated polyimides have been studied. These polymers were synthesized by a one step method in solution with non expensive commercially available monomers. For a structural point of view, these polymers are shown to be good candidates as model compounds in order to understand the structure-properties relationships in ionomer membranes. The dimension and the distribution of the ionic domains can be managed modifying the blockiness nature and the rigidity of the polymer chain as indicated by preliminary SANS experiments.

For an application point of view as proton exchange membrane for fuel cells (PEMFC), the naphthalenic SPIs are promising materials for PEMFC according to their mechanical and chemical stability in fuel cell experiments. These novel ion-exchange membranes could be also interesting materials in lot of electrochemical applications.

This presentation corresponds to an extended abstract of a paper presented at the second international symposium on new materials for fuel cell and modern batteries systems (Montreal, July 6-10, 1997).

---

[i] Proceedings of the *first international symposium on new materials for fuel cell systems*, Montreal, Quebec, Canada, July 9-13, (1995)

[ii] *Ionomers : Characterization, theory and Applications*, Schlick, S. (Ed), CRC Press, Boca Raton, Florida, (1996)

[iii] H.P. Dhar, *J.Electroanal.Chem*, **357** (1993) 237

[iv] A.E.Steck; Proceedings of the *first international symposium on new materials for fuel cell* systems, Montreal, Quebec, Canada, July 9-13, (1995) 74

[v] R.Nolte; K.Ledjeff; M.Bauer and R.Mulhaupt, J.Power Sources, **83** (1994) 211

[vi] F.Helmer-Metzman; F.Osan; A.Schneller; H.Ritter; K.Ledjeff; R.Nolte and R.Thorwirth; European patent; 574 791 (1993)

[vii] F. Buchi, B. Gupta, O. Haas, G.G. and Scherer, *Electrochimica Acta*, **40**, (1995) 345

[viii] G.Gebel, P.Aldebert, M.Pineri, *Polymer* **34** (1993) 333

[ix] S.Faure, PhD thesis, Grenoble (1996)
[x] A. L.Rusanov, *Adv.Polym.Sci.* **111** (1994) 116
[xi] *Perfluorinated Ionomer Membranes*, A. Eisenberg and H.L. Yeager Eds. ACS Symp. Series 180, American Chemical Society, Washington (1982)
[xii] C.Heitner-Wirguin, *J.Membrane Sci.* ; 120 (1996) 1
[xiii] K.D. Kreuer, T.Dippel and J.Maier, *Proc.Electrochem. Soc.* (1995) 95-23

Sulfonated Polyimides for Fuel Cell Applications

M. Pineri CEA/CEREM

Overview

- Driving forces for new membranes
- Short overview of programs under development.
- Polyimide synthesis
- Physico-chemical properties
  - Structure, swelling, conductivity
- Fuel cell experiments

Driving Forces for New Membranes

- Cost
- Methanol crossover
- High temperature work
  - CO poisoning
- EME improvements

Membranes Under Development

- Sulfonated aromatics:
  - Polytrifluorostyrene, polysulfonimides, polysulfones, polyether ketones
- Acid doped polybenzimidazoles
- Irradiation grafted membranes
- Polymer filled with conductive mineral
- Reinforced membranes

SYNTHETIC PATHWAY OF SULFONATED POLYIMIDES

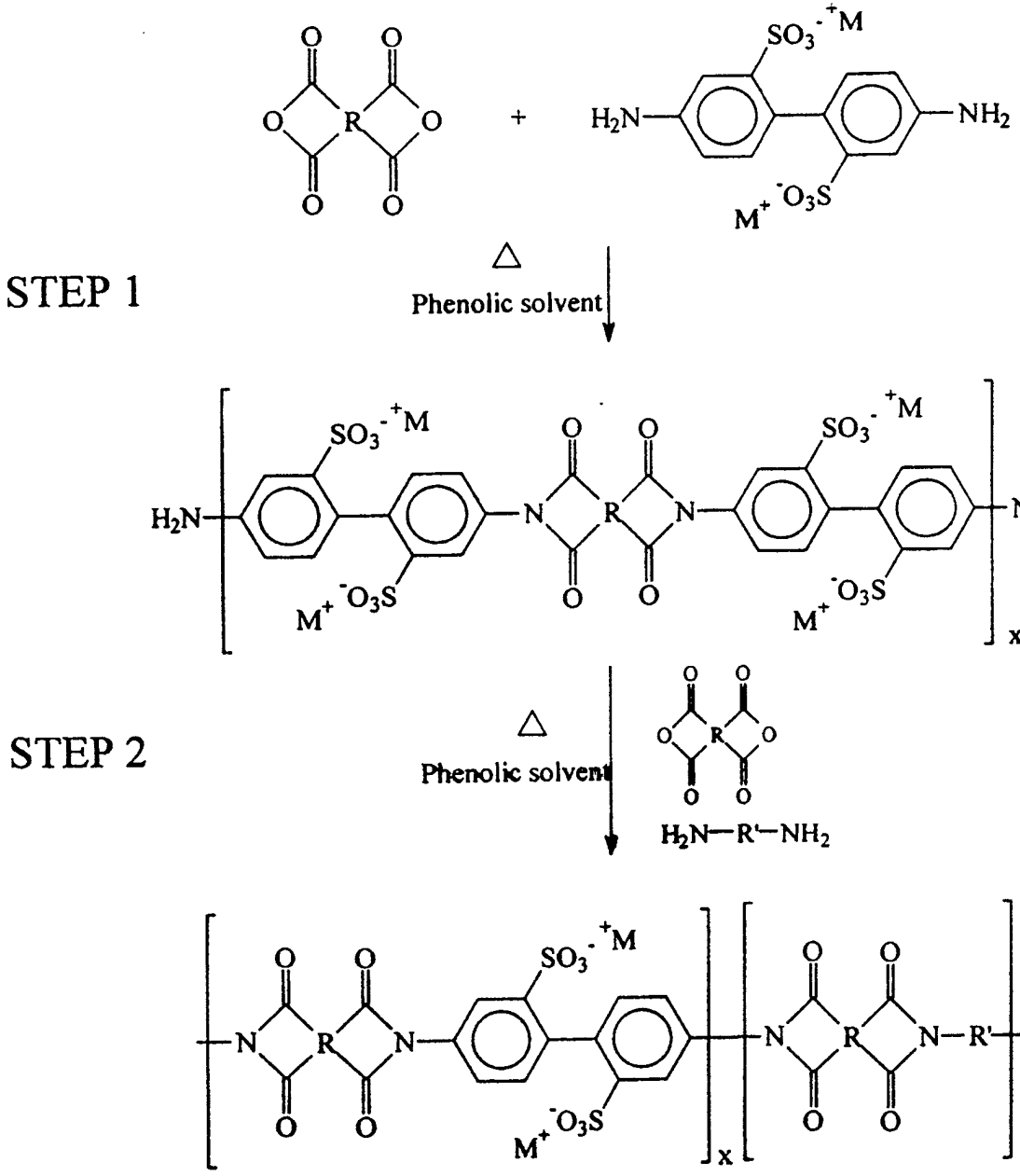

Sulfonated Diamine **A**	Dianhydride **B**	Diamine **C**
(BDSA) 4,4'-diamino-2,2'-biphenyl disulfonic acid 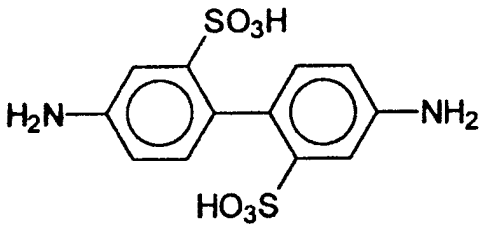	**(ODPA)** oxydiphtalic dianhydride 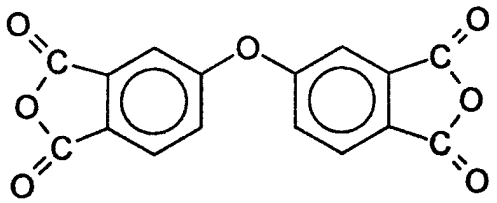	**(MDA)** 4,4'-diaminodiphenylmethane 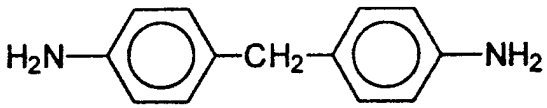
(OTDA) ortho-tolidine disulfonique acid 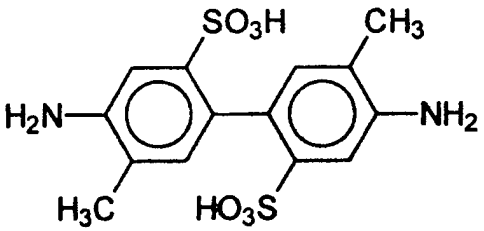	**(DNTA)** napthalene-1,4,5,8- tetracarboxylic acid anhydride 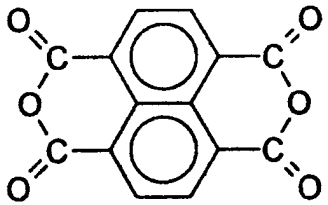	**(ODA)** 4,4'-oxydianiline or 4-aminophenylether 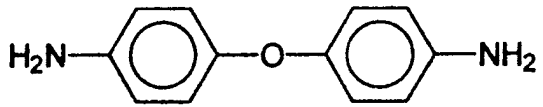

Table 1 : Monomers used for sulfonated polyimide synthesis

SULFONATED POLYIMIDES SYNTHESIS

Polymerization by the so-called one step method in a phenolic solvent

of unexpensive commercially available monomers

(excess of sulfonated diamine A) + (dianhydride B)

↓

(diamine endcapped sulfonated oligomer)

+ (dianhydride B) ↓ + (aromatic diamine C)

final sulfonated copolyimide in solution

COMPARISON BETWEEN NAPHTHALENIC AND PHTHALIC SULFONATED POLYIMIDES :

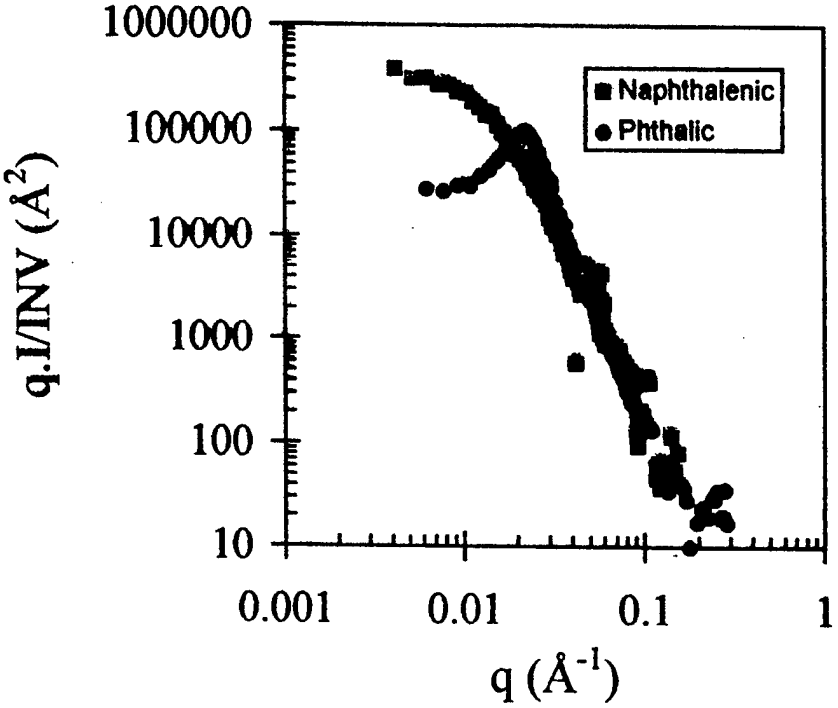

The naphthalenic sulfonated polymide does not exhibit an ionomer peak.
The level of the scattered intensity is large
The large angle behavior is identical

——> large ionic domains but different distribution

$$\lim_{q\to\infty} q^4 I(q) = 2\pi \cdot (\Delta\rho)^2 \cdot \Sigma = \frac{\Sigma \cdot INV}{\pi \cdot \phi \cdot (1-\phi)}$$

If the ionic aggregates are spherical, the surface over volume ratio is $\Sigma = 3\phi/R$
with the volume fraction $\phi = 36\%$ we obtain $R = 110$ Å

SMALL-ANGLE NEUTRON SCATTERING STUDY :

PAXE spectrometer, Léon Brillouin laboratory (Saclay, France)
Wavelength : λ=12Å, sample to detector distance : 5 m
$q=4\pi \sin(\theta)/\lambda$ where θ is the scattering angle

PHTHALIC SULFONATED POLYIMIDE AND PERFLUORINATED IONOMER (NAFION 117) :

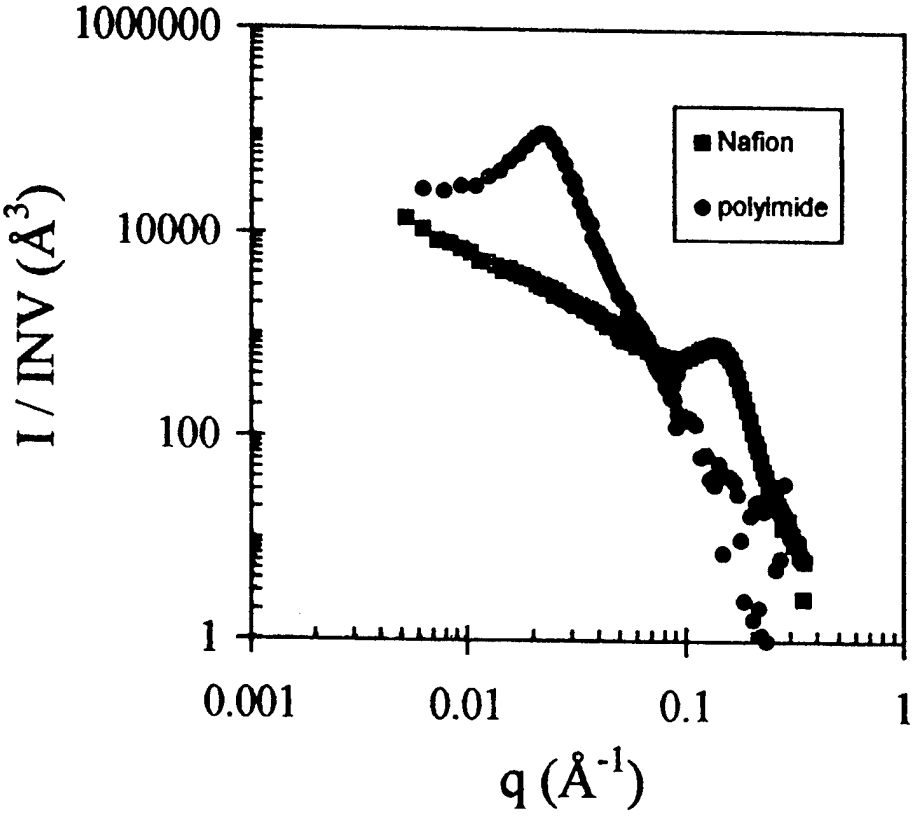

The scattering invariant is used to normalize the intensity :

$$INV = \int_0^\infty q^2 \cdot I(q) dq = (\Delta\rho)^2 \cdot \phi \cdot (1-\phi) \cdot 2\pi^2$$

An ionomer peak is observed
Its position is at lower q values compared to Nafion
Its intensity is very large
The intensity scales as q^{-4} at large q values,

SWELLING BEHAVIOR :

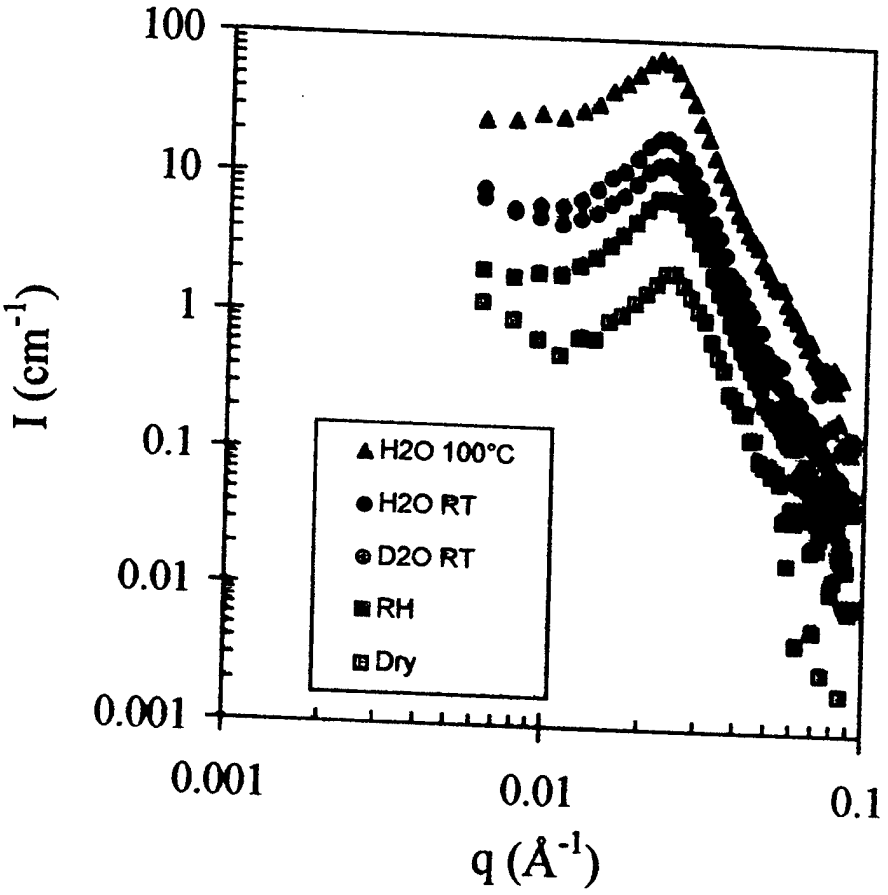

No shift of the ionomer peak but modification of the contrast factor

⟶ No modification of the structure occurs during the swelling process (filling of a nanoporosity)

This result is attributable to the high glass transition temperature

NAPHTHALENIC SULFONATED POLYIMIDE

Proton conductivity and dielectric relaxation properties as a function of the state of hydration of the membrane

λ=number of water molecules per sulfonated site

H=relative humidity at 323 K

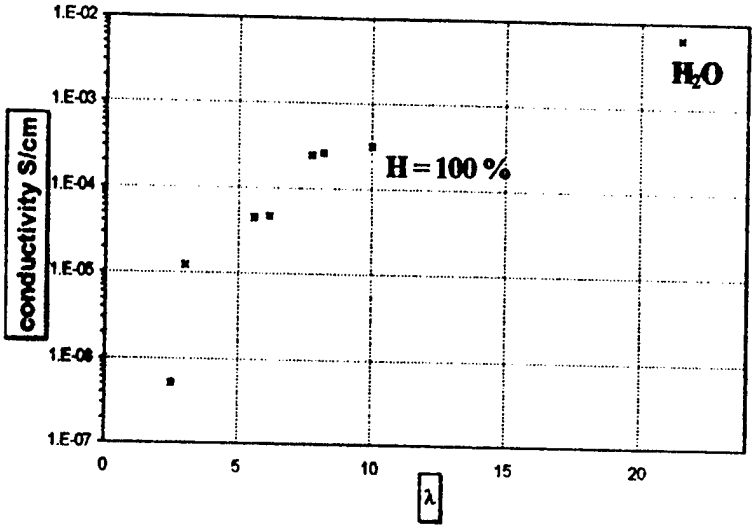

- Conductivity threshold at λ=3
- Conductivity similar to Nafion in water (6.10^{-3} S/cm)
- Important Schroeder paradox (λ=11 at H=100% ; λ=21 in water)

- Dielectric permittivity: $\varepsilon^* = \varepsilon' - i\varepsilon''$
- Dielectric loss factor: $\varepsilon'' = eR/[\omega\varepsilon_0 A(Re^2 + Im^2)]$
  - *e=membrane thickness*
  - *A=membrane superficy*
  - *ω=frequency (rad.s⁻¹)*
  - *Re=impedance real part*
  - *Im=impedance imaginary part*
  - *R=resistance*
- Relaxation peak related to local chain movement
- Raising of proton mobility with the increase of λ : increase of peak intensity and shift towards high frequencies

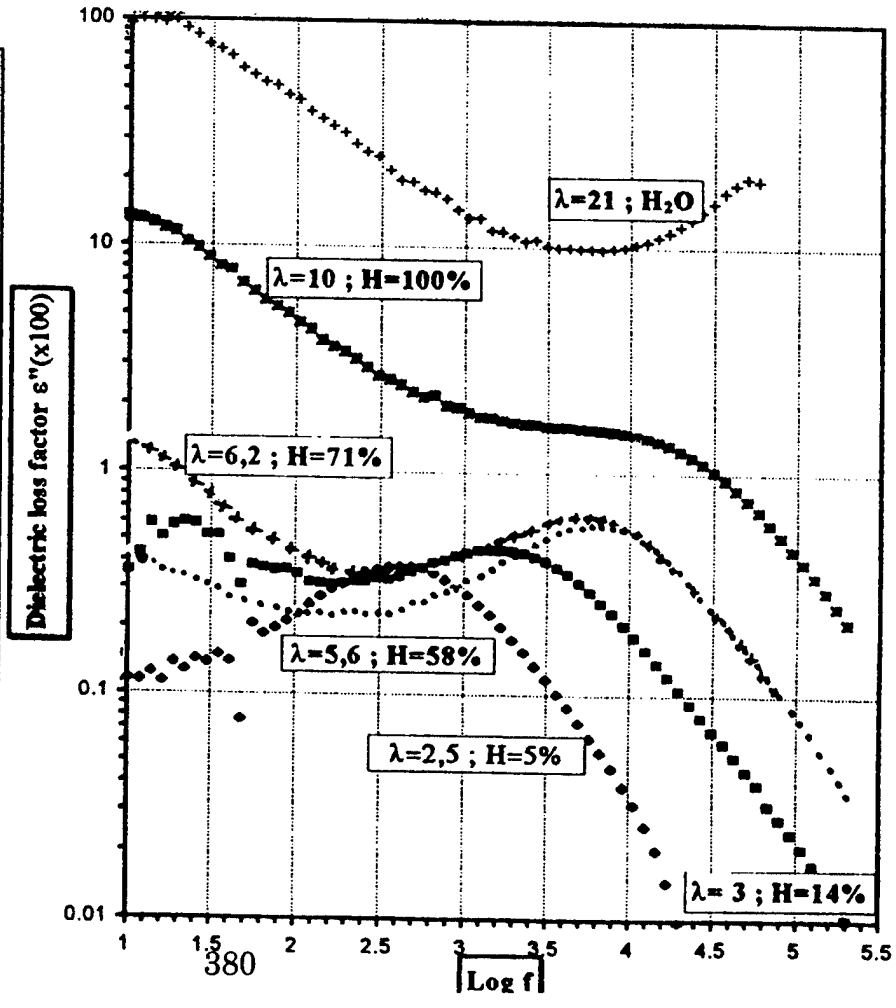

PHTHALIC SULFONATED POLYIMIDE

Proton conductivity as a function of membrane equivalent weight and sulfonated functions distribution

- Conductivity is measured by impedance spectroscopy
- Membranes are equilibrated 24 hours in water at 293K

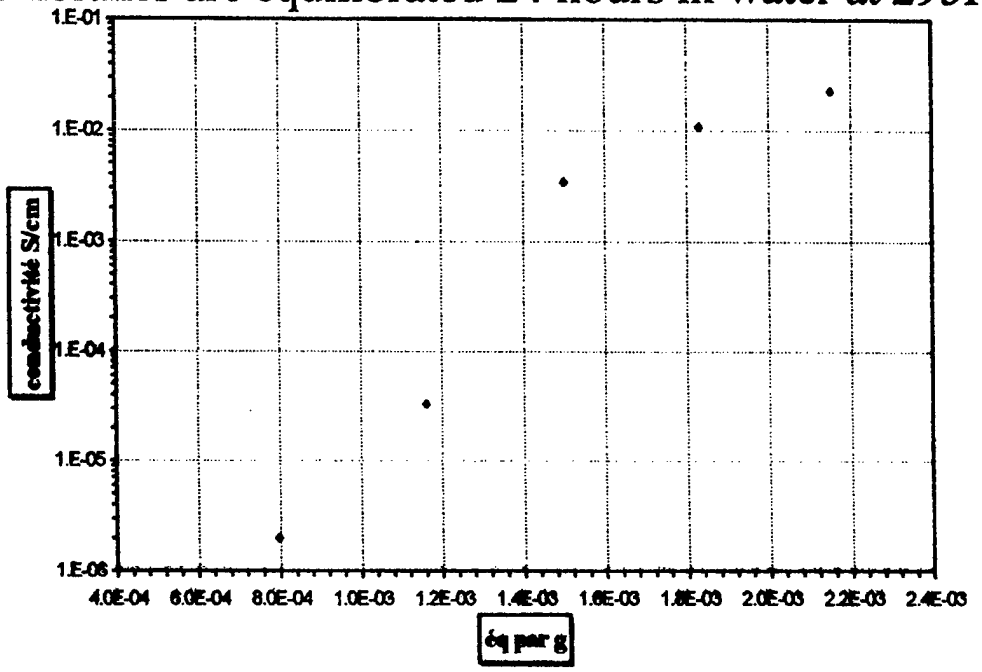

Ratio R1 (R2 = 30/70)	**Conductivity (S/cm)**
5 \ 4	**3.3E-05**
3 \ 2	**1.0E-04**
Statistical	**5.0E-07**

Modification of sulfonated functions distribution ⇒ Variation of distances between clusters and clusters dimension
Optimum of sulfonated functions distribution necessary to obtain higher conductivity ?

FUEL CELL TESTS

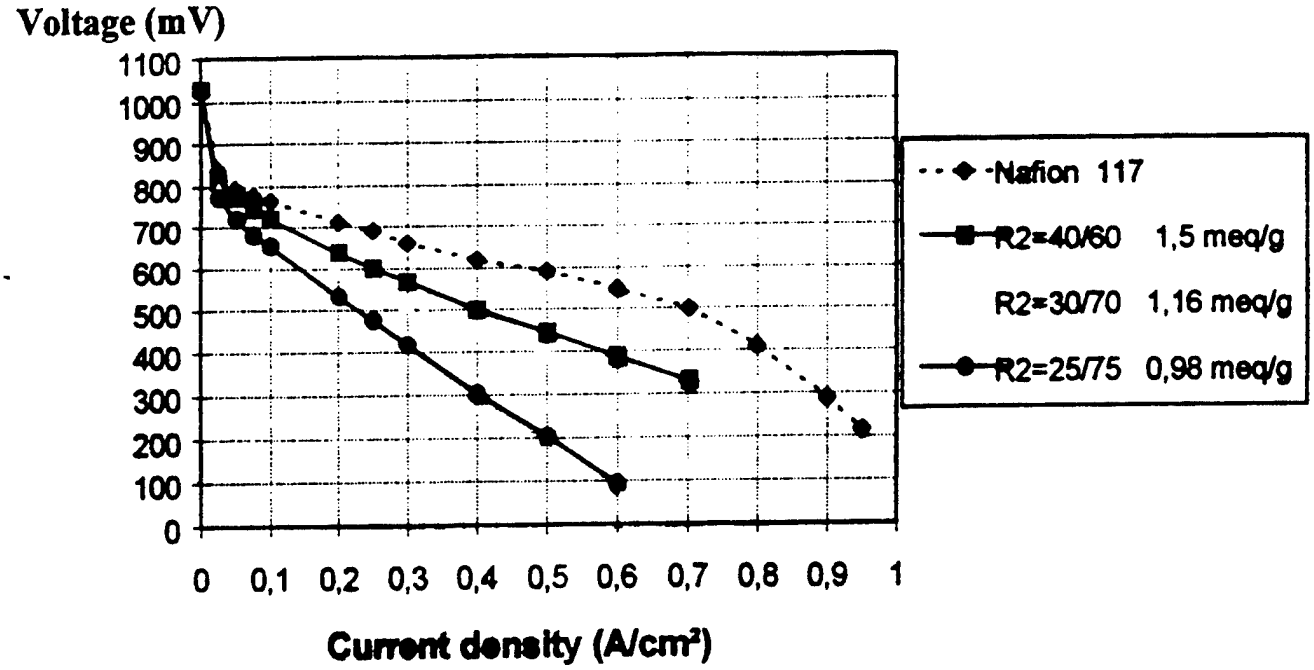

Polarization curves recorded at 60°C and $P(H_2) = P(O_2) = 3$ bar for phthalic sulfonated polyimide membranes of different equivalent weight in comparison with Nafion membrane

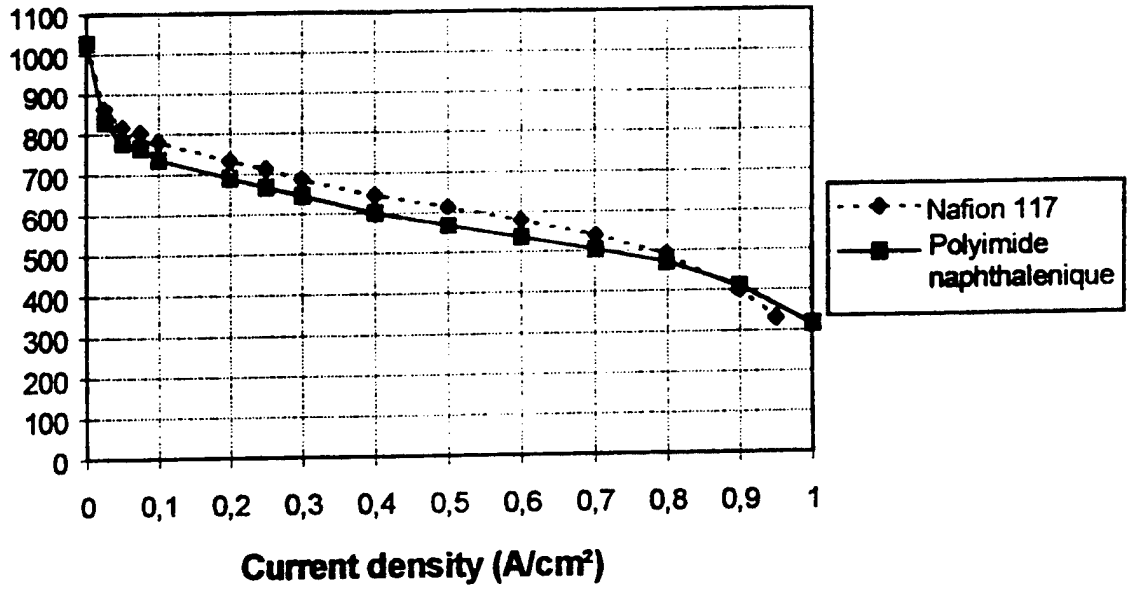

Polarization curves recorded at 70°C and $P(H_2) = P(O_2) = 4$ bar for the naphthalenic sulfonated membrane in comparison with Nafion membrane

CONCLUSION

- New low cost sulfonated polyimides were prepared
- Based on phthalic structures, problem of hydrolysis
- On the other hand, naphthalenic sulfonated polyimides

  seem to be a PROMISING MATERIAL for fuel cell
- New polyimides could be prepared in the future with certainly better performance than available expensive perfluorinated membranes

NARATIVE

HIGH TEMPERATURE POLYMER ELECTROLYTE FUEL CELLS

R. F. Savinell, J.S. Wainright and M. Litt
Ernest B. Yeager Center for Electrochemical Sciences
Case Western Reserve University
Cleveland, Ohio 44106

SLIDE 1

A 5-year DARPA University Research Initiative Grant that ended this past year supported this research. It continues to be a subject of interest at CWRU because of the advances made and the attractive features for these types of fuel cells. Before describing the CWRU approach, first we will review some of the potential advantages of operating a PEM fuel cell at higher temperatures.

SLIDE 2

A direct methanol fuel cell is a power delivery device having the advantages of the high energy density associated with liquid fuel. Some of the technical challenges facing development of this technology are indicated here. Operating at higher temperatures can mitigate the first three of these challenges, i.e., slow anode kinetics, catalyst poisoning, and methanol crossover.

SLIDE 3

A hydrogen fuel cell is the most efficient with highest power density because of the reversibility of the hydrogen electrode. Methanol can be reformed to hydrogen at an active catalyst surface at temperatures as low as 200 C. By reforming methanol, one can achieve the high efficiency of the hydrogen oxidation reaction while maintaining the advantages of a liquid fuel storage system.

SLIDE 4

A PEM fuel cell operating at higher temperatures can be directly integrated into the methanol reformer. The excess heat of the fuel cell can be available to meet the endothermic energy requirements of the reformer and to vaporize the fuel and water fed to the device.

SLIDE 5

First order estimates of the thermodynamic conversions in a reforming reactor and the energy balances have been estimated using a process simulation program. At 200 C the thermodynamic conversion of methanol with equal molar water/methanol feed is almost complete and the CO level is about 2.5 m%. In fact, with a little excess water this level of CO drops considerably to levels of about .1 m%. Of the heat available in the fuel

mixture, only about 8% is needed for the reformer and 20% for the fuel, water, and air preheating. By directly absorbing this energy within the fuel cell device the excess heat in need of dissipation becomes less. Consequently, with the smaller amount of waste heat and the higher temperature driving force, smaller heat exchange devices are needed.

SLIDE 6

A PBI fuel cell was operated on reformed hydrogen fuel. At 150 C with 1 m% CO the excess overpotential of the hydrogen anode is only about 5 mV. The excess overpotential becomes much less at higher temperatures. Lower platinum loading, comparable with those of PEM fuel cells with high platinum utilization, give excellent performance in the presence of CO at the higher temperatures. This means higher performance and lower cost.

SLIDE 7

The advantages of operating a PEM fuel cell at higher temperatures are summarized here. The properties and features of a polymer electrolyte required for fuel cell application are given. At CWRU we are pursuing a class of rigid rod polymers known as polybenzimidazoles (PBI). Two types of PBI have been investigated. The first is a commercially available material manufactured by Hoechst-Celanese Corporation. As will be seen, this material has properties that are very promising for fuel cell applications. In this presentation, we will describe the methods of preparation of these polymers, and summarize the chemical, mechanical, stability, and electrochemical properties that were measured in this research. Performance of the commercial PBI used in fuel cells has been reported by us elsewhere and will not be reported here.

SLIDE 8

PBI is available commercially from Hoechst-Celanese. As will be shown in the next slide, the mechanical properties necessary for good film formation will be enhanced by high molecular weight polymer. The polymer normally available has an inherent viscosity of about 0.7. The I.V. is a measure of the molecular weight of a polymer. A sample purchased from Aldrich had an I.V. considerably lower than that. We received material from Hoechst-Celanese with an I.V. of 0.91. This material has a broad molecular weight distribution. In order to increase the molecular weight, the lower MW fractions are extracted by fractionation in DMAc. The yield of high I.V. material decreases as the molecular weight increases. Our understanding is that high molecular weight material could be synthesized if the demand for it warrants the expense of process modifications.

SLIDE 9

PBI absorbs acid. Proton conduction requires oxo-acids. Sulfuric acid was originally investigated, but poor film mechanical properties led us to consider phosphoric acid. However, further investigation with different I.V. materials and casting methods may

warrant another look at this system. The first two phosphoric acids per repeat unit protonates the two benzimidazole groups, as shown by NMR. However, additional phosphoric acid is needed for good conductivity. The additional phosphoric acid is more weakly tied into the PBI structure, but relatively immobile. Still the polymer-acid system is single-phase.

SLIDE 10

Two methods were investigated for forming films of PBI with phosphoric acid. In the first method, the polymer is dissolved in DMAc and 1-2 wt% LiCl is added to maintain stability. The film is cast onto a glass plate, the solvent is evaporated, and then the film is washed in boiling water to remove the residual LiCl. Doping of the film is accomplished by submersion in concentrated phosphoric acid. The molarity of the acid determines the final acid loading in the membrane. For example, submersion in 11M acid solution gives a doping level of about 6 moles of acid per PBI repeat unit (this is called 600 m% doping level).

In the second method, PBI and acid are directly cast together from a co-solvent of TFA. The solvent is evaporated and the film is ready for use. The properties of the film formed by this process are substantially different than the DMAc method.

SLIDE 11

The mechanical properties of DMAc cast films are compared to TFA cast films. Films formed by the former method are normally stronger and tougher. The TFA films require a polymer of higher I.V. in order to acquire films of reasonable strength. The TFA films have much more crystallinity as compared to the DMAc films, and the surface texture is quite different. The TFA films are more rubbery and softer.

SLIDE 12

Although the mechanical properties of the TFA cast films are not as good as the DMAc cast films, the method of casting is simpler and the proton conductivity is greater. The proton conductivity of TFA films at dry conditions and temperatures exceeding 180C exceed that of Nafion (under Nafion's optimum operating conditions of 100% RH).

SLIDE 13

Several techniques have been used to measure the methanol permeability across PBI films. These techniques include close-volume membrane diffusion cells, limiting current methods, and mass spectroscopy methods. All techniques gave the same result. The crossover equivalent current (50 m% of methanol in feed at 1 atm pressure) for DMAc cast film is about 5-10 mA/cm^2, which is a factor of 10-20 times less than that reported for Nafion 117. For TFA cast films, the crossover is larger by a factor of 3, but still considerably less than Nafion 117. Of course, the low crossover is not unexpected

considering that the methanol activity is low in the gas phase at high temperatures and that PBI is a homogeneous phase system.

SLIDE 14

ABPBI is the second polymer in this class of polymers investigated at CWRU. The polymer is simple to synthesize by a condensation reaction. The presence of polyphosphoric acid scavenges the water production and helps to form high molecular weight material. Although the DABA starting material is available commercially, purification is critical for high molecular weight polymer. To date the highest I.V. we made was 4.27 and the preferred operating conditions are given here. Reports in the literature indicate that much higher molecular weights are achievable (I.V. up to 12-25).

SLIDE 15

Doping of acid into ABPBI is accomplished by submersion into phosphoric acid solution. By drying the film at 140 C before submersion, a higher doping level can be achieved. Annealing the film at temperatures of 150 C improves film strength to levels about that of PBI/TFA films. We expect better film properties with higher molecular weight material. A remarkable property of this material is the amount of strain before break. Some films have been stretched by a factor of 10 before breaking. Pre-stretched films are also stronger because of alignment of the molecular chains. This polymer is more conductive with lower amounts of acid as compared to PBI.

SLIDE 16

Oriented films of ABPBI were found to give greater strength. The films were first cast, doped, then stretched. The acid was remove before testing. These films had moduli that were 15 to 25 times greater than the un-doped and un-stretched films. The theoretical strength is about 300 Gpa so further improvement in strength can be expected.

SLIDE 17

The conductivity of ABPBI is greater than that of the PBI/DMAc and nearly equivalent to that of PBI/TFA. To compare acid loadings, a value of 1.3 Acid/Repeat in ABPBI is equivalent to 2.6 Acid/Repeat in PBI. ABPBI is an attractive polymer for fuel cell applications considering its high conductivity, its good mechanical properties for film formation, and its ease and control of synthesis.

SLIDE 18

We have only begun to develop the PBI-type polymers for fuel cell applications. Further work is needed to understand the conduction mechanism and to optimize the properties for film formation and electrode attachment. These polymers may also find other applications. Some examples include microfuel cells, sensors, electrochemical reactors for destruction of toxic volatile organic compounds.

This paper represents the contributions of a number of students and research associates in the Ernest B. Yeager Center for Electrochemical Sciences. Those directly involved with the data presented are acknowledged here.

HIGH TEMPERATURE POLYMER ELECTROLYTE FUEL CELLS

R. F. Savinell, J. S. Wainright, M. Litt

E. B. Yeager Center for Electrochemical Sciences
Case Western Reserve University
Cleveland, OH 44106

Acknowledgment:

This work was supported under a University Research Initiative Grant from the Defense Advanced Research Projects Agency, ONR grant #N00014-92-J-1848.

Direct Methanol/Air PEM Fuel Cell

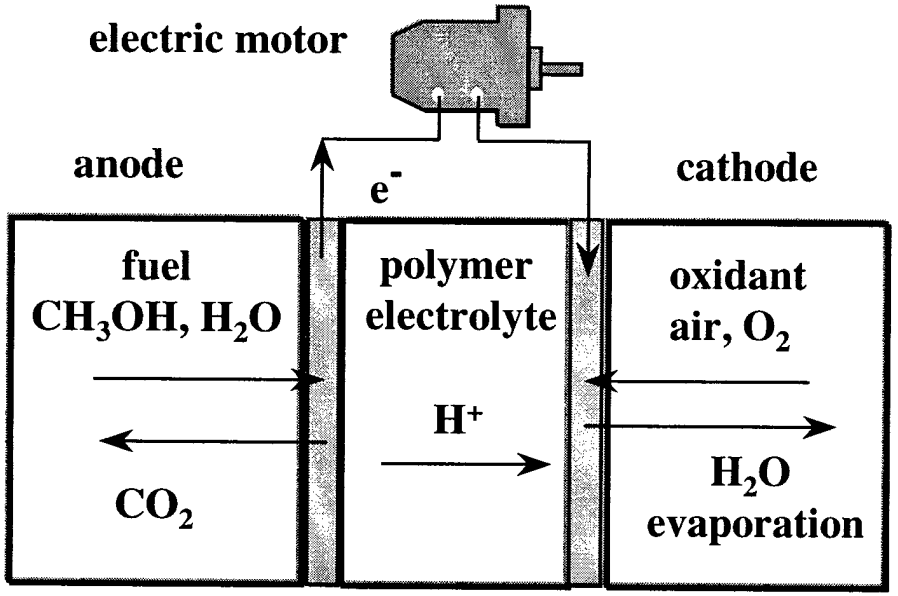

Anode: $CH_3OH + H_2O \longrightarrow CO_2 + 6\,H^+ + 6\,e^-$

Cathode: $O_2 + 4\,H^+ + 4\,e^- \longrightarrow 2\,H_2O$

Overall Reaction: $CH_3OH + 1.5\,O_2 \longrightarrow CO_2 + 2\,H_2O$

Challenges:

- Slow anode kinetics
- Catalyst Poisoning
- Methanol crossover lowers fuel utilization and lowers cathode performance
- Membrane and electrode cost

Hydrogen Fuel Cell & Methanol Fuel Cell

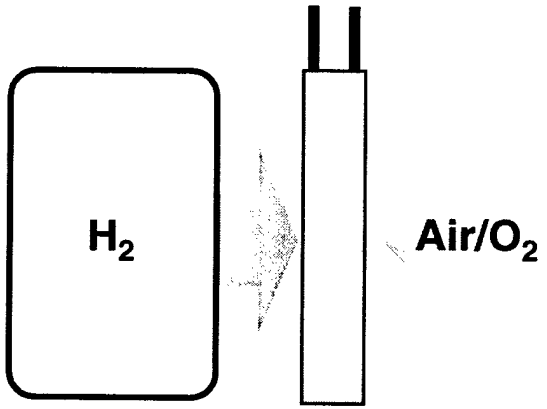

H_2/O_2 Fuel Cell

$$H_2 + 1/2\ O_2 \longrightarrow H_2O$$

- High power density
- Pollution free operation

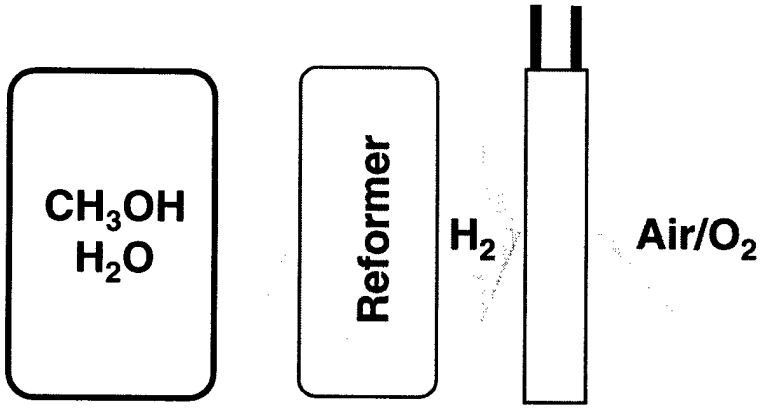

Methanol Fuel Cell

Reformer

$$CH_3OH + H_2O \xrightarrow{\text{Catalyst}} CO_2 + 3\ H_2$$

Fuel Cell

$$H_2 + 1/2\ O_2 \longrightarrow H_2O$$

- Liquid Fuel easy to store, handle and transport

PBI Fuel Cell Using Reformed Methanol

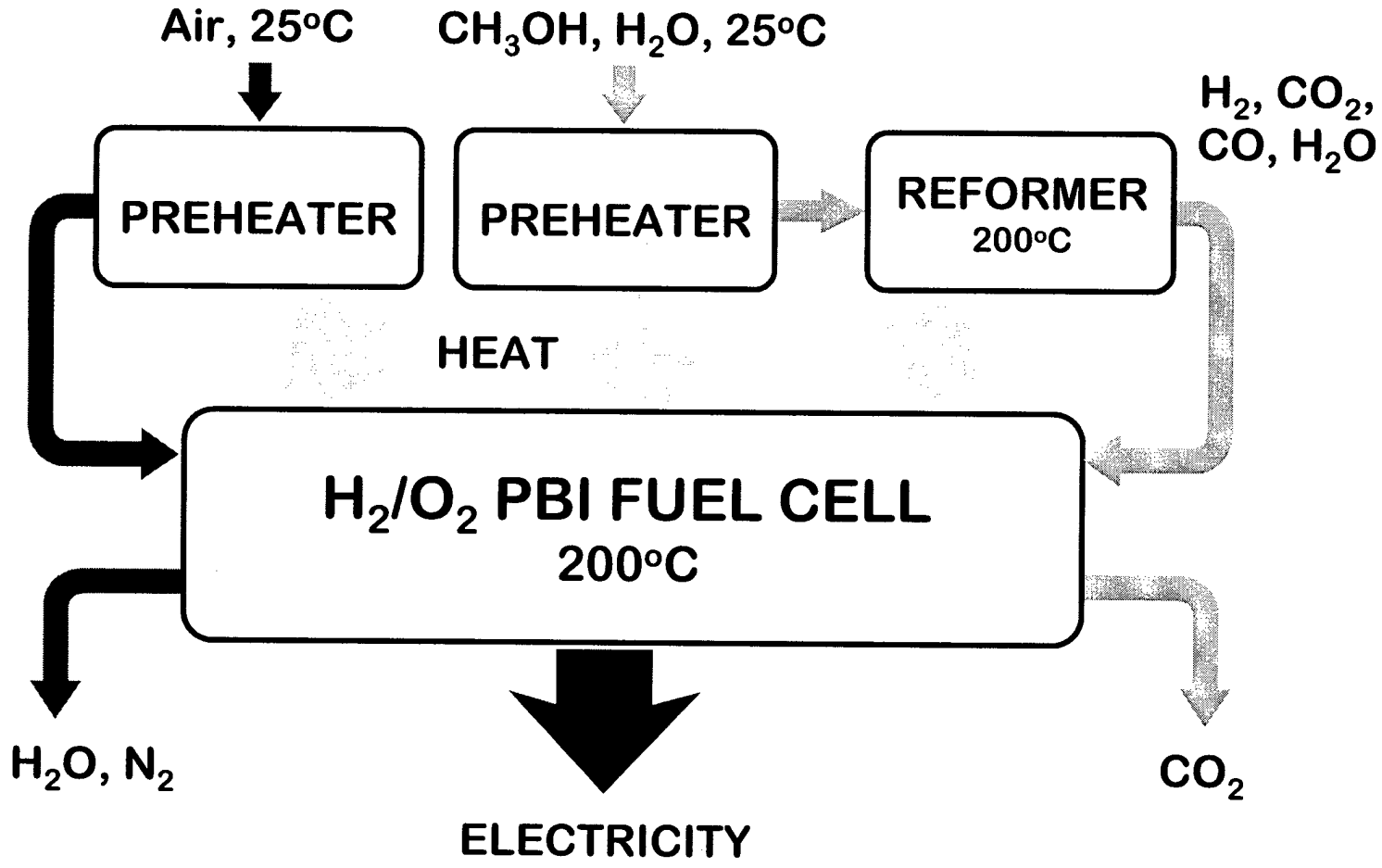

First Order Estimates of Conversion and Heat Flows (ChemCAD)

Conversion:

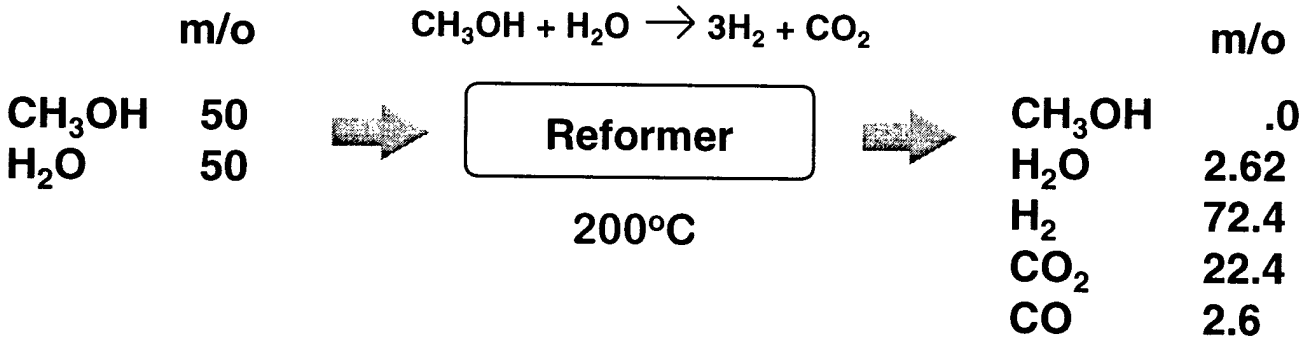

Energy Balance:

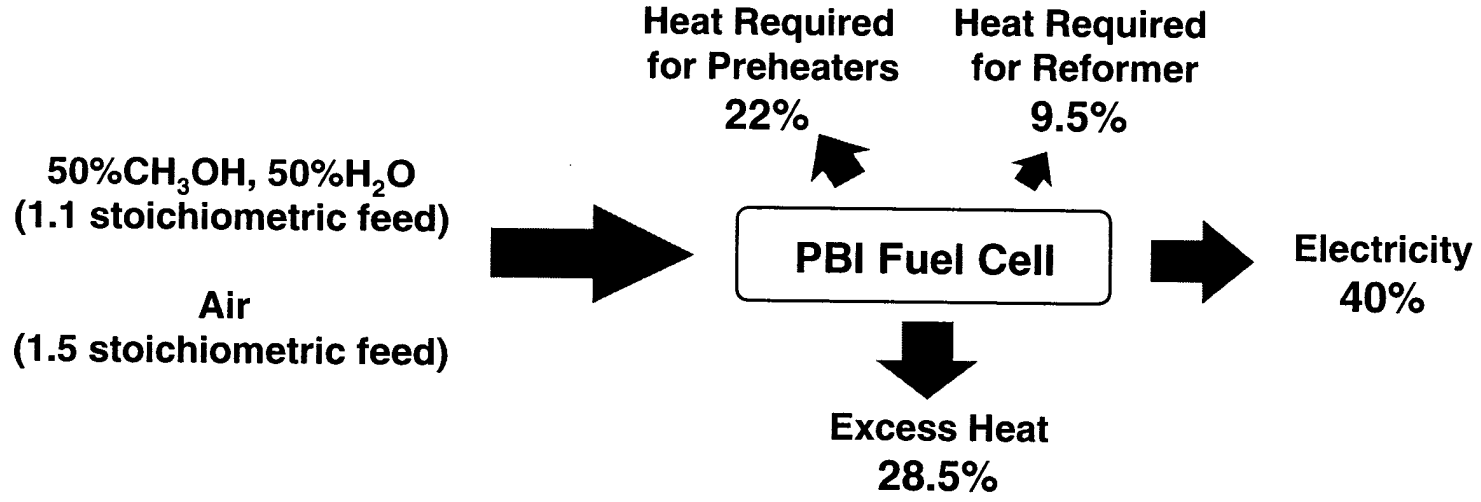

1% CO Effect on Anode Performance

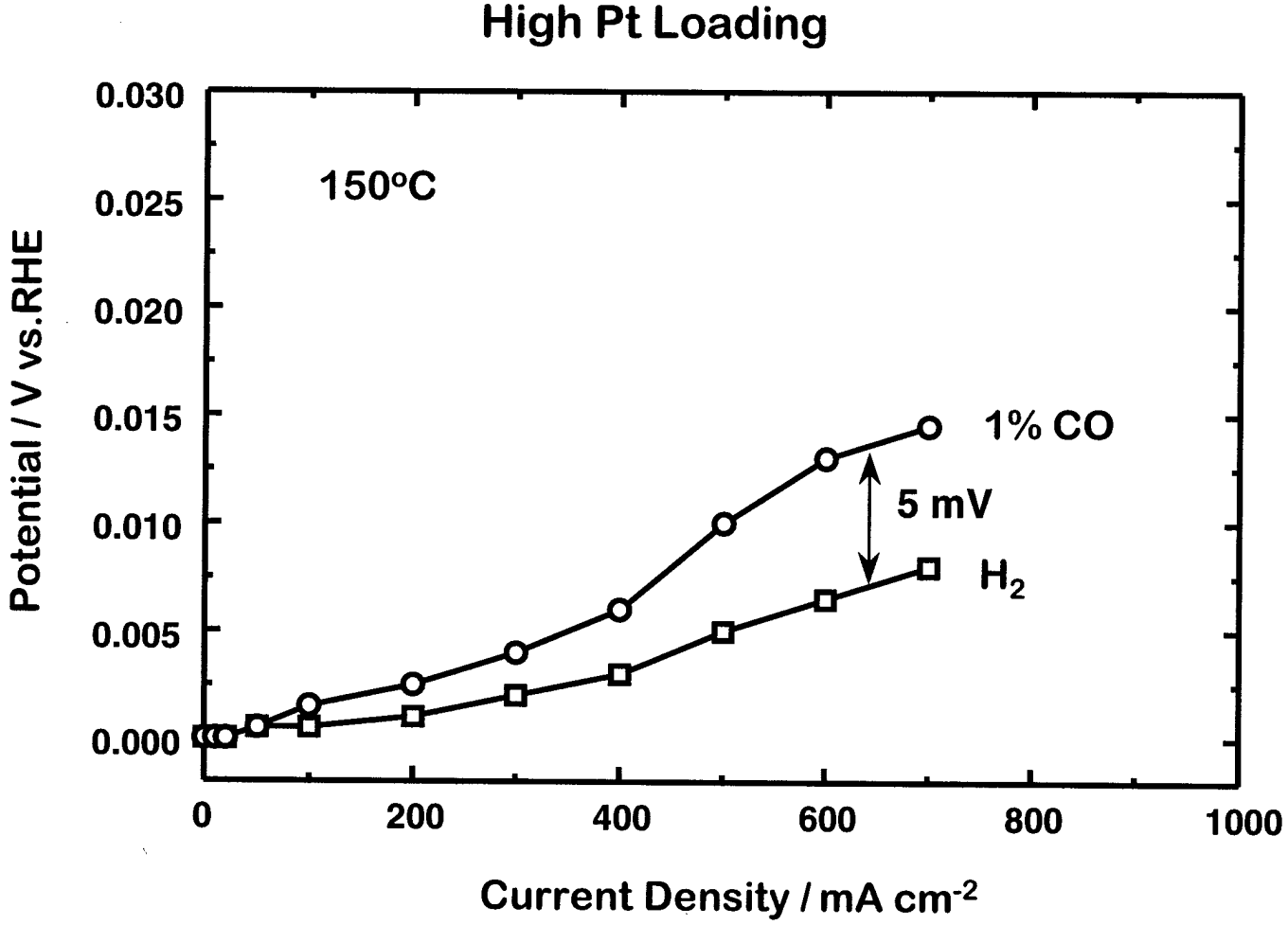

Electrode: 1mg/cm^2 Pt black. H_2 and H_2 w/ 1%CO , 1 atm, humidified at 65C.
Electrolyte: PBI/TFA membrane, 600 m/o H_3PO_4

HIGH TEMPERATURE POLYMER ELECTROLYTES

ADVANTAGES
- Improved electrode kinetics
- Minimize water balance issues
- Low fuel crossover

REQUIRED PROPERTIES
- High proton conductivity
- Favorable electrochemical environment
- Good film-forming mechanical properties
- High chemical/thermal stability
- Low cost

CWRU APPROACH

PBI
- Commercially Available
- High Chemical Stability
- Absorbs Acid

ABPBI
- Lower Equivalent Weight
- High Molecular Weight-Good Mechanical Properties
- Greater Control Over Synthesis-Lower Potential Costs
- Excellent Proton Conductivity

U.S. PATENT 5,525,436, Jan 11, 1996.
U.S. PATENT 5,716,727, Feb 10, 1998

PBI PROPERTIES AND CHARACTERISTICS

- HIGH TEMPERATURE RESISTANT
- GLASS TRANSITION TEMP ~450C
- SMALL MOLECULES ACT AS PASTICIZERS
- ABSORBS ACID, Pka~5.5

MOLECULAR WEIGHT AND INHERENT VISCOSITY (I.V.)

(5 WT% in concentrated sulfuric acid)

POLYMER	I.V. dl/g	M_n	M_w	MWD (M_w/M_n)
low	.3	6700	11200	1.7
avg	.68	18000	27200	1.5
high	.97	26300	50300	1.9

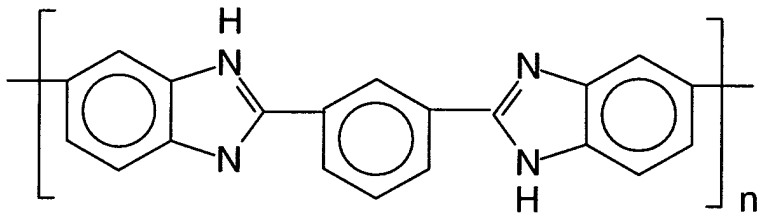

PBI FRACTIONATION IN DMAc - INITIAL I.V. = .91

(10 wt% PBI)

SAMPLE	FRACTIONATION TEMP. C	YIELD %	I.V. dl/g
A	160	23	1.42
B	130	41	1.28
C	110	53	1.19
D	94	69	1.14

Acid Doped Polybenzimidazole (PBI)

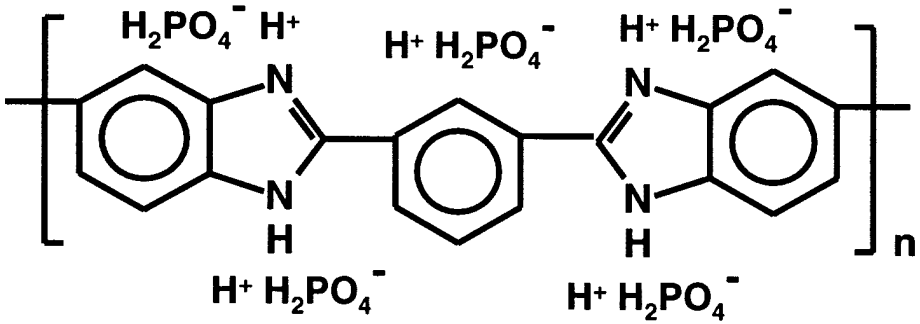

poly[2,2'-(m-phenylene)-5,5'-bibenzimidazole

- Doping level can be as high as 6 acid molecules per polymer repeat unit.
- Solid state NMR results show that there is an interaction between acid and polymer. Acid sorbed in PBI is relatively immobile compared to free acid.
- Stable in reducing and oxidizing environments to 600 C.

J. S. Wainright, et al. , J. Electrochem. Soc., 142, L121 (1995)

S.R. Samms, et al., J. Electrochem. Soc., 143, 1225 (1996)

PBI FILM FORMATION METHODS

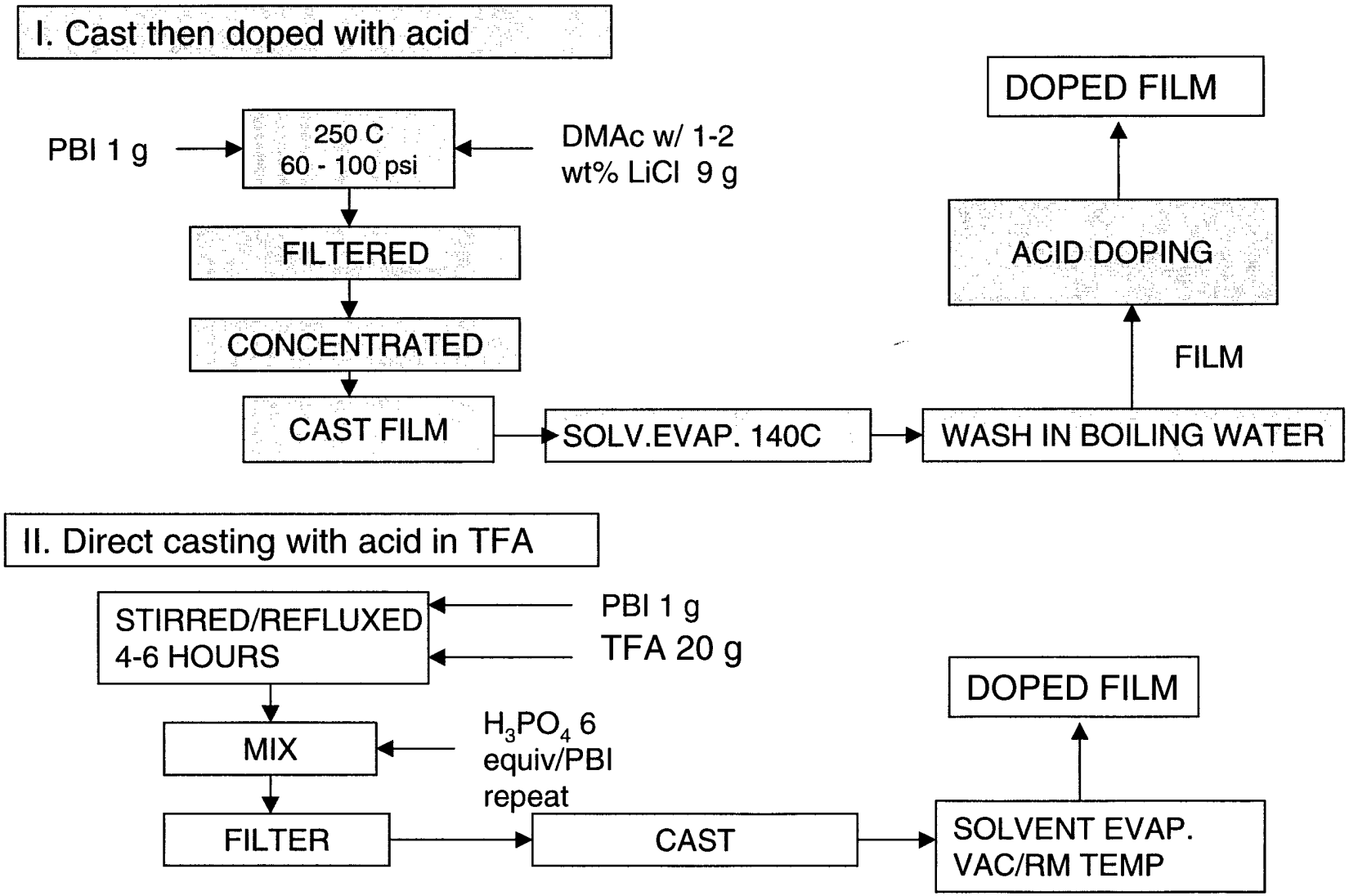

Mechanical Properties
TFA vs. DMAC Cast Films

•PBI/TFA has lower moduli and strength as compared to PBI/DMAC cast films (both acid doped)

	DMAC Cast (I.V. = 1)		TFA Cast (I.V. = .91)	
	Modulus 10^9 Pa	Toughness 10^6 Pa	Modulus 10^9 Pa	Toughness 10^6 Pa
Dry PBI	1.94	105.00	1.27	50
100% H_3PO_4	3.53	48.5	1.88	35

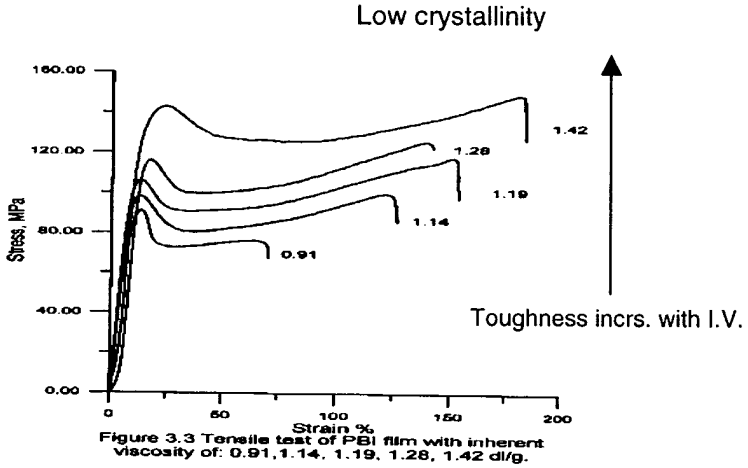

Figure 3.3 Tensile test of PBI film with inherent viscosity of: 0.91, 1.14, 1.19, 1.28, 1.42 dl/g.

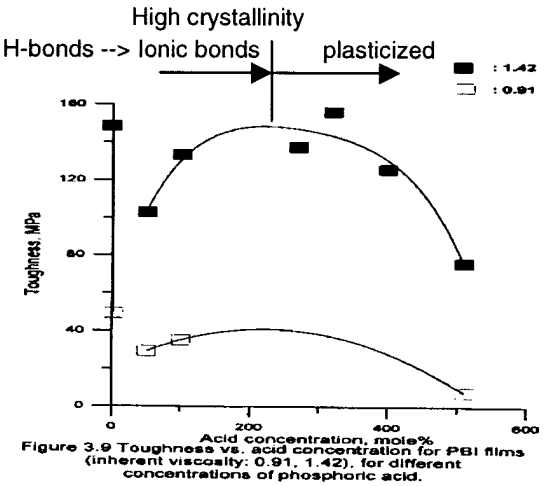

Figure 3.9 Toughness vs. acid concentration for PBI films (inherent viscosity: 0.91, 1.42), for different concentrations of phosphoric acid.

•TFA films need higher M.W. polymer for acceptable film properties

Conductivity of PBI Membranes

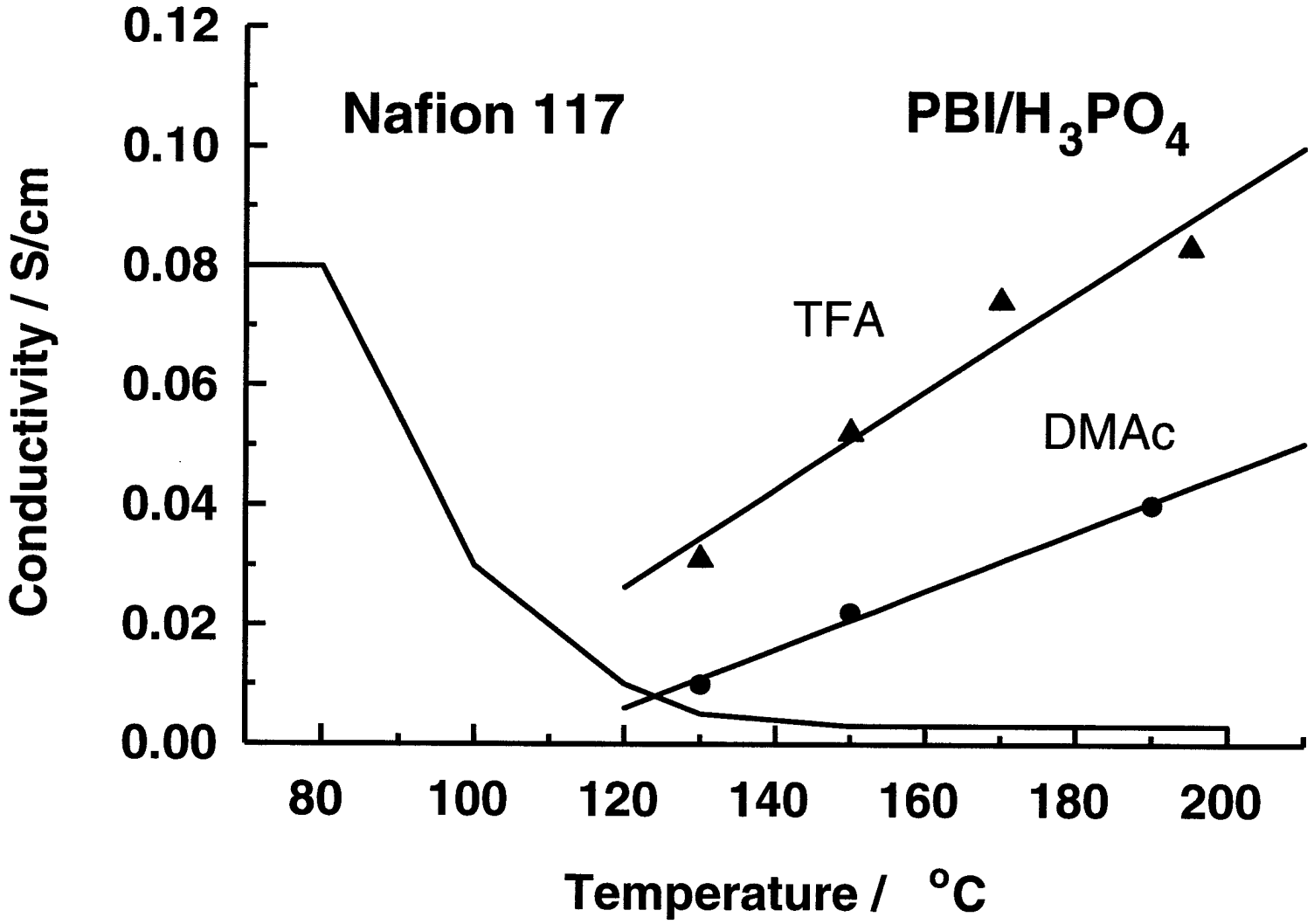

PBI/DMAc
METHANOL
PERMEABILITY

DMAc Cast
Membrane

Determination of the Methanol Crossover Rate by Mass Spectrometric Measurement

The methanol across through a membrane was swept by air and analyzed by the Mass Spectrometer.

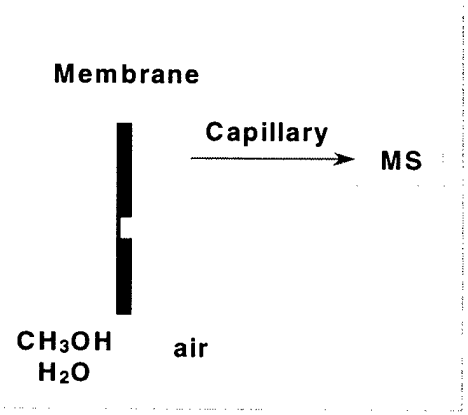

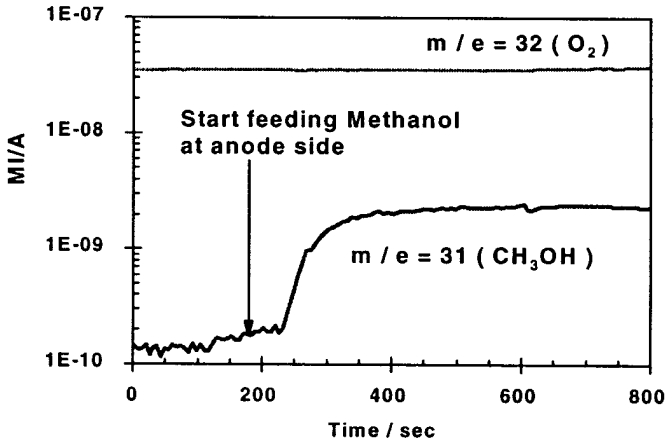

Methanol Crossover Rate Estimated From Mass Spectrometric Data Obtained Under Open Circuit Conditions

water/methanol mole ratio	methanol crossover rate / mA cm^{-2}	standard deviation / mA cm^{-2}
3	4.5	1.3
2	6.4	2.6
1	9.3	3.9
0 (pure methanol)	10.7	3.5

For each entry, five different values obtained varying the air flow rate were averaged.
Operating temperature: 160 °C
Cathode: 4 mg·cm^{-2} Pt-black
PEM: PBI doped with 500 mole% H_3PO_4, 0.011 cm thick

ABPBI
Poly (2,5-benzimidazole)

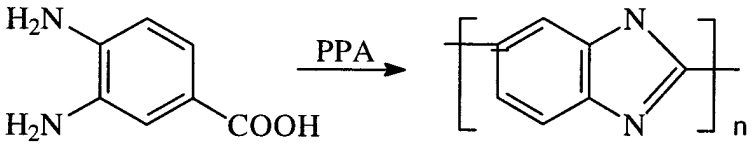

$+ 2nH_2O$

3,4 diaminobenzoic Acid (DABA)

Purified

$2\,H_2O + P_2O_5 \longrightarrow H_4P_2O_7$

Synthesis at 160 C

Excess P_2O_5,%	I.V.
50	.84
150	1.28
300	3.31

BEST SYNTHESIS CONDITIONS

200 C, 2 hours, DABA/P_2O_5/H_3PO_4 = 1/7/3.22

I.V. = 4.1 **M_w=71,000** **(Literature)**
I.V. = 4.27 **(this work)**

Yuan Wang, "The Synthesis and Properties of Poly (2,5-Benzimidizole)", M.S. Thesis, CWRU, May, 1998.

ABPBI
Stability and Mechanical Properties

Stability (T.G.A.) - 600°C

Soln. H_3PO_4 molar	H_3PO_4/Repeat	Annealing Temp.C	Modulus Gpa	Strain at Break,%
0	0	25	1.47	256
3	1.29	25	1.77	161
6	1.79	25	.25	437
6*	3.29	25	.069	872
"	"	100	.33	767
"	"	150	1.75	548

* Film dried at 140 C before acid doping

I.V. = 4.27, Measurements at 25 C

Figure 22 Modulus vs. Number of Phosphoric Acid Molecules per ABPBI Repeat Unit (IV=4.27)

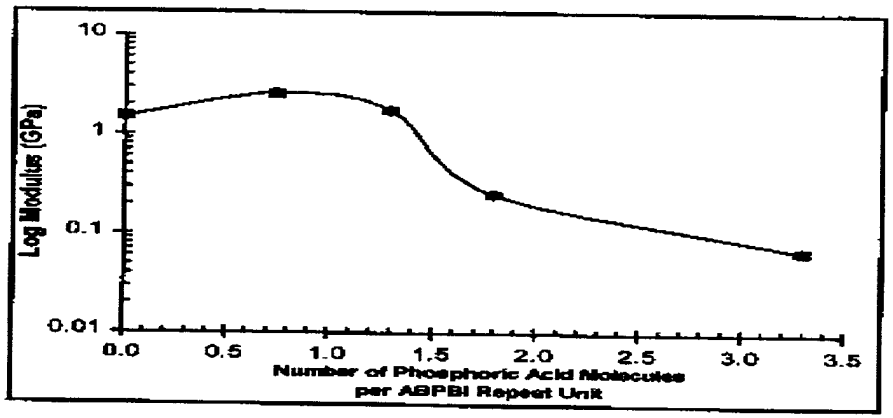

Figure 24 Modulus vs. Annealing Temperature of Doped ABPBI (Mole Ratio:3.3 H_3PO_4/ ABPBI, IV=4.27)

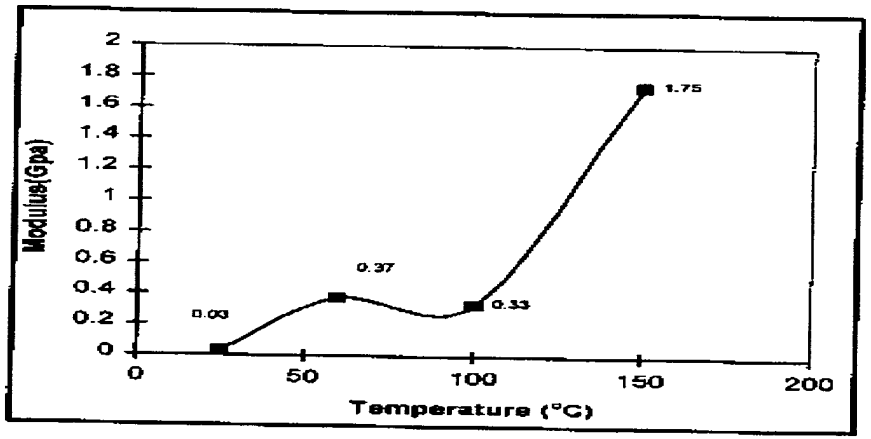

ABPBI

MECHANICAL AND ELECTROCHEMICAL PROPERTIES

ORIENTED FILMS HAVE GREATER STRENGTH

METHOD: Cast film, acid load, stretch, remove acid

Pre-stretch %	Modulus Gpa	Stress @ Brk Mpa	Strain @ Brk %
500	21.2	794	6.7
600	38.5	849	2.8

CONDUCTIVITY of ABPBI 1 atm water pressure, 150-200C

H_3PO_4/Repeat	Conductivity S/cm
1.3	.022
2.5	.05
3.29	.086

CHALLENGES FOR DEVELOPMENT OF PBI-TYPE POLYMERS

- **UNDERSTANDING THE MECHANISM OF CONDUCTION**
  - **DETERMIINE ROLE OF ACID STRUCTURE AND AMOUNT, OF WATER, OF POLYMER TYPE AND MW, OF POLYMER AND ACID CRYSTALLINITY**
  - **DETERMINE ROLE OF FILM CASTING METHOD**
- **INVESTIGATE OTHER NON-ADSORBING ANION ACIDS**
- **OPTIMIZE FILM MECHANICAL PROPERTIES WITH ELECTROCHEMICAL PROPERTIES**
- **OPTIMIZE ELECTRODE STRUCTURES FOR HIGH PERFORMANCE**
- **LIFE TESTING AND STABILITY ANALYSIS**

THE CWRU FUEL CELL GROUP

J.T. WANG D. WENG S SAMMS S. WASMUS H. MOEADDEL R. AMERI Z. BAO

Y. WANG S. SECEVIC

High Temperature Functional Fluoropolymers

Darryl D. DesMarteau, Department of Chemistry, Clemson University,
Hunter Hall, Box 341905, Clemson, SC 29634-1905

The fact that fuel cells are of increasing interest as electrochemical power sources is exemplified by reports in the popular press such as a recent announcement by Chrysler (**1**).* Worldwide research and development is intense and the prospect that mass produced PEM fuel cell power plants (**2**) will be used for electric and hybrid vehicular power early in the next century is very high. Nevertheless these prospects would be enhanced considerably if improved PEMs capable of operating at higher temperatures could be found. In this regard there are a number of issues that affect the development of new membrane materials (**3**).

Most of the development of PEM fuel cells is based on sulfonic acid ionomers. For overall performance and lifetime, the preferred ionomers are perfluorinated copolymers of TFE and functional vinyl ether monomers. If the limitations of perfluorinated ionomers of this type are to be overcome, new materials with alternative functional groups to the sulfonic acids must be considered.

Some possible solutions involving alternative acid functions are illustrated in (**4**). At Clemson University over the last 10 years we have carried out research on the preparation of new polymer materials containing the sulfonimide and sulfone acid functions. More recently under DOE/EPSCoR sponsorship, this program has been expanded to include a number of critical collaborations needed to make meaningful progress (**5**). A number of novel polymer materials under development are illustrated in (**6**). Some of the basis for selecting these materials is shown in (**7**). For this presentation, the focus will be on sulfonimide ionomers for which the largest effort and greatest progress has been made. To introduce these novel materials and to raise their specter as possible improved PEMs for fuel cells, an overview will be presented (**8**).

*Bold numbers in parenthesis refer to numbered copies of transparencies in the Appendix.

The background to these novel ionomers dates back to the mid-seventies. We were looking for novel ligands to bond to xenon and to create new examples of xenon-element bonds. With the successful isolation of the first xenon-nitrogen compound $FXeN(SO_2F)_2$ in 1974, other nitrogen ligands were actively sought after. Ultimately we were led to the synthesis of the new sulfonimide $(CF_3SO_2)_2NH$. This parent member of this class of compounds led us to an appreciation of the remarkable properties of this class of materials. This compound led to a second example of Xe-N bonds in $Xe[N(SO_2CF_3)_2]_2$, but more importantly we came to recognize its remarkable Bronsted acidity and related charge delocalization in covalent derivatives and the anion. While definitive solution acidities of this and other sulfonimides have not been determined, the gas phase acidities are the highest known (**9**). Even in neutral covalent compounds the delocalization of electron density in sulfonimides is clear as shown by the planar nitrogen in N-(4-methylphenyl)bis((trifluoromethyl)sulfonyl)imide (**10**). The sulfonimide anion is a multidentate ligand with metals giving rise to novel lamellar structures is illustrated for Cs salt of the difunctional acid $CF_3SO_2N(H)SO_2(CF_2)_4SO_2N(H)SO_2CF_3$ (**11**).

The real interest in this class of materials for electrochemical applications arose in part from work on molecular acids for use as aqueous electrolytes in phos-acid fuel cells under an alternative electrolyte program organized by the Gas Research Institute. Early test results with 75% $(CF_3SO_2)_2NH/H_2O$ showed outstanding performance in a typical phos-acid test fuel cell (**12**). This was confirmed by basic electrochemical studies which showed that sulfonimides had outstanding electrochemical properties. The GRI program led to many new sulfonimides and isoelectronic sulfones and the important discovery that such compounds had a remarkable effect as an additive to 85% phosphoric acid electrolyte in a phos-acid fuel cell (**13**). This discovery led to the desire to capture this enhanced fuel cell performance over long-term operation by incorporating these acid functions into fluoropolymers. Thus we began a program in 1989 to make fluorinated ionomers containing the sulfonimide and sulfone functions.

The preparation of polymers of course requires polymerizable monomers and we set out to develop a vinyl ether monomer containing the sulfonimide function (**14**). This was not an easy

task but it was ultimately reduced to practice. The major question was whether a water soluble monomer such as **1** (in **14**) would copolymerize with TFE. There was essentially no precedent for this in the literature. Fortunately **1** could be easily copolymerized with TFE by aqueous emulsion polymerization techniques using persulfate/bisulfite redox initiation (**15**). Similarly, we developed other novel monomers such as **2** (in **16**), which also underwent facile copolymerizations with TFE. From **2** one can appreciate the versatility of the sulfonimide function in enabling a fascinating variation of side chain structure in perfluorinated ionomers.

The copolymers of monomer **1** (polymer **A**) are well characterized as illustrated by its readily assignable ^{19}F NMR as shown in (**17**). The thermal stability of these polymers is outstanding as shown by TGA (**18**). For comparison a sample of Nafion® 117 is displayed, where one sees decomposition beginning at ca. 150°, compared to ca. 400°C for the sulfonimide. This is arguably the highest thermal stability for any known ionomer. The TGA of the sulfonimide polymer **A** in membrane form under various treatments is compared with the bulk polymer in (**19**). The degree of control in producing a completely random copolymer is illustrated by DSC (**20**) and TGA (**21**). In this case 94% of the polymer dissolved. The fraction that did not dissolve clearly contains some functionality but is rich in TFE. Our opinion is that the overall properties of the polymers would be improved if the polymerization can be more carefully controlled to eliminate the blocks of TFE.

The proton conductivity of polymer **A** is illustrated in (**22**). In general for comparable equivalent weights, the conductivity of **A** is higher than Nafion®. At elevated temperature according to our measurements under identical conditions polymer **A** clearly maintains a higher conductivity with increasing temperature at a fixed water pressure (**23**). The measurement of the conductivity of polymer **A** and other copolymers at higher temperatures is under active investigation.

The effect of the TFE blockiness on the properties of polymer **A** is illustrated in (**24**). A polymer membrane prepared from solutions of **A** clearly exhibits a higher conductivity with the

TFE-rich fraction removed. Although it is certainly true the dissolved polymer will have a somewhat lower equivalent weight and that this fact may increase the conductivity, we speculate that the effect is more complex than this. In morphologically complex materials such as these fluorinated ionomers, there are clearly many factors to consider in accessing the material performance.

Some insight into the microstructure of these ionomers has been obtained by time resolved fluorescence spectroscopy with various fluorescent probes. Ethidium bromide (**25**) is a sensitive probe for polarity and is a measure of the local environment of water in polymers. Comparisons of Nafion®, Dow PFSA and polymer **A** with comparable equivalent weights are illustrated in (**26**). In general the three types of ionomers are quite comparable with two distinctive regions in the ion clusters, different from bulk water as summarized in (**27**).

Conclusions

Sulfonimide polymers appear to be promising candidates for PEMs in fuel cells. Much more research will be required to determine if these polymer materials can solve some of the problems associated with existing PFSA ionomers. We are optimistic that this will be the case and we are hopeful that funding of our research on these novel materials will continue.

Acknowledgement

Funding for this work has been generously supplied by the Gas Research Institute, ARPA, DOD and DOE. Many excellent coworkers contributed to this work over the past 10 years and grateful acknowledgment is made to their untiring efforts. Special acknowledgment is made to Jing-Ji Ma whose experience in China on fluorinated ionomers was invaluable in the early years of this polymer research. Also Dr. Charles W. Martin, formerly of Dow Chemical, provided invaluable assistance in advancing this work. Finally the 3M Co. and Dow Chemical are acknowledged for generous donations of chemicals and equipment.

APPENDIX

High Temperature Functional Fluoropolymers

COPIES OF TRANSPARENCIES 1-27

Darryl D. DesMarteau
Department of Chemistry
Clemson University
Clemson, SC 29634-1905

Chrysler heralds major advance on electric car

By Brian S. Akre
AP AUTO WRITER

DETROIT — Chrysler Corp. Monday announced a major development in the search for a practical, long-range electric car — one that relies on inexpensive, low-grade gasoline instead of batteries.

Yes, a gasoline-powered electric car. What makes it possible is the development of a way to extract hydrogen from gasoline while the car is being driven.

It's called "fuel cell" technology. A fuel cell is a device that produces electricity from a chemical reaction between hydrogen and oxygen. The hangup for automotive use has been how to get and store hydrogen efficiently and inexpensively.

"We believe hydrogen needs to be processed from gasoline on board vehicles because hydrogen isn't a practical fuel choice today," said Francois Castaing, Chrysler vice president of vehicle engineering. "Simply put, there are not any filling stations supplying it to a mass market."

In Chrysler's system, a platinum catalyst and an on-board fuel processor break down the gasoline into hydrogen and water. The hydrogen is used by a series of fuel cells to produce enough electricity to power the car and its equipment.

Chrysler says the development will cut up to 10 years from the time it will take to create a practical prototype of a fuel-cell car. The No. 3 domestic automaker says it hopes to have a prototype as soon as 2005.

The car is expected to be at least 50 percent more fuel-efficient and 90 percent cleaner than a modern, gasoline-powered internal combustion engine, Chrysler advanced technologies specialist Christopher E. Borroni-Bird told a news conference at the North American International Auto Show.

"People will still refuel their vehicles the same way they always have, and the gas tanks on their vehicles may actually be smaller than they are today," Castaing said.

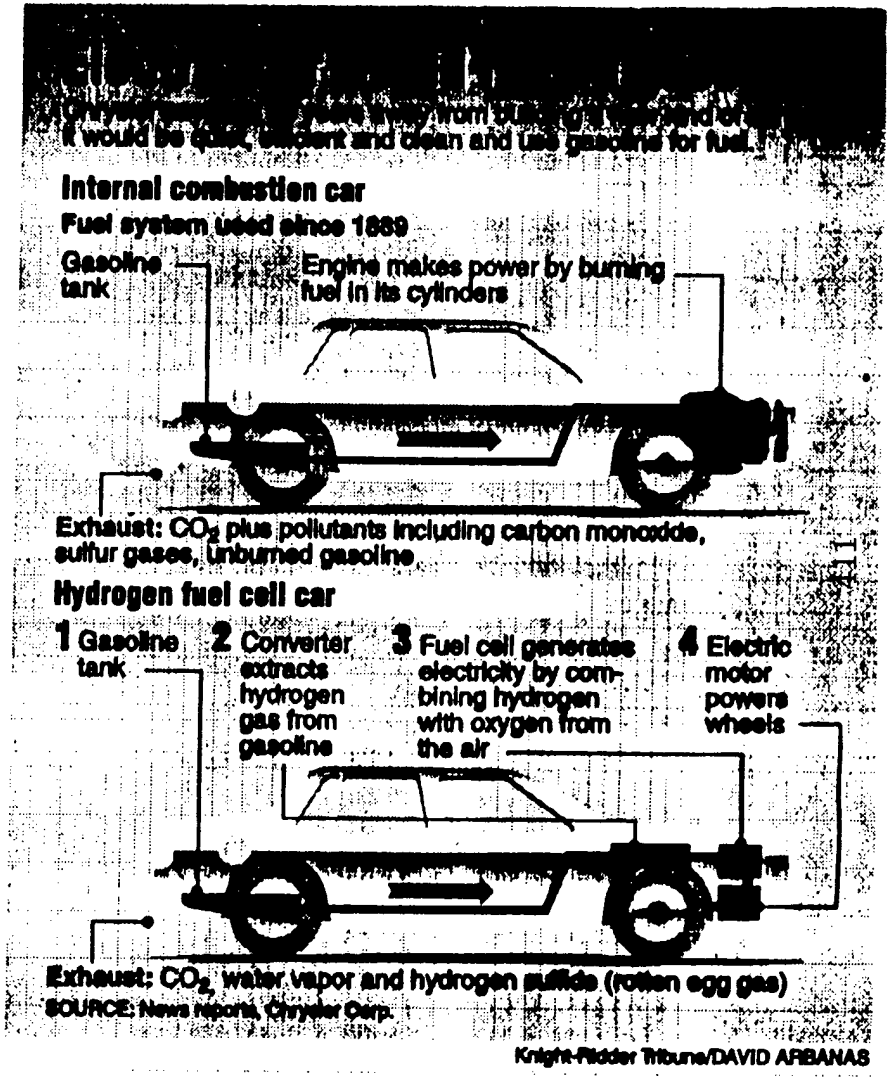

Knight-Ridder Tribune/DAVID ARBANAS

PEM Fuel Cell

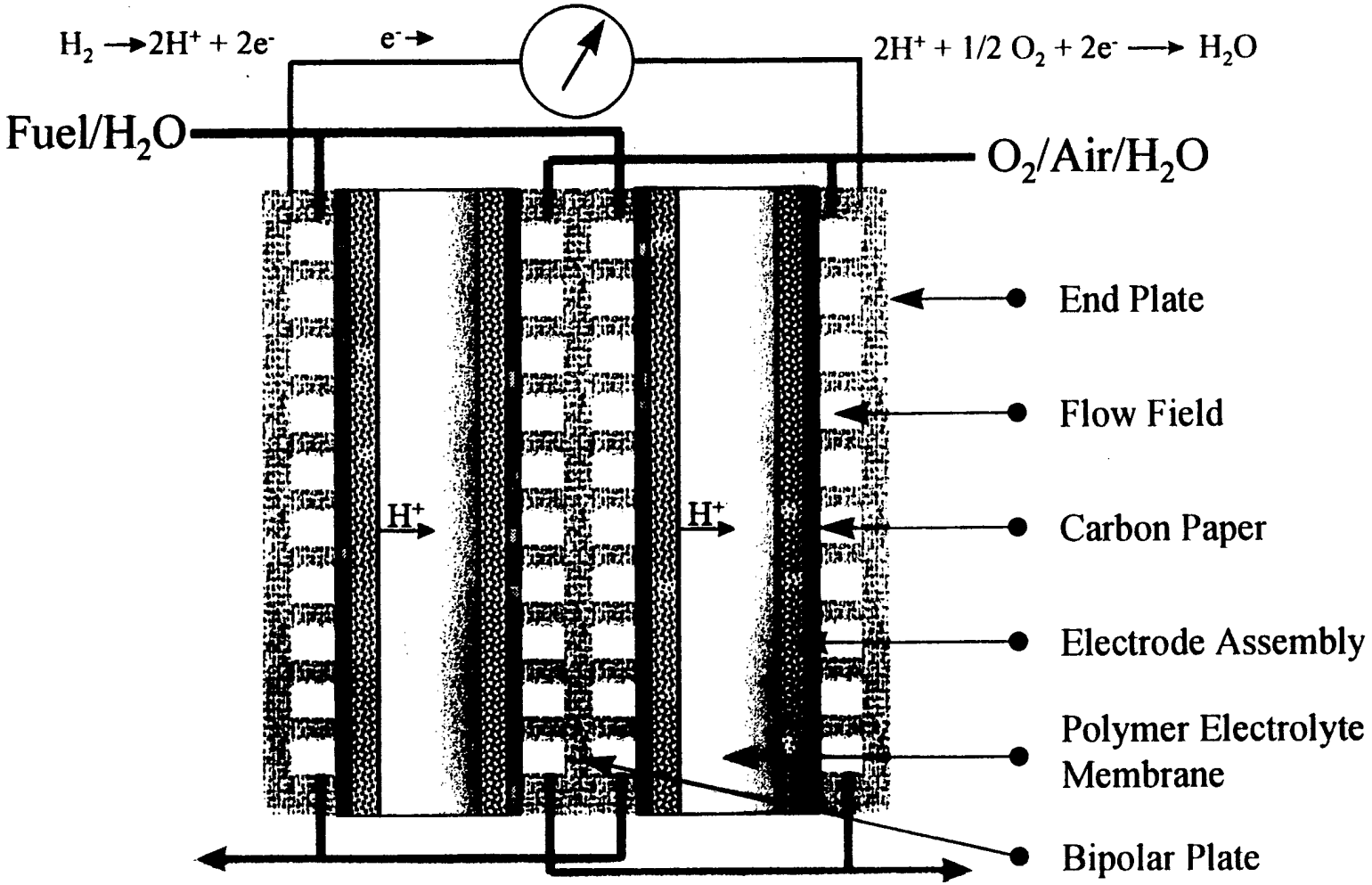

Some Issues

- Is there a perfluorinated ionomer capable of operating above 150°C in a PEM fuel cell?
- Sulfonic acid based ionomers begin to undergo thermal decomposition at ~150°C.
- Proton conductivity of sulfonic acid ionomers decreases rapidly above 100°C **without** pressurization to maintain hydration.
- Polymer structure for a given acid function, strongly influences polymer performance.

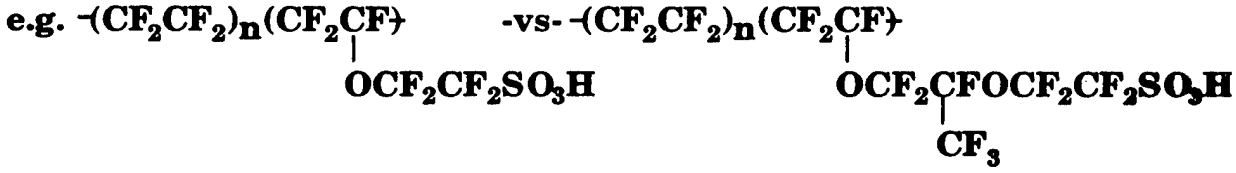

- Lower equivalent weights improve performance but lead to poor mechanical properties.

Some Possible Solutions

- **New acid functions:** $M-SO_2\overset{H}{N}SO_2R_f$;

  $M-SO_2\overset{H}{N}SO_2(CF_2)_xSO_2\overset{H}{N}R_f$; $M\text{-}PO(OH)_2$;

  $M\text{-}SO_2CH_2SO_2R_f$; other (?).

- **Crosslinking to improve mechanical properties at low equivalent weights.**

- **Composite materials, e.g. silica filled ionomers.**

- **Hybrid materials:** $M-SO_2\overset{H}{N}SO_2(CF_2)_xPO(OH)_2$;

  $M\text{-}SO_2NR_2H^+PO_4H_2^-$; 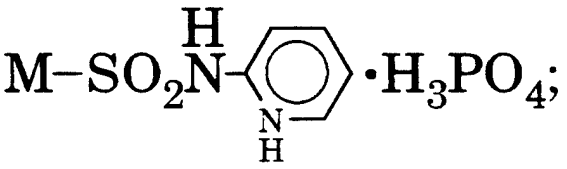

  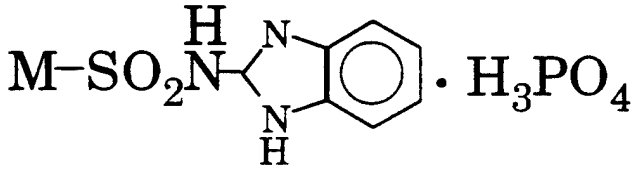

M=polymerizable fluorocarbon function such as $CF_2=\underset{\displaystyle OCF_2CF_2}{\underset{|}{CF}}$, $CF_2=\underset{\displaystyle OCF_2\underset{\displaystyle CF_3}{\underset{|}{C}}FOCF_2CF_2}{\underset{|}{CF}}$ *, etc.*

Clemson University Research in Fluorinated Ionomers

Program

- **Polymer synthesis, characterization and membrane fabrication** - D. DesMarteau & C. Martin
- **Electrochemical evaluation** - S. Creager
- **Structural characterization**

  X-Ray, WAXS, SAXS, SANS - W. T. Pennington

  Time-resolved and steady-state fluorescence spectroscopy - Y.-P. Sun

Goals

- **Improved PEMs for fuel cells and other applications**
- **Improved understanding of structure and structure-property-function in fluorinated ionomers**

Polymers Under Development

Copolymers of tetrafluoroethylene and the novel monomers:

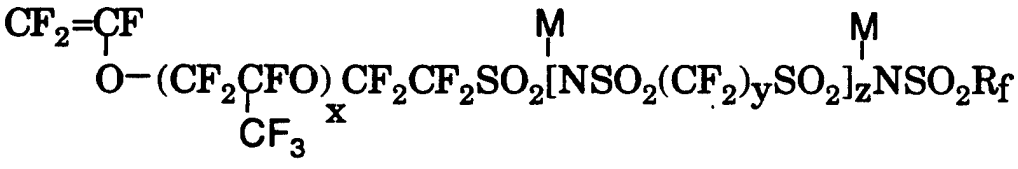

x=0,1; y=2,4,6,8, other; z=0,1,2
M=alkali metal, other
$R_f=C_nF_{2n+1}$

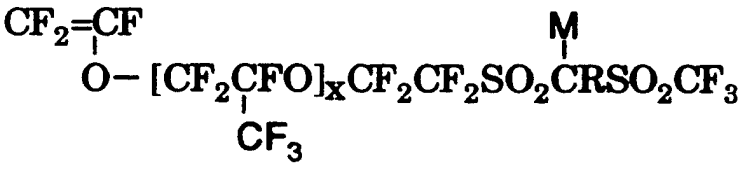

R=H,akyl,other

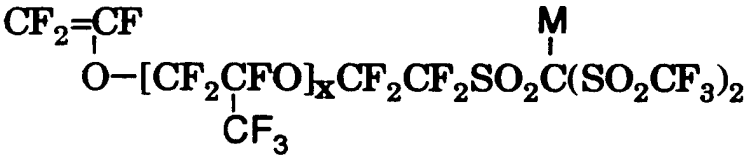

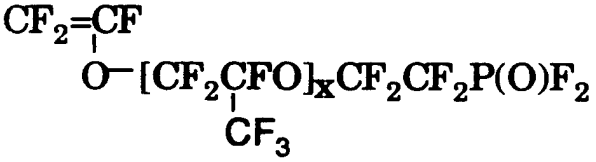

Some Relevant Information

- Phosphonic acid polymers

$$-(CF_2CF_2)_n(CF_2CF)-$$
$$\quad\quad\quad

A Brief Overview of Sulfonimide Ionomers

- Background
- Synthesis of monomers
- Copolymerizations with TFE
- Polymer Properties
- Membrane Properties

ΔGacid Values (k cal/mol) Derived from Gas Phase Proton-Transfer Equilibria

Acid	ΔGacid
CF_3CO_2H	316.6
CH_3SO_3H	315.0
$(CF_3CO)_2NH$	307.5
HI	309.2
$(CF_3SO_2)_2CH_2$	301.5
FSO_3H	299.8
CF_3SO_3H	299.5
$CF_3CONHSO_2C_4F_9$	296.9
$C_3F_7CONHSO_2C_4F_9$	294.3
$(CF_3SO_2)_2NH$	291.8
$CF_3SO_2NHSO_2C_3F_7$	290.3
$(C_2F_5SO_2)_2NH$	289.4
$(CF_3SO_2)_3CH$	289.0
$CF_3SO_2NHSO_2C_6F_{13}$	286.5
$(C_4F_9SO_2)_2NH$	284.1 (curent record holder)

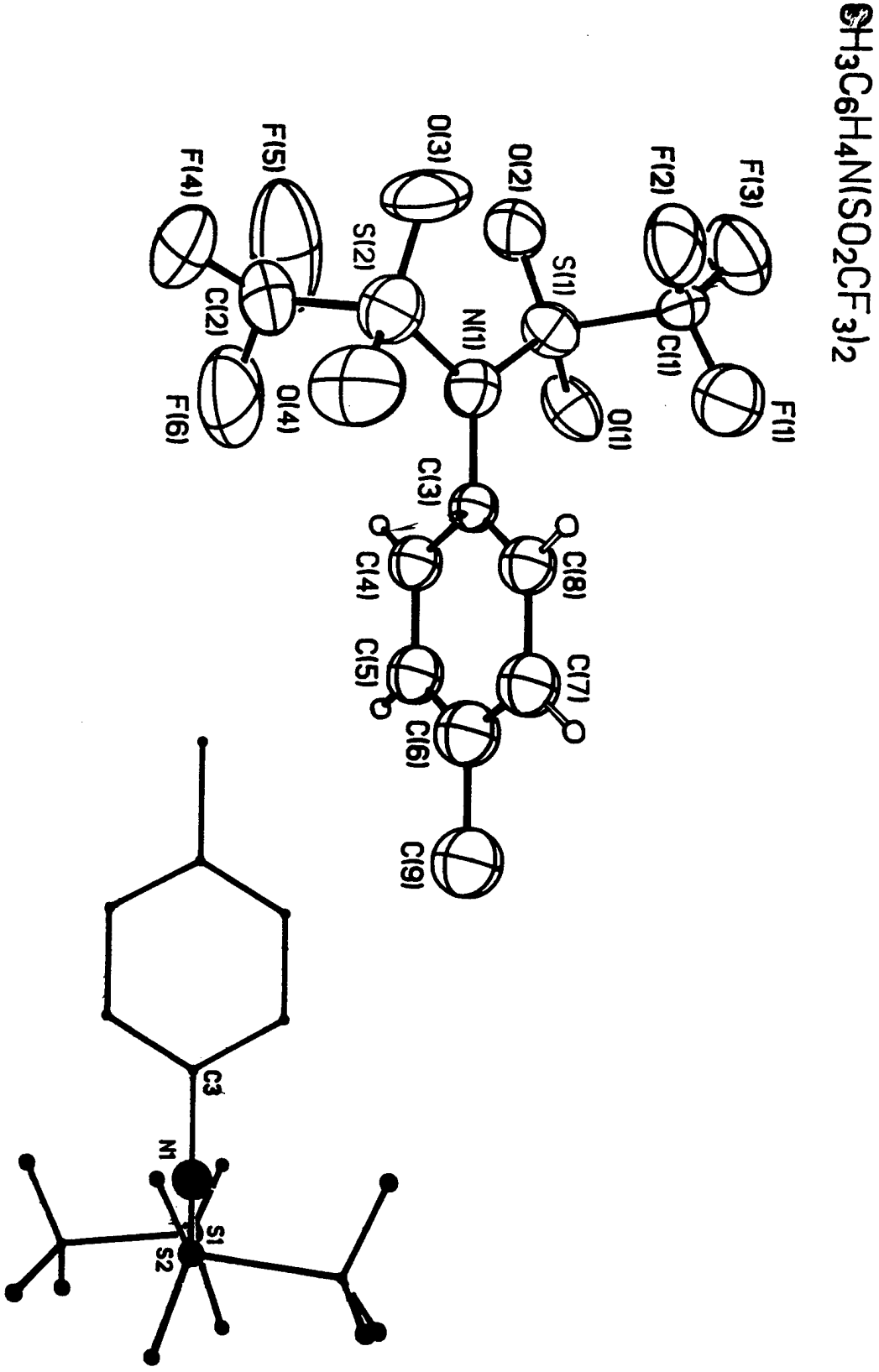
CH3C6H4N(SO2CF3)2
F(3)
F(2)
F(1)
O(3)
O(2)
F(5)
F(4)
S(2)
S(1)
C(2)
C(1)
N(1)
F(6)
O(4)
O(1)
C(3)
C(4)
C(8)
C(5)
C(7)
C(6)
C(9)
C3
M1
S1
S2

10

Figure 5

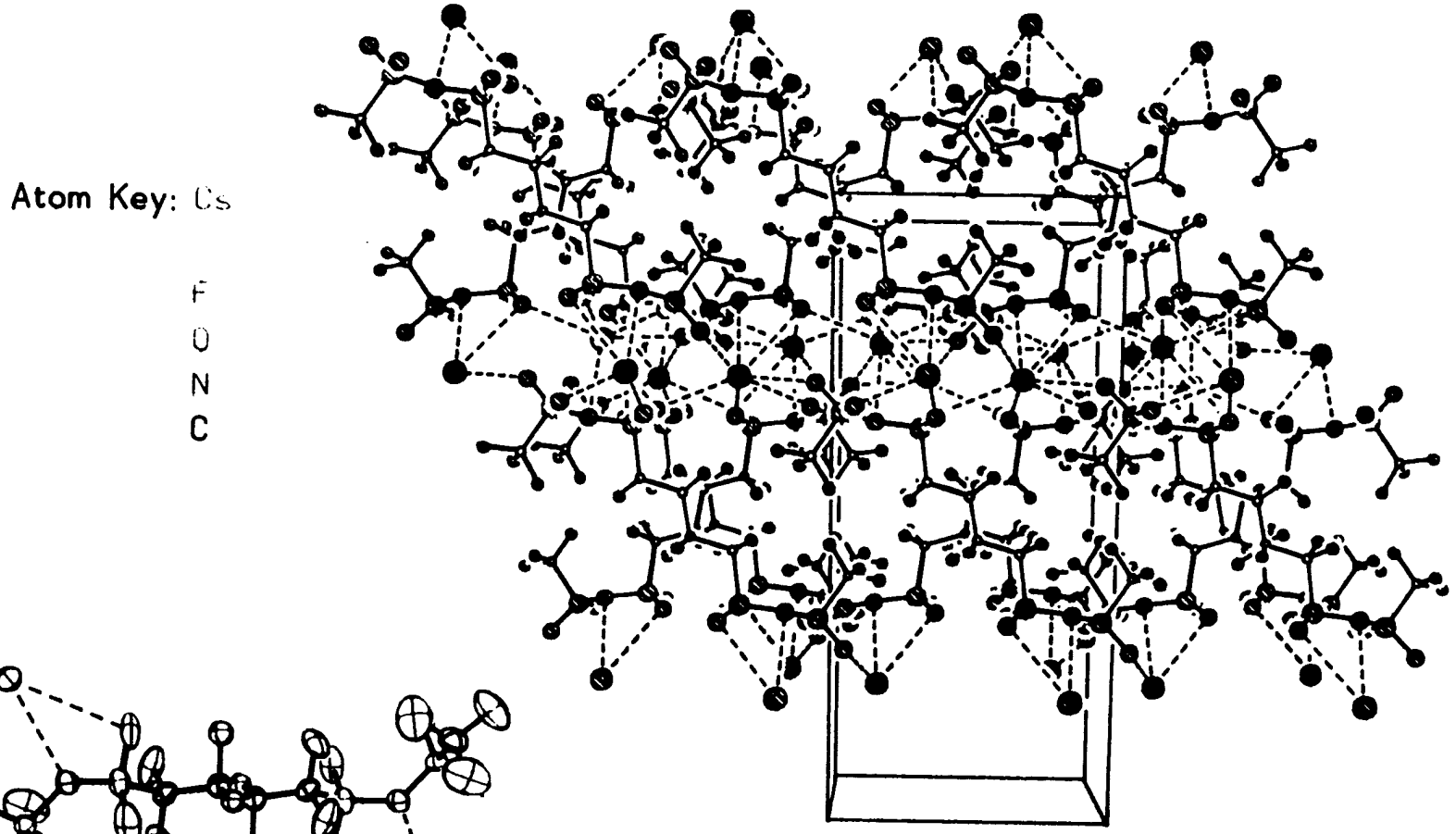

$Cs_2[CF_2CF_2SO_2NSO_2CF_3]_2$

Packing view parallel
to the c-axis

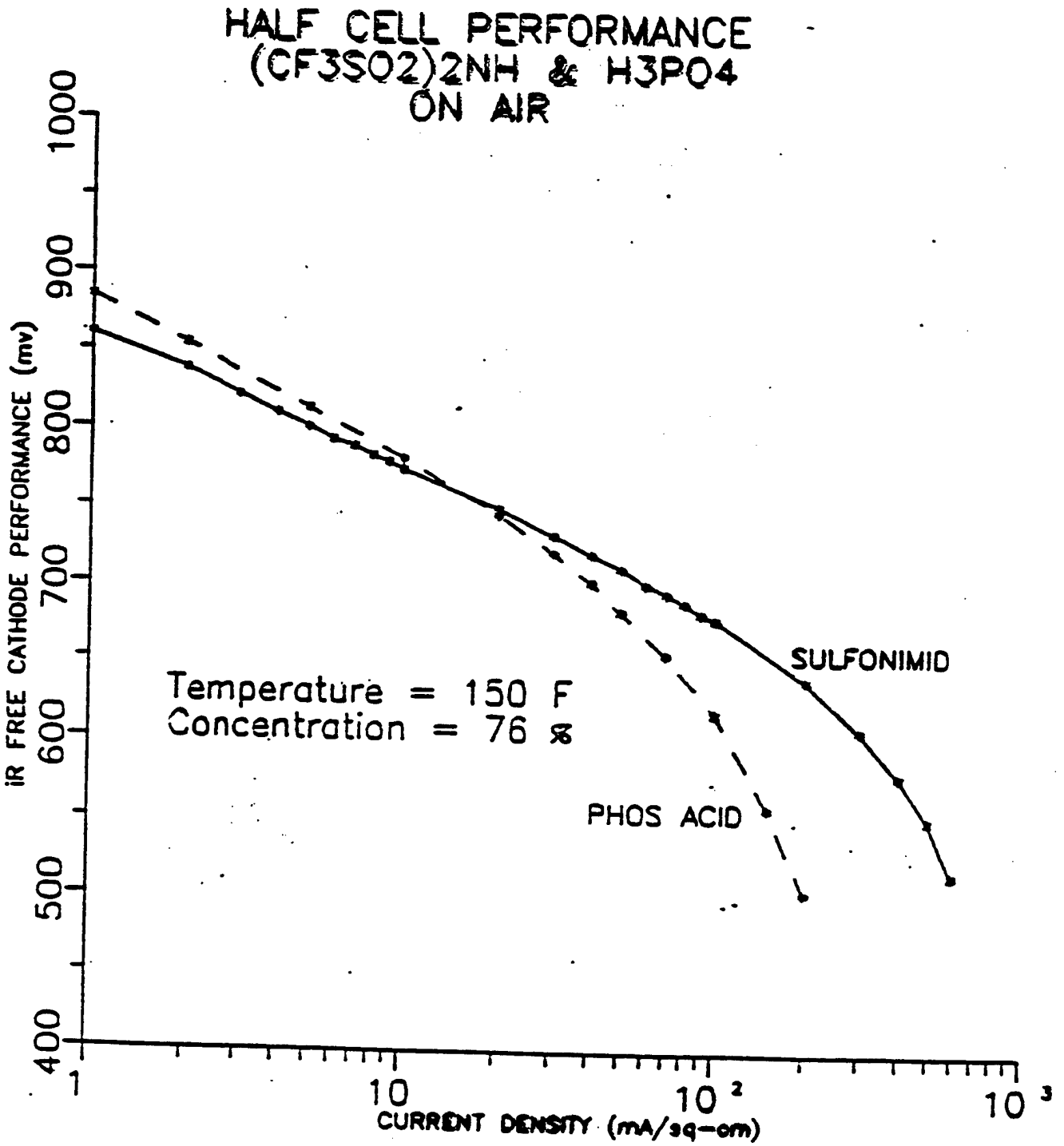

Figure 4

Courtesy: D. Maricle, International Fuel Cells

SULFONYL CARBON ACID ADDITIVE
$(CF_3SO_2CH_2SO_2CF_2CF_{2-})_2$
O_2 PERFORMANCE

- Tested as <0.1% solution at 350°F in 2" x 2" subscale cell
- Showed 43 mV performance enhancement over similar phosphoric acid cell
- High activity from such a low level of additive implies concentration of material on catalyst surface
- Additive approach attractive from cost perspective

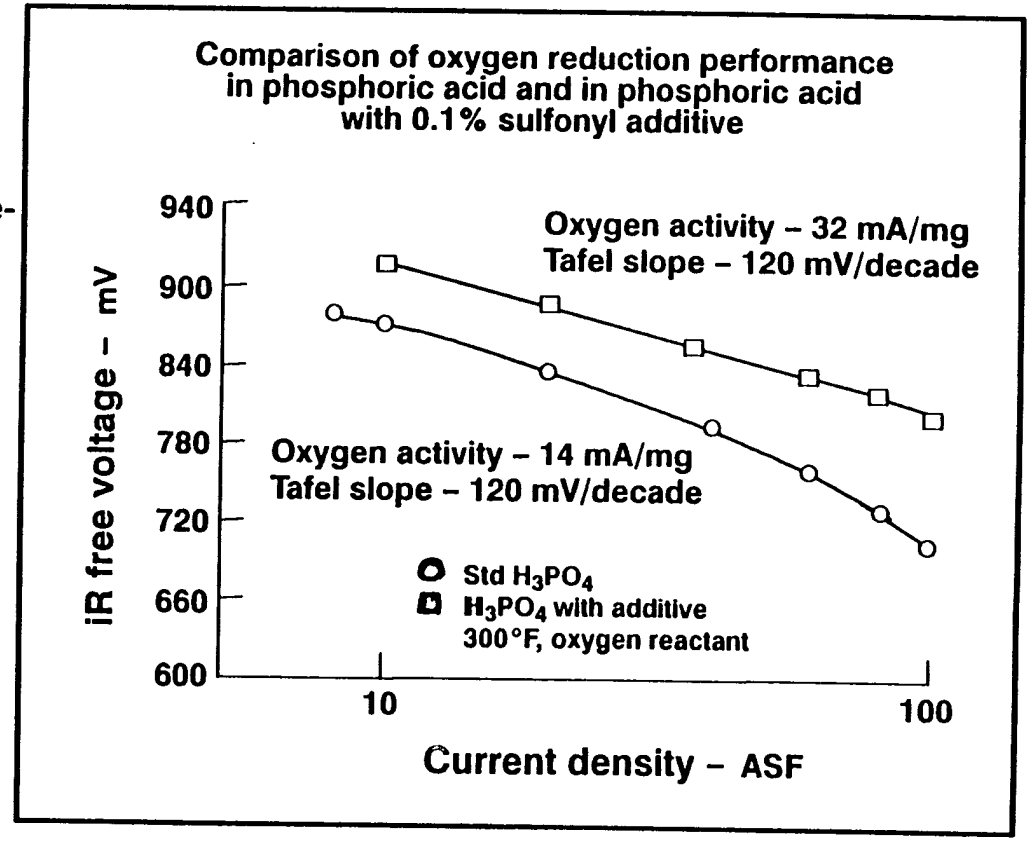

Synthesis of a Sulfonimide Monomer 1

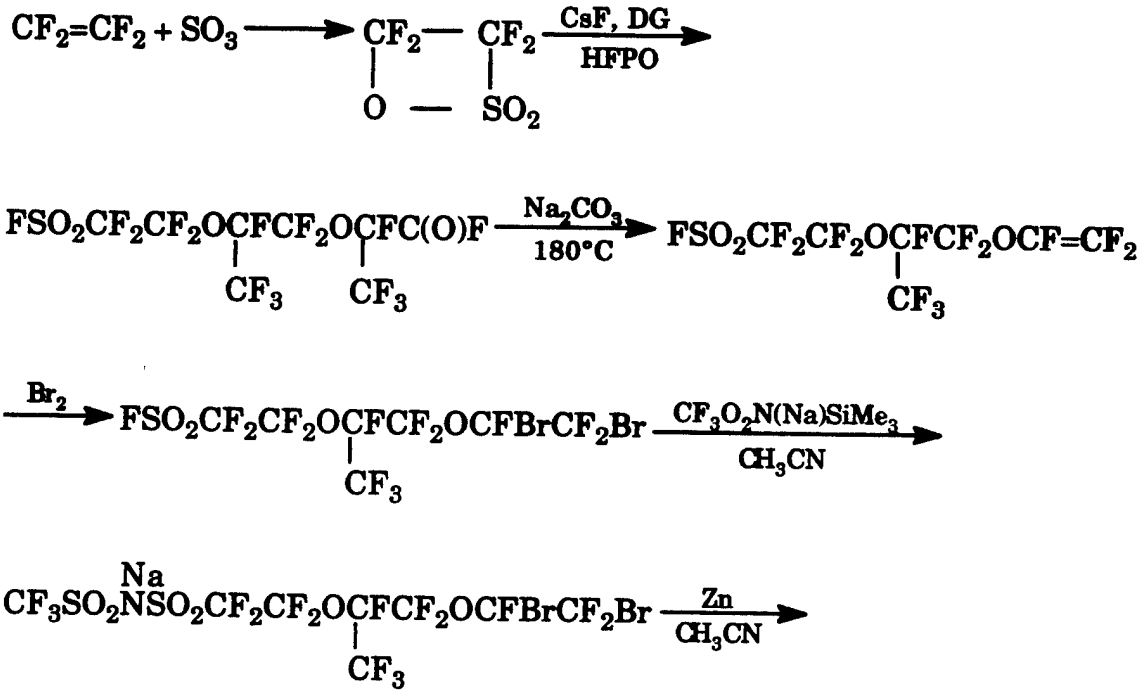

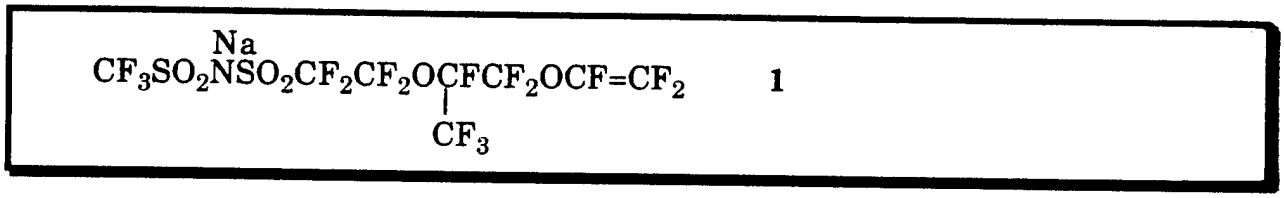

A Typical Small Scale Copolymerization

(450mL magnetically stirred Parr 316 ss autoclave)

Trial	1	2
Monomer in the autoclave (g)	2.00	2.00
$C_7F_{15}COONH_4$ (g)	2.00	2.00
$Na_2HPO_4 \cdot 7H_2O$ (g)	2.80	2.80
NaH_2PO_4 (g)	1.40	1.40
$(NH_4)_2S_2O_8$ (g)	0.30	0.30
$NaHSO_3$ (g)	0.27	0.27
H_2O (mL)	260	260
Pressure of TFE (psi)	150-5	150-5
Stirring speed (rpm)	650	650
Temperature (°C)	10±1	10±1
Reaction time (hour)	6.0	6.0
Total TFE drop (psi)	24	24
Average TFE drop rate (psi/hour)	4.0	4.0
Monomer addition rate through the metering pump (g/hour)	0.30*	0.30**
Added monomer (g)	1.8	1.8
Estimated monomer consumer (g)	1.6	1.8
Copolymer (g)	3.30	3.67
IEC (meq H/g)	0.81	0.83
EW	1235	1205

*The added monomer was not buffered with Na_2HPO_4/NaH_2PO_4.
**The added monomer was buffered with Na_2HPO_4/NaH_2PO_4.

Synthesis of a Difunctional Sulfonimide Monomer 2

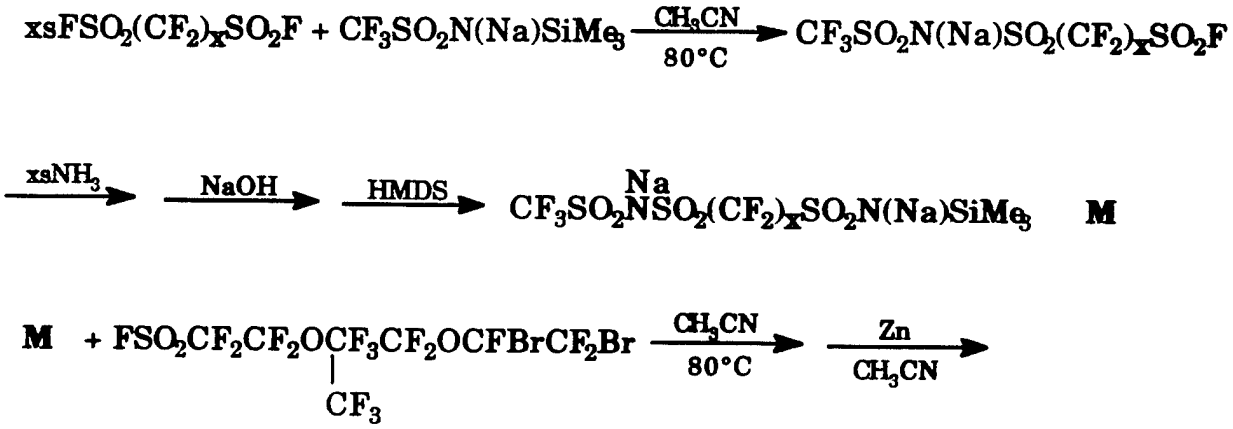

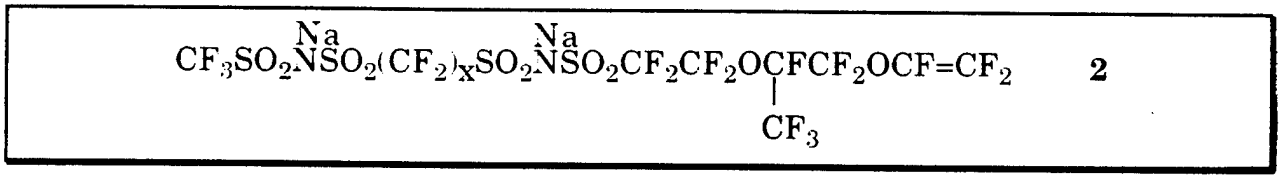

dissolution in H_2O/MeOH/i-PrOH at 275°C

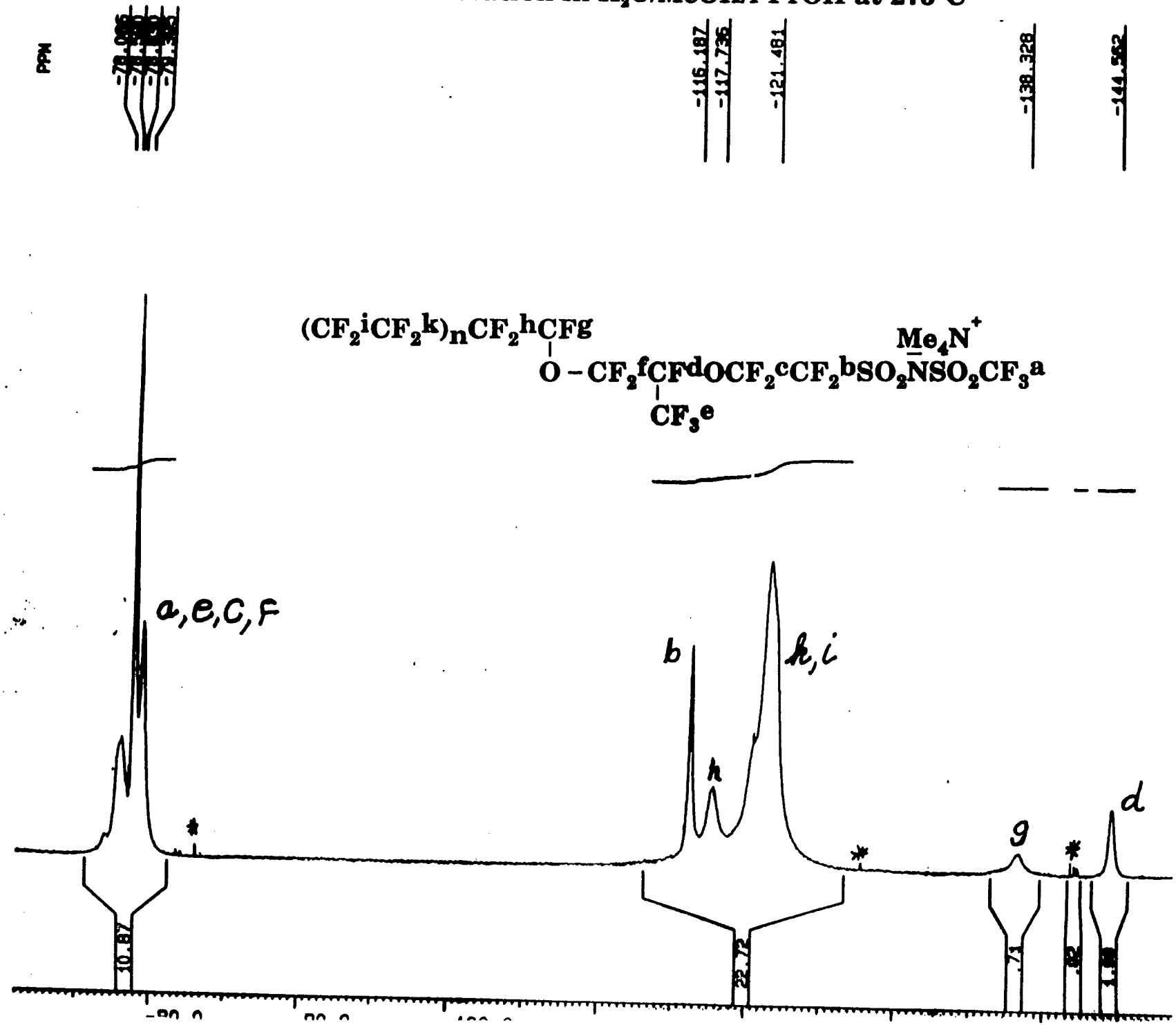

17

DATE 12-12-96

SF	188.313
SY	88.310000
O1	-8800.000
SI	65536
TD	65536
SW	88800.000
HZ/PT	1.907
PW	1.0
RD	2.000
AQ	.884
RG	100
NS	16380
TE	298
FW	78200
O2	3200.000
DP	63L PO
LB	.200
GB	0.0
CX	22.00
CY	10.000
F1	-71.032
F2	-148.788

Curve 1: TGA
File info: TU2112p Tue Jan 28 17:05:22 1997
Sample Weight: 3.636 mg
TFE/CF2=CFOCF2CF(CF3)OC2F4SO2NHSO2CF3

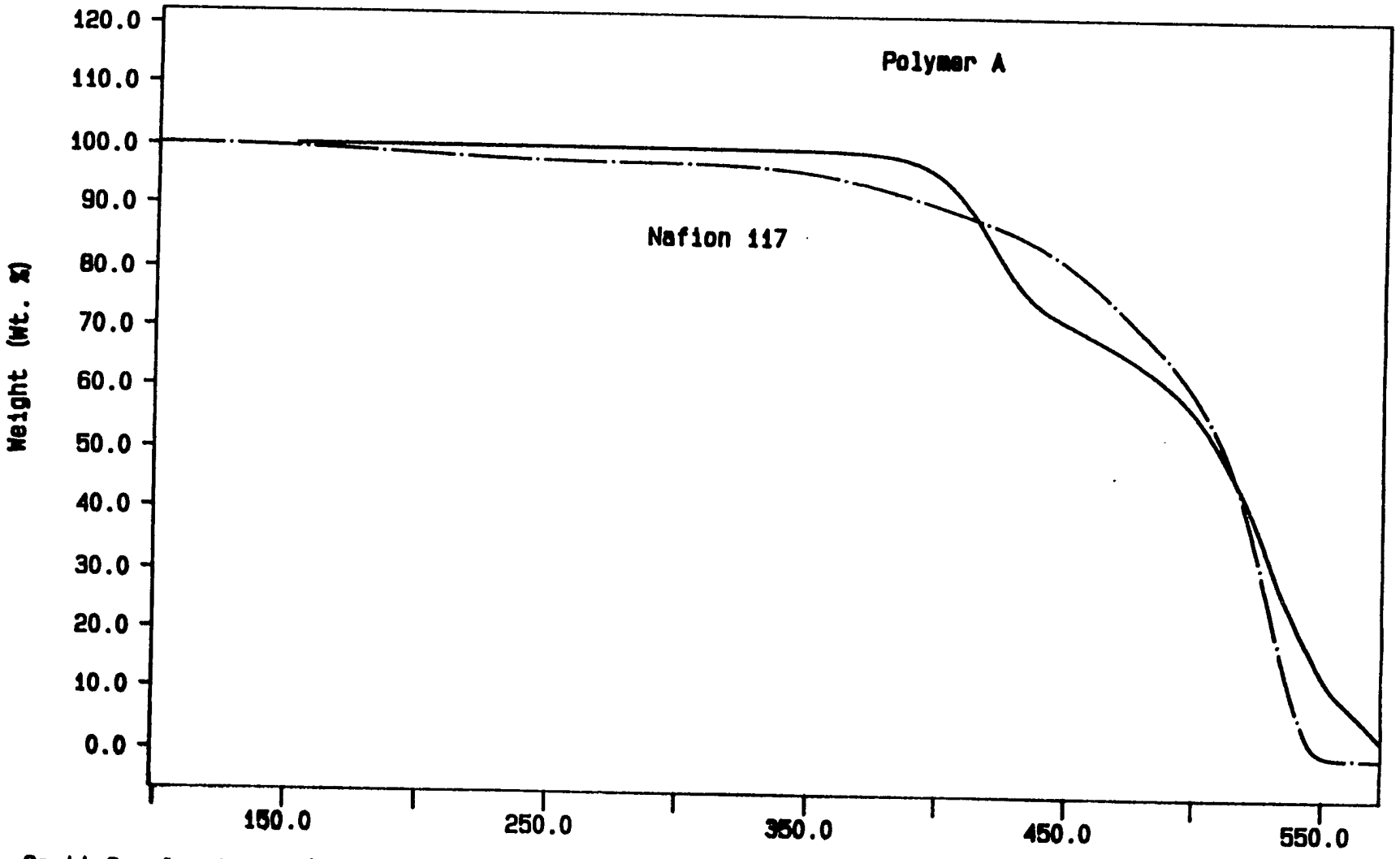

Conti.Copoly.at 10 C/IEC=0.83meqH/g

TEMP1: 150.0 C TIME1: 0.0 min RATE1: 10.0 C/min
TEMP2: 700.0 C

TU
PERKIN-ELMER
7 Series Thermal Analysis System
Thu Apr 23 09:19:49 1998

Curve 1: TGA
File info: TU2112p Tue Jan 28 17:05:22 1997
Sample Weight: 3.636 mg
TFE/CF2=CFOCF2CF(CF3)OC2F4SO2NHSO2CF3

TGA Polymer A(H⁺), IEC = 0.83

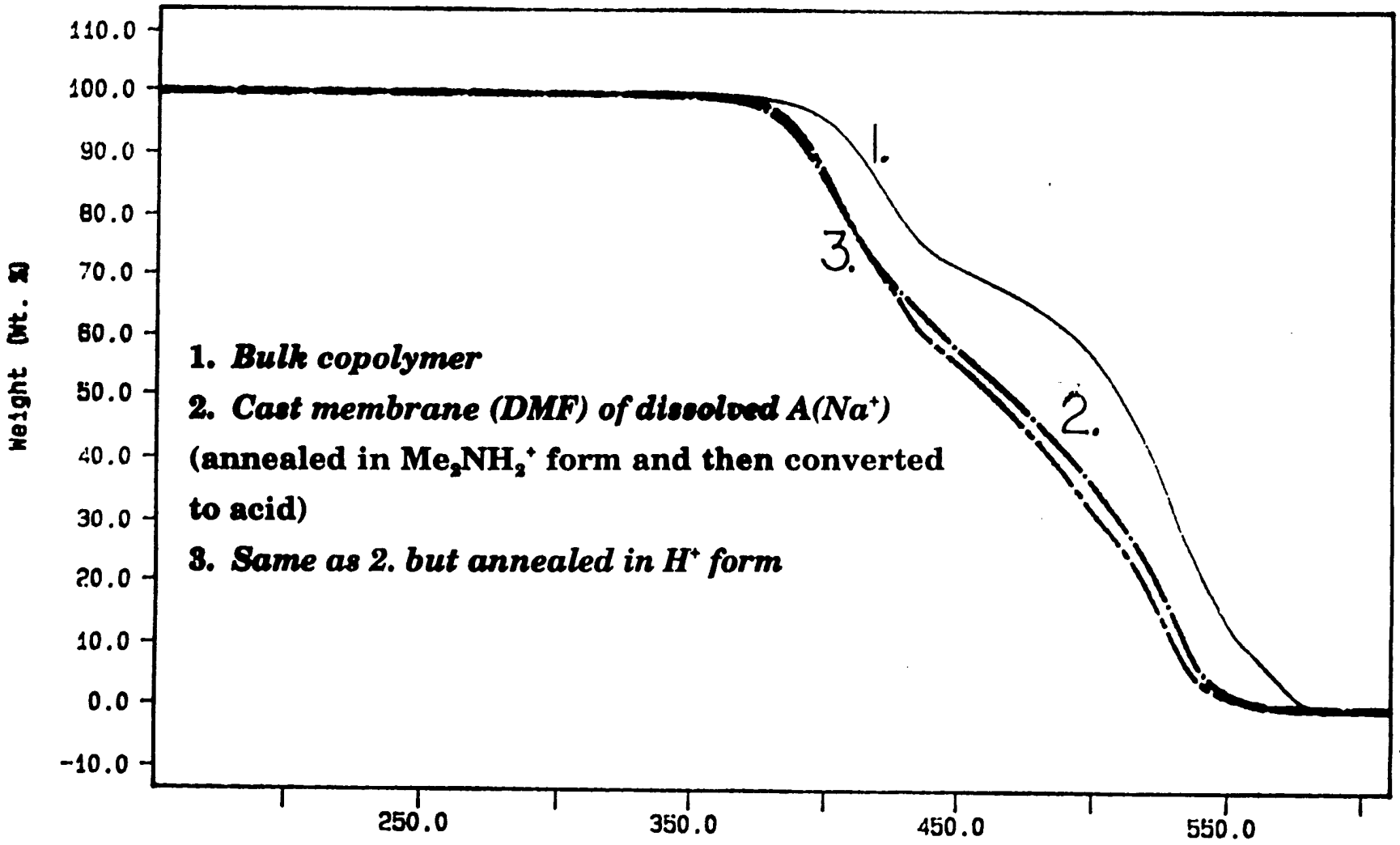

Conti.Copoly.at 10 C/IEC=0.83meqH/g
TEMP1: 150.0 C TIME1: 0.0 min RATE1: 10.0 C/min
TEMP2: 750.0 C

TU
PERKIN-ELMER
7 Series Thermal Analysis System
Thu Jun 19 09:50:42 1997

19

Curve 1: DSC
File info: TU2118-1 Tue Feb 18 12:50:45 1997
Sample Weight: 15.400 mg
TFE/CF2=CFOCF2CF(CF3)OC2F4SO2NHSO2CF3

DSC of Polymer A, IEC = 0.83

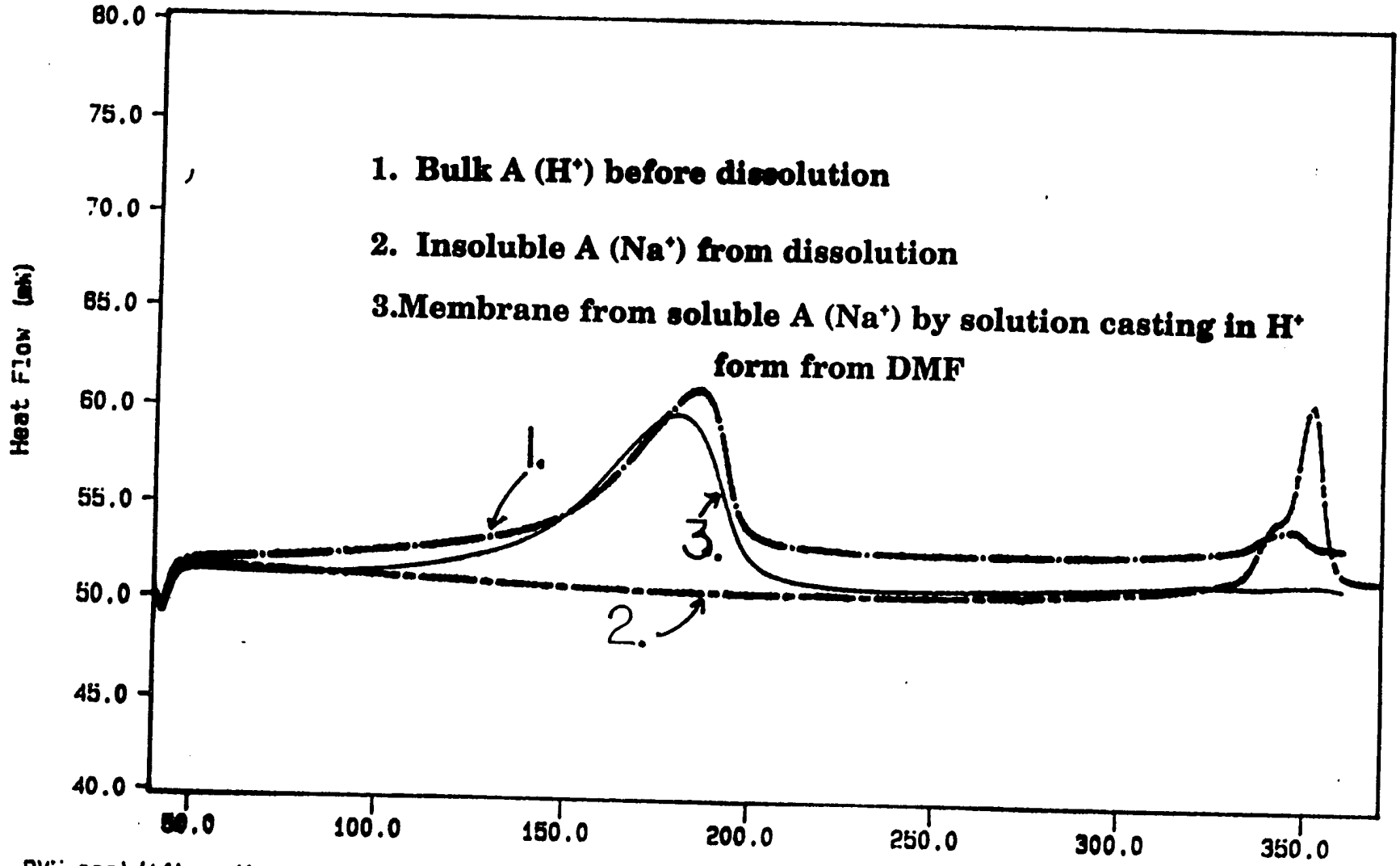

DMF cast/After dissolution/IEC=0.83
TEMP1: 48.8 C TIME1: 0.0 min RATE1: 10.0 C/min
TEMP2: 350.0 C
TU
PERKIN-ELMER
7 Series Thermal Analysis System
Thu Jun 19 08:45:55 2007

20

Curve 1: TGA
File info: TU2112Na Wed Feb 12 16:39:28 1997
Sample Weight: 3.523 mg
TFE/CF2=CFOCF2CF(CF3)OC2F4SO2NHSO2CF3

TGA of Polymer A, IEC = 0.83

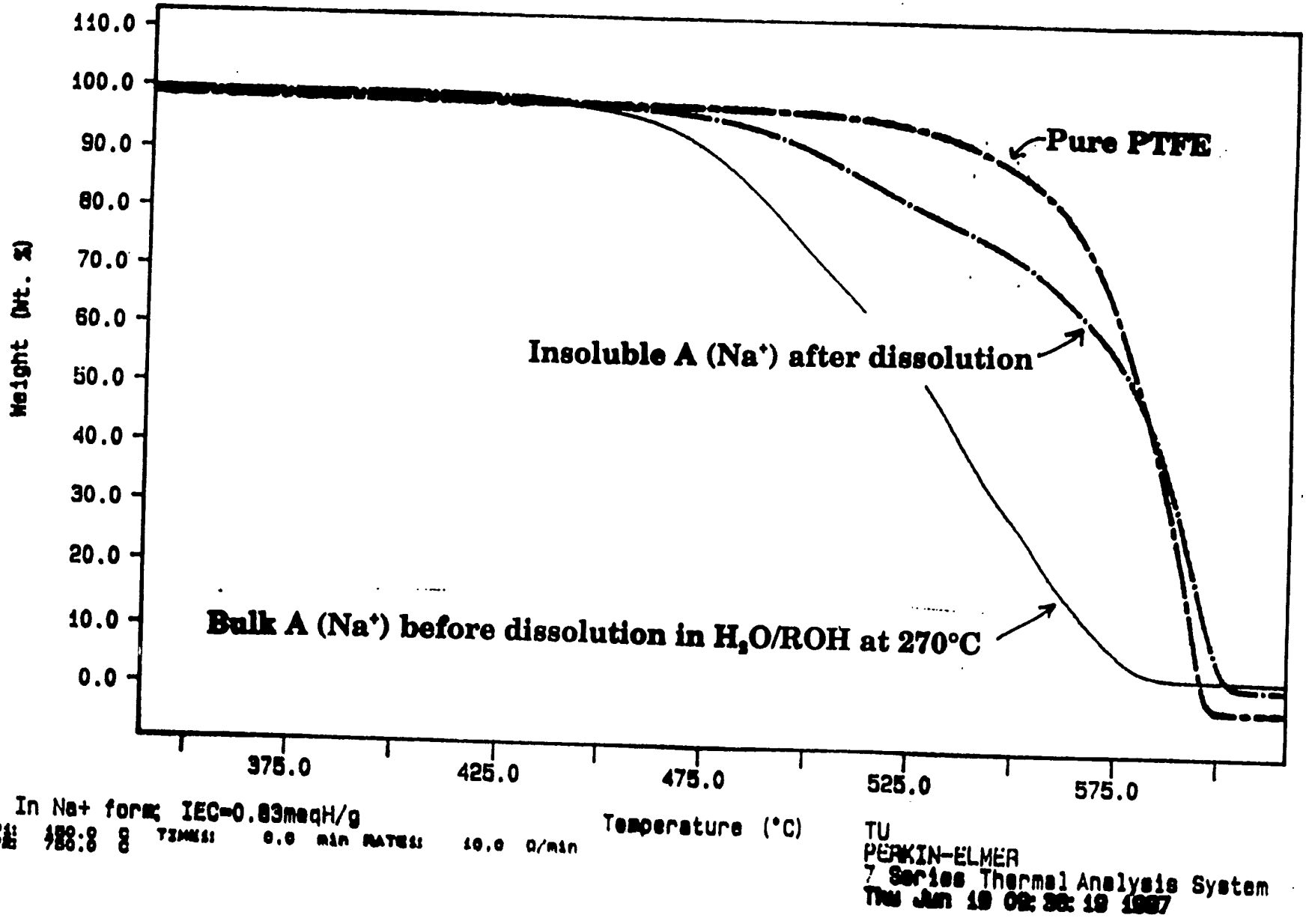

In Na+ form; IEC=0.83meqH/g

TEMP1: 150.0 C TIME1: 0.0 min RATE1: 10.0 C/min
TEMP2: 750.0 C

TU
PERKIN-ELMER
7 Series Thermal Analysis System
Thu Jun 19 08:38:19 1997

Conductivity vs. humidity at room temperature

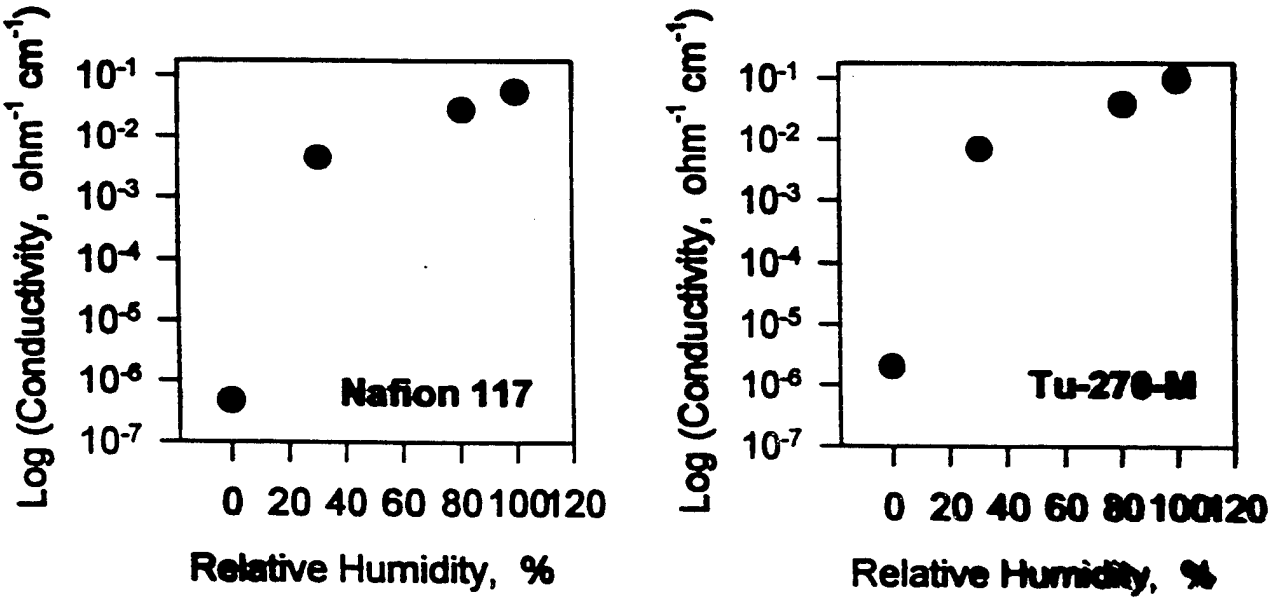

Relative humidity	Nafion 117	M-DP-5	M-DP-8	Tu-270-M
100 %	5.5×10^{-2}	1.0×10^{-1}	7.5×10^{-2}	9.6×10^{-2}
81%	2.8×10^{-2}	5.7×10^{-2}	4.1×10^{-2}	3.8×10^{-2}
31%	4.4×10^{-3}	8.9×10^{-3}	4.0×10^{-4}	6.9×10^{-3}
0 %	4.7×10^{-7}	5.7×10^{-6}	8.8×10^{-6}	2.1×10^{-6}

Conductivity vs. temperature at fixed water partial pressure (150 torr)

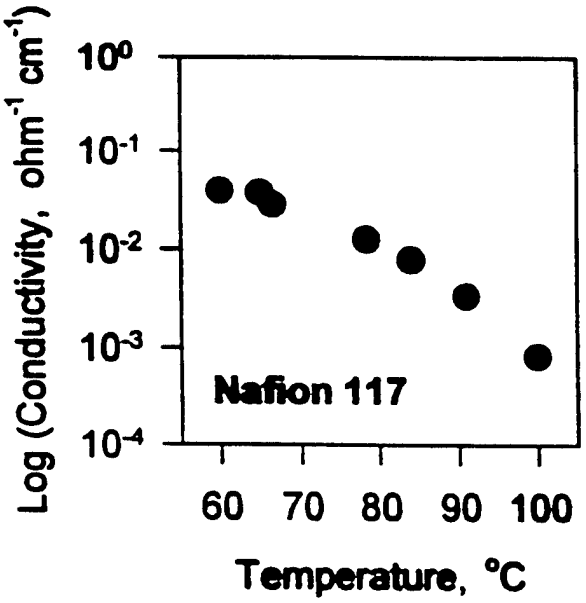

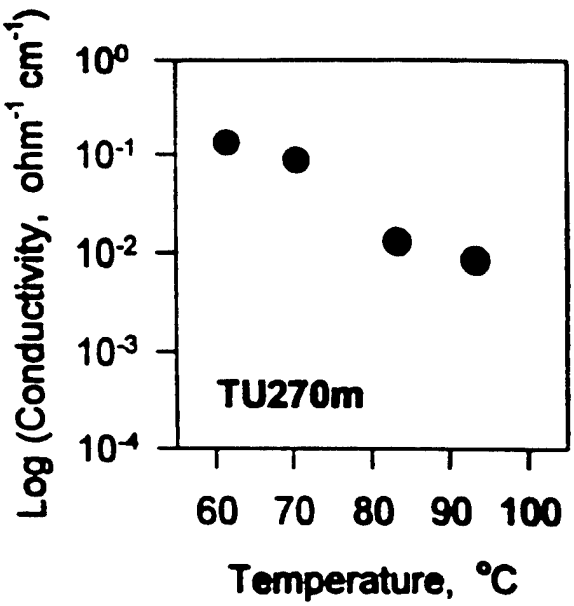

Nafion 117		Tu-270-M	
Temp. (°C)	Conductivity (ohm^{-1} cm^{-1})	Temp. (°C)	Conductivity (ohm^{-1} cm^{-1})
60	3.9×10^{-2}	62	1.3×10^{-1}
65	3.7×10^{-2}	71	8.8×10^{-2}
79	1.3×10^{-2}		
84	7.9×10^{-3}	83	1.3×10^{-2}
91	3.4×10^{-3}	93	8.5×10^{-3}
100	8.3×10^{-4}		

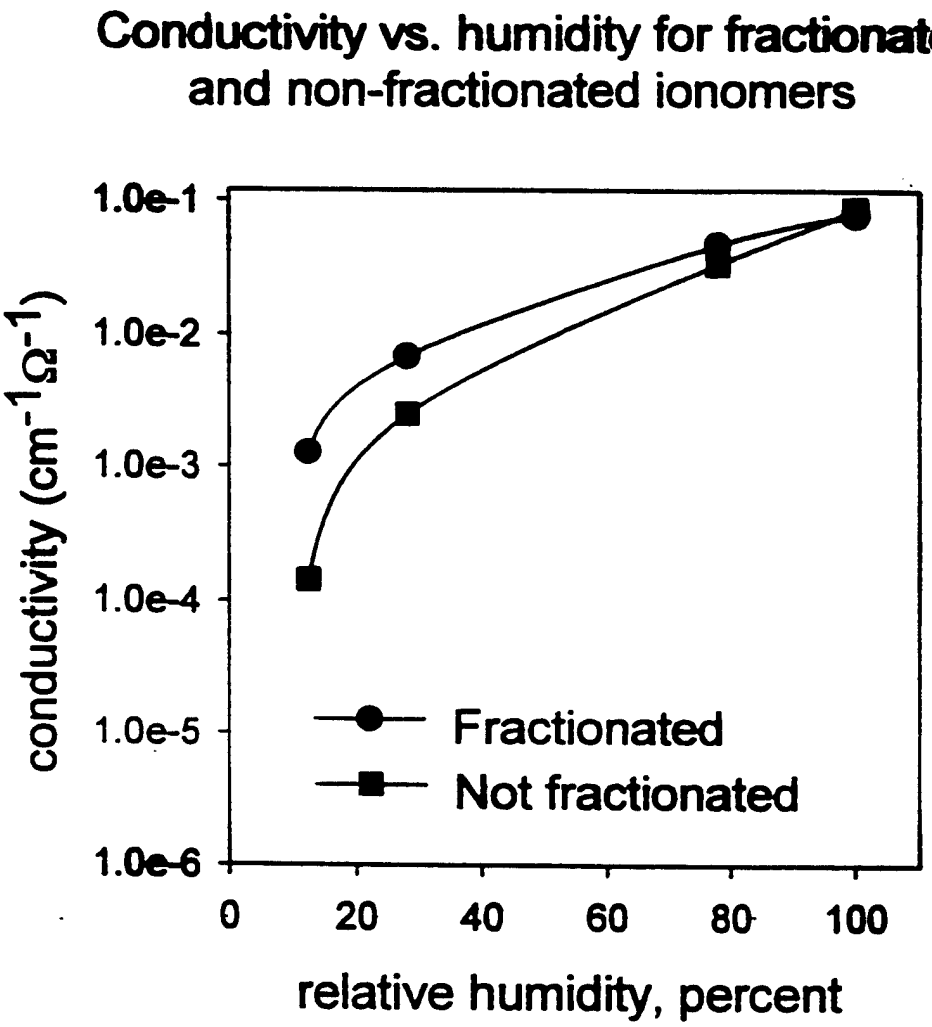
Conductivity vs. humidity for fractionated and non-fractionated ionomers
1.0e-1
1.0e-2
1.0e-3
1.0e-4
1.0e-5
1.0e-6
conductivity ($cm^{-1}\Omega^{-1}$)
0
20
40
60
80
100
relative humidity, percent
Fractionated
Not fractionated

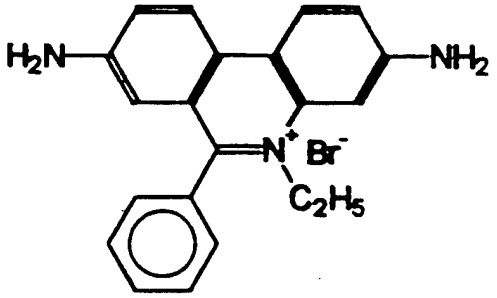

TABLE II: Comparison of the Ethidium Bromide Fluorescence Lifetimes, τ_f, and Intensity Ratios in Various Media Relative to H_2O.[a]

Medium	$\tau_f/\tau_f(H_2O)$	$I_f/I_f(H_2O)$
Me_2SO	2.8	2.7
D_2O	3.5	3.1
Ethanol	3.8	4.3
Acetone	5.1	5.0
10^{-4} M DNA/H_2O	12.5	11.2
10^{-5} M tRNA/H_2O	13.7	13.7[b]
10^{-4} M DNA/D_2O	20.8	20.0

[a] Estimated uncertainties, ±10%. [b] Corrected for contribution due to free ethidium bromide.

Olmsted, J., III; Kearns, D. R. *Biochemistry*, **1997**, *16*, 3647.

Luminescence Spectroscopic Probing of Microstructures and Properties of Perfluorinated Polyelectrolyte Membranes

Probe: Ethidium Bromide, Fluorescence Lifetimes

Fluorescence Lifetimes of Ethidium Cation in Ionomer Membranes

Membrane	Lifetime-1 (ns)	Lifetime-2 (ns)
Nafion	3.2	12
Dow	2.6	12.5
Sulfonimide	4.6	13.5
Bulk Water	1.7	
DNA Solution	22	

Conclusion

The presence of two distinctive regions in the membranes and both regions are significantly different from the bulk water phase.

Conclusions:

Nafion, Dow Chemical, and the sulfonimide membranes all yield similar spectroscopic results.

Observed polarities within the ion cluster structures are intermediate between water and hydrocarbon solvents.

Ethidium bromide indicates two distinct environments, one that is water-like and one that is much less accessible to water.

On the Development of Higher Temperature Proton-Exchange Membranes for Fuel Cells

Sanjiv Malhotra*, Tony Thampan[#] and Ravindra Datta[#]

Department of Chemical and Biochemical Engineering,
The University of Iowa, Iowa City, IA 52242, and
*H Power Corp., 60 Montgomery Street , Belleville NJ 07109
[#]Current address: Department of Chemical Engineering
Worcester Polytechnic Institute, Worcester MA 01609 – 2280.

ABSTRACT

There is a significant incentive for developing proton-exchange membrane for atmospheric fuel cells that can operate at temperatures higher than 120 °C and at low relative humidities. Higher temperature membranes can not only help to overcome the debilitating effects of CO poisoning of anode, but can also allow direct use of low-temperature reformable fuels such as methanol. The conventional perfluorosulfonic acid proton-exchange membranes have two limitations in this regard: 1) they require liquid water in their pores, and 2) their thermal stability is limited to less than 150°C. A solution to the first problem is to load the membranes with dopants of low volatility. The solution to the second problem requires the development of alternate ionomeric membranes with higher temperature stability.

INTRODUCTION

The current proton-exchange membranes (PEMs), in particular the perfluorosulfonic acid membranes such as Nafion®, are limited to an operating temperature of around 80°C for atmospheric fuel cells. This is because the conventional PEMs require water in their pores for proton conduction. Protons from the tethered sulfonic acid groups on the pore surface become detached and consequently mobile as a result of water hydration. These hydronium ions are responsible for proton conduction via ordinary diffusion and/or Grotthus chain hopping. The efficacy of this transport depends upon the amount of water present in their pores. At higher temperatures in fuel cells operating at atmospheric pressure, the relative humidity within the fuel cell can not be maintained at a level for adequate membrane hydration, causing a loss in membrane performance. This is illustrated in Figure 1, which shows the data of Malhotra and Datta (1997) on the effect of raising the fuel cell temperature from 80°C to 110°C while maintaining the humidifier temperature at 95°C. There is a precipitous drop in the fuel cell performance as a result of low proton conductivity due to a lack of membrane hydration .

Higher fuel cell temperatures are desirable since at the usual operating temperature of 80°C, even 10 ppm CO in the anode feed can significantly poison the platinum electrocatalyst commonly used at the anode. CO deactivates the catalyst by

preferentially occupying catalytic sites, thus making these sites unavailable for H_2 adsorption and the subsequent anode reaction. The dramatic influence of CO poisoning on the fuel cell performance is illustrated in Figure 2, which plots the data of Oetjen et al. (1996) for different CO levels in the H_2 feed. However, the chemisorption of CO is exothermic and decreases considerably at higher temperature. Further, CO may be removed at higher temperatures by reacting with water via water-gas shift reaction (WGSR). There is, thus, an incentive for the development of PEMs that can operate efficiently at temperatures at or above 120°C and at atmospheric pressure, i.e. under low relative humidities. Furthermore, this may eventually allow direct methanol or dimelthylether fuel cells based on *insitu* reforming. Although fuel cells with these fuels can be operated even at 80°C, the CO produced from their reforming occupies catalyst sites and can be further converted to H_2 and CO_2 via WGSR only at higher temperatures. It is shown here that PEMs such as Nafion® can be doped with low volatility dopants to provide adequate conductivity at higher temperatures and low relative humidities.

THEORY

Various structural models have been proposed for the describing the unique properties of the various PEMs. In the case of Nafion®, the incompatibility of the hydrophobic fluorocarbon component and the ionic component lead to microphase separation and a micellular structure. A Cluster - Network model proposes that ionic clusters interconnect through short narrow channels and provide a network for proton conduction that is dispersed throughout the fluorocarbon matrix. The conduction is related to water adsorbance through the clusters. Although the fluorocarbon phase is hydrophobic, the presence of the highly hydrophilic sulphonic group agglomerates causes the cluster to adsorb water. The cluster diameter and the number of exchange sites increase with the amount of water adsorbed.

Divisek et al. (1998) have recently studied the pore structure of the PEM. In the case of Nafion®, their results suggest a membrane that contains surface layers whose structure and hydrophobic/ hydrophilic properties are substantially different from the basic inner membrane. From standard porosity measurements, inner layer has pores ranging from 1 to 100 nm and the average pore radius is 2 nm. They propose a network of ultramicropores that are interconnected when the membrane is saturated with water. It is thought that high proton diffusion through the pores filled with water is responsible for high conductivities.

The following theoretical model is developed to investigate the effect of a generic dopant and the relative humidity on the conduction of protons through the membrane. The first step involved is the transfer of protons from the pendant side chains (HA) to the dopant, denoted as BH. For instance, in the case of water, B = OH. Conceptually, the proton transfer process is assumed to occur in two steps:

i) Deprotonation of the Brönsted acid group, HA :

$$HA \Leftrightarrow H^{\cdot} + A$$

for which the dissociation constant is

$$K_{HA} = \frac{a_{H^+} a_{A^-}}{a_{HA}} \tag{1}$$

ii) Protonation of the dopant BH, which acts as Brönsted base:

$$H^+ + BH \Leftrightarrow BH_2^+$$

for which the *dissociation* constant is

$$K_{BH_2^+} = \frac{a_{H^+} a_{BH}}{a_{BH_2^+}} \tag{2}$$

Combining Eqs. 1and 2, the concentration of protons, $c_{BH_2^+}$, can be expressed as

$$c_{BH_2^+} = \frac{10^{-H_0}}{K_{BH_2^+}} c_{BH} \tag{3}$$

where H_0 represents the Hammett acidity function, which is another measure for the ability of an acid to protonate a base. Values of the Hammett acidity function for various substances are available in the literature. For instance, for Nafion® $H_0 = -12$. H_0 is defined as follows:

$$H_0 \equiv -\log h_0 \tag{4}$$

where

$$h_0 = K_{HA} \left(\frac{\gamma_{BH}^C \gamma_{HA}^C}{\gamma_{BH_2^+}^C \gamma_{A^-}^C} \right) \frac{c_{HA}}{c_{A^-}} \tag{5}$$

with γ_i^C representing the activity coefficient of species i.

Equation (3) is, thus, a thermodynamic relationship that provides the concentration of proton carrier, $c_{BH_2^+}$, within the porous network in terms of the dopant concentration c_{BH}. The specific conductivity of the PEM for multiple charge carriers in a porous membrane of a given porosity ε and tortuosity τ is

$$\sigma = \sum_i^n \sigma_i = \left(\frac{\varepsilon}{\tau} \frac{F^2}{RT} \right) \sum_i^n z_i (D_i) c_i \tag{6}$$

where T is the temperature, z_i is the charge number of the ionic species i, D_i is the diffusion coefficient of i, accounting for Grotthus chain hopping as well as ordinary diffusion of the ion, F is the Faradays constant, and c_i is the concentration of the charge carrying species i.

Assuming that BH_2^+ is the sole charge carrier in the PEM ($t_{BH_2^+} = 1$),

$$\sigma_{BH_2^+} = \left(\frac{\varepsilon}{\tau}\frac{F^2}{RT}\right)\left(D_{BH_2^+}\right)c_{BH_2^+} \tag{7}$$

Finally, using Eq. (3) in (7) for $C_{BH_2^+}$, Eq. (8) is obtained:

$$\sigma_{BH_2^+} = \left(\frac{\varepsilon}{\tau}\frac{F^2}{RT}\right)\left(\frac{10^{-H_0}}{K_{BH_2^+}}\right)\left(D_{BH_2^+}\right)c_{BH} \tag{8}$$

For the usual case when the dopant, or Brönsted base, solvating the protons is water, i.e.,BH HOH , the conductivity becomes

$$\sigma_{H_3O^+} = \left(\frac{\varepsilon}{\tau}\frac{F^2}{RT}\right)\left(\frac{10^{-H_0}}{K_{H_3O^+}}\right)\left(D_{H_3O^+}\right)c_{H_2O} \tag{9}$$

According to Eq. (9), the conductivity of the PEM is proportional to the c_{H_2O} or λ defined as the number of water molecules per sulfonic acid site, i.e. $\lambda = N_{H_2O}/N_{SO_3H}$. This appears to be the case according to the data of Zawodzinski et al. (1997) plotted in Figure 3. However this linear dependence is approximate and not likely to hold for small λ, when the membrane structure ε and tortuosity τ, is dependent upon the level of hydration due to swelling.

PEM HYDRATION

While the results above describe PEM conductivity in terms of c_{H_2O} or λ, it is more convenient to relate conductivity directly to the relative humidity, i.e. the ratio of partial pressure to the vapor pressure of H_2O. This is done here by utilizing the n-layer BET equation (Adamson , 1997 ed. 6)

$$\lambda = \frac{\lambda_m\left(c\frac{a}{1-a}\right)\left(1-(n+1)a^n+na^{(n+1)}\right)}{1+(c-1)a-ca^{(n+1)}} \tag{10}$$

where a is the water vapor activity or the relative humidity, λ_m is the number of moles of water adsorbed per cation site that results in a monolayer. The temperature dependent constant, c, is the ratio of the enthalpies of adsorption of the first and higher layers, and n

is the number of adsorbed layers on the surface. Fitting this equation to the experimental data of Zawodzinski et. al. (1993) in Figure 4, these parameters for Nafion® are determined to be:

$c = 250$, $\lambda_m = 1.7$, and $n = 17$.

These parameters are infact physically reasonable. For example, the total height of the adsorbed layers is calculated at 4.7 nm, with 0.28 nm being the diameter of a water molecule, which is on the same order as the pore diameter of Nafion®. Combining the Figures 3 and 4, or the corresponding equations (9) and (10), conductivity can be predicted directly as a function of relative humidity.

HIGHER TEMPERATURE PEMs

A possible procedure for increasing the operating temperature of the PEM at low relative humidity is to replace water with an alternate dopant with a lower volatility for solvating the protons. Savinell et al. (1994) utilized BH = H_3PO_4 with Nafion®. They were thus able to develop a PEM with high conductivity at elevated temperature. In addition to hydronium ions as charge carriers, $H_3PO_4^+$ is also proton carrier. However $t_{BH_2^+}$ may decline due to the presence of dopant anions $B^- = H_2PO_4^-$ which also contribute to current. Furthermore H_3PO_4 has finite volatility at elevated temperatures.

Malhotra and Datta (1997) utilized phosphotungstic acid doped Nafion® to dramatically enhance PEM performance at 110°C at low relative humidities (humidifier temperature at 50°C.) as shown in Figure 5. This is promising since heteropolytacids are nonvolatile. However since heteropolyacids are highly soluble in water, excess water in the PEM will leach the acid out of the membrane. In other words, the relative humidity of a heteropolyacid doped PEM should be low for stability. Finally, Figure 6 shows that the deleterious effect of CO can be reduced by operating at higher temperature.

Although the discussion here has been limited to enhancing the conductivity of PEMs at higher temperature and using dopants as alternate proton carriers to lower the relative humidity, Eq. (8) suggests an alternative strategy for enhancing conductivity. If the Hammett acidity function can be increased beyond –12 either by increasing c_{HA} or by redesigning polymer linkages (e.g., Kotov et al. 1997), it could have a dramatic influence on the conductivity at low dopant concentrations or low relative humidity.

BIBLIOGRAPHY

1. Malhotra, S. and Datta, R., *J. Electrochem. Soc.*, **144**, L23, 1997.

2. H.F. Oetjen, V. M. Schmidt., U Stimming., F Trila., *J. Electrochem. Soc.*, **143**, 3838, 1996.

3. J. Divisek, M. Eikerling, V. Mazin, H. Schmitz, U. Stimming, Yu. M. Volfkovich. *J.Electrochem. Soc.*, **145,** 2677 1998.

4. T. A. Zawodzinski, Jr., C. Derouin, S. Radzinski, R. J. Sherman, V. T. Smith, T. E. Springer, S. Gottesfeld., *J. Electrochem. Soc.*, **140**, 1041, 1997.

5. Adamson A. *Physical Chemistry of Surfaces,* 1997, 6 th. Edition.

6. R. Savinell, E. Yeager, D. Tryk, U. Landau, J. Wainright, D. Weng, K. Lux, M. Litt, C. Rogers, *J. Electrochem. Soc.*, **141**, L46, 1994.

7. Zawodzinski et al., *J. Electrochem. Soc.*, **140**, 1041, 1993.

8. S.V Kotov,. S.D Pedersen, W. Qiu, Z. Qiu. and , D.J.Burton, *J. Fluorine Chem.*, **82**, 13, 1997.

On the Development of Higher Temperature Proton-Exchange Membranes for Fuel Cells

SANJIV MALHOTRA*, TONY THAMPAN
AND RAVINDRA DATTA

Department of Chemical and Biochemical Engineering, The University of Iowa, Iowa City, IA 52242-1219.

**H Power Corp., 60 Montgomery Street, Belleville, NJ 07109.*

Objectives

- Current proton-exchange membrane (PEM) fuel cells are limited to ~ 80 °C to avoid drying of perfluorosulfonic acid (Nafion®) membrane.
- At 80 °C, even 10 ppm CO can poison the anode electrocatalyst.
- ∴ Objective is to develop PEM that work at • 120 °C (to reduce CO poisoning) and at low relative humidity.
- At temperatures > 150 °C, low reforming fuels, e.g., methanol, dimethylether, may be used in fuel cell. However, Nafion® is thermally unstable in this range.
- Issues involved in the development of higher temperature PEMs are discussed.

Effect of Temperature

(Malhotra, S. and Datta, R., *J. Electrochem. Soc.*, **144**, L23, 1997.)

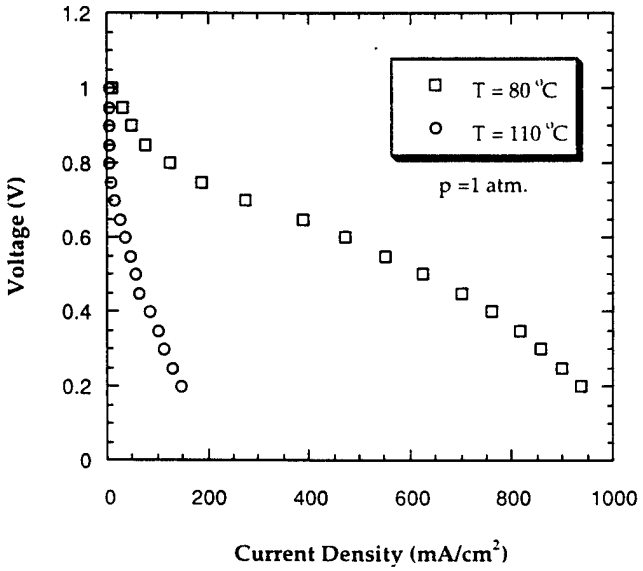

Figure 1: Fuel cell performance based on commercial (20% Pt-on-C, 0.35 mg Pt/cm^2) gas-diffusion electrodes (E-TEK), anode humidifier at 95 °C and cathode humidifier at 90 °C.

Effect of CO in Anode Feed

(Oetjen et al., *J. Electrochem. Soc.*, **143**, 3838, 1996.)

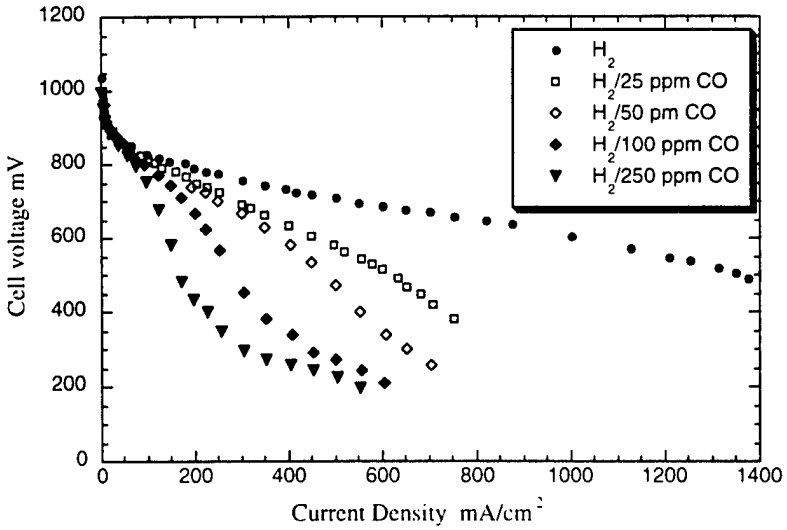

Figure 2: Steady-state voltage-current density plots for a PEM fuel cell with H_2/CO (25 to 250 ppm); anode and cathode: 30 w% Pt on Vulcan XC 72, Tcell = 80 °C; $p_{H_2} = 0.22$ MPc; $p_{O_2} = 0.24$ MPc. (Data of Oetjen et al., *J. Electrochem. Soc.*, **143**, 3838, 1996.)

Theory

AH = Sulfonic Acid; BH = Dopant ⊕ = H^+

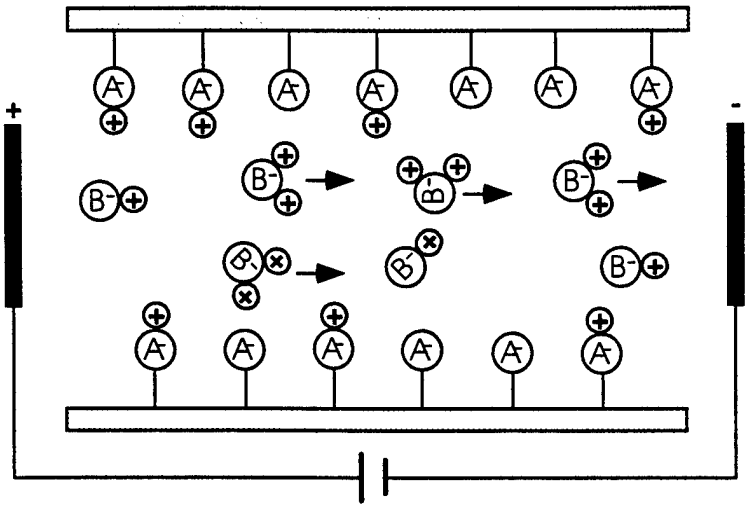

Proton Transfer to Dopant:

$$HA \Leftrightarrow A^- + H^+ \qquad ; K_{HA} = \frac{a_{A^-} a_{H^+}}{a_{HA}} \qquad (1)$$

$$H^+ + BH \Leftrightarrow BH_2^+ \qquad ; K_{BH_2^+} = \frac{a_{BH} a_{H^+}}{a_{BH_2^+}} \qquad (2)$$

From Eq. (2): $$c_{BH_2^+} = \left(\frac{10^{-H_0}}{K_{BH_2^+}} \right) c_{BH} \qquad (3)$$

Hammett Acidity Function:

In Eq. (3)

$$H_0 \equiv -\log h_0 \quad ; \text{where} \quad h_0 \equiv \left(\frac{\gamma^C_{BH}}{\gamma^C_{BH_2^+}} \right) a_{H^+} \tag{4}$$

Using Eq. (1): $$h_0 = K_{HA} \left(\frac{\gamma^C_{HA} \gamma^C_{BH}}{\gamma^C_{BH_2^+} \gamma^C_{A^-}} \right) \frac{c_{HA}}{c_{A^-}} \tag{5}$$

PEM Specific Conductivity:

$$\sigma = \sum \sigma_i = \left(\frac{\varepsilon}{\tau} \frac{F^2}{RT} \right) \sum z_i^2 D_i c_i \tag{6}$$

The proton conductivity (based on carrier BH_2^+):

$$\sigma_{BH_2^+} = \left(\frac{\varepsilon}{\tau} \frac{F^2}{RT} \right) \left(D_{BH_2^+} \right) c_{BH_2^+} \tag{7}$$

Using Eq. (3) in (7) for $c_{BH_2^+}$

$$\boxed{\sigma_{BH_2^+} = \left(\frac{\varepsilon}{\tau} \frac{F^2}{RT} \right) \left(\frac{10^{-H_0}}{K_{BH_2^+}} \right) \left(D_{BH_2^+} \right) c_{BH}} \tag{8}$$

Nafion® Conductivity with H_2O

For BH ≡ HOH, from Eq. (8), and hydronium ions as the lone charge carriers

$$\sigma_{H_3O^+} = \left(\frac{\varepsilon}{\tau}\frac{F^2}{RT}\right)\left(\frac{10^{-H_0}}{K_{H_3O^+}}\right)\left(D_{H_3O^+}\right)c_{H_2O} \qquad (9)$$

$D_{H_3O^+}$ includes Grotthus and ordinary diffusion.

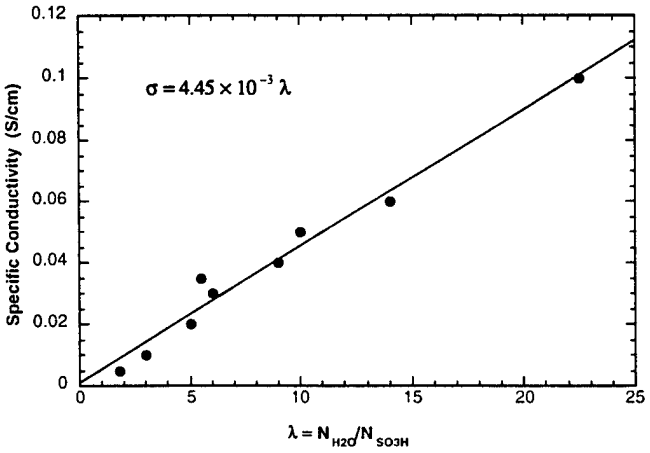

Figure 3: Nafion® 117 conductivity σ vs. water content λ (Data of Zawodzinski et al., *J. Electrochem. Soc.*, **140**, 1041, 1997).

Nafion® Hydration

n-Layer BET Model: ($\lambda \equiv N_{H_2O}/N_{SO_3H}$; $a = p_{H_2O}/p^{\circ}_{H_2O}$)

$$\frac{\lambda}{\lambda_m} = \frac{(ca/(1-a))(1-(n+1)a^n + na^{n+1})}{1+(c-1)a - ca^{n+1}} \qquad (10)$$

Parameters: $c = 250$, $\lambda_m = 1.7$, $n = 17$

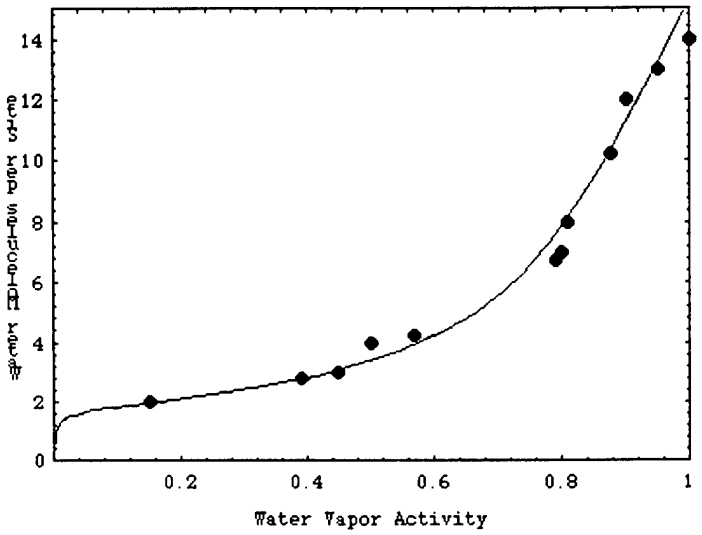

Figure 4: Equilibrium sorption of water in Nafion 117 as a function of water vapor activity (Data of Zawodzinski et al., *J. Electrochem. Soc.*, **140**, 1041, 1993).

Goals for the Development of Higher Temperature PEMs

1. Increasing PEM water retention at low relative humidities (e.g., by incorporating an oxide in PEM as done by Watanbe et al., *J. Electrochem. Soc.*, **143**, 3847, 1996).

2. Doping with low volatility acids BH to increase c_{BH} of alternate charge carriers (e.g., Nafion impregnated with H_3PO_4 used by Savinell et al., *J. Electrochem. Soc.*, **141**, L46, 1994). However, t_{H^+} may decline due to the presence of dopant anions B^- resulting from auto-dissociation

$$BH \Leftrightarrow B^- + H^+ \quad ; K_{BH} = \frac{a_{B^-} a_{H^+}}{a_{BH}}$$

3. Increasing $-H_0$ of PEM by increasing acid concentration c_{HA}, polymer/lnkages redesign, or by doping with appropriate materials.

4. Increasing thermal stability of PEM (e.g., perfluoro-phosphonic acid membranes developed by Kotov et al., *J. Fluorine Chem.*, **82**, 13, 1997).

Effect of Phosphotungstic Acid (PTA) Doping of Nafion®

(Malhotra, S. and Datta, R., *J. Electrochem. Soc.*, **144**, L23, 1997.)

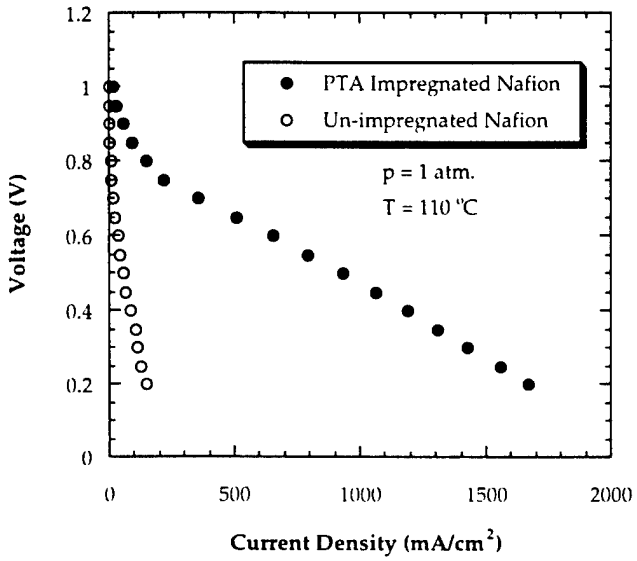

Figure 5: A comparison of unimpregnated Nafion® 117 and Nafion® impregnated with acetic acid solution of 12-phosphotungstic acid. $T_{humidifiers}$ = 50 °C for the impregnated Nafion® case.

Effect of CO at 120 °C with a PTA Doped Nafion®

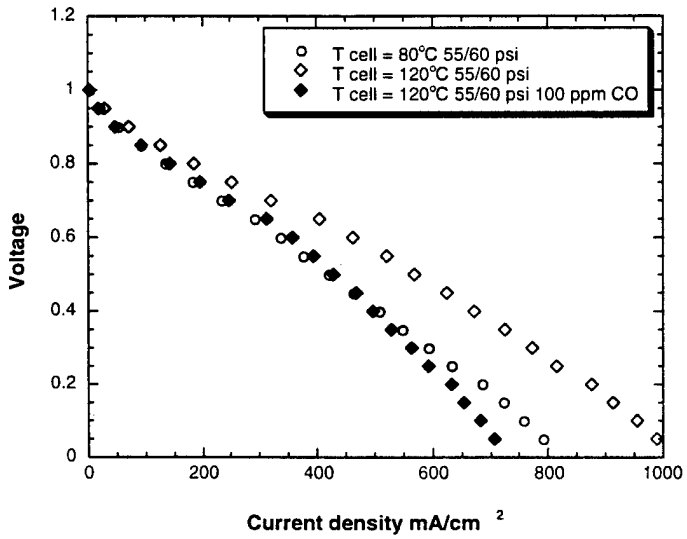

Figure 6: A Comparison of Performance for H_2 Feed with and without 100 ppm CO and Nafion® 117 Impregnated with 12-Phosphotungstic Acid (PTA) at 120 °C and 55-60 psi.

Improving Thermal Stability of PEM

Perfluorosulfonic Acid (T_g ~ 110 °C):

(Grot, W., *Encyclop. of Polym. Sci. and Eng.*, Vol. 16, 642, 1989.)

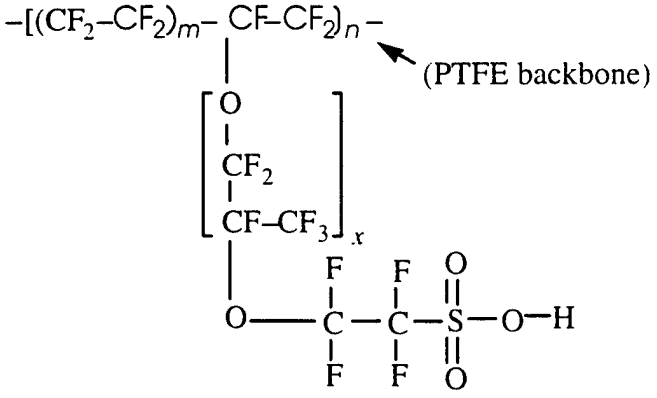

Perfluorophosphonic Acid (Better thermal stability):

(Kotov, S. V., Pederesen, S. D., Qui, W., Qui, Z.-M., and Burton, D. J., *J. Fluorine Chem.*, **82**, 13, 1997)

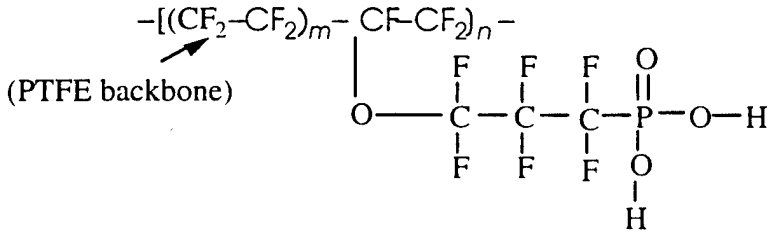

Title: **Sulfonated Polyphosphazenes: A New Class of PEM Materials**

Presenter: Peter N. Pintauro, Department of Chemical Engineering, Tulane University, New Orleans, LA 70118

Abstract

Cation-exchange membranes have been fabricated from selected phosphazene polymers by first sulfonating the base polymer with SO_3 and then solution-casting thin films. Polymer crosslinking was carried out by dissolving benzophenone photo-initiator in the membrane casting solution and then exposing dried films to UV light. One polyphosphazene, poly[bis(3- methylphenoxy)phosphazene], looks particularly promising for possible PEM fuel cell applications. A sulfonated and crosslinked membrane from this polymer, with an ion-exchange capacity of 1.4 mmol/g (an equivalent weight of 714), swelled less than Nafion 117 in both water and methanol and its proton conductivity (for a fully hydrated 200 μm thick film at temperatures between 25°C - 65°C) was approximately 70% of that for Nafion 117. Additionally, water and methanol diffusivities in the polyphosphazene membrane were low ($< 10^{-7}$ cm^2/s). The sulfonated phosphazene polymer was found to be thermally stable up to 350°C. Sulfonated/crosslinked membranes showed no signs of mechanical failure (softening) up to 170°C and did not degrade in the presence of hydrogen peroxide.

Introduction

Over the past decade, studies of proton exchange membranes for polymer electrolyte fuel cells have focused, for the most part, on perfluorosulfonic acid membranes such as DuPont's Nafion® and Dow's Developmental Membrane, because they exhibited high ionic conductivity, good mechanical strength and chemical stability, and reasonably low water swelling. The high electro-osmotic water flows and methanol crossover rates in these materials, coupled with their high cost, have stimulated research into alternative polymers for proton exchange membranes, including those composed of polybenzimidazole, polystyrene-divinylbenzene mixtures radiation-grafted to poly(fluoroethylene-co-hexafluoropropylene), Nafion impregnated microporous PTFE (the Gore-Select™ membranes), and sulfonated Kraton.

Polyphosphazene-based cation exchange membranes are attractive materials for PEM H_2/O_2 and direct methanol fuel cells because of their reported chemical and thermal stability[1] and due to the ease of chemically attaching various side chains onto the -P=N- polymer backbone. Although polyphosphazenes have been explored for use as solvent-free solid polymer electrolytes in lithium batteries, no one has examined this class of polymers for proton exchange membrane fuel cells.

Prior studies by Pintauro and co-workers have shown that poly[(3-methylphenoxy) (phenoxy)phosphazene] and poly[bis(3-methylphenoxy)phosphazene] can be sulfonated using SO_3 to a high ion-exchange capacity (near 2.0 mmol/g) with no detectable polymer degradation.[2,3] Solution-cast sulfonated polymer membranes (100-200 μm thick) exhibited good mechanical

properties in both the dry and water-swollen states for ion-exchange capacities ≤1.4 mmol/g. Additionally, we have shown that methylphenoxy-substituted phosphazene polymers could be photocrosslinking using UV light (via a hydrogen abstraction mechanism) and benzophenone as the photoinitiator in dry-film form.[4,5]

Below, we report on our evaluation of a membrane composed of sulfonated and crosslinked poly[bis(3-methylphenoxy)phosphazene]. The membrane was characterized in terms of ion-exchange capacity, equilibrium swelling in water, methanol, and water/methanol mixtures, water and methanol diffusivity, proton conductivity, and chemical/thermal stability.

Experimental

Poly[bis(3-methylphenoxy)phosphazene] (henceforth denoted as POP) was purchased from *,technically,* Inc., Andover, MA and used as the base polymer without further purification. The molecular weight of this polyphosphazene, as determined by gel permeation chromatography (Waters Styragel HT 6E column in THF), was 2.0×10^6 Daltons.

The polyphosphazene was sulfonated with SO_3 in 1,2-dichloroethane (DCE) solvent at 0°C, using procedures described elsewhere.[2] The polymer product was washed thoroughly with deionized and distilled water, pre-conditioned by soaking sequentially in water, 0.1 M NaOH, water, 0.1 M HCl, and water over a 10 day period, and then dried thoroughly. The ion-exchange capacity (IEC) of the sulfonated polymer was 1.4 mmol/g (as compared to an IEC of 0.909 mmol/g for Nafion 117). Membranes were solution-cast from a mixture of 3 w/v% polymer in N,N-dimethylacetamide. In some cases, 15 mol% benzophenone (BP) photoinitiator was added to the casting solution for eventual polymer crosslinking. Membranes were dried in the dark and under vacuum at 45°C for 3 days. Membranes containing benzophenone were irradiated with UV light (365 nm wavelength, 2.8 mW/cm^2 intensity) under an Argon atmosphere at 25°C for 15-20 hours. The final dry membrane thickness for both crosslinked and non-crosslinked films was ~200 μm.

Equilibrium membrane swelling by water and methanol and the diffusion coefficients of water and methanol in polyphosphazene films were determined under controlled vapor activity conditions using a McBain quartz spring sorption apparatus. All measurements were made on membrane samples in the H^+ form. Swelling was first calculated as the % increase in the dry membrane weight and then was converted to units of solvent molecules per sulfonic acid site. For unit activity water swelling, a membrane was equilibrated in deionized and distilled liquid water. Water and methanol diffusion coefficients were determined by a weight loss method, using a thick polyphosphazene membrane (400-600 μm) to minimize surface drying effects. After a membrane sample was fully equilibrated with water vapor at an activity of 0.95 or methanol vapor at an activity of either 0.80 or 0.90, the vapor activity was lowered by 5% and the membrane weight loss was recorded with time. The diffusion coefficient was then computed from the initial slope of a weight loss vs. square-root of time plot according to the following equation[6]

$$D = \frac{\pi\delta^2 (\text{slope})^2}{16}$$

The electrical conductivity of protons in a water-equilibrated polyphosphazene membrane in the H^+ form was determined using an AC impedance method. Membrane samples were first soaked in deionized and distilled water for 24 hours. The conductivity was measured using a pair of pressure-attached, high surface area platinum electrodes, as described elsewhere.[7] The mounted sample was immersed in deionized and distilled water at a given temperature and measurements were made from 1Hz to 10^5Hz using a PAR Model 5210 amplifier and a PAR Model 273 potentiostat/galvanostat. Both real and imaginary components of the impedance were measured and the real Z-axis intercept was closely approximated. The cell constant was calculated from the spacing of the electrodes, the thickness of the membrane (200 μm), and the area of the platinum electrodes.

Results and Discussion

The equilibrium water sorption vs. water activity data at 30°C was correlated in terms of the number of water molecules per sulfonic acid site. At water vapor activities less than 0.6, the 1.4 IEC and 1.4 IEC/crosslinked polyphosphazene membranes swelling was less than that for Nafion 117 (0.909 IEC). For water activities greater than 0.6, the un-crosslinked polyphosphazene membrane swelled more than Nafion. When equilibrated in liquid water (unit activity), the number of water molecules per sulfonic acid site was 14 (for Nafion 117), 20 (for the 1.4 IEC polyphosphazene without crosslinking) and 12 (for the 1.4 IEC polyphosphazene with crosslinking). Although the concentration of fixed charges in the polyphosphazene membrane was greater than that in Nafion, polymer crosslinking was prevented excessive swelling. Equilibrium membrane swelling of the crosslinked polyphosphazene membrane in methanol vapor at 30°C was also measured and compared to that for Nafion. Again, the polyphosphazene membrane swelled less than Nafion, with an equilibrium swelling of 12.5 wt% (2.8 methanol molecules per sulfonic acid site) at a vapor activity of 0.9, as compared to 15.1 wt% (5.1 methanol molecules per sulfonic acid site).

The measured water and methanol diffusion coefficients in a crosslinked and sulfonated polyphosphazene membrane at 30°C and 45°C are listed in Table. The water diffusivity in the polyphosphazene membrane was considerably lower than that in Nafion due probably to the combined effects of: (i) Stronger molecular-level interactions of the water with the P-N polymer backbone, as compared to the highly hydrophobic PTFE backbone in Nafion (for example, hydrophilic -N-H^+ complexes may be present in the membrane, due to the presence of backbone nitrogens with unpaired electrons) and (ii) lower solvent swelling that increased the tortuous pathway for species diffusion. The pure methanol diffusivity in the polyphosphazene membrane was also very low and comparable to that of water.

Table 1. The diffusion coefficients of water and methanol in a sulfonated/crosslinked poly[bis(3-methylphenoxy)phosphazene] membrane.

	Water Diffusion Coefficient (cm^2/s)	Methanol Diffusion Coefficient (cm^2/s)
Crosslinked polyphosphazene (IEC=1.40 mmol/g)	6.72×10^{-8} (at 30°C; activity= 0.98) 9.85×10^{-8} (at 45°C; activity=0.98)	1.62×10^{-8} (at 30°C; activity=0.80) 7.50×10^{-8} (at 45°C; activity=0.80) 8.50×10^{-8} (at 45°C; activity=0.90)
Nafion 117 (IEC=0.909 mmol/g)	4.50×10^{-6} (at 30°C; activity=0.98)	

The proton conductivity in a liquid-water-equilibrated polyphosphazene membrane (1.4 IEC, crosslinked, and in the H^+ form) was measured at temperatures ranging from 30°C to 65°C and the results were compared with literature data[8] for Nafion 117. The conductivity of the phosphazene membrane was high, at approximately 70% that of Nafion, throughout the temperature range under investigation. The high conductivity results have been attributed to: (i) The close proximity of SO_3^- groups on the polyphosphazene's methylphenoxy side chains (approximately 30% of the methylphenoxy groups were sulfonated for an IEC of 1.4 mmol/g, with a side-chain/side-chain distance of approximately 4.7-4.9 Å) and (ii) the clustering of sulfonated polymer domains in the polyphosphazene (small angle x-ray scattering experiment revealed ion clustering in hydrated polyphosphazene membranes with a characteristic cluster dimension of 65 Å). It is anticipated that electro-osmotic drag coefficient will be small in the polyphosphazene membrane, based on the high proton conductivity and low water diffusivity results (such experiments have not yet been performed).

The mechanical stability of sulfonated and sulfonated/crosslinked polyphosphazene ion-exchange membranes was determined by thermal mechanical analysis (TMA), where data was collected in the penetration mode with a load of 0.5 N. In these experiments, the membrane was bathed in N_2 gas and heated at 10°C/min. The TMA results showed that the un-crosslinked, 1.4 IEC polyphosphazene membrane began to soften at 75°C, whereas the crosslinked film exhibiting no softening for temperatures up to 174°C.

The chemical stability of the polyphosphazene membranes was evaluated by a soaking membrane sample in an aqueous 3% H_2O_2 solution containing 4 ppm Fe^{2+} at 68°C . Periodically, over a 24 hour period, the membrane was removed from the peroxide solution, wiped with filter paper to remove excess liquid, and weighed. No membrane weight loss was observed, confirming our hypothesis and literature references regarding the excellent chemical stability of phosphazene polymers. For comparison purposes, a Nafion 117 membrane and a commercially available

polystyrene sulfonate membrane (crosslinked with divinyl benzene) were also subjected to the peroxide degradation test. As expected, the Nafion film showed essentially no weight loss over the 24 hour test period, whereas the polystyrene-based cation exchange membrane showed severe degradation, with a weight loss of about 50% (corrected for the presence of an inert polymer webbing material) after 8 hours of peroxide exposure.

Acknowledgments

This work was funded by the National Science Foundation (Grant Nos. ARI-9512258 and CTS-9632079) and the U.S. Department of Energy (Grant No. DE-FG01-93EW532023, "Hazardous Materials in Aquatic Environments of the Mississippi River Basin") through the Tulane/Xavier Universities' Center for Bioenvironmental Research.

REFERENCES

1. H. R. Allcock and R. J. Fitzpatrick, *Chem. Mater.*, **3**, 1122 (1991).
2. R. Wycisk and P. N. Pintauro, *J. Membr. Sci.*, **119**, 155 (1996).
3. H. Tang, P. N. Pintauro, Q. Guo, and S. O'Connor, *J. Appl. Polym. Sci.* (in press).
4. R. Wycisk, P. N. Pintauro, W. Wang, and S. O'Connor, *J. Appl. Polym. Sci.*, **59**, 1607 (1996).
5. R. Graves and P. N. Pintauro, *J. Appl. Polym. Sci.*, **68**, 827 (1998).
6. J. Crank, The Mathematics of Diffusion, Oxford Press, London, p. 228 (1956).
7. T. A. Zawodzinski, M. Neeman, L. O. Sillerud, and S. Gottesfeld, *J. Phys. Chem.*, **95**, 6040 (1991).
8. T. A. Zawodzinski, J. Thomas, E. Springer, J. Davey, R. Jestel, C. Lopez, J. Valerio, and S. Gottesfeld, *J. Electrochem. Soc.*, **140**, 1981 (1993).

Sulfonated Polyphosphazenes:

A New Class of PEM Materials

Peter N. Pintauro
Department of Chemical Engineering
Tulane University
New Orleans, Louisiana 70118

Workshop on
Advanced Fuel Cell Membranes for Non-conventional Fuels

April 28-May 1, 1998

Why Polyphosphazenes?

1. Polymers have good chemical and thermal stability.

2. There are practically unlimited possibilities to functionalize the polymer.

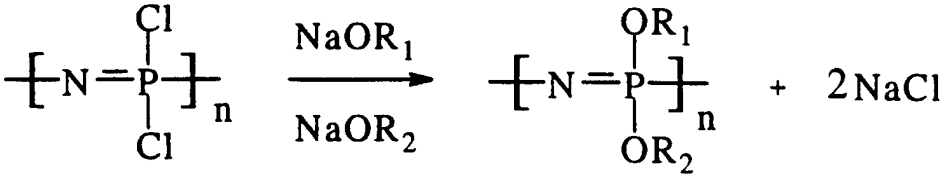

3. Prior use of polyphosphazenes - polymer electrolytes in solid-state lithium batteries, membranes for organic/water pervaporation separation, low temperature gaskets.

Approach

Base polymer: Poly[bis(3-methylphenoxy) phosphazene). MW=2 x 10^6 daltons; purchased from *,technically,* Inc., Andover, MA.

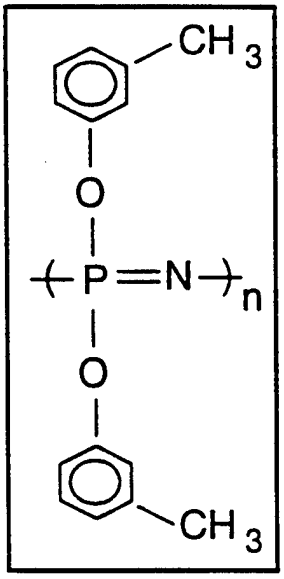

Examine sulfonated and sulfonated/crosslinked membranes.

Base polymer is semi-crystalline with a low glass transition temperature (T_g=-28.3°C).

Methyl groups on the phenoxy sidechains activate the ring for sulfonation and can be used for crosslinking (with UV light and a photoinitiator).

Sulfonation of Poly[bis(3-methylphenoxy)phosphazene] with SO_3

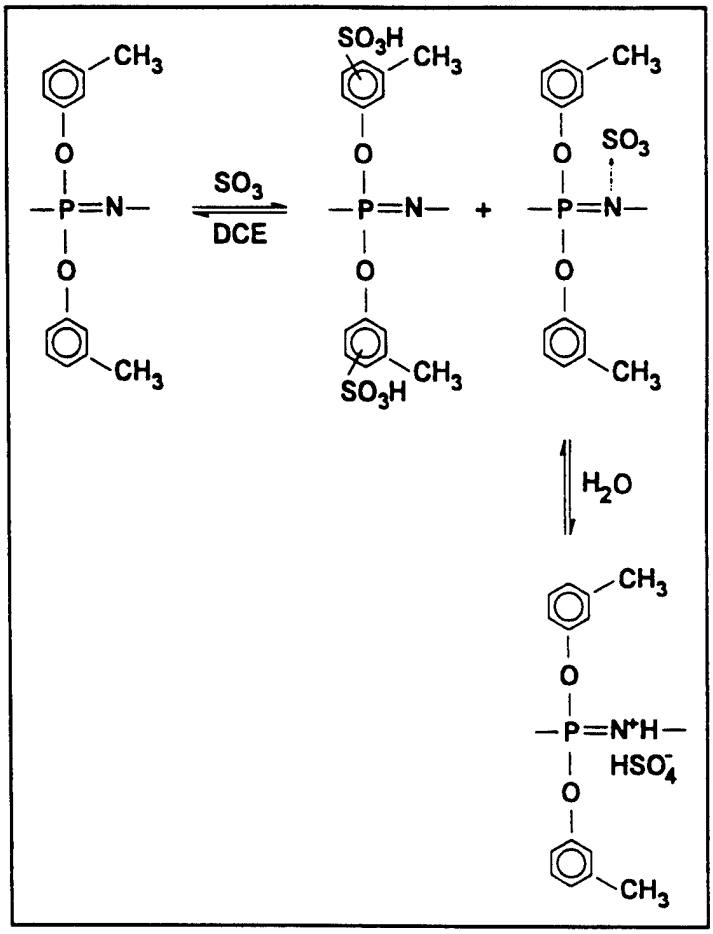

- One gram of polymer was dissolved in 40 cm^3 of dichloroethane.
- SO_3 in dichloroethane was added dropwise at 0°C and in a dry nitrogen atmosphere.
- Resulting precipitate was stirred for 3 hours at 0°C, then the reaction was terminated by addition of a dilute NaOH/water/methanol solution.
- Polymer was pre-conditioned by soaking in distilled water, 0.1M NaOH, distilled water, 0.1 M HCl, and distilled water (48 hours for each soak).
- Polymer was then dried, dissolved in dimethylacetamide, and cast on a polypropylene plate (final membrane thickness was 100-200 μm).

Photocrosslinking Mechanism

1. **Generation of macroradicals with benzophenone and UV radiation.**

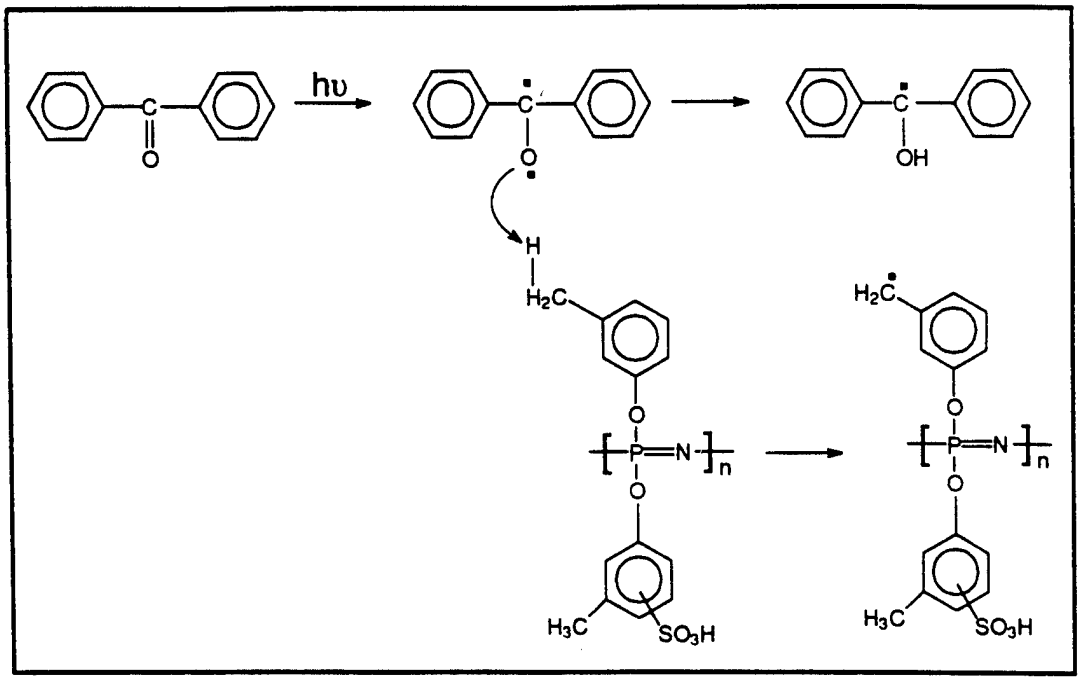

2. **Recombination of macroradicals.**

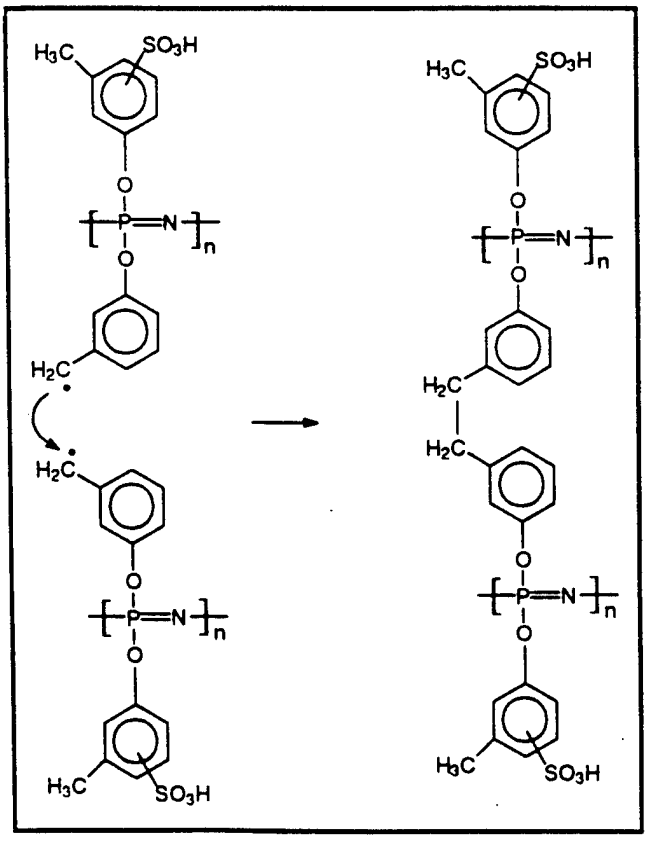

Effect of Added SO_3 on the Polymer Ion-Exchange Capacity

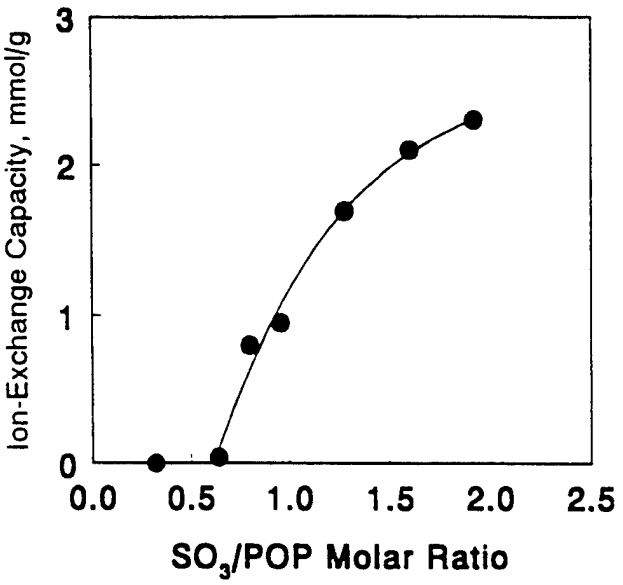

- Aromatic C-sulfonation began at a SO_3/POP between 0.64 and 0.8, with a gradual increase in IEC with added SO_3.
- Sulfonated polymers with an IEC < 2.1 mmol/g were water insoluble.
- Yield for SO_3^- site creation varied from 1.6% at SO_3/POP = 0.64 to 44% at SO_3/POP = 1.6.
- IR analysis of sulfonated polymers showed no change in the P=N and P-O-Ph stretching bands for SO_3/POP molar ratios < 1.92 (above 1.92, P=N band decreased).
- Solid-state ^{13}C NMR analysis showed para-position sulfonation for SO_3/POP $\leq$ 1.0 and non-specific carbon sulfonation for SO_3/POP > 1.0.
- Wide-angle x-ray diffractograms showed a loss in 3-D crystallinity but the presence of a 2-D ordered phase after polymer sulfonation.

Elemental Analysis of Sulfonated Poly[bis(3-methylphenoxy)phosphazenes]

SO_3/POP Molar Ratio	IEC (mmol/g)	Elemental analysis (% w/w)				mole % C-Sulfonation (a)	mole % $\equiv N \rightarrow SO_3$ Complex (b)	mole % $\equiv N^+H$ Complex (b)
		N	C	H	S			
0.64	0.04	5.38	64.58	5.39	0.33	0.52	1.63	---
0.96	0.95	4.76	57.11	4.89	4.74	14.0	9.86	5.75
0.96 (c)	0.95	4.88	58.59	5.00	3.89	13.6	4.43	3.18
1.28	1.69	4.36	52.36	4.58	7.59	27.1	13.9	7.97
1.60	2.10	4.18	50.11	4.44	8.95	35.2	14.7	8.63

466

(a) Mole % of sulfo groups attached to methylphenoxy side groups, related to the total moles of phenoxy rings.

(b) Related to total nitrogen functions.

(c) Additional soaking of membrane sample for six days in HCl, water, and NaCl (48 hours for each soaking).

Glass Transition and Thermal Analysis of the Sulfonated Phosphazene Polymers

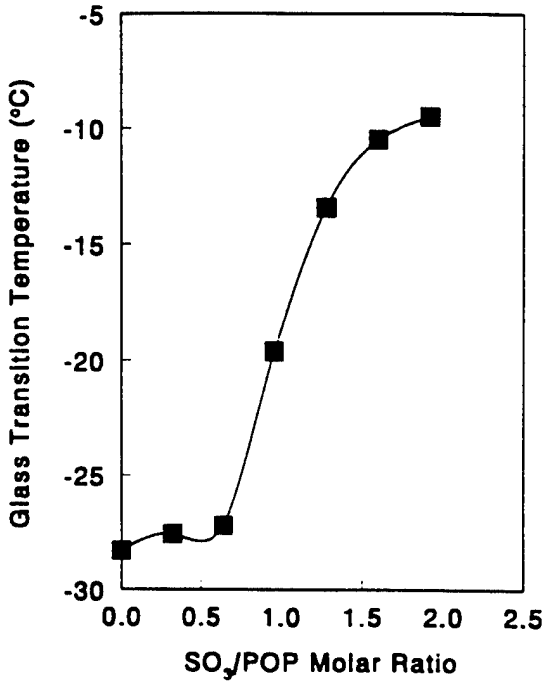

- T_g increased monotonically (from -28.3°C to -10.0°C) with added SO_3 for SO_3/POP > 0.64.

- Thermal Stability - of dry polymer samples (from IR analysis)
  - P-N backbone and aromatic ring C-C degradation at 450°C for non-sulfonated POP.
  - For sulfonated POP, P=N, C-C, and S=O stretching bands decreased for polymer heating above 350°C.

- Polymer DSC Heating Curves
  - For non-sulfonated polymer - two mesophase transitions were observed between 40°C and 100°C.
  - For sulfonated polymers - a broad peak in the heating curve (at 95°C) and an x-ray peak at 11.54-11.56Å indicate a 2-D ordered phase.

Chemical Stability of Sulfonated/Crosslinked Polyphosphazene Membranes

Membrane Soaking in a 3% H_2O_2 Solution Containing 4 ppm Fe^{2+} at 68°C

Tests run on:

a. 1.4 mmol/g crosslinked polyphosphazene membrane.
b. Nafion 117
c. Commercial sulfonated polystyrene membrane (crosslinked with divinylbenzene).

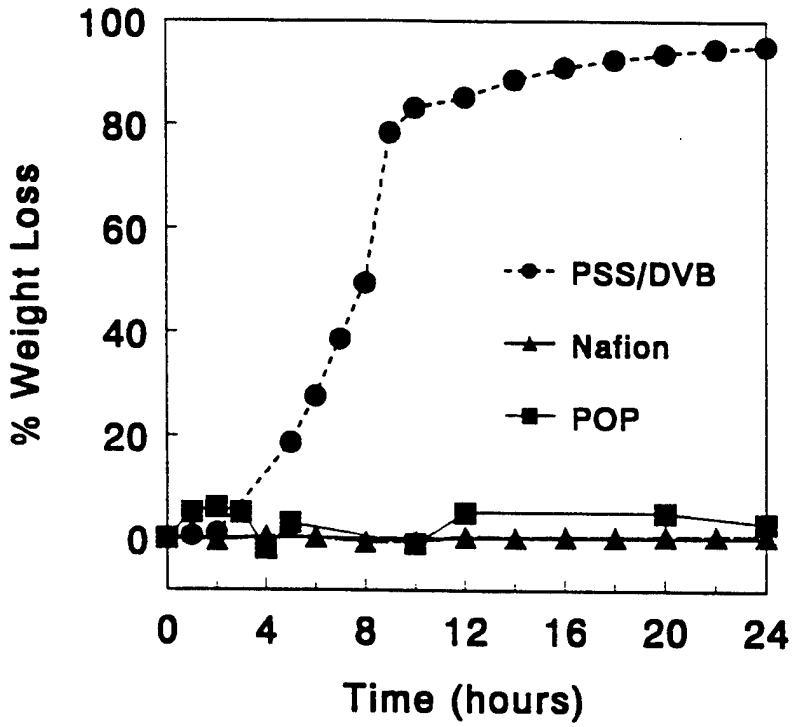

Thermomechanical Analysis (TMA) of Crosslinked/Sulfonated Polyphosphazene Films

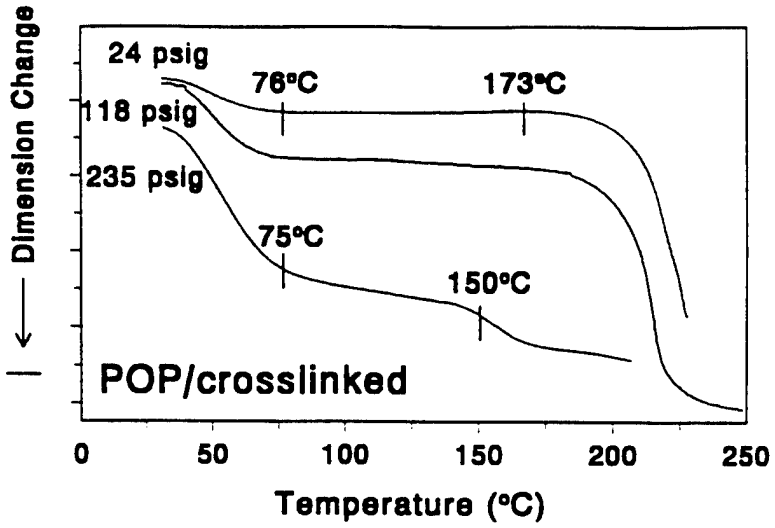

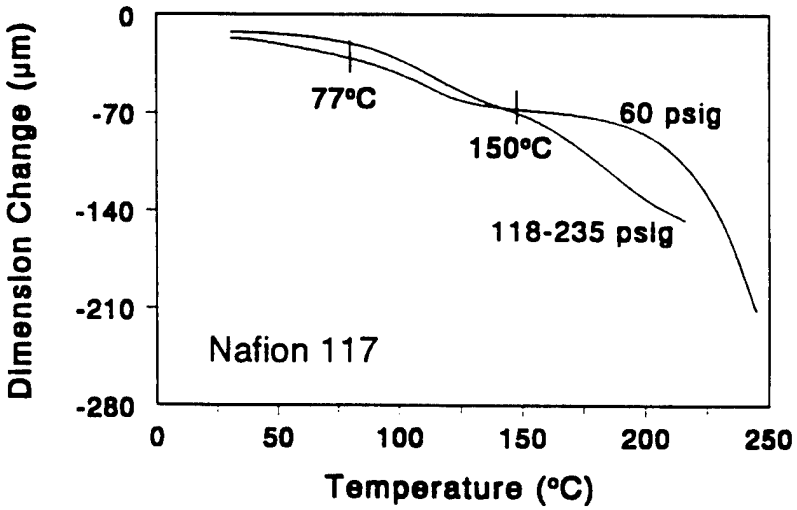

- Penetration mode experiments were used to measure the compressive property (softening) of membranes. Heating rate of 10°C/min in air.
- Typical MEA hot-pressing conditions (1000 psig and 125°C) may irreversibly alter the sulfonated/crosslinked polyphosphazene.
- Non-crosslinked POP began to soften at 31°C with full probe penetration at 89°C.

Proton Conductivity in Sulfonated Poly[bis(3-methylphenoxy)phosphazene] Membranes

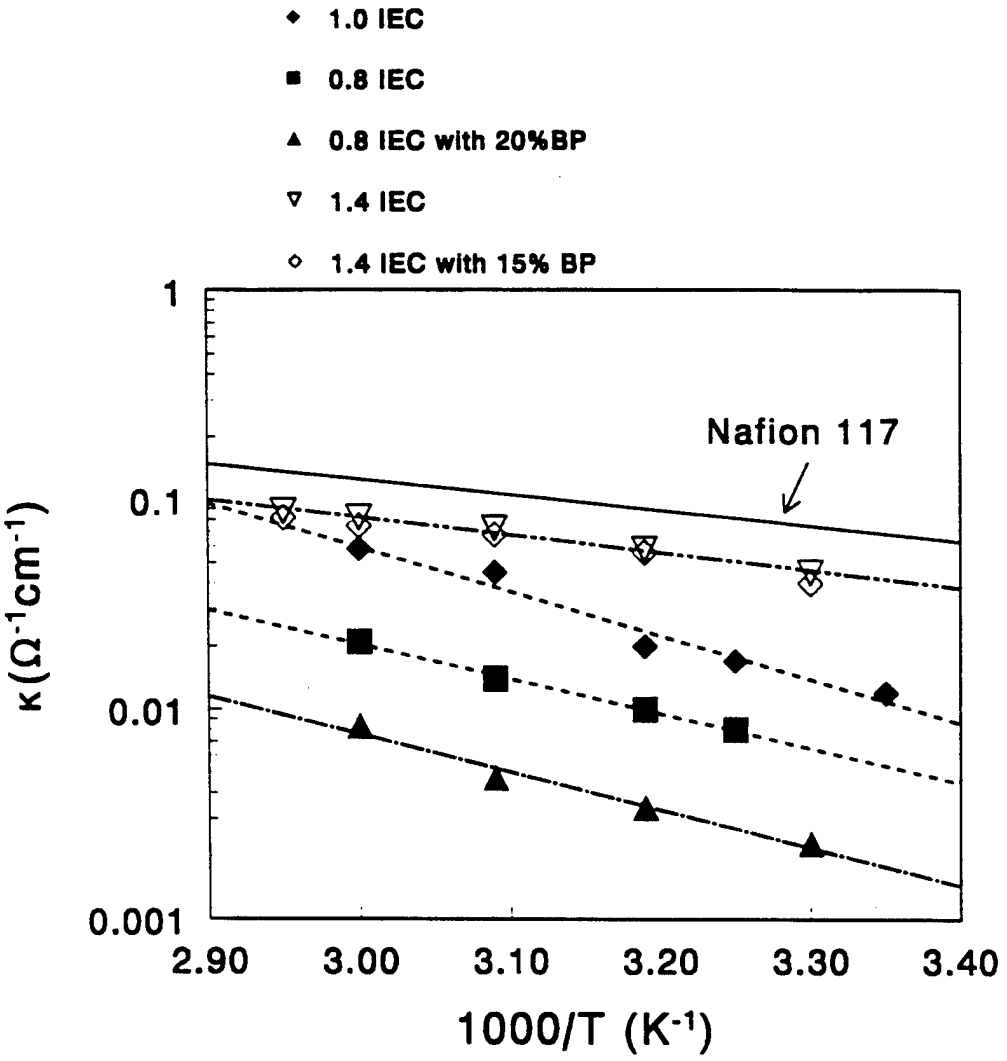

- Longitudinal (x-y) conductance was determined by AC impedance, on membranes in the H^+ form and equilibrated in distilled water.
- Conductivity of membranes increases with increasing temperature (25°C-65°C) and increasing IEC.
- Conductivity of polyphosphazene membranes increases with increasing IEC. Highest measured conductivity: 0.083-0.088 $\Omega^{-1}cm^{-1}$ at T=65°C for 1.4 IEC with/without crosslinking.

Equilibrium Water Swelling of 1.4 IEC Sulfonated Polyphosphazene Films

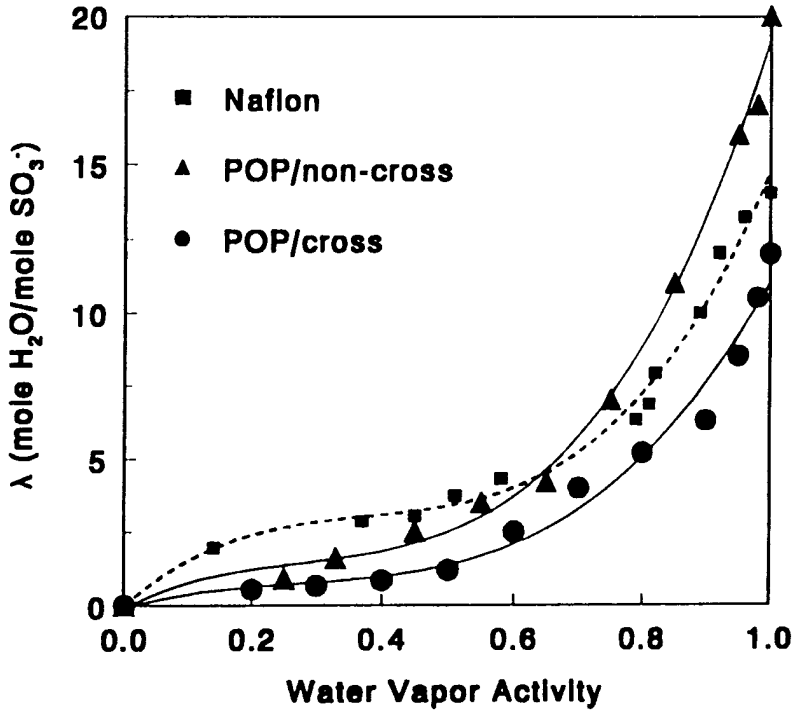

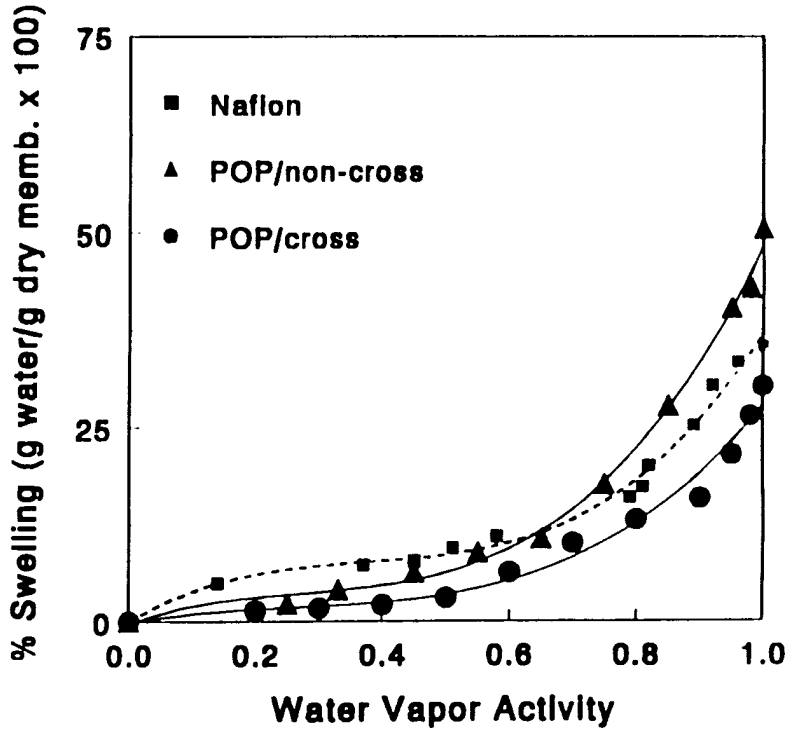

Equilibrium Methanol and Methanol/Water Swelling of 1.4 IEC Sulfonated and Croslinked Polyphosphazene Films

Methanol Vapor Swelling at 30°C

Methanol Vapor Activity	% Methanol Swelling (dry membrane basis)	λ (methanol molecules per SO_3^- Sites)
Polyphosphazene		
0.6	5.4	1.2
0.8	10.5	2.3
0.9	12.5	2.8
Nafion 117		
0.6	9.2	3.2
0.8	12.8	4.4
0.9	15.1	5.2

Selective Absorption of Methanol from External Methanol/Water Solutions (membranes in H^+ form and pre-hydrated)

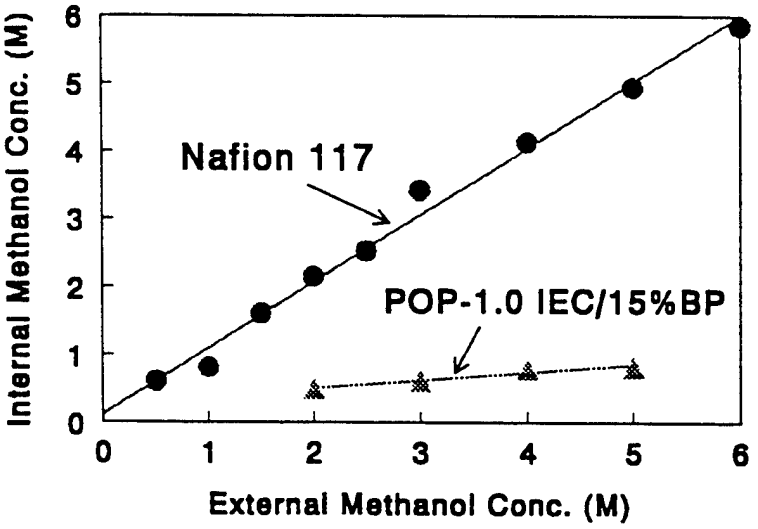

Water Diffusivity in Sulfonated Polyphosphazene Membranes

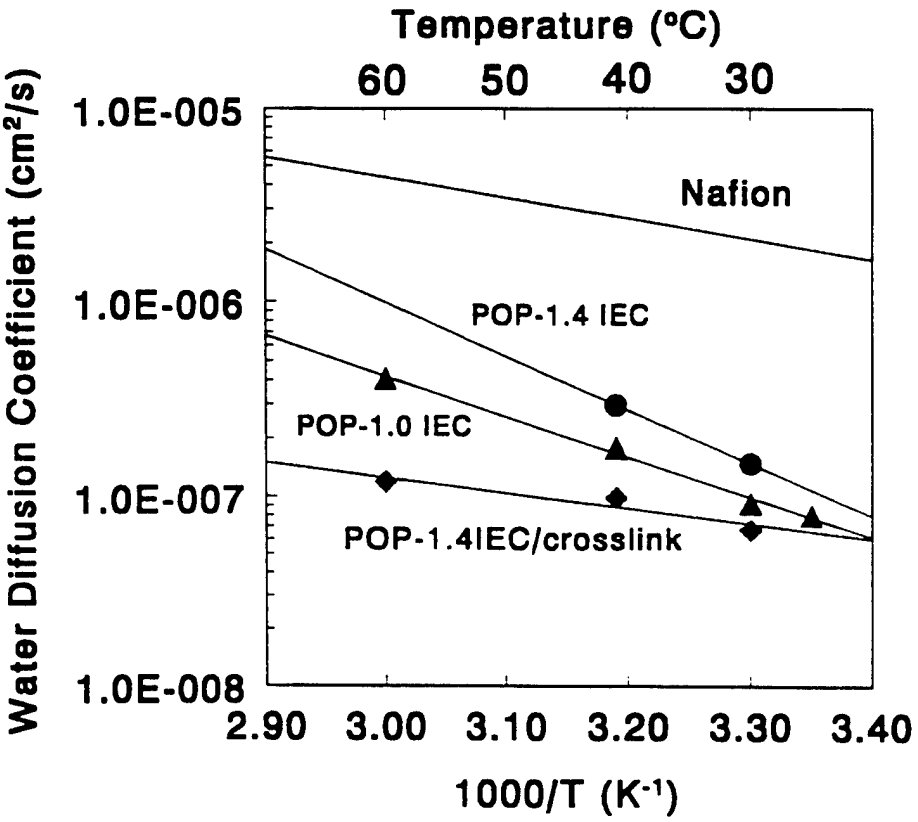

- Diffusivities were measured using a weight loss method, with a quartz spring microbalance, a 600 μm thick POP membrane, and a water vapor activity of 0.98 (0.93 activity during desorption).
- At 60°C, the water diffusivity in a 1.4 mmol/g crosslinked polyphosphazene membrane is 33 times lower than that in Nafion.
- Preliminary methanol diffusion data for a 1.4 IEC/crosslinked membrane - 8.5×10^{-8} cm^2/s at 45°C and a methanol vapor of 0.90.

Future Work

- *Hot-press gas diffusion electrodes onto POP membranes and obtain cell polarization curves for direct methanol/air fuel cell* - Identify MEA hot-pressing conditions; determine methanol crossover; examine long-term membrane stability.

- *Measure membrane physical properties* - Methanol diffusivity (pulsed field gradient NMR method) for methanol/water solutions; electro-osmotic drag coefficient of water; water/polymer and methanol/polymer interactions (ATR-FTIR).

- *Optimize the ion-exchange capacity and degree of crosslinking* - for poly[bis(3-methylphenoxy)phosphazene].

- *Investigate new phosphazene polymers for sulfonation and crosslinking* - Thermally crosslinked polymers; block copolymers, the use of star crosslinkers.

- *Investigate interpenetrating polymer networks (IPNs)* - With sulfonated/crosslinked polyphosphazenes.

ACKNOWLEDGMENTS

Co-Workers: Dr. Hao Tang, Dr. Ryszard Wysick, Richard Graves, and Roy Carter
Department of Chemical Engineering
Tulane University

Dr. Qunhui Guo and Professor Sally O'Connor
Department of Chemistry
Xavier University, New Orleans, LA 70125

Funding Provided by: -Office of Naval Research
-National Science Foundation
-U.S. Department of Energy, through the Tulane/Xavier Center for Bioenvironmental Research

An Overview of Ionomer Membrane Stability – a commentary on the slides presented at the Workshop on Advanced Fuel Cell Membranes, Las Vegas, NV, April 28, 1998. Charles W. Martin.

A quantitative, critical evaluation of ionomer membrane life via a review of the literature is quite difficult. While a significant amount of information has been reported on various membrane structures, it tends to be in the form of conclusions with limited backup data and experimental detail. Also, side-by-side comparisons of performance and life are somewhat problematic since the optimum operating conditions for different membrane vary significantly depending on structure, equivalent weight, membrane thickness, etc.

Slides 1-3. The challenges and issues of membrane stability can be well illustrated by comparing the literature on the three membrane materials listed on Slide 3. They run the gamut from a pure hydrocarbon ionomer through the perfluorinated Nafion®.

Slide 4. Partially sulfonated polystyrene was one of the first PEM fuel cell membranes used for the Gemini space program. At lower temperatures, it has a significant operating life but above 80° C the operating life is measure in hundreds of hours depending on the extent of crosslinking. Crosslinking raises the molecular weight and slows the loss of membrane mass due to oxidative cleavage. Grafting polystyrene on to a more stable, partially fluorinated backbone also gives improved but still limited stability (Slide 7).

Slide 5. Sulfonated poly-α,α,β-trifluorostyrene represented the next generation of membranes with dramatically improved stability. General Electric patented this membrane and demonstrated operating lifetimes of over 8000 hours in a fuel cell at 80° C. While the chemical stability was improved, the physical properties were quite poor. In recent years, the properties of α,α,β-trifluorostyrene-based ionomers have been improved by grafting onto an ethylene-tetrafluoroethyene copolymer backbone (Slide 6, Ramion®, Chlorine Engineers Corp.). The resulting membrane has shown stable

operation for 10,000 hr. in electrolysis mode (Slide 12). At last check, development of Ramion has been terminated by CEC. Ballard Technologies is currently developing an improved version of this class of membrane by co-polymerization of α,α,β-trifluorostyrene with one or more ring substituted monomers (Slide 8). An operating life in excess of 14,000 hr. at 80° C, 500 asf in a fuel cell has been demonstrated (Slide 9).

Slide 10. The longest-lived membrane material tested to date is Nafion®, a perfluorinated sulfonic ionomer membrane. Operating lifetimes of 100,000 hr. have been reported. Interestingly, the operating life has been correlated with the small amount of fluoride present in the product water. This clearly indicates that even the perfluorinated materials are chemically degraded at a finite rate in an operating fuel cell. The degradation rate is temperature dependent with an activation energy of 18 kcal/mole measured over the range of 60-100° C (Slide 11).

The chemical degradation of ionomer membranes in a fuel cell or electrolysis cell is an asymmetric phenomenon. The degradation is most rapid near the electrode that is consuming (fuel cell) or producing (electrolysis cell) hydrogen (Slide 13,14). This is well illustrated by the electrolysis study reported by Scherrer and coworkers shown on Slide 15 & 16. In this work, several thin layers of a membrane were compressed between electrodes and operated for an extended time in an electrolysis cell. The membrane layers were then separated and analyzed for degradation. The results clearly show that the rate of degradation is inversely related to the distance from the hydrogen cathode. This and other studies have led to the hypothesis outlined on Slide 17. According to this proposal, hydrogen radicals form at the electrode and combine with oxygen that has diffused through the membrane to form hydrogen peroxide. The hydrogen peroxide then diffuses into the membrane until it encounters a trace metal contaminate, especially iron, which catalyzes the formation of peroxyl and hydroxyl radicals. These highly reactive species then attack the polymer. In support of this mechanism, the in-cell stability of ionomer membranes has been shown to correlate with their resistance to the iron catalyzed oxidation with hydrogen peroxide (Fenton's reagent) as illustrated in Slide 18.

As the operating temperature of a fuel cell increases, thermal degradation also becomes a concern. The desulfonation of aromatic sulfonic groups (Slide 21) is an acid catalyzed process and is therefore auto-catalytic. The rate increases with increasing temperature and decreasing hydration. Sulfonated aromatic ion exchange resins are known to have limited life above 100° C. The thermal stability of sulfonated poly-α,α,β-trifluorostyrene has not been reported.

Perfluorinated sulfonic acid membranes also undergo a thermal degradation process. A proposed mechanism based on known chemistry of perfluorinated alkyl sulfonic acids is outlined on slide 22. Since the first step is a reversible loss of water to form a sulfonic anhydride, this process would also be auto-catalytic and very dependent on the amount of water in the system. Under anhydrous conditions, perfluorinated alkyl sulfonic acids have been reported to lose sulfur dioxide at temperatures as low as 180° C.

Physical strength and resistance to dimensional changes are also an important consideration at higher temperatures. In the absence of reinforcement, the physical properties of a membrane are dependent on the glass transition (Tg), crystallinity, and covalent crosslinking. In the absence of crystallinity or covalent crosslinking, the long term operating temperature of a membrane will be limited by the glass transition (Slide 23,24).

Clearly, the design of membranes for high temperature fuel cells involves multiple challenges beyond the problem of conductivity in a low hydration environment. Chemical, thermal and physical stability are all critical questions that must be addressed by the scientists and engineers working to advance fuel cell technology.

Stability of Proton Exchange Membranes

An Overview

479

Overview of Presentation

- Illustrate using three of membranes
- Compare operating life
- Mechanism of chemical degradation
- Mechanisms of thermal degradation
- Morphological and dimensional stability

480

Membrane Types

- Polystyrene based membranes
  - Homopolymer, partially sulfonated
  - Grafted & sulfonated
- α,α,β-Trifluorostyrene based membranes
  - Homopolymer, partially sulfonated
  - Copolymers, partially sulfonated
  - Grafted & sulfonated
- Perfluorinate sulfonic polymers (Nafion®)

481

Sulfonated Polystyrene

- SPS membranes were among the first PEM
  - Used in Gemini Space Program
- Useful life below 60° C
  - "Several thousand hours", 70 mw/cm^2
  - Rapid degradation above 80° C
- Life extended by
  - Crosslinking
  - Grafting to more stabile backbone

482

Sulfonated α,α,β-Trifluorostyrene

- Homopolymer
  - Greatly improved operating life vs SPS
  - 8000 hr @ 80° & 70 mw/cm^2
  - Very poor physical properties
- Grafted on PVDF (Raymion®)
  - >10,000 hr (electrolysis) @ 80° & 1 a/cm^2
- Ballard copolymer
  - >13,000 hr in PEMFC @ 80° & 500 asf

483

Raymion Structure

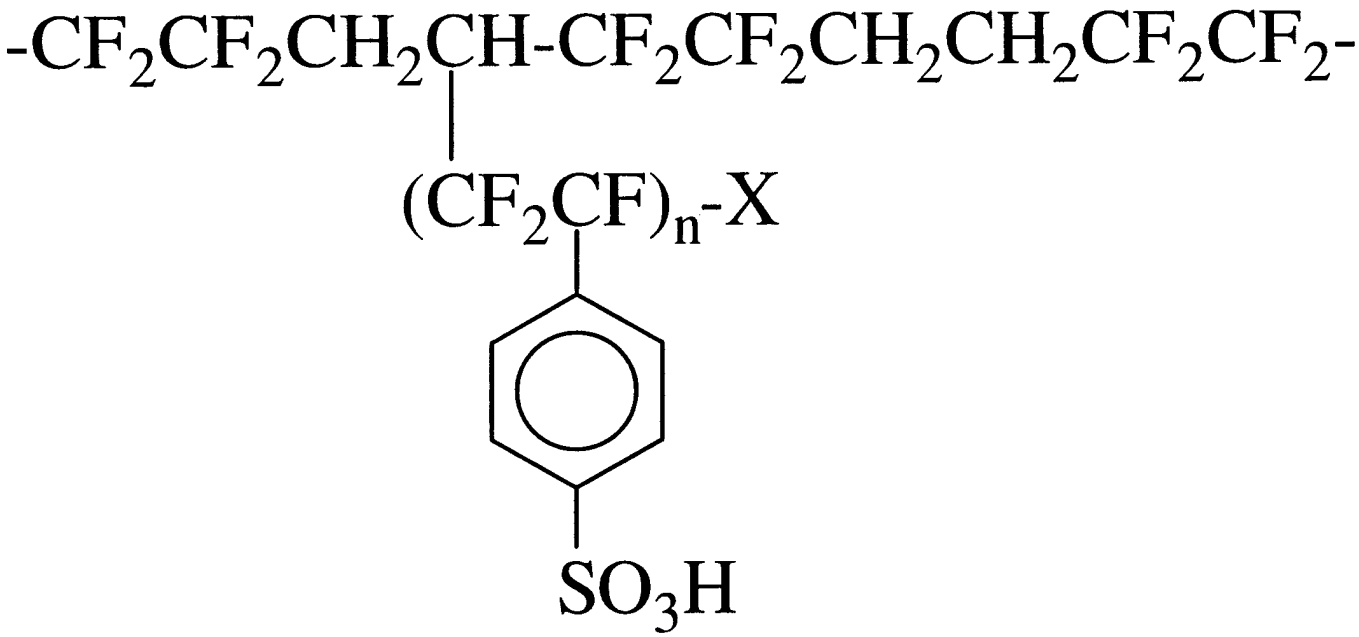

484

Permion 4010 Structure

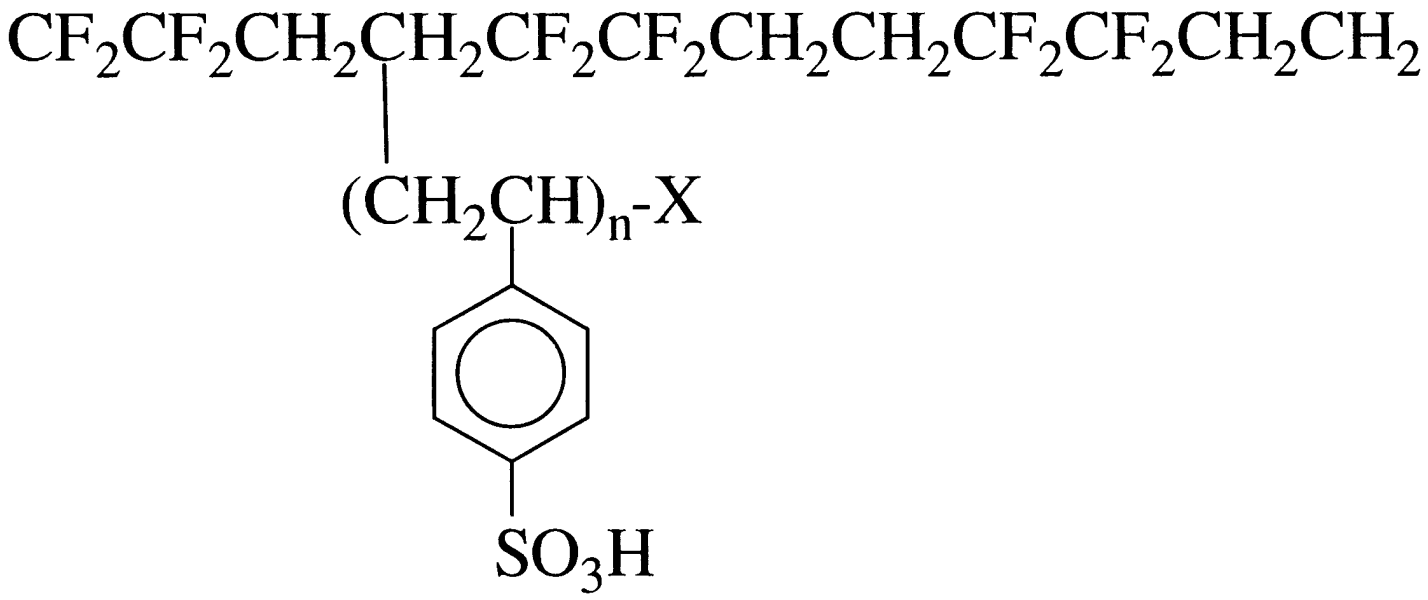

485

Generalized Formula for BAM3G

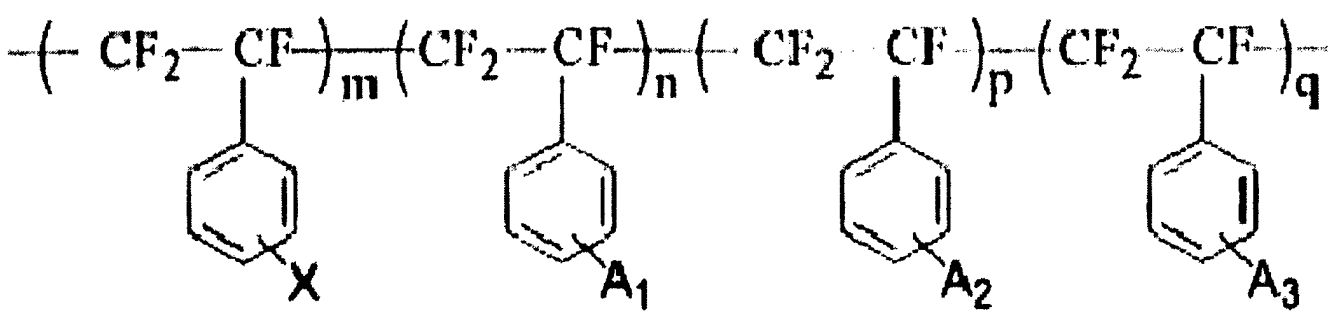

In this generalized formula, at least two of m, n, p and q are greater than zero, with X selected as SO_3H. The groups A_1, A_2 and A_3 are selected from the series consisting of alkyl, perfluoroalkyl, halogen, etc.

486

BAM Membrane Performance in MK5 Hardware

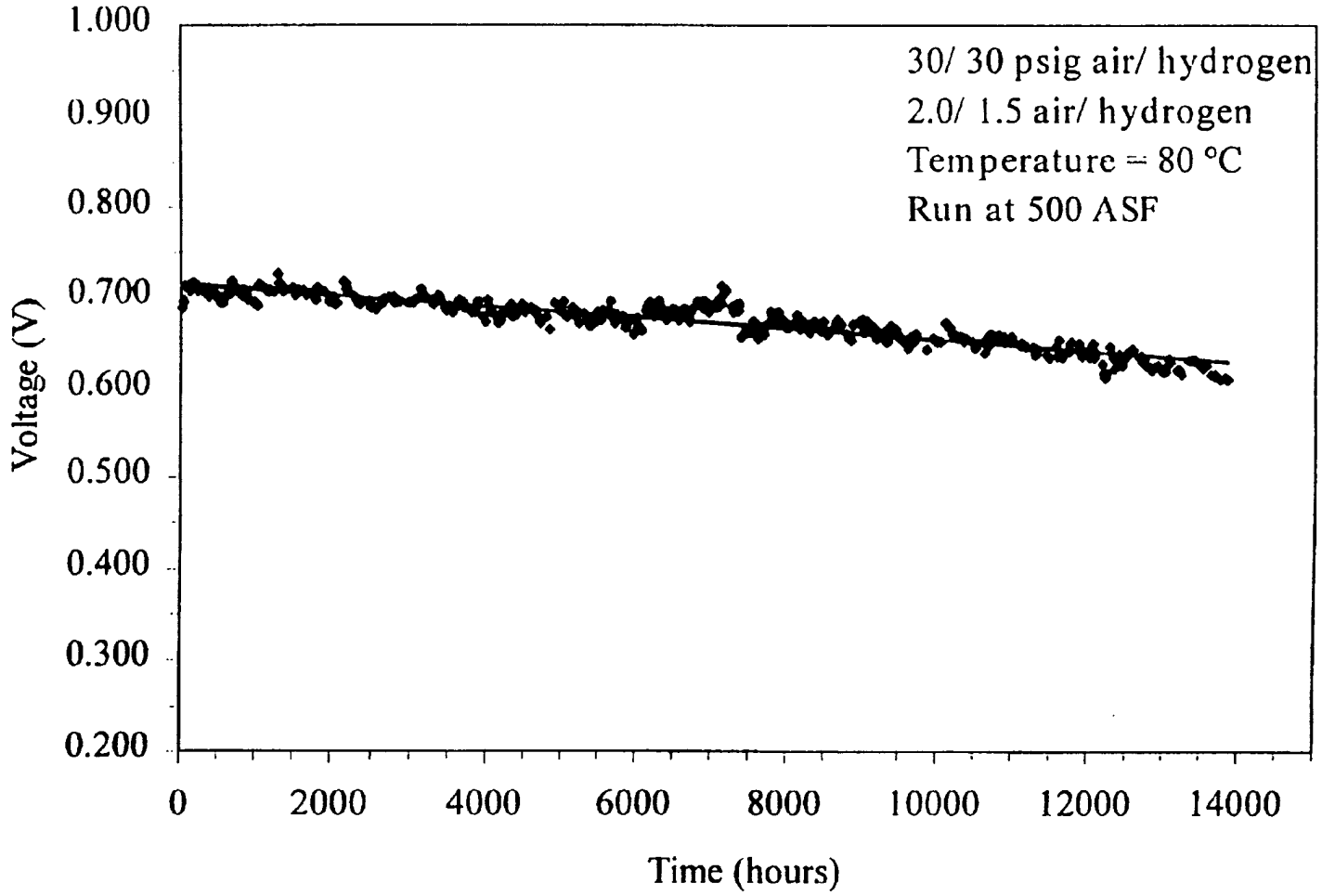

487

Perfluorinated Sulfonic polymers

- Longest lived membrane - 100,000 hr.
  - Most of the data on Nafion®
- Life correlated with F^- in effluent.
  - Even perfluorinated polymers chemically degradation in a fuel cell.

488

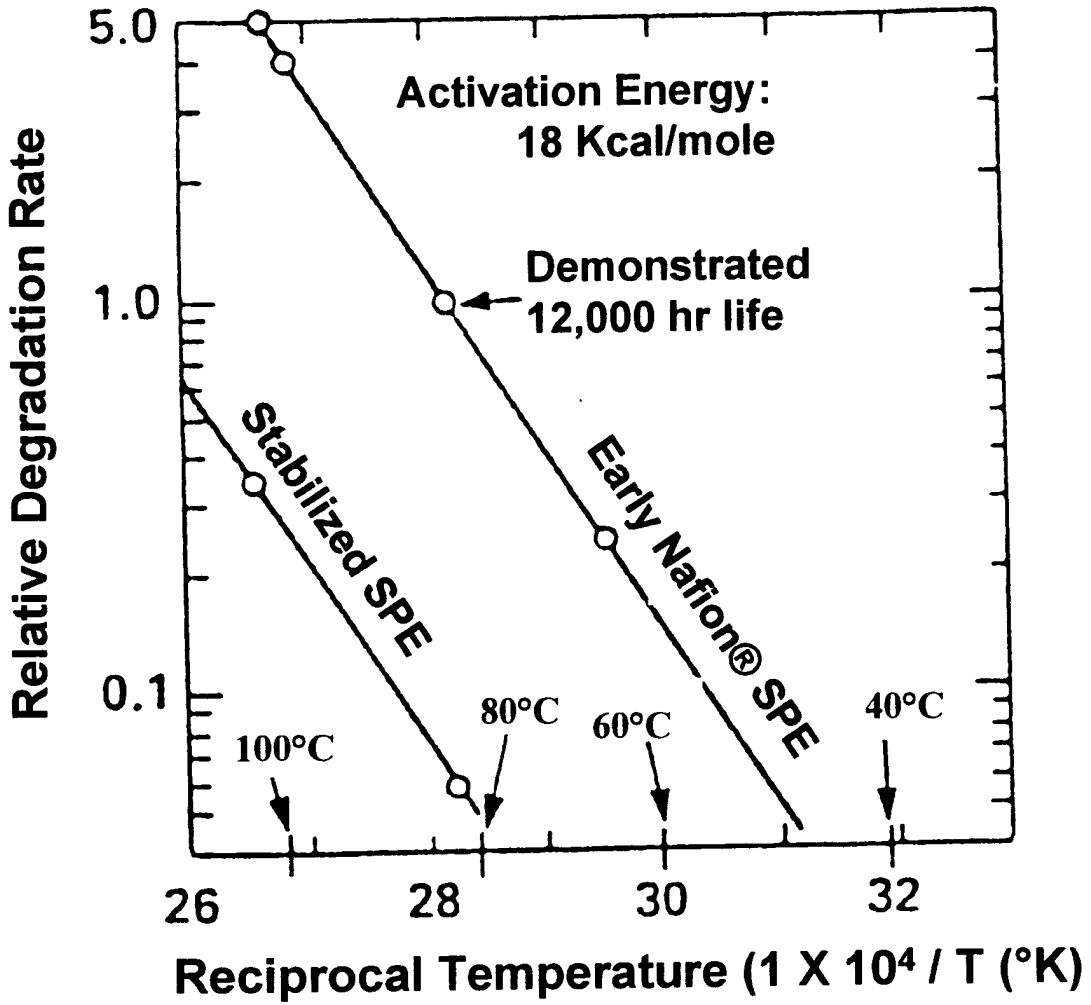

Adapted from A. B. LaConti, A. R. Fragala, & J. R. Boyack, in "Proc. of the symp on electrode materials and processes for energy conversion and storage", p 354, eds. D. E. McIntyre, S. Srinivasan, and F. G. Will. The Electrochem. Soc., 77-6, 1977

Electrolysis Cell Performance

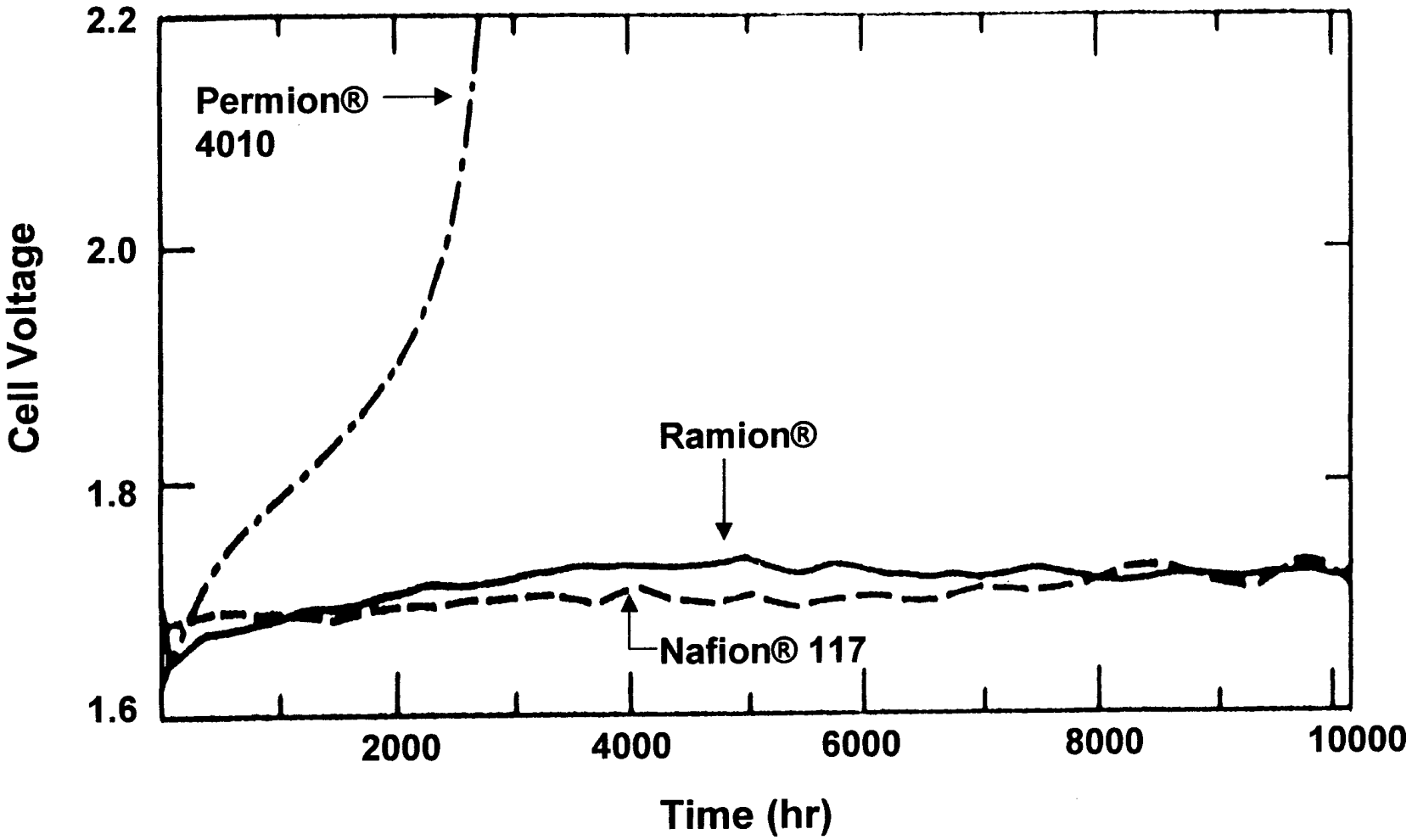

Adapted from G. G. Scherer; Ber. Bunsen-Ges. Phys. Chem., 94(9), 1008-14 "Polymer membranes for fuel cells"

490

Degradation Mechanism

- In-cell degradation is asymmetric
- Occurs near the hydrogen electrode
  - Fuel cell anode
  - Electrolysis cell cathode

491

Asymmetric Degradation*

- Five identical membrane layers stacked between electrodes in an electrolysis cell.
- Permion® 4010
  - 1 A/cm^2, 80°C, 1000 hr.
- Nafion ® 117
  - 1 A/cm^2, >100°C, several thousand hours.
- Measure membrane thickness and Ion Exchange Capacity (IEC)

*G. G. Scherer; Ber. Bunsen-Ges. Phys. Chem., 94(9), 1008-14 "Polymer membranes for fuel cells"

492

Asymmetric Degradation - Permion® 4010

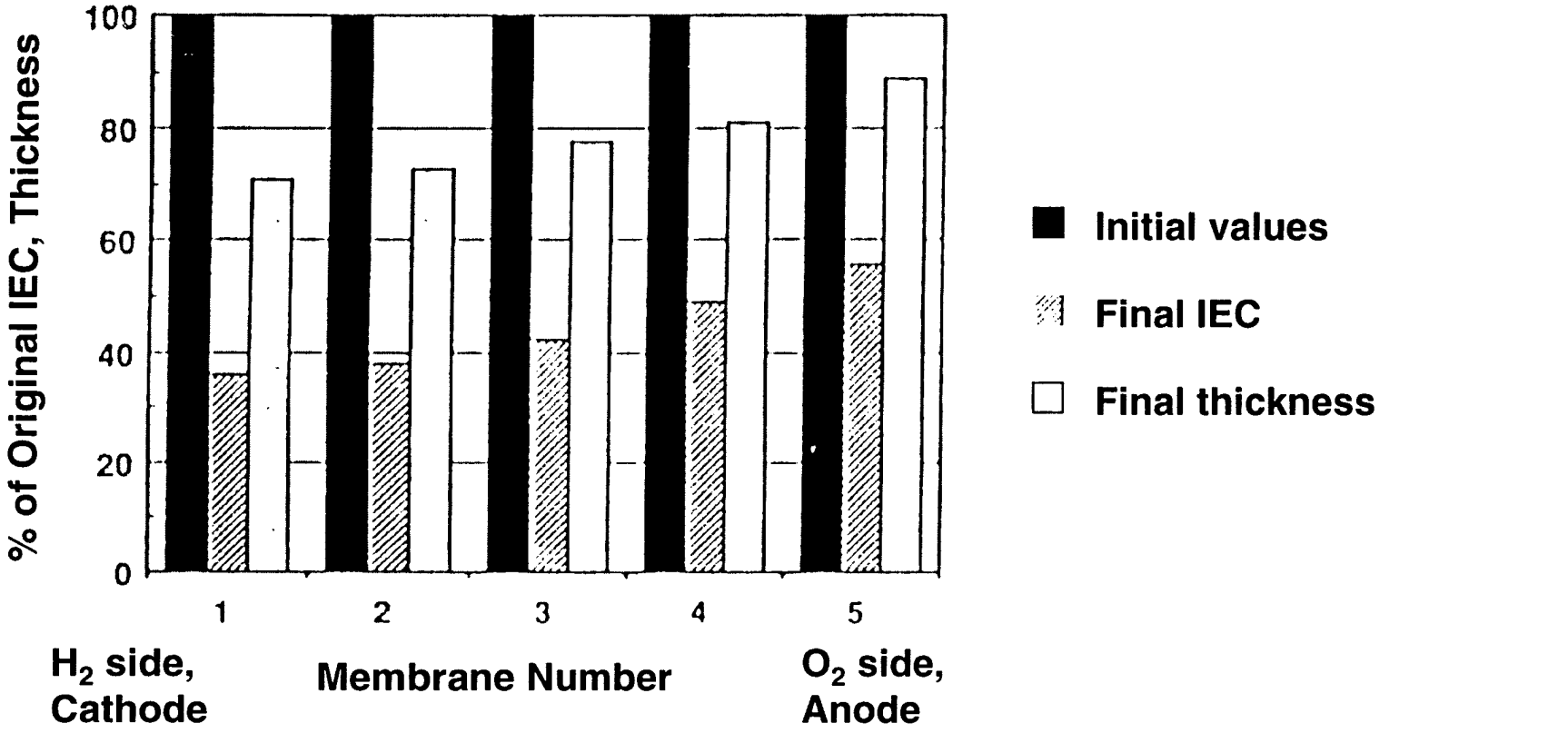

493

Adapted from G. G. Scherer; Ber. Bunsen-Ges. Phys. Chem., 94(9), 1008-14 "Polymer membranes for fuel cells"

Asymmetric Degradation - Nafion® 117

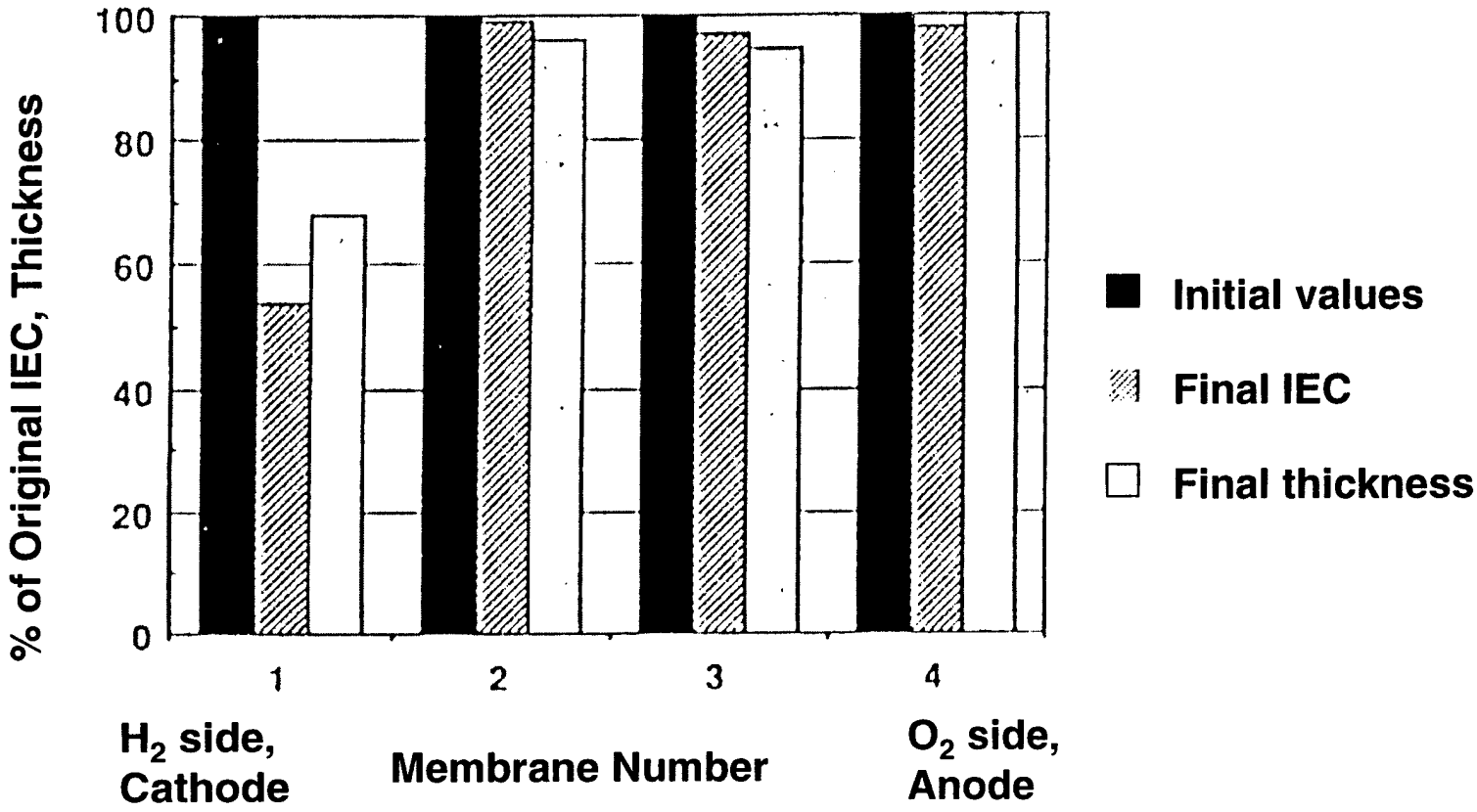

494

Adapted from G. G. Scherer; Ber. Bunsen-Ges. Phys. Chem., 94(9), 1008-14 "Polymer membranes for fuel cells"

Proposed Mechanism (simplified)

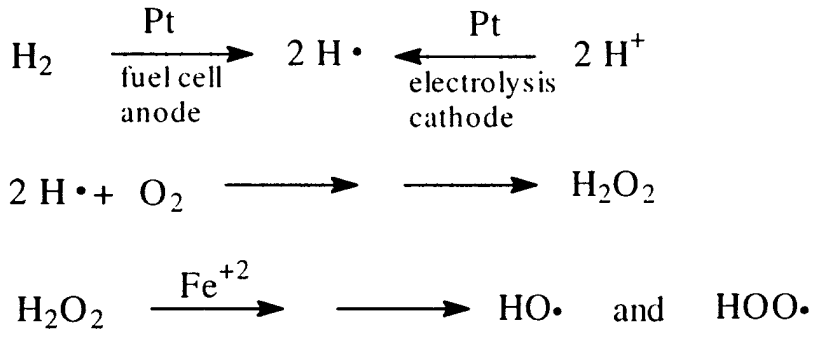

- Oxygen diffuses through the membrane
- Combines with hydrogen radicals to form H_2O_2
- Hydrogen peroxide migrates into the membrane.
- Metal catalyzed decomposition gives HO• and HOO•
- Radicals degrade polymers

495

Degradation of Ionomers with Fenton's Reagent*

Giner, Inc.

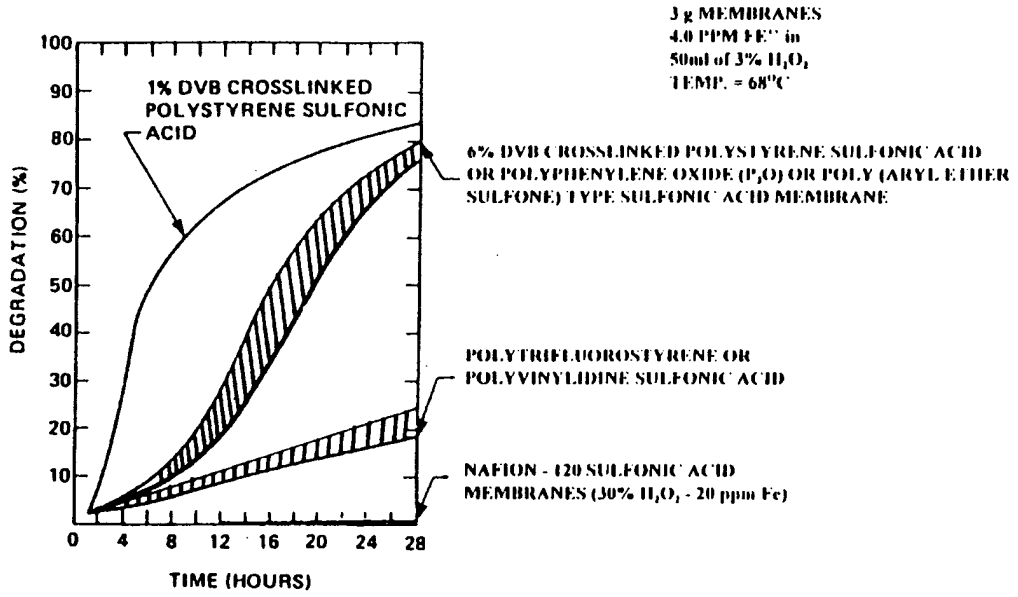

Figure 5. Degradation Rate of Certain Sulfonic Acid Membranes in H_2O_2/Fe^{++} Media

*From A. B. LaConti, "Disposable Fuel Cells and Lifetimes", Workshop on Disposable Fuel Cells, W. H. Smyrl and P. S. Fedkiw, eds., Minneapolis, MN, April 11-12, 1996, p. 109 with permission from the author.

Important Variables

- Oxygen diffusion rate
- Temperature
- Trace metal contaminants (especially Fe^{+2})
- Reactivity of polymer backbone

497

Thermal Degradation

- Functional group degradation.
- Loss of sulfonic group most common

498

Aromatic Desulfonation

- Mechanism

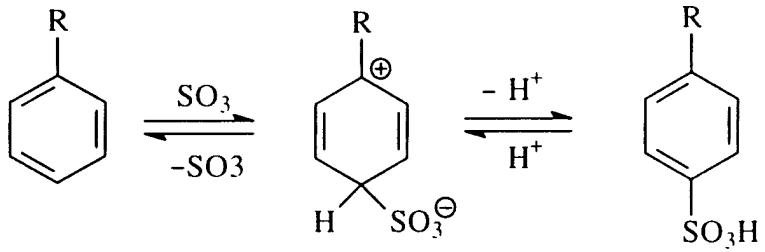

- Rate depends on temperature, hydration, substituent effects.

499

Perfluoroalkyl Sulfonic Acid Degradation

$$2\ R_fCF_2\text{-}SO_2\text{-}OH \xrightarrow[[-\ H_2O]]{H^+} R_fCF_2\text{-}SO_2\text{-}O\text{-}SO_2\text{-}CF_2R_f$$

$$R_fCF_2\text{-}SO_2\text{-}O\text{-}SO_2\text{-}CF_2R_f \xrightarrow[180^oC]{H^+} R_fCF_2\text{-}SO_2\text{-}O\text{-}CF_2R_f + SO_2$$

$$R_fCF_2\text{-}SO_2\text{-}O\text{-}CF_2R_f \xrightarrow[H_2O]{H^+} R_fCF_2\text{-}SO_2\text{-}OH + R_fCOF + HF$$

$$R_fCOF + \xrightarrow[H_2O]{H^+} \longrightarrow R_fH + CO_2 + HF$$

Rate depends on temperature and hydration.

500

Membrane Physical Properties

- Amorphous Tg
  - Amorphous phase becomes thermoplastic
- "Ionic" Tg
  - Ionic phase becomes mobile
  - Nafion ionic Tg ≅ 105° C.
  - Dow PFSA Tg ≅ 155° C
- Crystalline melt point
- Covalent crosslinking

501

COMPARISON OF STORAGE MODULI FOR 800 EW PERFLUOROSULNATE:
PRECURSOR, ACID, AND IONOMER AT 10 RAD/S

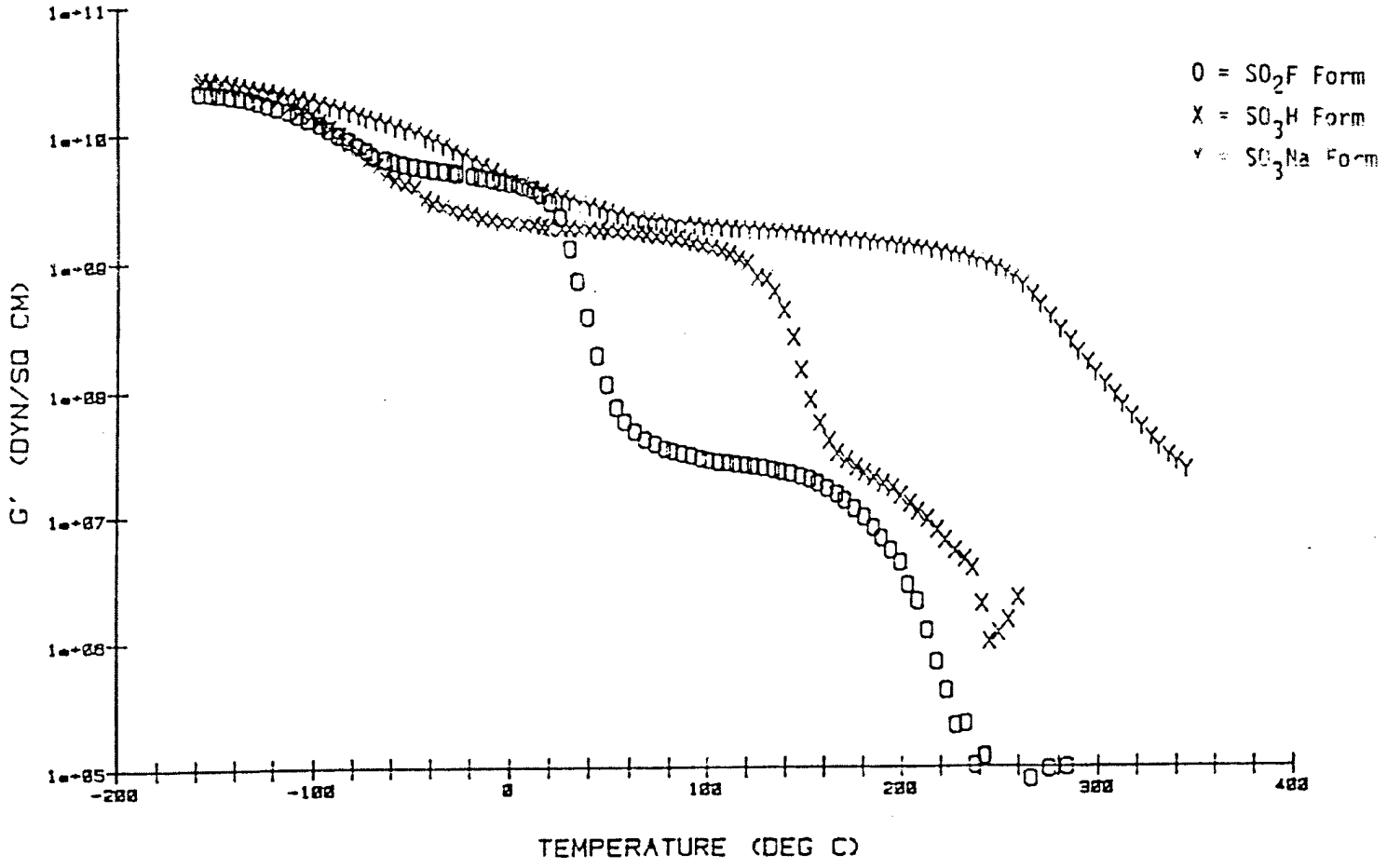

502

Conclusions

- Multiple challenges in the design of advanced membranes.
- Chemical, thermal and physical stability are all critical considerations.
- Study of "classical" membrane structures has provided a good understanding of the challenges.

503